EUROCVD / Baltic ALD 2023

ABSTRACT BOOK

29 May – 2 June
Leuven, Belgium

Conference program

Monday, 29 May 2023

12:00pm - 1:15pm	**Welcome coffee & registration**	Jubilee Hall
1:15pm - 1:30pm	**Welcome**	Auditorium 1, Promotion Hall
1:30pm - 3:00pm	**Precursor design I** Session Chair: Miika Mattinen	Auditorium 1, Promotion Hall
3:00pm - 3:30pm	**Coffee break & Sponsor Exhibition**	Jubilee Hall
3:30pm - 5:00pm	**Characterization I** Session Chair: Neil Dasgupta	Auditorium 1, Promotion Hall
5:00pm - 6:30pm	**Welcome reception**	Historical Town Hall Leuven

Tuesday, 30 May 2023

8:00am - 8:30am	**Welcome coffee & registration desk is open**	Jubilee Hall
8:30am - 10:00am	**Functional materials I** Session Chair: Henrik Sønsteby	Auditorium 1, Promotion Hall
8:30am - 10:00am	**ASD I / organic** Session Chair: Anjana Devi	Auditorium 2, Maria-Theresiacollege
10:00am - 10:30am	**Coffee break & Sponsor Exhibition**	Jubilee Hall
10:30am - 12:00pm	**Characterization II** Session Chair: Joachim Schnadt	Auditorium 1, Promotion Hall
10:30am - 12:00pm	**Functional materials II** Session Chair: Elisabeth Blanquet	Auditorium 2, Maria-Theresiacollege
12:00pm - 1:30pm	**Lunch & Sponsor Exhibition**	Jubilee Hall
1:30pm - 3:00pm	**Energy-related applications and catalysis I** Session Chair: Geoffrey Hyett	Auditorium 1, Promotion Hall
1:30pm - 3:00pm	**Metals** Session Chair: Ageeth A. Bol	Auditorium 2, Maria-Theresiacollege
3:00pm - 3:30pm	**Coffee break & Sponsor Exhibition**	Jubilee Hall
3:30pm - 5:00pm	**Semiconductor and nanomaterials I** Session Chair: Erwin Kessels	Auditorium 1, Promotion Hall
3:30pm - 5:00pm	**Energy-related applications and catalysis II** Session Chair: Andreas Georgiou Kafizas	Auditorium 2, Maria-Theresiacollege
5:00pm - 8:00pm	**Poster session I (with reception)**	Jubilee Hall

Wednesday, 31 May 2023

8:00am - 8:30am	**Welcome coffee & registration desk is open**	Jubilee Hall
8:30am - 10:00am	**Modeling** Session Chair: Sean Thomas Barry	Auditorium 1, Promotion Hall
10:00am - 10:30am	**Coffee break & Sponsor Exhibition**	Jubilee Hall
10:30am - 12:00pm	**Organic and hybrid materials** Session Chair: Michael Nolan	Auditorium 1, Promotion Hall
12:00pm - 1:30pm	**Lunch & Sponsor Exhibition**	Jubilee Hall
1:30pm - 5:00pm	**Social activities**	
1:45pm	Guided city tour through Leuven	steps of the Historic City Hall of Leuven
2:00pm	University library tour an tower	University Library
3:00pm	AB Inbev brewery tour	Visitors entrance AB Inbev
6:00pm	**Conference dinner**	Faculty Club Leuven

Thursday, 1 June 2023

8:00am - 8:30am	**Welcome coffee & registration desk is open**	Jubilee Hall
8:30am - 10:00am	**Energy-related applications and catalysis III** Session Chair: Caroline Knapp	Auditorium 1, Promotion Hall
9:00am - 10:00am	**Industry** Session Chair: Adriaan J.M. Mackus	Auditorium 2, Maria-Theresiacollege
10:00am - 10:30am	**Coffee break & Sponsor Exhibition**	Jubilee Hall
10:30am - 12:00pm	**Precursor design II** Session Chair: Patrik Hoffmann	Auditorium 1, Promotion Hall
10:30am - 12:00pm	**Semiconductor and nanomaterials II** Session Chair: Alfonso Sepulveda Marquez	Auditorium 2, Maria-Theresiacollege
12:00pm - 1:30pm	**Lunch & Sponsor Exhibition**	Jubilee Hall
1:30pm - 3:00pm	**ASD II** Session Chair: Christophe Detavernier	Auditorium 1, Promotion Hall
1:30pm - 3:00pm	**Functional materials III** Session Chair: Anna Maria Coclite	Auditorium 2, Maria-Theresiacollege
3:00pm - 3:30pm	**Coffee break & Sponsor Exhibition**	Jubilee Hall
3:30pm - 5:00pm	**Dielectrics I** Session Chair: Aile Tamm	Auditorium 1, Promotion Hall
5:00pm - 8:00pm	**Poster session II (with reception)**	Jubilee Hall

Friday, 2 June 2023

8:00am - 8:30am	**Welcome coffee & registration desk is open**	Jubilee Hall
8:30am - 10:00am	**Dielectrics II** Session Chair: Sven Van Elshocht	Auditorium 1, Promotion Hall
10:00am - 10:30am	**Coffee break & Sponsor Exhibition**	Jubilee Hall
10:30am - 12:00pm	**Novel concepts** Session Chair: Naoufal Bahlawane	Auditorium 1, Promotion Hall
12:00pm - 12:15pm	**Closing & announcement of best oral and poster awards (and price)**	Auditorium 1, Promotion Hall
12:15pm - 1:30pm	**Lunch & Sponsor Exhibition**	Jubilee Hall

TABLE OF CONTENTS:

PRECURSOR DESIGN I 1

– **Small Molecule Inhibition on Surfaces: The Role of Carbenes and Other Ligands**
Barry, Sean Thomas; Ragogna, Paul; Crudden, Cathleen*

– **From Molecules to Materials: Precursor Design for the Deposition of Conductive Metals**
*Knapp, Caroline**

– **New non-Pyrophoric metalorganic precursors for CVD and ALD of IGZO**
Schmickler, Marcel; Preischel, Florian; Zanders, David; Klimars, Jacqueline; Devi, Anjana*

– **New Precursors for the Atomic Layer deposition of p-type SnO**
*Johnson, Andrerw**

– **Iron and and cobalt second-generation precursors for the vapor-phase deposition of Fe2O3 and Co3O4 systems**
*Barreca, Davide; Seraglia, Roberta; Jandl, Christian; Pöthig, Alexander; Fois, Ettore; Tabacchi, Gloria; Roverso, Marco; Bogialli, Sara; Callone, Emanuela; Dirè, Sandra; Gasparotto, Alberto; Maccato, Chiara**

CHARACTERIZATION I 10

– **Real-time monitoring of the surface chemistry of ALD processes by ambient pressure x-ray photoelectron spectroscopy**
*Schnadt, Joachim**

– **In-Situ characterization of CVD processes where plasma electrons are utilized as reducing agents**
Niiranen, Pentti; Kapran, Anna; Nadhom, Hama; Čada, Martin; Hubička, Zdeněk; Lundin, Daniel; Pedersen, Henrik*

– **Controlling the Hydrogen Source in zinc, titanium, and aluminum oxides deposited via Atomic Layer Deposition**
Putz, Barbara; Guerra-Nunez, Carlos; Bernardi, Alex; Döbeli, Max; Micher, Johann; Utke, Ivo*

– **Ambient pressure XPS setup for studying in situ ALD**
Kokkonen, Esko; Jones, Rosemary; Schnadt, Joachim*

FUNCTIONAL MATERIALS I 17

– **Vapour deposition of functional semiconductor and heterojunction (nano-)materials for gas sensing**
*Blackman, Chris**

– **Chemical vapor deposition and high-resolution patterning of a highly conductive two-dimensional coordination polymer film**
Rubio Giménez, Víctor; Arnauts, Giel; Wang, Mingchao; Oliveros Mata, Eduardo Sergio; Huang, Xing; Lan, Tianshu; Tietze, Max L.; Kravchenko, Dmitry E.; Smets, Jorid; Wauteraerts, Nathalie; Khadiev, Azat; Novikov, Dmitri V.; Makarov, Denys; Dong, Renhao; A*

– **Gradient polymer coatings deposited via initiated chemical vapor deposition (iCVD) for anti-icing applications**
Hernández Rodríguez, Gabriel; Coclite, Anna Maria*

– **ALD GST industrial processing, scaling to 300mm challenges and outcomes**
Innocent, Jerome; Illiberi, Andrea; Givens, Michael; Sharma, Varun; Nyns, Laura; Hody, Hubert; Delabie, Annelies; Devulder, Wouter; Garbin, Daniele; Luca Donadio, Gabriele; Peissker, Tobias*

– **Extraordinary slippery liquid-repellent surfaces by vapor-deposition of self-assembled monolayers**
Ras, Robin; Lepikko, Sakari; Morais Jaques, Ygor; Junaid, Muhammad; Backholm, Matilda; Lahtinen, Jouko; Julin, Jaakko; Jokinen, Ville; Sajavaara, Timo; Sammalkorpi, Maria; Foster, Adam*

ASD I / ORGANIC 26

– **Area-selective atomic layer deposition of nitrides and oxides using small molecule inhibitors**
*Mackus, Adriaan J.M.**

– **The Importance of Small Molecule Inhibitor Dosing Conditions during Area-Selective ALD Studied with Infrared Spectroscopy**
Bolkenbaas, Olaf C.A.; Maas, Joost F.W.; Merkx, Marc J.M.; Tezsevin, Ilker; Yu, Pengmei; Sandoval, Tania E.; Kessels, Wilhelmus M.M.; Mackus, Adriaan J.M.*

– **Insight into Mechanism of Area-Selective Atomic Layer Deposition of Germanium Telluride**
Sinha, Jyoti; Delabie, Annelies; Nyns, Laura*

– **Bridging the Synthesis Gap: Ionic Liquids Enable Solvent-Mediated Reaction in Vapor-Phase Deposition**
*Shi, Jingwei; Seo, Seunggi; Schuster, Nathaniel; Kim, Hyungjun; Bent, Stacey**

CHARACTERIZATION II 33

– **Interface formation chemistry in ALD of charge transport layers for perovskite solar cells**
*Hultqvist, Adam; Rakheja, Bhavya; Törndahl, Tobias**

– **Gas-phase reactions of Zr(tmhd)4: New insights from microreactor studies using synchrotron radiation**
*Grimm, Sebastian; Hemberger, Patrick; Atakan, Burak**

– **Al2O3 growth in PMMA by SIS: in-situ thickness evolution and mass uptake investigation**
Perego, MIchele; Seguini, Gabriele; Wiemer, Claudia; Caligiore, Federica; Cianci, Elena*

– **Tailoring microstructural features of industrial CVD Ti(C,N) thin hard coating**
El Azhari, Idriss; Garcìa, José; Valle, Nathalie; Barrirero, Jennifer; Pauly, Christoph; Engstler, Michael; Soldera, Flavio; Llanes, Luis; Mücklich, Frank*

FUNCTIONAL MATERIALS II 42

– **Towards fabrication of 1D BN/Carbon Van der Waals heterostructures by atomic layer deposition**
Hossain, Ali; Okuno, Hanako; Journet, Catherine; Marichy, Catherine*

– **ALD of Unique Magnetic Thin Films**
Jussila, Topias; Philip, Anish; Karppinen, Maarit*

– **CVD processing of high quality ferromagnetic CoS2 layers**
Glauber, Jean-Pierre; Wree, Jan-Lucas; Zanders, David; Ney, Andreas; Devi, Anjana*

– **Single-Step PEDOT deposition by oxidative chemical vapor deposition for opto-electronic applications**
Sekkat, Abderrahime; Breig, Benjamin; Salemor, Diane; Poupaki, Eleni; Doxas, Panagiotis; Caussé, Nicolas; Vergnes, Hugues; Vahlas, Constantin; Caussat, Brigitte*

– **Epitaxial LiNbO3 thin film with controlled nonstoichiometry for acoustic wave devices**
Bartasyte, Ausrine; Astié, Vincent; Boujnah, Sondes; Arapan, Lilia; Micard, Quentin; La Spina, Léa; Boulet, Pascal; Margueron, Samuel; Decams, Jean-Manuel*

ENERGY-RELATED APPLICATIONS AND CATALYSIS I 52

– **Interfacial Engineering of Batteries and Solar Energy Materials using Atomic Layer Deposition**
*Dasgupta, Neil P.**

– **Atomic Layer Deposition of Lithium Borate and Borophosphate Thin Films for Lithium-ion Battery Applications**
Verhelle, Tippi; Dhara, Arpan; Henderick, Lowie; Dendooven, Jolien; Detavernier, Christophe*

– **Spatial ALD on porous substrates for energy applications**
*Frijters, Corne; Poodt, Paul**

– **Optimizing a Ni-Fe phosphate catalyst for the Oxygen Evolution Reaction using ALD**

Blomme, Ruben; Ramesh, Rahul; Henderick, Lowie; Detavernier, Christophe; Dendooven, Jolien*

METALS 59

– **Integrity of Graphene in Functional Nanostructures Represented by Resistively Switching Media Grown by ALD**
*Tamm, Aile**

– **MOCVD of highly active metallic iridium films using new amidinate-based precursors for water splitting**
Boysen, Nils; Wree, Jan-Lucas; Zanders, David; Rogalla, Detlef; Devi, Anjana*

– **Effect of thermal induced strain on electrical properties off-stoichiometric Cu2/3 Cr4/3O2 delafossite**
Moreira, Marco; Lunca Popa, Petru; Fleming, Yves; Polesel, Jérôme; Leturcq, Renaud*

– **Superconducting ultrathin TaCxN1-x films for quantum applications enabled by plasma-enhanced ALD with ion-energy control**
Peeters, Silke A.; Lennon, Ciaran T.; Hadfield, Robert H.; Verheijen, Marcel A.; Kessels, Wilhelmus M. M.; Knoops, Harm C. M.*

SEMICONDUCTOR AND NANOMATERIALS I 66

– **Precise doping and alloying of 2D transition metal dichalcogenides using plasma-enhanced atomic layer deposition**
*Bol, Ageeth A.**

– **Advanced Process Design for Low-Temperature PEALD of 2D Transition Metal Dichalcogenides**
Mattinen, Miika; Verheijen, Marcel; Kessels, Erwin; Bol, Ageeth*

– **Transition metal dichalcogenides grown by Direct-Liquid Injection MOCVD**
Astié, Vincent; Wasem-Klein, Felipe; Makhlouf, Houssin; Decams, Jean-Manuel; Paillet, Matthieu; Landois, Périne; Juillaguet, Sandrine; Contreras, Sylvie; Voiry, Damien*

– **Improving Interfacial Properties of 2D Transition Metal Dichalcogenide Gate Stacks by GdAlOx Atomic Layer Deposition**
Lin, Zaoyang; Wu, Xiangyu; Cott, Daire; Groven, Benjamin; Morin, Pierre; Lin, Dennis; Asselberghs, Inge; Delabie, Annelies*

ENERGY-RELATED APPLICATIONS AND CATALYSIS II 73

– **Low-temperature CVD process for Cu2O thin-film growth: applications as photodetectors and HTL for solar cells**
Pellegrino, Anna Lucia; Lo Presti, Francesca; Malandrino, Graziella*

– **Steps towards atomic-layer additive manufacturing for rapid prototyping of solar cells**
*Stefanovic, Sonja; Tymek, Sarah; Kundrata, Ivan; Plakhotnyuk, Maksym; Bachmann, Julien**

– **Electric transport through CVD Molybdenum oxide films. Why these films are excellent hole transfer layers in organic light-emitting diodes?**
*Soultati, Anastasia; Filippatos, Petros-Panagis; Chroneos, Alexander; Vasilopoulou, Maria; Davazoglou, Dimitris**

– **Chemical deposition of Cu2O films with ultra-low resistivity: Correlation with the defect landscape**
Muñoz-Rojas, David; Sekkat, Abderrahime; Weber, Matthieu; Rapenne, Laetitia `; Bellet, Daniel*

POSTER SESSION I 81

– **Transition metal oxide nanoheterostructures by hybrid CVD routes as heterogeneous photocatalysts for air purification**
Barreca, Davide; Fragoso, Javier; Gasparotto, Alberto; Sada, Cinzia; Lebedev, Oleg I.; Modin, Evgeny; Pavlovic, Ivana; Sánchez, Luis; Maccato, Chiara*

– **Resistive switching in memristor structures with multilayer dielectrics**
Merisalu, Joonas; Viskus, Toomas Daniel; Aarik, Jaan; Kukli, Kaupo*

– **The effect of dopant element on mechanical and optical properties of Cr2O3 thin films.**
Salari Mehr, Mahtab; Aarik, Lauri; Jõgiaas, Taivo; Tarre, Aivar; Kasikov, Aarne; Mändar, Hugo*

– **Molybdenum-carbide and tungsten-carbide CVD coatings obtained by Avinit vacuum-plasma technologies.**
Sagalovych, Olexiy V.; Sagalovych, Vladislav V.; Dudnik, Stanislav.F.; Popov, Viktor V.; Popenchuk, Roman P.*

– **Nano-tailored morphology of La2NiO4+δ thin films using PI-MOCVD**
*Stangl, Alexander; Riaz, Adeel; Rapenne, Laetitia; Panisset, Silvere; Burriel, Monica; Jiménez, Carmen**

– **Impact of precursor reactivity on growth of self-assembled 3D architectures**
Ziegler, Mario; Zanders, David; Ripka, Valentin; Wagner, Hanjörg; Devi, Anjana; Hübner, Uwe*

– **Conformal and superconformal chemical vapor deposition of silicon carbide coatings**
Huang, Jing-Jia; Militzer, Christian; Wijayawardhana, Charles A.; Forsberg, Urban; Pedersen, Henrik*

– **Encapsulating TiO2 thin films grown via Atomic Layer Deposition for biocompatible UV-activated neuronal interfaces**
El Habra, Naida; Famengo, Alessia; Sagrini, Giacomo; Canton, Patrizia; Boldrini, Stefano; Ferrario, Alberto; Galenda, Alessandro; Natile, Marta Maria; Sada, Cinzia; Leparulo, Alessandro; Maschietto, Marta; Losurdo, Maria; Vassanelli, Stefano*

– **Synthesis of graphene nanoribbons via atmospheric-pressure CVD: understanding the process parameters roles through spectroscopy**

Osipov, Vasilii; Weitkamp, Philipp; Reimer, Max; Han, Yi; Müllen, Klaus; Hertel, Dirk; Meerholz, Klaus*

– **Enhancing corrosion protection properties of steel by phase control of CVD processed ZrO2 films**

Glauber, Jean-Pierre; Beer, Sebastian M.J.; Samélor, Diane; Etzkorn, Johannes; Kostka, Aleksander; Vahlas, Constantin; Devi, Anjana*

– **The use of silver CVD nanostructured substrates in analysis of low molecular weight compounds**

Radtke, Aleksandra; Piszczek, Piotr; Sagandykova, Gulyaim; Pomastowski, Paweł*

– **Ruthenium Sulfide Thin Films - a New Route via MOCVD**

Obenlüneschloß, Jorit; Zanders, David; Wree, Jan-Lucas; Selvakumar, Ilamparithy; Devi, Anjana*

– **KNbO3 thin film growth with advanced CVD precursors**

Labbaveettil Basheer, Ishamol; Peddagopu, Nishant; Lo Presti, Francesca; Ouhabaz, Merieme; Margueron, Samuel; Astié, Vincent; Decams, Jean-Manuel; Malandrino, Graziella; Bartasyte, Ausrine*

– **SALD deposition of ZnO coatings for flexible, transparent electrodes for localized heating of lab-on-chip devices**

Muñoz-Rojas, David; Papanastasiou, Dorina; Sekkat, Abderrahime; Nguyen, Viet; Jimenez, Carmen; Bruckert, Franz; Bellet, Daniel*

– **Rare-earth sulfide thin films for magneto-optical applications**

Preischel, Florian; Beer, Sebastian M. J.; Debus, Joerg; Ney, Andreas; Parala, Harish; Shashindra, Ravindra; Baspinar, Silan; Devi, Anjana*

– **Single source precursor approach towards MoS2 thin films via MOCVD**

Wilken, Martin; Shashindra, Ravindra; Becher, Malte; Ostendorf, Andreas; Devi, Anjana*

– **Synthesis of Self-Cleaning Window Glass for Photocatalytic Oxidation of NOx: Effect of APCVD Synthesis Conditions**

Lin, Zhipeng; Li, Yuankai; Kafizas, Andreas*

– **Vapour Phase Infiltration: an efficient strategy to tune microporous Metal Organic Frameworks**

Marichy, Catherine; De, Siddhartha; Quan, Gian Co; Gikonyo, Ben; Martineau Corcos, Charlotte; Bousige, Colin; Veyre, Laurent; Devic, Thomas; Fateeva, Alexandra*

– **Atomic-molecular layer deposition of hybrid multilayers of AlN straddled with hydroquinone nanolayers.**

Mpofu, Pamburayi; Rowe, Collin; Ramanath, Ganpati; Pedersen, Henrik*

– **Depositing ALD-oxides on MLD-metalcones: enhancing initial growth through O2 plasma densification.**

Santo Domingo Peñaranda, Juan; Minjauw, Matthias M.; Vandenbroucke, Sofie Sarah Titia; Petit, Robin; Li, Jin; Dendooven, Jolien; Detavernier, Christophe*

– **Engineering Biomimetic Biocompatible and Selectively Antibacterial Ultrathin Films by Vapor Phase Chemistry**
Ashurbekova, Karina; Alonso-Lerma, Borja; Ashurbekova, Kristina; Muriqi, Arbresha; Barandiaran, Leire; Šarić, Iva; Modin, Evgenii; Perez-Jimenez, Raul; Petravić, Mladen; Nolan, Michael; Knez, Mato*

– **MOCVD of spinel ferrite film for applications in photoelectrochemical cells**
Bombaci, Matteo; Pellegrino, Anna Lucia; Malandrino, Graziella*

– **Towards perovskite solar cells made by atomic layer deposition**
Kemell, Marianna; Popov, Georgi; Weiß, Alexander; Ritala, Mikko; Leskelä, Markku*

– **Atomic Layer Deposition of Li4Ti5O12: Towards High-Capacity 3D Thin-Film Batteries**
Speulmanns, Jan; Bönhardt, Sascha; Czernohorsky, Malte; Weinreich, Wenke*

– **Macroscopically uniform distribution of platinum over mesoporous γ-alumina by a scalable atomic layer deposition process**
Saedy, Saeed; Järvilehto, Jänis; Gonsalves, Christine; Velasco, Jorge; Grehl, Thomas; Brüner, Philipp; van Ommen, J. Ruud; Puurunen, Riikka L.*

– **Interplay between coordination sphere engineering and properties of nickel precursors for NiO thin films**
Benedet, Mattia; Barreca, Davide; Fois, Ettore; Seraglia, Roberta; Tabacchi, Gloria; Roverso, Marco; Pagot, Gioele; Invernizzi, Cristiano; Gasparotto, Alberto; Heidecker, Alexandra; Pöthig, Alexander; Callone, Emanuela; Sada, Cinzia; Dirè, Sandra; Bogial*

– **Stabilized Aluminum Hydride Complexes as Potential Precursors for Vapor Phase Deposition Processes**
Huster, Niklas; Devi, Anjana*

– **ZnS Buffer Layers: Novel Precursors for AA-CVD**
*Robson, Max Edward**

– **New Precursors to Printed Electronic Metal Oxides**
Vokes, Elinor T; Johnson, Andrew L*

– **Development of Single-Source Precursors for Chemical Vapour Deposition of Lithium Sulfide (Li2Sx)**
Mason, Daniel M.; Johnson, Andrew L.*

– **Investigation of Bismuth ALD precursors**
Charvot, Jaroslav; Bureš, Filip*

MODELING 149

– **Mechanisms of atomic level processing from first principles simulations**
Nolan, Michael; Liu, Ji; Muriqi, Arbresha; Mullins, Rita*

– **Predicting microstructural changes in a CVD reactor thanks to CFD simulation of the local supersaturation**
Gallou, Yann; Dubois, Marie; Reboud, Roman; Chichignoud, Guy; Potier, Alexandre; Hassant, Cyril; Chaussende, Didier*

– **Diffusion-reaction model for conformality evolution in ALD on spherical porous catalyst particles**
Heikkinen, Niko; Lehtonen, Juha; Yim, Jihong; Puurunen, Riikka L.*

– **DFT Modeling Study: Inhibition of Silica by Small Molecule Inhibitors in the AS-ALD of Al2O3**
*Wellmann, Philipp**

ORGANIC AND HYBRID MATERIALS 158

– **Vapor-Phase Synthesis and Modification of Porous Framework Thin Films**
*Zhao, Junjie**

– **Molecular layer deposition of zeolitic imidazolate framework 8 films**
Smets, Jorid; Rubio-Giménez, Víctor; Cruz, Alexander John; Ameloot, Rob*

– **Towards high throughput spatial molecular layer deposition of alucone films**
*Jain, Hardik; Creatore, Mariadriana; Poodt, Paul**

– **Organic-Component and Ln-Ion Tailored White-Light Emitting Lanthanide-Organic Thin Films via ALD/MLD**
Ghazy, Amr; Lastusaari, Mika; Karppinen, Maarit*

– **Organic-inorganic hybrid thermoelectric materials through a new concept of vapor phase infiltration (VPI)**
Ashurbekova, Kristina; Knez, Mato*

ENERGY-RELATED APPLICATIONS AND CATALYSIS III 166

– **Studying processing parameters in the CVD of TiO2 coatings on glass for NOx remediation**
*Wong, Yanda; Li, Yuankai; Lin, Zhipeng; Kafizas, Andreas Georgiou**

– **Protection of platinum electrocatalysts for water electrolysis using atomic layer deposition of silicon dioxide**
Li, Ming; Saedy, Saeed; Kortlever, Ruud; van Ommen, Ruud*

– **Tin and Indium Sulfide by Plasma-Enhanced Atomic Layer Deposition for CO2 Electroreduction**
Mathew, Femi; Hoek, Järi Van Den; Poonkottil, Nithin; Rampelberg, Geert; Daems, Nick; Hereijgers, Jonas; Hens, Zeger; Breugelmans, Tom; Detavernier, Christophe; Dendooven, Jolien*

– **Effect of Processing Parameters and Electrolyte Concentration on the Electrochemical Performance of Spray Deposited LiFePO4**
*Floraki, Christina; Androulidaki, Maria; Spanakis, Emmanuel; Vernardou, Dimitra**

INDUSTRY 174

– **Dielectric gap-fill material and process challenges for future semiconductor technology**
Sepulveda, Alfonso; Premkumar Peter, Antony; Kumar Channam, Venkat Sunil; Morin, Pierre; Swerts, Johan*

– **Green CVD—Toward a sustainable philosophy for thin film deposition by chemical vapor deposition**
Pedersen, Henrik; Barry, Seán T.; Sundqvist, Jonas*

PRECURSOR DESIGN II 178

– **Designing large aromatic molecules: Bringing colour to MLD**
Hansen, Per-Anders; Purohit, Bhagyesh; Sørensen, Silje Holm; Desbois, Nicolas; Gros, Claude; Nilsen, Ola*

– **Development of new Li-Nb precursors for DLI-CVD process of thin LiNbO3 films**
TACNET, Anthony; BARTASYTE, Ausrine; MICARD, Quentin; DECAMS, Jean-Manuel; ASTIE, Vincent; DANIELE, Stephane*

– **Atmospheric pressure vapor phase deposition of MgF2 thin films: precursor thermal properties and their applications**
Lo Presti, Francesca; Pellegrino, Anna Lucia; Muñoz-Rojas, David; Malandrino, Graziella*

– **Cost-analysis and optimization of ALD and CVD processes for halide perovskites**
Popov, Georgi; Weiß, Alexander; Ritala, Mikko; Kemell, Marianna*

– **Alkali β-Diketonate Glyme Adducts as Precursors for alkali niobate films: Synthesis, Characterization and Functional Validation**
*Lo Presti, Francesca; Peddagopu, Nishant; Pellegrino, Anna Lucia; Labbaveettil Basheerb, Ishamol; Micard, Quentin; Rossi, Patrizia; Paoli, Paola; Bartasyte, Ausrine; Malandrino, Graziella**

SEMICONDUCTOR AND NANOMATERIALS II 189

– **Nucleation and initial growth in CVD of epitaxial Boron Nitride**
Sharma, Sachin; Palisaitis, Justinas; Pedersen, Henrik; Högberg, Hans*

– **Improving the quality of hexagonal boron nitride thin films grown on Ge(001)/Si substrates by CVD**
Franck, Max; Dabrowski, Jarek; Schubert, Markus Andreas; Batista Pessoa, Walter; Vignaud, Dominique; Achehboune, Mohamed; Colomer, Jean-François; Henrard, Luc; Wenger, Christian; Lukosius, Mindaugas*

– **AlScN/GaN heterostructures grown by metal-organic chemical vapour deposition using novel Sc-Precursors**
Streicher, Isabel; Leone, Stefano; Manz, Christian; Kirste, Lutz; Straňák, Patrik; Prescher, Mario; Waltereit, Patrick; Quay, Rüdiger; Ambacher, Oliver*

– **Group III-Nitride semiconductor materials made by low temperature plasma based Atomic Layer Deposition**
Adjeroud, Noureddine; Polesel, Jérôme; Fleming, Yves*

– **ALD-AlOx Monolayers for Modulation-Doping of Silicon Nanowires**
Hiller, Daniel; Nagarajan, Soundarya; Ratschinski, Ingmar; Shams, Somayeh; Mikolajick, Thomas; Trommer, Jens; König, Dirk*

ASD II 200

– **Is HV-CVD best for all coating challenges ?**
Hoffmann, Patrik; Szmyt, Wojciech*

– **Area-Selective Etching of Polymers for Self-Aligned Patterning**
Lasonen, Valtteri; Zhang, Chao; Vehkamäki, Marko; Vihervaara, Anton; Ritala, Mikko*

– **Area-selective ALD involving sputter yield amplification by heavy elements**
de Jong, Arthur; Merkx, Marc; Chittock, Nicholas; Kessels, Wilhelmus; Mackus, Adriaan*

– **Selective ALD-Deposition of IrOx on Platinum Neural Electrodes**
Simon, Nicolai; Stieglitz, Thomas; Bucher, Volker*

FUNCTIONAL MATERIALS III 209

– **Self-healing of Metal Oxides enabled by Vapor Phase Infiltration**
*Yurkevich, Oksana; Modin, Evgeny; Saric, Iva; Peter, Robert; Petravic, Mladen; Knez, Mato**

– **Thick ZrO2 thermal barrier coatings produced by DLI-MOCVD on plastic molds**
Jaud, Alexandre; Montalban, Laura; Samélor, Diane; Sadowski, Daniel; Sekkat, Abderrahime; Vergnes, Hugues; Brulez, Anne Catherine; Boschard, Cédric; Vahlas, Constantin; Benayoun, Stephane; Caussat, Brigitte*

– **Y2O3 and YF3 thermal ALD for anti-corrosion coating**
Kamimura, Sunao; Teramoto, Takashi; Ono, Takashi; Dussarrat, Christian; Blasco, Nicolas; Gosset, Nicolas; Nikiforov, Grigory*

DIELECTRICS I 215

– **Metastable nickelates by ALD - Advantages of low temperature epitaxy**

Sønsteby, Henrik H.; Amedjkouh, Yani L.; Verne, Mathilde I. N.; Nilsen, Ola*

– **Effects of Interlayer Formation by Oxidants and Substrates on Properties of ALD ZrO2 Thin Film**
Park, Seonyeong; Na, Seunggyu; Lee, Yujin; Chung, Seung-min; Kim, Hyungjun*

– **HfZrO-based structures by ALD for embedded ferroelectric non-volatile memories**
Mallmann Tonelli, Amanda; Mercier, Julien; François, Léonard; Gauthier, Nicolas; Grenouillet, Laurent; Jousseaume, Vincent; Bedjaoui, Messaoud*

– **Evaluation of ALD Films of Y2O3, Al2O3 and Their Combinations for Hydrogen Permeation Barrier Applications**
Pavel, Alexandru Cezar; Dekkers, Harold; Morin, Pierre; Swerts, Johan; Franquet, Alexis; Spampinato, Valentina; Meersschaut, Johan*

POSTER SESSION II 223

– **SMI layer decomposition - a theoretical investigation on the deposition of Al2O3**
Maue, Patrick; Tonner-Zech, Ralf*

– **Area-selective ALD/MLD of noble metals and polyimide through surface-dependent film nucleation and growth**
Zhang, Chao; Ritala, Mikko; Leskelä, Markku*

– **Correlating In-Situ Photoluminescence and Ellipsometry: A Novel approach to Analyze ALD Materials for Photovoltaic Applications**
HARADA, Nao; LEVTCHENKO, Alexandra; COUTANCIER, Damien; DONSANTI, Frederique; GOFFARD, Julie; DOMENEGHETTY, Corentin; GUILLEMOLES, Jean-François; SUCHET, Daniel; DELPORT, Géraud; SCHNEIDER, Nathanaëlle*

– **Electronic structure, optical and electrical properties of APCVD SnO2 films. Influence of thermal cycling**
*Petaroudis, Christos; Ioannis, Kostis; Filippatos, Petros-Panagis; Chroneos, Alexander; Soultati, Anastasia; Vasilopoulou, Maria; Davazoglou, Dimitris**

– **Thin film conformality characterization using imaging spectroscopic ellipsometry with the PillarHall LHAR-method**
Philip, Anish; Mirhamed, Arash; Kinnunen, Jussi; Utriainen, Mikko*

– **In Vacuo XPS Study of Al2O3 ALD Deposition Processes on GaN**
Vandenbroucke, Sofie S. T.; Treidel, Eldad B.; Tadmor, Liad; Brusaterra, Enrico; Plate, Paul; Bickel, Nicole; Brunner, Frank; Würfl, Joachim; Hilt, Oliver; Dendooven, Jolien; Detavernier, Christophe*

– **Specific characterization of III-nitride thin film deposits by Plasma Enhanced Atomic Layer Deposition**
Fleming, Yves; Philippe, Adrian-Marie; Guillot, Jérôme; Vergne, Christèle; Adjeroud, Noureddine; Polesel, Jérôme*

– **Characterization Method of Sticking Probability for Various ALD Chemistries Relevant for Artificial Solid Electrolyte Interphases**
Lapeyre, Léo; Mackosz, Krzysztof; Szmyt, Wojciech; Laszlo, Pethö; Michler, Johann; Raynaud, Patrice; Utke, Ivo*

– **Alumina layer deposited by atomic layer deposition with different precursors for different microelectronic application**
Dill, Pauline; Kolkovsky, Vladimir; Franz, Mathias*

– **In-situ investigation of the physico-chemical mechanisms driving Al2O3 growth into PMMA during sequential infiltration synthesis**
Motta, Alessia; Seguini, Gabriele; Wiemer, Claudia; Perego, Michele*

– **Evidence of a twin mediated growth in CVD of polycrystalline silicon carbide (3C-SiC)**
Gallou, Yann; Dubois, Marie; Potier, Alexandre; Chaussende, Didier*

– **Comprehensive study of the early growth stages of copper films**
Maćkosz, Krzysztof; Minzoni, Camilla; Szkudlarek, Aleksandra; Klejna, Sylwia; Sikora, Marcin; Utke, Ivo*

– **High resolution imaging optical thickness metrology for ALD**
Sütő, Attila; Binderiya, Oyunbolor; Defranoux, Christophe*

– **Ion beam analysis of ALD and CVD thin films and nanostructures**
*Meersschaut, Johan**

– **Development of a cobalt atomic layer deposition process using Co2(CO)6HC≡CC5H11 as precursor**
Franz, Mathias; Daniel, Marcus; Schulz, Stefan E.*

– **Conformality of plasma-enhanced atomic layer deposition of silver films into lateral high aspect ratio microstructures**
Leturcq, Renaud; Wack, Sabrina; Lunca Popa, Petru; Adjeroud, Noureddine; Vergne, Christèle*

– **Growth and Nucleation Study of ALD Copper Thin Films**
Minzoni, Camilla; Mackosz, Krzysztof; Utke, Ivo; Hoffmann, Patrik; Sikora, Marcin*

– **Twovalent Ru diazadienyls: A promising precursor class for the MOCVD of low resistivity thin films**
Zanders, David; Obenlüneschloß, Jorit; Huster, Niklas; Gock, Michael; Unkrig-Bau, Michael; Devi, Anjana*

– **Scanning-Tunneling Microscopy Simulation through an Online Platform**
Engelund, Mads; Kharitonov, Stanislav; Graf, Georg; Laubenthal, Horst*

– **The automatic modelling system for reaction mechanisms using multi-objective optimization algorithms**
Takahashi, Takahiro; Arai, Tenichiro; Kubota, Shinsuke; Nakazawa, Eisuke*

– **Using SOLIDWORKS Simulation to optimise the deposition pattern of a combinatorial air pressure CVD**
*Li, Yuankai**

– **Flash lamp enabled atomic layer deposition of titanium oxide employing titanium isopropoxide as single-source precursor**
Cui, Yuanhe; Deltschew, Rumen; Mikolajick, Thomas; Knaut, Martin*

– **Mechanical Behavior upon Annealing-induced Blistering of Atomic Layer Deposited Alumina Thin Film Layered with Tantala**
Piirsoo, Helle-Mai; Jõgiaas, Taivo; Kukli, Kaupo; Tamm, Aile*

– **Minority carrier lifetime of more than 1.2ms for commercial Cz-Si(111) wafers, through ALD Al2O3 passivation**
Dsouza, Namitha; Singh, Ashish K; Maurya, Rajesh; Rath, Jatindra K*

– **Wafer scale growth of transition metal dichalkogenide films by MOCVD**
Pasko, Sergej; Krotkus, Simonas; Mischke, Jan; Ounis, Moez; Tang, Haonan; Wockel, Cornelia; Henning, Alexander; Heuken, Michael*

– **Titanium Nitride Thin Film Fabricated by Atomic Layer Deposition with Hydrazine and Metal-Organic Precursors**
*Spiegelman, Jeffrey**

– **Functionalization of gCN-based electrocatalysts with metal and metal oxide nanoparticles for the enhancement of OER**
Benedet, Mattia; Barreca, Davide; Gasparotto, Alberto; Rizzi, Gian Andrea; Maccato, Chiara*

– **Development of Ternary ALD Chalcogenides for Memory Applications**
Peissker, Tobias; Devulder, Wouter; Pallem, Venkateswara R.; Girard, Jean-Marc; Nyns, Laura*

– **Nucleation and initial growth stages of MoS2 by plasma ALD**
Schulpen, Jeff J.P.M.; Kessels, Wilhelmus M.M.; Bol, Ageeth A.*

– **Fast Plasma ALD for Quantum: Superconducting NbN**
Besprozvannyy, Dmytro; Powell, Michael; Bailey, Louise; Knoops, Harm; Kurek, Agnieszka; Renzas, Russ; Newton, Andrew*

DIELECTRICS II 275

– **Atomic Layer Deposition of Functional Complex Oxides for Next-generation Electronics?**
Napari, Mari; Caruana, Andrew; Heikkilä, Mikko; Huotari, Simo; Julin, Jaakko; Kinane, Christy; Kinnunen, Sami; Mustonen, Otto; Stenning, Gavin*

– **Plasma Enhanced-Atomic Layer Deposition of nanolaminates and nanocomposites Al2O3/HfO2 layers on wide band gap semiconductors**

Galizia, Bruno; Fiorenza, Patrick; Schilirò, Emanuela; Greco, Giuseppe; Di Franco, Salvatore; Saggio, Mario; Giannazzo, Filippo; Roccaforte, Fabrizio; Malandrino, Graziella; Lo Nigro, Raffaella*

– **Tuning the crystallinity of Boron Nitride using Chemical Vapor Deposition**
Souvignet, Thomas; Toury, Bérangère; Journet, Catherine; Marichy, Catherine*

– **Comparison of Thermal and Plasma Enhanced ALD growth of Al2O3/AlN dielectric stacks on silicon carbide**
Lo Nigro, Raffaella; Galizia, Bruno; Fiorenza, Patrick; Schilirò, Emanuela; Greco, Giuseppe; Fogarassy, Zsolt; Pecz, Bela; Malandrino, Graziella; Saggio, Mario; Giannazzo, Filippo; Roccaforte, Fabrizio*

NOVEL CONCEPTS 282

– **Synthesis of mixed anion oxynitride thin films as visible light active self-cleaning photocatalytic coatings**
Hyett, Geoffrey; Cosham, Samuel; Kulak, Alexander; Iborra-Torres, Antonio; Rees, Kelly; Kaye, Karl; Platt, Nathanya*

– **Stimuli-responsive thin films and their applications as actuators and on-skin sensors**
*Coclite, Anna Maria**

– **Competitive diffusion as a route to enhance step coverage in CVD**
Choolakkal, Arun Haridas; Niiranen, Pentti; Högberg, Hans; Birch, Jens; Pedersen, Henrik*

– **Superconductivity in Chromium Oxide Thin Films Embedding Silver**
Otsus, Markus; Kunakova, Gunta; Jõgiaas, Taivo; Erts, Donāts; Kozlova, Jekaterina; Kukli, Kaupo; Tamm, Aile*

– **Novel metal-polymer interface engineering via combined atomic layer and physical vapor deposition**
Byloff, Johanna; Renault, Pierre-Olivier; Faurie, Damien; Husain, S. Altaf; Edwards, Thomas E. J.; Putz, Barbara*

Precursor design I

Chair: Mattinen, Miika (University of Helsinki)

Time: 5/29/2023 1:30:00 PM
Location: Auditorium 1, Promotion Hall, Naamsestraat 22, Leuven

Small Molecule Inhibition on Surfaces: The Role of Carbenes and Other Ligands

Seán T. Barry[a,*], Paul J. Ragogna[b], Cathleen M. Crudden[c]

[a] *Carleton University, 1125 Colonel By Drive, Ottawa, ON, K1S 5B6, Canada*
[b] *Western University, 1151 Richmond Street, London ON, N6A 3K7, Canada*
[c] *Queen's University, 99 University Avenue, Kingston ON, K7L 3N6, Canada*

Carbenes are unusual ligands in metal-organic chemistry: they are neutral ligands bearing a carbon with a lone pair of electrons. They have a unique bonding mode that is particularly selective for coinage metal ions (Cu, Ag, Au) and metallic surfaces. We have been working on carbenes to be used as small molecule inhibitors for area-selective deposition.
Generally, carbenes are difficult to isolate, and we have overcome this by generating the free carbene in the gas phase through thermal fragmentation of an imidazolium bicarbonate (Figure 1a). These are independent thermodynamic events that occur prior to the evaporation (Figure 1b).

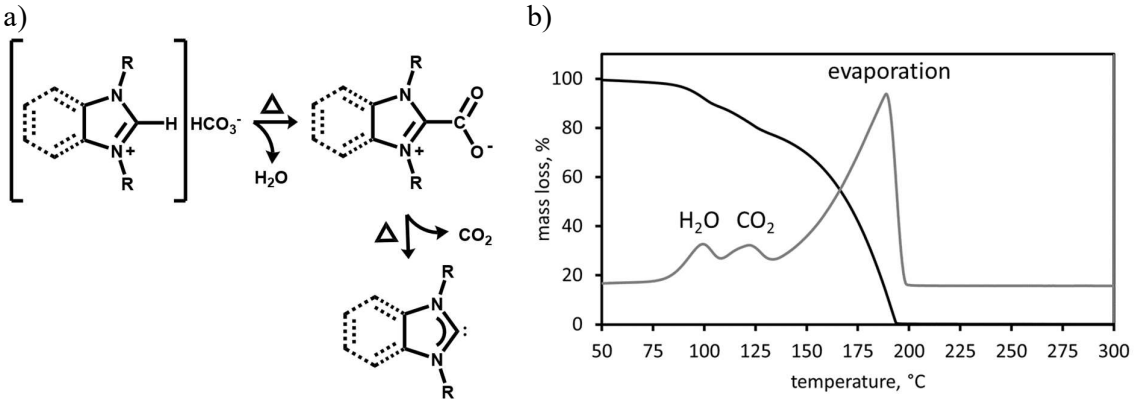

Figure 1. Generation of a free carbene in the gas phase by thermal fragmentation. a) Step-wise evolution of water and then carbon dioxide from an imidazolium bicarbonate, b) Thermogravimetric analysis highlighting the stepwise fragmentation to produce volatile carbene.

The carbenes that are generated bind specifically to metal surfaces, leaving dielectric surfaces unmasked. The carbene is a strong "sigma-donor" due to hyperconjugation of the central carbene by the adjacent nitrogen electrons (Figure 2a). This selectivity can be seen on Si/SiO2 wafers patterned with metal lines (Figure 2b).

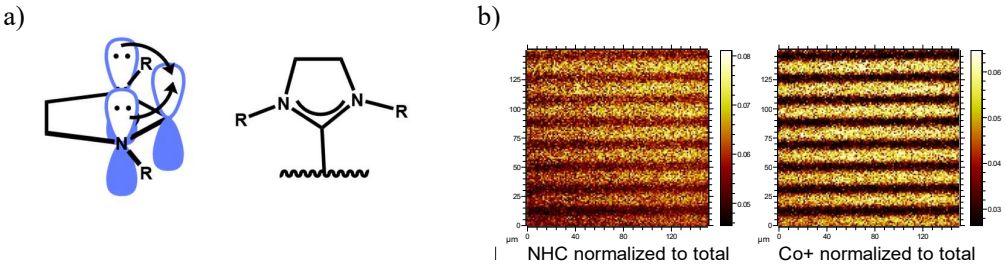

Figure 2. Generation of a free carbene in the gas phase by thermal fragmentation. a) Step-wise evolution of water and then carbon dioxide from an imidazolium bicarbonate, b) Thermogravimetric analysis highlighting the stepwise fragmentation to produce volatile carbene.

An overview of the carbene ligand will be discussed, and a summary of preceding precursors and processes where carbenes appear will be presented. Recent results of carbene surface chemistry will be compared to small molecule inhibition results from the literature, and selectivity and coverage will be shown as characterised by X-ray photoelectron spectroscopy, time-of-flight secondary ion mass spectrometry, and quartz crystal microbalance analysis.

From Molecules to Materials: Precursor Design for the Deposition of Conductive Metals

Caroline E. Knapp[a]*

[a] *Department of Chemistry, University College London, 20 Gordon Street, London, WC1H 0AJ*

With the market for inorganic electronics predicted to reach $60 billion by 2030, advances in the manufacture of large scale flexible electronics has resulted in the efficient, environmentally friendly roll to roll process, employing inkjet printing. This leap in technology has come hand-in-hand with the requirement for precursors that will decompose cleanly, at low temperature and high speed. The Knapp group are working to create 'metal-organic decomposition (MOD) inks' that can be deposited in air, then treated at temperatures below 200 °C, to give conductive metallic features.[1]

Recent work has highlighted that the careful selection of ligands can aid reduction of the metal complexes to leave conductive metals (e.g. Cu, Ag, Al).[2-4] Facile formulation of these compounds into inks allows for inkjet printing and subsequent low temperature reduction (via thermal sintering) yielding highly conductive features which can be incorporated into electronic devices. MOD inks are an emerging alternative to the industrial standard nanoparticle (NP) inks.

Here we discuss the chemistry of precursor development and report our work on printed metal tracks. Using careful ligand design we can attune the properties of the resultant precursor at the molecular level, making precursor functionality fully adjustable. We describe the synthesis, characterisation and printing of a library of novel compounds; selected to produce various deposits fulfilling the required specification – with particular focus on sintering methods, including thermal and plasma enhanced.

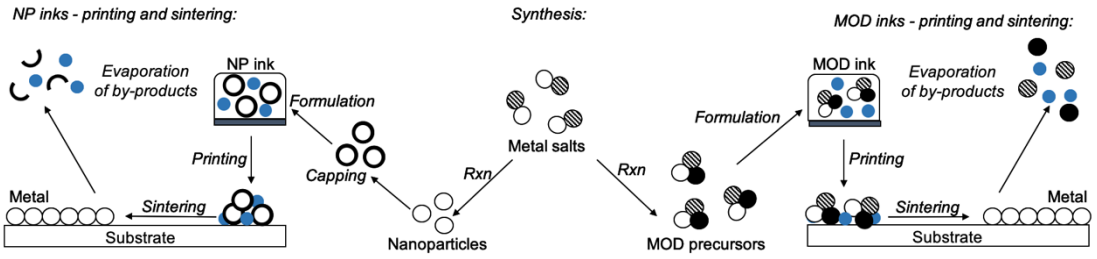

Figure 1: MODs vs. NP: From the centre, schematic illustration showing the different synthetic routes to either NP (to the left) or MOD precursors (to the right), bookended by the process involved in printing and sintering metal coatings.[1]

References

1. S. P. Douglas, S. Mrig, C. E. Knapp. MODs vs. NPs: Vying for the Future of Printed Electronics. Chemistry–A European Journal, (2021), **27**, 31, 8062-8081.
2. S. P. Douglas, C. E. Knapp. Low Temperature Deposition of Highly Conductive Aluminium Metal Films on Flexible Substrates using Liquid Alane MOD Precursors. ACS Appl. Mater. Interfaces. (2020), **12**, 26193.
3. C. E. Knapp, E. A. Metcalf, S. Mrig, C. Sanchez-Perez, S. P. Douglas, P. Choquet, N. D. Boscher. Precursors for Atmospheric Plasma-Enhanced Sintering: Low-Temperature Inkjet Printing of Conductive Copper. Chem. Open, (2018), **7**, 850. Cover feature.
4. C. E. Knapp, J.-B. Chemin, S. P. Douglas, D. Abessolo Ondo, J. Guillot, P. Choquet, N. D. Boscher. Room-Temperature Plasma-Assisted Inkjet Printing of Highly Conductive Silver on Paper. Advanced Mater. Technol. (2018), **3**, 1700326.

* *Corresponding author e-mail:* caroline.knapp@ucl.ac.uk

New non-Pyrophoric metalorganic precursors for CVD and ALD of IGZO

Marcel Schmickler[a,*], Florian Preischel[a], David Zanders[a], Jacqueline Klimars[a], Anjana Devi[a]

[a] *Inorganic Materials Chemistry, Ruhr University Bochum, Universitätsstraße 150, Bochum, 44801, Germany*

Indium-gallium-zinc oxide (IGZO) is a transparent, flexible semiconductor with excellent field-effect mobility. Since Nomura et al. reported the first fabrication of a flexible thin film transistor (TFT) using IGZO as active layer in 2004, it has become a frequently used material for screens, displays, OLEDs, and sensors etc.[1,2] Physical vapor deposition (PVD) methods are commonly used to deposit uniform IGZO thin films on a large scale at low costs.[2] Yet, PVD deposition techniques are not suitable for complex surfaces due to their line-of-sight feature, and instead, chemical vapor deposition (CVD) and atomic layer deposition (ALD) processes are favored. Notably, CVD and ALD alike rely strongly on the precursors used in the respective process as chemical surface reactions enable film growth.

The predominantly used precursors for group III element oxides (Ga_2O_3, In_2O_3) and zinc oxide (ZnO) are the respective alkyls namely TMG, TMI, and DEZ. Although volatile and reactive, these precursors suffer from high pyrophoricity, and thus special measures are needed to handle them. Schumann et al. developed the synthesis for a series of volatile and less pyrophoric group III metal-organic complexes using the (3-(dimethylamino)propyl (DMP) ligand in the early 1990s.[3] This ligand can intramolecularly coordinate and thus stabilize otherwise highly reactive metal centers. Mai et al recently unearthed this work and successfully applied DMP containing Al complexes for ALD of Al_2O_3.[4] In addition, Mai and Zanders et al. used this ligand to synthesize and apply [$Zn(DMP)_2$] and [$Sn(DMP)_4$] in ALD.[5,6,7]

Following the notable success of our previous studies with the use of the DMP ligand, we extended the concept of intramolecularly stabilizing ligands to the main group metals namely gallium and indium, resulting in the synthesis of a series of promising precursor candidates with heteroleptic ligand combinations. The synthesis of (3-(dimethylamino)propyl)dimethyl gallium ([$Ga(DMP)Me_2$]) is one representative example. Other new complexes include [$Ga(DMP)H_2$] and [$InMe(DMP)_2$]. The thermal properties of these compounds were investigated via thermogravimetric analysis (TGA), revealing promising thermal properties (Figure 1). In this presentation, we focus on gallium and indium complexes that are promising precursor candidates for gas-phase deposition methods, potentially advancing the development of IGZO applications.

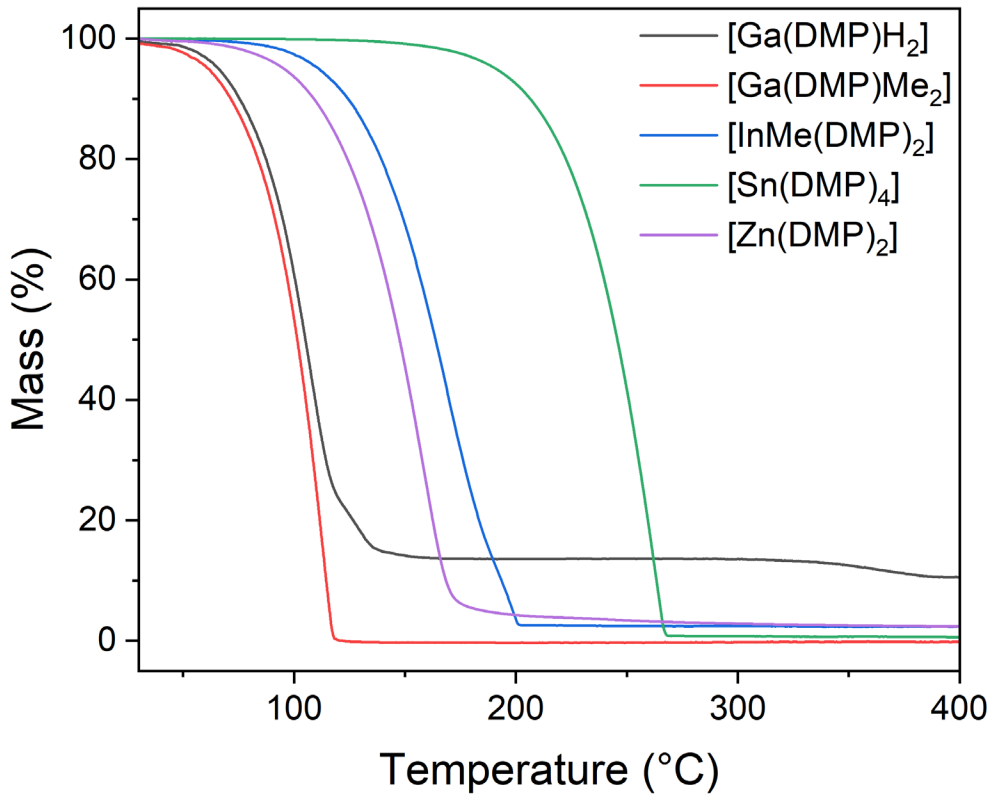

Figure 1: Thermogravimetric analysis of [Ga(DMP)H_2] (black), [Ga(DMP)Me_2] (red), [InMe(DMP)$_2$] (blue), [Sn(DMP)$_4$] (green) and [Zn(DMP)$_2$] (violet)

References

1. K. Nomura *et al.*, Nature **432**, 488 (2004).
2. Y. Zhu *et al.*, J. Semicond. **42**, 31101 (2021).
3. H. Schumann *et al.*, Polyhedron **9**, 353 (1990).
4. L. Mai *et al.*, Chem. Eur. J. **23**, 10768 (2017).
5. D. Zanders *et al.*, Chem. Mater. **33**, 5045 (2021).
6. L. Mai *et al.*, Small, **16**, e1907506 (2020).
7. L. Mai *et al.*, ACS Appl. Mater. Interfaces **11**, 3169 (2019).

** Corresponding author e-mail:* marcel.schmickler@rub.de

New Precursors for the Atomic Layer deposition of p-type SnO.

Andrew L. Johnson

[a] *Department of Chemistry, University of Bath, Bath. United Kingdom*

Over the past decade, significant research effort has been directed towards the development of p-type oxide semiconductor materials for realization of complementary metal oxide semiconductor (CMOS) circuits. Of the potential p-type oxide materials researchers have investigated tin(II) monoxide (SnO) has received the great interest due to it disperse valence band maximum due to hybridization between O 2p and Sn 5s orbitals, allowing a relatively high hole mobility [1]. While sputtering method has been widely used for SnO, atomic layer deposition (ALD) has not been widely reported [2].

Despite the attractiveness of ALD as a deposition technique, due to its precision on stoichiometry, its repeatability and its conformality over a large substrate area [3], its application is often limited by the availability of viable precursors. In the case of SnO, very few ALD precursors are available. As such, the design of new precursors is fundamental to the progression of ALD, with feature such as increased volatility, reactivity, durability, alongside faster growth rates all seen as important features in precursor development.

Here we report our recent work on the development of SnO precursors, for application in spatial ALD (sALD) and temporal ALD processes.[4,5] As an example, we have recently we have described the application of the novel liquid precursor tin(II)-bis(tert-amyloxide), i.e. $[Sn\{OCMe_2Et\}_2]_2$ ($Sn(TAA)_2$) in the deposition of SnO thin films, using the novel Sn precursor (with H_2O as a co-reactant) in a cross-flow wafer scale ALD reactor. Compared to previously reported temporal ALD precursors and chemistries for the deposition of SnO, deposition rates of up to 19.5 times higher are obtained using $Sn(TAA)_2$ as a precursor in combination with atmospheric pressure sALD (Fig 1). This serves to highlight the vital importance of precursor development in the establishment of ALD as a viable industrial process.

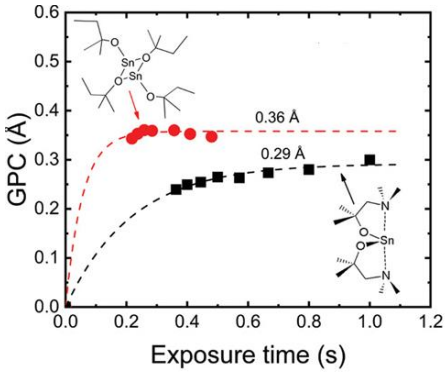

Figure 1: A plot showing the growth per cycle (GPC) of SnO as function of the overall exposure time, using $Sn(TAA)_2$ (red-circles), $Sn(dmamp)_2$ (black-squares) and H_2O as a co-reactant, at a deposition temperature of 160 °C in a sALD process.

References

1. (a) Z.-W. Shang, H.-H. Hsu, Z.-W. Zhang, C.-H. Cheng, Nanotechnology Reviews, **8**, 422-443 (2019). (b) A. L. Johnson, J. D. Parish, "Recent developments in molecular precursors for atomic layer deposition", *Organometallic Chemistry*: 2018, Volume 42, (Eds., N.J. Patmore, P.I.P. Elliott).
2. J. H. Han, Y. J. Chung, B. K. Park, S. K. Kim, H.-S. Kim, C. G. Kim, and T.-M. Chung, *Chemistry of Materials,* vol. 26, no. 21, pp. 6088-6091, 2014.
3. P.O. Oviroh, R. Akbarzadeh, D. Pan, R.A.M. Coetzee, T.C Jen, *Sci. Technol. Adv. Mater.*, **20**(1), 465-496 (2019).
4. A. Mameli, J.D. Parish, T. Dogan, G. Gelinck, M. W Snook, A.J. Straiton, A.L Johnson, A.J Kronemeijer, *Adv. Mater. Interfaces*, **9**(9) (2022) 2101278.
5. N.C.A van Fraassen, K.M, Niang, J.D. Parish, J.D. A.L. Johnson, A.J. Flewitt, *Sci Rep* **12**, (2022) 16111.

* *Corresponding author e-mail:* a.l.johnson@bath.ac.uk

Iron and and cobalt second-generation precursors for the vapor-phase deposition of Fe_2O_3 and Co_3O_4 systems

Davide Barreca,[a] Roberta Seraglia,[a] Christian Jandl,[b] Alexander Pöthig,[b]
Ettore Fois,[c] Gloria Tabacchi,[c] Marco Roverso,[d] Sara Bogialli,[a,d]
Emanuela Callone,[e] Sandra Dirè,[e] Alberto Gasparotto,[a,d] Chiara Maccato[a,d,*]

[a] *CNR-ICMATE and INSTM, Department of Chemical Sciences, Padova University, Via Marzolo 1, 35131 Padova, Italy*
[b] *Catalysis Research Center & Department of Chemistry, Technische Universität München, Lichtenbergstr. 4, 85748 Garching, Germany*
[c] *Department of Science and High Technology, Insubria University and INSTM, Via Valleggio 11, 22100 Como, Italy*
[d] *Department of Chemical Sciences, Padova University and INSTM, Via Marzolo 1, 35131 Padova, Italy*
[e] *Klaus Müller Magnetic Resonance Laboratory, Department of Industrial Engineering, Trento University, Via Sommarive 9, 38123 Povo (TN), Italy*

The importance of metal oxides nanostructures as versatile multi-functional systems is mainly due to their considerable potential in view of various technological end-uses. In particular, low-cost iron and cobalt oxides feature a rich variety of chemico-physical properties paving the way to manifold applications, among which magnetic systems, gas sensing devices, photocatalysts for pollutant degradation, and water splitting photoelectrodes for clean H_2 production [1,2]. Among the possible synthetic approaches for their production in the form of thin films/supported nanosystems, chemical vapor deposition (CVD) is an appealing choice thanks to its inherent versatility and the possibility of finely tuning the resulting material characteristics through tailored variations of processing parameters. Yet, its successful implementation is critically dependent on the availability of improved precursors with good stability under manipulation and vaporization conditions, suitable volatility and reactivity, and sufficient temperature window between volatilization and decomposition.
In this context, the present contribution is focused on the preparation, chemico-physical characterization and functional validation of heteroleptic diketonate diamine adducts of general formula $M(tfa)_2TMEDA$ [M = Co(II), Fe(II); tfa = 1,1,1-trifluoro-2,4-pentanedionate; TMEDA = N,N,N',N'-tetramethylethylenediamine]. Both complexes have been subjected to a thorough investigation of their structural, electronic, thermal and fragmentation properties by an integrated theoretical-experimental approach [1,2]. The obtained compounds, monomeric and characterized by a fully saturated M(II) octahedral coordination sphere (Figs. 1a, 2a), feature a high stability to air and moisture under laboratory conditions and a quantitative vaporization at moderate temperatures (Fig. 1b). Electrospray ionization-high resolution mass spectrometric (ESI-HRMS) data evidenced a clean fragmentation, dominated by the loss of the tfa radical and the TMEDA radical cation from the radical molecular ion (Figs. 2b-c). Overall, these features render the target compounds attractive candidates for the vapor phase growth of the corresponding metal oxide nanomaterials. In fact, thermal CVD validation processes yielded high purity β-Fe_2O_3 and Co_3O_4 nanosystems, which were fully characterized from a structural, compositional and morphological point of view (Figs. 1c, 2d-e). Photoelectron spectroscopy analyses highlighted the surface occurrence of adventitious carbon and chemisorbed carbonates (bands at 284.8 and 288.0 eV, Fig. 2e), that could be easily removed upon erosion. The O1s signal resulted from the contribution of lattice oxygen and of hydroxyl species chemisorbed on O defects (bands at 529.9 eV and 531.6 eV, Fig. 2f). The data confirmed the successful obtainment of phase-pure systems free from other Fe or Co oxides in appreciable amounts (Fig. 2g). Taken together, the present results open the door to further fundamental and applicative research developments. The promising physico-chemical properties of the proposed compounds render them attractive candidate as precursors even for atomic layer deposition (ALD) processes. In addition, efforts will be dedicated to an advanced optimization of the deposition process through controlled variations of chemico-physical properties, aimed at tailoring material functional behaviour, in particular towards the obtainment of heterostructured/composite systems for energy and environmental applications.

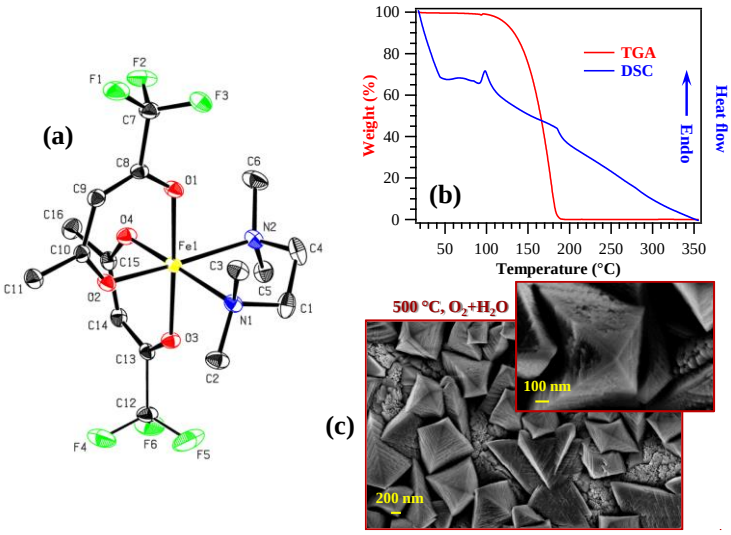

Figure 1. (a) Molecular structure of $Fe(tfa)_2TMEDA$. (b) Thermoanalytical characterization of $Fe(tfa)_2TMEDA$. (c) FE-SEM micrographs for a representative Fe_2O_3 sample grown on Si(100) at 500°C in O_2+H_2O atmosphere [1].

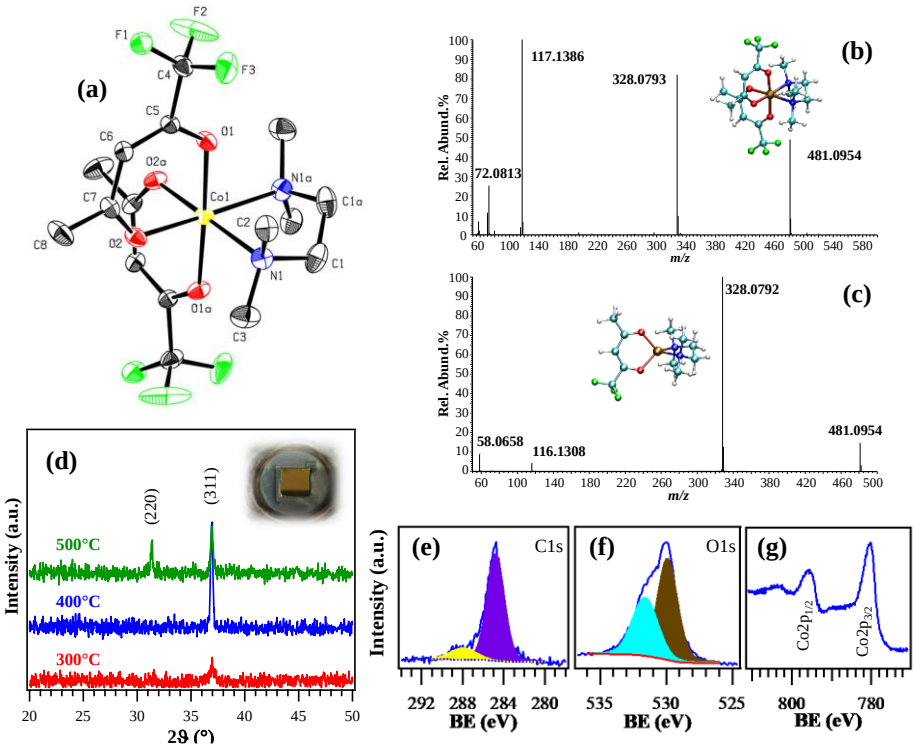

Figure 2. (a) Molecular structure of $Co(tfa)_2TMEDA$. (b) Positive ion ESI-HRMS spectrum of $Co(tfa)_2TMEDA$ in acetonitrile solution. (c) ESI-HRMS^2 mass spectrum of the ion at *m/z* = 481.0954. (d) X-ray diffraction (XRD) patterns of Co_3O_4 films grown under a wet O_2 atmosphere. X-ray photoelectron spectroscopy (XPS) analysis for a sample grown at 400°C in the same reaction environment: C1s (e), O1s (f), and Co2p (g) peaks [2].

References

1. D. Barreca, L. Bigiani, M. Klotzsche, A. Gasparotto, R. Seraglia, C. Jandl, A. Pöthig, E. Fois, L. Vanin, G. Tabacchi, M. Roverso, S. Bogialli, E. Callone, S. Dirè, C. Maccato, Mater. Chem. Phys. **277**, 125534 (2022).
2. M. Klotzsche, D. Barreca, L. Bigiani, R. Seraglia, A. Gasparotto, L. Vanin, C. Jandl, A. Pöthig, M. Roverso, S. Bogialli, G. Tabacchi, E. Fois, E. Callone, S. Dirè, C. Maccato, Dalton Trans. **50**, 10374 (2021).

* *Corresponding author e-mail: chiara.maccato@unipd.it*

Characterization I

Chair: Dasgupta, Neil (University of Michigan)

Time: 5/29/2023 3:30:00 PM
Location: Auditorium 1, Promotion Hall, Naamsestraat 22, Leuven

Real-time monitoring of the surface chemistry of ALD processes by ambient pressure x-ray photoelectron spectroscopy

Joachim Schnadt[a,*]

[a] *Lund University, Department of Physics and MAX IV Laboratory, Box 118, 221 00 Lund, Sweden*

Today, atomic layer deposition (ALD) is one of the primary methods for the deposition of ultrathin films with atomic-scale precision [1-3]. At the same time, important aspects of the underlying surface chemistry remain unclarified for many ALD processes [4,5]. The time-resolved monitoring of ALD processes, e.g. by quartz crystal microbalance measurement [6], quadrupole mass spectrometry [7], pyroelectric calorimetry [8] and ellipsometry [9], can provide much deepened insight into ALD surface reaction mechanisms. Only relatively recently, two chemically sensitive methods for the time-resolved characterisation of ALD processes have been become available, namely infrared spectroscopy [10] and ambient pressure x-ray photoelectron spectroscopy (APXPS) [11-14]. These two methods are capable of following the ALD surface chemistry in real time and at processing pressures equal or similar to those in an ALD reactor. Indeed, while conventional x-ray photoelectron spectroscopy (XPS) is limited to vacuum pressures of 10^{-5} mbar and below, APXPS can be carried out at realistic pressure. Today, most APXPS machines can operate at pressures up to the 10 mbar regime, which is an ideal match to the pressure regime used in standard ALD reactors.

In my presentation, I would like to show how the use of time-resolved APXPS, not least when combined with theoretical calculations, can contribute to the understanding of ALD reaction mechanisms, taking as example the ALD of hafnium and titanium oxides from amido complexes and water on a variety of different supports. From time-resolved APXPS data such as shown in Fig. 1 detailed insight can be gained into the nature of surface species, that may or may not be in agreement with widely accepted reaction schemes, and their time evolution. Likewise, information is provided on the presence or absence of oxygen ion transport and its relevance for the oxide ALD. General findings from our APXPS studies include that reaction pathways exist that are not included in the standard models of ALD surface chemistry (cf. Fig. 2) [13,14], that surface hydroxylation is not a prerequisite for oxide ALD to take place [13,14], and that on reducible support oxygen transport may play a major role for the oxide formation of the initial phases of ALD [12,13].

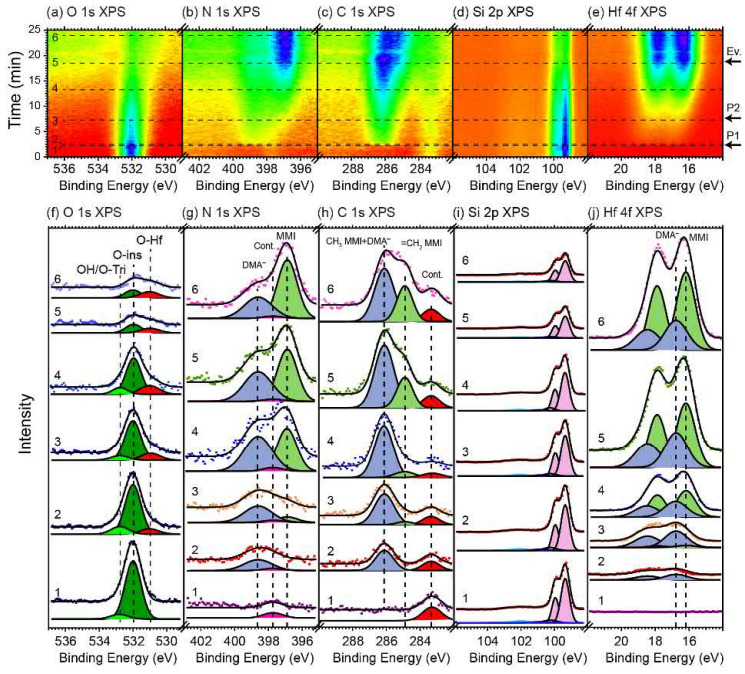

Fig. 1. Series of O 1s, N 1s, C 1s, Si 2p and Hf 4f APXPS data measured during the first half-cycle of ALD of hafnium oxide from tetrakis(dimethylamido) hafnium and water on a SiO_2 surface [14]. The different core levels were measured in sequence, and a full set of spectra was obtained during 13 s. (a−e) Image plots of the indicated core levels. The intensity is represented by a false color scale, where violet represents maximum and red minimum intensity. The times of TDMAHf dosing (pulses P1 and P2) and pump-out (Ev.) are indicated. (f−j) Selected spectra as indicated by the numbered dashed lines in (a−e).

Already today, APXPS is a powerful tool for the study of the ALD surface chemistry. In my presentation I will also address current efforts to render the experimental conditions of APXPS even more similar to those encountered in ALD reactors. These efforts include, in particular, the development of dedicated setups for APXPS investigations [15] as well as the development of time-resolved APXPS experiment with a high sampling rates beyond the Hz

rates achieved already today [16]. Work is also underway that addresses other ALD processes, including, e.g. metal ALD and photo-ALD.

Hence, APXPS provides us with entirely new insight into the surface reaction mechanisms of ALD, well needed for the future optimization of ALD materials and processes.

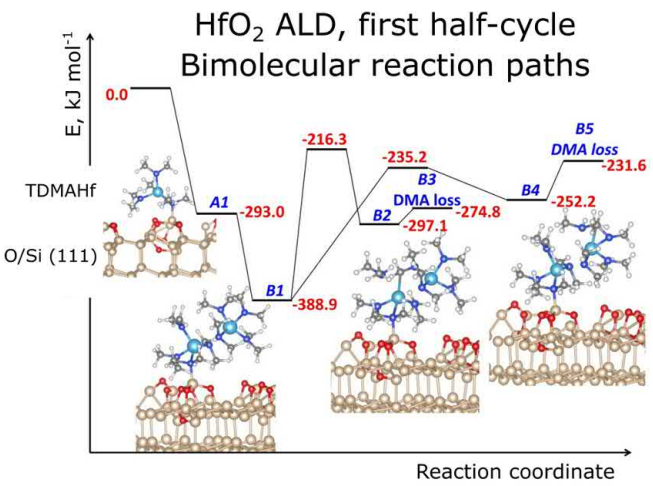

Fig. 2. DFT calculations of bimolecular reaction paths in the ALD of HfO_2 on SiO_2 [14]. On the stoichiometric SiO_2 surface, which cannot be hydroxylated, the depicted reaction mechanisms represent the only viable pathways towards ALD. Kinetic modelling shows that these pathways are realistic at reaction temperature, in spite of relatively high activation barriers. Once sufficient hydroxylation of the deposited Hf layer is achieved, a ligand exchange reaction mechanism becomes more favourable.

References

1. V. Miikkulainen, M. Leskelä, M. Ritala and R. L. Puurunen, J. Appl. Phys. **113**, 021301 (2013).
2. R. W. Johnson, A. Hultqvist and S. F. Bent, Mater. Today **17**, 236 (2014).
3. C. S. Hwang (Ed.), Atomic Layer Deposition for Semiconductors (Springer, Berlin, Heidelberg, 2014).
4. F. Zaera, Coord. Chem. Rev. **257**, 3177 (2013).
5. N. E. Richey, C. De Paula and S. F. Bent, J. Chem. Phys. **152**, 1 (2020).
6. J. R. Schneider, C. de Paula, N. E. Richey, J. G. Baker, S. T. Oyakhire, and S. F. Bent, Chem. Mater. **34**, 5584 (2022).
7. H.-E. Nieminena and M. Ritala, J. Vac. Sci. Technol. A **40**, 022401 (2022).
8. A. R. Bielinski, E. P. Kamphaus L. Cheng and A. B. F. Martinson, J. Am. Chem. Soc. **144**, 14203 (2022).
9. U. Kumar, C. Feit, S. N. Berriel, A. Arunachalam, T. S. Sakthivel, K. Basu, P. Banerjee and S. Seal, J. Vac. Sci. Technol. A **39**, 060504 (2021).
10. B. A. Sperling, J. Hoang, W. A: Kimes, J. E. Maslar, K. L. Steffens and N. V. Nguyen, J. Vac. Sci. Technol. A **32**, 031513 (2014).
11. R. Timm, A. R. Head, S. Yngman, J. V. Knutsson, M. Hjort, S. R. McKibbin, A. Troian, O. Persson, S. Urpelainen, J. Knudsen and A. Mikkelsen, Nat. Commun. **9**, 1412 (2018).
12. G. D'Acunto, E. Kokkonen, P. Shayesteh, V. Boix, F. Rehman, Z. Mosahebfard, E. Lind, J. Schnadt and R. Timm, Faraday Discuss. **236**, 71 (2022).
13. G. D'Acunto, R. Jones, L. P. Ramírez, P. Shayesteh, E. Kokkonen, F. Rehman, F. Lim, F. Bournel, J.-J. Gallet, R. Timm and J. Schnadt, J. Phys. Chem. C **126**, 12210 (2022).
14. G. D'Acunto, R. Tsyshevsky, P. Shayesteh, J.-J. Gallet, F. Bournel, F. Rochet, I. Pinsard, R. Timm, A. R. Head, M. Kuklj and J. Schnadt, Chem. Mater. **35**, 529 (2023).
15. E. Kokkonen, M. Kaipio, H.-E. Nieminen, F. Rehman, V. Miikkulainen, M. Putkonen, M. Ritala, S. Huotari, J. Schnadt and S. Urpelainen, Rev. Sci. Instrum. **93**, 013905 (2022).
16. J. Knudsen, T. Gallo, V. Boix, M. Døvre Strømsheim, G. D'Acunto, C. Goodwin, H. Wallander, S. Zhu, M. Soldemo, P. Lömker, F. Cavalca, M. Scardamaglia, D. Degerman, A. Nilsson, P. Amann, A. Shavorskiy and J. Schnadt, Nature Commun. **12**, 6117 (2021).

* *Corresponding author e-mail:* joachim.schnadt@sljus.lu.se

In-Situ characterization of CVD processes where plasma electrons are utilized as reducing agents

Pentti Niiranen[a]*, Anna Kapran[b], Hama Nadhom[a,c], Martin Čada[b], Zdeněk Hubička[b], Daniel Lundin[a,c], Henrik Pedersen[a]

[a] *Department of Physics, Chemistry and Biology (IFM), Linköping University, Linköping, Sweden*
[b] *Institute of Physics of the Czech Academy of Sciences, Na Slovance 2, 18221 Prague, Czech Republic*
[c] *Ionautics AB, Kabelgatan 9B, 943 31, Öjebyn, Sweden*

Deposition of metallic films by CVD typically require a reducing agent to supply electrons to reduce the metal center of the precursor molecule. For more electropositive metals, the reduction of the metal center is thermodynamically unfavorable, requiring strong reducing agents and/or high temperatures. Very strong reducing agents for electropositive metals are scarce and are, per definition, highly reactive and can thus be challenging to synthesize, handle and scale up to mass production. As an alternative, a plasma discharge has been used as a source of electrons for reduction of Fe, Co, and Ni in CVD, where the deposition process has been shown to be selective to low resistivity areas. [1,2]

While the process has been demonstrated, little understanding of its mechanisms has been uncovered. In this contribution we address two key research challenges: 1) identification of growth mechanisms, and 2) characterization of the electron dynamics. The film growth has been studied using a new electrically modified quartz crystal microbalance (QCM) sensor, capable of allowing a flux of negative charge carriers (*e.g.*, electrons) to the surface of the QCM, while still studying the film growth.[3] By time-resolving the deposition with the QCM, *i.e.*, temporally resolving the precursor flow and the plasma pulses, we are able to separate the adsorption step and the reduction step, which generates sequences that appears to resemble saturation in the surface chemistry. This approach also gives us knowledge in what is going on in the deposition chamber during the plasma exposure. Additional studies of the film growth were carried out through optical emission spectroscopy (OES), which showed emission lines corresponding to Co, Fe, Ni and also C_2 and CO species which appears to be plasma power dependent. To study the gas composition during film deposition, a quadrupole mass spectrometer (QMS) was connected to the exhaust of the deposition chamber. Through the QMS we were able to detect both the unreacted precursor and fragments originating from it and by time-resolving the process, we were able to distinguish between fragments originating from plasma volume reactions and those from surface chemical reactions.

To characterize the electron dynamics, we carried out measurements through a radio frequency Sobolewski probe and observed that the electron density and electron temperature is affected by the introduction of precursor to the deposition chamber. Spatial variations of the electron temperature and electron density has also been observed.

To further improve this process, it is critical for us to understand the deposition chemistry. Because of this, we believe that the combination of these kind of measurements provides pieces of the deposition chemical puzzle and will be combined with theoretical studies of the precursor decomposition and surface chemistry.

References

1. Nadhom, H., Lundin, D., Rouf, P. & Pedersen, H. Chemical vapor deposition of metallic films using plasma electrons as reducing agents. *J. Vac. Sci. Technol. A* **38**, 033402 (2020).
2. Nadhom, H., Boyd, R., Rouf, P., Lundin, D. & Pedersen, H. Area selective deposition of metals from the electrical resistivity of the substrate. *J. Phys. Chem. Lett.* **12**, 4130–4133 (2021).
3. Niiranen, P. *et al.* Biased quartz crystal microbalance method for studies of CVD surface chemistry induced by plasma electrons. Rev. Sci. Instrum. (2023) Accepted manuscript.

* *Corresponding author e-mail:* pentti.niiranen@liu.se

Controlling the Hydrogen Source in zinc, titanium, and aluminum oxides deposited via Atomic Layer Deposition

Barbara Putz[a,b]*, Carlos Guerra-Nunez[c], Alex Bernardi[a], Max Döbeli[c], Johann Michler[a], Ivo Utke[a,]*

[a] *Laboratory for Mechanics of Materials and Nanostructure, EMPA, Swiss Federal Laboratories for Materials Science and Technology, Feuerwerkerstrasse 39, CH-3602 Thun, Switzerland*
[b] *Department of Materials Science, University of Leoben, Franz-Josef Strasse 18, AT-8700 Leoben, Austria*
[c] *Swiss Cluster AG, Feuerwerkerstrasse 39, CH-3602 Thun, Switzerland*
[d] *ETHZ, Ion Beam Physics, HPK H32, Schafmattstrasse 20, CH-8093 Zürich, Switzerland*

In this comparative work, we quantitatively elucidated and compared the hydrogen source in the atomic layer deposition (ALD) of ZnO, TiO_2 and Al_2O_3. The precursors diethylzinc $Zn(C_2H_5)_2$ (DEZ), titanium tetraisopropoxide $Ti(OC_3H_7)_4$, (TTIP), and trimethyl $Al(CH_3)_3$, (TMA), were cycled with water at different temperatures (40 °C – 220 °C), to study the impact on the overall chemical composition and density. We replaced the ^1H_2O precursor with deuterated water (^2H_2O) to use as a tracer and distinguish between the incorporated hydrogen coming from unreacted metal precursor ligands or hydroxyl (^2HO) groups from ^2H_2O. Hydrogen content, stoichiometry, and density of the films were characterized as a function of growth temperature. Fig. 1 shows elastic recoil detection measurements with helium ions (He-ERDA) and contextualizes our results with respect to the hydrogen content reported in literature for all three metal oxides. The hydrogen concentration decreases by increasing temperature, and the total hydrogen content in Al_2O_3 is significantly higher than the other metal oxides, reaching up to ~20 at.% at temperatures below 100 °C, compared to 10 at.% from TiO_2 and ~7 at.% from ZnO. Fig. 2a details that the major source of hydrogen in Al_2O_3 comes from unreacted water hydroxyl groups ^2HO that remained inside the film due to steric hindrance mechanisms, predominantly at low temperatures. For ZnO we observed a $^1H/^2H$ ratio of about 6:1 (6at.% vs 1at.%) and for TiO_2 1:1 (5at. % each) at the lowest growth temperatures, indicating that part of the H may originate from the organic ligands. However, the film carbon content does not match the amount of H that could be incorporated by unreacted CH_3 groups. We therefore assume that deuterium ^2H was replaced through exchange reactions with ^1H from ambient moisture in the time period between deposition and ERDA measurements.

Furthermore, the off-stoichiometry of the oxides scales directly and the film density scales inversely with the hydrogen content (not shown). The magnitude of hydrogen and carbon contamination is ZnO < TiO_2 < Al_2O_3. The same applies for the off-stoichiometry and density. The observed trends do not scale with the number of ligands in the precursor molecules (2 vs 4 vs 3) nor with the number of C and H contained in the molecules (4&10 vs 12&28 vs 3&9). Associating unreacted hydroxyl groups due to steric hindrance with the shape of the molecules does not seem to fully explain the behaviour either: DEZ as pseudo linear molecule has least steric hindrance, the TTIP is 3D with potentially highest steric hindrance, while the TMA monomer is pseudo planar (potentially less hindrance than TTIP). Below 75°C the 3D dimer $(TMA)_2$ is dominant in the gas phase and is probably comparable to TTIP in steric hindrance.

We will discuss further Al_2O_3 ALD experiments performed using thermal and plasma enhanced (PE) ALD in an ALD system from Swiss Cluster (SC-1), equipped with a larger purging capacity which can efficiently purge with higher flows and lower pressures. These films show considerably lower hydrogen content <4at.% in the films at 50°C, see Fig. 3. This points towards desorption of water from the surface as limiting factor/source for hydrogen incorporation in the films. This mechanism was evoked only recently in the scope of spatial ALD [9] and seems to be controllable by adjusting purge gas flow properly.

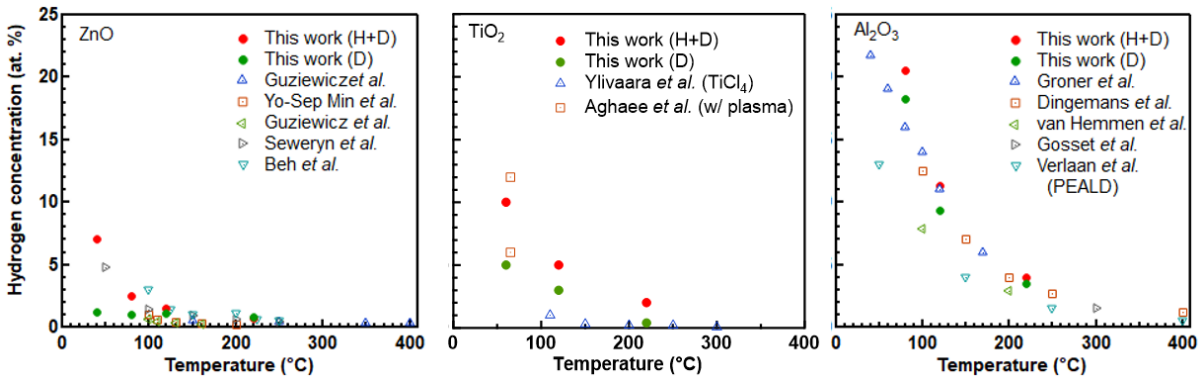

Fig 1. The hydrogen content of ZnO, TiO_2, and Al_2O_3 for different deposition temperatures. References for ZnO [1-5], TiO_2 [6,7], and Al_2O_3 were adapted from [8]. Data of this work show the H+D content since deuterated water was used; H and D stand for hydrogen ^1H and deuterium ^2H, respectively.

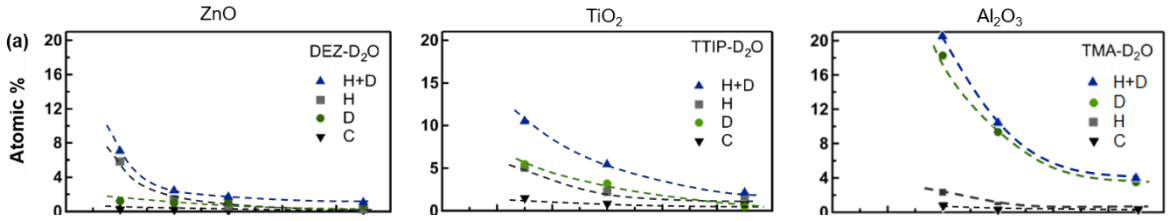

Fig 2. Comparison of the chemical composition between ZnO, TiO_2, and Al_2O_3 films at different deposition temperatures using D_2O as the second precursor. (a) He-ERD values of the concentrations of H and D, and heavy ion ERDA values of C content at different temperatures.

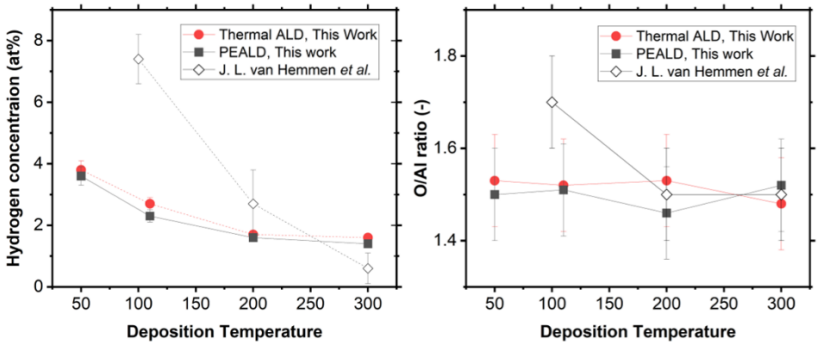

Fig. 3. ERDA measurements of thermal and PE-ALD Al_2O_3 films grown with TMA and water with optimized purge gas flow in the SC-1 reactor. Reference for Al_2O_3 [10].

References

1. E. Guziewicz, M. Godlewski, L. Wachnicki et al., Semicond. Sci. Technol. **27**, 074011 (2012).
2. E. Guziewicz, T. A. Krajewski, E. Przezdziecka et al., physica status solidi (b) **257**, 1900472 (2020).
3. Y-S. Min, C-J. An, S-K. Kim, J-W. Song et al., Bull. Korean Chem. Soc. **31**, 2503 (2010).
4. A. Seweryn, R. Pietruszka, B. S. Witkowski, A. Wierzbicka et al., Crystals **9** (2019).
5. H. Beh, D. Hiller, M. Bruns, A. Welle et al., J. Appl. Phys. **122**, 025306 (2017).
6. O. M. E. Ylivaara, L. Kilpi, X. Liu, S. Sintonen et al., J. Vac. Sci. Technol. A **35**, 01B105 (2017).
7. M Aghaee, J. Verheyen, A. A. E. Stevens et al., Plasma Processes and Polymers **16** (2019).
8. C. Guerra-Nuñez, M. Döbeli, J. Michler, and I. Utke, Chem. Mater. **29**, 8690 (2017).
9. S. Kinnunen, T. Sajavaara, Surf et al., Surf. Coat. Technol. **441**, 128456 (2022).
10. J. L. van Hemmen, S. B. S. Heil, J. H. Klootwijk et al., J. Electrochem. Soc. **154**, (2007).

* *Corresponding authors' e-mail:* barbara.putz@empa.ch, ivo.utke@empa.ch

Ambient pressure XPS setup for studying *in situ* ALD

Esko Kokkonen[a] *, Rosemary Jones[b], Joachim Schnadt[a,b]

[a] *MAX IV Laboratory, Lund University, Lund, Sweden*
[b] *Division of Synchrotron Radiation Physics, Department of Physics, Lund University, Lund, Sweden*

Ambient pressure X-ray photoelectron spectroscopy (APXPS) is a powerful tool to study surfaces in elevated pressure and temperature conditions. We have recently developed an ambient pressure cell (AP cell) dedicated for ALD research. The cell allows real-time XPS study of the surface of a substrate where ALD reactions take place. The cell is intended for chemical characterization of intermediate products that are short-lived and might not be present on the surface once saturation of the surface has been achieved and therefore are not visible in post-process XPS identification. Experiments such as these have gained noticeable traction within a few years. [1,2,3,4]

The system is installed on the SPECIES beamline [5] at the MAX IV Laboratory in Lund, Sweden. SPECIES beamline is a soft X-ray beamline with one beam branch dedicated for APXPS. The beamline offers a wide photon energy range of 30-1500 eV, which enables to study most core-levels using XPS, but also makes it possible to focus on valence band investigations using UPS and lower photon energies and high photon flux. The endstation consists of different equipment for sample characterization and preparation, with the main instrument being an electron analyser capable of high energy and time resolution.

The ALD cell has been designed with realistic gas flow dynamics in mind. The cell can operated with a maximum pressure of 20 mbar, with the intention of creating a laminar-like flow across the substrate surface that is being investigated using XPS. Two mass spectrometers located in different locations in the endstation can be used to probe the gaseous reaction products. The mass spectrometers allow to simultaneously follow masses of important ligands and synchronize this data acquisition with the XPS data. [1]

Here, we will give a brief overview of the system including its design and operating parameters. Some results from example cases are given which demonstrate the capability of the ALD cell for studying substrates during ALD reactions.

References

1. Kokkonen, E., et al. *Rev. Sci. Instrum.* 93.1, 013905 (2022)
2. D'Acunto, Giulio, et al. *ACS Appl. Electron. Mater.* 2.12, 3915-3922 (2020)
3. D'Acunto, Giulio, et al. *Faraday Discuss.* 236, 71-85 (2022)
4. D'Acunto, Giulio, et al. *J. Phys. Chem. C* 126.29 12210-12221 (2022)
5. Kokkonen, Esko, et al. *J. Synch. Rad.* 28.2, 588-601 (2021)

* *Corresponding author e-mail:* esko.kokkonen@maxiv.lu.se

Functional materials I

Chair: Sønsteby, Henrik (University of Oslo)

Time: 5/30/2023 8:30:00 AM
Location: Auditorium 1, Promotion Hall, Naamsestraat 22, Leuven

Vapour deposition of functional semiconductor and heterojunction (nano-)materials for gas sensing

Chris Blackman[a]

[a] *Department of Chemistry, University College London, 20 Gordon Street, London, WC1H 0AJ, UK*

Materials such as complex oxides (doped, quaternary, etc) and heterojunctions are finding wide application in fields such as solar devices, heterogenous catalysis and gas sensing, amongst numerous others. The controlled and reproducible synthesis of such materials are obviously therefore key to progress in these fields. Amongst competing synthesis technologies chemical vapour deposition techniques (CVD, ALD) allow reproducible synthesis of a wide range of thin and ultra-thin film materials, and nanomaterials, and provides direct integration of the functional material with a device platform. Here I will discuss our use of vapour deposition techniques for synthesis of functional gas sensing semiconductor and heterojunction (nano-)materials.

Chemical vapor deposition and high-resolution patterning of a highly conductive two-dimensional coordination polymer film

Víctor Rubio-Giménez,[a,*] Giel Arnauts,[a] Mingchao Wang,[b] Eduardo Sergio Oliveros Mata,[c] Xing Huang,[b] Tianshu Lan,[b] Max L. Tietze,[a] Dmitry E. Kravchenko,[a] Jorid Smets,[a] Nathalie Wauteraerts,[a] Azat Khadiev,[d] Dmitri V. Novikov,[d] Denys Makarov,[c] Renhao Dong,[b] and Rob Ameloot[a,*]

[a] *Centre for Membrane Separations, Adsorption, Catalysis and Spectroscopy (cMACS), Katholieke Universiteit Leuven, Celestijnenlaan 200F, 3001 Leuven, Belgium*
[b] *Center for Advancing Electronics Dresden (cfaed) & Faculty of Chemistry and Food Chemistry, Technische Universität Dresden, 01062 Dresden, Germany*
[c] *Institute of Ion Beam Physics and Materials Research, Bautzner Landstrasse 400, 01328 Dresden, Germany*
[d] *Deutsches Elektronen-Synchrotron DESY, Notkestraße 85, 22607 Hamburg, Germany*

Integration of metal-organic frameworks (MOFs) and coordination polymers (CPs) into functional devices will require suitable processing methodologies. Robust thin film deposition methods are key in providing control over the material properties and ensuring standardization.[1,2] Yet, current solution-based methods to produce MOGs thin films lack control over nucleation and crystal growth, and the resulting coatings are typically rough and far from pinhole-free. Apart from particle contamination due to homogeneous nucleation, solution-based synthesis methods can lead to corrosion due to metal salts and surface-tension-related issues.[1,3] Chemical vapor deposition (CVD) of MOFs and CPs is a solvent-free methodology that avoids these problems by reacting a metal-containing precursor film with a ligand in the vapor phase to yield the desired material. This technique was pioneered for zeolitic imidazolate frameworks[4] and has since been extended to other MOFs and CPs.[3] The absence of solvent during this approach limits metal ion mobility during crystallization, enabling the conversion of patterned oxide precursors with high fidelity in bottom-up lithography procedures.[4,5] In contrast, solvent-based syntheses typically yield poorly defined edges,[6,7] leaving top-down patterning methodologies as the only option.

Figure 1. a) Top view of the Cu-BHT crystal structure showing the Kagome-type planar lattice with the chemical formula $[Cu_3(C_6S_6)]_n$. Cu, C, and S atoms are colored green, grey, and yellow, respectively. b) Scheme of the 2-step CVD procedure to prepare Cu-BHT nanofilms: a CuO layer is deposited via RF sputtering, followed by exposure to H_6BHT vapor. c) Photograph of glass substrates (3x3 cm^2) with a CuO layer before (top) and after CVD conversion into Cu-BHT (bottom). d) AFM topographic image of a homogeneous CVD Cu-BHT nanofilm and; e) a manually scratched area of the same film. d) CVD Cu-BHT film thicknesses obtained from CuO precursor films with different thicknesses. Black line is a linear fit of the data. g) Confocal microscopy image of a Hall bar microdevice (Cu-BHT Hall bar and Au electrodes) made with additive lithography.

Here, we report the CVD of Cu-BHT films (BHT = benzenehexanothiolate, Figure 1a) using an copper oxide precursor layer (Figure 1b).[10] Cu-BHT is a two-dimensional coordination polymer composed by Kagome-type layers MOGs. Furthermore, it is a metallic conductor with the highest conductivity reported for a metal-organic compound.[8,9] Thus far, Cu-BHT has mainly been synthesized through interfacial liquid-liquid reactions yielding inhomogeneous and rough films. In contrast, our CVD Cu-BHT nanofilms (Figure 1c-e) are homogeneous over large areas and smooth while maintaining a high crystallinity, electrical conductivity and charge carrier mobility. Moreover, the conversion from a CuO precursor layer allows for controlling the final Cu-BHT film thickness over a broad nanometric range (20-85 nm, Figure 1d), and is fully compatible with additive lithography processes (e.g., lift-off patterning) with a resolution down to the µm range. This approach facilitates the fabrication of well-defined, micrometric Hall bar devices that were used to accurately measure the conductivity parameters (Figure 1g). The demonstrated deposition and patterning fabrication flow showcases the advantages of vapor-phase methods and brings the integration of metal-organic nanofilms into microelectronic devices closer.

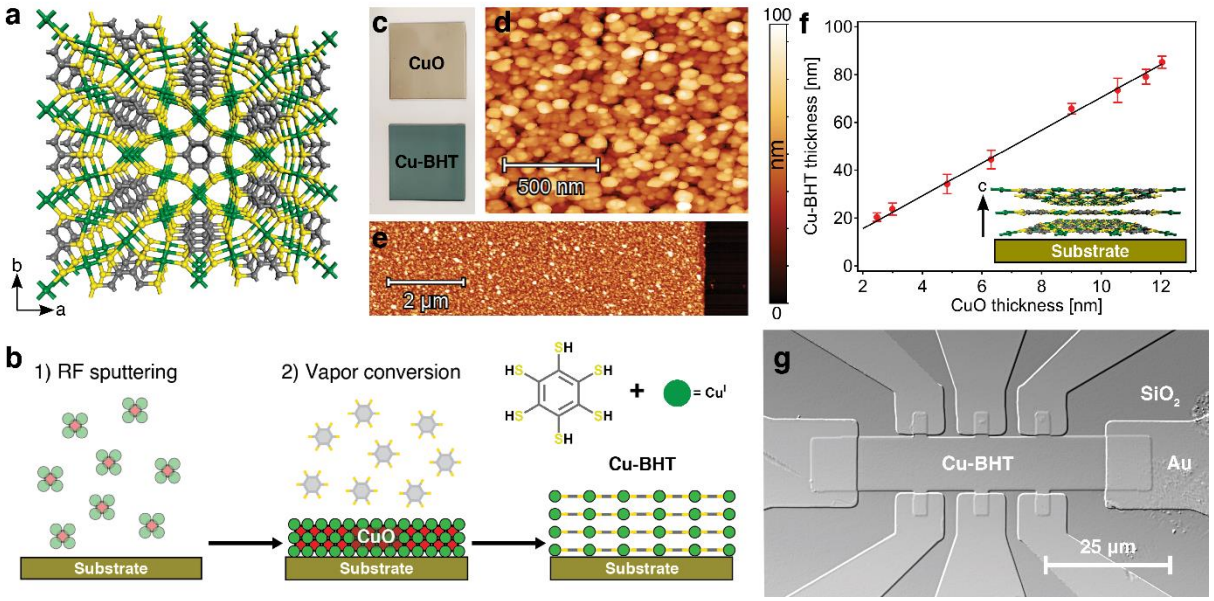

References

1. I. Stassen, N. Burtch, A. Talin, P. Falcaro, M. Allendorf, and R. Ameloot, *An Updated Roadmap for the Integration of Metal-Organic Frameworks with Electronic Devices and Chemical Sensors*, Chem. Soc. Rev. **46**, 3185 (2017).
2. V. Rubio-Giménez, S. Tatay, and C. Martí-Gastaldo, *Electrical Conductivity and Magnetic Bistability in Metal–Organic Frameworks and Coordination Polymers: Charge Transport and Spin Crossover at the Nanoscale*, Chem. Soc. Rev. **49**, 5601 (2020).
3. P. Su, M. Tu, R. Ameloot, and W. Li, *Vapor-Phase Processing of Metal–Organic Frameworks*, Acc. Chem. Res. **55**, 186 (2022).
4. I. Stassen, M. Styles, G. Grenci, H. V. Gorp, W. Vanderlinden, S. D. Feyter, P. Falcaro, D. D. Vos, P. Vereecken, and R. Ameloot, *Chemical Vapour Deposition of Zeolitic Imidazolate Framework Thin Films*, Nat. Mater. **15**, 304 (2016).
5. M. Krishtab, I. Stassen, T. Stassin, A. J. Cruz, O. O. Okudur, S. Armini, C. Wilson, S. De Gendt, and R. Ameloot, *Vapor-Deposited Zeolitic Imidazolate Frameworks as Gap-Filling Ultra-Low-k Dielectrics*, Nat. Commun. **10**, 3729 (2019).
6. P. Falcaro, R. Ricco, C. M. Doherty, K. Liang, A. J. Hill, and M. J. Styles, *MOF Positioning Technology and Device Fabrication*, Chem. Soc. Rev. **43**, 5513 (2014).
7. C. L. Ruiz-Zambrana, M. Malankowska, and J. Coronas, *Metal Organic Framework Top-down and Bottom-up Patterning Techniques*, Dalton Trans. **49**, 15139 (2020).
8. X. Huang et al., *A Two-Dimensional π-π Conjugated Coordination Polymer with Extremely High Electrical Conductivity and Ambipolar Transport Behaviour*, Nat. Commun. **6**, 7408 (2015).
9. X. Huang, S. Zhang, L. Liu, L. Yu, G. Chen, W. Xu, and D. Zhu, *Superconductivity in a Copper(II)-Based Coordination Polymer with Perfect Kagome Structure*, Angew. Chem. Int. Ed. **57**, 146 (2018).
10. V. Rubio-Giménez, G. Arnauts, M. Wang, E. S. Oliveros Mata, X. Huang, T. Lan, M. L. Tietze, D. E. Kravchenko, J. Smets, N. Wauteraerts, A. Khadiev, D. V. Novikov, D. Makarov, R. Dong, and R. Ameloot, *Chemical vapor deposition and high-resolution patterning of a highly conductive two-dimensional coordination polymer film*, J. Am. Chem. Soc. **accepted** (2022).

* *Corresponding author e-mail: victorrubio.gimenez@kuleuven.be; rob.ameloot@kuleuven.be*

Gradient polymer coatings deposited via initiated chemical vapor deposition (iCVD) for anti-icing applications

Gabriel Hernández Rodríguez[a], Anna Maria Coclite[a,*]

[a] *Institute of Solid State Physics, Graz University of Technology, Petersgasse 16, 8010 Graz, Austria*

The development of coatings using initiated chemical vapor deposition iCVD represents a promising alternative to the current demand for icephobic technology that can be potentially incorporated into existing anti-icing systems. In this study, we propose a design of gradient polymer coatings via iCVD for anti-icing applications. The icephobicity was tested through different experiments with the aim of showing how icephobic properties can be enhanced when the design of the gradient polymer is tailored.

The gradient polymer design contemplated monomers of different nature and properties a highly fluorinated compound and an organosilicon, namely, perfluorodecyl acrylate (PFDA) and tetravinyl tetramethyl cyclotetrasiloxane (V4D4). The gradient polymer consisted of a discontinuous vertical structure where a section rich in pV4D4 lies on the bottom, in contact with the substrate, a progressive change forms a copolymer in the middle section to finally end with a section rich in pPFDA, which forms the surfaces exposed to the environment. The structure results in three regions: two homopolymers on each end and a copolymer in between, connected in a continuous structure (Fig 1.1). The multiple vinyl groups of V4D4 form a highly cross-linked network that provides strong adhesion to the substrates, whereas the PFDA fluorinated groups produce low-energy surfaces with potential icephobic properties. The appeal of this concept is the complete retention of the functionality of the monomers selected, in contrast with the typical copolymerization approach. Using iCVD is the only way in creating such complex structures, moreover, they are created with high precision, in one step, and without any usage of solvents. Gradient polymers with different thicknesses of the pPFDA top section were deposited.

After deposition, spotless and defect-free surfaces were obtained indicating uniform coverage. Cross hatch adhesion tests confirmed strong adhesion to the substrate. Atomic force microscopy exhibited that gradient polymers resulted in rougher surfaces due to spherical islands, in contrast to smoother surfaces observed when conventional structures were deposited. A significant difference in static water contact angle between samples was a direct consequence of the nature of the surface. Additionally, gradient polymers revealed a high pinning effect as a result of the high contact angle hysteresis. To assess the feasibility of the gradient polymers for anti-icing systems the surface properties and surface events were observed and analyzed under different icing experiments. Observations on the nucleation and propagation of ice over the films were done by analyzing the condensation frosting process (Fig 1.2). Single droplet freezing experiments provided information regarding the freezing delay and ice detachment experiments showed a reduction of ice adhesion to the coating surface of at least 25 times compared to the reference silicon sample, without damaging the coating (Fig 1.3). Finally, supercooled droplet impact experiments tested the coatings in different environmental conditions, revealing the endurance and feasibility of the gradient polymer films as anti-icing materials.

In conclusion, we showed that gradient polymer coatings are actively delaying frost formation, influencing the nature of the resulting frost avoiding a densely packed structure and decreasing the ice adhesion, exhibiting promising ice mitigation properties vital for anti-icing systems.

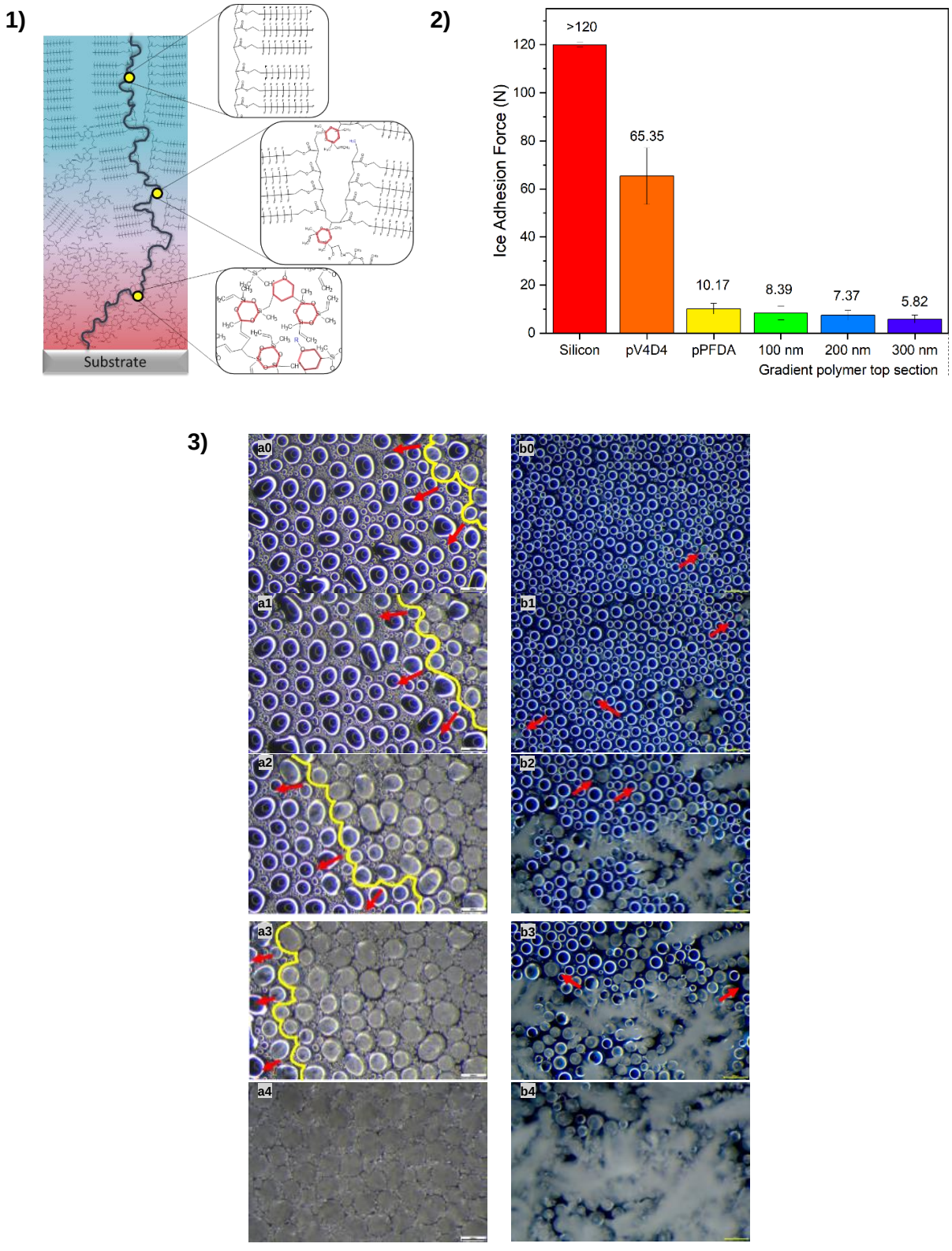

Figure 1.- 1) Schematic representation of the molecular architecture that conforms a gradient polymer, highlighting three sections: two homopolymers in each end and a copolymer in the middle. 2) Ice adhesion force of gradient polymers with different top section thicknesses compared with reference samples. 3) Evolution of the condensation frosting process at different surfaces: a) bare silicon and b) gradient polymer.

* *Corresponding author e-mail:* ghernandezrodriguez@tugraz.at

ALD GST industrial processing, scaling to 300mm challenges and outcomes

Jerome Innocent[a], Andrea Illiberi[a], Michael Givens[a], Varun Sharma[a], Laura Nyns[b], Hubert Hody[b], Annelies Delabie[b], Wouter Devulder[b], Daniele Garbin[b], Gabriele Luca Donadio[b] and Tobias Peissker[b]

[a] *ASM International, Kapeldreef 75, Leuven, 3001, Belgium*
[b] *Imec, Kapeldreef 75, Leuven, 3001, Belgium*

Phase change memory (PCM) has long been viewed as a potential low cost, low energy non-volatile storage class memory solution. A material central to and historically intertwined to with PCM is germanium antimony telluride (GST). Sandwiched between two contacts and with the aid of joule heating, GST can be cycled between its high resistance amorphous and low resistance crystalline phases. This on/off relationship can be manipulated as a binary readout and as such GST, with a up to seven orders of magnitude difference in its resistance, is ostensibly an ideal PCM material.[1]

In order to keep unit cost low PCM memory has begun to scale vertically.[2] With multiple device stacks and higher aspect ratios this means the constraints for deposition are becoming even greater. ALD where both conformal and selective growth of GST are possible is therefore a key technology in accessing the GST based PCM market.

In this work, GST ALD has been upscaled to 300mm wafers on a 300mm production ALD reactor. The process has been engineered to maximize throughout and reliability and with it demonstrated that ALD grown GST can perform equivalently to PVD GST on blanket test materials. Furthermore, the pitfalls when moving to 3D high aspect ratio (HAR) devices have been catalogued and the key ALD precursor and material criteria when moving toward 3D PCM applications are presented.

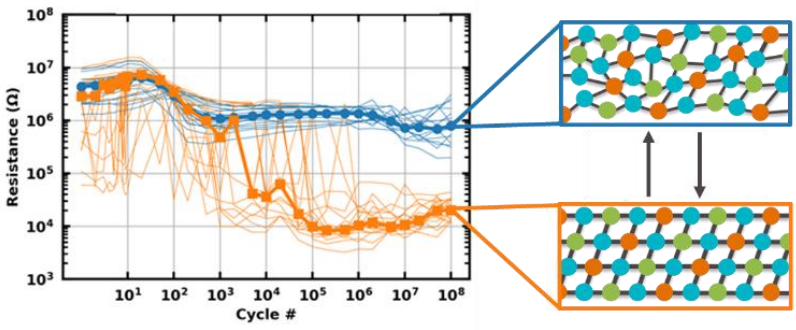

Figure 1. Cartoon of the change in crystal structure of GST and its associated switch in resistance.

References

1. S. Raoux, M. Ritala, PCRAM. In: Hwang, C. (eds) Atomic Layer Deposition for Semiconductors. (2014).
2. P. Fantini, *J. Phys. D: Appl. Phys,* **53,** 283002 (2020)

* *Corresponding author e-mail:* jerome.innocent@asm.com

Extraordinary slippery liquid-repellent surfaces by vapor-deposition of self-assembled monolayers

Sakari Lepikko[a], Ygor Morais Jaques[a,c,e], Muhammad Junaid[a], Matilda Backholm[a], Jouko Lahtinen[a], Jaakko Julin[b], Ville Jokinen[c], Timo Sajavaara[b], Maria Sammalkorpi[c,d,e], Adam S. Foster[a,f], Robin H. A. Ras[a,e*]

[a] *Department of Applied Physics, Aalto University, P.O. Box 15100, 02150 Espoo, Finland*
[b] *Department of Physics, University of Jyväskylä, P.O. Box 35, 40014 University of Jyväskylä, Finland*
[c] *Department of Chemistry and Materials Science, Aalto University, P.O. Box 16100, 02150 Espoo, Finland*
[d] *Department of Bioproducts and Biosystems, Aalto University, P.O. Box 16100, 02150 Espoo, Finland*
[e] *Center of Excellence in Life-Inspired Hybrid Materials, Aalto University, P.O. Box 15100, 02150 Espoo, Finland*
[f] *Nano Life Science Institute (WPI-NanoLSI), Kanazawa University, Kakuma-machi, 920-1192 Kanazawa, Japan*

Water-repellent surfaces have the attractive property of staying dry, and find applications in self-cleaning, anti-icing, anti-fogging and much more. These surfaces stay dry because water droplets experience low friction and slide off easily at low tilt angles.[1]

Liquid-repellent surfaces, especially smooth solid surfaces with covalently grafted flexible brushes or alkyl monolayers, are the focus of an expanding research area.[1] Surface-tethered flexible species are highly mobile at room temperature, giving solid surfaces a unique liquid-like quality and unprecedented dynamical repellency towards various liquids regardless of their surface tension. The liquid-like molecular layer controls many important interface properties, such as slip, friction and adhesion, which may enable novel functions and applications that are inaccessible with conventional solid coatings.

Here we challenge two common assumptions on liquid-repellency with the use of vapor-deposited self-assembled monolayers (SAMs) (Figs. 1+2).[2]

- It is generally assumed that achieving low sliding angles on water-repellent surfaces requires hydrophobicity, in other words high water contact angle like for example teflon. Here we challenge this assumption and demonstrate a hydrophilic alkyltrichlorosilane SAM featuring the unusual combination of low sliding angle and low contact angle.
- Surface heterogeneity is generally acknowledged as the major cause of increased contact angle hysteresis and friction of droplets. Here we challenge this long-standing premise for chemical heterogeneity at the molecular length scale.

Furthermore, we demonstrate world's most slippery surface, by combining SAMs and surface structuring.

We form SAMs by vapor deposition in a specially designed ALD reactor, where operando ellipsometry allows us to monitor the SAM while it grows. Findings obtained from a range of characterization techniques and molecular dynamics simulations reveal a yet unknown and counterintuitive mechanism for slipperiness, opening new avenues for enhancing the mobility of droplets.

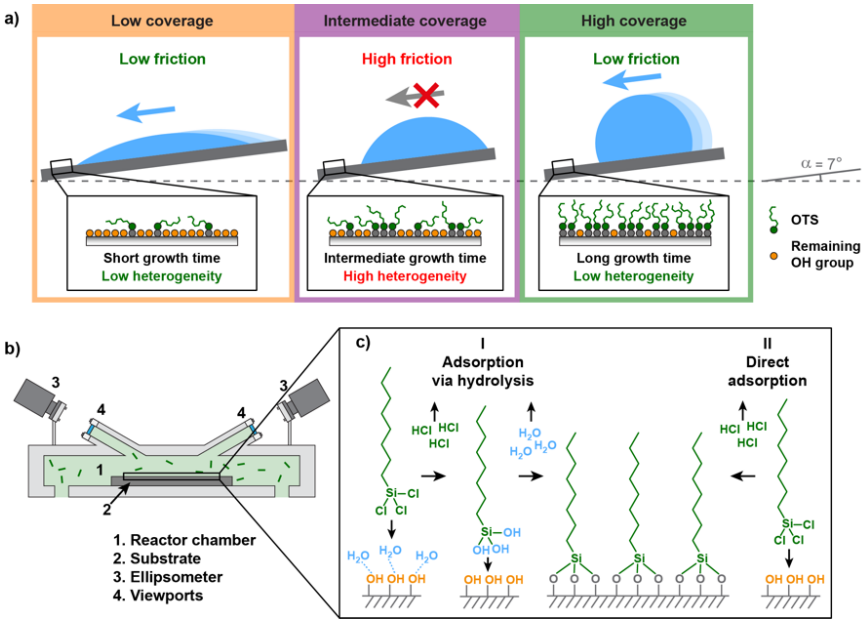

Figure 1. Controlling contact line friction CLF by tuning surface hydrophobicity with SAM. a) We observe that CLF depends on heterogeneity of the SAM and has lowest values both at low and high SAM coverage regimes, and highest values at intermediate coverages. b) Schematics of the vapor deposition reactor chamber for growing SAMs, featuring operando spectroscopic ellipsometry for continuous in-situ monitoring the growth of SAM films. c) Adsorption mechanisms of SAM on hydroxyl rich surfaces.

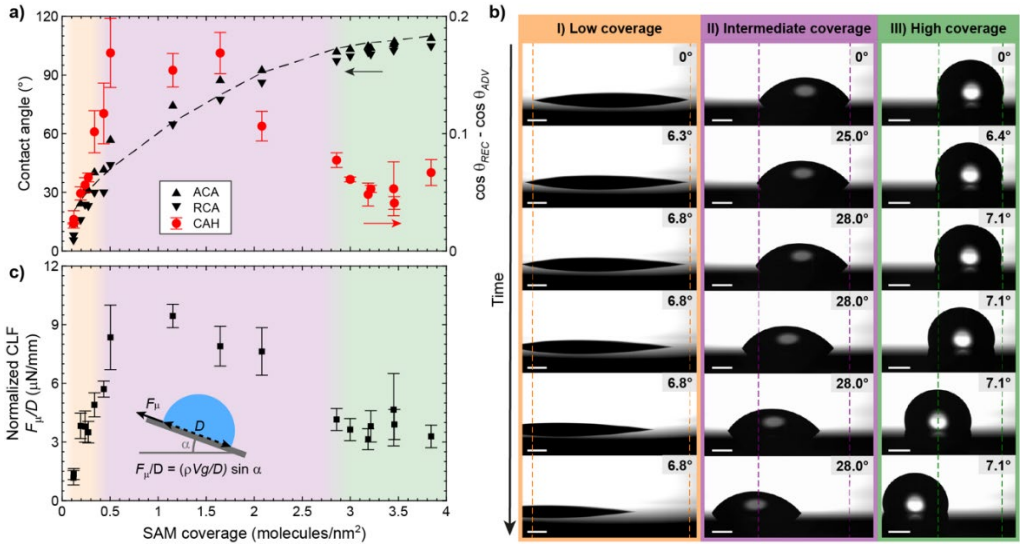

Figure 2. SAM wetting properties. a) Advancing contact angle ACA, receding contact angle RCA, and contact angle hysteresis CAH as function of SAM coverage. b) Snapshots of 10 μl droplets sliding on low (0.1 molecules/nm^2), intermediate (0.5 molecules/nm^2), and high-coverage (3.2 molecules/nm^2) SAMs. Surface tilt is shown in the top-right corner of each frame and dashed lines show initial location of droplet. Droplet started sliding at second frame from top. Scale bars represent 1 mm. c) Normalized CLF calculated from sliding angles.

References

1. L. Chen, S. Huang, R. H. A. Ras, X. Tian, Omniphobic liquid-like surfaces, Nature Chemistry Reviews, (2023) 123-137 https://doi.org/10.1038/s41570-022-00455-w
2. S. Lepikko, Y. Morais Jaques, M. Junaid, M. Backholm, J. Lahtinen, J. Julin, V. Jokinen, T. Sajavaara, M. Sammalkorpi, A. S. Foster, R. H. A. Ras, Droplet slipperiness despite surface heterogeneity at molecular scale, Nature Chemistry, in review – revised version submitted.

* *Corresponding author e-mail:* robin.ras@aalto.fi

ASD I / organic

Chair: Devi, Anjana (Ruhr-Universität Bochum)

Time: 5/30/2023 8:30:00 AM
Location: Auditorium 2, Maria-Theresiacollege, St. Michael's Street 6, Leuven

Area-selective atomic layer deposition of nitrides and oxides using small molecule inhibitors

A.J.M. Mackus*

Eindhoven University of Technology, P O. Box 513, 5600 MB Eindhoven, The Netherlands

With top-down fabrication approaching its limits, area-selective deposition (ASD) processes are currently being developed for a variety of applications in the semiconductor industry, allowing for novel bottom-up and self-aligned fabrication schemes. Selectivity during atomic layer deposition (ALD) is typically obtained by functionalizing the surfaces on which no growth is desired with inhibitor molecules. In addition to self-assembled monolayers (SAM), in recent years there is especially interest in vapor-phase dosing of small molecule inhibitors (SMI), [1,2] because of the compatibility with industrial processing flows.

In this contribution, results will be presented for area-selective ALD processes of nitrides and oxides, two important classes of materials in semiconductor fabrication. The mechanisms of how SMIs block precursor adsorption will be discussed based on insights from simulation and experimental studies. Generally, it is more challenging to block ALD growth using SMIs as compared to SAMs. As a result of vapor-phase dosing, inhibitor molecules sequentially adsorb at random sites, leaving relatively large gaps in between the inhibitor molecules, where precursor molecules can potentially interact with the surface.[3] In addition, it was found that not all SMIs react in the same way, but adsorb in different bonding configurations. The consequences of these surface reaction mechanisms will be discussed by comparing two ALD processes as case studies: (*i*) silicon oxide using acetylacetone (Hacac), and (*ii*) tantalum nitride using aniline as SMI.

References:
1. A.J.M. Mackus, M.J.M. Merkx, W.M.M. Kessels, *Chemistry of Materials* **31**, 2 (2019).
2. J. Yarbrough, A.B. Shearer, and S.F. Bent, *Journal of Vacuum Science & Technology A* **39**, 021002 (2021)
3. J. Li, I. Tezsevin, M.J.M. Merkx, J.F.W. Maas, W.M.M. Kessels, T.E. Sandoval, and A.J.M. Mackus*, J. Vac. Sci. Technol. A* **40**, 062409 (2022)

* *Corresponding author e-mail: a.j.m.mackus@tue.nl*

The Importance of Small Molecule Inhibitor Dosing Conditions during Area-Selective ALD Studied with Infrared Spectroscopy

O.C.A. Bolkenbaas[a,*], J.F.W. Maas[a], M.J.M. Merkx[a], I. Tezsevin[a], P. Yu[a], T.E. Sandoval[b], W.M.M. Kessels[a], A.J.M. Mackus[a]

[a] *Eindhoven University of Technology, P. O. Box 513, 5600 MB Eindhoven, The Netherlands*
[b] *Universidad Técnica Federico Santa María, Av. Vicuña Mackenna 3939, Santiago, Chile*

Area-selective atomic layer deposition (AS-ALD) has gained much interest recently due to its potential in facilitating the further downscaling of semiconductor devices. One mechanism for achieving AS-ALD is the use of small molecule inhibitors (SMIs) that selectively block deposition on certain materials. However, AS-ALD processes generally lose their selectivity after a certain number of cycles. A mechanism contributing to this loss of selectivity is that the SMI adsorbs in a mixture of bonding configurations, that have different stability and do not necessarily all block deposition effectively [1]. In this work, we investigate the influence of dosing conditions on SMI adsorption configuration using in-situ reflection adsorption infra-red spectroscopy (RAIRS) and a model based on reaction rate equations.

To investigate SMI adsorption, acetylacetone (Hacac) adsorption on an Al_2O_3 non-growth area is studied as a model system. It is known that Hacac initially adsorbs in the monodentate configuration, binding to the surface through a single O atom. Subsequently, it can convert to the chelate configuration, after which it bonds to the surface with both O atoms (Fig. 1), releasing water as a byproduct. The molecules in the monodentate configuration are expected to be a cause for the loss of selectivity [2]. For such a two-step adsorption mechanism, reaction rate equations can be set up and solved numerically for different dosing conditions. The solutions to the equations showed that dosing at low partial pressure can increase selectivity since this leads to a high coverage of acac adsorbates in the chelate configuration (Fig. 2) and saturation coverage is achieved at lower exposures. This behavior is confirmed experimentally by in-situ RAIRS measurements. When dosing using 0.5 s, low pressure pulses of Hacac, the surface saturates after a total exposure of 0.26 Torr·s, while when using higher pressure pulses of 1 s, the saturation is only reached after a total exposure of 1 Torr·s. Furthermore, a shift of the C-O peak towards lower wavenumbers for low pressure dosing is observed when comparing the spectra of the saturated surfaces (Fig. 3). This coincides with the expected increase of adsorbates in the chelate configuration, indicating that the ratio between monodentate and chelate adsorbate products can be tuned by changing the dosing conditions. Therefore, the inhibitor dosing conditions are important for achieving a high selectivity.

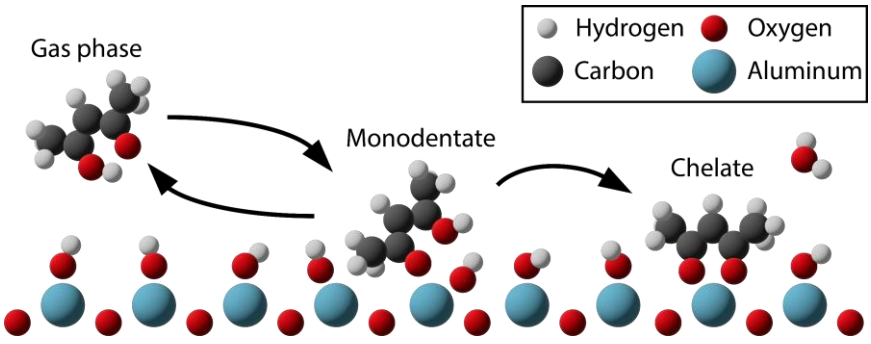

Figure 1: The reaction mechanism of Hacac on an Al_2O_3 surface. First, the Hacac reversibly binds to an Al atom in the monodentate configuration. Then, the molecule reacts with the -OH group forming the chelate configuration and water as a reaction product.

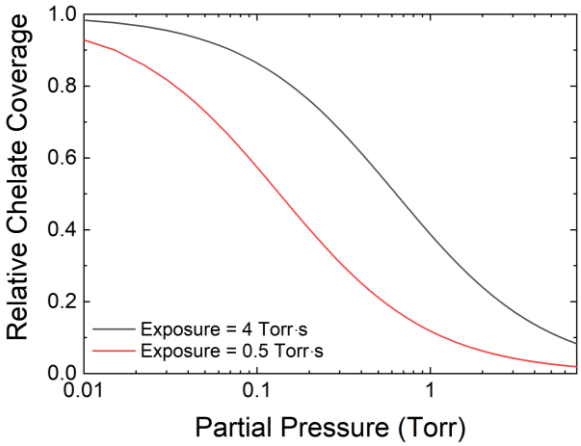

Figure 2: Numerical solutions of the reaction rate equations. The fraction of molecules adsorbed in the chelate configuration as a function of partial pressure for two fixed exposures. The model shows that when dosing at a lower partial pressure, the fraction of adsorbates in the chelate configuration is higher. Therefore, a lower SMI partial pressure during dosing is predicted to be beneficial for selectivity.

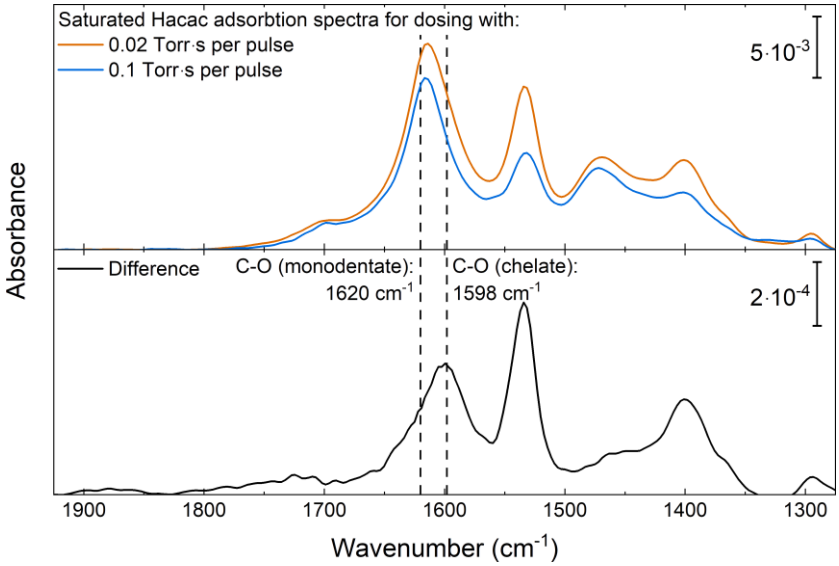

Figure 3: RAIRS adsorption spectra for an Al_2O_3 surface saturated with Hacac after pulses with an exposure of 0.02 Torr·s per pulse and 0.1 Torr·s per pulse, in orange and blue respectively. In black the difference between the two spectra is shown. The shift of the C-O peak around 1618 cm^{-1} towards lower wavenumbers coincides with the expected increase of adsorbates in the chelate configuration when dosing at low pressures.

References:

1. M. J. M. Merkx, T. E. Sandoval, D. M. Hausmann, W. M. M. Kessels, and A. J. M. Mackus, “Mechanism of precursor blocking by acetylacetone inhibitor molecules during area-selective atomic layer deposition of SiO_2,” *Chemistry of Materials*, **32**, 3335 (2020).
2. A. Mameli, M. J. M. Merkx, B. Karasulu, F. Roozeboom, W. M. M. Kessels, and A. J. M. Mackus, “Area-selective atomic layer deposition of SiO_2 using acetylacetone as a chemoselective inhibitor in an ABC-type cycle,” *ACS Nano*, **11**, 9, 9303 (2017).

* *Corresponding author e-mail:* o.c.a.bolkenbaas@tue.nl

Insight into Mechanism of Area-Selective Atomic Layer Deposition of Germanium Telluride

Jyoti Sinha[a, b], Laura Nyns[b], Annelies Delabie[a, b]*

[a] *Department of Chemistry, KU Leuven (University of Leuven), Leuven, 3001, Belgium*
[b] *IMEC, Leuven, 3001, Belgium*

The phase change material $Ge_2Sb_2Te_5$ (GST) has emerged as promising candidate for non-volatile storage class memory (SCM) [1]. As advanced SCM devices consist of 3D high-aspect ratio structures, it is crucial to develop highly conformal GST deposition processes. In addition, area-selective deposition is a promising technique to reduce the number of etch and patterning steps and as such the fabrication cost of advanced nano-electronic devices [2,3]. Area-selective atomic layer deposition (ALD) of GST is therefore of great interest. The reaction chemistry of an ALD process for GST has been reported, where cycles of GeTe and Sb_2Te_3 are combined to deposit the desired composition $Ge_2Sb_2Te_5$ [4,5]. Hence, insight in the growth behaviour and selectivity mechanism of GeTe ALD is a first step to understand and improve the selectivity of $Ge_2Sb_2Te_5$ ALD. In this study, we describe the selectivity mechanism of GeTe ALD. TiN and SiO_2 are selected as growth surface and non-growth surface, respectively, as TiN acts as the electrode while SiO_2 is used as the insulating material in typical phase change memory devices [6]. The passivation of SiO_2 is achieved using an aminosilane small molecule inhibitor, namely dimethylamino-trimethylsilane (DMA-TMS), while TiN remains reactive after DMA-TMS treatment [7]. GeTe is deposited on blanket TiN and SiO_2 using $GeCl_2.C_4H_8O_2$ and $Te(Si(CH_3)_3)_2$ as precursors, with a growth-per-cycle of 0.06 nm/cycle (Fig. 1(a), mass measurements). Deposition of GeTe on TiN is not much affected by the DMA-TMS pretreatment and a GPC of 0.05 nm/cycle is achieved (Fig. 1(a)). On the other hand, we observe a nucleation delay of ~240 cycles on DMA-TMS treated SiO_2, confirming that SiO_2 could act as a non-growth area during selective GeTe deposition (Fig. 1(a)). After extended cycles, selectivity loss occurs due to nanoparticle growth (Fig. 2). The selectivity of GeTe deposition is calculated using the following equation (Eq. 1):

$$Selectivity\ (S) = \frac{n_G + n_{NG}}{n_G - n_{NG}} \qquad (1)$$

where n_G and n_{NG} denotes the thickness of the material deposited on growth and non-growth surface, respectively [3]. The selectivity of 10 nm GeTe is 0.95 and decreases with increasing thickness to reach 0.88 for 17 nm GeTe for blanket substrate (Fig. 1(b)). The Ge:Te ratio for a 20 nm GeTe film on both surfaces is 1:1 as confirmed by Rutherford Backscattering Spectrometry (RBS) (Fig. 2).The mechanism of selectivity loss is analyzed further from the scanning electron microscopy (SEM) images. The number and size of nanoparticles increase with ALD cycles and agglomeration of nanoparticles contributes to the increased sizes (Fig. 2). The composition of GeTe nanoparticles is Ge rich, which indicates that DMA-TMS affects the surface chemistry on the SiO_2 substrate (Fig. 3). To investigate the mechanism, we studied the individual reactions of $GeCl_2.C_4H_8O_2$ and $Te(Si(CH_3)_3)_2$ on DMA-TMS treated SiO_2, and measure the concentration of elements by Total reflection X-Ray Fluorescence (T-XRF) spectroscopy. Ge is present in a concentration of 1.9×10^{14} atoms/cm^2. In contrast, in case of Te precursor reaction, no trace of Te is detected using T-XRF. This indicates that the Ge adspecies on DMA-TMS treated SiO_2 act as reactive site for the incoming Te precursor, which degrades the overall selectivity. Finally, GeTe is deposited on SiO_2-TiN line-space patterns with a SiO_2 line height of 65 nm and pitch of 90 nm. The transmission electron microscope shows that 20 nm of GeTe could be selectively deposited on the TiN area of the line-space pattern which is important for selective deposition on complex device structures (Fig. 4). Overall, we have demonstrated the selective deposition of GeTe on the line-space pattern and established that the Ge precursor adsorption is responsible for loss in selectivity of GeTe. The insights from this study will be helpful to understand the selectivity loss mechanism for $Ge_2Sb_2Te_5$.

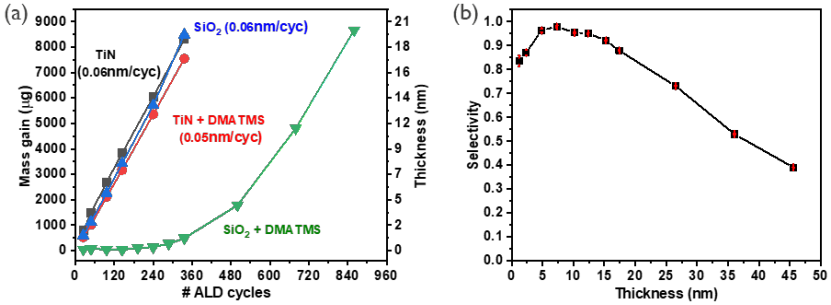

Figure 1 (a)Mass gain of GeTe with ALD cycle and (b) Selectivity of GeTe as function of thickness

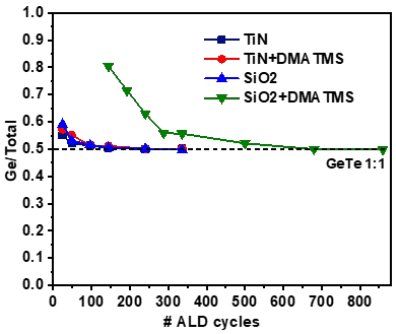

Figure 2 Composition of GeTe analyzed using RBS, showing the Ge content as function of ALD cycles

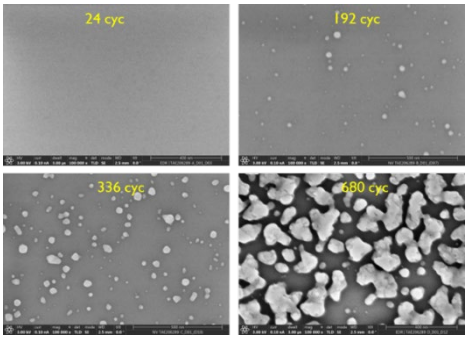

Figure 3 GeTe nanoparticles on SiO2-DMA-TMS by SEM

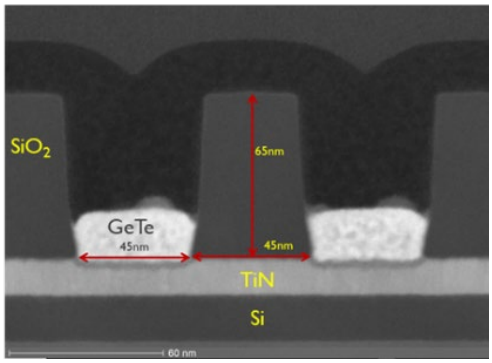

Figure 4 Selective deposition of GeTe on line-space patterns (TEM)

Acknowledgement
Authors would like to thank Andrea Illiberi, Michael Givens and Jerome Innocent from ASM for their support in process development.

References

1. P. Kowalczyk et al., “Impact of Stoichiometry on the Structure of van der Waals Layered GeTe/Sb2Te3 Superlattices Used in Interfacial Phase-Change Memory (iPCM) Devices,” Small, vol. 14, no. 24, p. 1704514, Jun. 2018, doi: 10.1002/SMLL.201704514.
2. T. Gwon et al., “Atomic Layer Deposition of GeTe Films Using Ge{N[Si(CH 3) 3] 2 } 2 , {(CH 3) 3 Si} 2 Te, and Methanol,” 2016, doi: 10.1021/acs.chemmater.6b03704.
3. G. N. Parsons and R. D. Clark, “Area-Selective Deposition: Fundamentals, Applications, and Future Outlook,” Chemistry of Materials, vol. 32, no. 12, pp. 4920–4953, Jun. 2020, doi: 10.1021/acs.chemmater.0c00722.
4. V. Pore, T. Hatanpää, M. Ritala, and M. Leskela, “Atomic layer deposition of metal tellurides and selenides using alkylsilyl compounds of tellurium and selenium,” J Am Chem Soc, vol. 131, no. 10, pp. 3478–3480, Mar. 2009, doi: 10.1021/JA8090388/SUPPL_FILE/JA8090388_SI_002.CIF.
5. K. Knapas, T. Hatanpää, M. Ritala, and M. Leskelä, “In situ reaction mechanism studies on atomic layer deposition of Sb 2Te3 and GeTe from (Et3Si)2Te and chlorides,” Chemistry of Materials, vol. 22, no. 4, pp. 1386–1391, Feb. 2010, doi: 10.1021/CM902180D/ASSET/IMAGES/LARGE/CM-2009-02180D_0008.JPEG.
6. K. Aryana et al., “Interface controlled thermal resistances of ultra-thin chalcogenide-based phase change memory devices,” Nat Commun, vol. 12, no. 1, Dec. 2021, doi: 10.1038/s41467-020-20661-8.
7. J. Soethoudt, S. Crahaij, T. Conard, and A. Delabie, “Impact of SiO2 surface composition on trimethylsilane passivation for area-selective deposition,” J Mater Chem C Mater, vol. 7, no. 38, pp. 11911–11918, 2019, doi: 10.1039/c9tc04091a.

* *Corresponding author e-mail:* Annelies.Delabie@imec.be

Bridging the Synthesis Gap: Ionic Liquids Enable Solvent-Mediated Reaction in Vapor-Phase Deposition

Jingwei Shi[a], Seunggi Seo[a,c], Nathaniel J. Schuster[b], Hyungjun Kim[c], Stacey F. Bent[a,*]
[a] *Department of Chemical Engineering, Stanford University, Stanford, CA, 94305 USA*
[b] *Department of Chemistry, Stanford University, Stanford, CA, 94305 USA*
[c] *School of Electrical and Electronic Engineering, Yonsei University, Seoul 03722, Republic of Korea*

Atomic layer deposition (ALD) and molecular layer deposition (MLD) are technologically important methods to grow thin inorganic and organic films with high conformality and excellent thickness control from vapor phase precursors. The thin film materials that can be grown by MLD and ALD are valued for their diversity and tunability. However, there is still a need to broaden the ALD and MLD synthesis methods. For example, most MLD growth chemistries are constrained to those reacting by nucleophilic addition or substitution mechanisms, limiting those materials to primarily substituted carbonyl backbone polymers. Moreover, the development of new thermal ALD processes is also often limited by precursor reactivity and stability, with reaction temperature and precursor design being among the few variables available to achieve higher reactivity in gas-phase reactions. A limiting factor in each of these vapor processes is the absence of a solvent, which plays a role in traditional synthesis, where the use of solvent and/or a catalyst can promote a desired reaction. To bridge this synthesis gap between vapor-phase and solution-phase, we demonstrate the use of an ultrathin coating layer of a vapor phase-compatible solvent an ionic liquid (IL) on the growth substrate to enable both MLD and ALD. By performing the surface reactions inside of an IL, solvent effects are replicated inside the vacuum system, broadening the possible reactions to a wider suite of chemistries.

Using this strategy, the MLD of polyetherketoneketone (PEKK), an industrially and research-relevant, high-performance thermoplastic, is demonstrated. PEKK films are grown with diphenyl ether and isophthaloyl dichloride and catalyzed by aluminum chloride, in a thin IL layer of 1-ethyl-3-methylimidazolium chloride, notable because these precursors are the same as those utilized in the solution synthesis of PEKK. The results show that the IL-MLD process exhibits the three essential properties of MLD: conformality, surface limited (not bulk) reaction, and linear and saturating growth. Examination of the PEKK film by infrared spectroscopy and x-ray photoelectron spectroscopy (XPS) shows excellent agreement with reference spectra for PEKK.

We also describe studies of IL-assisted ALD of SnO. Successful SnO deposition is achieved using tin acetylacetonate and water, a process that otherwise would require a stronger counter-reactant such as ozone. The layer of IL allows a solvent-mediated reaction mechanism to take place on the growth substrate. We report a growth per cycle of 0.7 Å/cycle at a deposition temperature of 100 °C in an IL comprised of 1-ethyl-3-methylimidazolium hydrogen sulfate. Characterization of the ALD films confirms the SnO film composition, and ^{1}H and ^{13}C NMR are used to probe the solvent-mediated ALD reaction, suggesting a solvent-mediated addition-elimination type mechanism forming acetone and acetate. Thus, the IL-ALD and IL-MLD methods enable new vapor deposition chemistries to be achieved.

[*] *Corresponding author e-mail:* sbent@stanford.edu

Characterization II

Chair: Schnadt, Joachim (Lund University)

Time: 5/30/2023 10:30:00 AM
Location: Auditorium 1, Promotion Hall, Naamsestraat 22, Leuven

Interface formation chemistry in ALD of charge transport layers for perovskite solar cells

Adam Hultqvist[a], Bhavya Rakheja[a], Tobias Törndahl[a,*]

[a] *Div. Solar Cell Technology, Dept. of Materials Science and Engineering, Uppsala University, Box 35 SE-751 03 Uppsala, Sweden*

The current world record for a single junction perovskite device is 23.7% (> 1 cm^2), [1] where the most promising point of entry for the perovskite technology to the solar cell market is as a top cell in tandem with a bottom cell using established technologies such as Si and Cu(In,Ga)Se_2 (CIGS). [2, 3] Figure 1 shows the general material stack used for the perovskite top cell in two terminal tandem high efficiency devices with Si, CIGS and perovskite bottom cells. Here, an ALD-SnO_x electron transport layer (ETL) is commonly used in all of these stacks together with an organic ETL. In doing so, the perovskite is protected from the ALD process and the organic ETL is protected from sputter deposition of the high quality transparent conducting oxide (TCO). Omitting the organic ETL would not only reduce the cost, but also improve the stability of the solar cells, as organic layers are susceptible to damage by the high-energy photons of the sun spectra over time. Furthermore, by using a single ETL or hole transport layer (HTL) made by ALD, the conduction band (E_C) or valence band (E_V) positions can be varied to suit different perovskite materials.

No vacuum-based techniques have been able to deposit inorganic contact materials successfully directly on the metal halide perovskites (ABX_3 structure) while maintaining the solar cell performance. The main reason for this is that the perovskites are both temperature and chemically sensitive, which easily lead to material deterioration and poor-quality interfaces. Therefore, it is imperative to study the surface chemistry at these interfaces in order to find ALD processes that are compatible with metal halide perovskites. This abstract treats studies of ALD processes and precursors (M-L_n) in combination with some different metal halide perovskite materials.

One example of a non-ideal perovskite/SnO_x interface that acts as a transport barrier for the light-generated current is that of direct deposition ALD-SnO_x from TDMASn and water. [4] The interface formation during the initial ALD-SnO_x growth on the perovskite was studied by QCM monitor crystals coated by partial p−i−n solar cell stacks, and by soft and hard X-ray photoelectron spectroscopy (PES) measurements for the same structures (Fig. 2). From QCM, a mass loss was observed prior to ALD for growth temperatures above 60 °C, suggesting the decomposition of the perovskite. In addition, a mostly irreversible mass gain was observed during the first exposure to the TDMASn precursor that is independent of growth temperature, and which disrupts the mass gain of the following 20−50 ALD cycles. The chemical environments of the buried interface were analyzed by PES for a sample with 50 ALD cycles of SnO_x on the perovskite. Although measurements on the perovskite bulk below and the SnO_x film above did not show chemical changes, additional chemical states for Pb, Br, and N as well as a decrease in the amount of I were observed in the interfacial region.

References

1. J. Peng, *et al*, Science, **371**, 390 (2021).
2. M. A. Green, et al, Prog. Photovolt Res Appl., **31**, 3, (2023).
3. M. Jost, et al, ACS Energy Lett., **7**, 1298 (2022).
4. A. Hultqvist, *et al*, Appl. Energy Mater., **4**, 510, (2021)

* *Corresponding author e-mail:* tobias.torndahl@anstrom.uu.se

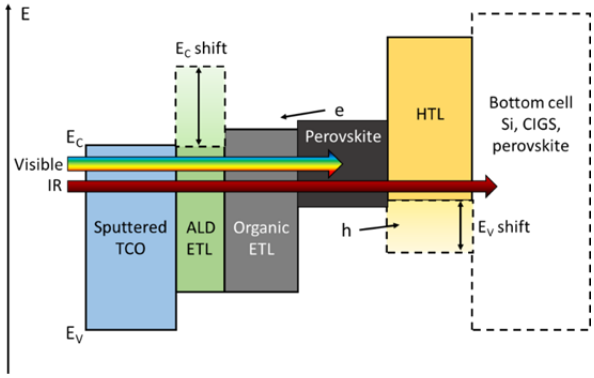

Figure 1: Energy band diagram of the metal halide perovskite top cell in a two terminal tandem device structure. Coloured arrows show the direction from which light enters the respective cells, whereas black arrows indicate the conduction paths for the photo excited electrons and holes.

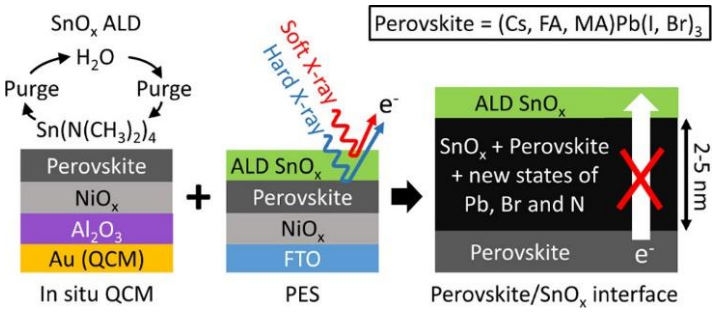

Figure 2: (Left) Set-up with a partial solar cell structure deposited on a QCM monitor crystal, (Middle) solar cell structure for photoelectron spectroscopy (PES) analysis of a buried interface, and (Right) model showing the resulting perovskite/SnO_x interface and its impact on solar cell performance.

Gas-phase reactions of $Zr(tmhd)_4$: New insights from microreactor studies using synchrotron radiation

S. Grimm[a*], P. Hemberger[b], B. Atakan[a],

[a] *Thermodynamics and CENIDE, University of Duisburg-Essen, Lotharstraße 1, Duisburg, 47057, Germany*
[b] *Paul Scherrer Institute (PSI), Forschungsstrasse 111, Villigen, 5232, Switzerland*

Metal-β-diketonate complexes are widely used as precursors for chemical vapor deposition for various applications. [1] This is mainly because of their superior physical and chemical properties such as the volatility and inertness, which can be customized by changing the β-diketonate group attached to the respective metal centre. [2]
In deposition processes, often gas-phase reactions are the initial steps, but gaseous intermediates can lead to unwanted film morphology and unsatisfactory purity or a depletion of the precursor, and consequently a reduction in growth rate. Understanding the decomposition mechanism, especially the sequence of bond dissociation steps, is important for improving and modelling such processes.
Consequently, the analysis of the initial stages of growth is important and requires analytical techniques with sufficiently low detection limits for elusive gas-phase species. Because of limitations in experimental techniques, it was until recently not possible to detect most of the postulated intermediate species; their temperature-dependent kinetics often remained unknown.[3]
We have overcome some of these challenges and demonstrated for various metal-organic precursors, that by using a microreactor coupled to a very mild ionization source we are capable to detect and characterize elusive species, especially metal-containing intermediates with short lifetimes below 50 µs. [4-6]
Building up on previous work on acetylacetonate complexes, we present insights into the reactions of a 2,2,6,6-tetramethyl-3,5-heptanedionate (tmhd) compound. The vacuum pyrolysis of zirconium 2,2,6,6-tetramethyl-3,5-heptanedionate ($Zr(tmhd)_4$) with and without oxygen is investigated here.
In brief, the precursor is sublimated, subsequently transported by helium as carrier gas, and expanded through a pinhole into a resistively heated 1 mm inner diameter SiC-microreactor of 10 mm length (see Fig.1). Species leaving the reactor are ionized by tuneable vacuum ultraviolet (VUV) synchrotron radiation and characterized by imaging photoelectron photoion coincidence spectroscopy (i^2PEPICO) and mass spectrometry at the Swiss Light Source. We recorded photoionization efficiency curves (PIE) and threshold photoelectron spectra (TPES) at photon energies of 6.3-11.5 eV, which give us direct evidence for the characterization of reactive intermediates and products.
In the experiments, hydrocarbons, oxygenated and metal-containing species were detected and characterized unambiguously in the gas-phase at temperatures from 450-950 K, which provides insights in the underlying decomposition mechanisms. Most importantly, we detected and characterized $Zr(C_{11}H_{19}O_2)(C_{11}H_{15}O_2)$ as major initial decomposition product in the gas-phase at temperatures above 650 K. Additionally, several hydrocarbons and oxygenated species were detected and unambiguously assigned as decomposition species for the first time, i.e. *m/z* 166 $C_{10}H_{14}O_2$, *m/z* 100 pinacolone ($C_6H_{12}O$), three isomers on *m/z* 57 (C_4H_9), the tert-butyl radical, 1-butyl and i-butyl (see Fig. 2). Their detection gives hints on the remaining Zr-residues formed in the gas-phase or on the surface. The temperature-dependent formation mechanisms of the assigned species will be discussed and compared to previous results on $Zr(acac)_4$.

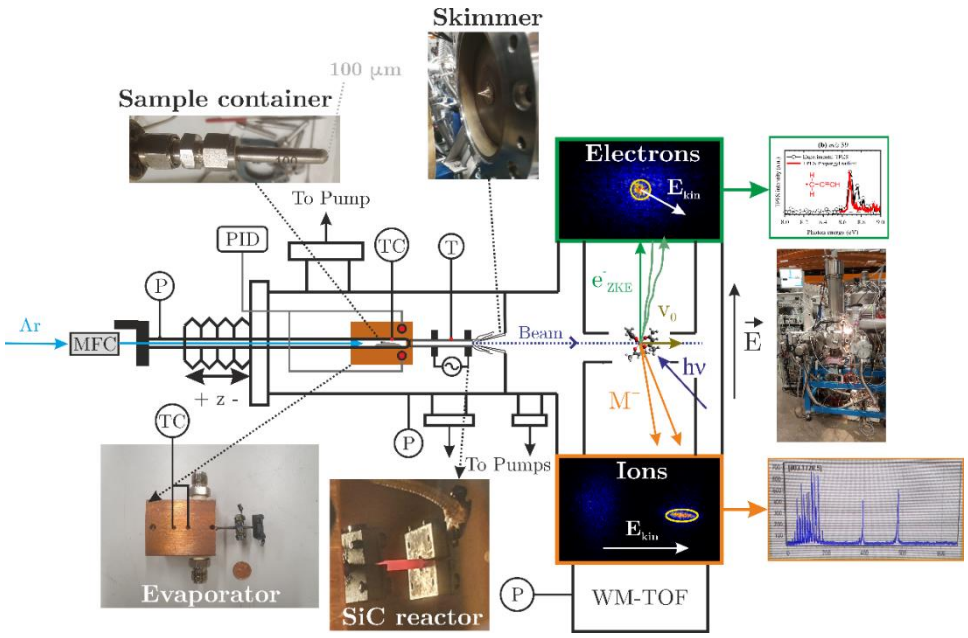

Figure 2: Vacuum apparatus of CRF-PEPICO endstation at the X04DB VUV beamline at the SLS synchrotron facility with embedded images of the most important parts of the pyrolysis reactor setup. The schematic in the background is taken from a recent publication [4].

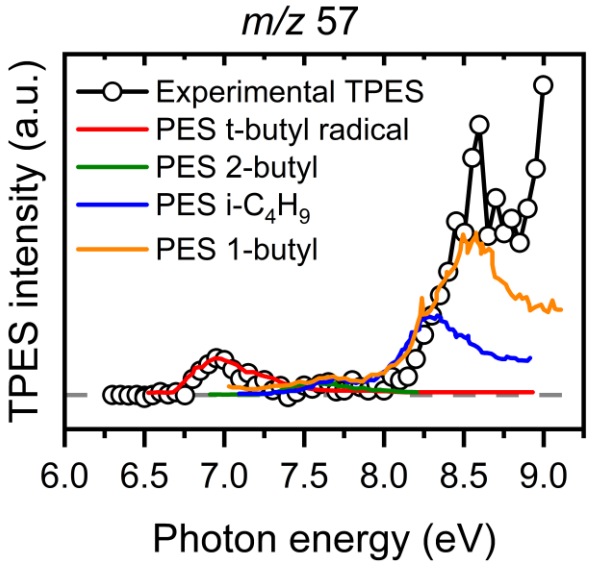

Figure 1: Exemplary mass-selected threshold photoelectron spectrum (ms-TPES) of *m/z* 57 recorded at 796 K. The literature photoelectron spectra (PES) are as follows: t-butyl [7], 2-butyl [8], i-C_4H_9 [8], 1-butyl [8].

References

1. A.L. Pellegrino, G. Lucchini, A. Speghini and G. Malandrino, *J. Mater. Res.*, 2020, **35**(21), 2950.
2. G.G. Condorelli, G. Malandrino and I.L. Fragalà, *Coord. Chem. Rev.*, 2007, **251**(13-14), 1931.
3. Y. Jiang, M. Liu, Y. Wang, H. Song, J. Gao and G. Meng, *J Phys. Chem. A*, 2006, **110**(50), 13479.
4. S. Grimm, S.-J. Baik, P. Hemberger, A. Bodi, A.M. Kempf, T. Kasper and B. Atakan, *Phys. Chem. Chem. Phys.*, 2021, **23**(28), 15059.
5. S. Grimm, S.-J. Baik, P. Hemberger, T. Kasper, A.M. Kempf and B. Atakan, *J. Mat. Res.*, 2022, **37**(9), 1558.
6. S. Grimm, P. Hemberger, T. Kasper and B. Atakan, *Adv Materials Inter*, 2022, **9**(22), 2200192.
7 F. A. Houle and J. L. Beauchamp, *J. Am. Chem. Soc.,* 1979, **101**, 4067.
8 J. C. Schultz, F. A. Houle, and J. L. Beauchamp, *J. Am. Chem. Soc.,* 1984, **106**, 3917.

* *Corresponding author e-mail:* sebastian.grimm@uni-due.de

Al_2O_3 growth in PMMA thin films by sequential infiltration synthesis: in-situ thickness evolution and mass uptake investigation

Michele Perego[a,*], Gabriele Seguini[a], Claudia Wiemer[a], Federica E. Caligiore[a], Elena Cianci[a]

[a] *CNR-IMM, Unit of Agrate Brianza, Via C. Olivetti 2, I-20864 Agrate Brianza, Italy*

Sequential infiltration synthesis (SIS), also referred to as vapor phase infiltration (VPI), is a quite simple approach to grow inorganic materials into polymeric films through the penetration of gaseous precursors into the polymer matrix [1]. In particular SIS has been proposed as a powerful tool to create an organic-inorganic hybrid material or to fabricate inorganic nanostructures by infiltration in patterned polymer templates like, for instance, in self-assembled block copolymer thin films.[2,3] Depending on the specific morphology of the block copolymer template, different inorganic nanostructures can be obtained, providing a simple and cost effective tool to generate periodic inorganic nanostructures over large areas [3]. However, several fundamental aspects of the SIS process are still not fully understood [4,5]. In this work, *in-situ* and *ex-situ* spectroscopic ellipsometry (SE) analysis and *ex-situ* X-ray reflectrometry (XRR) are used to offer a complete and comprehensive picture of polymer film evolution and Al_2O_3 incorporation in poly(methyl methacrylate) (PMMA) thin films as a function of the number of SIS cycles. In particular, the SIS process is performed in a standard ALD reactor operating at 90°C in quasi-static mode, using trimethylaluminum (TMA) and water (H_2O) as precursor and co-precursor, respectively. *In-situ* dynamic (SE) is used for real time monitoring of the SIS process. Time resolution of SE system guarantees acquisition of information about intra-cycle sample evolution as demonstrated by Cianci *et al.* in a previous work.[6] In addition, SE analysis offers the possibility of *in situ* monitoring the thickness (H) and refractive index (n) evolution during the whole SIS process (figure 1). Accordingly, two different growth regimes can be clearly distinguished. Initially, Al_2O_3 incorporation determines a marked swelling of the polymer film upon each SIS cycle (figure 1a). Subsequently, no significant variation of the polymer film thickness is observed, despite Al_2O_3 mass uptake at each SIS cycle is clearly highlighted by the gradual increase of *n* values (figure 1b). According to the *in-situ* SE data, after few SIS cycles, Al_2O_3 incorporation into the volume of the polymer film results in the formation of a rigid inorganic-organic structure. Precursor penetration determines further incorporation of Al_2O_3 within the volume of this hybrid material during subsequent SIS cycles, without any significant swelling of the film. This interpretation is well supported by *ex-situ* SE and XRR analyses of the infiltrated polymer films and of the residual Al_2O_3 films left over the substrate upon removal of the organic matrix. The thickness values of the residual Al_2O_3 film upon O_2 plasma are measured by SE and XRR (Figure 2a). The data clearly highlight a linear increase of the film thickness cycle after cycle, confirming that the incorporation of Al_2O_3 continues even when no swelling of the polymer film is detected during *in situ* SE analysis. the values of electronic density as a function of the number of SIS cycles for each sample are obtained by analysis of the XRR data (Figure 2b). The electronic density increases over the first 3 cycles achieving a saturation value of 0.7 e/Å. This value is significantly lower than the one obtained in the case of samples grown by a standard ALD process at 90°C. An additional thermal treatment in N_2 atmosphere at 900°C for 600 s determines a significant shrinking of the Al_2O_3 films (Figure 2a). According to the linear fitting (dashed line) of the experimental data, the growth per cycle is determined to be 0.62 nm ± 0.09 nm/cycle. The growth per cycle value obtained by this analysis is significantly higher than the one obtained by standard ALD at 90°C, confirming that Al_2O_3 growth takes places within the volume of the PMMA film. In conclusion, monitoring in real-time the thickness of the polymer film by *in-situ* SE allows to fully characterize the evolution of the system during the SIS process, providing information to better tailor the process parameters.

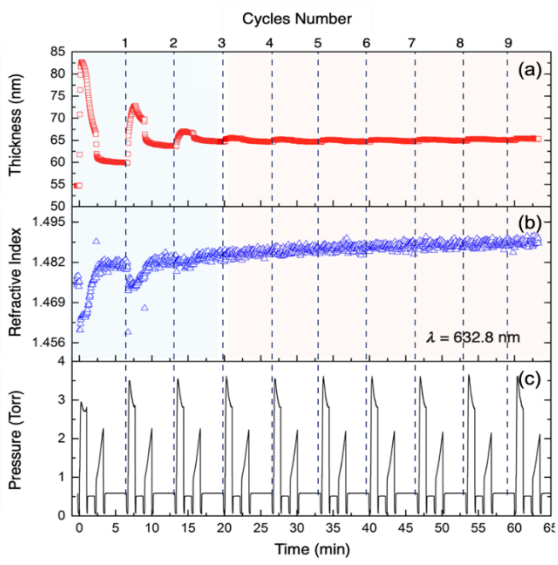

Figure 1. *(a) Thickness and (b) refractive index of a 55 nm thick PMMA film during a 10 cycle SIS process performed at 90 °C using TMA and H_2O as metal and oxygen precursors, respectively. Data are reported as a function of the processing time. The values were obtained from the average of the thickness and refractive index measured by in situ spectroscopic ellipsometry data acquired in real time during the SIS process. (c) pressure in the main chamber during the SIS process.*

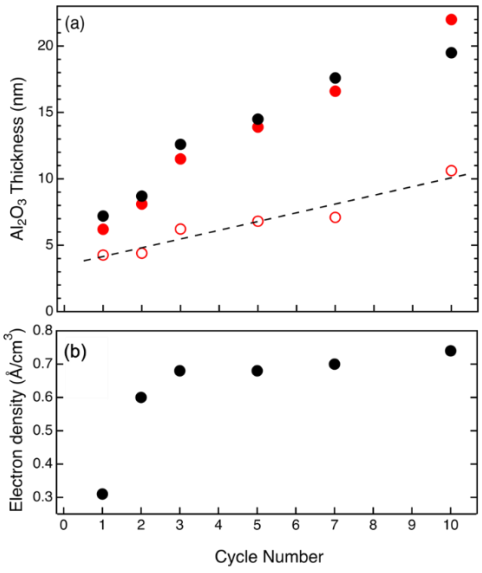

Figure 2. *(a) Thickness of the Al_2O_3 films obtained upon infiltration into 45 nm thick PMMA films and subsequent removal of the organic phase by O_2 plasma. Thickness values were obtained by SE (red closed symbols) and XRR (black closed symbols) analysis of the same samples. Thickness (red open symbols) of the same Al_2O_3 films upon annealing in N_2 atmosphere at 900°C for 600s are reported as well. (c) electron density of the Al_2O_3 films before the densification thermal treatment*

References

1. E. Barry *et al.*, J. Mater. Chem. A, 5, 2929 (2017)
2. J. Frascaroli *et al.*, ACS Appl. Mater. Interfaces 8, 33933 (2016)
3. G. Seguini *et al.,* ACS Appl. Nano Mater. 5, 9818−9828 (2022)
4. C.Z. Leng, Phys.Chem.Chem.Phys. 20, 21506 (2018)
5. F.E. Caligiore et al., Adv. Mater. Interfaces, 1900503 (2019)
6. E. Cianci *et al.*, Adv. Mater. Interfaces, 1801016 (2018)

**Corresponding author: michele.perego@cnr.it*

Tailoring microstructural features of industrial CVD Ti(C,N) thin hard coating.

Idriss El Azhari [a,b*], José García [c], Nathalie Valle [d], Jenifer Barrirero [a], Christoph Pauly [a], Michael Engstler [a], Flavio Soldera [a], Luis Llanes [b], Frank Mücklich [a]

[a] Chair of Functional Materials, Department of Materials Science, Saarland University, Campus D 3.3, D-66123 Saarbrücken, Germany

[b] CIEFMA - Department of Materials Science and Engineering, EEBE – Campus Diagonal Besòs, Universitat Politècnica de Catalunya - BarcelonaTech, 08019 Barcelona, Spain

[c] AB Sandvik Coromant R&D, Lerkrogsvägen 19, SE-126 80 Stockholm, Sweden

[d] Materials Research and Technology Department, Luxembourg Institute of Science and Technology, 41 rue du Brill, 4422 Belvaux, Luxembourg

*Corresponding author: idriss.elazhari@uni-saarland.de

Abstract

During the last two decades, Ti(C,N) is one of the most used thin hard coating in metal cutting industry. In previous works of the authors, a multi-scale testing and characterization campaign was carried out in which industrial cutting inserts coated with Ti(C,N) is contrasted to Zr(C,N) wear resistant hard coating. The objective was to shed light on the microstructural features that influence their mechanical behavior for cutting applications. It was revealed that the more compatible coefficient of thermal expansion of Zr(C,N) with the substrate, the better cohesive strength at the grain boundaries and the plastic deformation were found to assign to the Zr(C,N) coated hardmetal better structural integrity and fracture toughness in comparison to Ti(C,N) [1,2]. In the present work, unexplored other microstructural characteristics related to the grain boundary complexions and crystal shapes of Ti(C,N) are investigated. State of the art characterization techniques were used such as high-resolution secondary ion mass spectrometry imaging (nano-SIMS) and atom probe tomography (APT) to investigate compositional variations and segregations with increasing deposition temperature (885°C and 930°C) using a moderate temperature CVD process (MT-CVD). It is shown that segregation of chlorine at the grain boundaries is affecting not

only the grain size of the columnar crystals, but texture and crystal shapes are indeed affected and modified as the chlorine concentration is decreasing. Approaches to tailor the microstructure of these compounds are discussed and suggested.

Bilbliography

[1] I. El Azhari, J. Barrirero, J. García, F. Soldera, L. Llanes, F. Mücklich, Atom Probe Tomography investigations on grain boundary segregation in polycrystalline Ti(C,N) and Zr(C,N) CVD coatings, Scripta Materialia. 162 (2019) 335–340. https://doi.org/10.1016/j.scriptamat.2018.11.041.

[2] I. El Azhari, J. Barrirero, N. Valle, J. García, L. von Fieandt, M. Engstler, F. Soldera, L. Llanes, F. Mücklich, Impact of temperature on chlorine contamination and segregation for Ti(C,N) CVD thin hard coating studied by nano-SIMS and atom probe tomography, Scripta Materialia. 208 (2022) 114321. https://doi.org/10.1016/j.scriptamat.2021.114321.

Functional materials II

Chair: Blanquet, Elisabeth (CNRS)

Time: 5/30/2023 10:30:00 AM
Location: Auditorium 2, Maria-Theresiacollege, St. Michael's Street 6, Leuven

Towards fabrication of 1D BN/Carbon Van der Waals heterostructures by atomic layer deposition

Ali Hossain[a,b], Hanako Okuno[b], Catherine Journet[a], Catherine Marichy[a,*]

[a] *LMI, UMR CNRS 5615, Univ Lyon, Université Claude Bernard Lyon 1, F-69622 Villeurbanne, France*
[b] *IRIG/MEM/LEMMA, CEA-Grenoble, 17 Avenue des Martyrs, 38054 Grenoble Cedex 09 France*

In line with the spectacular improvement and emergence of new physical properties in two-dimensional (2D) van der Waals (VdW) heterostructures, the curvature and confinement effects provided by the reduced dimensionality of 1D VdW heterostructures make them highly attractive. Fabricating these high quality heterostructures requires a synthesis approach capable of controlling the epitaxial deposition at the atomic scale. Based on self-limiting gas-surface reactions, Atomic Layer Deposition (ALD) has proven to be ideally suited for the fabrication of functional hetero-nanostructures, such as carbon nanotube (CNT)-based materials [1]. We have previously reported the use of a two-step ALD process of hexagonal BN (hBN) for the elaboration of hBN/CNT heterostructures [2]. Briefly, multi-wall CNTs were successfully coated with a controlled layer of polyborazine within the first ALD step and then annealed at high temperatures to convert the polyborazine into crystalline hBN [3].

Herein, the fabrication and advanced characterization of 1D VdW heterostructures made of single-wall CNTs coated with hBN will be discussed. It is worth mentioning that no functionalization of the starting material is performed before ALD. Particular attention will be paid to the influence of the starting single-wall CNTs, especially the effect of their curvature, crystallinity and bundle packing on the hBN layer in terms of quality and coverage. For instance, advanced analytical transmission electron microscopy and Electron Energy Loss Spectroscopy (EELS) allow us to observe a complete and homogeneous coverage of the bundles around their circumference. However, when CNTs are detached from the bundle after ALD, they are not homogeneously covered, which suggests that the precursors do not diffuse to the individual CNTs within the bundle (Figure 1). Furthermore, features of the EELS spectra permit to highlight the high-quality of the BN layer.

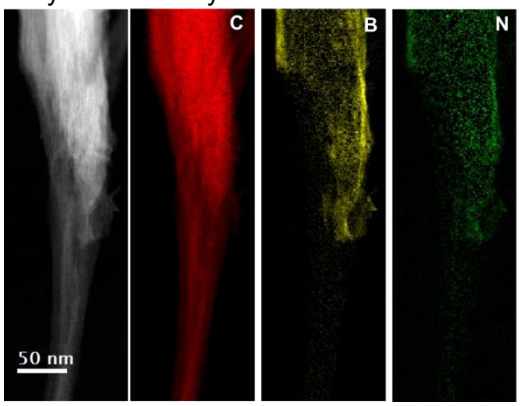

Figure 1. Scanning TEM images of torn bundle of BN coated single-wall CNTs and its corresponding C (red), B (yellow) and N (green) elemental EELS mapping.

References

1. Marichy C. et al., Coordination Chemistry Reviews **257**, 3232-3253 (2013).
2. Hao W. et al., ChemNanoMat **3**, 656–63 (2017).
3. Matsoso B. et al., Journal of Physics: Materials **3**, 034002 (2020).

* *Corresponding author e-mail:* catherine.marichy@univ-lyon1.fr

ALD of Unique Magnetic Thin Films

Topias Jussila[a,*], Anish Philip[a], Maarit Karppinen[a]

[a] *Department of Chemistry and Materials Science, Aalto University, Kemistintie 1, Espoo, FI-00076 Aalto, Finland*

Magnetic and multiferroic thin films are vital for next-generation electronic and spintronic devices. For instance, room-temperature multiferroic materials could enable high-density magnetic memory devices where data would be written electrically and read magnetically. However, the state-of-the-art magnetic and multiferroic materials typically have complex chemical composition including critical elements and their (room-temperature) functional properties do not meet the requirements of the next-generation applications. Fortunately, there is one highly promising multiferroic material, namely, ε-Fe_2O_3, which has a unique set of material properties; it is an ultra-hard room-temperature ferromagnet, ferroelectric, and it exhibits magnetoelectric coupling and zero-field ferromagnetic resonance.[1] Moreover, this simple iron oxide is composed of Earth-abundant, low cost, and biocompatible elements. The only drawback is the metastability of the ε-Fe_2O_3 polymorph; it is easily transformed to the more stable α-Fe_2O_3 (hematite) and γ-Fe_2O_3 (maghemite) phases. Therefore, the synthesis of phase-pure ε-Fe_2O_3 has been notoriously challenging which has hindered its potential for practical applications. Excitingly, the atomic layer deposition (ALD) technique has turned out to be superiorly suited for the deposition of in-situ crystalline and amazingly stable ε-Fe_2O_3 thin films from simple precursors ($FeCl_3$ and H_2O) in the temperature range of 260 – 300 °C.[2]

Here we first of all demonstrate the excellent quality of the ALD-grown ε-Fe_2O_3 thin films, using a variety of characterization techniques. ^{57}Fe Mössbauer spectroscopy measurements, realized by piling multiple ε-Fe_2O_3 films deposited on gamma-ray-transparent polyimide substrate to achieve sufficient signal, show that the hematite impurity level in the films was only ~2% (Fig. 1a).[3] This is most important not to affect the magnetic properties of the film. The room-temperature magnetic coercivity of our ALD-grown ε-Fe_2O_3 films is appreciably high, 2 kOe, which is in the range required for magnetic data storage devices. Moreover, through our simple ALD process, the ε-Fe_2O_3 films can be deposited on 3D substrates which creates new possibilities in terms of nanostructuring and modifying the fine magnetic properties through dimensional effects. The deposition process is also independent of the substrate material used (Si, glass, polymer). Furthermore, the magnetic properties of ε-Fe_2O_3 can be modified through metal substitution by utilising other metal halide precursors such as $AlCl_3$.

Optical switching of magnetic devices is a topic of high interest, as it could enable ultra-fast and high-efficiency control over magnetic state of individual magnetic grains through light irradiation. Typically, this has been pursued through molecular metalorganic magnets with intrinsic magnetic properties significantly inferior to inorganic magnetic materials. Combination of molecular layer deposition (MLD) and ALD provides an extremely exciting alternative approach to optical switching. We have demonstrated the deposition of ε-Fe_2O_3:azobenzene superlattice thin films using azobenzene-4,4'-dicarboxylic acid as the organic precursor.[4] The ALD/MLD-grown ε-Fe_2O_3:azobenzene thin films are highly crystalline (ε-Fe_2O_3 phase; Fig. 1b) and stable in ambient conditions and, importantly, the hard ferromagnetism is not lost upon inserting the organic monolayers in the inorganic matrix. Amazingly, in consequence of the reversible trans-cis photoisomerization of azobenzene, the magnetic properties of the ε-Fe_2O_3:azobenzene films can be reversibly controlled through UV/Vis irradiation (Fig. 1c). Thus, the ALD/MLD-grown inorganic-organic superlattices offer a prospective solution to achieve simultaneously both optical switching and the excellent magnetic properties of ε-Fe_2O_3-based thin films.

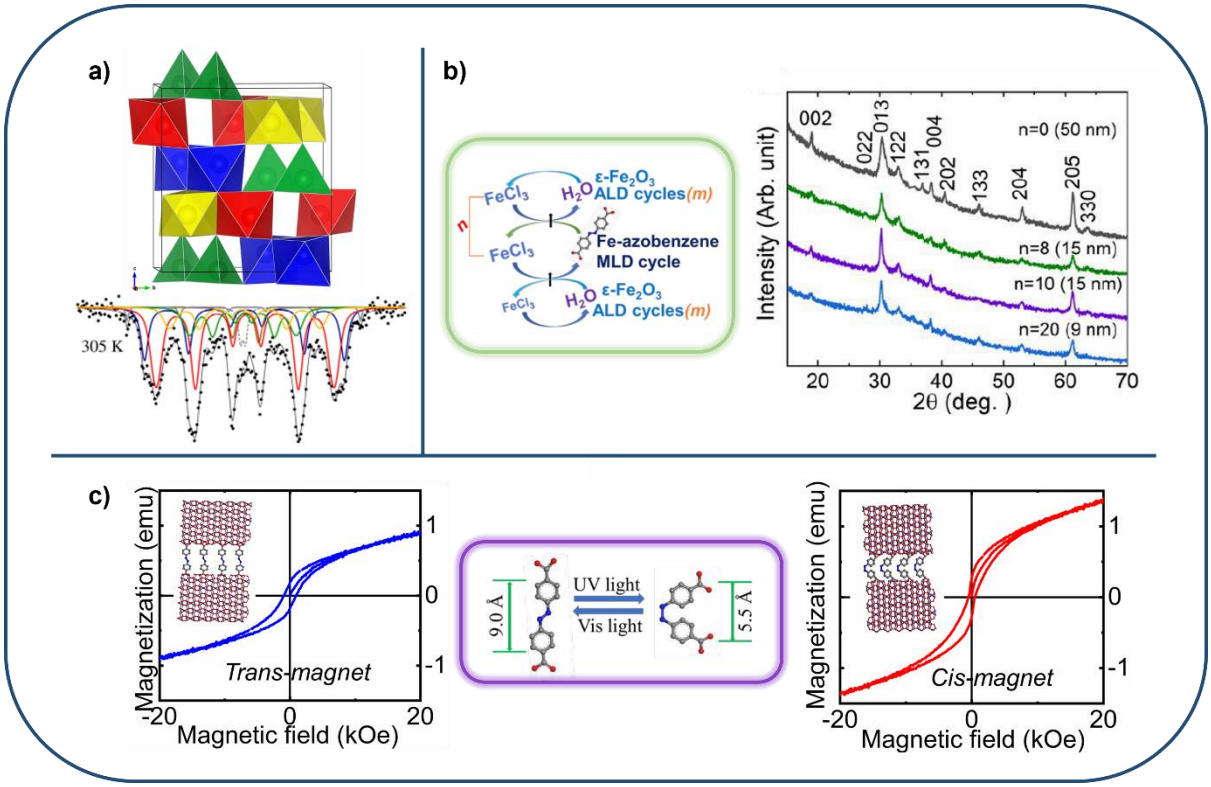

Figure 1. a) Polyhedral representation and Mössbauer spectrum of ε-Fe_2O_3. Blue, green, red, and yellow colours of the spectral lines correspond to the different Fe sites of the ε-Fe_2O_3 crystal structure. The weak grey line corresponds to the small hematite impurity. **b)** Illustration of ALD/MLD supercycle sequence and GIXRD patterns of the ε-Fe_2O_3:azobenzene superlattices (n refers to the number of supercycles, and thus, number of organic monolayers; m refers to the number of ε-Fe_2O_3 ALD cycles within each supercycle, which determines the thickness of each individual ε-Fe_2O_3 block in the superlattice structure (written in brackets for each GIXRD pattern)). **c)** Effect of UV/Vis exposure on magnetic properties; both magnetic coercivity and remanent magnetization are increased by UV exposure and decreased back to the original state by visible light irradiation.

References

1. J. Tuček, R. Zbořil, A. Namai, and S.-i. Ohkoshi, Chem. Mater. **22**, 6483 (2010).
2. A. Tanskanen, O. Mustonen, and M. Karppinen, APL Mater. **5**, 056104 (2017).
3. T. Jussila, A. Philip, J. Lindén, and M. Karppinen, Adv. Eng. Mater., 2201262 (2022).
4. A. Philip, Y. Zhou, G. C. Tewari, S. van Dijken, and M. Karppinen, J. Mater. Chem. C **10**, 294 (2022).

* *Corresponding author e-mail: topias.jussila@aalto.fi*

CVD processing of high quality ferromagnetic CoS_2 layers

Jean-Pierre Glauber*[a], Jan-Lucas Wree[a], David Zanders, Andreas Ney[b], Anjana Devi[a]

[a] *Inorganic Materials Chemistry, Ruhr University Bochum, Bochum, 44801, Germany*
[b] *Institute of Semiconductor and Solid State Physics, Johannes Kepler University, Linz, 4040, Austria*

Cobalt disulfide (CoS_2) is known for its intrinsic magnetic properties and was recently identified as a Weyl-semimetal, which makes it an appealing material for advanced spintronic devices with potential applications for the development of spin to charge conversions.[1] This application requires high-quality, phase pure CoS_2, which is challenging to realize due to the numerous stable cobalt sulfide phases that can co-exist, namely CoS_2, Co_2S_3, Co_3S_4, $Co_{1-x}S$, CoS, Co_9S_8 and Co_4S_3.

Although chemical vapor deposition (CVD) is capable of fabricating large area, highly quality and conformal films, the phase control with this method is demanding and is strongly dependent on deposition temperature and precursor choice. To date, there has been only one report on an aerosol assisted CVD process that yielded phase pure CoS_2.[2]

This motivated us to develop a new MOCVD processing route for phase pure CoS_2. The precursors that have priorly been used for cobalt sulfides are sulfur coordinated with poor volatility and thus are usually employed in AACVD conditions. In our recent study, we employed an all-nitrogen-coordinated cobalt precursor, namely [Co(*g*DAS)$_2$] (**1**) (Figure 1 a)), and elemental sulfur as the co-reactant in the MOCVD process.[3]

Process optimization was carried out on Si(100) to obtain crystalline and phase pure CoS_2 and was validated by XRD, Raman spectroscopy, RBS/NRA and XPS. These measurements revealed that phase pure polycrystalline CoS_2 was deposited at temperatures between 350 °C and 400 °C. Increasing the temperature beyond 400 °C, led to formation of mixed sulfide phases (Figure 1 b)).

Superconducting quantum interference device (SQUID) measurements were performed to determine the magnetic moment and the Curie temperature (T_C), which is significantly affected by small deviations of the sulfur content. A ferromagnetic behavior below a T_C of 128 (5) K and a magnetic moment of 0.85 μ_B per Co atom were estimated, which are in accordance with literature reported values for phase pure and crystalline CoS_2. (Figure 1 c) and d)). These magnetic measurements further confirmed the formation of phase pure CoS_2 layers. The new processing CVD route to obtain large area phase pure CoS_2 is a very promising development in the field of transition metal sulfides for magnetic applications and may help to pave the way of transition metal sulfide MOCVD processing in the context of advanced spintronics.

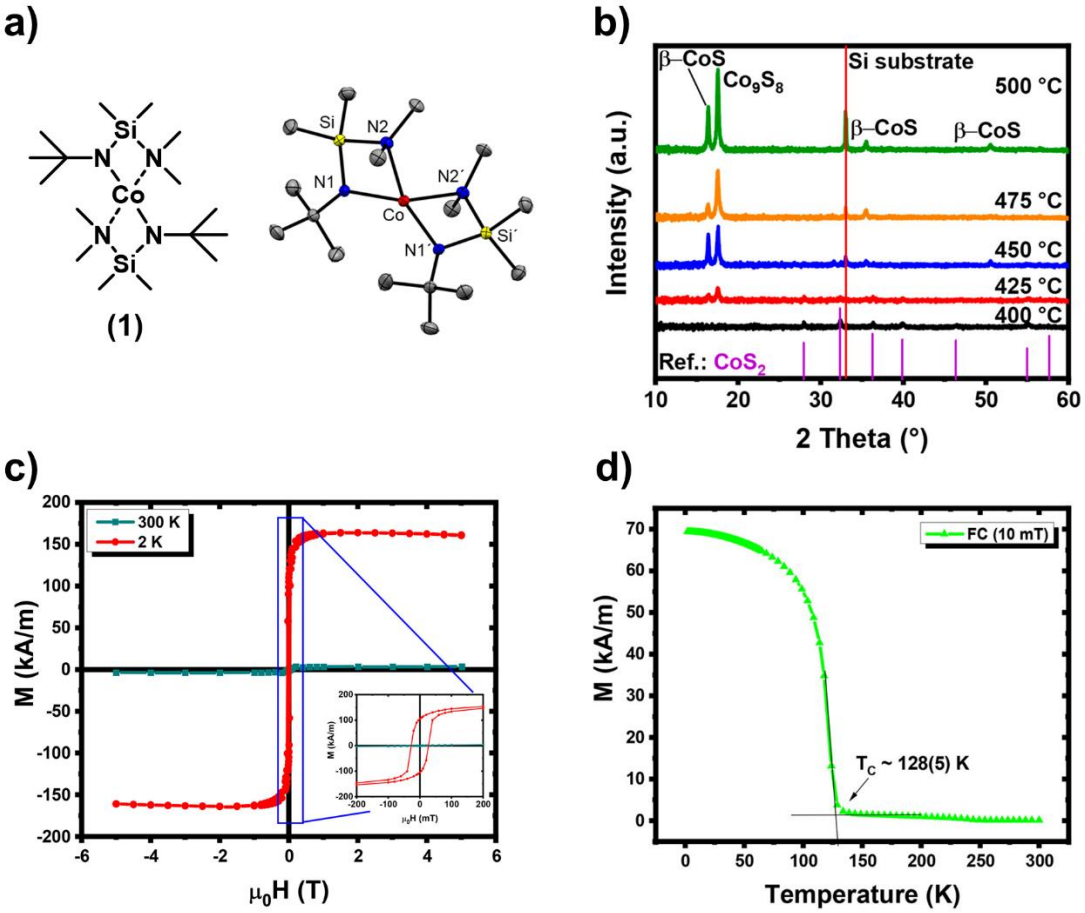

Figure 1. a) Lewis structure and solid state structure of [Co(*g*DAS)$_2$] (**1**). The H atoms are omitted for the sake of clarity. b) XRD patterns of cobalt sulfide thin films grown on Si(100) as a function of deposition temperature. Assignment of the obtained reflexes was done with reference patterns for CoS_2, β-$CoS_{1.097}$ and Co_9S_8 taken from PDF no. 00-041-14711, PDF no. 00-019-0366 and PDF no. 00-019-0364), respectively. SQUID measurements of cobalt disulfide film: c) *M(H)* hysteresis curve at 2 K and 300 K with the enlarged view between −200 mT and 200 mT in the inset. d) The graphical estimation of the Curie temperature (Tc).

References

1. Schröter, N. B. M. et al., Sci. Adv. **6**, 51 (2020)
2. Srouji, F. et al., Chem. Vap. Deposition **11**, 91 (2005)
3. J.-L. Wree, J.-P. Glauber, D. Zanders, D. Rogalla, M. Becher, M. B. E. Griffiths, A. Ostendorf, S. T. Barry, A. Ney and A, Devi, ACS Appl. Electron. Mater. **4**, 3772 (2022)

* *Corresponding author e-mail: jean-pierre.glauber@rub.de*

Single-Step PEDOT deposition by oxidative chemical vapor deposition for opto-electronic applications

Abderrahime Sekkat[a,*], Benjamin Breig[a], Diane Samelor[b], Eleni Poupaki[a], Panagiotis Doxas[b], Nicolas Causse[b], Hugues Vergnes[a], Constantin Vahlas[b], Brigitte Caussat[a,*]

[a]*LGC, Université de Toulouse, CNRS, Toulouse, France.*
[b]*CIRIMAT, Université de Toulouse, CNRS, Toulouse, France*

Conjugated polymer Poly (3,4-ethylenedioxythiophene) PEDOT represents an excellent candidate as transparent conducting material (TCM) due to its high optical transparency, high electrical conductivity, and promising mechanical flexibility[1,2]. This was demonstrated in previous works from our group, where an emerging approach, known as oxidative chemical vapor deposition (oCVD), was used to develop stable PEDOT thin films through gas phase injection of 3,4-ethylene dioxythiophene (EDOT) as monomer and oxidants (i.e. $FeCl_3$ or $SbCl_5$) [3-5]. It is a dry, one-step technique that allows for the precise deposition of high-quality PEDOT films at low temperature (20-200°C) and under reduced pressure (50-70 Pa), allowing conformal coatings on complex substrates and effective device integration while avoiding solvent-substrate issues[5,6]. A thorough correlation between deposition conditions and film structure, using the cheapest and least toxic molecules $SbCl_5$, has revealed a panel of promising properties including a high optical transmittance (>90% at 550 nm) and quite smooth surfaces (RMS ranging from 4 nm to 8 nm) [3]. Further, these works highlight the importance of the reaction chamber design, precursor delivery system and deposition conditions on the properties of the resulting layers[3,4].

Herein, we have developed a tubular hot wall oCVD reactor, using EDOT as monomer and $SbCl_5$ as oxidant (**Figure 1a**). Seven glass (B, D, E, and F) and silicon (A, C, and G) substrates are placed all along the reactor length (**Figure 1b**). Further, we have extensively investigated the influence of some key deposition conditions (substrate temperature and coating time) on the deposit morphology, structure, chemical composition, and deposition rate and on their optical transparency and electrical conductivity. Among the numerous results obtained, it can be emphasized that deposition rates are uniform along the reactor length for specific temperatures. The electrical conductivity is spatially uniform for all the temperatures tested. These findings correlate with an in-depth analysis of the film structure and composition, in particular with XRD results demonstrating a strong face-on orientation of the films, corresponding to the quinoid conductive form of PEDOT. FTIR spectra confirm the presence of a quinoid structure related the C=C asymmetric stretching vibration at ~ 1520 cm^{-1} and a successful polymerization of intact EDOT monomer units. This paves the way for improving the intrinsic properties of PEDOT thin films allowing efficient integration into next-generation solar cells and OLED devices.

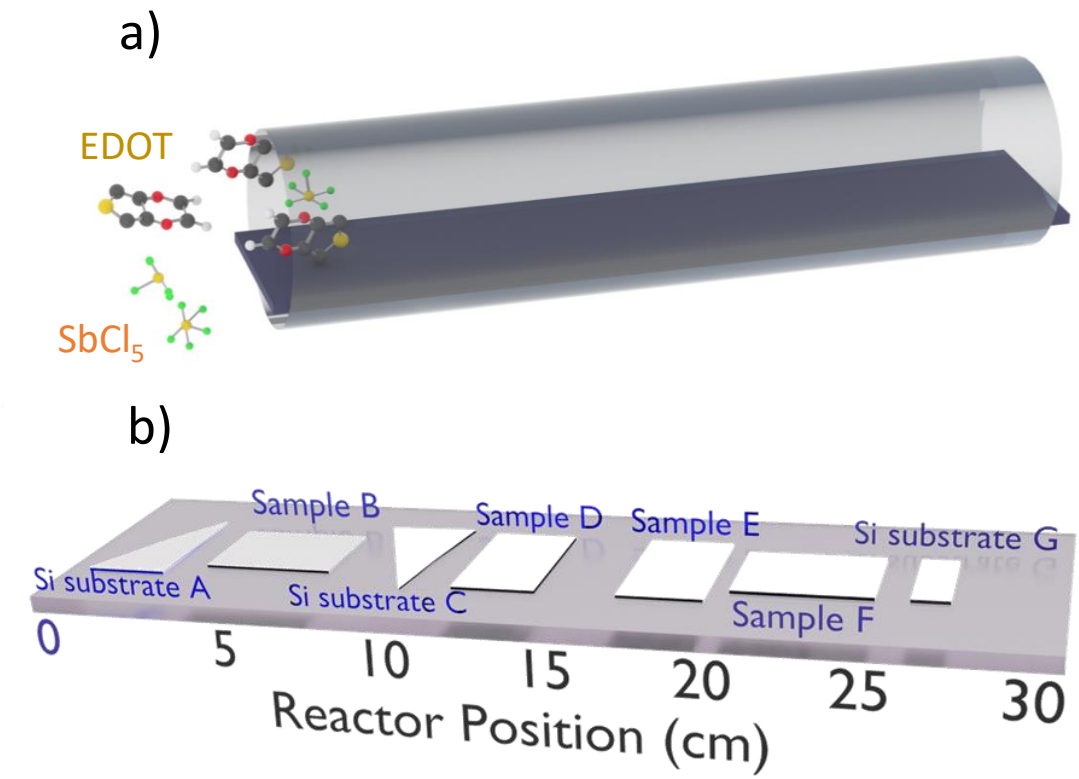

Figure 1. a). Schematic of the oCVD system used for the deposition of PEDOT thin films with EDOT and $SbCl_5$ inside the hot wall reactor, and **b).** Schematic view of the 30 cm platen on which seven samples are placed, samples A, C and G being silicon substrates and samples B, D, E and F being borosilicate glass substrates.

References

1. Krieg, L. *et al.* Toward three-dimensional hybrid inorganic/organic optoelectronics based on GaN/oCVD-PEDOT structures. *Nat. Commun.* **11**, (2020).
2. Gueye, M. N., Carella, A., Faure-Vincent, J., Demadrille, R. & Simonato, J. P. Progress in understanding structure and transport properties of PEDOT-based materials: A critical review. *Prog. Mater. Sci.* **108**, 100616 (2020).
3. Mirabedin, M., Vergnes, H., Caussé, N., Vahlas, C. & Caussat, B. Liquid antimony pentachloride as oxidant for robust oxidative chemical vapor deposition of poly(3,4-ethylenedioxythiophene) films. *Appl. Surf. Sci.* **554**, (2021).
4. Mirabedin, M., Vergnes, H., Caussé, N., Vahlas, C. & Caussat, B. An out of the box vision over oxidative chemical vapor deposition of PEDOT involving sublimed iron trichloride. *Synth. Met.* **266**, (2020).
5. Caussat, B. *et al.* Diode Electroluminescente Organique Comprenant une Couche d'Anode de PEDOT. Patent under review (2022).
6. Heydari Gharahcheshmeh, M., Robinson, M. T., Gleason, E. F. & Gleason, K. K. Optimizing the Optoelectronic Properties of Face-On Oriented Poly(3,4-Ethylenedioxythiophene) via Water-Assisted Oxidative Chemical Vapor Deposition. *Adv. Funct. Mater.* **31**, 1–12 (2021).

* *Corresponding author e-mail:* abderrahime.sekkat@toulouse-inp.fr *and* brigitte.caussat@toulouse-inp.fr

Epitaxial $LiNbO_3$ thin film with controlled nonstoichiometry for acoustic wave devices

Ausrine Bartasyte[a,b*], Vincent Astié[c], Sondes Boujnah[a], Lilia Arapan[a], Quentin Micard[a,c], Léa La Spina[a], Pascal Boulet[d], Samuel Margueron[a], and Jean-Manuel Decams[c]

[a] *FEMTO-ST Institute, Université de Franche-Comté, ENSMM, 25030 Besançon, France*
[b] *Institut Universitaire de France*
[c] *Annealsys, 34000 Montpellier, France*
[d] *Institut Jean Lamour, Université de Lorraine, CNRS, 54011 Nancy, France*

Radio-frequency (RF) filters are widely used in the field of telecommunications (smart phones, wi-fi, Bluetooth, automotive navigation, etc.). The next generation of radiofrequency (RF) telecom applications urgently requires filters operating at frequencies above 3 GHz, particularly operating in the C-Band (4–6GHz). The conventional RF surface acoustic wave (SAW) filters are presently mainly fabricated on $LiNbO_3$ (LN) and $LiTaO_3$ (LT) single crystal substrates. The frequency of SAW devices is defined by the period of interdigitated transducers (IDTs) and by the SAW phase velocity. So far, the frequency of RF SAW filters, produced at the industrial scale, is limited to about 3.2 GHz. New low-loss materials with sufficiently high electro-mechanical coupling (K^2) and high acoustic velocities are needed to achieve SAW filters at the above-mentioned frequencies. A promising approach to satisfy this demand is to use guided acoustic waves in the piezoelectric layers. Combining composite wafers with an epitaxial piezoelectric layer and a said high velocity and acoustic quality substrate is a promising way to answer those demands. However, the fabrication of high-quality $LiNbO_3$ films with reproducible physical properties is complicated by the difficulty in controlling volatile Li_2O incorporation into the film and of measuring its composition [1]. So far, large-scale production of films with physical properties suitable for the targeted applications is not available. The deposition of alkaline niobate-based films with good piezoelectric properties is still not satisfactory due to deviations in stoichiometry and loss of volatile alkali oxides during preparation.

Direct liquid injection metalorganic chemical vapor deposition (DLI-CVD, Annealsys) technique was used to grow LN thin films on various substrates using tetramethylheptanedionate precursors, Li(thd) and $Nb(thd)_4$. In the case of SAW devices, proper propagation axis is demanded. Thus, particular effort was done to achieve growth of films with single crystallographic orientation. Epitaxial relationships and structural properties of the deposited films are investigated using X-ray diffraction (XRD) and scanning electron microscopic (SEM) techniques. Single crystalline quality films were obtained on sapphire substrates with the mosaicity comparable to that of the substrates. As lithium nonstoichiometry in $LiNbO_3$ films is critical parameter defining high acoustical performance, Li incorporation in the films was studied in details by varying deposition conditions. Li concentration in the films was estimated by means of Raman spectroscopy. Particular effort was done to achieve films with controlled Li_2O composition (Fig. 1a) and homogeneous distribution over 4 inch wafers.

Extremely high acoustic performance (quality factor, Q, up to 700, K^2 up to 8%) in SAW devices based on Z-$LiNbO_3$ thin films was achieved in the frequency range from 3.7 GHz to 5.3 GHz (Fig. 1 b) [2]. This quality of the layers makes it possible to manufacture SAW filters operating around 6 GHz using standard industrial technology.

The demands of the RF filter market are pushing for the development of new piezoelectric materials also for bulk acoustic wave (BAW) devices to meet the challenges of modern telecommunications. BAW filters withstand better high-power densities, necessary at high-frequencies, than SAW filters. BAW filter technology requires integration of $LiNbO_3$ layers with Si-based heterostructures including bottom electrode to replace devices based on standard AlN layers limited in electromechanical coupling, K^2, (= narrow bandwidth) at high frequency for high-frequency broadband or agile low-frequency filters of 5th generation (5G) telecommunications. In the literature, only layers of $LiNbO_3$ oriented along the c-axis, offering a K_2 equivalent to AlN, have been obtained by deposition methods on Si structures. Therefore, top-down methods (ion slicing or wafer bonding-polishing techniques) are considered for this purpose although the presicion control of thickness (definition of frequency) and its homogeneity remains a challenge. We have demonstrated a direct textured growth of 33°Y-LN on BAW structures using a patented buffer layer [3]. The K^2 of the longitudinal mode of 33°Y-LN is almost four times higher than that of the standard AlN layer. The HBAR resonators based on deposited 33°Y-LN films were fabricated up to frequencies of 7.5 GHz (Fig. 2).

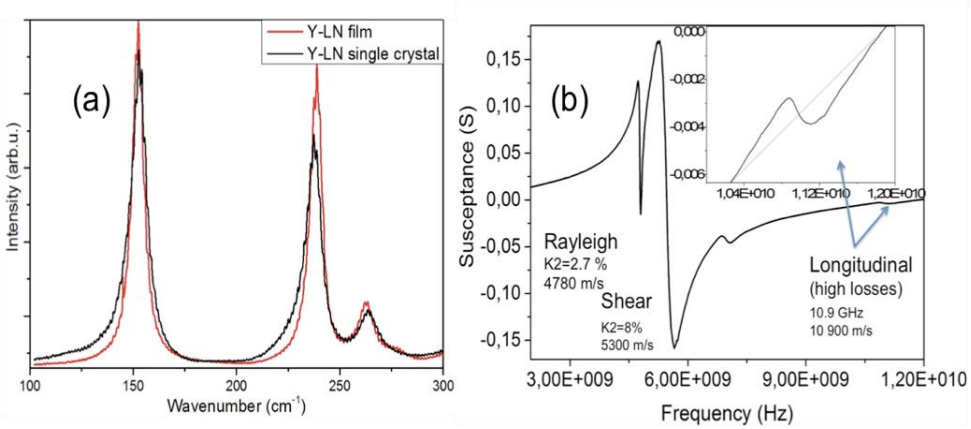

Fig.1 (a) Comparison of the Raman spectra of the LN layer with the almost stoichiometric composition and of the LN single crystal with the congruent composition. The width of the modes is dependent on the concentration of nonstoichiometry defects. (b) High-frequency acoustic response of a single-port SAW resonator based on a thin layer of Z-LN on sapphire [2].

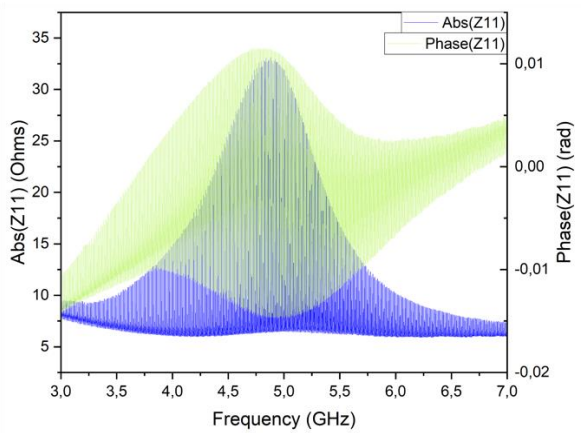

Fig. 2 HBAR resonator based on deposited 33°Y-LN films, operating at ~ 5GHz.

References

1. A. Bartasyte, S. Margueron, T. Baron, S. Oliveri, P. Boulet, Adv. Mater. Interfaces 1600998, 2017.
2. A. Almirall, S. Oliveri, W. Daniau, S. Margueron, T. Baron, P. Boulet, S. Ballandras, S. Chamaly, A. Bartasyte, Appl. Phys. Lett. 114, 162905 (2019).
3. A. Bartasyte, S. Kuprenaite, V. Astié, Layered solid element comprising a ferroelectric layer and a method for manufacturing the same, Patent EP20 305575 (2020).

* *Corresponding author e-mail:* ausrine.bartasyte@femto-st.fr

Energy-related applications and catalysis I

Chair: Hyett, Geoffrey (University of Southampton)

Time: 5/30/2023 1:30:00 PM
Location: Auditorium 1, Promotion Hall, Naamsestraat 22, Leuven

Interfacial Engineering of Batteries and Solar Energy Materials using Atomic Layer Deposition

Neil P. Dasgupta[a,b,*]

[a] *Department of Mechanical Engineering, University of Michigan, Ann Arbor, MI 48109, USA*
[b] *Department of Mechanical Engineering, University of Michigan, Ann Arbor, MI 48109, USA*

Nanomaterials offer several advantages for energy conversion and storage devices including high surface areas, short transport distances, and tunable material properties. However, the ability to precisely control the properties of surfaces and heterogeneous interfaces limits the performance of many applications. To address these challenges, in this talk, I will describe key advances in the application of Atomic Layer Deposition (ALD) for the atomically-precise modification of surfaces and interfaces.

I will demonstrate how ALD modifications can allow for rational control of interactions at heterogeneous interfaces, which can be used to tune the optical, electronic, thermal, and mass transport properties of integrated material systems. This enables exquisite control of energy, charge, and mass transfer processes across physical and chemical boundaries. I will describe examples of the ALD process for modification of electrode-electrolyte interfaces with an emphasis on advanced batteries [1-3] and solar photochemistry [4-5], and provide a perspective on the design and manufacturing of energy material systems at length scales ranging from atoms to meters.

References

1. E. Kazyak, K.-H. Chen, A. L. Davis, S. Yu, A. J. Sanchez, J. Lasso, A. R. Bielinski, T. Thompson, J. Sakamoto, D. J. Siegel, and N. P. Dasgupta, *J. Mater. Chem. A* **6**, 19425 (2018).
2. E. Kazyak, K.-H. Chen, Y. Chen, T. H. Cho, N. P. Dasgupta*, Adv. Energy Mater.* **12**, 2102618 (2022).
3. E. Kazyak, M. Shin, W. S. LePage, T. H. Cho, N. P. Dasgupta, *Chem. Commun.* **56**, 15537 (2020).
4. A. R. Bielinski, A. J. Gayle, S. Lee, N. P. Dasgupta, *ACS Appl. Mater. Interfaces* **13**, 52063 (2021).
5. A. J. Gayle , Z. J. Berquist, Y. Chen, A. J. Hill, J. Y. Hoffman, A. R. Bielinski, A. Lenert, N. P. Dasgupta, *Chem. Mater.* **33**, 5572 (2021).

[*] *Corresponding author e-mail:* ndasgupt@umich.edu

Atomic Layer Deposition of Lithium Borate and Borophosphate Thin Films for Lithium-ion Battery Applications

Tippi Verhelle[a], Arpan Dhara[a], Lowie Henderick[a], Jolien Dendooven[a] and Christophe Detavernier[a,*]

[a] *Department of Solid State Sciences, COCOON group, Ghent University, Ghent, Belgium*

Undesired side-reactions at the electrode-electrolyte interface (such as e.g. electrolyte oxidation) form a major challenge towards further performance enhancements for lithium-ion batteries (LIB's). In literature, the use of atomic layer deposition (ALD) to apply a conformal and ultra-thin protective coating (such as e.g. Al_2O_3) on the electrode surface has shown to be a promising approach to circumvent these unwanted side-reactions [1]. Metal phosphates have shown to be an interesting class of materials to this end, due to their high stability. Several metal phosphates have been deposited by ALD [2], and for crystalline Li_3PO_4 films deposited by ALD a lithium-ion conductivity of 1.4×10^{-10} S cm^{-1} with an activation energy of 0.92 eV has been reported by Put et al. [3]. This relatively poor conductivity may hamper lithium transport through a coated electrode. Although the use of a sub-nanometre thickness limits the impact of the poor ionic conductivity, it is important to note that it is never completely suppressed [4]. For that reason, we want to boost the inherent ionic conductivity of the protective coating by exploring borates and borophosphate mixtures. It has been shown, although using other deposition techniques, that the inclusion of borate species can enhance the ionic conductivity of lithium phosphate [5]. The downside of metal borates is their smaller stability window compared to that of corresponding metal phosphates. Hence, we aim to combine the good ionic conductivity property of borates and stability of phosphates, into an intermixed lithium borophosphate coating, for which the composition and thus electrochemical properties can be steered by ALD.

For lithium borates, so far only one ALD process has been reported by Kazyak et al [6]. However, they observed considerable carbon contamination and were not able to deposit pure lithium borate. In this work, an ALD process is developed for the deposition of lithium borate with approximately < 5 at.% contaminants, which is then combined with lithium phosphate for the deposition of lithium borophosphate protective LIB coatings.

By combining lithium bis(trimethylsilyl)amide (LiHMDS), H_2O and trimethylborate (TMB), linear growth with a growth of 0.04 nm/cycle is obtained at 250 °C. At this temperature, growth saturation is observed for LiHMDS, H_2O and TMB, indicating ALD like growth (Fig. 1). XPS measurements confirm the successful deposition of a lithium borate thin film, including only a small amount of contaminants, e.g. C (~2 at.%), Si (~1 at.%) and N (~1 at.%) originating from the precursor. By measuring the resistance using through-plane impedance spectroscopy measurements, the conductivity of a lithium borate thin film of 81 nm deposited at 250 °C is calculated to be $1.60 \pm 0.03 \times 10^{-7}$ S cm^{-1} at 30 °C, with an activation energy of 0.58 ± 0.01 eV. Initial results indicate that the borate/phosphate ratio affects the stability of the film (Fig. 2). To obtain an idea of the stability of the film, cyclic voltammetry was used. At higher voltages, electrolyte oxidation and thus unwanted side-reactions will occur. By depositing a lithium borophosphate coating on top of the electrode, we want to prevent this electrolyte oxidation as long as possible, meaning we should be able to cycle the thin films to an as high as possible voltage. As seen from figure 2, the stability of the coating decreases as the amount of lithium borate cycles increase. These promising results therefore indicate that finding the optimal coating will be a trade-off between the conductivity and the stability and will depend on the intended application.

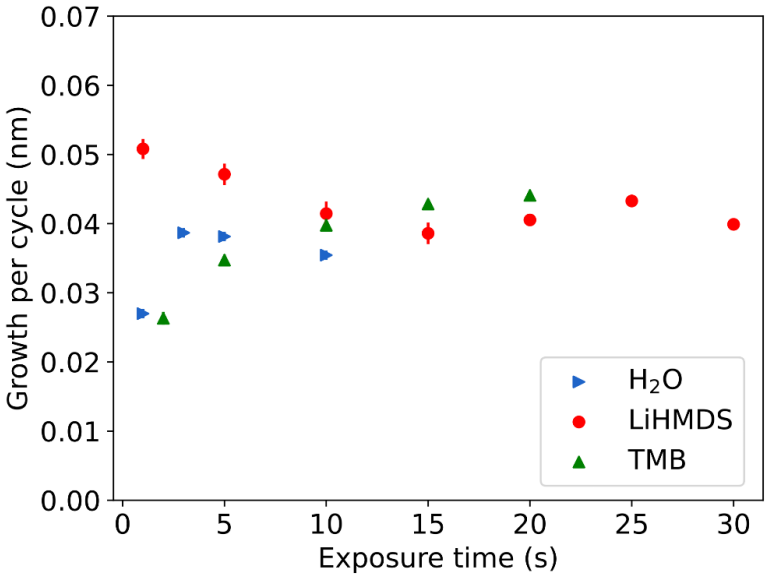

Figure 1: Saturation behavior of LiHMDS, H_2O and TMB during the deposition of lithium borate at 250°C

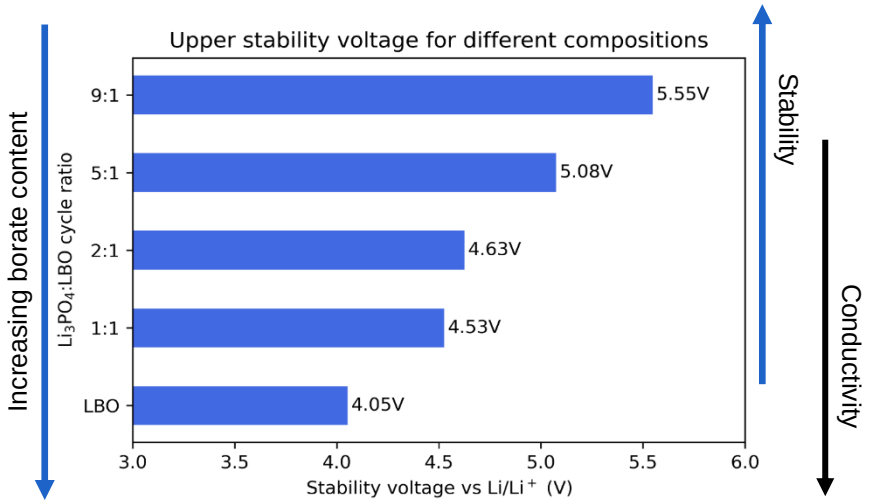

Figure 2: Upper stability voltage for lithium borate (LBO) and different borophosphate compositions (x:y). x:y represents the Li_3PO_4 to lithium borate ALD cycles ratio, e.g. 9:1, meaning 9 LiHMDS and TMP ALD cycles to 1 LiHMDS, H_2O and TMB ALD cycle.

References

1. Jung, Y. S., J. Electrochem. Soc. **157**, A75 (2009).
2. Henderick, L., Appl. Phys. Rev. **9**, 011310 (2022).
3. Put, B., J. Electrochem. Soc. **166**, A1239 (2019).
4. Mattelaer, F., Adv. Mater. Interfaces **4**, 1601237 (2017).
5. Magistris, A., J. Power Sources **14**, 87 (1985).
6. Kazyak, E., J. Mater. Chem. A **6**, 19425 (2018).

* *Corresponding author e-mail:* christophe.detavernier@ugent.be

.

Spatial ALD on porous substrates for energy applications

Corné Frijters, Paul Poodt*

SparkNano B.V., Esp 266, 6533AC Eindhoven, the Netherlands

One of the greatest challenges for the coming decade is the transition to a sustainable way of generating, storing, and converting energy. High performance batteries, fuel cells, electrolyzers and solar cells are part of the solution, but still face many challenges that need to be solved. Efficiencies and capacities need to increase, the use of scarce and expensive materials needs to reduce and the life-time needs to improve. There are many examples where ALD has been used to improve on these aspects. For example, by applying thin and highly conformal films on porous substrates using ALD, the lifetime of Li-ion batteries can be improved, the loading of expensive catalyst materials in fuel cells and electrolyzers can be reduced and new devices such as 3D solid state batteries are enabled.

In order to enable large-scale mass production of these applications, Spatial ALD can be used for high deposition rates on both large substrates (square meters) and roll-to-roll. Scaling-up Spatial ALD processes on large area porous substrates, however, can lead to problems with supply limitation; i.e. when the required precursor flow to cover a high surface area substrate exceeds the amount of precursor that can actually be supplied, e.g. due to a low vapor pressure. Furthermore, in case of very expensive precursors, it is required to maximize the precursor efficiency to minimize costs.

The dependency of the precursor dose on aspect ratio, sticking coefficient and reactor pressure has been studied in great detail before. However, when substrate sizes and throughput increase beyond lab-scale, the effective surface area of porous substrates becomes the most important parameter. Furthermore, transport of precursor from the inlet towards the substrate and exhausts must be taken into account. We have developed a numerical model to solve the diffusion-convection-reaction equation for porous substrates in a spatial ALD reactor. The model combines parameters such as the porosity and effective area of the substrate with reactor dimensions, gas flow rates and deposition rate requirements to calculate and optimize the required precursor dose, precursor mass flow and utilization efficiency.

We will discuss several important results from this model and introduce revised scaling laws for the precursor dose required to conformally coat pores. We will demonstrate how the model can help to optimize S-ALD processes and equipment. We will apply the model to two model cases: 1) Very high throughput, roll-to-toll S-ALD of battery electrode interface layers, where there is a significant risk that the deposition rate is limited by the precursor flow, and 2) S-ALD of IrO_2 catalyst layers on porous supports for PEM electrolysis, where the Ir-precursor efficiency has to be maximized because of the extremely high precursor costs.

* *Corresponding author e-mail:* paul.poodt@spark-nano.com

Optimizing a Ni-Fe phosphate catalyst for the Oxygen Evolution Reaction using ALD

Ruben Blomme[a], Rahul Ramesh[a], Lowie Henderick[a], Christophe Detavernier[a] and Jolien Dendooven[a,*]

[a] *Department of Solid State Sciences, Ghent University, Krijgslaan 281 S1, 9000 Gent, Belgium*

In the current drive for making our world sustainable new technologies are being researched and old technologies are being remade to fit into a sustainable model. Green hydrogen is an inevitable necessity for making large industrial processes sustainable and has been recognized as such by the EU [1]. However electrochemical water splitting for the production of hydrogen is currently still not a very efficient process. The main cause for this inefficiency lies on the oxygen evolution (OER) half-reaction of the process. This half-reaction involves the transfer of four electrons and is hampered by sluggish kinetics resulting in a significant overpotential [2].

In an attempt to overcome this problem, catalysts of transition metals garnered a lot of interest due to their availability, pricing and more environmentally friendly nature compared to classical OER catalysts based on Ir and Ru [3]. Oxides as well as phosphates of transition metals have been explored; the latter in some cases outperforming the former [4][5]. Nickel has shown to be one of the more OER-active transition metals, and doping or combining it with iron seems to further increase its performance [6]. Inspired by these results, atomic layer deposition (ALD) was used in this work to deposit and finetune the properties of a Ni-Fe ternary phosphate for its use as an OER-catalyst material.

This material was deposited by alternating ALD cycles of Ni- and Fe-phosphate (denoted here as NiPO and FePO) at a substrate temperature of 300°C, where the resulting composition could be altered by varying the NiPO-to-FePO cycle ratio. Both separate processes have already been reported in literature and start with a 15 s trimethylphosphate plasma step (TMP*) followed by a 10 s oxygen plasma step (O_2*). For NiPO, this is followed by a 15 s nickelocene ($NiCp_2$) pulse [7], while for FePO, it is followed by a 15 s tert-butyl ferrocene (TBF) step [8]. These processes both have a GPC of approx. 0,2 nm/cycle. A peculiar effect occurs where deposition of Ni becomes more favorable when NiPO is co-deposited with FePO as is shown in Fig 1. The XPS results also indicate that even though the GPC for both processes is similar the final deposited layers are rich in Ni (approx. 70% Ni for a 2 to 1 FePO to NiPO supercycle) as is clear in Fig 2.

Ni-Fe phosphates with varying composition and thickness were deposited on a planar wafer with a conducting Ni-surface and tested in a rotating-disc electrode (RDE) set-up to quantify their electrochemical performance. Applying a coating with a selected composition of 4 NiPO to 1 FePO cycles improves the performance over a bare Ni-PVD substrate (Fig 3). A current density of 91 mA/cm^2 at 0.685 V vs Hg/HgO is obtained for this material which is 75% higher than the uncoated nickel disk (51 mA/cm^2). It has also been observed that the pulsing order of the two sub-processes within a super-cycle has an important impact on the resulting layer's performance. If the FePO sub-cycle is pulsed last, the current density improves to approx. 150 mA/cm^2.

These results indicate that ALD is a promising technique for the deposition of catalytic materials due to the precise control that can be exerted over the thickness and composition of the material. Specifically the option to exert high control over the surface of the catalyst can be a big asset in researching catalytic materials.

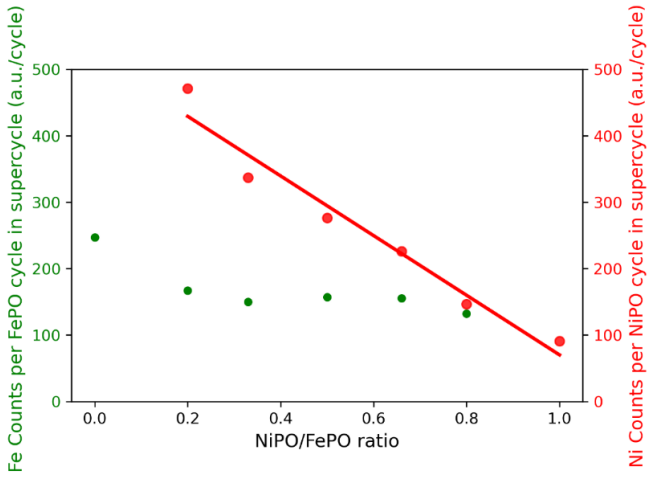

Figure 1: Graph showing the increase in deposited nickel per cycle when the amount of NiPO in supercycles decreases. Fe content, added per ALD cycle, seems to remain more or less constant. All data in this figure was measured on samples with a film thickness between 10 and 20 nm.

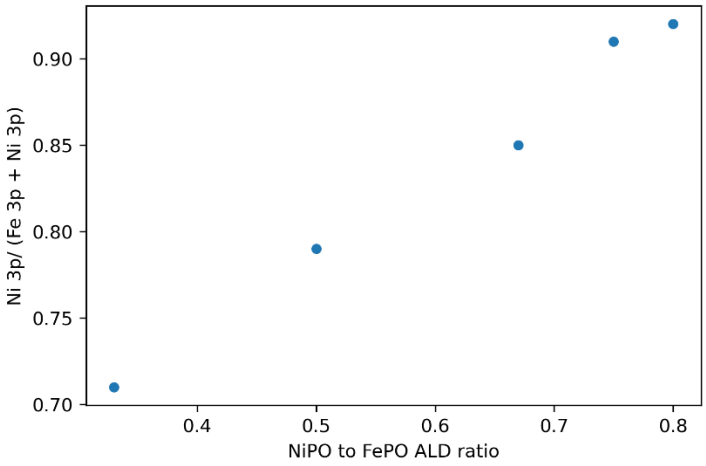

Figure 2: Ni/(Ni+Fe) ratio of the materials according to XPS measurements. The displayed trend is not in line with what is expected for two processes with very similar growth rates [9].

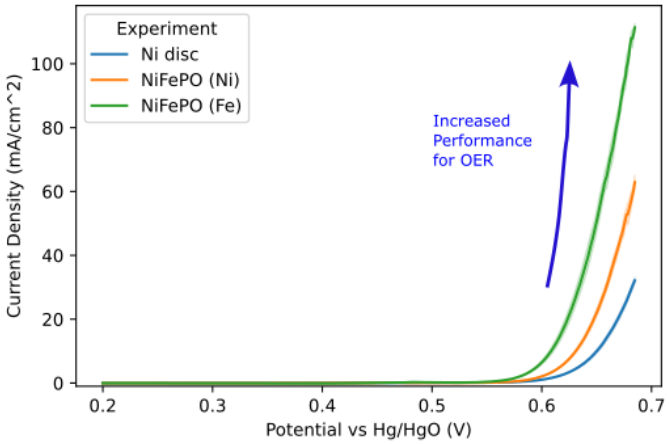

Figure 3: Cyclic Voltammograms of the $NiFePO_x$ (4 NiPO for 1 FePO) materials with different surface terminations.

References

1. https://eur-lex.europa.eu/legal-content/EN/TXT/?uri=CELEX:52020DC0301
2. X. Xie, Adv. Funct. Mater., **32**, 2110036 (2022)
3. C.C.L. McRory,J. Am. Chem. Soc., **137**, 13, 4347–4357 (2015)
4. J. Rongé, Nanoscale Adv., **1**, 4166-4172 (2019)
5. R. Zhang, ACS Catal., **11**, 5, 2774–2785 (2021)
6. F. Diongini, Adv. Energy Mater., **6**, 1600621(2016)
7. L. Henderick, Dalton Trans., **51**, 2059(2022)
8. T. Dobbelaere, Chem. Mater., **28**, 10, 3435-3445(2016)
9. A. J. M. Mackus, Chemistry of Materials, **31**, 4, 1142-1183(2019)

* *Corresponding author e-mail:* Jolien.Dendooven@ugent.be

Metals

Chair: Bol, Ageeth A. (University of Michigan)

Time: 5/30/2023 1:30:00 PM
Location: Auditorium 2, Maria-Theresiacollege, St. Michael's Street 6, Leuven

Integrity of Graphene in Functional Nanostructures Represented by Resistively Switching Media Grown by ALD

Aile Tamm [a]*

[a] *Institute of Physics, University of Tartu, W. Ostwaldi 1, Tartu 50411, Estonia*

Dramatic growth of information density and data related to the development of artificial intelligence (AI) necessitates increment in computing performance. Neuromorphic computing could, in addition, decrease the power consumption [1]. Electronic switches, also characterized by rather simple structure, are searched upon research and development of next-generation nonvolatile resistive random-access memory (RRAM) prototypes. Artificial mixing of different oxides and graphene as interface layer order to tailor their useful physical properties could allow the extension of their application areas including potential memory materials [2].

Chemical vapor deposited graphene can be transferred to Si/SiO_2 or Si/TiN substrates or different metal oxide films. Thin layers of metal oxides, such as Al_2O_3, HfO_2, ZrO_2 or Ta_2O_5 can then be grown by plasma-assisted atomic layer deposition (ALD) on transferred graphene. Nanostructures containing graphene were, thus, synthesized and analysed, keeping in mind their potential applications in nanoelectronics (RRAM), and also nanosensors, electrodes for energy storage and harvesting devices. The metal oxide films have been deposited either in a commercial PicosunTM R-200 Advanced ALD system or in low-pressure flow-type home-build reactors. Graphene sheets were grown on commercial 25 µm thick polycrystalline copper foils in an in-house built chemical vapour deposition (CVD) reactor, and transferred onto Si/SiO_2 or Si/TiN or Si/TiN/metal oxide substrates by using a wet chemical transferring process described by Kahro *et al*. [3]. Thereafter, metal oxide layers could be grown on top of graphene in plasma-assisted processes without destruction of its integrity.

According to the Raman analysis carried out after the ALD of metal oxides on top of the graphene, the G and 2D bands, as fingerprints of graphene, were slightly broadened, and the defect-related D-band remained of low significance (Fig. 1). Stacked nanostructures with graphene layer intermediating metal oxide insulators, devised as resistive switching media between top Ti, or Au, and bottom TiN electrodes, were studied comparatively with and without graphene interlayers. The switching processes could, apparently, be promoted in the devices supplied with conductive graphene interlayer, compared with the media consisting of insulating dielectric oxide films only.

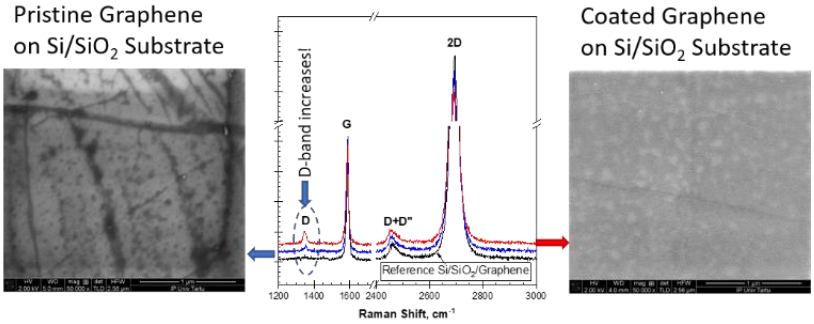

Figure 1. Micro-Raman spectra and Scanning electron microscope images of graphene-based nanostructures Si/SiO_2/G and Si/SiO_2/metal oxide. The deposition of the metal oxide film causes the increase of the D-band and by changing the precipitation parameters of ALD process we could to reduce the damage of graphene.

Our findings have highlighted the correlation between ALD process parameters, appearance of structural defects in graphene, and electrical performance of stacked junctions containing graphene.

References

1. Y. Lee, J. Jang, B. Jeon, K. Lee, D. Chung, S. Kim. *Materials* **15**, 7520 (2022).
2. S. Maji, A.D. Paul, P. Das, S. Chatterjee, P. Chatterjee, V.R. Dhanak, A.K. Chakraborty, R. Mahapatra. *J Mater Sci: Mater Electron*, **32**, (2021), 2936–2945.
3. T. Kahro, A. Tarre, T. Käämbre, H.-M. Piirsoo, J. Kozlova, P. Ritslaid, A. Kasikov, T. Jõgiaas, G. Vinuesa, S. Dueñas, H. Castán, A. Tamm, K. Kukli. *ACS Appl. Nano.Mater.* **4**, (2021) 5152-5153.

* *Corresponding author e-mail:* aile.tamm@ut.ee

MOCVD of highly active metallic iridium films using new amidinate-based precursors for water splitting

Nils Boysen*[a], Jan-Lucas Wree[a], David Zanders[a], Detlef Rogalla[b], Anjana Devi[a]

[a] *Inorganic Materials Chemistry, Ruhr University Bochum, 44801 Bochum, Germany*
[b] *RUBION, Ruhr University Bochum, 44801 Bochum, Germany*

Owing to the valuable intrinsic properties of iridium metal, namely high chemical inertness, high mechanical strength, low electrical resistivity and high catalytic activity, nanostructured iridium thin films have been exploited in numerous applications. These properties of Ir metal are particularly useful for electro-catalytic water splitting applications and especially for the hydrogen evolution reaction (HER). One promising method to produce such nanostructured iridium metal thin films is metal-organic chemical vapor deposition (MOCVD). Yet, highly reactive, thermally stable, and volatile Ir precursors remain a scarcity in the available precursor library. In pursuit of better performing Ir precursors, we designed and developed three new and closely related volatile Ir(I)-1,5-cyclooctadiene complexes bearing all-nitrogen coordinating (di-*iso*-propyl)-guanidinate (DPDMG), (di-*iso*-propyl)-amidinate (DPAMD) and (di-*iso*-propyl)-formamidinate (DPfAMD) ligands (Fig. 1). [1] They were analyzed by nuclear magnetic resonance (NMR) spectroscopy, X-ray diffraction (XRD) and mass spectrometry (MS), which evidenced the structural motifs of the complexes in the liquid, solid and gaseous phase. The structural investigations confirmed the high purity of the obtained complexes and indicated a dinuclear nature of $[Ir(COD)(DPfAMD)]_2$ even in the gaseous phase, while the complexes [Ir(COD)(DPDMG)] and [Ir(COD)(DPAMD)] retained a mononuclear nature. The evaporation properties of the Ir(I) complexes, highly relevant for MOCVD experiments, were investigated by thermogravimetry (TG) experiments. [Ir(COD)(DPAMD)] was found to be the most volatile, features highest thermal stability among the three complexes and cleanly decomposes to iridium metal at higher temperatures (> 210 °C) (Fig. 2). Consequently, [Ir(COD)(DPAMD)] was chosen as precursor in MOCVD experiments for the deposition of Ir metal thin films in a broad temperature range of 300 °C to 800 °C with and without O_2 as the co-reactant (Fig. 3). With the addition of O_2 as co-reactant, the resulting films are dense, highly crystalline with a predominant (100) orientation and exhibit a smooth surface. Rutherford backscattering spectrometry (RBS) and X-ray photoelectron spectroscopy (XPS) measurements revealed a high iridium content of greater than 90 at.% at deposition temperatures reaching from 400 °C to 600 °C, while the films are approaching the bulk resistivity of Ir (5.33 μΩ·cm) in this temperature range. The electrochemical activity (HER) of the Ir films on FTO-coated glass substrates were evaluated. An outstanding performance with overpotentials of 53 mV and 50 mV at –10 $mA \cdot cm^{-2}$ could be achieved for films grown at 400 °C to 500 °C, which strongly underlines the quality of the obtained iridium films. This is a first example of evaluating CVD grown layers for HER applications. The present results set a new milestone in the applicability of metallic iridium films deposited by MOCVD for water splitting applications using tailor-made Ir precursors.

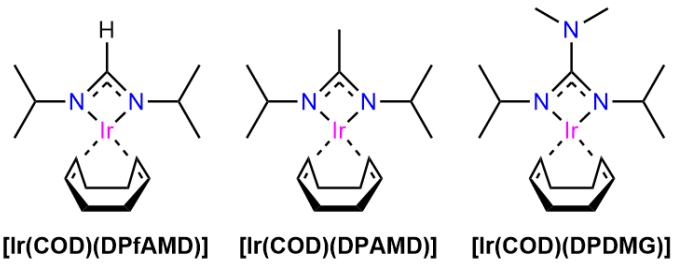

[Ir(COD)(DPfAMD)] **[Ir(COD)(DPAMD)]** **[Ir(COD)(DPDMG)]**

Figure 1. Schematic drawings of the different molecular structures of the precursors investigated in this study.

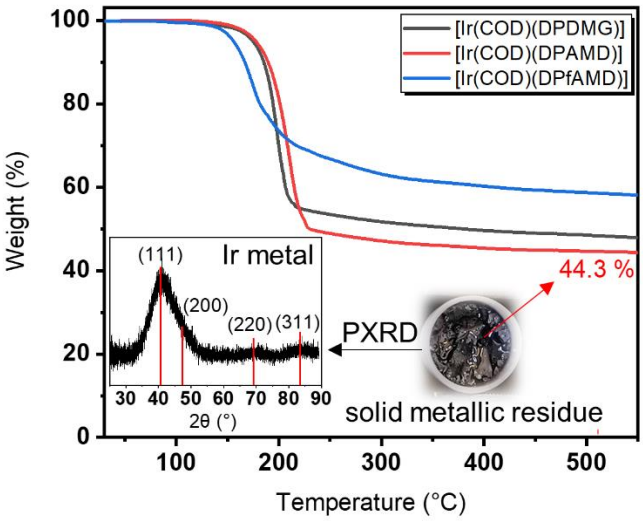

Figure 2. TG analysis of the three different potential precursors from RT to 500 °C at atmospheric pressure. As insets, a picture of the metallic residues from [Ir(COD)(DPAMD)] after heating to 550 °C and the corresponding XRD pattern which indicates metallic iridium formation.

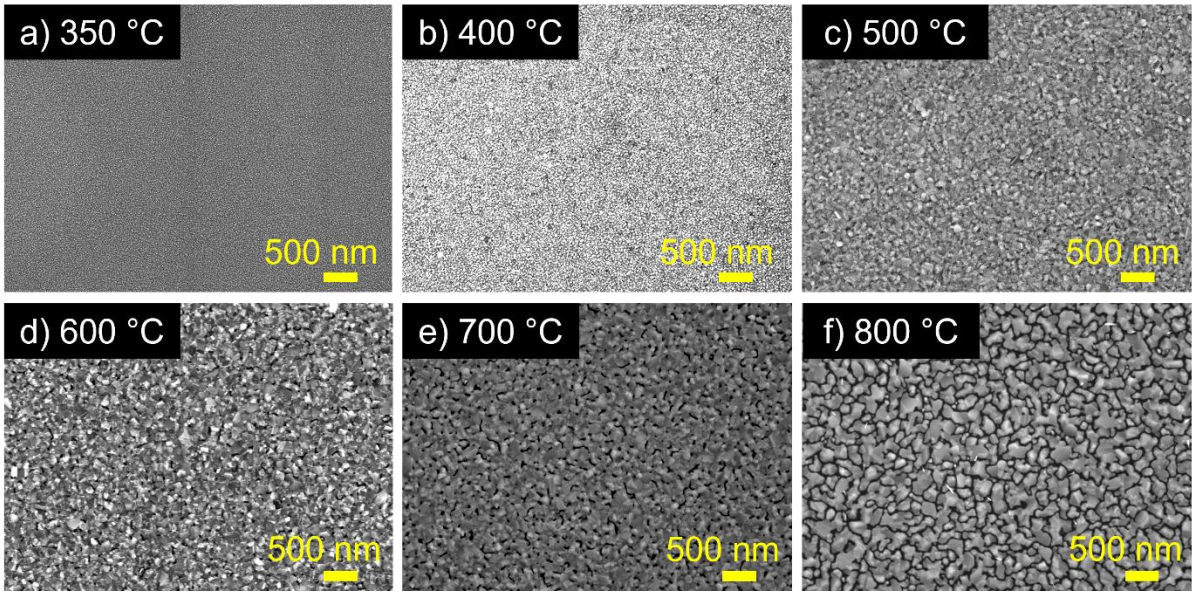

Figure 3. Scanning electron micrographs of films deposited at different deposition temperatures by MOCVD using [Ir(COD)(DPAMD)] and O_2 as precursors.

References:

1. N. Boysen, J.-L. Were, D. Zanders, D. Rogalla, D. Öhl, W. Schuhmann, A. Devi, *ACS Appl. Mater. Interfaces* **14**, 46, 52149–52162 (2022).

* *Corresponding author e-mail:* nils.boysen@rub.de

Effect of thermal induced strain on electrical properties off-stoichiometric $Cu_{2/3}$ $Cr_{4/3}O_2$ delafossite

Marco Moreira [a*], Petru Lunca Popa[a], Yves Fleming[a], Jérôme Polesel[a], Renaud Leturcq[a]

[a]*Luxembourg Institute of Science and Technology (LIST), Materials Research and Technology (MRT) Department, 44 Rue du Brill, L-4422, Belvaux, Luxembourg*

Our group reported previously [1] off-stoichiometric copper-chromium delafossite ($Cu_{2/3}Cr_{4/3}O_2$) with long chains of copper vacancies as source of high p-type electrical conductivity and adequate optical transparency. The small polaron conduction mechanisms present in this class of materials leads to low values of mobilities (< 0.1 cm^2/ (V.s) – Bosman-Van Daal limit). One way to ameliorate this is to engineer the energetic band structure by the means of induced strain. For this purpose, delafossite thin films were grown by metal organic chemical vapour deposition (MOCVD) on substrates with different thermal expansions and to evaluate the effect of induced thermal strain on delafossite thin films (caused by the mismatch between the coefficients of thermal expansion of the substrate and the delafossite) was evaluated. Seebeck coefficient and resistivity measurements were performed on the range of 300-850 K. The Arrhenius relation has shown two different electrical conductivity behaviours over temperature with two distinct activation energies; this crossover point lies around the deposition temperature (Figure 1), where the transition from tensile to compressive strain takes place. These results might open the possibility of tunning the electrical properties of TCOs by engineering of the substrate-film interface.

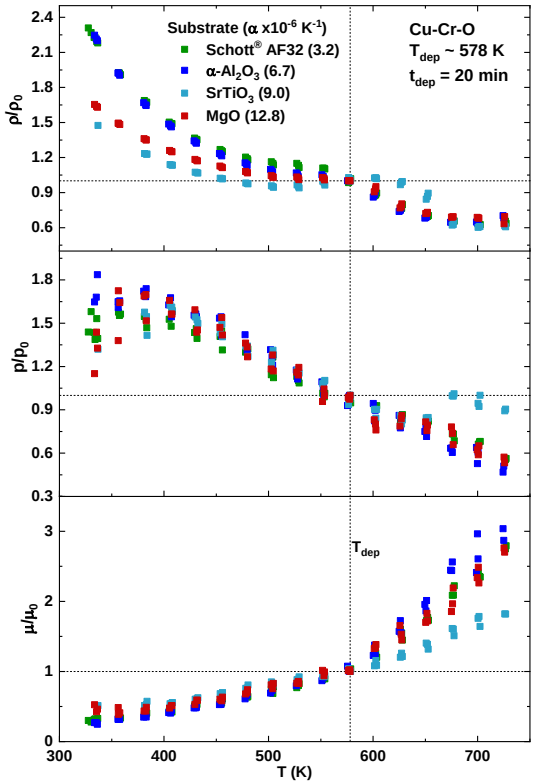

Figure 1 – Normalised Electrical resistivity (ρ/ρ_0), carrier concentration (p/p_0) and mobility (μ/μ_0) as function of temperature.

* marco.moreira@list.lu

[1] P. Lunca-Popa, J. Afonso, P. Grysan, J. Crêpellière, R. Leturcq, and D. Lenoble, "Tuning the electrical properties of the p-type transparent conducting oxide Cu1-xCr1+xO2 by controlled annealing," *Sci. Rep.*, vol. 8, no. 1, pp. 1–8, 2018, doi: 10.1038/s41598-018-25659-3.

Superconducting ultrathin TaC_xN_{1-x} films for quantum applications enabled by plasma-enhanced ALD with ion-energy control

S.A. Peeters[a, *], C.T. Lennon[b], R.H. Hadfield[b], M.A. Verheijen[a], W.M.M. Kessels[a], H.C.M. Knoops[a,c]

[a] *Eindhoven University of Technology, P.O. Box 513, Eindhoven, 5600 MB, Netherlands*
[b] *University of Glasgow, University Avenue, Glasgow, G12 8QQ, Scotland*
[c] *Oxford Instruments Plasma Technology, North End, Bristol, BS49 4AP, England*

The emerging field of quantum technology introduces revolutionary methods of computation, communication, and sensing. Notably, quantum computers are envisioned to provide a leap in capabilities, such as the simulation of extremely complex systems in chemistry and materials science. However, the transition from the current, noisy, intermediate stage to large-scale, fault-tolerant quantum systems requires major material advances. Among the leading architectures to realize large-scale systems are superconducting quantum circuits, where low defectivity, low impurity levels, and sharp interfaces are key. In addition, scalable fabrication methods must be developed, keeping in mind the downscaling of circuit features necessary to make these systems viable.

To this end, the atomic-level growth control and compatibility with large-scale fabrication of atomic layer deposition (ALD) show great promise. Yet, the number of studies on ALD of superconducting materials for quantum circuits remains comparably low. Moreover, preparation of highly-conductive metal (nitrides) by ALD remains challenging, even with the additional energy supplied to the growing surface in plasma-enhanced ALD (PEALD).

To prepare high-quality superconducting films, we apply an RF bias to the substrate to enhance the energy of the bombarding ions in PEALD. The ion-energy control, here investigated in the ~25 – 250 eV range, can be employed as a tuning knob for various material properties, leading to significant improvements in e.g. film microstructure and conductivity [1,2]. The studied material is TaC_xN_{1-x}, motivated by the record coherence times achieved with Ta in superconducting qubits [3,4]. As co-reactants the TBTDMT precursor and an Ar-H_2 plasma are used at a deposition temperature of 250 °C.

Through extensive characterization, we observe a clear trend of beneficial effects of energetic ions on the material properties, followed by an onset of material degradation for excessive ion-energy enhancement. For example, for ~19 nm films prepared without RF substrate biasing a lateral room-temperature resistivity of 1.4×10^4 μΩ cm is measured, while a 20 W RF bias power yields 239 μΩ cm. An increase of the bias power to 35 W results in a slightly higher resistivity of 283 μΩ cm. The mass density as measured by XRR also displays an optimum around 20 W. TEM imaging reveals energetic ions promote a larger grain size and coalescence. In addition, XPS measurements show mitigation of O impurity incorporation and tunability of the TaC_xN_{1-x} composition through ion-energy control. Ion-energy enhancement is also essential for the preparation of ultrathin superconducting films. For 11 - 40 nm films prepared with 20 W RF bias power a consistently high critical temperature (T_c) for superconductivity of around 7 K is found. Considering the absence of a decay in T_c when moving to 11 nm thin films, this process is particularly promising for the fabrication of ultrathin low-loss superconducting devices.

In this contribution, we will discuss how ion energy-control in PEALD can be used to tune material properties, including the relation with the superconducting transition. In addition, the suitability of the prepared ultrathin superconducting films for quantum circuits will be considered.

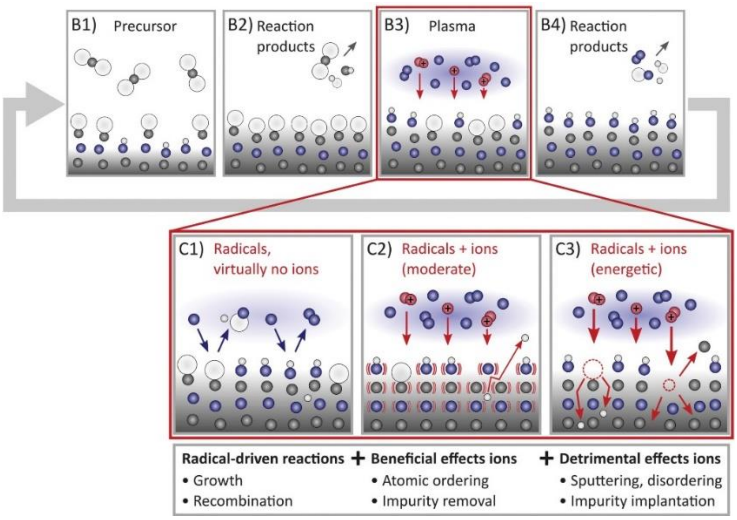

Figure 1 Schematic of a generic PEALD cycle (B1- B4), with a zoom of the plasma step depicting three degrees of ion bombardment: (C1) virtually no ions, (C2) beneficial effects of ions, such as atomic ordering and impurity removal, and (C3) potential detrimental effects of ions. Figure taken from [2].

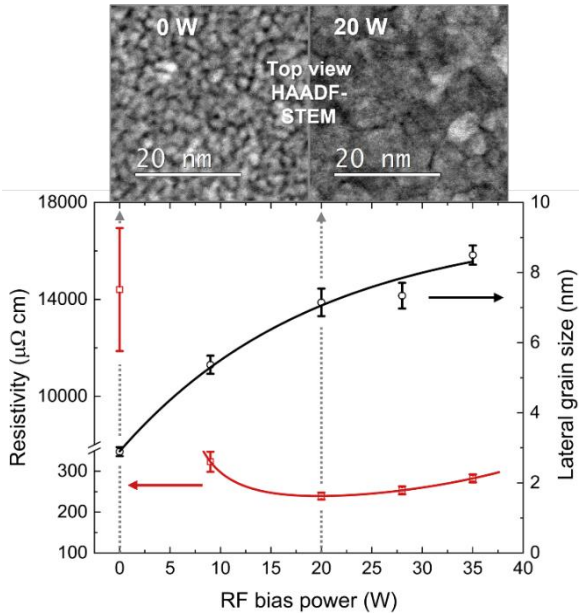

Figure 2 Improved resistivity (red) and grain size (black) by ion-energy enhancement through RF substrate biasing. For 0 W and 20 W RF bias power top-view HAADF-STEM images are shown, depicting film closure as a result of energetic-ion bombardment.

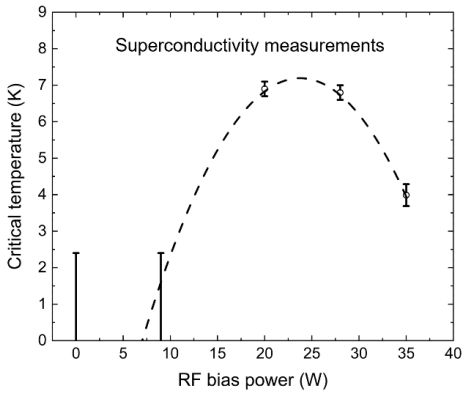

Figure 3 Superconductivity in ~19 nm TaC_xN_{1-x} films achieved through RF substrate biasing, displaying an optimum in ion-energy enhancement. The error bars for 0 W and 9 W RF bias power indicate no superconducting transition was recorded above a temperature of 2.4 K.

References
1. T. Faraz *et al*., ACS Appl. Mater. Interfaces **10**, 13158 – 13180 (2018).
2. K. Arts *et al.*, Plasma Sources Sci. Technol. **31**, 103002 (2022).
3. A. P. M. Place *et al*. Nat. Commun. **12**, 1779 (2021).
4. C. Wang *et al*. npj Quantum Inf. **8**, 3 (2022).

* *Corresponding author e-mail: s.a.peeters@tue.nl*

Semiconductor and nanomaterials I

Chair: Kessels, Erwin (Eindhoven University of Technology)

Time: 5/30/2023 3:30:00 PM
Location: Auditorium 1, Promotion Hall, Naamsestraat 22, Leuven

Precise doping and alloying of 2D transition metal dichalcogenides using plasma-enhanced atomic layer deposition

Ageeth A. Bol

Department of Chemistry, University of Michigan, Ann Arbor, MI

2D transition metal dichalcogenides (TMDs) have many unique properties such as high electronic mobilities and a large surface-to-volume ratio, making them promising materials for various applications in, for example, nanoelectronics and catalysis. In particular, alloys of 2D TMDs or doped 2D TMDs hold great potential due to their composition-controlled properties, making them more versatile than pure TMDs. Atomic layer deposition can be used to synthesize thin films of such ternary TMDs with sub-monolayer growth control, making this method relevant for applications that demand fine control over material structure and properties such as nanoelectronics and catalysis.

Here I will present how we employ plasma enhanced atomic layer deposition (ALD) to achieve highly controllable growth of the ternary 2D TMDs $Mo_xW_{1-x}S_2$, $Nb_xW_{1-x}S_2$, and $Al_xMo_{1-x}S_2$ at low deposition temperatures (< 400 ℃). Pure MoS_2 and WS_2 are both semiconductors and their transition metals are isovalent, making $Mo_xW_{1-x}S_2$ a good case study for a bandgap-tunable semiconductor alloy [1]. On the other hand, NbS_2 is a metallic TMD and Nb is a group-5 transition metal whereas W is a group-6 transition metal, such that $Nb_xW_{1-x}S_2$ is a relevant case study for electronic applications for which a doping effect is desired. Al, being a group 13 element, is a somewhat unlikely dopant for MoS_2, but we have shown that Al doping of MoS_2 leads to sough after p-type doping [2].

The ternary 2D TMDs are grown directly onto thermal oxide silicon wafers by alternating deposition cycles of the constituent TMDs in a supercycle scheme. In this way, we observe near-ideal growth in all three cases without heteronucleation delays. Furthermore, the composition of the alloys is found to be in line with the ideal rule of mixtures. This well-behaved nature of the deposition process and the cyclic nature of ALD enable us to control the *atomic ordering* of the alloys both in-plane and out-of-plane. We demonstrate this directly by atomic resolution HAADF-STEM imaging. In addition, the potential of these 2D alloys synthesized by ALD for application in nanoelectronics and electrocatalysis will be demonstrated.

[1] J. J. P. M. Schulpen *et al. 2D Mater.* (2022), **9,** 025016
[2] V. Vandalon *et al. ACS Appl. Nano Mater.* (2020), **3,** 10200

Advanced Process Design for Low-Temperature PEALD of 2D Transition Metal Dichalcogenides

Miika Mattinen[a,b*], Marcel Verheijen[a], Erwin Kessels[a], Ageeth Bol[a,c]

[a] *Eindhoven University of Technology, PO Box 513, 5600 MB Eindhoven, The Netherlands*
[b] Present address*: Department of Chemistry, University of Helsinki, PO Box 55, 00014, Finland*
[c] *Department of Chemistry, University of Michigan, 930 N. University Ave, Ann Arbor, MI, 48109, USA*

Two-dimensional transition metal dichalcogenides (TMDCs) have a broad range of potential applications as a result of their extraordinary electronic, optical, and mechanical properties. The diverse TMDC family contains both semiconductors (e.g. MoS_2, WS_2) and (semi)metallic materials (e.g. TiS_2, NbS_2). However, synthesis of high-quality, wafer-scale TMDC films under industrially relevant conditions remains a challenge. To this end, several TMDC (PE)ALD processes compatible with back-end-of line semiconductor processing (T ≤ 450 °C), have been developed by us[1,2] and others.[3] In contrast, considerably fewer options are available for direct deposition on plastic substrates for flexible applications (T ≤ 150 °C).

Recently, we demonstrated deposition of TMDCs including MoS_2, TiS_2, and WS_2 at record-low temperatures down to 100 °C by controlling plasma chemistry.[2] The key to this is the addition of a sufficient amount of H_2 into H_2S-based plasma, which prevents incorporation of excess sulfur into the films. With the correct stoichiometry thus reached, crystalline films can be deposited on SiO_2/Si as well as plastic substrates. However, extensive characterization of MoS_2 films showed that some of the hydrogen incorporates into the films and acts as a dopant. In addition, the most crystalline films also present a rough morphology (Fig. 1, top part).

To better tailor films for applications including electronics and electrocatalysis, we set to design advanced ABC type processes consisting of two separate plasma steps. This allows for different atomistic processes such as ligand removal, sulfur incorporation, and enhancement of crystallinity by low energy ions to be more effectively decoupled. As an example, we introduced an additional hydrogen plasma step (C step) instead of mixing it into the H_2S/Ar plasma (B step). This results in MoS_2 films with improved crystallinity, decreased H impurity incorporation, and improved semiconducting characteristics, including increased carrier mobility and decreased carrier density (Fig 1, bottom part).

The ABC approach offers many opportunities for tailoring film growth and properties via use of different plasma gases and conditions. For example, using an Ar plasma C step instead of H_2 plasma further decreases H impurities and carrier density, albeit at a cost of decreased crystallinity and throughput. As another example, applying an H_2 plasma C step only every 10 ALD cycles instead of every cycle results in smooth, crystalline multilayer TMDC films, as formation of out-of-plane oriented “fins” is suppressed. Besides tailoring of film properties, I will describe our mechanistic understanding of advanced PEALD processes operating at conditions compatible with flexible electronics as well as other applications with a low thermal budget.

References

1. *Thermal ALD*: Mattinen et al., Adv. Mater. Interfaces **4**, 1700213 (2017). Mattinen et al., Small **14**, 1800547 (2018). Mattinen et al., Chem. Mater. **15**, 5713 (2019). Mattinen et al., 2D Mater **7**, 011003 (2020).
2. *PEALD*: Sharma et al., Nanoscale **10**, 8615 (2018). Balasubramanyam et al., Chem. Mater. **31**, 5104 (2019). Basuvalingam et al., Chem. Mater. **31**, 9354 (2019). Schulpen et al., 2D Mater. **9**, 025016 (2022).
3. *Review on ALD TMDCs*: Mattinen et al., Adv. Mater. Interfaces **8**, 2001677 (2021).
4. Mattinen et al., Chem. Mater. **34**, 7280 (2022).

* *Corresponding author e-mail: miika.mattinen@helsinki.fi (MM), aabol@umich.edu (AB)*

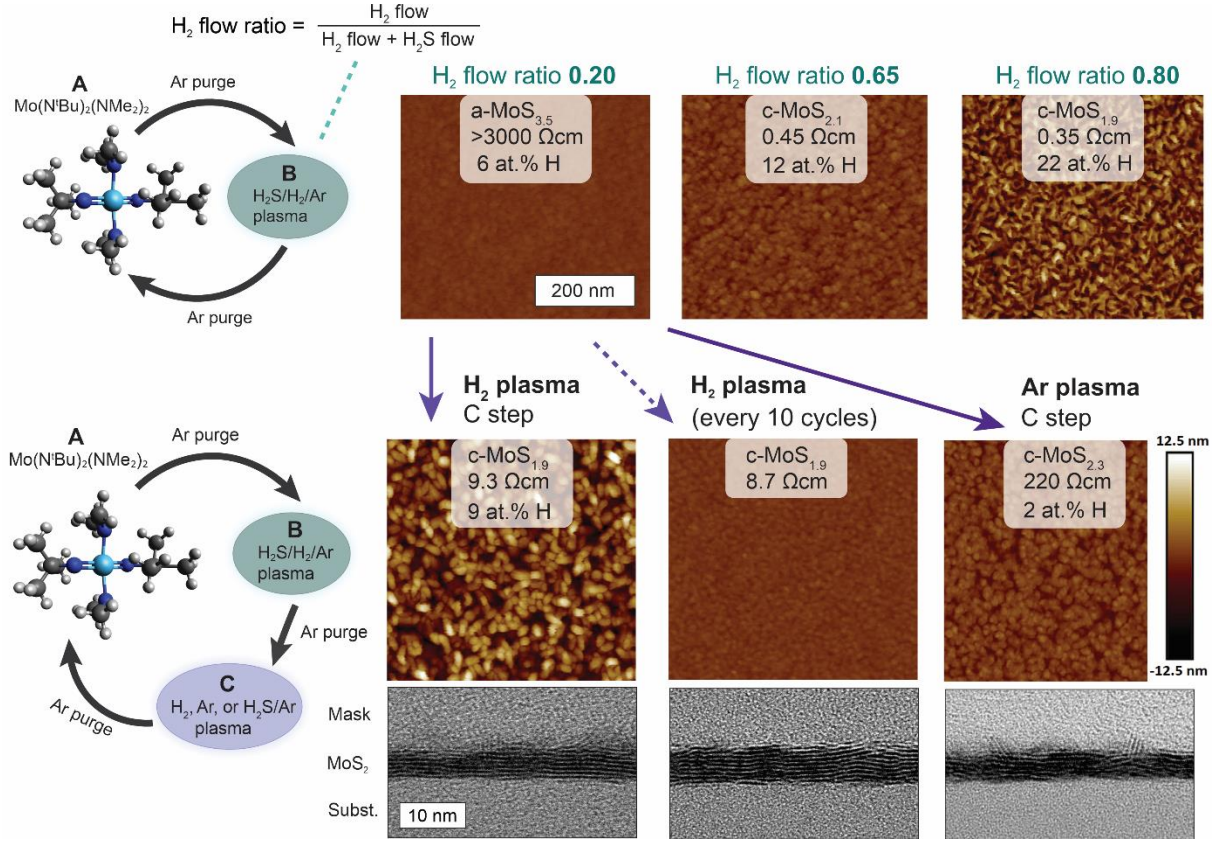

Figure 1. Schematic and selected film properties using advanced MoS_2 PEALD processes at 150 °C. **Top row**: AB type processes where H_2 flow ratio of plasma feed gas was varied.
Bottom row: ABC type processes using H_2 and Ar plasma C steps (B step with H_2 flow ratio 0.20). The characteristics include crystallinity (c = crystalline, a = amorphous; Raman spectroscopy), stoichiometry (X-ray photoelectron spectroscopy), resistivity (four-point-probe - in general, we found a decrease in resistivity to indicate an increase in carrier concentration and vice versa), H impurity content (elastic recoil detection), morphology (atomic force microscopy), and cross-sectional microstructure (transmission electron microscopy). The properties were measured from films deposited on SiO_2/Si using 140 ALD cycles (6–20 nm in thickness)

Transition metal dichalcogenides grown by Direct-Liquid Injection MOCVD

Vincent Astié[a,*], Felipe Wasem-Klein[b], Houssin Makhlouf[b], Matthieu Paillet[b], Sandrine Juillaguet[b], Sylvie Contreras[b], Damien Voiry[c], Périne Landois[b] and Jean-Manuel Decams[a]

[a] *Annealsys, 139 rue des Walkyries, 34000 Montpellier, France*
[b] *Laboratoire Charles Coulomb, CNRS UMR 5221, Université Montpellier, 34000 Montpellier, France*
[c] *Institut Européen des Membranes, CNRS UMR 5635, Université Montpellier, 34000 Montpellier, France*

Transition Metal Dichalcogenides (TMDs) have attracted considerable attention in the scientific community due to several remarkable properties, including high flexibility [1] and tunable bandgap [2]. Particularly, the properties of a selection of TMDs change dramatically when their thickness is reduced to a monolayer [3]. For example, monolayer molybdenum disulfide MoS_2 is of particular interest in optoelectronic applications since it becomes a direct bandgap semiconductor with very high photoluminescence quantum yield [3]. In the last few years, top-down methods have generated excellent proof of concept devices, yet, major drawbacks such as irreproducibility and limited spatial area still hinders its transfer to larger scales. Bottom-up approaches, among which MOCVD is a strong candidate, are still either irreproducible, lengthy, result in non-continuous films, present toxic hazards, or result in films with large sulfur vacancies leading to degraded performances [4].

In this talk, the Direct Liquid Injection Metalorganic Chemical Vapor Deposition (DLI-MOCVD) of MoS_2 on SiO_2/Si substrates using low-toxicity precursors will be presented. Indeed, in a Direct Liquid Injection system, the precursors are injected in liquid form before being flash evaporated and transported to the substrate area, thus expending the range of available chemistry. Therefore, the effect of the precursor molecule and the injection flow rate on the quality of the deposited material will be discussed (Fig. 1). Similarly, reproducibility and scalability will be addressed with large-scale integration in mind (Fig. 2).

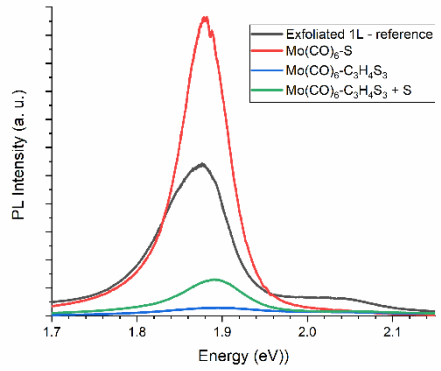

Figure 1 PL spectra of MoS_2 monolayer grown with different precursors and an exfoliated reference sample

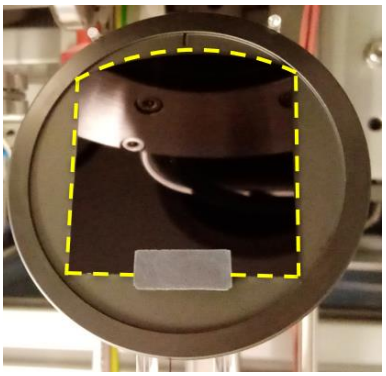

Figure 2 Photography of a 35x35mm SiO_2/Si substrate after MoS_2 deposition. The sample is outlined for clarity.

References

1. Lee, Gwan-Hyoung, et al. "Flexible and transparent MoS_2 field-effect transistors on hexagonal boron nitride-graphene heterostructures." ACS nano **7**, 7931 (2013)
2. Conley, Hiram J., et al. "Bandgap engineering of strained monolayer and bilayer MoS_2." *Nano letters* **13**, 3626 (2013)
3. Splendiani, Andrea, et al. "Emerging photoluminescence in monolayer MoS_2." *Nano letters* **10**, 1271 (2010)
4. Tian, Zi-Liang, et al. "Optimization of defects in large-area synthetic MoS_2 thin films by CS_2 treatment for switching and sensing devices." ACS Applied Nano Materials **2**, 7810 (2019)

* *Corresponding author e-mail:* vastie@annealsys.com

Improving Interfacial Properties of 2D Transition Metal Dichalcogenide Gate Stacks by $GdAlO_x$ Atomic Layer Deposition

Z. Lin[a,b], X. Wu[a], D. Cott[a], B. Groven[a], P. Morin[a], D. Lin[a], I. Asselberghs[a] and A. Delabie[a,b,*]

[a] *imec, Kapeldreef 75, Leuven, 3001, Belgium*
[b] *Department of Chemistry, Celestijnenlaan 200F, Leuven, 3001, Belgium*

Introduction The two-dimensional transition metal dichalcogenides (2D TMDs), such as MoS_2 and WS_2, have attracted significant interest because of their scalability for the next generation transistors [1]. One of the major challenges in building transistors with 2D TMDs is the formation of high-quality gate stacks. Atomic layer deposition (ALD) of gate dielectrics on 2D TMDs is difficult due to the lack of dangling bonds on their basal planes [2]. Various techniques have been developed to facilitate the precursor adsorption on 2D TMDs [3,4,5]. However, literatures report degradation of carrier mobility after the deposition of the top gate dielectrics [6], possibly due to defects and the increase of surface roughness introduced during the formation of seeding layers.

In this work, we study the growth of gadolinium aluminate ($GdAlO_x$) interfacial layers (IL) by ALD on AlO_x seeding layers formed by physisorption on monolayer (ML) WS_2. The impact of the $GdAlO_x$ ILs on device performance have been evaluated on dual gate (DG) MoS_2 field effect transistors (FETs).

Experimental A schematic illustration of the gate stack structure is shown in Fig. 1(a). ML WS_2 was grown on 300 mm SiO_2/Si wafers by MOCVD at 950ºC in a commercial epi chamber [7]. A surface physisorption-based process was applied to form an AlO_x seeding layer on WS_2 to facilitate the following ALD by exposing WS_2 to trimethylaluminium (TMA) at high partial pressure in an ALD reactor at 100ºC. $Gd(^iPrCp_3)$, TMA, and H_2O were used as precursors for the growth of $GdAlO_x$. The Gd:Al mole fraction within the film can be tuned by changing the $Gd(^iPrCp_3)$/[$Gd(^iPrCp_3)$+TMA] precursor pulse ratio (Fig. 1(b)). The temperature of the $Gd(^iPrCp_3)$ precursor canister and process chamber were set at 200 ºC and 250 ºC, respectively. The detailed fabrication process of DG MoS_2 FETs can be found elsewhere [8].

Results and Discussion Fig. 2(a) shows the Gd areal density as a function of $Gd(^iPrCp_3)$ pulse number at different Gd:Al precursor ratios on AlO_x/WS_2 and SiO_2 surface, as measured by Rutherford backscattering spectrometry (RBS). The linear growth curves at given ratio indicate no growth inhibition of $GdAlO_x$ ALD after the TMA treatment on WS_2 surface. This is confirmed by the identical deposited amount of Gd on both pretreated WS_2 and SiO_2 surfaces at given cycle number. However, the amount of deposited Gd per $Gd(^iPrCp_3)$ cycle increases with higher Gd:Al ratios. One possible explanation is that more unreacted H_2O remains in the film at higher Gd:Al ratio due to the hygroscopicity of Gd_2O_3 [9, 10]. This unreacted H_2O will react during the following Gd precursor pulse. Fig. 2(b) shows the relationship between the Gd:Al precursor ratio and mole fraction of the film subtracting the contribution from AlO_x seeding layer. We obtain $GdAlO_3$ and $Gd_{1.6}Al_{0.4}O_3$ at Gd:Al precursor ratio 2:1 and 4:1, providing a possibility to tune the gate stack electrical characteristics (threshold voltage, etc.). The measured κ-value 15 for $GdAlO_3$ is 15, close to the value for amorphous HfO_2.

To investigate the nucleation during ALD, we evaluate the morphology by atomic force microscopy (AFM) measurements. Fig. 3(a) shows the AFM image of 1-nm-thick $GdAlO_3$ on the WS_2 ML with AlO_x seeding layer. The film appears to be closed. AFM shows no preferential decoration of WS_2 crystal edges as we see a similar height difference on the 2nd ML WS_2 crystal edge and basal plane. The surface roughness (RMS) slightly increases after dielectrics deposition (with ~0.1 nm). The RMS value for Al_2O_3 and $GdAlO_3$ ALD are similar.

Next, we investigate the influence of $GdAlO_x$ deposition on the WS_2 properties. The Raman E` and $A_1$` characteristic peaks of WS_2 are maintained after $GdAlO_x$ deposition (Fig. 4(a)). The XPS W 4f spectra of WS_2 after dielectrics deposition shows no peaks corresponding to WO_x formation (Fig. 4(b)). Both of observations suggest the WS_2 physical and chemical properties are well maintained after $GdAlO_x$ ALD.

The impact of the $GdAlO_x$ IL on the 2D TMD device performance has been evaluated on DG MoS_2 FETs (Fig. 5). With the 1 nm $GdAlO_3$ insertion, higher 2-point mobility has been measured compared with devices with direct HfO_2 deposition on AlO_x seeding layer. A similar top-gate capacitance-equivalent-thickness (CET) of ~2.2 nm has been maintained. The possible mechanisms of this improvement can be the mitigation of interface/oxide defects and/or the reduction of surface potential fluctuation close to the WS_2 channel.

Conclusion In conclusion, we have demonstrated the integration of $GdAlO_x$ into 2D TMD gate stacks. ALD provides nm-thin and continuous $GdAlO_x$ film on AlO_x-seeded synthetic WS_2. Because of the mild process condition, the underlying WS_2 ML is well preserved as confirmed by Raman and XPS measurement. We achieve higher mobility MoS_2 DG FETs by adding the 1 nm $GdAlO_3$ IL while maintaining similar electrical thickness as compared to devices with direct HfO_2 deposition.

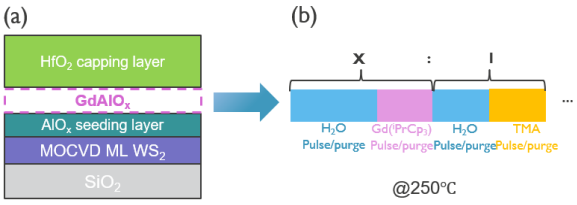

Fig. 1: (a) Schematic illustration of the gate stack structure. (b) the $GdAlO_x$ ALD pulse scheme of this study.

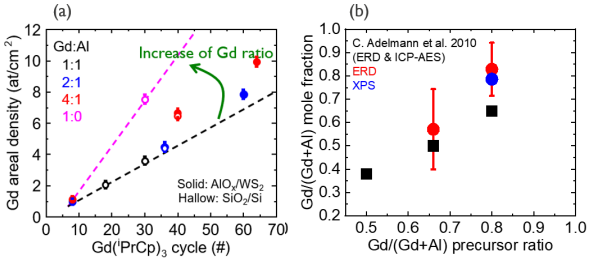

Fig. 2: (a). Relationship between Gd precursor cycle and Gd areal density. (b). Gd/(Gd+Al) mole fraction as a function of Gd/(Gd+Al) precursor pulse ratios of the $GdAlO_x$ film. Film thickness is fixed at 10 nm to exclude the contribution from the AlO_x seeding layer.

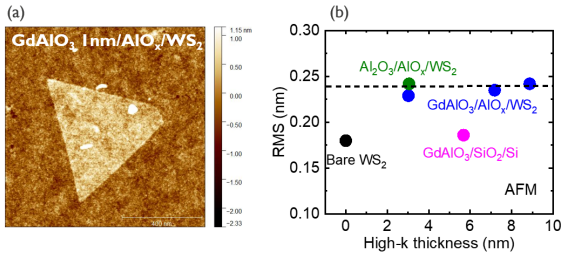

Fig. 3: (a).AFM image of 1nm $GdAlO_3$/AlOx/WS_2 structure. The scale is 1×1 µm. (b). RMS surface roughness as a function of the layer thickness for different stacks.

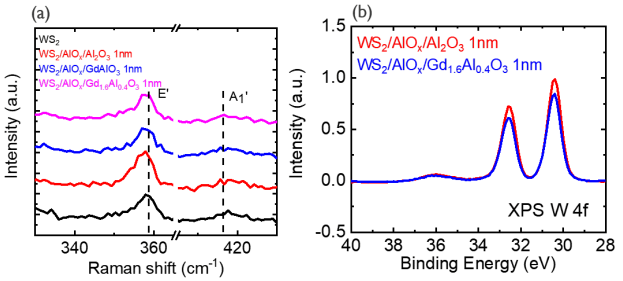

Fig. 4: (a). Raman and (b). XPS spectra of WS_2 deposited with different dielectrics after AlO_x seeding layer formation.

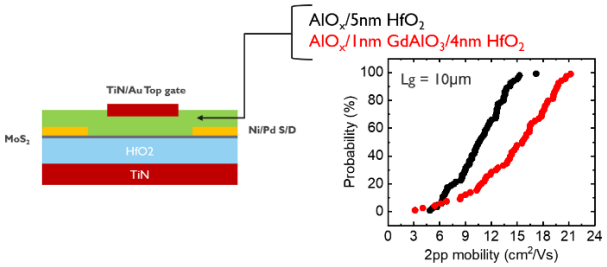

Fig. 5: Schematic structure of the DG MoS_2 FET and the 2-point mobility extracted with AlO_x/5nm HfO_2 and AlO_x/1nm $GdAlO_3$/4nm HfO_2 gate stacks. Top-gate CET is measured to be very similar for these 2 conditions (~2.2 nm)

References

1. D. Akinwande et al., Nature **573**, 507 (2019).
2. S. McDonnell et al., ACS Nano **7**, 10354 (2013).
3. W. Li et al., Nature Electronics **2**, 12 (2019).
4. H. Zhang et al., Chem. Mater. **29**, 6772 (2017).
5. B. Huang et al., ACS Appl. Mater. Interfaces **11**, 35438 (2019).
6. S. Kurabayashi et al., Nanoscale **9**, 13264 (2017).
7. D. Lin et al., IEDM (2020).
8. X. Wu et al., IEDM (2021).
9. S. Jeon et al., Journal of Applied Physics **93**, 6393 (2003).
10. C. Adelmann et al., Chem. Vap. Deposition **16**, 170 (2010).

* *Corresponding author e-mail: Annelies.Delabie@imec.be*

Energy-related applications and catalysis II

Chair: Kafizas, Andreas Georgiou (Imperial College London)

Time: 5/30/2023 3:30:00 PM
Location: Auditorium 2, Maria-Theresiacollege, St. Michael's Street 6, Leuven

Low-temperature CVD process for the Cu_2O thin film growth: applications as photodetectors and HTL for solar cells

Anna Lucia Pellegrino [a], Francesca Lo Presti [a], Graziella Malandrino [a,*]

[a] *Dipartimento di Scienze Chimiche, Università degli Studi di Catania, INSTM UdR Catania, Viale Andrea Doria 6, Catania, 95125, Italy.*

Copper-oxide compounds represent one of the most studied classes of semiconducting materials due to their main advantages of easily tuning the optical and electronic properties within the semiconducting behavior. For this reason, copper oxide materials in form of thin films play a significant role in many technological applications, ranging from batteries to catalysis, from photodetectors to solar cell devices. In particular, among the three most common and stable copper oxide phases, Cu_2O, Cu_4O_3, and CuO, named cuprite, paramelaconite and tenorite, respectively, the cuprite phase (Cu_2O) has been intensively studied and applied as p-type semiconducting material in many technological fields. In fact, Cu_2O represents an attractive material, due to copper abundance, nontoxicity, a wide variety of synthetic strategies and low-cost production.
In literature, Cu_2O as a thin film layer has been synthesized by several vapor and solution methods, including hydrothermal, electrodeposition, sputtering, atomic layer deposition, and chemical vapor deposition. Among these approaches, metalorganic chemical vapor deposition (MOCVD) represents one of the most promising techniques due to its tunability processes, easy scaling up and industrial applicability. Moreover, the CVD approach offers the possibility of fine-tuning the composition of the Cu–O phases by easily altering the operating conditions and the chemical nature of the precursors [1].

Herein, we report an in-depth study of the metalorganic chemical vapor deposition (MOCVD) process for the fabrication of both cuprite Cu_2O and tenorite CuO copper oxide thin films starting from the commercial, quite low-cost β-diketonate copper (II) precursor, i.e. $Cu(tmhd)_2$ bis(2,2,6,6-tetramethyl-3,5-heptanedionate) [2-3]. The present approach represents a simple, easily scalable and industrially appealing process for the production of compact and homogeneous copper oxide films at relatively low temperature. The capability to operate at 250 °C, using a process that is already industrially applied on a large scale, represents a breakthrough for the production of solar cells on plastic flexible supports. X-ray diffraction (XRD), field-emission scanning electron microscopy (FE-SEM) and atomic force microscopy (AFM) analyses allowed an accurate determination of the physico-chemical properties of deposited layers. Operative conditions of fabrication strongly affect both composition and morphologies of the copper oxide thin films. In particular, deposition temperature has been accurately monitored through XRD analyses in order to stabilize and to produce selectively and reproducibly the cuprite Cu_2O and/or tenorite CuO phases (Fig.1). Moreover, the FE-SEM characterizations allowed also to correlate morphologies and thickness of the layers as a function of deposition temperatures (Fig. 2).
Furthermore, as preliminary studies, two main applications have been tested: i) the use of Cu_2O thin films as hole transporting layer for the hybrid perovskite (methylammonium lead iodide, MAPI) based solar cell devices [2]; ii) a core-shell system of all-oxide ZnO-Cu_2O n-p junction as fast and stable self-powered photodetectors [3]. Morphology, crystalline and electronic structure of the Cu_2O thin film materials play a crucial role in determining the main functional parameters of both applications.

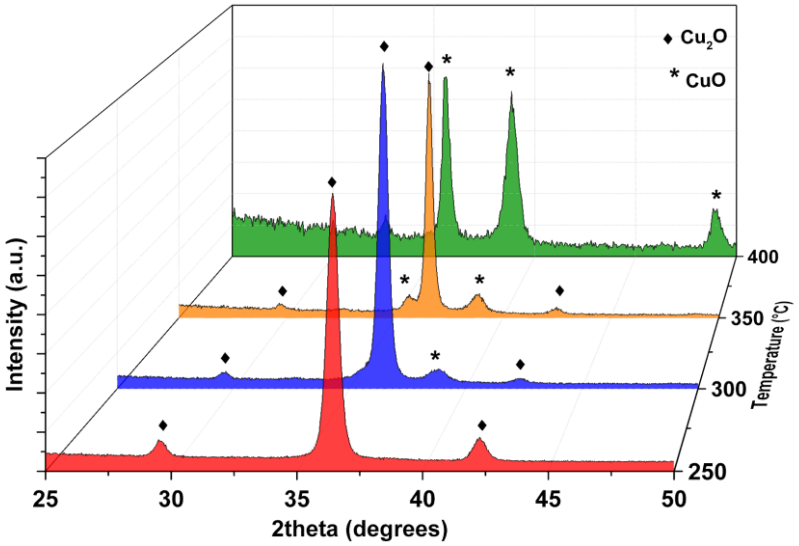

Figure 1. X-ray diffraction patterns of the Cu_2O and CuO thin films prepared by MOCVD at different temperatures from 250 °C to 400°C.

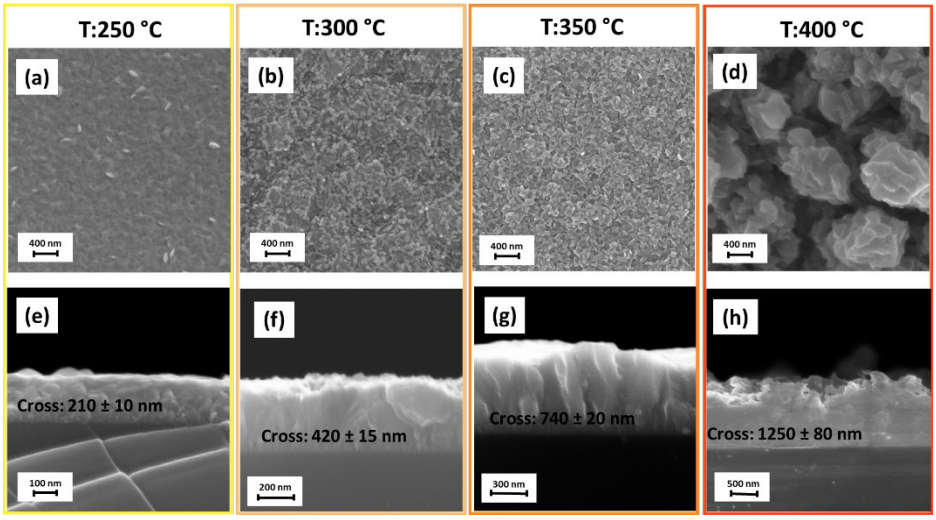

Figure 2. FE-SEM images of Cu_2O and CuO thin films on Si substrate deposited at 250 °C (a,e), 300 °C (b,f), at 350 °C (c,g) and at 400 °C (d,h).

References

1. G. G. Condorelli, G. Malandrino, I. Fragalà, Chem. Vap. Depos. **5**, 21 (1999).
2. A. L. Pellegrino, F. Lo Presti, E. Smecca, S. Valastro, G. Greco, S. Di Franco, F. Roccaforte, A. Alberti, G. Malandrino, Materials **15**, 7790 (2022).
3. P. Ghamgosar, F. Rigoni, S. You, I. Dobryden, M. G. Kohan, A. L. Pellegrino, I. Concina, N. Almqvist, G. Malandrino, A. Vomiero, Nano Energy **51**, 308 (2018).

* *Corresponding author e-mail:* gmalandrino@unict.it

Steps towards atomic-layer additive manufacturing for rapid prototyping of solar cells

Sonja Stefanovic,[a] Sarah Tymek,[a] Ivan Kundrata,[b] Maksym Plakhotnyuk,[b] Julien Bachmann[a,b,*]

[a] *Friedrich-Alexander-Universität Erlangen-Nürnberg, Chemistry of Thin Film Materials, IZNF, Cauerstr. 3, 91058 Erlangen, Germany*

[b] *ATLANT 3D Nanosystems, Mårkærvej 2, 2630 Taastrup, Denmark*

Atomic-layer additive manufacturing (ALAM) combines the advantages of ALD and 3D printing for the direct deposition of materials in patterns. It is realized by delivering ALD precursors in a spatially constrained manner from a nozzle and moving the nozzle over the substrate surface. [1] Just like additive manufacturing accelerates prototyping in classical manufacturing fields, we envision that ALAM will enable rapid prototyping of semiconductor-based devices by circumventing the need for cumbersome lithographic processing. One potential area of application is thin-film photovoltaics, where the thickness of each layer must be optimized systematically.

In a first step towards this goal, we demonstrated that the characteristics of ALAM still conform to the principles of self-limited surface chemical control that underpin ALD. Growth rates are transferrable, if the values of growth per cycle (ALD) are compared with those of growth per pass (ALAM). Thickness can therefore be controlled with sub-nanometer precision. Non-planar substrates are coated conformally. Material properties are similar. However, ALAM can generate much more than blanket coatings, namely straight and curved lines with sharp edges, rectangular patches, and thickness gradients.

Secondly, we have started adapting ALD processes for the generation of the material types needed for building a PV stack to ALAM processes: hole conductor, electron conductor, light absorber, metal contact, and insulator. Our results here highlight the reduced consumption of precursor in ALAM. The comparison of processing parameters exhibits lower evaporation temperatures needed to achieve well-behaved growth than in ALD. Other parameters such as the temperature window of self-saturation behavior remain essentially unchanged.

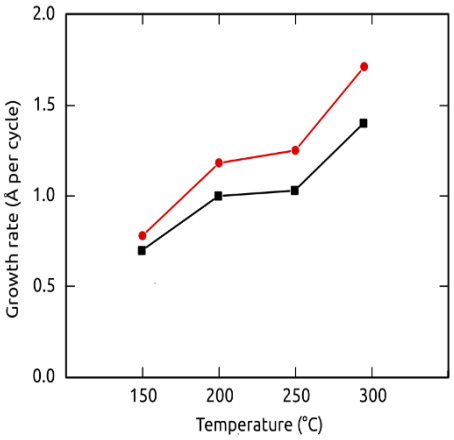

Thirdly, we have built up the experimental infrastructure required for the deposition of all materials in distinct patterns on one single prototype ALAM setup. This includes the integration of a large number of individual precursor lines, the build of an inert-atmosphere enclosure needed to prevent surface oxidation, and the automation enabling for the precise positioning of all material layers into functional devices.

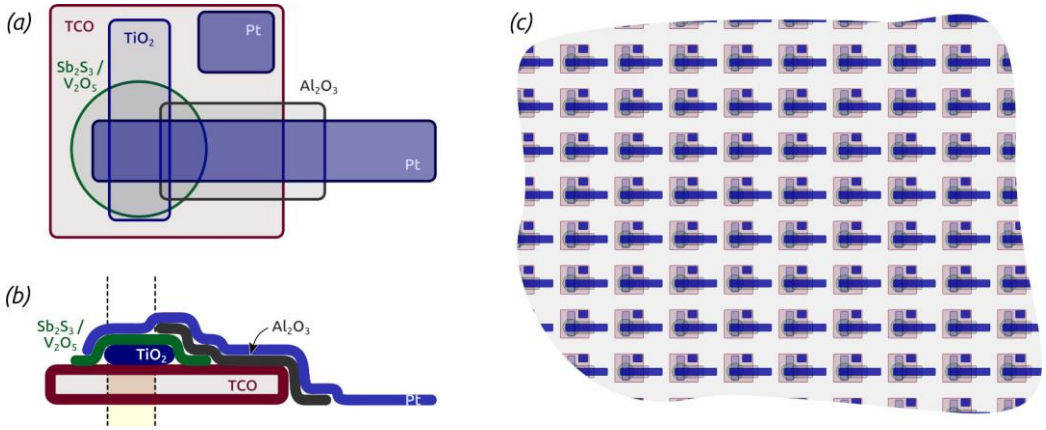

With this, we have established the tools that will enable us to ALAM-print arrays of miniaturized PV devices in which the statistics of device performance can be tested and the optimization of individual layer parameters carried out systematically and quickly. These tools will be applicable to other fields of materials and device research in which thickness control in the sub-nanometer range is of utmost importance and optimization of performance based on film thickness must be explored systematically.

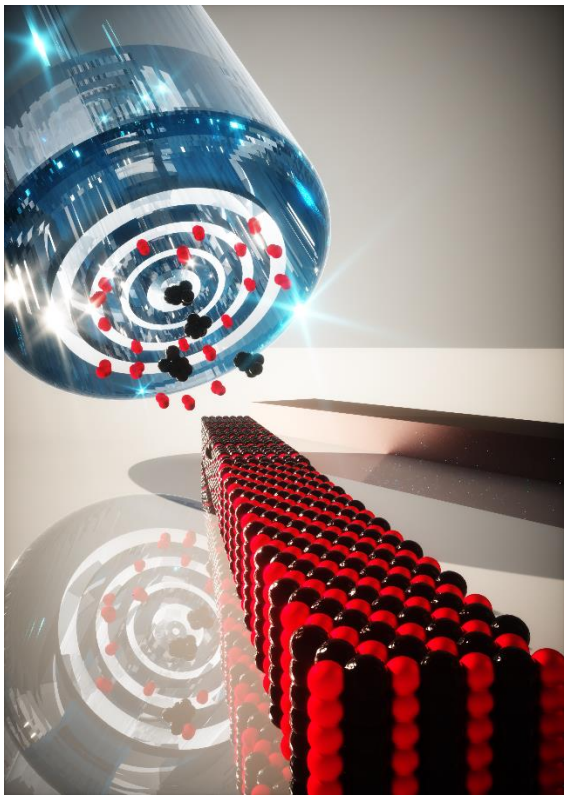

References

1. I. Kundrata, M. K. S. Barr, S. Tymek, D. Döhler, B. Hudec, P. Brüner, G. Vanko, M. Precner, T. Yokosawa, E. Spiecker, M. Plakhotnyuk, K. Fröhlich, J. Bachmann, Small Methods **2022**, 2101546 (2022).

* *Corresponding author e-mail:* julien.bachmann@fau.de

EElectric transport through CVD Molybdenum oxide films. Why these films are excellent hole transfer layers in organic light-emitting diodes?

Anastasia Soultati[a], Petros-Panagis Filippatos[a,b], Alexander Chroneos[b], Maria Vasilopoulou[a] and Dimitris Davazoglou[a*]

[a]NCSR "Demokritos", Institute of Nanoscience and Nanotechnology, POB 60228, 15310 Agia Paraskevi, Greece
[b]Department of Electrical and Computer Engineering, University of Thessaly, Volos, 38333, Greece

In recent years molybdenum oxide films are being extensively used as hole transfer layers (HTLs) in organic and inorganic opto-electronic devices such as solar cells [1, 2]. In an optoelectronic device the HTL must exhibit two basic requirements: (i) it must repulse electrons so as to suppress electron-hole recombination which, e.g., in photovoltaic cells, leads to losses of the photo-generated carriers and therefore to a decrease of the short-circuit current, I_{sc}. The second (ii) requirement that must be fulfilled is that the HTL must exhibit p-type conductivity. In order to repulse electrons, a semiconducting HTL must exhibit states within its band gap where electrons are trapped, therefore negatively charging the layer. Gap states must also be located near the edge of the valence band to insure p-type conductivity. In this work we investigated the charge transport in molybdenum oxide layers deposited by hot-wire chemical vapor deposition (HWCVD) using current-voltage (I-V) measurements on devices of the kind Al/MoOx/Al in air and at temperatures up to 400 ^{o}C. As deposited films were known to be sub-stoichiometric in oxygen (x=2,7) and heating, obviously caused their oxidation. In order to investigate the temperature evolution of the electronic structure of these films spectroscopic ellipsometry (SE) measurements were performed at every temperature simultaneously with the I-V measurements. To investigate the role of the atomic ordering in films (crystallinity) similar electrical and optical measurements were also made as the temperature decreased. Such measurements were made at two thermal cycles.

In Fig. 1 is seen the dispersion of the imaginary part of refractive index of a MoOx film measured at various temperatures. The absorption threshold, corresponding to electronic transitions between valence and conduction band (VB, CB) is observed at wavelengths below 350 nm. Sub-band gap absorption is also observed above 450 nm due to electronic transitions between an intermediate band (IB) located within the band gap [3] and the CB as shown in Fig. 2(a). At -10V the Fermi level of the Al electrode at the left side of the device is raised and electrons are injected in the CB. Due to the disorder the wavefunctions there are localized, their mobility is limited, so they are finally captured by states at the IB. This process is represented with the dotted arrows in Fig. 2 (left) and gives rise to the increase of current as the applied voltage decrease observed in Fig. 3 (upper left panel) between -10 and -5 V. Moreover, due to this capturing of electrons the layer is charged negatively. At positive voltages, holes are pushed to the electrode on the right of the device giving a V^2 dependence of the current, characteristic of the presence of a space charge. At 200 ^{o}C the sample is more oxidized relatively to the as-deposited and now the density of states at the IB decreases considerably (see Fig.'s 1 and 2(b)). Now electrons and holes within the CB and IB respectively contribute equally to the transport giving rise to a "symmetric" I-V curve shown in Fig. 3 (upper right panel). At 400 ^{o}C the sample is almost completely oxidized, the IB fainted out (Fig. 2(c)) and the sub-gap absorption almost vanished as seen in Fig. 1. Now the I-V curve takes the familiar form of an n-type semiconductor as seen in Fig. 3 (lower left panel). From the above it may be concluded that MoOx films act as good HTLs provided that (i) they are disordered, so as to be able to trap electrons at gap states and therefore to charge negatively, and (ii) they are sub-stoichiometric in oxygen, so as to form an IB that insures p-type transport. It is noted though that an excessive oxygen sub-stoichiometry may render the layer metallic thus losing all its good properties as HTL.

It is also noted that as MoOx films cool down they reduce again as seen in Fig. 1, where the sub-gap absorption re-appears upon cooling due to the re-formation of the IB. The presence of the IB gives rise to unexpected phenomena related to the transport. This is shown in Fig. 3 (lower right panel) where at negative voltages, as the temperature drops from 400 and down to 170 ^{o}C the current decreases as expected for a semiconductor, while at lower temperatures it increases again similarly to a metal.

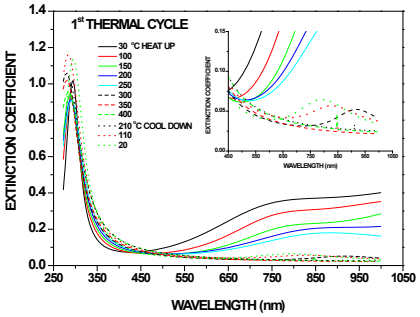

Fig. 1. Temperature evolution of the dispersion of the extinction coefficient of an initially amorphous and sub-stoichiometric molybdenum oxide film. At the insert the evolution of EC during heating above 300 °C and during cooling down to room temperature is shown in magnification.

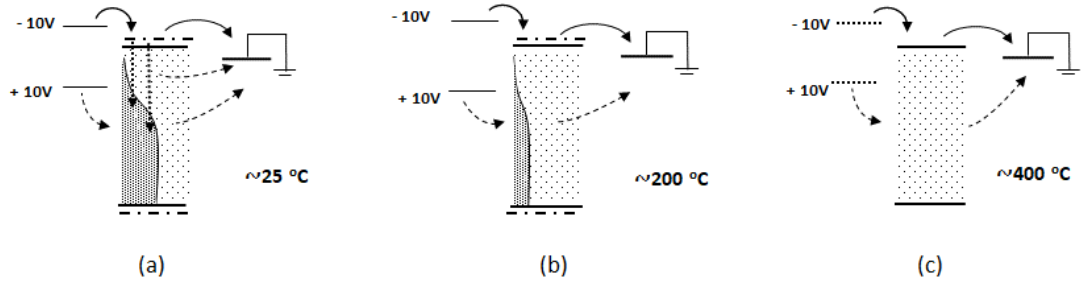

Fig. 2. (a) The energy diagram of the Al/$MoO_{2.7}$/Al structure. At -10 V the Fermi level of Al at the biased contact (left) is shifted upwards and electrons (solid arrows) are injected in the CB whose bottom is composed by localized orbitals and are captured by gap states (dotted arrows). At positive voltages, holes (dashed arrows) are pushed to the grounded Al electrode. (b) As the temperature increases, due to the oxidation of MoOx the density of states at the IB decrease. Now both electrons and holes contribute to the transport. (c) At high temperatures the IB vanishes and the I-V curve becomes as that expected for an ordinary (highly leaky) n-type semiconductor.

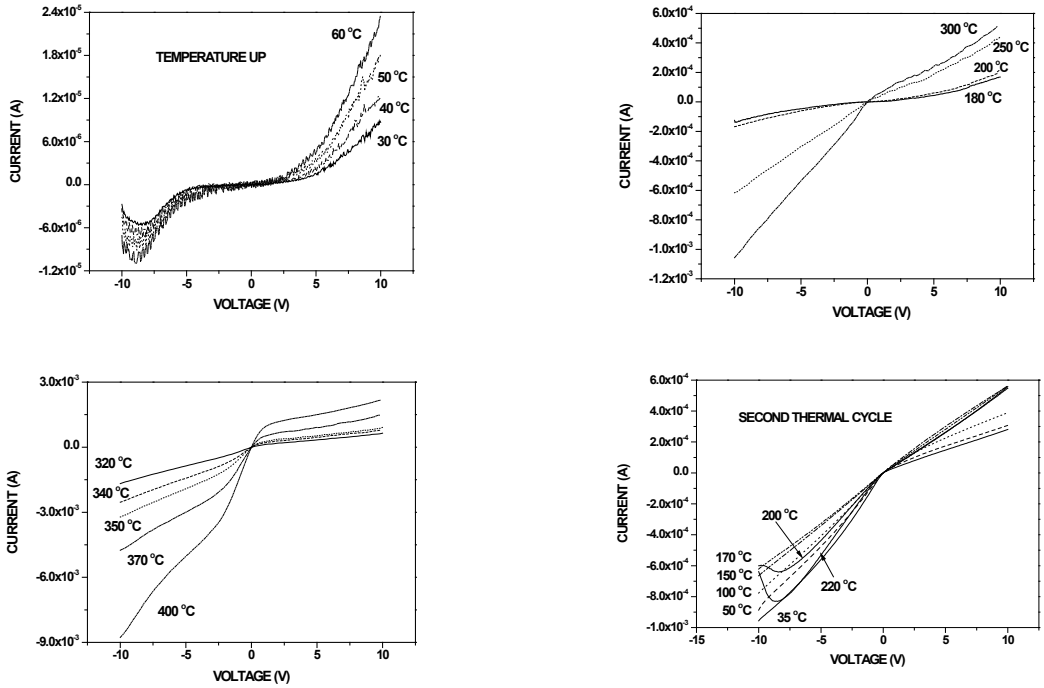

Fig. 3. Current-Voltage characteristics taken on an Al/MoOx/Al sample at temperatures up to 400°C.

References

1. Soultati, et al, J. Mater. Chem. C, 4 (2016) 7683-7694.
2. Battaglia, et al Nano let., 14 (2014)
3. Kostis et al, J. Phys. Chem. C, 117(35), pp. 18013-18020

* *Corresponding author e-mail:* d.davazoglou@inn.demokritos.gr

Chemical deposition of Cu_2O films with ultra-low resistivity: Correlation with the defect landscape

Abderrahime Sekkat[a], Matthieu Weber[a], Laetitia Rapenne[a], Daniel Bellet[a], David Muñoz-Rojas[a,*]

[a] *Univ. Grenoble Alpes, CNRS, Grenoble INP, LMGP, 38000 Grenoble, France*

Cuprous oxide (Cu_2O) is a promising p-type semiconductor material for many applications. So far, the lowest resistivity values are obtained for films deposited by physical methods and/or at high temperatures (~1000 °C), limiting their mass integration. Here, Cu_2O thin films with ultra-low resistivity values of 0.4 Ω.cm were deposited at only 260 °C by atmospheric pressure spatial atomic layer deposition, a scalable chemical approach. The carrier concentration (7.10^{14}-2.10^{18} cm^{-3}), mobility (1- 86 $cm^2/V.s$), and optical bandgap (2.2-2.48 eV) are easily tuned by the choice of precursor and adjusting the fraction of oxygen used during deposition.[1,2] The properties of the films are correlated to the defect landscape, as revealed by a combination of techniques (positron annihilation spectroscopy (PAS), Raman spectroscopy and photoluminescence). Our results reveal the existence of large complex defects and the decrease of the overall defect concentration in the films with increasing oxygen fraction used during deposition. The optimized Cu_2O films are implemented in all-oxide PV harvesters and silicon heterojuntion solar cells. [1,3] Finally, we show that it is possible to selectively obtain Cu, Cu_2O or CuO thin films in our open-air SALD approach from the same Cu precursor by propoer choice of coreactant. [4]

References

1. Open-Air Printing of Cu_2O Thin Films with High Hole Mobility for Semitransparent Solar Harvesters. Abderrahime Sekkat, Viet Huong Nguyen, César Arturo Masse de La Huerta, Laetitia Rapenne, Daniel Bellet, Anne Kaminski-Cachopo, Guy Chichignoud, and David Muñoz-Rojas* Communications Materials (Nature), 2021, volume 2, Article number: 78.
2. Chemical deposition of Cu_2O films with ultra-low resistivity: Correlation with the defect landscape. A. Sekkat*, M. O. Liedke, V. H. Nguyen, M. Butterling, F. Baiutti, J. D. S. Veru, M. Weber, L. Rapenne, D. Bellet, G. Chichignoud, A. Kaminski-Cachopo, E. Hirschmann, A. Wagner, and D. Muñoz-Rojas* Nature Communications, 2022, 13, Article number: 5322
3. Open-Air, Low-Temperature Deposition of Phase Pure Cu_2O Thin Films as Efficient Hole-Transporting Layers for Silicon Heterojunction Solar Cells. Van Son Nguyen, Abderrahime Sekkat, Daniel Bellet, Guy Chichignoud, Anne Kaminski-Cachopo, David Muñoz-Rojas* and Wilfried Favre* J. Mater. Chem. A, 2021, 9, 15968-15974.
4. Selective spatial atomic layer deposition of Cu, Cu_2O and CuO thin films in the open air: reality or fiction? Abderrahime Sekkat, Matthieu Weber, Jesús López-Sánchez, Hervé Rabat, Dunpin Hong, Juan Rubio-Zuazo, Daniel Bellet, Guy Chichignoud, Anne Kaminski-Cachopo, and David Muñoz-Rojas* Submitted.

* *Corresponding author e-mail:* david.munoz-rojas@grenoble-inp.fr

Poster session I

Time: 5/30/2023 5:00:00 PM
Location: Jubilee Hall, Naamsestraat 22, Leuven

Transition metal oxide nanoheterostructures by hybrid CVD routes as heterogeneous photocatalysts for air purification

Davide Barreca[a,*], Javier Fragoso[b], Alberto Gasparotto[a,c], Cinzia Sada[d], Oleg I. Lebedev[e], Evgeny Modin[f], Ivana Pavlovic[b], Luis Sánchez[b], Chiara Maccato[a,c]

[a] *CNR-ICMATE and INSTM, Department of Chemical Sciences, Padova University, Via Marzolo 1, 35131 Padova, Italy*
[b] *Department of Inorganic Chemistry and Chemical Engineering, Córdoba University, Campus de Rabanales, Edificio Marie Curie, 1° Planta, 14071 Córdoba, Spain*
[c] *Department of Chemical Sciences, Padova University and INSTM, Via Marzolo 1, 35131 Padova, Italy*
[d] *Department of Physics and Astronomy, Padova University and INSTM, Via Marzolo 8, 35131 Padova, Italy*
[e] *Laboratoire CRISMAT, ENSICAEN-CNRS UMR6508, 6 boulevard Marechal Juin, 14050 Caen Cedex 4, France*
[f] *CIC nanoGUNE BRTA, Tolosa Hiribidea, 76, 20018 Donostia - San Sebastian, Spain*

Among the most common air pollutants, nitrogen oxides (NO_x; x = 1,2) have an adverse impact on both environment and human health, and their efficient removal from atmosphere (De-NO_x action) has become an imperative and urgent task. In this regard, photo-assisted NO_x degradation with the aid of oxygen and water has emerged as an amenable technology, and has triggered numerous research efforts worldwide aimed at the development of low-cost, green and efficient photocatalysts activated by Vis-light [1,2]. To this aim, the use of supported inorganic nanosystems offers a broader perspective for property tailoring and an easier post-use recovery than their powdered counterparts.

In this work we report on nanoheterostructures based on first-row transition metal oxides as De-NO_x photocatalysts. The target materials were fabricated by hybrid preparation routes involving the initial chemical vapor deposition (CVD) of *host* systems on Si(100) substrates, followed by their functionalization with suitable *guests* by radio frequency (RF)-sputtering under mild conditions. In particular, the case studies dealt with herein concern nanomaterials based on: (i) Co_3O_4 *hosts* + SnO_2 or Fe_2O_3 *guests* [1]; (ii) Fe_2O_3 *hosts* (based on the less studied β polymorph) + CuO or WO_3 *guests* [2]. After a multi-technique chemico-physical characterization of the developed materials, their De-NO_x properties were investigated, providing a preliminary assessment on the possibility of tailoring functional performances through modulations of the system composition. The photocatalytic De-NO_x process mechanism was elucidated by combined *in-situ* and *ex-situ* complementary analytical tools.

As concerns case (i), transmission electron microscopy (TEM) and electron diffraction (ED) revealed the formation of columnar Co_3O_4 arrays uniformly decorated by very thin and conformal overlayers (Fig. 1a-b). Bare Co_3O_4 systems yielded appealing performances for NO_x degradation, with a very limited production of toxic NO_2. The functional behavior of Co_3O_4-SnO_2 and Co_3O_4-Fe_2O_3 heterostructured systems (Fig. 1c) was directly influenced by the concurrent contribution of the system composition and the overlayer morphology. Taken together, the obtained results revealed the occurrence of charge transfer events between the single oxide constituents, in the framework of type-II and *Z*-scheme heterojunctions [1], which had a key role in determining the material photocatalytic behavior.

Regarding case (ii), the adopted route enabled the obtainment of high-purity systems endowed with a pyramidal morphology, an inherent oxygen defectivity and a uniform ultra-dispersion of CuO or WO_3 (Fig. 2a-b). A tiny amount of the latter was sufficient to boost the photocatalytic activity of β-Fe_2O_3, yielding the best performances for WO_3-containing materials. Indeed, the resulting large surface area nanostructures maximize both surface exposure and mass transfer. As a consequence, the observed De-NO_x behavior is competitive with the best non-titania transition metal photocatalysts in terms of both photoactivity and selectivity towards nitrates formation. These outcomes are of considerable importance, since the potential toxicity and low De-NO_x selectivity are common drawbacks of numerous photocatalysts utilized for NO abatement. These favorable issues, mainly rationalized basing on the enhanced charge carrier separation enabled by the high density of heterocontacts between the single oxides, candidate the proposed route as an effective strategy to improve the intrinsic activity of β-Fe_2O_3 nanostructures.

In perspective, the synthesis protocol described in this work provides important guidelines for the nanoscale engineering of active and economically viable photocatalysts, triggering knowledge-based research towards the development of improved platforms for air purification. In addition, the reproducibility and versatility of the proposed preparation route, which is simple, cost-effective and potentially amenable for an eventual scale-up, act as future pointers for future research advancements in the field of green materials for an improved eco-sustainability.

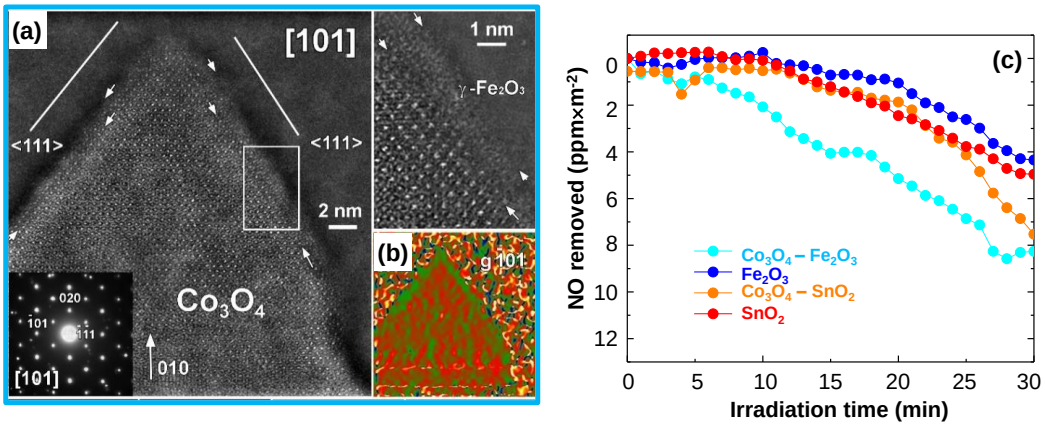

Figure 1. (a) High resolution (HR)-TEM micrograph of a single [101]-oriented Co_3O_4 column and corresponding ED pattern. Upper right corner: magnified image of the area framed by the white box. White arrows mark the Fe_2O_3 overlayer. (b) Color geometric phase analysis (GPA) image for *g*-101 diffraction spot. The color gradient indicates the change in lattice spacing along the [-101] direction. (c) Photodegradation profiles for gaseous NO on functionalized Co_3O_4 photocatalysts in comparison to Fe_2O_3 and SnO_2 obtained by RF-sputtering on Si(100) [1].

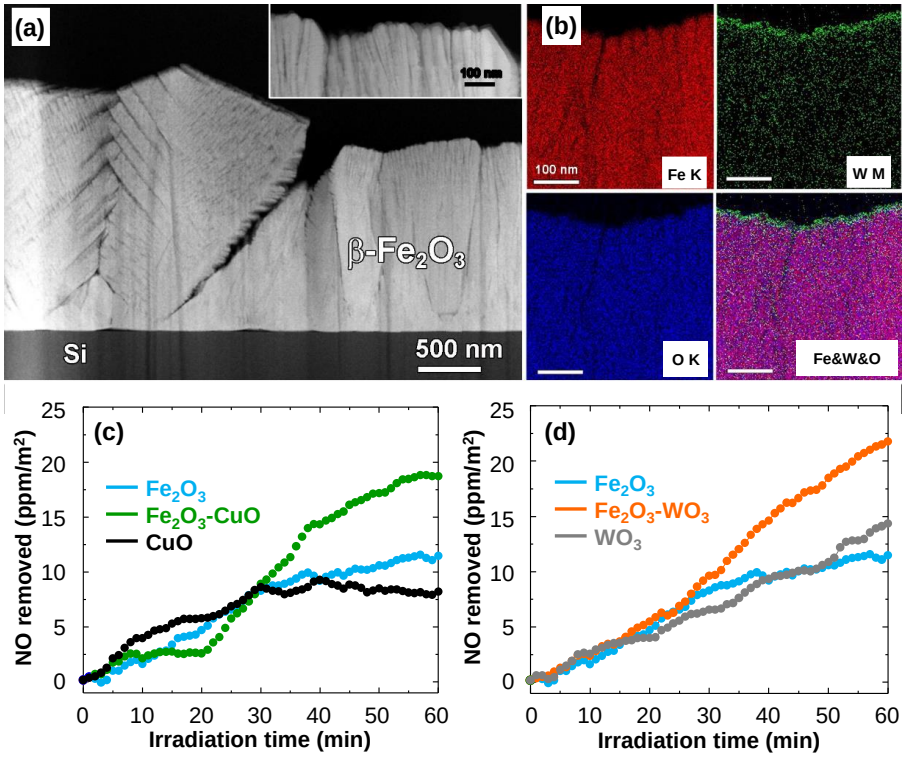

Figure 2. TEM analysis for a Fe_2O_3-WO_3 sample: (a) low magnification cross-section micrograph and magnified near-surface image; (b) energy dispersive X-ray spectroscopy (EDXS) elemental mapping. (c,d) Concentration profiles obtained during NO photodegradation for bare Fe_2O_3, Fe_2O_3-CuO and Fe_2O_3-WO_3. Curves pertaining to CuO and WO_3 obtained by RF-sputtering on Si(100) are also displayed for comparison [2].

References

1. J. Fragoso, D. Barreca, L. Bigiani, C. Sada, O.I. Lebedev, E. Modin, I. Pavlovic, L. Sánchez, C. Maccato, ACS Appl. Mater. Interfaces **13**, 44520 (2021).
2. J. Fragoso, D. Barreca, L. Bigiani, A. Gasparotto, C. Sada, O.I. Lebedev, E. Modin, I. Pavlovic, L. Sánchez, C. Maccato, Chem. Eng. J. **430**, 132757 (2022).

* *Corresponding author e-mail: davide.barreca@unipd.it*

Resistive switching in memristor structures with multilayer dielectrics

Joonas Merisalu*, Toomas Daniel Viskus, Jaan Aarik, Aile Tamm, Kaupo Kukli

Institute of Physics, University of Tartu, W. Ostwaldi 1, Tartu 50411, Estonia

Resistive switching (RS) is one of the most promising future electronic memory technologies, especially for neuromorphic computing. Neuromorphic computing, i.e. brain-like processing, can bring the next technological evolution. Besides the fast processing of large amounts of data, it could help us to understand the human brain better than ever. The technology is based on a single important component, the memristor. In the search for RS media of memristors we have studied different multilayer and multicomponent dielectric oxides deposited by atomic layer deposition (ALD). This report gives an overview of studies focused on RS dielectrics grown in ALD processes using halide-based precursors, which are known to reduce the risk of carbon contamination and material degradation, for instance, in possible application of electrolyte-gated neuromorphic synapse transistors [1].

First, we demonstrated that it was possible to reduce currents in high resistance state (HRS) and increase the high to low resistance ratio of rutile-phase TiO_2 host media with thicknesses of around 10 nm applying a novel Al_2O_3 doping method. The RS media were deposited at 350 °C using $TiCl_4$, $Al(CH_3)_3$ and H_2O as the precursors [2]. In a parallel study, we tested a similar approach with the same doping method using $ZrCl_4$ as the precursor for deposition of the host ZrO_2 medium at 300 °C [3]. As the continuation of the work on TiO_2-based RS media, we also investigated the RS performance of TiO_2:HfO_2 nanolaminates, deposited by ALD at 350 °C from $TiCl_4$, $HfCl_4$, and H_2O as the precursors. The results obtained revealed that in a relatively wide composition range, these RS media crystallized in orthorhombic phase of hafnium titanate, which demonstrated well-defined shape of RS I-V characteristics (Fig. 1 a) and RS cyclic endurance of more than 3×10^3 cycles (Fig. 1 b) with nearly 80% of contact yield. Additionally, application of ALD in synthesis of different RS structures based on SiO_2/graphene/HfO_2, SnO_2:HfO_2, and TiO_2:SiO_2 media has been of interest in our studies.

The results obtained in this research have demonstrated that high to low resistance ratios, resistive switching voltages, multilevel switching ability, endurance and retention characteristics could be modified by changes in ALD chemistry as well as in the composition and structure of RS media.

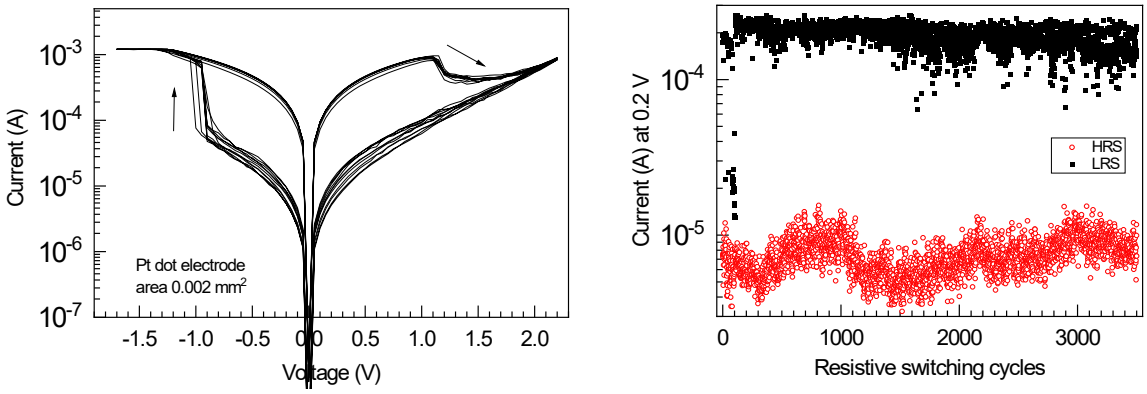

Figure 1. Resistive switching (a) I-V and (b) cyclic endurance characteristics of a memristor cell with orthorhombic hafnium titanate dielectric deposited by applying ALD cycle sequence 80 × (3 × TiO_2 + 1 × HfO_2) at 350 °C

References

1. D.-H. Kim, S.-M. Yoon *Mater Sci Semicond Process.* **153**, 107182 (2022)
2. J. Merisalu, T. Arroval, A. Kasikov, J. Kozlova, M. Rähn, P. Ritslaid, J. Aarik, A. Tamm, K. Kukli *Mater. Sci. Eng. B* **282**, 115797 (2022)
3. J. Merisalu, T. Jõgiaas, T.D. Viskus, A. Kasikov, P. Ritslaid, T. Käämbre, A. Tarre, J. Kozlova, H. Mändar, A. Tamm, J. Aarik, K. Kukli *Coatings* **12**, 431 (2022)

* *Corresponding author e-mail: joonas.merisalu@ut.ee*

The effect of dopant element on mechanical and optical properties of Cr_2O_3 thin films.

Mahtab Salari Mehr[a,*], Lauri Aarik, Taivo Jõgiaas, Aivar Tarre, Aarne Kasikov, Hugo Mändar

Institute of Physics, University of Tartu, W. Ostwaldi Str. 1, Tartu, 50411, Estonia

Chromium oxide is technologically important material owing to the convergence of a variety of mechanical, physical, and chemical properties that offer interesting opportunities in both in fundamental research and technological applications [1]. According to the previous research reports, doping of chromium oxide with suitable elements enables to tailor its properties, for instance: adjusting both p- and n-type semiconductor behavior in form of thin films [2], enhance of hardness and corrosion resistance [3,4] or optical absorption [5], thermal stability for photo-thermal conversion applications [6]. In the current research study, we investigate how the doping of chromium oxide with TiO_2 and Al_2O_3 at different composition influence phase composition, mechanical (hardness and elastic modulus) and optical properties (refractive index and band gap values) of the films.

The films were grown on Si (100) substrate using CrO_2Cl_2-CH_3OH and $Cr(thd)_3$-O_3 as Cr_2O_3; TMA-O_3 as Al_2O_3 and $TiCl_4$-O_3 as TiO_2 precursors, respectively, by atomic layer deposition technique (ALD). XRF analyses revealed the enhanced growth of the TiO_2 and Al_2O_3 during the first ALD cycle on Cr_2O_3 being 2.4 and 2.5 times higher than on binary component.

According to the GIXRD the impact of Al_2O_3 and TiO_2 on the crystallinity of films was different. The $Cr_xTi_{1-x}O_y$ films were crystalline containing α-Cr_2O_3 eskolaite phase that showed a decrease in size of crystallites when increasing the concentration of Ti atoms and a strong preferred growth in (001) plane, however, the $Cr_xAl_{1-x}O_y$ films were X-ray amorphous regardless of the doping rate (Fig. 1 (a)). The hardness of films increased from 14 ± 0.8 GPa for binary Cr_2O_3 to 20.9 ± 1.6 GPa for Ti doped Cr_2O_3 films (Ti/(Ti+Cr) = 0.24) that was related to the decrease in crystallite size explained by Hall-Petch hardening mechanism. The hardness of 17.8 ± 1.2 GPa was observed for Al doped Cr_2O_3 films (Al/(Al+Cr) = 0.29) (Fig. 1 (b)). Spectroscopic ellipsometry analysis showed remarkable dependence of band gap energy values of the Cr_2O_3 films on the concentration of Ti and Al dopant elements.

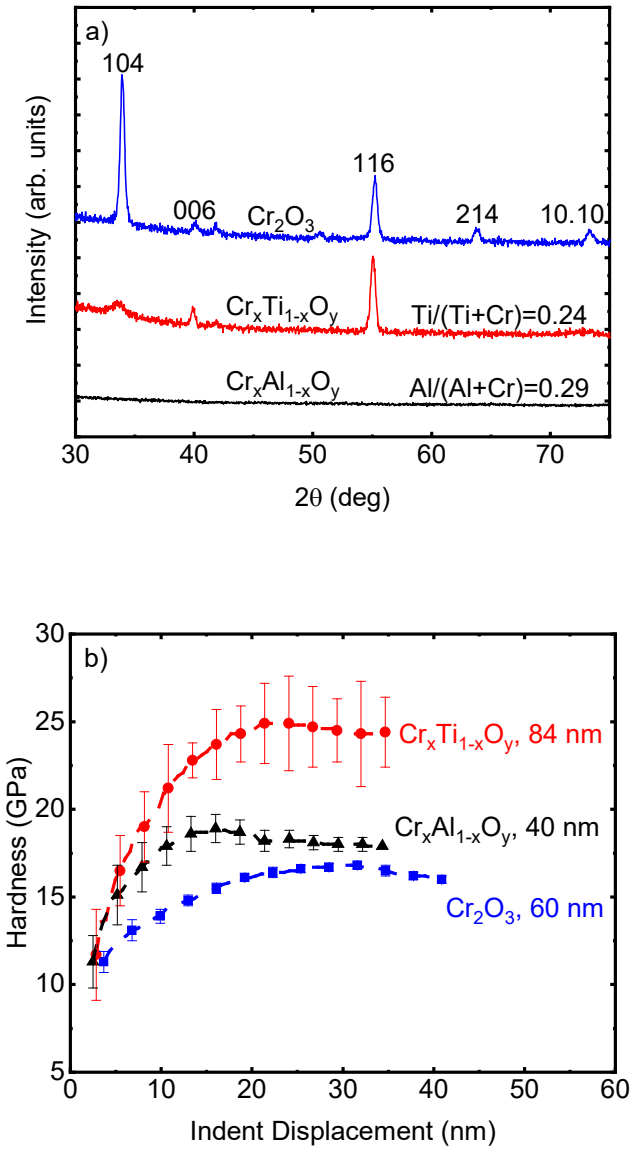

Fig. 1. a) Grazing incidence X-ray diffraction patterns and b) hardness of the undoped and doped Cr_2O_3 films. Diffraction reflections are labelled by Miller indices of corresponding lattice planes.

References:
1. K. Sekizawa, K. Oh-ishi, T. Morikawa, Dalton Transactions, 49, 659-666 (2020).
2. P. Qin, G. Fang, N. Sun, X. Fan, Q. Zheng, F. Chen, J. Wan, X. Zhao, Thin Solid Films, 519 (13), 4343-4341 (2011).
3. M. Mohammadtaheri, Y. Li, J. Corona-Gomez, Q. Yang, Surf. Coat. Technol, 375, 694-700 (2019).
4. A. Bahrami, A. Delgado, C. Onofre, S. Muhl, S. E. Rodil, Surf. Coat. Technol, 374, 690-699 (2019).
5. A. Zekaik, H. Benhebal, B. Benrabah, High Temp. Mater. Proc, 38, 806-812 (2019).
6. H. D. Liu, Q. Wan, B. Z. Lin, L. L. Wang, X. F. Yang, R. Y. Wang, D. Q. Gong, Y. B. Wang, F. Ren, Y. M. Chen, X. D. Cheng, B. Yang, Sol. Energy Mater. Sol. Cells, 122, 226-232 (2014).

* *Corresponding author e-mail address:* mahtab.salari.mehr@ut.ee

Molybdenum-carbide and tungsten-carbide CVD coatings obtained by *Avinit* vacuum-plasma technologies.

A. Sagalovych, V. Sagalovych, V. Popov, S. Dudnik, R. Popenchuk.

Abstract.

The process of gas-phase deposition of Mo-C and W-C multilayer coatings by pyrolysis of molybdenum and tungsten hexacarbonyls on heat-treated technical steel X155CrVMo12-with high class of surface finish (>10) has been studied.

Metallographic research confirms the possibility of low-temperature deposition of high quality coatings with microhardness from ~ 11000 MPa to 20000 MPa at coating deposition rate of 40...170 mkm/h. This provides good adhesion to the substrate materials without reducing the strength characteristics of steel and without deteriorating the purity class of the original surface.

The conducted tribological tests reveal high tribological characteristics of the developed coatings and testify to the prospects of their use for increase of wear resistance and reduction of sliding friction coefficient of friction pairs (steel - coating and coating) of precision units in mechanical engineering.

Comparison of the properties of the developed coatings with the characteristics of electrolytic hard chromium coatings showed that molybdenum-carbide and tungsten-carbide CVD coatings, obtained by vacuum-plasma technology ***Avinit***, are not inferior to chromium coatings in friction values, can surpass them in hardness up to two times, and in resistance to abrasive wear up to 10 times.

According to the aggregate properties, molybdenum coatings can not only compete with electrolytic hard chromium coatings, as hardening and tribological coatings, but also be considered as an alternative to chromium coating in the environmental aspect.

On the basis of the conducted research the technological bases of the processes of applying metallic and metal-carbide CVD coatings on the basis of molybdenum and tungsten have been worked out, which are the base for the development of industrial technologies for precision parts of aggregate and engine construction and machine building.

Examples of application of the developed coatings in production conditions are given.

Keywords: Vacuum-plasma multicomponent multilayer coatings ***Avinit***, CVD, tribology.

Chemical vapor deposition (CVD) methods for coating have become quite widespread in modern technology [1-6]. Compared to other methods, they are distinguished by the relative technological simplicity of the process, the absence of high vacuum requirements (in many cases, the processes take place at atmospheric pressure). The high surface mobility of adsorbed metal-containing compounds allows in CVD processes to obtain a coating with a density close to the theoretical one at temperatures ~ 0.15-0.3 from the melting temperature of the material, which is unavailable for other coating methods.

Among the well-known methods of applying high-quality coatings, CVD methods are very effective in coating powders and other loose materials, as well as in impregnation (sealing) of porous structures.

For many years, we have been carrying out scientific and technological work in the field of development and practical implementation of the latest nanomaterials and nanotechnologies of multicomponent coatings (mono- and multilayer, nanostructured, gradient) of various functional purposes to improve the operational characteristics of materials, assemblies and parts of machines and mechanisms using the method chemical deposition from the gas phase [7-12].

We have developed technological cycles of applying multi-layer coatings based on refractory materials that have high corrosion properties.

Composite materials with such coatings were tested for corrosion resistance in environments typical for pharmaceutical industries, which are hydrofluoric acid and its mixtures with hydrochloric and sulfuric acids, mixtures of organic and inorganic acids, alkalis and various salts with acidity in the range of 1 < pH < 14, hydrogen-rich environments at temperatures of 20 -100 °C. As a result of the performed works and a set of tests of the corrosion resistance of materials, it was established [13] that composite materials with W, Mo coatings, obtained by the developed technologies, are practically resistant to the corrosive effects of all aggressive environments studied in the work, and their corrosion resistance is much higher than stainless steels.

Corrosion tests of titanium samples with a molybdenum coating with a thickness of 10...15 microns were also carried out in a hydrogen environment at a pressure of 600 mm Hg at a temperature of 60±2 ºC [14]. The results of the tests proved that the gas-phase method of forming such coatings ensures their necessary quality and can be recommended for practical use in the protection of materials actively interacting with hydrogen in hydrogen-rich environments.

The results of research on the corrosion resistance of metal coatings in drug synthesis environments showed the prospects of using coatings made of refractory metals to protect against corrosion the equipment of pharmaceutical and other industries exposed to aggressive environments. According to their mechanical and technological characteristics, composite materials with W and Mo coatings are superior to materials with enamel coatings. The corrosion resistance of such materials in conditions of elevated temperature and relative humidity is 10 -15 times higher than that of galvanic coatings [13]. The established resource of work in aggressive environments of capacitive equipment and technological equipment for the synthesis of drugs made of composite materials with W, Mo coatings, according to technical regulations, is at least 5 years with a coating thickness of at least 150-200 microns [15]. This makes it possible to replace expensive alloys with less scarce materials (including "black" steels that have good manufacturability) with highly corrosive protective coatings. In fig. 1 - 4 show photos of various samples with gas-phase coatings with W, Mo, obtained by the developed technologies.

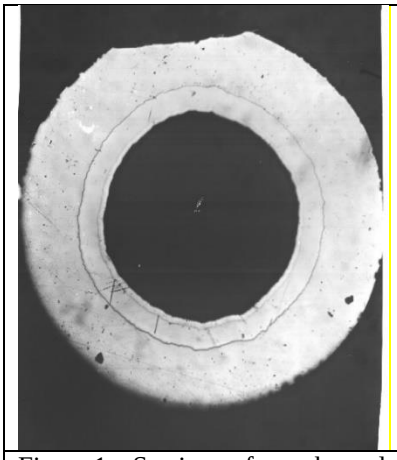

Figer 1. Section of a channel (steel) with an internal coating of Mo (l/d = 300, d = 1 mm)

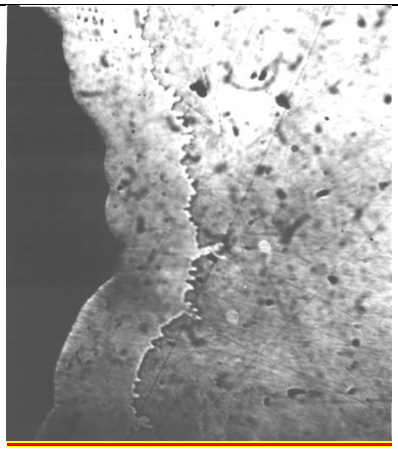

Figer 2. Penetration of the coating into the cavity of the substrate

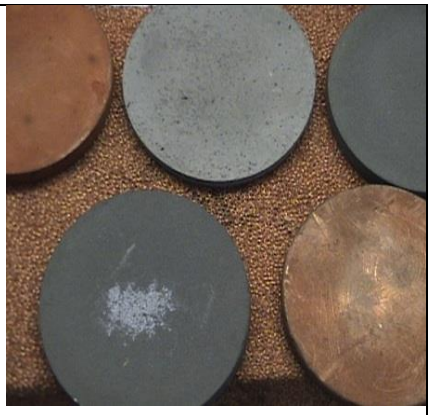

Figer 3. Metal-ceramic filter elements obtained by the method of CVD impregnation of porous structures.

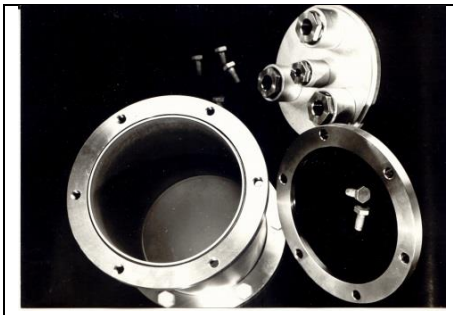

Figer 4. Elements of polyfunctional reactor made of structural materials 1.0038 and stainless 1.4541 with protective coatings W, Mo.

Recently, we have developed experimental and technological equipment for the application of functional multilayer composite coatings - the automated vacuum-plasma cluster ***Avinit***, which allows the implementation of complex coating methods (plasma-chemical CVD, vacuum-plasma PVD (vacuum-arc, magnetron), processes of ion saturation and ion surface treatment) [16-19]. A component of the Avinit vacuum-plasma cluster is the ***Avinit V*** unit for applying coatings to the external and internal surfaces of parts by thermal decomposition of organometallic compounds, mainly hexacarbonyls Mo, W, Re, Cr and their compounds with nitrogen, carbon, etc.

When applying CVD coatings using ***Avinit*** technologies, it becomes possible to carry out technological operations of ion-plasma cleaning of the surfaces of parts before applying coatings, if necessary, the creation of matching metal layers by PVD methods to increase adhesion, plasma support by methods of low-temperature unbalanced plasma in one technological cycle, which ensures obtaining high-quality tightly bonded coatings on the surface of parts.

The purpose of this work is to conduct research on the development of processes for applying multilayer, high-quality, tightly bonded Mo-C and W-C coatings by the gas-phase deposition method and conducting tribological tests to assess the prospects for use in friction pairs ("steel-coating" and "coating-coating") with increased wear resistance and a low coefficient of friction in precision engineering units.

Previously, in works [11, 12], we conducted studies of the process of gas-phase application of Mo - C coatings from molybdenum carbonyl.

The coating was applied to samples of heat-treated steels of technical purpose X155CrVMo12-1 and 24CrMoV55 with a high class of purity of surface treatment (> 10). These steels are widely used in aircraft construction, and the improvement of their structural properties in the future leads to a significant increase in the service life of aircraft units. Samples of 24CrMoV55 steel were polished according to factory technologies to a roughness of class 8 (Ra = 0,32 μm), and samples of steel X155CrVMo12-1 56...61HRC - to a roughness of class 10 (Ra = 0,063 μm).

Technological data of the coating process on steel 24CrMoV55 and X155CrVMo12-1 are presented in the table 1.

Table 1.

Technological data of the process of applying Mo coatings

T, °C	P, Pa	δ, μm	V, μm/ min	Adhesion
350	5,20	8	0,80	+++
	10,00	7	0,70	+++
	5,30	17	1,13	+++
	11,00	10	0,67	+++
	8,80	25	0,83	+++
	11,00	31	1,03	++
400	5,60	3	0,60	++
	5,40	8	0,80	+
	5,50	6	0,60	+
	6,10	8	0,80	+
	5,00	10	0,67	+
	5,40	12	0,80	+
450	7,60	6	1,20	+++
	5,30	17	1,13	+++
	7,20	20	1,33	+++
	5,10	12	0,40	+++

+++ - the coating is removed only by etching; ++ - minor cracks; + - many chips.

The microhardness of HB coatings increased from 16670 MPa at an application temperature of 450 °C to 21575 MPa when the temperature decreased to 350°C. At 450 °C, the coating had good

adhesion to the base, at a lower temperature, a weakening of the adhesion to the original sample was observed. In fig. 5 shows a cross section of coatings on X155CrVMo12-1 and 24CrMoV55 steel samples obtained at different temperatures with marked analysis zones, and the chemical composition of the analysis zones.

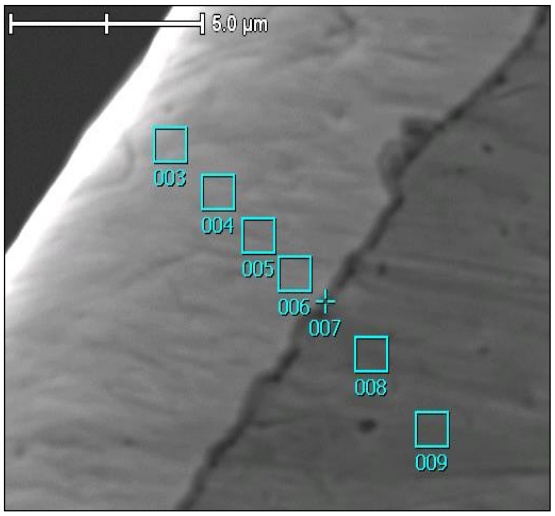

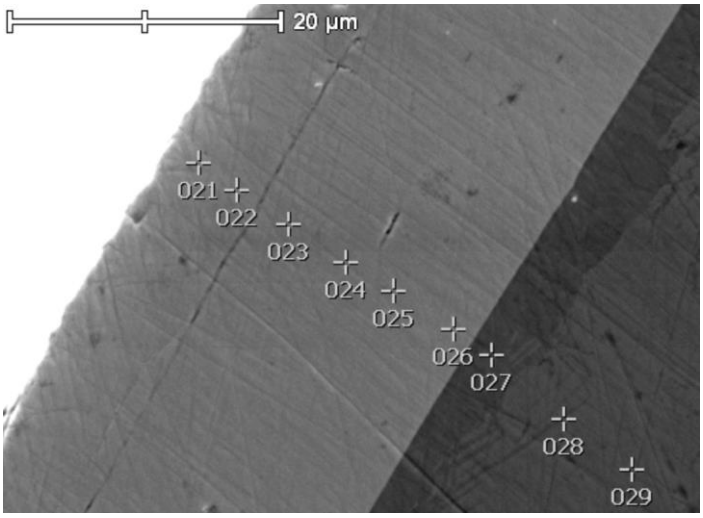

Point No.	Si	Cr	Fe	Ni	Mo	C
003					97.0	3.0
004					96.5	3.5
005			2.21		94.79	3.0
006			3.17		94.83	2.0
007		10.13	22.67	9.90	55.31	2.0
008	0.21	6.85	92.13			0.8
009	0.34	7.13	91.73			0.8

a

Point No.	Si	Cr	Fe	Ni	Mo	C
021				3.40	94.12	2.48
022				3.32	94.01	2.67
023				3.05	95.61	1.34
024				3.40	94.80	1.80
025				3.18	94.64	2.18
026			2.72	1.98	93.69	1.57
027	0.17	1.93	97.69	0.22		
028	0.25	1.88	97.55	0.32		
029	0.27	1.67	97.86	0.19		

b

Figer 5. Appearance of Mo coating with marked analysis zones and chemical composition of the analyzed zones on steels: a) X155CrVMo12-1 (T = 350 °C, P = 8,8 Па); б) 24CrMoV55 (T = 450 °C, P = 7,6 Па).

For comparative tribological tests, cubes (steel X155CrVMo12-1, 56...61HRC) were coated with CVD Mo-C. The parameters of the CVD coating process and their characteristics are given in table. 2.

Table 2.

Parameters of the CVD coating process and their characteristics.

№	Cubes	CVD process parameters		Coating characteristics		Notes
		T, °C	*t*, min	Thickness h, µm	microhardness H_vMPa	
1	Cube № 23 - CVD Mo-C	410-440	10,00	15	24520	Finishing with ACM7/3 diamond paste with an allowance of 0.004-0.006 mm to restore flatness. After finishing - h=5...10 µm.
2	Cube № 24 – CVD Mo-C	360-370	10,00	10	176500	
3	Cube № 25 – CVD Mo-C	290,00	10,00	10	24520	

Tribological tests of samples with coatings were carried out with friction and wear machine 2070 SMT-1 under the scheme "cube" - "roller" test. The linear slip velocities - 1.3 m/s. Time of tests in each cycle – 150 seconds. Operating fluid was fuel TS-1, GOST 10227-86. Fig. 6 - 8 show the results of tribological tests of pairs "Mo-C coating/ steel 24CrMoV55" "Mo-C coating/ Avinit Mo-N and Avinit Ti-Al-N coating", which are widely used in the production of FED JSC.

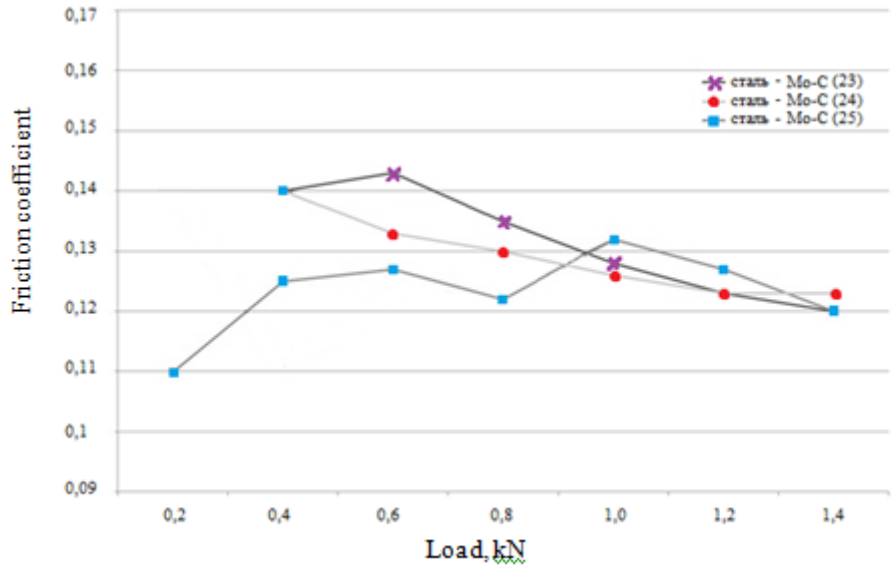

Fiiger 6. Dependence of the friction coefficient on the load for Mo-C/steel 24CrMoV55 friction pairs.

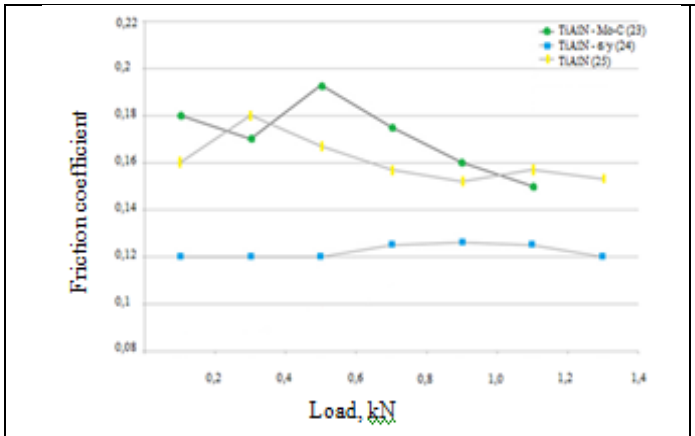

Figer 7. Dependence of the friction coefficient on the load for the Mo-C/Ti-Al-N friction pair.

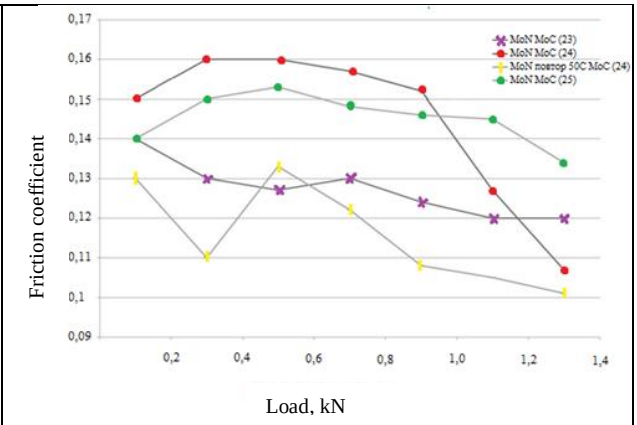

Figer 8. Dependence of the friction coefficient on the load for Mo-C/Mo-N friction pairs.

Studies of the application process of Mo coatings and their properties showed the possibility of low-temperature application with sufficient adhesion to substrates made of 24CrMoV55, X155CrVMo12-1 steels of high-hardness Mo-C coatings, and also showed that such coatings may have the prospect of application for precision components of aircraft assembly construction. Therefore, in this work, the studies of the processes of applying molybdenum-carbide and tungsten-carbide coatings were continued at higher (≥ 480 °C) pyrolysis temperatures of molybdenum and tungsten hexacarbonyls. The experiments were performed on the ***Avinit V*** gas-phase unit, which is part of the ***Avinit*** vacuum-plasma cluster. The coating was applied to cubic substrates made of X155CrVMo12-1 steel. Samples of this shape made it possible to use them in tribological studies of the properties of the obtained coatings according to the "cube" - "roller" test scheme. The conditions for conducting such studies did not differ from those given above.

Methods of applying coatings, studying their metallographic and tribological properties are described in detail in works [16-19].

In fig. 9, 10 present graphs of the dependence of the growth rate of Mo coatings on temperature and pressure in the reaction volume.

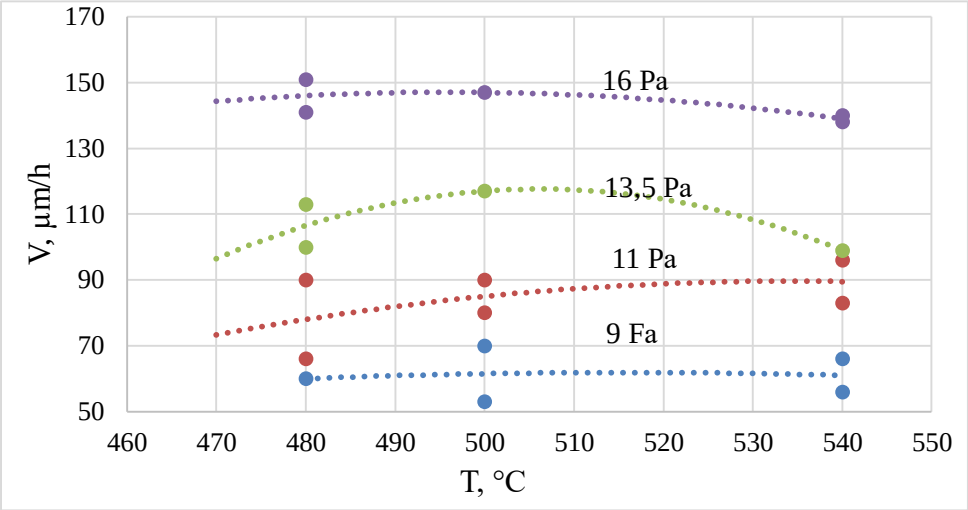

Figer 9. Dependence of the growth rate of Mo coatings on the deposition temperature at different pressure values.

As can be seen on the curves of the dependence of the growth rate of the coating on the temperature at different pressure values (Fig. 9), there is a tendency for the growth rate to increase up to a certain temperature, and then its decrease. For different pressure values, the region of maximum deposition rate occurs in the temperature range of ≈ (500 – 530) °C. The presence of a maximum in the curves of the coating growth rate versus temperature is typical for CVD processes. This is due to the fact that upon reaching a certain temperature of the substrate, the decomposition reaction of the metal-containing compound begins to proceed not only on the surface of the substrate, but partly already in the gas phase near the substrate, i.e., a homogeneous process of thermal dissociation of $Mo(CO)_6$ becomes possible as a result of reaching temperature required for this in the near-surface layer of the gas medium with a substrate. This leads to a decrease in the concentration of molybdenum carbonyl directly above the substrate surface and, accordingly, the growth rate of the coating.

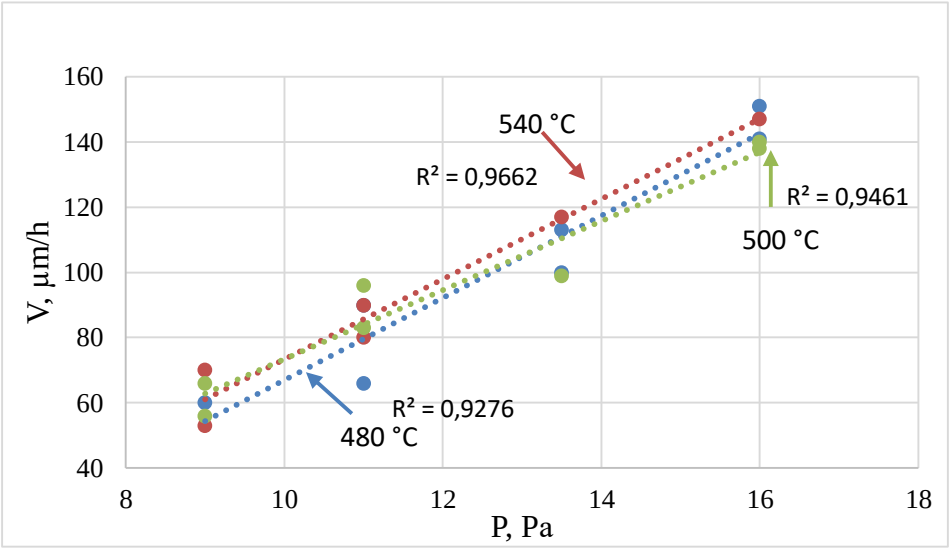

Figer 10. Dependence of the growth rate of Mo coatings on the pressure in the reaction volume at different temperature.

The growth rate of Mo coatings at different deposition temperatures (Fig. 10) is quite well approximated by a linear dependence on the pressure in the reaction volume. At the same time, the deposition curves lie within the range of experimental data for different temperatures. This indicates that the growth rate in the investigated temperature range is primarily controlled by the mass transfer processes of the gas phase components in the near-surface layer above the coating deposition surface, and not by the temperature of the substrate.

The study of the surface morphology of molybdenum coatings showed that depending on the temperature and pressure in the chamber during their deposition, it can differ significantly.

At a deposition temperature of 480 °C (fig. 11) it has a globular structure for all pressure values from 9 Pa to 16 Pa. At a temperature of 500 °C, the coating surface had a globular structure only for a pressure of 16 Pa. At lower pressure values and an increase in the deposition temperature to 540 °C, the structure of the surface of the coatings takes the form of a collection of crystallites of irregular shape and different sizes (Fig. 12).

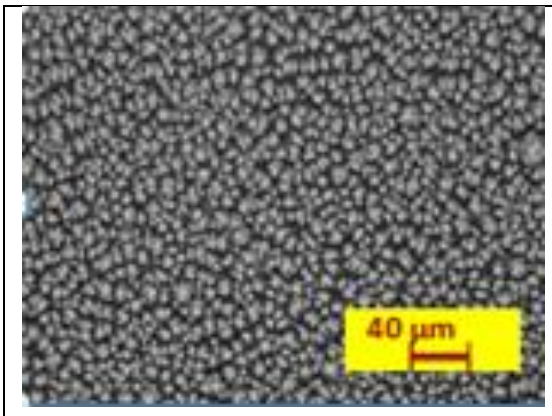

Figer 11. Surface structure of molybdenum coating, T = 480℃, P =16 Pa.

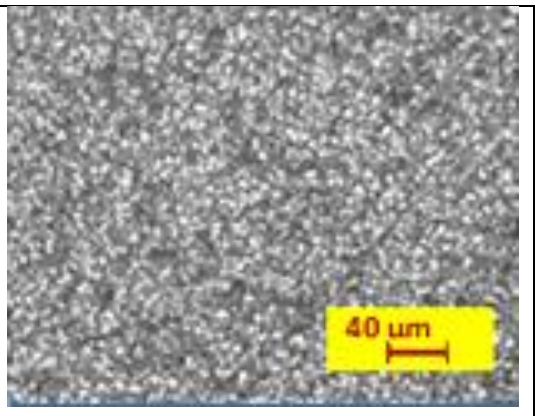

Figer 12. Surface structure of molybdenum coating, T = 540℃, P = 9 Pa.

The microstructure of the coatings obtained under different conditions had a columnar character and differed mainly only in the size of the crystallites, which to a certain extent adjusted to the sizes of the structural elements of the surface of the given coating. In fig. 13 shows a photo of a section of one of the samples with molybdenum coating.

Figer 13. The structure of the Mo coating obtained at a temperature of 500 °C and a pressure of 16 Pa.

Surface roughness Ra of samples with molybdenum coatings was in most cases in the range of 0.12 - 0.25 microns and did not exceed the value of 0.49 microns. Coatings can withstand filleting operations well. After the filleting operation, the roughness decreased to Ra = 0,11-0,15 µm, and in some cases even to 0,07-0,08 µm.

Studies of the microhardness of molybdenum coatings showed that it decreased with increasing temperature and increased with increasing pressure. Fig. 14 presents the results of these studies for different values of temperature and pressure with approximation by curves corresponding to the power law.

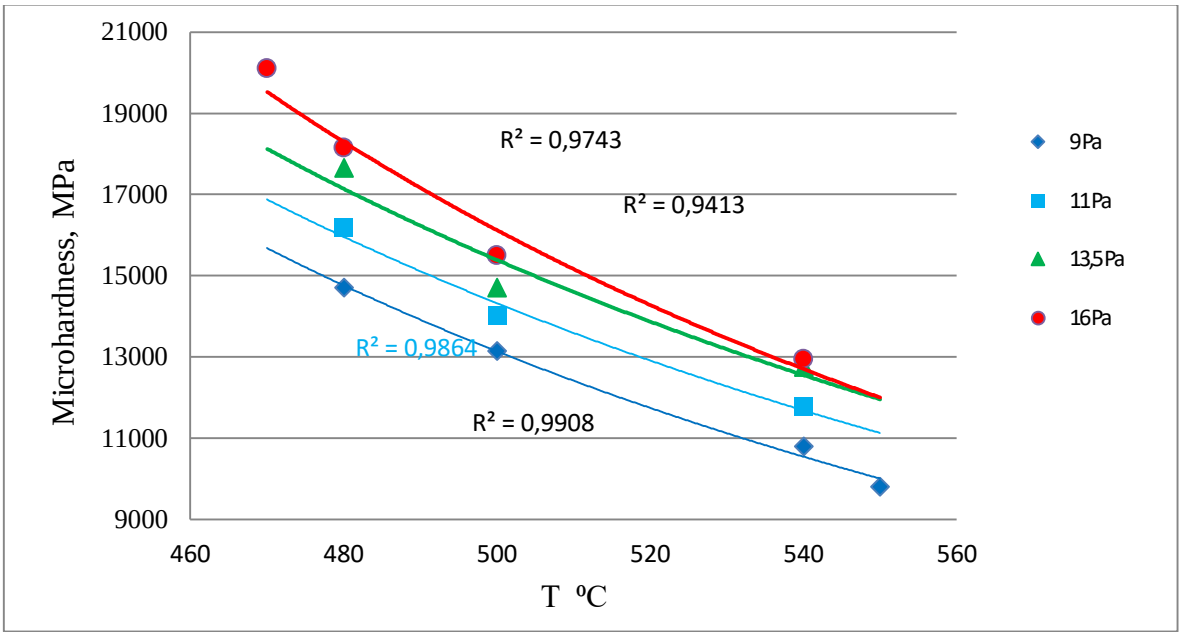

Figer 14. Graph of dependence of microhardness of Mo coatings on temperature at different values of pressure.

This character of the dependence of microhardness on the conditions of their deposition has an explanation related to the interaction of molybdenum carbonyl decomposition products with the growing coating and reactions in the gas phase described in works [2, 4]. Yes, in addition to the main reaction of thermal dissociation of molybdenum carbonyl:

$$Mo(CO)6 \rightarrow Mo+6CO \quad (1)$$

other reactions also occur:

$$CO \leftrightarrow CO_2+C \quad (2);$$

$$2Mo+CO \leftrightarrow MoO+MoC \quad (3);$$

$$Mo+CO \leftrightarrow MoO+C \quad (4);$$

$$Mo+2CO \leftrightarrow MoC+CO_2 \quad (5)$$

The rate of flow of the main reaction of thermal dissociation of molybdenum carbonyl increases with increasing temperature, while the equilibrium of reaction (2) shifts to the left with increasing temperature, which leads to a decrease in the degree of CO conversion. Since the change in hardness within wide limits during the production of metal coatings is primarily associated with their contamination with various impurities, the decrease in hardness of molybdenum coatings with increasing temperature can be explained primarily by the decrease in contamination of the coating with products of incomplete decomposition of molybdenum hexacarbonyl according to reaction (1) and respectively, by carbon according to reaction (2). The consequence of increasing the pressure in the gas phase, according to Le Chatelier's principle, will be a shift in the equilibrium of reactions (1), (3-5) to the right, which will lead to an increase in contamination of the molybdenum coating and an increase in its hardness.

A study of the abrasive wear resistance of Mo coatings with different hardness was conducted. The test was carried out with the supply of abrasive to the contact zone according to the Brinell scheme (II) under a load of 0,05 kN along a friction path of 60 m at a sliding speed of 0,78 m/s. Quartz sand fraction 0,25-0,4 mm was used as an abrasive. The counterbody was a "disc" made of polytetrafluoroethylene (fluoroplastic-4) with a diameter of 50 mm. The amount of wear was determined by the weight method with an accuracy of $1x10^{-4}$ g. To compare the wear of different

coatings, this study also used a sample with a galvanic coating of hard chromium, which is widely used as a strengthening and wear-resistant coating in friction pairs with different materials. In fig. 15 shows the graph of the dependence of wear of coatings depending on their hardness.

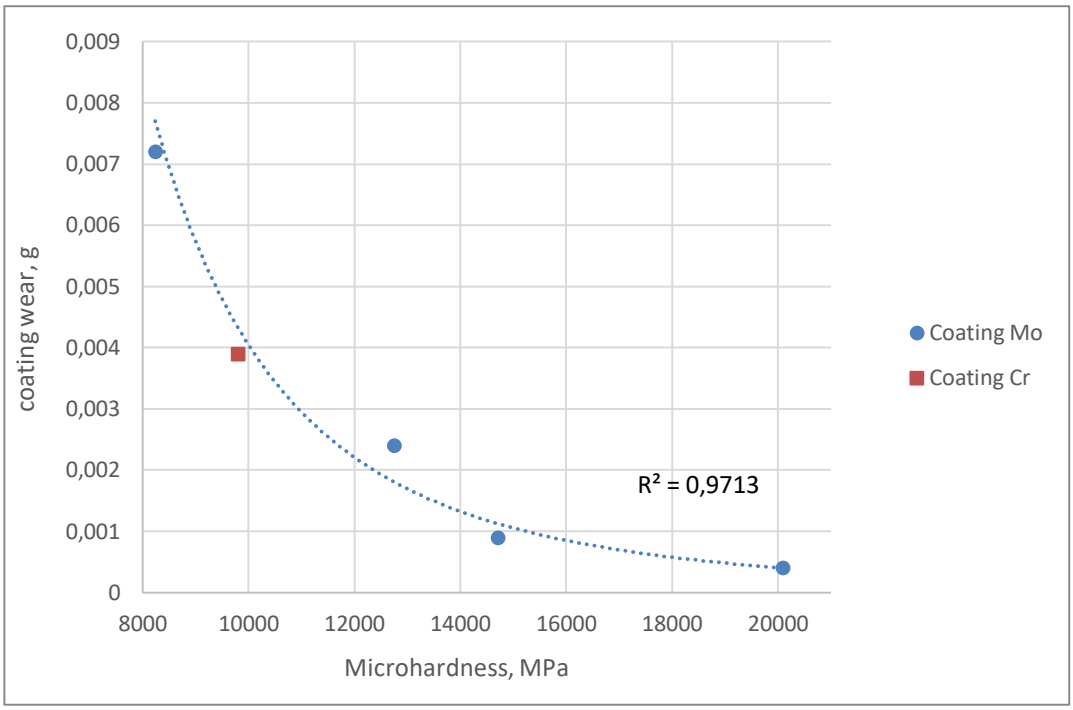

Figer 15. Dependence of wear of Mo coatings depending on their hardness.

The results of the study of the abrasive wear of Mo coatings depending on their hardness do not contradict the well-known fact that the wear resistance increases with the hardness of the coating. For this set of coatings, this dependence of wear on the value of microhardness can be fairly well approximated by the curve described by the equation $y = 4E+0.7x^{-3.321}$. The value of wear value for galvanic coating made of hard chrome, as can be seen from the graph, practically lies on the curve of dependence of wear of Mo coatings. If we take into account that the maximum hardness of galvanic hard chrome is at the level of 10790 MPa, then the wear resistance of Mo-C coatings under conditions of abrasive wear can be up to 10 times higher compared to hard chrome coatings.

The tribological properties of molybdenum coatings with a hardness of 17950 MPa and below were investigated in friction pairs with nitrided steel 20Cr3MoWV and with bronze VB-23NTS (Pd 18–22 %, Ni 3–4 %, Zn 3–4 %, Sb 3 –4 %, P 0.15–0.3).

To carry out tribological studies of gas-phase molybdenum coatings, samples were used that differed primarily in hardness and temperature of production (Table 3). The surface of the coatings after deposition and before conducting tribological studies was not subjected to any type of treatment.

Table 3.

Characteristics of Mo coatings for tribological research.

№	Substrate temperature, ℃	Pressure in the cell, Pa	$H\mu$, MPa	Notes
1	550	9	9810	Paired with bronze
2	540	13,5	12750	
3	480	13,5	17800	

4	Galvanic hard chrome		9810	
5	540	9	10790	Paired with steel
6	540	16	12950	
7	480	13,5	17950	

In fig. 16 presents the results of tribological studies of coatings under the numbers corresponding to the numbers in table 4.

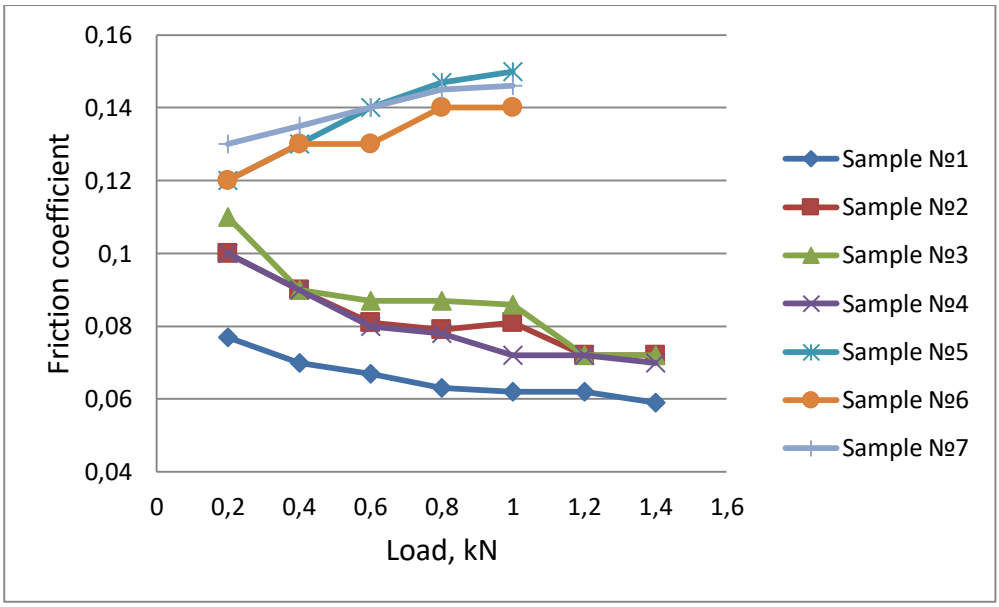

Figer 16. Dependence of the friction coefficient on the load for friction pairs Mo - bronze (samples No. 1 - No. 4) and Mo - nitrided steel 20Cr3MoWV (samples No. 5 - No. 7).

The conducted studies showed that the changes in the coefficients of friction Mo of coatings with nitrided steel 20Cr3MoWV and bronze VB - 23NTS with increasing load had the opposite character. Thus, if the friction coefficient of Mo with bronze decreased with increasing load, which usually occurs as a result of running-in of pairs in the process of testing to a certain stable value, then for the friction pair of Mo with steel, on the contrary, the coefficient of friction increased. In view of this, the maximum value of the load in the experiments for the Mo friction pair - nitrided steel 20Cr3MoWV was limited to 1 kN. The increase in the coefficient of friction of Mo with nitrided steel 20Cr3MoWV indicates insufficient time to reach a stationary mode of friction in these tests. This may be due to the use of samples with the original structure of the surface of the coatings without its preliminary treatment before the machining tests. The conducted studies did not reveal a certain dependence of the coefficients of friction of Mo coatings with nitrided steel 20Cr3MoWV on the hardness of the coating, and the value of the coefficients of friction itself was within the limits of the values indicated above for Mo coatings with higher hardness during tribological studies with other materials (Figs. 6-8).

The coefficients of friction in the friction pair of Mo with bronze for coatings with a hardness of 12750 MPa and 17800 MPa in the friction pair of Mo with bronze did not have a significant difference at a load of up to 1 kN, and at a higher load, they had the same value of 0.072. A noticeable decrease in the coefficient of friction in the entire range of loads was observed when testing a sample of Mo coating with a hardness of 9810 MPa, including, and compared to a chrome coating with the same hardness value.

The conducted experiments showed that in the studied range of conditions for applying molybdenum coatings, their hardness can vary from 9810 kgf/mm2 to 20100 MPa. For comparison, the hardness of hard chromium electrolytic coatings is 8825 -10890 MPa. A comparison of the

properties of molybdenum coatings with the characteristics of electrolytic coatings made of solid chromium, obtained under similar test conditions, showed that molybdenum coatings are not inferior to chromium coatings in terms of the friction value, can exceed them in hardness up to two times, and in terms of resistance to abrasive wear up to 10 times. If we take into account that "hexavalent" chromium (CrVI)) is among the most toxic substances that affect nature and human health, and its use is already limited by the European Union directive (RoHS) in the production of a large list of industrial products, then, according to the set of properties, molybdenum coatings can not only compete with electrolytic coatings made of solid chromium, as strengthening and tribological coatings, but also be considered as an alternative to chrome coatings in the environmental aspect.

The processes of thermal dissociation of tungsten carbonyl have many features in common with the processes of thermal dissociation of molybdenum carbonyl, except that they occur at higher temperatures. In fig. 17 presents a graph of the dependence of the growth rate of the tungsten coating on the temperature at different pressure values in the reaction volume.

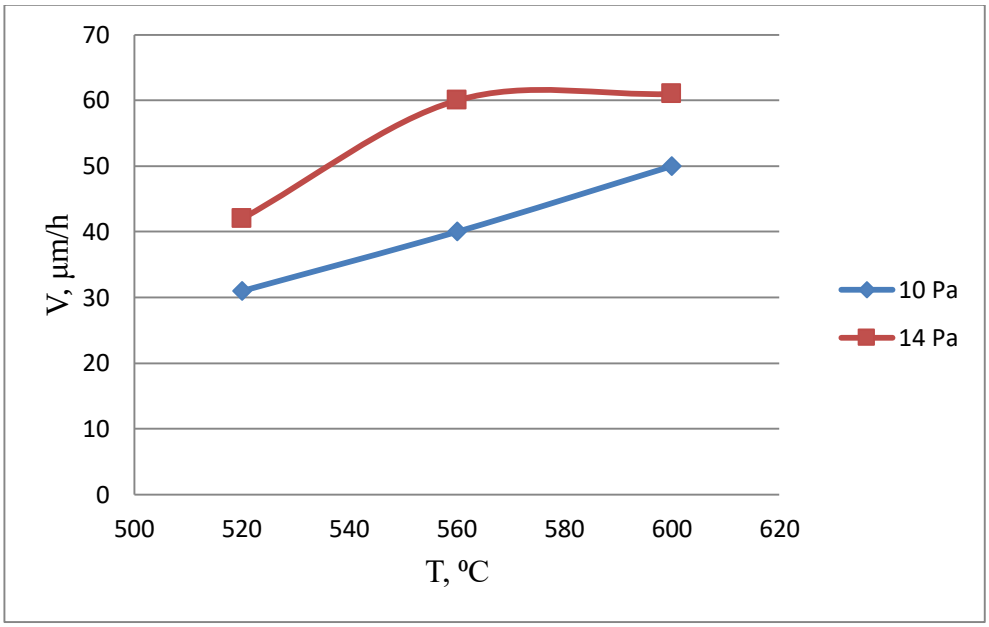

Figer 17. Dependence of the growth rate of W coatings on the deposition temperature at different pressure values.

As can be seen from the given graph, the growth rate of the coating in the studied range of parameter changes depends on both temperature and pressure in the reaction volume.

Studies of the surface morphology of CVD W coatings showed that in the studied range of process parameters at a deposition temperature of 520 ℃, the structure has the same regularities as for CVD Mo coatings.

The surface has a globular structure with a characteristic size of a single globule at the level of 1 - 4 microns, which form globular conglomerates with large sizes (Fig. 18). At higher temperatures (560-600 ℃), the surface of the coatings also has a globular structure with dimensions at the level of 1 μm, but without the formation of large conglomerates (Fig. 19).

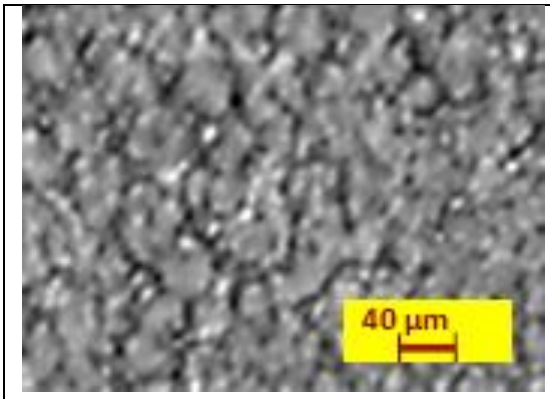

Figer 18. Surface structure of tungsten coating, T = 520℃

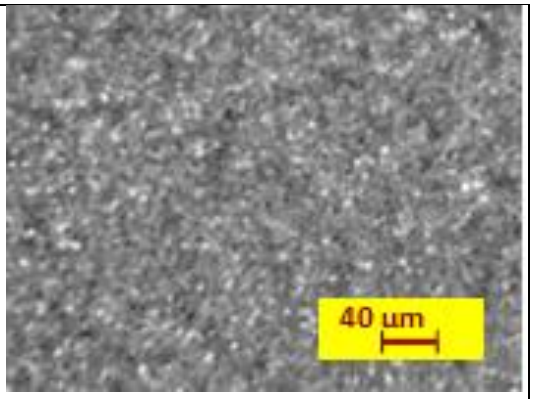

Figer 19. Surface structure of tungsten coating, T= 560℃.

At the coating growth temperature of 600 ℃ and 560 ℃, the grains in the form of columns have dimensions in diameter of 1 µm throughout the thickness of the coating. At a temperature of 520 ℃, grain boundaries are less visible, especially closer to the substrate.

In fig. 20 presents a graph of the dependence of the hardness of tungsten coatings obtained in different modes with approximation by curves corresponding to the power law.

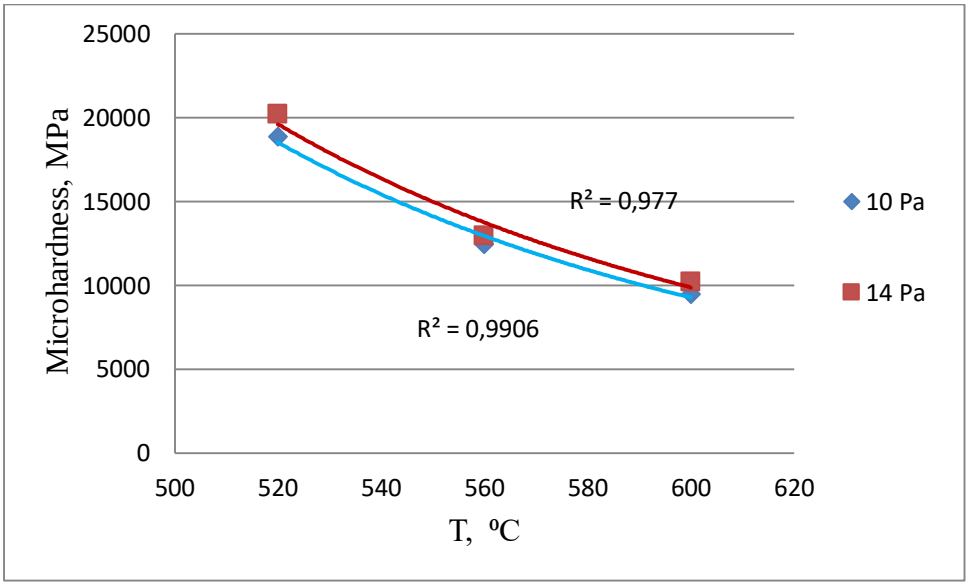

Figer 20. Dependence of the hardness of tungsten coatings on temperature at different pressure values in the reaction volume.

The obtained dependences of the hardness on the process parameters show that its values practically do not depend from the pressure in the reaction volume, but depend, first of all, on the temperature of the coating growth.

As with studies of tribological properties of molybdenum coatings, samples that differed in hardness and temperature were used to conduct tribological studies of gas-phase tungsten coatings with nitrided steel 20Cr3MoWV and bronze VB-24 (Table 4).

Table 4.

Characteristics of W coatings for conducting tribological studies*.

№	Substrate temperature,℃	Pressure in the cell, Pa	$H\mu$, MPa	E, ГПа
1	520	10	18880	441
2	560	10	12945	486
3	560	14	13090	470
4	560	14	13240	463
5	600	14	10400	516

*The hardness and Young's modulus of the coatings were determined using the MST3 scratch tester.

Table 5.

Values of coefficients of friction of gas-phase tungsten coatings with bronze VB-24 and with nitrided steel 20Cr3MoWV (in parentheses - values of coefficients of friction with nitrided steel 20Cr3MoWV).

№	The value of coefficients of friction under load P, kN				
	0,2	0,4	0,6	0,8	1,0
1	0,120 (0,110)	0,120 (0,115)	0,113 (0,120)	0,112	0,116
2	0,120 (0,108)	0,120 (0,120)	0,113 (↑)	0,107	0,104
3	0,130 (0,110)	0,120 (0,120)	0,113 (0,123)	0,107	0,118
4	0,130 (0,108)	0,120 (0,123)	0,113 (0,127)	0,137	0,120
5	0,130 (0,110)	0,120 (0,112)	0,113 (0,120)	0,105	0,100

The conducted tribological tests of samples with tungsten coatings did not reveal certain dependences of the value of the coefficients of friction on the modes of obtaining the coatings, as well as the values of their hardness and modulus of elasticity. The friction pair "tungsten-nitrided steel" showed relatively low values of the coefficient of friction at the first load with a load of 0,2 kN. As the load increased, the friction coefficients increased, and the friction pair with sample No. 2 at a load of 0,6 kN developed a burr (↑).

The "tungsten-VB-24" friction pair showed a decrease in friction coefficients in the case of an increase in load up to 0,6 kN. At the same time, if the friction coefficients for different samples had small differences at the initial load of 0,2 kN, then at subsequent loads of 0,4 kN and 0,6 kN, the friction coefficients for different samples completely coincided. At a load of 0,8 kN, a further decrease in the coefficient of friction was observed for samples, except for sample No. 4, and at a load of 1,0 kN, this trend was preserved only for samples No. 2 and No. 5, although their values no longer coincided in magnitude. The results of these tests show that in the friction pair of the tested samples with VB-24 bronze there is wear of the rubbing surfaces in the range of loads up to 0,6 kN with a corresponding decrease in the coefficient of friction.

At higher loads, an increase in the coefficient of friction was observed for several tested samples, which, in the process of operation of such a pair, could lead to the formation of burrs. This

may be due to the need for more time for the preliminary run-in of such pairs at lower loads and when working under conditions of higher loads.

The conducted studies confirmed the possibility of obtaining highly hard both Mo-C and W-C coatings at temperatures ≥ 480 °C, as well as obtaining new information about the tribological properties of such coatings in friction pairs with nitrided steel 20Cr3MoWV and bronzes VB 24, VB - 23NTS. The results of previously performed studies and studies in this work indicate the prospects of their use as reinforcements, to increase wear resistance and reduce the coefficient of sliding friction in friction pairs with different materials.

Elucidation of the possibility of practical application of such coatings as coatings of various functional purposes and in various conditions of their operation will require further research of a much larger volume and time to be carried out. Therefore, in order to speed up the obtaining of information about the possibility of practical application of such coatings in production, the process of applying Mo-C coatings to several types of parts of precision assemblies of JSC "Fed" products was carried out. In fig. 21 shows photos of details that were used during the development of the process of applying Mo-C coatings.

a

b

Figer 21. Details used in real designs of products of FED JSC: a – piston; b - stock .

The study of the characteristics of the Mo coatings obtained on the piston (Fig. 21a) in the optimized conditions of the process showed that the thickness of the coatings on the entire controlled surface did not exceed 10 % of the average value of 66 μm, and the microhardness was 15550 MPa with a deviation of about 5 %.

When molybdenum coatings were applied to the working surface of parts with a fairly simple geometry, such as a rod (Fig. 21b), even greater uniformity was achieved both in terms of thickness and microhardness. Thus, deviations in coating thickness did not exceed 2% of the average value of 40 μm, and the microhardness was 14810MPa with a deviation of up to 2.5% from this value.

The high uniformity of the coatings allows applying them with minimal tolerances and subsequent mechanical processing to size or grinding and polishing of the surface to a roughness of Ra < 0,08. Coatings have sufficient adhesion, withstand processing by felting and grinding without breaking the integrity or delamination, ensuring the necessary cleanliness of the processing of the coated surfaces.

The obtained parts with Mo-C coatings will allow testing them in accordance with the test program for these parts in force at the enterprise and determine the advantages or disadvantages of using such coatings, including the possibility and prospects of their use as an alternative to galvanic coatings made of hard chrome.

The results of the conducted research can be used in working out the technological foundations of the processes of applying metal and metal-carbide CVD coatings based on molybdenum and tungsten and serve as a basis for the development of industrial technologies for precision parts of aggregate and engine construction and mechanical engineering.

References.

1. Пауэлл К. Осаждение из газовой фазы / К. Пауэлл, Дж. Оксли, Дж. Блочер мл.. //Пер. с англ. //М.—Атомиздат.—1970.

2. Сыркин, В.Г. CVD-метод. Химическая парофазная металлизация: монография/В. Г. Сыркин. - М.: Наука, 2000. - 496 с.

3. K.L. Choy. Chemical vapour deposition of coatings. Progress in Materials Science 48 (2003) 57–170. https://doi.org/10.1016/S0079-6425(01)00009-3.

4. Конаков С. Технология микрореакторного осаждения тонких пленок и наноструктур – новый подход к исследованию процесса химического осаждения из газовой фазы. Наноиндустрия, в. №4/2017, стр. 76-82. DOI: 10.22184/1993-8578.2017.75.4.76.82.

5. Wen-Cheng J. Wei and Ming-Hung Lo. Processing and Properties of (Mo,Cr) Oxycarbides from MOCVD. Applied Organometallic Chemistry, v. 12, 201–220 (1998).

6. Douard A, Maury F. ets. Reactivity of $Cr(CO)_6$ in atmospheric pressure CVD processes for the growth of various metallurgical coating. Rev.Adv.Mater.Sci. 15(2007) 24-32

7. Иванов В.Е., Нечипоренко Е.П., Криворучко В.М., Сагалович В.В. Кристаллизация тугоплавких металлов из газовой фазы. М., Атомиздат, 1974.

8. Сагалович А.В. Композиционные материалы с покрытиями и их использование в высокотемпературных технологических процессах / А.В. Сагалович, С.Ф. Дудник, В.В. Сагалович. //Оборудование и инструмент. —2006. — т. 2.— С. 15— 16.

9. Сагалович А.В. Экспериментальные исследования покрытий типа *Avinit* / [А.В. Сагалович, А.В. Кононыхин, В.В. Попов и др.]. //Авиационно-космическая техника и технология. Технология производства летательных аппаратов.—2011.—т. 1.— С. 5-15. Sagalovych, A. V., Kononyhin, A. V., Popov, V. V., Dudnik, S. F., Sagalovych, V. V. (2011). Experimental investigations of "Avinit" type coatings. Aviatsionno-kosmicheskaya tekhnika i tekhnologiya, 3, 5–15. Available at: http://nbuv.gov.ua/UJRN/aktit_2011_3_3.

10. Sagalovych A. The Tribological Investigation of Multicomponent Multilayered Ion-plasma Coatings ***Avinit*** / [A. Sagalovych, V. Sagalovych, A. Kononyhin ea]. //Tribology in industry.—2011.—v 33.— No. 2.—P. 79-86. Available at: https://www.tribology.rs/journals/2011/2011-2/5.pdf.

11. Сагалович А.В. Нанесение покрытий на сложнопрофильные прецизионные поверхности газофазным методом (CVD) / [А.В. Сагалович, А.В. Григорьев, А.В. Кононыхин и др.]. //Физическая инженерия поверхности.—2011.—т. 9.—№ 3.—С. 229-236. Sagalovich, A. V., Grigor'ev, A. V., Kononyhin, A. V., Popov, V. V., Sagalovich, V. V. (2011). Nanesenie pokrytiy na slozhnoprofil'nye precizionnye poverhnosti gazofaznym metodom (CVD). Fizicheskaya inzheneriya poverhnosti, 9 (3), 229–236. Available at: http://dspace. nbuv.gov.ua/bitstream/handle/123456789/76903/04-Sagalovich.pdf? sequence=1

12. Sagalovych A. Mo-C multilayered CVD coatings / [A. Sagalovych, V. Sagalovych]. // Tribology in industry.—2013.—v 35.— No. 4.—P. 219-227. //.Sagalovych, A., Sagalovych, V. (2013). Mo-C multilayered CVD coatings. Tribology in industry, 35 (4), 261–269. Available at: https://www.tribology.rs/journals/2013/2013-4/2.pdf Available at: https:// 1library.org/document/oy89d3wq-mo-c-multilayered-cvd-coatings.html.

13. Сагалович В.В., Дудник С.Ф., Кірюхін М.М., Чернов А.М., Забашта Л.О. та ін. Створення корозійно-стійкого малотонажного багатофункціонального обладнання для хіміко-фармацевтичних виробництв II. Вивчення корозійної стійкості конструкційних сталей з металевими покриттями при синтезі лікарських засобів. Вісник фармації, № 1-2, 1994, сс. 47-50.

14. Дудник С.Ф. Применение металлических покрытий для защиты от коррозии в водородсодержащих середах / [С.Ф.Дудник, А.В. Сагалович, В.В. Сагалович и др.]. // Вестник Харьковского политехнического университета" (Новые решения в современных технологиях). — 2001. — в. 14. С. 237 — 250..

15. Сагалович О.В. Розробка і впровадження в фармацевтичне виробництво сучасних технологій, обладнання і оснастки. / [О.В. Сагалович, В.В. Сагалович, А.М. Чернов та ін.].

//Фармація України. Погляд у майбутнє.—Матеріали VII Національного з'їзду фармацевтів України.—Харків.—15–17 вересня 2010.—т. 1.— С. 207-208.

16. Sagalovych, A., Popov, V., Sagalovych, V., Dudnik, S., Popenchuk, R. (2020). Development of the chemical vapor deposition process for applying molybdenum coatings on the components in assembly and engine construction. Eastern-European Journal of Enterprise Technologies, 2 (12 (104)), 6–15. doi: https://doi.org/10.15587/1729-4061.2020.201540

17. Popov V., Sagalovych A., Sagalovych V. Improving the performance, reliability and service life of aviation technology products based on the innovative vacuum-plasma nanotechnologies for application of ***Avinit*** functional coatings and surfaces modification: monograph / Sagalovych V. (Ed.). Tallinn: Scientific Route OÜ, 2020. 102 p. doi: https://doi.org/10.21303/978-9916-9516-1-3.

18. Sagalovych, A., Sagalovych, V., Popov, V., Dudnik, S.; Sagalovych, V. (Ed.) (2021). Vacuum-plasma multilayer protective coatings for turbine blades. Tallinn: Scientific Route OÜ, 91. doi: https://doi.org/10.21303/978-9916-9516-5-1.

19. Sagalovych A., Sagalovych V., Popov V., Dudnik, S. Olijnyk A; (2021). ***Avinit*** vacuum-plasma technologies in transport machine building. Tallinn: Scientific Route OÜ. doi: https://doi.org/10.21303/978-9916-9516-7-5.

Nano-tailored morphology of La2NiO4+δ thin films using PI-MOCVD

Alexander Stangl *[a], Adeel Riaz [a], Laetitia Rapenne [a], Silvère Panisset [a], Mónica Burriel [a] and Carmen Jiménez[a]

[a] *Univ. Grenoble Alpes, CNRS, Grenoble INP, LMGP, 38000 Grenoble, France*

The morphology is a key parameter in the performance optimisation of thin film electrodes for micro solid oxide cells, where surface reactions are limiting the overall activity. We will show, that the pulsed-injection (PI) MOCVD growth technique gives access to different growth regimes by changing the deposition temperature, leading to distinct microstructures.

In this study, we have selected La2NiO4+δ (L2NO4), a very promising cathode material for intermediate and low temperature solid oxide cell applications, due to its good electronic and ionic conductivity, paired with its high oxygen exchange activity with a low activation energy. Oxygen incorporation and transport in La2NiO4+δ thin films is limited by surface reactions. Hence, tailoring the surface morphology allows to significantly enhance the electrode performance.

Thin film samples were synthesized by PI-MOCVD on different single crystal substrates with thicknesses ranging between 33 and 2000 nm. The microstructure was thoroughly characterised by SEM, TEM and XRD. By varying the deposition temperature (600 - 750 °C) we were able to tune the morphology of the films. In agreement with the structure zone model, originally developed for metallic thin films, we obtained a nano-columnar microstructure, with open porosity and a significantly enlarged specific surface area by reducing the deposition temperature. On the other hand, a dense microstructure prevails at higher temperatures. A multi-step growth process enables complex hetereo-microstructures, e.g. a nano-columnar structure rooted in a dense bottom layer, serving as electronic and ionic conduction pathway, or capped nano-porous films with largely increased oxygen storage capacity.

This research is completed with the analysis of electrode performance of derived thin films by electrical conductivity relaxation measurements. We studied the effect of different microstructures and found remarkably enhanced surface activity in thicker, nano-architectured films, as compared to thin, dense ones. As we will show, this can be understood in large parts due to the increase of the exposed surface area.

Overall, the growth of nano-architectured La2NiO4 thin film cathodes by PI-MOCVD resulted in a substantial enhancement of the oxygen exchange activity and opens up a new route towards the optimisation of electrode materials for intermediate to l
ow temperature devices.

References

1. Stangl , J. Mater. Chem. A 10, 2528-2540 (2022) https://doi.org/10.1039/D1TA09110G

* *Corresponding author e-mail: carmen.jimenez@grenoble-inp.fr*

Impact of precursor reactivity on growth of self-assembled 3D architectures

Mario Ziegler[a,*], David Zanders[b], Valentin Ripka[a], Hanjörg Wagner[a], Anjana Devi[b], Uwe Huebner[a]

[a] *Leibniz Institute of Photonic Technology Jena (IPHT), Albert-Einstein-Str. 9, 07745 Jena, Germany*
[b] *Inorganic Materials Chemistry, Ruhr University Bochum, Universitätsstr. 150, 44081 Bochum, Germany*

For most light-driven catalytic applications, large surface areas are favourable and can be realized for instance in complex 3D architectures. The fabrication of 3D nanostructures is still challenging by using classical microfabrication processes. Here, self-assembly approaches offer the opportunity to fabricate sophisticated 3D nanostructures with superior properties without the need for several, complex process steps or expensive lithography tools. By doing so, sophisticated structures such as nanoparticles, nanoflowers or nanopillars are easily manufacturable with good quality and controllability on a large scale. Typically, atomic layer deposition (ALD) or chemical vapor deposition (CVD) processes are not the methods of choice as these techniques are dedicated to 2D layer depositions and are in need for a 3D scaffold to generate 3D structures.

In contrast, metastable ALD (MS-ALD) enables to fabricate complex 3D nanostructures exploiting a self-assembly approach without the need for pre-structured or pre-defined 3D substrates (Fig. 1 a). In our recently established approach, a planar silver layer is oxidized in the ALD reactor to a metastable silver oxide and subsequently decomposes to elemental silver and reactive oxygen. So, the silver acts as a time-limited precursor container and to favourable side-reactions, resulting in 3D architectures such as porous sponges, nanoparticle like structures or nanowires [1]. The morphology of the structures can easily be adjusted by tuning the respective parameters of the ALD process. In an already established MS-ALD process, the resulting structures consisted of silver nanoparticles and silica originating from the silver template and the ALD of silica (AgNP@SiO_2), respectively. Optical optimized structures revealed high performance absorption characteristics above 99.5 % over a broad wavelength range from 220 nm up to 4000 nm. This offers the opportunity for applications in stray light reduction, water evaporation systems to generate fresh water [2] or photo thermoelectric power generation [3].

Nevertheless, so far optimized structures were only investigated using the ALD of silica to generate AgNP@SiO_2. This material combination is not applicable for industrially relevant catalytic applications such as plasmon-induced water splitting or direct solar-driven energy conversion due to the dielectric function of the silica. Consequently, the non-conductive scaffold SiO_2 has to be substituted by conductive layers such as titania (TiO_2) or zinc oxide (ZnO) to fabricate AgNP@TiO_2 or Ag-NP@ZnO nanostructures. As precursors TTIP, DEZ and $Zn(DMP)_2$ [4] were used (Fig. 1 b-d). Structures generated using DEZ exhibited nanoparticle-like structures and no favourable 3D structure, which was associated with the too high reactivity of DEZ. We found that the side-reactions were dependent on the reactivity of the first precursor. The DEZ reactivity led to a coverage of the silver layers and thus, supressed the formation of metastable silver oxide, which is crucial for the self-assembled formation of the 3D architectures. $Zn(DMP)_2$ reveals a slightly lower reactivity compared to DEZ and stability, which facilitated the controllability within the MS-ALD process. By doing so, elevated sponge-like structures were fabricated. So far optimized structures revealed absorptions efficiencies in visible spectra of 94 % and 80 % in near infrared (Fig. 2).

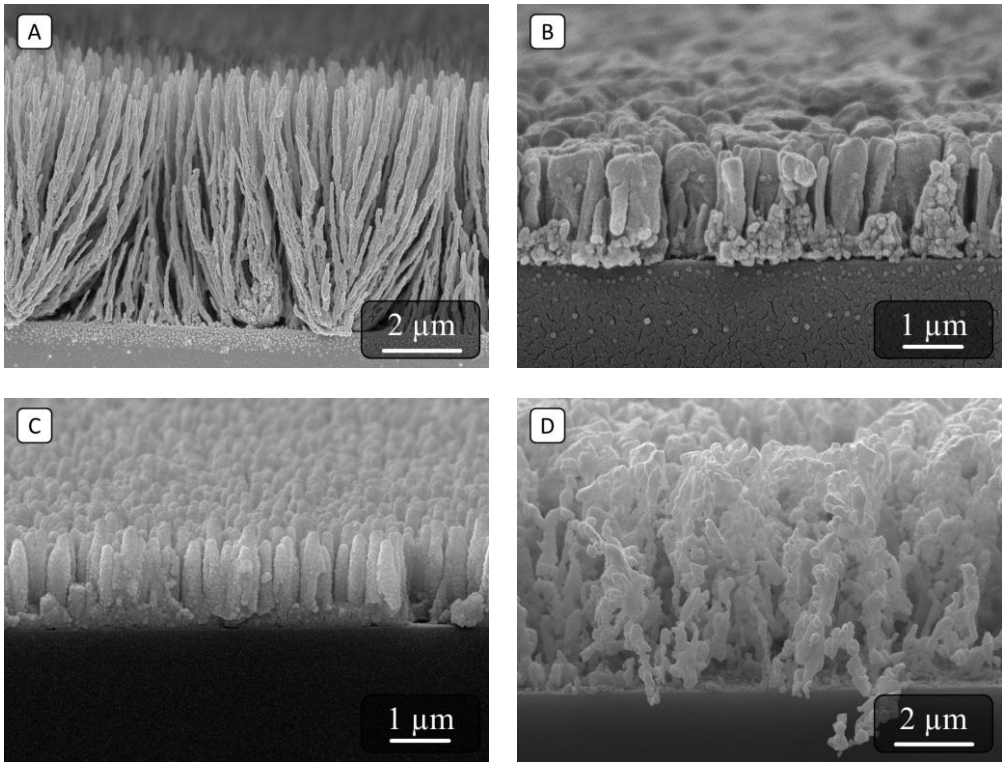

Fig. 1: SEM cross section images of 3D structures generated using different precursors: a) TDMAS, b) TTIP, c) DEZ and d) Zn(DMP)2

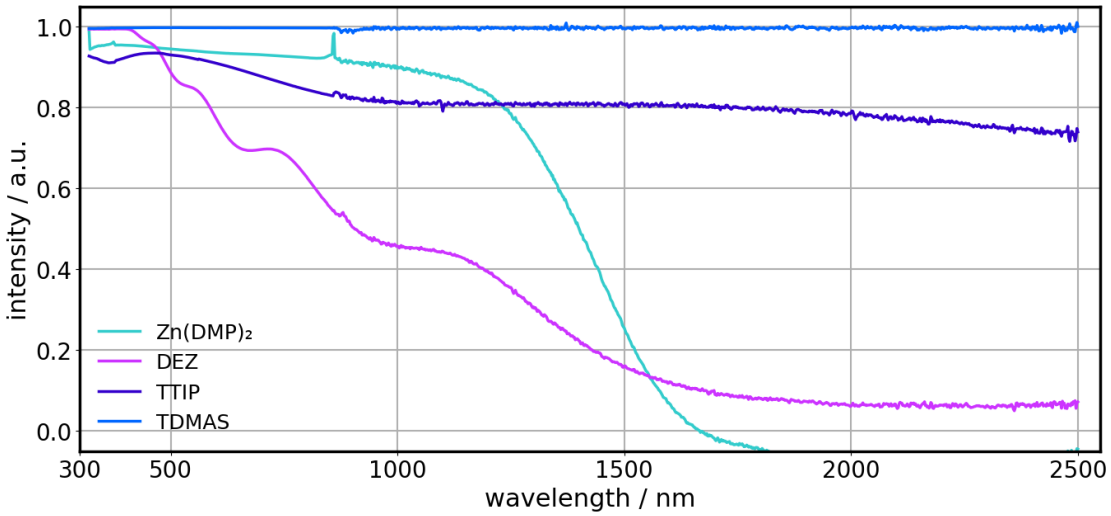

Fig. 2: Absorption spectra of so structures generated using DEZ, TTIP and Zn(DMP)2 in comparison to high performance MS-ALD structures using TDMAS.

References

1. Ziegler, M., Thamm, S., Stolle, H. L. K., Dellith, J., Hübner, U., Wang, D. & Schaaf, P. *Applied Surface Science* **514**, 145770 (2020).
2. Cheng, P., Ziegler, M., Ripka, V., Wang, D., Wang, H., van Aken, P. A. & Schaaf, P. *Applied Materials Today* **25,** 101238 (2021).
3. Cheng, P., Ziegler, M., Ripka, V., Wang, H., Pollok, K., Langenhorst, F., Wang, D. & Schaaf, P. *ACS applied materials & interfaces* **2022**.
4. Mai, L., Mitschker, F., Bock, C., Niesen, A., Ciftyurek, E., Rogalla, D., Mickler, J., Erig, M., Li, Z., Awakowicz, P., Schierbaum, K. & Devi, A. *Small* **16,** e1907506 (2020).

* *Corresponding author e-mail:* mario.ziegler@leibniz-ipht.de

Conformal and superconformal chemical vapor deposition of silicon carbide coatings

Jing-Jia Huang[a,b,*], Christian Militzer[b], Charles A. Wijayawardhana[a,b], Urban Forsberg[a], Henrik Pedersen[a]

[a] *Department of Physics, Chemistry and Biology, Linköping University, Linköping, SE-58328, Sweden*
[b] *SGL Carbon GmbH, Drachenburgstraße 1, Bonn, DE-53170, Germany*

Conformal and superconformal growth of silicon carbide (SiC) coatings on structured graphite substrates has been achieved by both continuous and pulsed chemical vapor deposition (CVD) at a total pressure of 1 kPa and at temperatures between 950 °C and 1200 °C using silicon tetrachloride ($SiCl_4$) and ethylene (C_2H_4) as the precursors. Several approaches to conformal growth via continuous CVD have been reported in the work of Abelson and Girolami [1], albeit with focus on film deposition at low temperatures (200 – 300 °C), low pressures (10 – 10^{-8} Pa), and primarily for electronic applications. In the current study, we extend their concepts of conformal CVD to depositions that are performed at elevated temperatures and a moderate pressure, which is commonly utilized in hard coating CVD processes, e.g., SiC.

Step coverage (SC), which is defined as the ratio of the growth rate at the lower sidewall near the bottom of a recessed feature to that at the upper sidewall near the opening, is a conventional way to assess the coating conformality. SC < 1 denotes a non-conformal coating, whereas SC =1 and SC > 1 indicates a conformal and a superconformal coating, respectively. With the continuous CVD, we were able to improve the conformality of SiC coatings in a trench with a width-to-depth ratio of 3.3 from nearly conformal (SC= 0.98) to superconformal (SC= 2.6) by reducing the deposition temperature, increasing the partial pressure of $SiCl_4$ and a minute addition of hydrogen chloride (HCl) as a growth inhibitor [2]. Surprisingly, with the pulsed CVD, where the precursors were pulsed alternately into the growth chamber and were separated by a hydrogen (H_2) purge gas, the deposited coatings exhibited SCs between 3.75 and 9 at 1200 °C. At this temperature, the continuous CVD only resulted in non-conformal SiC coatings [3].

The primary factor leading to improved conformality in the SiC growth by the continuous CVD is reported to be the reduction of the surface reaction probability, β. A reduced β can be realized either by decreasing the deposition temperature or by the surface-site blocking effect. In the current study, the latter was achieved by increasing the precursor partial pressure or by adding HCl as a growth inhibitor. In terms of the SiC growth by the pulsed CVD, the high degree of conformality at elevated temperatures was assumed to be a result of enhanced inhibition effect due to a much higher surface coverage of Cl species during the $SiCl_4$ pulse. On the other hand, the pronounced superconformal growth seen in the pulsed CVD process may originate from a stronger inhibition effect close to the opening of the trench because the HCl producing from the SiC growth reaction at the bottom would diffuse upwards, leading to an increase of HCl partial pressure at the upper part of the trench, and therefore a stronger inhibition effect was resulted.

Our findings in improving the SiC coating conformality at elevated temperatures and a moderate pressure could potentially benefit numerous hard coating CVD processes using chlorinated precursors because these coatings are often deposited under such conditions.

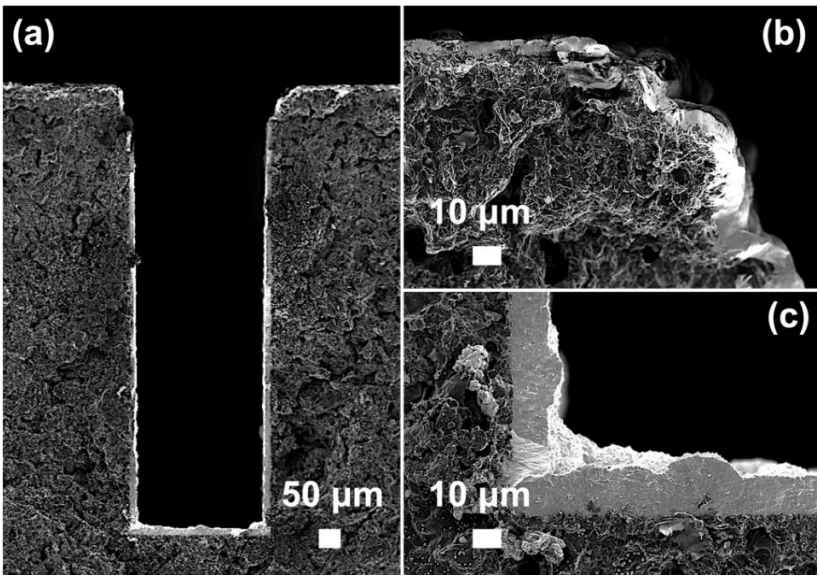

Figure 1. The cross-sectional SEM micrographs of the overall view (a), upper (b) and lower corner (c) of a SiC coated trench with a width-to-depth ratio of 3.3. The SiC coating was deposited by continuous CVD at 950 ℃ and 1 kPa with p_{SiCl_4}= 20 Pa, $p_{C_2H_4/SiCl_4}$= 1 and $p_{added\ HCl}$= 10 Pa [2].

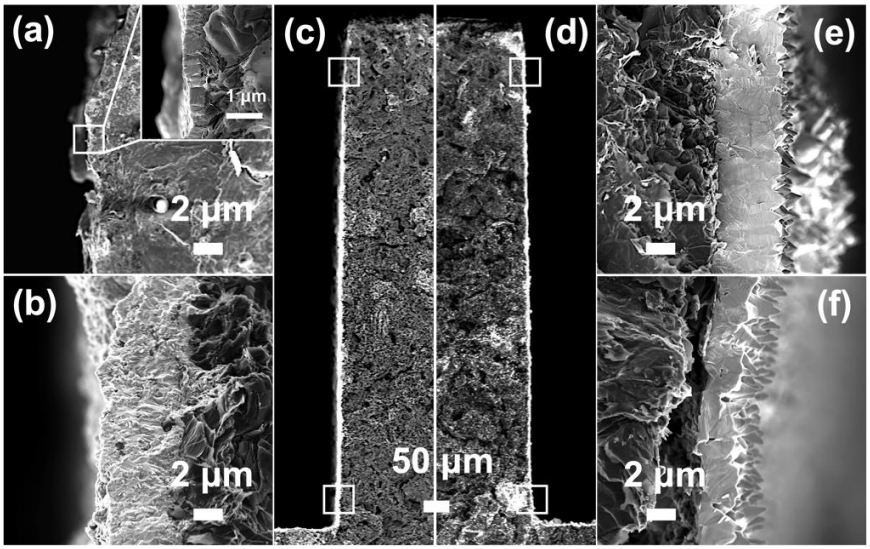

Figure 2. The cross-sectional SEM micrographs of two SiC coated trenches with a width-to-depth ratio of 4 by continuous CVD (a)(b)(c) and pulsed CVD (d)(e)(f). (c)(d) are the overall views of the deposited trenches, and (a)(e) and (b)(f) are the upper and lower sidewalls, respectively. The sample prepared via continuous CVD was deposited at 1200 ℃, 1 kPa with p_{SiCl_4}= 20 Pa, $p_{C_2H_4/SiCl_4}$= 1 and $p_{added\ HCl}$= 0. Although the sample prepared via pulsed CVD was deposited in the same ambient conditions, the precursors were pulsed alternately into the growth chamber and were separated by a H_2 purge [3].

References

1. J. R. Abelson and G. S. Girolami, J. Vac. Sci. Technol. A **38**, 030802 (2020)
2. J.-J. Huang, C. Militzer, C. Wijayawardhana, U. Forsberg and H. Pedersen, J. Vac. Sci. Technol. A **40**, 053402 (2022)
3. J.-J. Huang, C. Militzer, C. Wijayawardhana, U. Forsberg and H. Pedersen, ChemRxiv (2023). This content is a preprint and has not been peer-reviewed.

* *Corresponding author e-mail:* Jing-Jia.Huang@liu.se

Encapsulating TiO_2 thin films grown via Atomic Layer Deposition for biocompatible UV-activated neuronal interfaces

Naida El Habra[a,*], Alessia Famengo[a], Giacomo Sagrini[b], Patrizia Canton[b], Stefano Boldrini[a], Alberto Ferrario[a], Alessandro Galenda[a], Marta Maria Natile[c], Cinzia Sada[d] Alessandro Leparulo[e], Marta Maschietto[e], Maria Losurdo[a], Stefano Vassanelli[a, e]

[a]*Institute of Condensed Matter Chemistry and Technologies for Energy, National Research Council (ICMATE-CNR), Corso Stati Uniti 4, Padova, 35127, Italy*

[b]*Department of Molecular Sciences and Nanosystems, Ca' Foscari University of Venice, 30170, Venezia-Mestre, Italy*

[c]*Institute of Condensed Matter Chemistry and Technologies for Energy, National Research Council (ICMATE-CNR), c/o Department of Chemical Sciences, University of Padova, via F. Marzolo 1, Padova, 35131, Italy*

[d]*Department of Physics, University of Padova, Via F. Marzolo 8, Padova, 35131, Italy*

[e]*Department of Biomedical Sciences, University of Padova, via F. Marzolo 3, Padova, 35131, Italy*

The development of smart implantable medical devices, focused to neuro-stimulation and/or recording with high resolution and long-term neuronal activity, are gaining a powerful importance in Neuroscience, aiming to a deep study of cerebral functions and in the treatment for neurodegenerative diseases, which are closely linked to an increase in the number of elderly people. Alzheimer, senile dementia, Parkinson's movement disorders, and other dyskinetic pathologies are constantly increasing and strongly connected to age, slowly evolving, characterized by a progressive and irreversible degeneration of neuronal system [1]. Others, such as epilepsy, cerebral stroke, and spinal injuries have recently encountered important and powerful advances in neurostimulation for therapy and rehabilitation. Currently, there are no specific therapies with a heavy impact on caregivers, health, and care system [2,3]. However, in the recent years, neurostimulation has gained more and more importance as a complementary approach or, in some cases, replacement of drug treatments. In the wider framework of bioelectronics, the present work tackles the urgent need of miniaturized interfaces between living and artificial systems (neuronal cell/CMOS-based specimen), consisting of highly biocompatible materials for applications in smart biosensors, characterized by long-term endurance and stability to mimic as better as possible the natural interaction with the native organ to restore functionality (*neurobiohybrids*) [4,5]. Specifically, thanks to the exploitation of Nanotechnology, the proposed research aims to understanding the ALD potentialities for downscaling synthesis of highly conformal and biocompatible dielectric TiO_2 thin films, both focusing the attention on material biocompatibility at neuron/biomaterial interface, as well as satisfying the dielectric properties of the interfaces. The deposition and characterization of nanostructured dielectric TiO_2 coatings via Low Pressure-ALD (LP-ALD) with a controlled composition, structure, and conformality have been carried out. The control of all the film properties combined with the development of an easy UV surface functionalization protocol to induce highly wettable and encapsulating surfaces was of crucial importance for the response of the prototype titania interfaces to be tested. Wettability, biocompatibility, preliminary electrochemical, and electrophysiological behavior of the materials were analyzed. Moreover, the optical properties of the grown thin films were analyzed by spectroscopic ellipsometry to infer porosity and photoactive defects that can also play a role in biocompatibility.

Aiming to evaluate the functional biomedical applications of the ALD-deposited TiO_2, neuronal biocompatibility *in-vitro* tests were probed. In this regard, to study the influence on cell adhesion, growth, and progress, the simple surface functionalization method by using UVC radiation has been developed obtaining highly wettable surfaces. *In-vitro* neuronal biocompatibility of the encapsulating titania was tested by plating rat hippocampi neurons and monitoring their development and morphology in culture before and after UV exposure. TiO_2 thin films subjected to UV pre-treatment were highly biocompatible: neurons displayed a development and morphology comparable to neurons seeded on standard Petri dishes. To establish the efficacy of the capacitive behavior of the deposited prototypes, a preliminary electrochemical characterization was carried out in Simulated Body Fluid (SBF) solutions at physiological temperature and pH. The electrochemical characterization was also preliminary investigated as function of surface wettability of titania surfaces. TiO_2 thin films demonstrated a non-faradaic range and a cathodic threshold voltage, which were suitable for an implantable electrode, together with high dielectric constant, *k*, of primary importance for capacitive communication devices.

Electrophysiological studies, through patch-clamp protocol, demonstrated a great action potentials and activity passive properties, like resting potential ($V_{resting}$), much closer to physiological values for neurons on UV-exposed TiO_2 deposits. The investigated neuron passive properties differ greatly in relation to the presence or absence of the UV exposure, showing a difference in the maturation of the neurons, characterized by an enhanced neuronal compatibility on UV treated-TiO_2 surfaces.

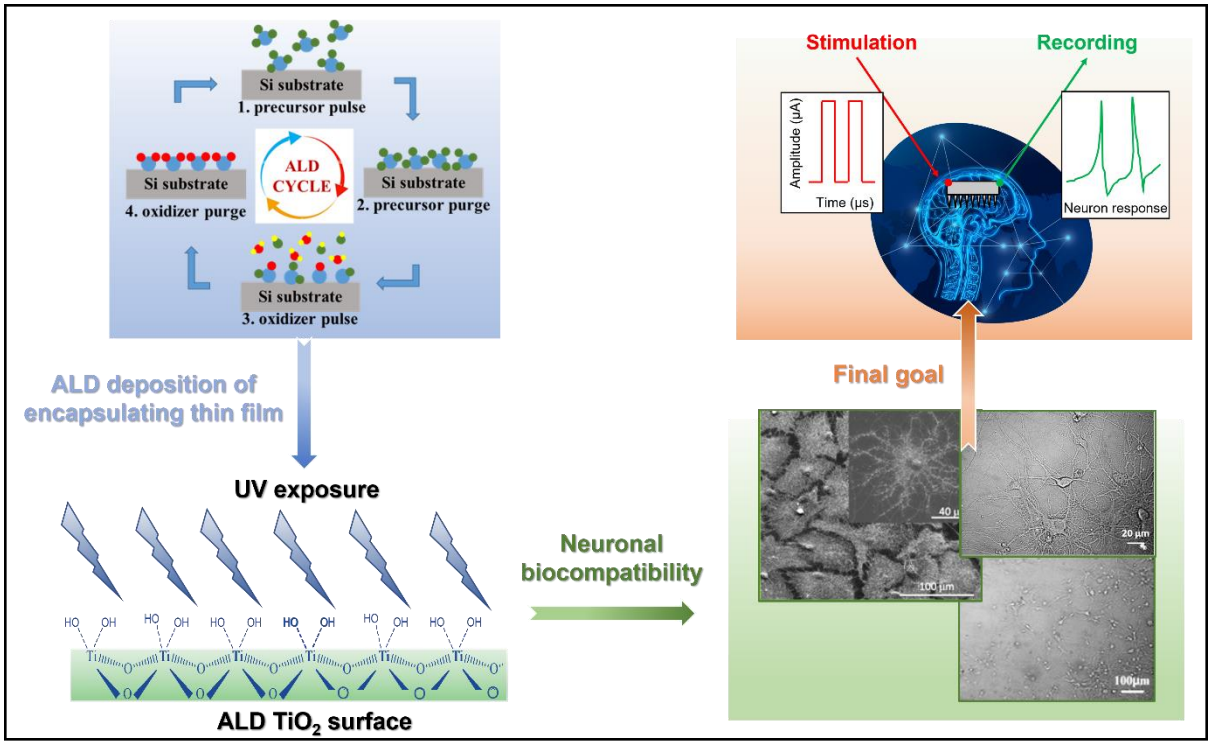

Figure 1. Schematic representation of the developed process.

References

1. J. Rivnay, H. Wang, L. Fenno, K. Deisseroth, G.G. Malliaras, Sci. Adv. **3**, e1601649 (2017).
2. D. Rozgic, V. Hokhikyan, W. Jiang, I. Akita, S. Basir-Kazeruni, H. Chandrakumar, D. Markovic, IEEE Trans. Biomed. Circuits Syst. **13**, 38 (2019).
3. R. Bhimani, Rehabil. Res. Pract. article ID 718527 (2014).
4. S. Vassanelli, M. Mahmud, Front Neurosci. **10**, article 438 (2016).
5. R. Thewes, G. Bertotti, N. Dodel, S. Keil, S. Schroder, K.H. Boven, G. Zeck, M. Mahmud, S. Vassanelli, IEEE International Symposium on Circuits and Systems; Conference paper 1826 (2016).

* *Corresponding author e-mail:* naida.elhabra@cnr.it

Synthesis of graphene nanoribbons *via* atmospheric-pressure CVD: understanding the process parameters roles with help of spectroscopic methods

Vasilii Osipov*, Philipp Weitkamp, Max Reimer, Yi Han, Klaus Müllen, Dirk Hertel and Klaus Meerholz

University of Cologne, Chemistry department, Greinstr. 4-6, Cologne, 50939, Germany

Graphene nanoribbons (GNRs), i.e. quasi one-dimensional stripes of graphene with typical widths of several carbon atoms and lengths in range of 10 nm – 100 nm, are an interesting class of materials for various applications due to their tuneable electronic structure depending on nanoribbon width, edge type, and (in case of doped GNRs) dopant nature [1]. *Inter alia*, GNRs look promising as templating substrate for ordered growth of organic semiconductor (OS) molecules that are deposited on top. The state-of-the-art methods of GNRs synthesis are bottom-up processes involving polymerization of precursor molecules, which determine the core structure of the GNRs being synthesized, atop catalytic surfaces (commonly crystalline gold), and are typically performed either under ultra-high vacuum (UHV) conditions [2, 3] or by atmospheric pressure chemical vapor deposition (APCVD) technique [4]. Despite leading to GNR layers of reduced quality, the APCVD method, compared to the UHV one, possesses the advantages of simplicity and better scalability, which makes it a promising option for testing new types of precursors and developing corresponding routes of GNRs synthesis.

This work is aimed at gaining a better understanding of the GNRs synthesis by APCVD and gaining insights into how the process parameters influence the product for further optimization of the process. For that, we focus on one of the best-described GNRs synthesis routes, 7-atoms-wide armchair-type GNRs (7-ANGRs) made from the precursor 10,10′-dibromo-9,9′-bianthracene (DBBA) and control the results through mass- and Raman spectroscopy. Eventually, this effort may contribute to the development of CVD-based synthesis of 2D functional materials useful for modern organic electronics.

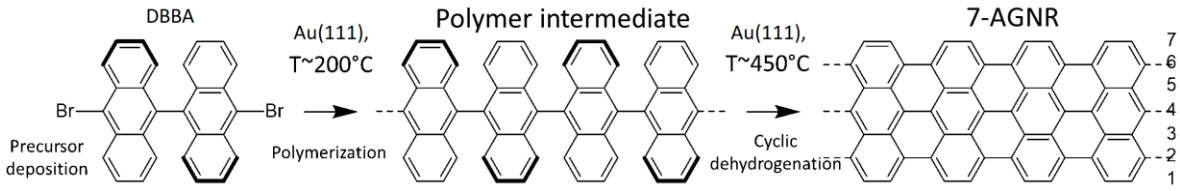

Fig. 1. Scheme of the 7-AGNRs synthesis from DBBA via on-surface catalytic reaction

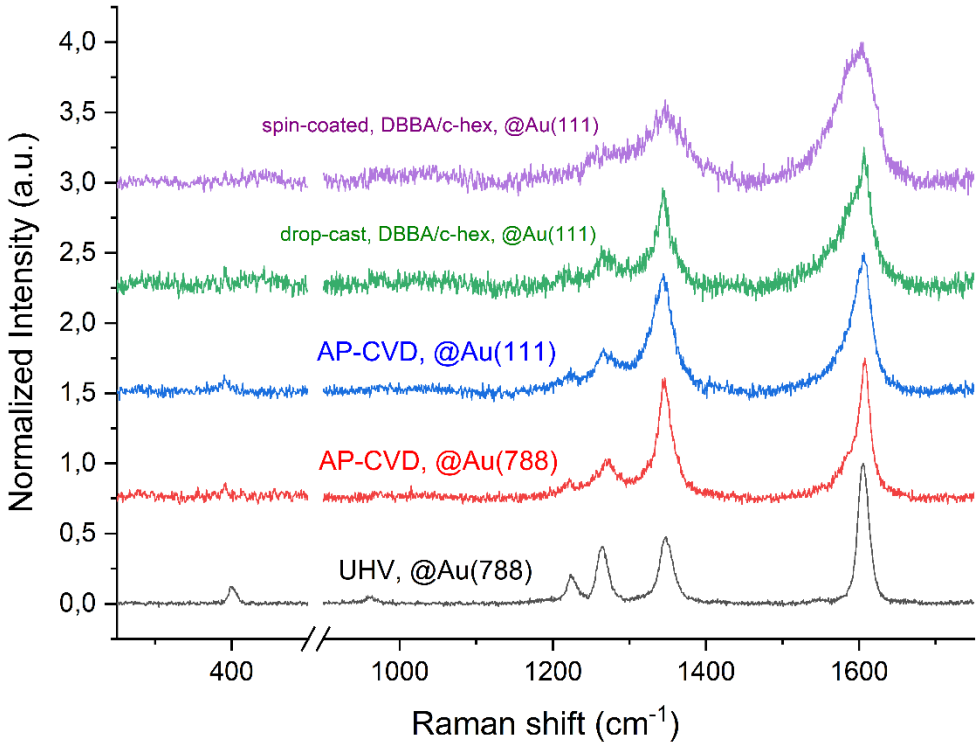

Fig. 2. Raman spectra of 7-AGNRs@Au(111) produced by AP-CVD and 7-AGNRs@Au(788) by UHV showing the characteristic peaks

References

1. R. S. Koen Houtsma, J. de la Rie and M. Stöhr, Chem. Soc. Rev. **50,** 6541-68 (2021)
2. G. Borin Barin *et al.*, ACS Appl. Nano Mater. **2**, 2184−92 (2019)
3. B.V. Senkovskiy *et al.*, Nano Lett. **17**, 4029–37 (2017)
4. Z. Chen *et al.*, J. Am. Chem. Soc. **138**, 47, 15488–96 (2016)

* *Corresponding author e-mail:* vosipov1@uni-koeln.de

Enhancing corrosion protection properties of steel by phase control of CVD processed ZrO_2 films

Jean-Pierre Glauber*[a], Sebastian M.J. Beer[a], Diane Samélor[b], Johannes Etzkorn[c], Aleksander Kostka[d], Constantin Vahlas[b], Anjana Devi[a]

[a] *Inorganic Materials Chemistry, Ruhr University Bochum, Bochum, 44801, Germany*
[b] *CIRIMAT - CNRS, Université de Toulouse, Toulouse Cedex 4, France*
[c] *Chemistry and Materials Engineering, Fachhochschule Dortmund, 44139 Dortmund, Germany*
[d] *Center for Interface Dominated Materials (ZGH), Ruhr University Bochum, 44801 Bochum, Germany*

Zirconium dioxide (ZrO_2) is an attractive material for protective coatings due to its low thermal conductivity, high erosion resistance, high thermal robustness, and mechanical strength. Furthermore, ZrO_2 features a thermal expansion coefficient that is similar to many metals which makes it an appealing material for thermal barrier coatings.[1] In addition, the great inertness towards extreme pH and oxidation environments of cubic ZrO_2 also enables its use as corrosion protection coatings (CPC).[2]

Growth of ZrO_2 via chemical vapor deposition (CVD) method features advantages that are important for protective coatings such as conformal film growth on large and complex substrate geometries while allowing a precise structure control.

Although, there are several reports on CVD processes of ZrO_2, the number of reports investigating the growth of ZrO_2 as a CPC on stainless steel substrates is rather limited, arguably due to challenging processing on these substrates, which are prone to oxidation. This motivated us to develop a direct liquid injection chemical vapor deposition (DLI-CVD) process involving the heteroleptic $[Zr(O\textit{i}Pr)_2(tbaoac)_2]$ (**1**) compound (Figure 1 a)) and oxygen as the co-reactant.[3] The growth characteristics of ZrO_2 on Si and AISI 304 stainless-steel substrates at varied deposition temperatures were investigated in detail by means of GIXRD, SAED, TEM, AFM and SEM. Compositional analysis was conducted by XPS, RBS/NRA and FT-IR followed by determination of the corrosion protection performance of ZrO_2 on AISI 304 utilizing electrochemical impedance spectroscopy (EIS).

Structural analysis revealed that the deposition temperature significantly influences the growth characteristics: while at 500 °C to 700 °C polycrystalline monoclinic and cubic ZrO_2 was deposited, at 400 °C an amorphous and compact film with cubic crystalline domains at the interfacial region was obtained (Figure 1 b) and c)). To correlate the corrosion protection capabilities of the ZrO_2 films on stainless steel with the structure, electrochemical impedance spectroscopy (EIS) measurements of the processed films were conducted. The mainly amorphous film grown at 400 °C, outperforms the ones deposited at elevated temperatures (500 °C – 700 °C) as shown by the Bode plots in Figure 1 d). The findings on the growth characteristics and CPC properties of ZrO_2 on stainless steel substrates serves as a benchmark for future application on steel tools in industry.

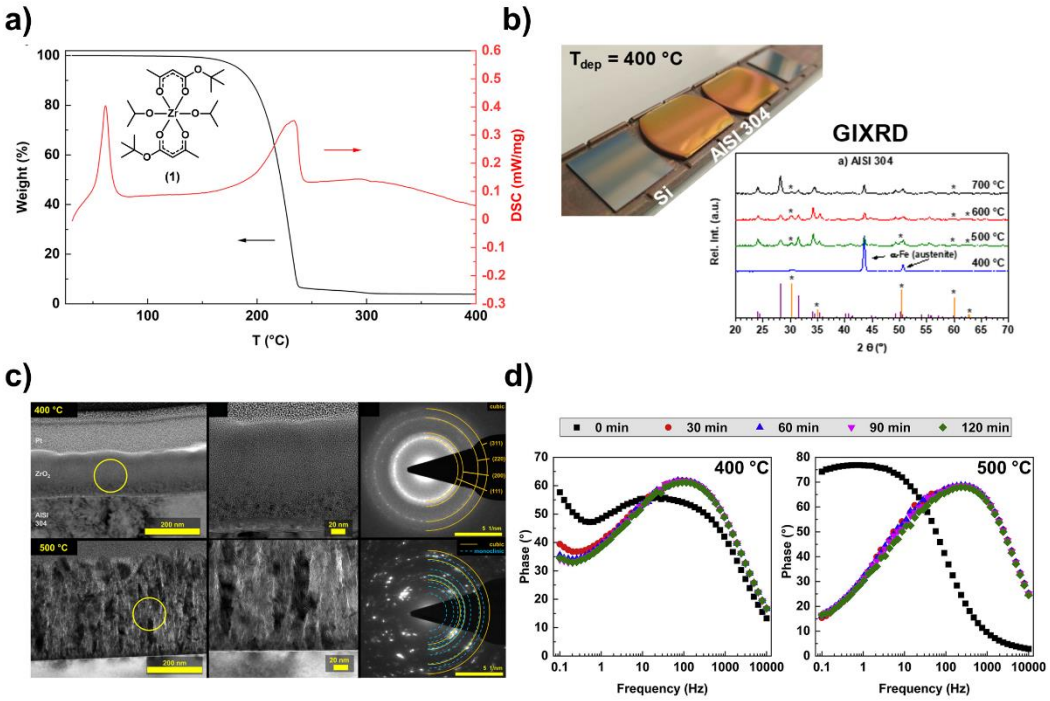

Figure 1. a) Thermal analysis of $[Zr(OiPr)_2(tbaoac)_2]$ (**1**). b) Photograph of ZrO_2 thin films on Si and stainless steel (AISI 304) substrates and GIXRD patterns of ZrO_2 on steel substrates. c) High resolution TEM measurements of ZrO_2 deposited on AISI 304. d) Bode plots with different immersion times for ZrO_2 on AISI 304.

References

1. G. Thurn, et al., Surf. Coat. Technol. **123**, 147 (2000).
2. M. Atik, et al., J. Mater. Sci. Lett., **14**,178 (1995).
3. S. M. J. Beer, D. Samelor, A. Abdel Aal, J. Etzkorn, D. Rogalla, A. E. Turgambaeva, J. Esvan, A. Kostka, C. Vahlas, A. Devi, J. Mater. Res. Technol., **13**, 1599 (2021).

* *Corresponding author e-mail: jean-pierre.glauber@rub.de*

The use of silver CVD nanostructured substrates in analysis of low molecular weight compounds

Aleksandra Radtke[a]*, Piotr Piszczek[a], Gulyaim Sagandykova[b], Paweł Pomastowski[b]

[a] *Faculty of Chemistry, Nicolaus Copernicus University in Toruń, Gagarina 7, 87-100 Toruń, Poland*
[b] *Centre for Modern Interdisciplinary Technologies, Nicolaus Copernicus University in Toruń, Wileńska 4, 87-100 Toruń, Poland*

Introduction

Mass spectrometric techniques can provide data on the composition of a studied sample, utilizing both targeted and untargeted approaches to solve various research problems. Analysis of compounds in the low mass range has practical implications in many areas of research and industry. Laser desorption ionization techniques are utilized for the analysis of molecules in a low mass region using low sample volume, providing high sensitivity with low chemical background. The fabrication of substrates based on nanostructures to assist ionization with well-controlled morphology may improve LDI-MS efficiency for silver nanoparticles with plasmonic properties. In this presentation, we report an approach for the preparation of silver nanostructured substrates applied as laser desorption ionization (LDI) plates, using the chemical vapor deposition (CVD) technique [1].

Materials and Methods

For the synthesis of the LDI plates, stainless steel (H17) was cut to pieces 2.5 × 7.5 cm. The surfaces of the steel samples (substrates) were covered by the silver coating, consisting of densely packed silver nanoparticles and microparticles (AgPs). For this purpose, a chemical vapor deposition (CVD) technique was used. In our CVD experiments, $[Ag_5(O_2CC_2F_5)_5(H_2O)_3]$ has been used as a precursor. The morphology of created coatings was studied using a scanning electron microscope. The structure of the AgPs films was investigated using an energy-dispersive X-ray diffractometer with a copper monochromator and CuKα radiation (λ = 0.15418 nm). XRD patterns were collected in the 2Θ range 10–80°, step 0.02° and time 20 sec. For the purposes of the NALDI experiments, Ag films were prepared in real time, and the storage time of samples (in a closed box, at room temperature and with limited access to light) was not longer than 2–3 days.

The LDI-MS performance of the synthesized plates was evaluated by using stock solutions at concentration of 1 mg/mL and standard mixtures of various lipids. Stock solutions of adonitol, glucose, fructose, shikimic acid, methionine, serine, alanine and phenylalanine were prepared by dissolving a powder of each standard in water. Stock solutions of cholesterol, oleic acid, palmitic acid and PC were prepared by dissolving a powder of each standard in chloroform. The standard mixtures of the various lipids were sonicated for 5 min prior to spotting to the target plate to avoid precipitation of lipids during storage. Subsequently, 1 µL of the stock solution of each compound and standard mixture was spotted to the synthesized LDI plates. LDI-MS analysis of low molecular weight compounds was carried out in both positive and negative ion-reflectron modes with the utilization of laser power at 80% in the mass range of *m*/*z* 60–1500. Analysis was performed using an UltrafleXtreme II MALDI-TOF-MS apparatus equipped with a modified neodymium-doped yttrium aluminium garnet (Nd:YAG) laser operating at 355 nm and frequency 2 kHz. Mass calibration was performed using signals of silver using quadratic and cubic enhanced calibration methods individually for each spectrum. Theoretical *m*/*z* values of the analyzed compounds were calculated by using ChemCalc program.

Results and Discussion

Our main idea was to study the dependency between the size of the deposited silver particles (AgPs), the coatings' surface morphology and the LDI plates' sensitivity to various low molecular weight compounds. For this purpose, the plates were subjected to characterization using scanning electron microscopy (SEM) (Fig.1) and X-ray diffraction (XRD) techniques (Fig 2). The use of different masses of solid Ag precursor and similar deposition conditions enabled controlling the surface morphology of the deposited layers as well as controlling the size of the AgPs deposited. The presented approach allows for the synthesis of LDI plates with tunable sensitivity for various classes of small biomolecules. The utilization of a chemical vapor deposition technique with various values of the mass of the precursor resulted in the formation of structures with sizes 50–330 nm and up to 1 µm with irregular shapes. Small biomolecules were detected at nanomolar concentrations, while lipids were detected at the picomolar level with a reduced chemical background (Fig.3).

Conclusions

Depending on the mass of used CVD precursor, the approach allowed the synthesis of LDI plates with tunable sensitivity for various low molecular weight compounds in both ion-positive and ion-negative modes. Reduced chemical background and sensitivity to small biomolecules of various classes (fatty acids, amino acids and water-soluble metabolites) at nanomolar and picomolar detection levels for lipids such as triacylglycerols, phosphatidylethanolamines and lyso-phosphatidylcholines represent an emerging perspective for applications of LDI-MS plates for the collection of molecular profiles and targeted analysis of low molecular weight compounds for various purposes.

Acknowledgments

This study was supported by the National Science Center (Preludium 16; 2018/31/N/ST4/02210 (2019–2022)

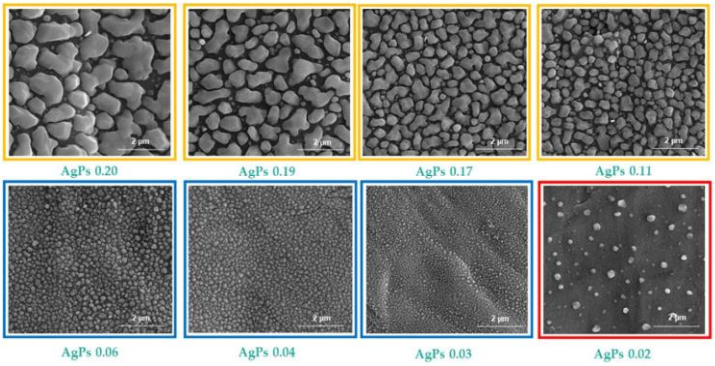

Fig.1. SEM images of CVD AgPs films deposited on stainless

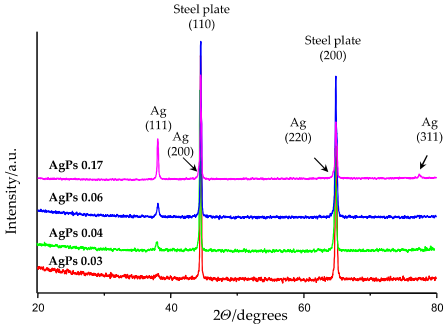

Fig.2. XRD spectra of CVD AgPs

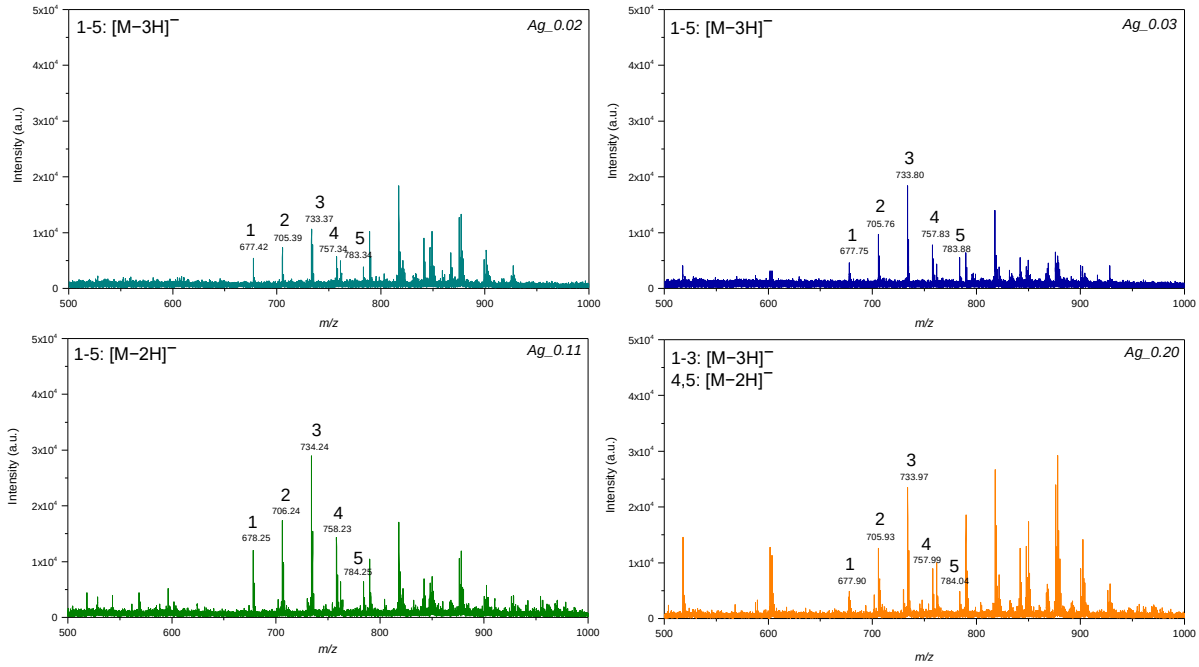

Fig.3. LDI-MS spectra of the standard mixture of phosphatidylethanolamines for the

References

1. G. Sagandykova, et al., Materials **15**, 4660 (2022)

* *Corresponding author e-mail:* aradtke@umk.pl

Ruthenium Sulfide Thin Films - a New Route via MOCVD

Jorit Obenlüneschloß[a*], David Zanders[a], Jan-Lucas Wree[a], Ilamparithy Selvakumar[a], Anjana Devi[a]

[a] *Inorganic Materials Chemistry, Ruhr University Bochum, Universitätsstraße 150, Bochum, Germany 44780*

Ruthenium sulfide (RuS_2) or laurite, is known as a very active catalyst for hydrodesulfurization and for the hydrogenation of organic compounds.[1,2] With the advent of renewable energy and the need to utilize new energy carriers hydrogen is among the top candidates. Its production via water splitting however requires effective catalysts.[3] RuS_2 is anticipated to be a very efficient catalyst for this application and has already been successfully tested.[4,5] RuS_2 is further said to be corrosion resistant and in addition is a very promising semiconducting material.
To this day, the fabrication of this desirable material has been mostly limited to solution chemical approaches for nanoparticles and physical vapor deposition (PVD) methods for films, omitting the advantages chemical vapor deposition (CVD) provides.[6,7] With CVD the coating of large area and topographically challenging substrates can be realized, which is advantageous for catalysis applications.

In this work, we venture into closing this gap with by developing a new MOCVD process for RuS_2. The combination of the proven CVD ruthenium precursor $Ru(CO)_2(^{tBu}AMD)_2$ in combination with elemental sulfur (S_8) was chosen. The use of toxic H_2S, generally employed in the CVD as well as PVD of metal sulfides, was readily circumvented due to the favorable reactivity of the amidinate ligands of the Ru precursor with S_8 under the applied process conditions.[8,9] Herein, comprehensive CVD process development was undertaken and is explored in this study to investigate new pathways to obtain RuS_2. The deposited thin films were thoroughly characterized in terms of their crystallinity, morphology, optical properties, and composition to establish an understanding of the influence of the process conditions on the forwarded material.

While the threshold temperature for continuous film formation was as low as 350°C, the optimal deposition temperature was found to be 600°C on Si(100) substrates. The as-deposited films were homogeneous and smooth with a pronounced degree of crystallinity (Fig. 1). Additionally, at 600°C high purity and stochiometric layers were formed (Fig. 2), proving the high quality of the deposited material. For the different deposition temperatures employed the interesting observation was a change in band gaps. For an increase in deposition temperature not only an improved purity was observed, but both the direct and indirect band gaps increased notably. Preliminary studies on the use of these layers as catalysts for hydrogen evolution reaction is underway and seem promising

With this study the library for CVD processes for Ru containing materials has been enriched with another valuable material system. The capability of careful process design and precursor choice to finetune the material properties has thus been proven.

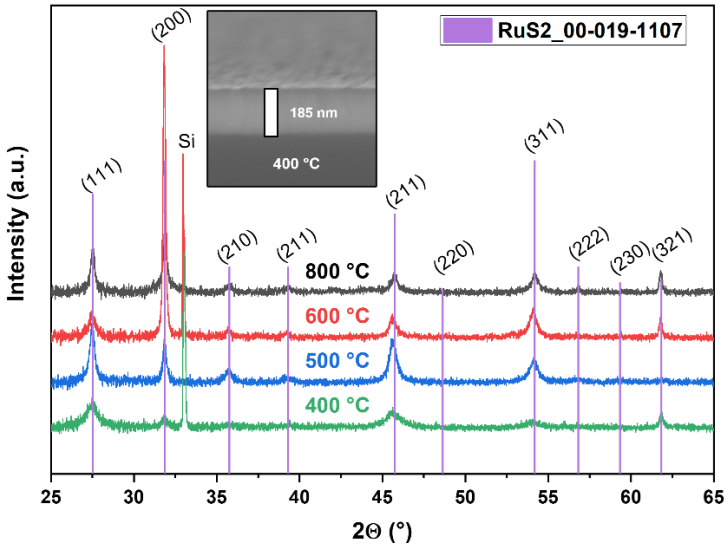

Fig. 1: X-ray diffractograms of RuS_2 thin films deposited at different deposition temperatures. The inset shows a cross-sectional SEM of a film deposited at 400°C.

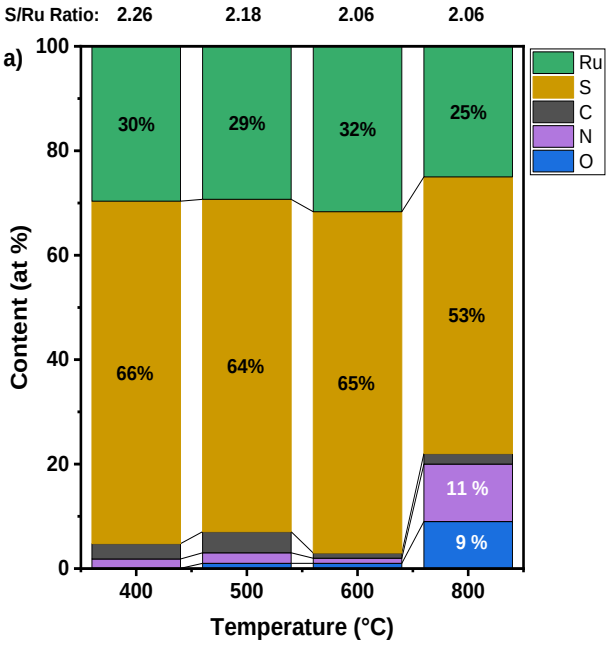

Fig. 2: Composition of RuS_2 thin films deposited at different temperatures depicted with corresponding S/Ru ratios. Atomic percentages were obtained from fitting RBS and NRA spectra.

References

1. M. Lacroix, N. Boutarfa, C. Guillard, M. Vrinat, M. Breysse, *J. Catal.* **1989**, *120*, 473–477.
2. J. A. De Los Reyes, *Appl. Catal., A* **2007**, *322*, 106–112.
3. "Hydrogen Basics," can be found under https://www.nrel.gov/research/eds-hydrogen.html, **n.d.**
4. Z. Zhang, C. Jiang, P. Li, K. Yao, Z. Zhao, J. Fan, H. Li, H. Wang, *Small* **2021**, *17*, 2007333.
5. Y. Xia, W. Wu, H. Wang, S. Rao, F. Zhang, G. Zou, *Nanotechnology* **2020**, *31*, 145401.
6. Y. Li, N. Li, K. Yanagisawa, X. Li, X. Yan, *Mater. Res. Bull.* **2015**, *65*, 110–115.
7. S. Brunken, A. Kratzig, P. Bogdanoff, S. Fiechter, K. Ellmer, *Thin Solid Films* **2013**, *527*, 16–20.
8. P. Bogdanoff, C. Zachäus, S. Brunken, A. Kratzig, K. Ellmer, S. Fiechter, *Phys. Chem. Chem. Phys.* **2013**, *15*, 1452–1459.
9. N. P. Dasgupta, X. Meng, J. W. Elam, A. B. F. Martinson, *Acc. Chem. Res.* **2015**, *48*, 341–348.

* *Corresponding author e-mail:* Jorit.obenlueneschloss@rub.de

$KNbO_3$ thin film growth with advanced CVD precursors

Ishamol Labbaveettil Basheer[a*], Nishant Peddagopu[b] , Francesca Lo Presti[b], Merieme Oubahaz[a], Samuel Margueron[a], Vincent Astié[c], Jean-Manuel Decams[c], Graziella Malandrino[b], Ausrine Bartasyte[a,d]

[a] *FEMTO-ST Institute, Université de Franche-Comté, ENSMM, 25030 Besançon, France*
[b] *Dipartimento di Scienze Chimiche, Universita' di Catania, and INSTM UdR Catania, 95125 Catania, Italy*
[c] *Annealsys, 34000 Montpellier, France*
[d] *Institut Universitaire de France*

Among the large family of ferroelectrics, the perovskite-type $KNbO_3$ has attracted considerable interest in the field of agile dielectric devices for its electro-optic and acoustic properties. However, the synthesis of $KNbO_3$ single crystals is very challenging, and only very expensive single crystals with small sizes are available at present. To bring this material towards industrial applications, the only remaining possibility is to use the grown $KNbO_3$ thin films. Nevertheless, the growth of $KNbO_3$ is far from being a routine process due to the high volatility and reactivity of K_2O. Various approaches have been used in the literature for KN thin films growth, including (i) using excess alkali metal oxides during synthesis; (ii) thermal annealing of deposited films in an alkali metal oxide atmosphere; and (iii) low-temperature synthesis and reduction of crystallization temperatures to suppress or reduce the volatility of alkali metal oxides [1], [2]. The composition of multicomponent oxide films changes due to volatile constituents as a function of layer thickness, growth direction, and deposition conditions. Controlling thin film stoichiometry using physical deposition methods (pulsed laser deposition, RF sputtering, etc.) is particularly difficult due to increased volatility at high vacuum conditions. As with chemical deposition methods, the homogeneous composition of such thin films can be much more easily adjusted by changing the ratio between different element precursors. The major challenges identified in most literature works appear to be control of potassium content in films, repeatability of depositions, and difficulty in locating a reliable K precursor.

To overcome these challenges, pulsed-injection metalorganic chemical vapor deposition (PI MOCVD), a technique that allows for digital control of the film deposition and K content, and consequently stoichiometry, was used in the current study to deposit $KNbO_3$ thin films on C-sapphire, R-sapphire, and 36°Y-$LiNbO_3$ substrates (supplied by Roditi) [3]. $KNbO_3$ films were obtained by growing mixtures of potassium and niobium precursors that were dissolved in 1,2-dimethoxyethane. A heated evaporator received microdoses of the solution at a frequency of 0.5 Hz, and a gas combination of Ar and O_2 (33%) carried the vapor to a hot substrate. 700°C was used as the deposition temperature.

For potassium, two distinct precursors—a commercially available K(tmhd) and a laboratory-produced K_4(hfa)$_4$tetraglyme— were considered [4]. Nb(tmhd)$_4$ precursor was used for niobium. TGA was used to study the evaporation/decomposition behavior of the precursor mixtures. In the precursor mixtures, as the molar ratio between K_4(hfa)$_4$tetraglyme : Nb(tmhd)$_4$ increases, the volatility behavior is better with single-step decomposition. In contrast, as the amount of K(tmhd) increases, the volatility of the K(tmhd): Nb(tmhd)$_4$ tends to decrease. The phase composition and texture have been examined by using X-ray diffraction, (XRD). Through the use of energy-dispersive X-ray analysis (EDX) and surface scanning microscopy (SEM), the elemental composition and surface morphology were investigated. According to EDX and XRD analyses, films grown using the K(tmhd) - Nb(tmhd)4 precursor combination consisted of a variety of K-poor phases ($K_4Nb_6O_{17}$, $K_3Nb_7O_{19}$, $K_6Nb_{10.88}O_{19}$, KNb_3O_8, etc.) even at very high K precursor excess. This may be because the inner coordination sphere is unsaturated in K(tmhd), which results in low volatility or high instability under ambient conditions.

On the other hand, the thin films grown by using advanced K_4(hfa)$_4$tetraglyme and standard Nb(tmhd)$_4$ precursors with molar ratio of K/Nb=8, presented a K/Nb ratio close to 1, as indicated by EDX analysis. In the K_4(hfa)$_4$tetraglyme precursor molecule, the potassium in the center is saturated with a polydentate coordinating ligand and the precursor is more stable compared to K(tmhd) and has a suitable volatility leading to cleaner decomposition inside the CVD reactor. The phase composition and the texture have been analyzed utilizing X-ray diffraction (XRD) and the thin films consisted of a single orthorhombic $KNbO_3$ phase. The film texture and morphology were highly dependent on the substrate (Fig. 1). In the case of R-sapphire substrates, a mixture of (110) & (001) with the presence of (111) orientation have been obtained. The morphology of these films consisted mainly of crystallites with square shape rotated by 90° and 45° in the substrate plane with respect to each other. In the case of C-sapphire, the dominating $KNbO_3$ orientation was (201), which presents triangular growth symmetry, which can be

identified in its stereographic projection (Fig. 1i) as well. The purest (001) growth texture was obtained on 36°Y-LN substrates, which is identified from the homogenously oriented squares in the morphology (Fig. 1e). SEM cross-section of the thin films revealed a dense films.

Better control of K composition in $KNbO_3$ films has been demonstrated by using $K_4(hfa)_4$tetraglyme precursors with respect to the industrially available K(thd) precursor. This enabled the growth of pure $KNbO_3$ films and their epitaxial growth on different substrates. Efforts to grow high-quality KN on bottom electrode are ongoing to realize the electromechanical properties of the films.

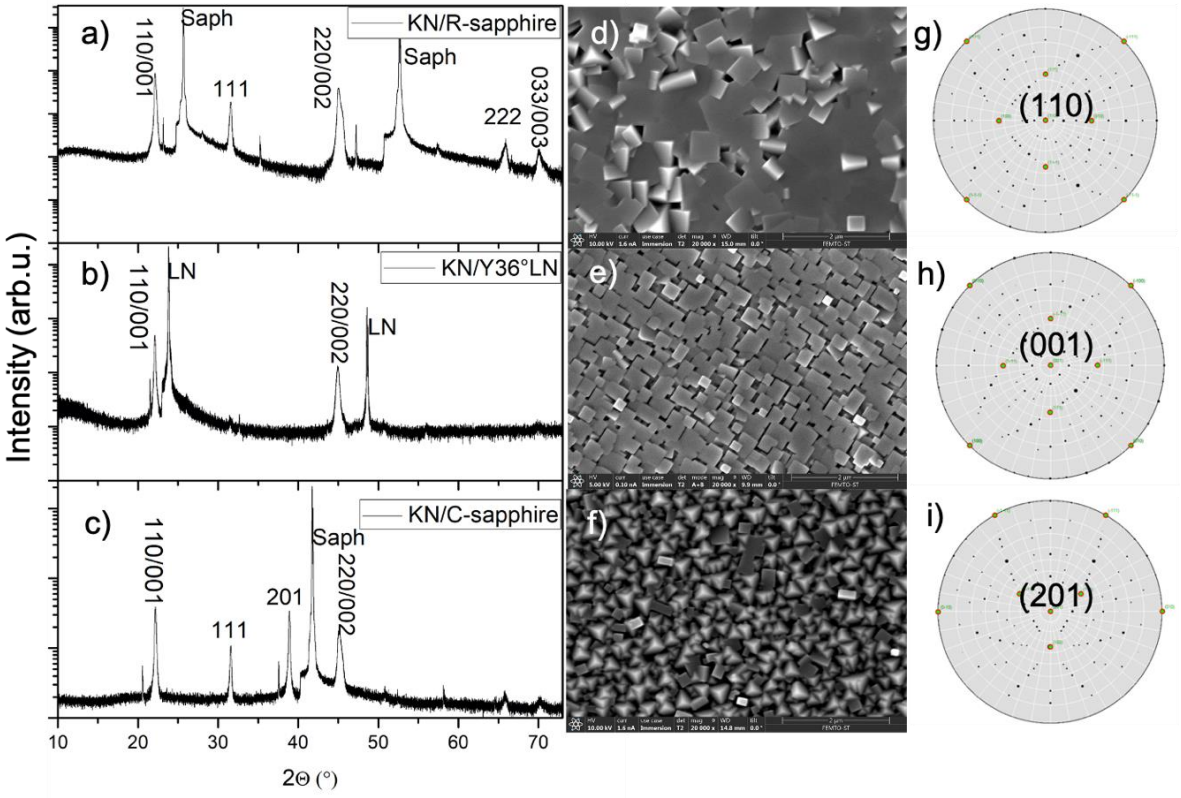

Fig. 1: XRD patterns (a, b, c) and SEM images of morphology (d, e, f) of $KNbO_3$ films grown on R-sapphire, 36°Y-LN, and C-sapphire substrates, respectively. Stereographic projections of (110), (001), and (201) planes of orthorhombic $KNbO_3$ (g, h, and I, respectively).

References

1. J. Wu, D. Xiao, and J. Zhu, “Potassium–Sodium Niobate Lead-Free Piezoelectric Materials: Past, Present, and Future of Phase Boundaries,” *Chem. Rev.*, vol. 115, no. 7, pp. 2559–2595, Apr. 2015, doi: 10.1021/cr5006809.
2. M. V. Romanov, I. E. Korsakov, A. R. Kaul, S. Y. Stefanovich, I. A. Bolshakov, and G. Wahl, “MOCVD of KNbO3 Ferroelectric Films and their Characterization,” *Chem. Vap. Depos.*, vol. 10, no. 6, pp. 318–324, Dec. 2004, doi: 10.1002/cvde.200306302.
3. V. Astié, C. Millon, J. Decams, and A. Bartasyte, “Chapter 2 Direct Liquid Injection Chemical Vapor Deposition.,” 2019.
4. N. Peddagopu, S. Sanzaro, P. Rossi, P. Paoli, and G. Malandrino, “A One-Pot Synthesis of ‘K(hfa) glyme’ Adducts: Effect of the Polyether Length on the Ion Coordination Sphere,” *Eur. J. Inorg. Chem.*, vol. 2021, no. 36, pp. 3776–3780, 2021, doi: 10.1002/ejic.202100553.

* *Corresponding author e-mail:* ishamol.labbaveetti@femto-st.fr

SALD deposition of ZnO coatings for flexible, transparent electrodes for localized heating of lab-on-chip devices

D. T. Papanastasiou[a], A. Sekkat[a], V. H. Nguyen[b], M. C. Jiménez[a], D. Muñoz-Rojas[a*], F. Bruckert[a], D. Bellet[a]

[a] *Univ. Grenoble Alpes, CNRS, Grenoble INP, LMGP, 38000 Grenoble, France*
[b] *Faculty of Materials Science and Engineering, Phenikaa University, 12116 Hanoi, Vietnam*

In situ biological observations require stable, accurate and local temperature control of specimen. Several heating elements are coupled with microfluidic systems, but few of them are transparent to visible light and therefore compatible with microscopic observation. Traditional transparent electrodes such as indium tin oxide, still suffer from high fabrication cost and brittleness, which is not fully compatible to emerging microfluidic devices. Here, we propose a lightweight, low-cost, flexible transparent heater [1] based on percolating silver nanowire networks, protected with a transparent zinc oxide film deposited by Spatial Atomic Layer Deposition (SALD),[2,3] for the *in situ* monitoring of biological experiments. Using the fluorescence of dyes bound to double-stranded DNA to monitor its temperature *in situ*, we demonstrate that such nanocomposites allow rapid and reproducible heating under low applied voltage.[4] Furthermore, selective heating is achieved in different zones of the same microchannel or for adjacent with a single transparent heater and bias.

References

1. Papanastasiou, D. T.; Schultheiss, A.; Muñoz-Rojas, D.; Celle, C.; Carella, A.; Simonato, J.-P.; Bellet, D. Transparent Heaters: A Review. Advanced Functional Materials 2020, 30 (21), 1910225. https://doi.org/10.1002/adfm.201910225.
2. Sannicolo, T.; Lagrange, M.; Cabos, A.; Celle, C.; Simonato, J.-P.; Bellet, D. Metallic Nanowire-Based Transparent Electrodes for Next Generation Flexible Devices: A Review. Small 2016, 12 (44), 6052–6075. https://doi.org/10.1002/smll.201602581.
3. Khan, A.; Nguyen, V. H.; Muñoz-Rojas, D.; Aghazadehchors, S.; Jiménez, C.; Nguyen, N. D.; Bellet, D. Stability Enhancement of Silver Nanowire Networks with Conformal ZnO Coatings Deposited by Atmospheric Pressure Spatial Atomic Layer Deposition. ACS Applied Materials & Interfaces 2018, 10 (22), 19208–19217. https://doi.org/10.1021/acsami.8b03079.
4. Dorina T. Papanastasiou, Abderrahime Sekkat, Viet H. Nguyen, Carmen Jiménez, David Muñoz-Rojas, Franz Bruckert*, Daniel Bellet*. Stable flexible transparent electrodes for localized heating of lab-on-a-chip devices, Advanced Materials Technologies, accepted.

* *Corresponding author e-mail: david.munoz-rojas@grenoble-inp.fr*

Rare-earth sulfide thin films for magneto-optical applications

Florian Preischel[a,*], Sebastian M. J. Beer[a], Joerg Debus[b], Andreas Ney[c], Harish Parala[a], Ravindra Shashindra[a], Silan Baspinar[a], Anjana Devi[a]

[a] *Inorganic Materials Chemistry, Ruhr University Bochum, Universitätsstr. 150, Bochum, 44801, Germany*
[b] *Experimental Physics, TU Dortmund University, Otto Hahn Str. 4a, 44277, Dortmund, Germany*
[c] *Institute of Semiconductor and Solid State Physics, Johannes Kepler University, Altenberger Str. 69, Linz, 4040, Austria*

Owing to their unique 4f-electron shell configuration, rare earth (RE) containing thin films possess highly interesting properties. In particular, RE sulfides (RES) show promising magneto-optical properties and may be used in new technologies such as spintronics[1] and quantum sensing devices.[2,3] However, due to the oxophilicity of RE metals[4], the fabrication of RES thin films is challenging and the research that has been done on this topic so far is limited. To obtain a comprehensive understanding of these materials and to advance this field of research, metalorganic chemical vapor deposition (MOCVD) as a versatile gas-phase method is well suited.

In this context we have developed a new MOCVD process for the growth of crystalline EuS and Eu_3S_4 thin films.[5] Facilitated by the employment of closely related Eu(III) precursors containing the amidinate and guanidinate ligands in combination with elemental sulfur, EuS_x films were deposited on Si substrates at moderate process conditions apart from avoiding the toxic H_2S that is commonly used for metal sulfide film growth. From XRD measurements, it was inferred that the crystalline phase (EuS or Eu_3S_4) depends on the temperature and the type of precursor used (Fig. 1). EuS films deposited on Si(100) showed optical properties comparable to bulk EuS (Fig. 2, left), and superconducting quantum interference device (SQUID) magnetometry measurements revealed the ferromagnetic character of these films (Fig. 2, right). This demonstrates the high-quality of the CVD grown EuS films that seem promising for future magneto-optical and magnetic devices as well as potential applications in spintronics. Subsequently, we extended the concept to deposit Er_2S_3 and Gd_2S_3 thin films using amdinate-type Er(III) and Gd(III) precursors with elemental sulfur. The Gd_2S_3 layers were found to be crystalline above 700 °C, while the Er_2S_3 films were amorphous for temperatures ranging from 400 °C to 800 °C. The ongoing studies are focused on phase control via varying CVD process parameters and on investigating the magnetic and magneto-optical properties of the RES films.

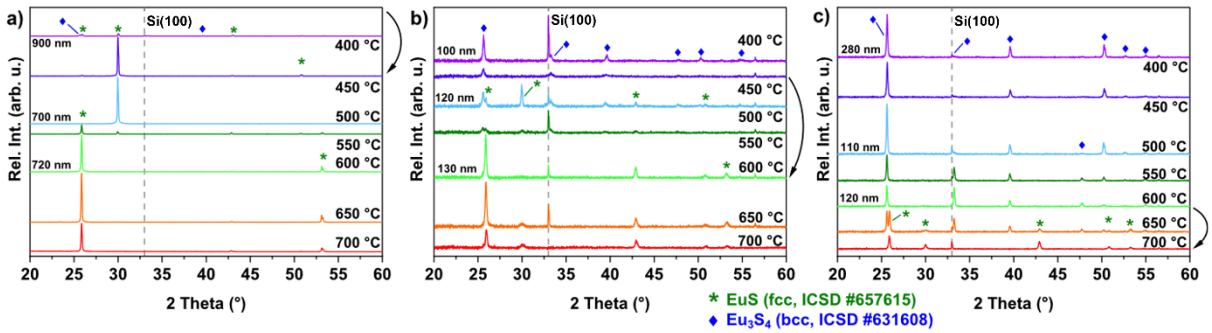

Figure 1. Structure of EuS_x thin films determined by XRD. The phase change from Eu_3S_4 to EuS is indicated by arrows.

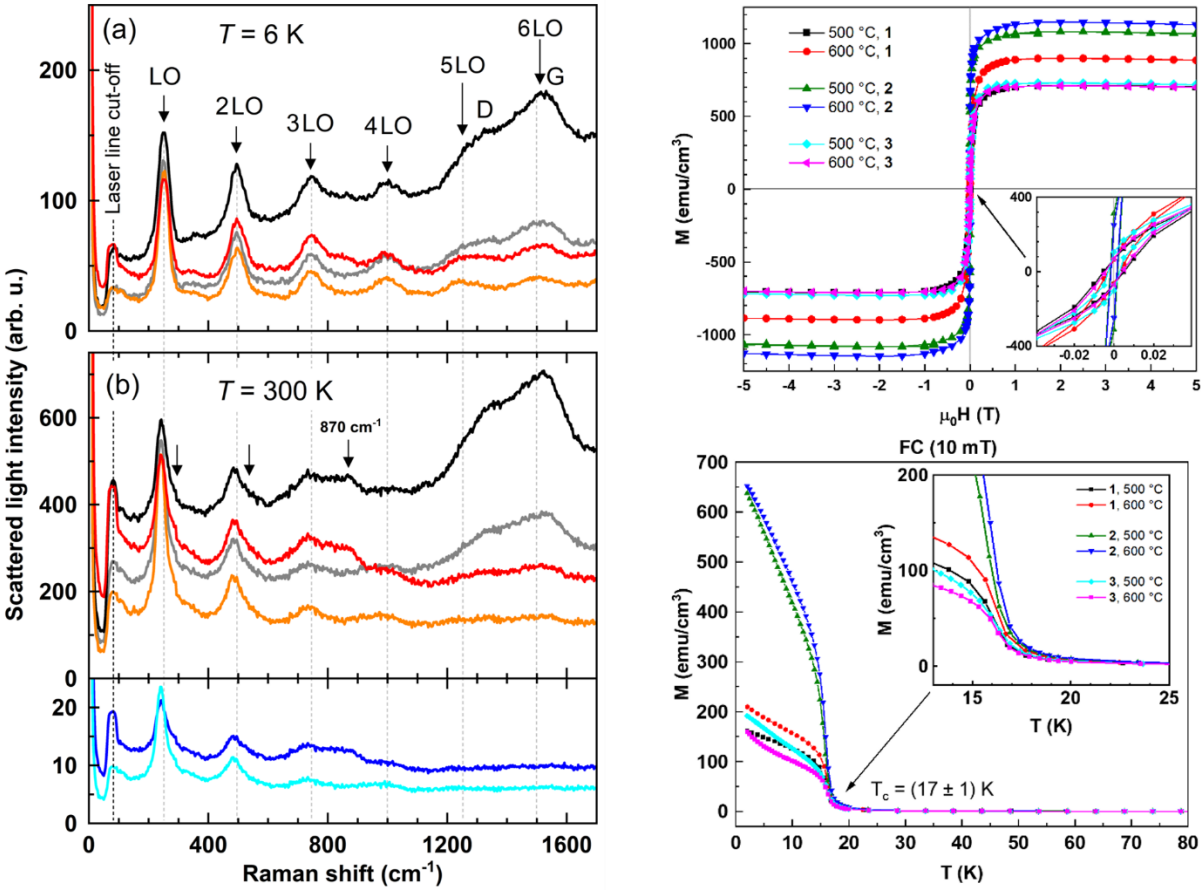

Figure 2. EuS film properties: (left) optical properties via Raman spectroscopy and (right) magnetic properties via SQUID magnetometry measurements.

References

1. G.-X. Miao and J. S. Moodera, Appl. Phys. Lett. **94**, 182504 (2009).
2. M. Hatanaka and S. Yabushita, Theor. Chem. Acc. **133** (2014).
3. C. L. Degen, F. Reinhard, and P. Cappellaro, Rev. Mod. Phys. **89** (2017).
4. F. Ortu, Chem. Rev. **122**, 6040 (2022).
5. S. M. J. Beer, J. Debus, A. Ney, A. Devi *et al.*, Chem. Mater. **34**, 152 (2022).

* *Corresponding author e-mail: florian.preischel@rub.de*

Single source precursor approach towards MoS_2 thin films via MOCVD

Martin Wilken[a*], Ravindra Shashindra[a], Malte Becher[b], Andreas Ostendorf[b] and Anjana Devi[a]

[a] *Inorganic Materials Chemistry, Ruhr University Bochum, Universitätsstr. 150 44801 Bochum, Germany*

[b] *Applied Laser Technologies, Ruhr University Bochum, Universitätsstr. 150, 44801 Bochum, Germany*

2D materials such as molybdenum disulfide (MoS_2) have attracted a lot of research interest due to their unique structural and (opto)electronic properties. As a result they are proposed to be suitable for a variety of applications that include their implementation in next-generation electronic devices such as thin film transistors (TFT), photovoltaics, batteries, sensors, or as catalysts for the electrocatalytic hydrogen evolution reaction (HER).[1] Most of the reports on 2D-MoS_2 are either via exfoliation routes or the classical chemical vapor deposition (CVD) routes involving the sulfurization of molybdenum oxide or the use of metal halides in combination with H_2S.[2] Although exfoliation yields high quality 2D-materials, the scale up of this route is limited and in this context, CVD is a preferred processing route for crystalline large area growth with thickness control.

In classical CVD routes, precursors like molybdenum halides (e.g. $MoCl_5$, MoF_6) with H_2S as co-reactant or the direct conversion of molybdenum oxides with H_2S have been used to grow MoS_2.[2] Beside halide incorporation, high deposition temperatures are needed and additionally the use of the highly toxic H_2S.[3] To grow large area crystalline MoS_2 at lower temperatures, metalorganic precursors containing Mo can be employed to grow films at moderate process conditions .[4] One other approach to grow MoS_2 is to use single source precursor (SSP) which contain both Mo and S. This pathway can also simplify the CVD processing of MoS_2 without an additional sulfur source and can also yield films at moderate process conditions.

Herein we report the development of a new MOCVD process using the single source precursor $[Mo(S^tBu)_4]$ where Mo is surrounded by a sulfur coordinated ligand [5]. The role of the precursor on morphology, structure, composition and optical properties is thoroughly investigated using complementary analysis namely SEM, RBS/NRA, XPS, XRD and Raman spectroscopy to elucidate the structure, composition and quality of the MoS_2 layers. Figure 1 (XRD and Raman analysis) confirms the formation of hexagonal phase of MoS_2 using the SSP-MOCVD approach. Further results obtained are promising in terms of large area deposition of stoichiometric and high purity thin crystalline MoS_2 layers at moderate process conditions. The obtained results are compared to previously reported aerosol assisted (AA) CVD using SSPs and MOCVD processes for MoS_2 thin film growth using other metalorganic precursors.

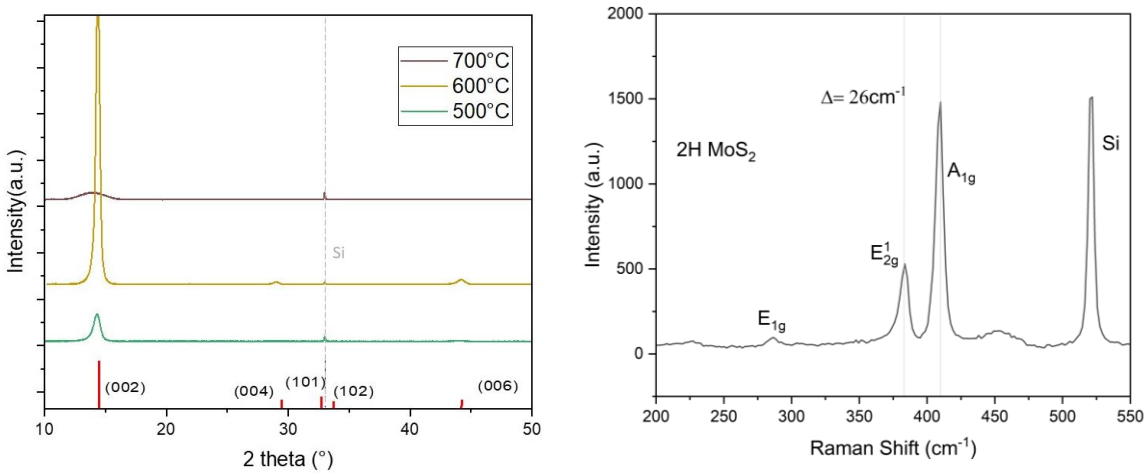

Figure 1. (left) XRD patterns of MoS_2 layers grown on Si(100) at different deposition temperatures. (Red reference pattern PDF no. 00-037-1492 molybdenite-2H phase). (right) Raman measurement for a MoS_2 film deposited on Si(100) at 600 °C.

References

1. a) S. Manzeli *et al.*, Nat Rev Mater **2** (2017); b) K. Chang, X. Hai, and J. Ye, Adv. Energy Mater. **6**, 1502555 (2016).
2. L. Seravalli and M. Bosi, Materials (Basel) **14** (2021).
3. J. Park *et al.*, Appl. Phys. Lett. **106**, 12104 (2015).
4. S. Cwik *et al.*, Adv. Mater. Interfaces **5**, 1800140 (2018).
5. J. Cheon, J. E. Gozum, and G. S. Girolami, Chem. Mater. **9**, 1847 (1997).

* *Corresponding author e-mail: martin.wilken@rub.de*

Synthesis of Self-Cleaning Window Glass for Photocatalytic Oxidation of NO_x: Effect of APCVD Synthesis Conditions on Photocatalytic Performance

Zhipeng Lin[a], Yuankai Li[a], Andreas Kafizas[a,*],

[a] *Department of Chemistry, Imperial College London, United Kingdom*

Human activities are escalating the rise of NO_x concentration in atmosphere, resulting in an emerging global environmental challenge. Many effective strategies have been developed over past decades to control the NO_x emissions at emission sources, such as physical adsorption and three-way catalyst-assisted degradation [1] Countries and regions have enacted stringent legislation to limit NO_x emissions originating from industry and human activities in recent years. For instance, the UK has implemented the revised Convention on Long-Range Transboundary Air Pollution (CLRTAP) and National Emission Ceilings Regulations (NECR), mandating a reduction in NO_2 emissions to 73% of the 2005 levels by 2030 [2]. Despite these efforts, global NO_x emissions remain in the range of 2-8 TgN/year and continue to increase annually [3].

Employing self-cleaning surfaces with TiO_2 coatings can remediate anthropogenic NO_x that escapes into the atmosphere by a photocatalytic process, where toxic NO_x can be converted into comparatively benign nitric acid. However, self-cleaning surface coated on glass has yet to demonstrate satisfactory NO_x removal performance, particularly when it compares to the remarkable performances of TiO_2 when coated on concrete, ceramic, and other surfaces. The diminished photocatalytic activity is not only attributed to the inherent drawbacks of semiconducting TiO_2, such as a high electron-hole recombination rate and low solar energy utilization, but also the manufacturing process of commercial self-cleaning glass via Atmospheric Pressure Chemical Vapor Deposition (APCVD) [4]. The physicochemical properties and coating thickness of TiO_2 on the glass substrate are significantly influenced by synthesis parameters like gas flow rate, reaction time, and saturated vapor pressure of the precursor, all of which determine the product's photocatalytic activity [5]. However, there are no articles that have carried out a comprehensive study on the relationship between APCVD synthesis conditions efficiency of TiO_2 coated glass and NO_x removal efficiency.

In our work, 58 samples were synthesised by APCVD under various experimental conditions. The investigated parameters included CVD deposition temperature (350°C - 600°C), synthesis time (1- 27 mins), precursor selection (titanium tetraisopropoxide: TTIP, titanium ethoxide: TiEt and titanium butoxide: TiBu) and precursor bubbler temperature (100°C - 220°C). The synthesized samples were subsequently assessed for their NO_x conversion (**Figure 1**) and NO_2 selectivity based on the ISO 22197-1:2016 testing procedure [6]. The optimal sample exhibited a NO_x conversion of ~22.7%, which was significantly higher than that achieved by commercial Activ™ self-cleaning glass (~0.27%). The 58 synthesized samples were all analyzed by using XRD, UV-Vis, AFM, SEM, and TAS techniques to investigate their crystal structures, optical properties, surface characteristics, and photogenerated charge kinetics, respectively. The relationship between CVD synthesis conditions on the physicochemical properties of the TiO_2 formed, as well as the NO_x remediation performance, were then evaluated using various machine learning models. Among them, we found employing linear regression models can effectively predict and demonstrate the relationships between material properties and NOx conversion. Specifically, charge kinetics and surface roughness exhibit strong positive correlations, while optical properties display a pronounced negative correlation, and crystal properties do not demonstrate a significant relationship with material performance.

**Corresponding author e-mail: a.kafizas@imperial.ac.uk*

References

[1] J. Gao *et al.*, Journal of Cleaner Production **288**, 125647 (2021).
[2] K. Pedrosa and B. Vanheusden, in *Research Handbook on EU Environmental Law*, edited by M. Peeters and M. Eliantonio (Edward Elgar Publishing, 2020), p. 296.
[3] B. A. Nault *et al.*, Geophysical Research Letters **44**, 9479 (2017).
[4] K. D. Sanderson *et al.*, 46th Annual Society of Vacuum Coaters Technical Conference (2003).
[5] H. M. Yates, P. Evans, and D. W. Sheel, ECS Trans. **25**, 781 (2009).
[6] A. Mills *et al.*, Journal of Photochemistry and Photobiology A: Chemistry **400**, 112734 (2020).

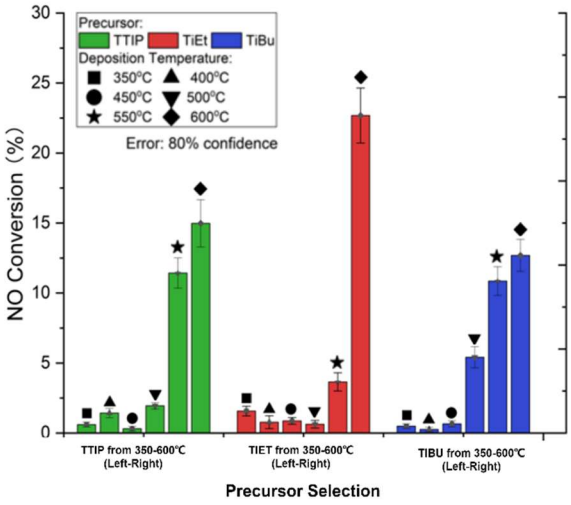

Figure 1. Effect of APCVD synthesis temperature on the photocatalytic NO conversion efficiency of TiO_2 coatings on glass

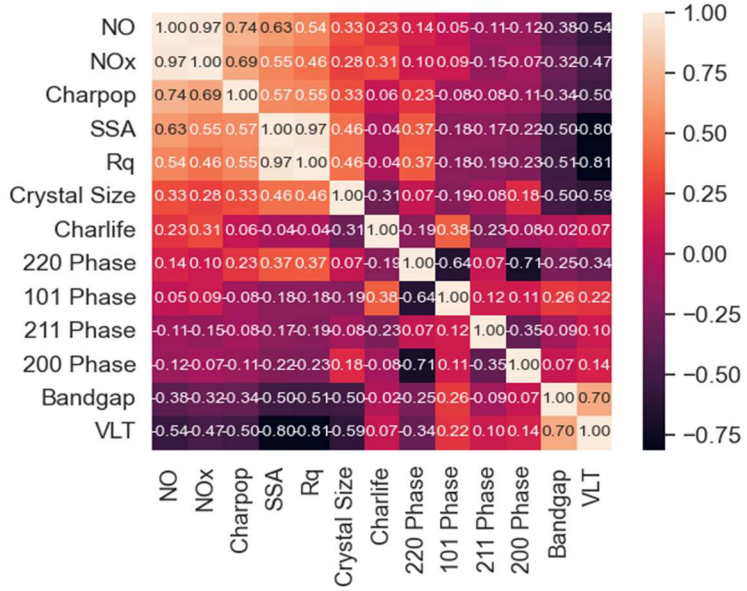

Figure 2. Pearson Coefficient between each tested properties and NO/NOx Conversion

Vapour Phase Infiltration: an efficient strategy to tune microporous Metal Organic Frameworks

Catherine Marichy[a*], Siddhartha De[a], Gia Co Quan[a], Ben Gikonyo[a], Charlotte Martineau Corcos[b], Colin Bousige[a], Laurent Veyre[c], Thomas Devic[d], and Alexandra Fateeva[a]

[a] *Laboratoire des Multimatériaux et Interfaces, CNRS/Université Claude Bernard Lyon 1, Villeurbanne, France*
[b] *Université de Versailles St-Quentin en Yvelines, Université Paris Saclay*
[c] *Laboratoire de Chimie, Catalyse, Polymères et Procédés, Université Lyon, Villeurbanne, France*
[d] *Institut des Matériaux Jean Rouxel, Université de Nantes, UMR CNRS 6502, 44322 Nantes, France*

Metal-organic frameworks (MOFs) are a class of crystalline materials composed of metal ions/clusters as nodes bridged by organic moieties. These materials often exhibit remarkably high accessible specific surface areas, uniform and tunable pore volumes, and chemical modularity. Post-synthesis modification (PSM) can be performed to adjust the MOF properties, providing new functionalities while preserving the network structure. The vapor phase infiltration (VPI) is a promising PSM strategy, which has been demonstrated enabling the insertion of metal cation into mesoporous MOFs such as NU-1000 and UiO-66.[1-4]

Herein, post-synthesis modification of microporous porphyrin-based MOFs by VPI will be introduced. Using a single precursor, isolated metallic entities are successfully installed in the stable Zr(IV)-based porphyrinic bulk MIL-173(Zr), evidencing that VPI is not restricted to mesoporous materials.[5] From trimethylaluminum (TMA) and diethylzinc (DEZ), respectively, Al and Zn metals are inserted in a saturated manner in the MOF on the available chemical sites. Indeed MIL-173(Zr) presents two types of reactive sites originating from the porphyrinic ligand: the pyrrolic porphyrin core (free base), and one of the phenolic groups, which remains protonated (Fig. 1a and c). Furthermore, the high chemical stability of MIL-173(Zr) allows VPI with these highly reactive precursors without altering the MOF structure.

In the present contribution, the advantage of VPI compare to classical solution PSM and the porosity prerequisite for efficient vapor-phase PSM will be highlighted. The structural characterizations and the spectroscopic properties of the VPI-modified MOF will be presented. A particular attention will be given to the controlled alteration of the optical properties of MIL-173(Zr) as a function of the number of VPI cycles (Fig. 1b).

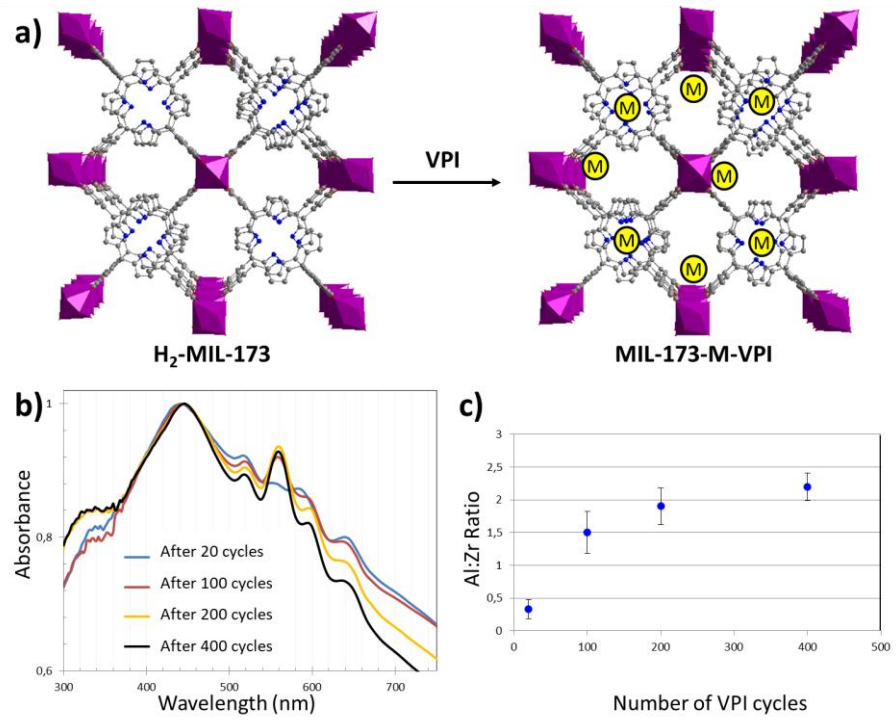

Figure 1. (a) Scheme of VPI of the MIL-173 structure, colour code: Zr (purple), inserted metal cations after VPI (yellow), N (blue), C (grey). (b) UV-Visible spectra of MIL-173 after infiltration with TMA and

(c) the corresponding Al:Zr ratio, determined by EDS analyses, as a function of the number of VPI cycles. (c) The Al:Zr ratio tends to a maximum value of 2.5.

References

1. J. Mondloch *et al.*, J. Am. Chem. Soc. **135**, 10294 (2013).
2. P. C. Lemaire *et al.*, ACS Appl. Mater. Interfaces, **9**, 22042 (2017).
3. K. Tan *et al.*, Chem. Mater. **31**, 2286 (2019).
4. M. Rimoldi *et al.*, Chem Mater. **29**, 1058 (2017).
5. S. De *et al.*, Inorg. Chem. **59**, 10129 (2020).

* *Corresponding author e-mail:* catherine.marichy@univ-lyon1.fr

Atomic-molecular layer deposition of hybrid multilayers of AlN straddled with hydroquinone nanolayers.

Pamburayi Mpofu[a,*], Collin Rowe[b], Ganpati Ramanath[a,b] and Henrik Pedersen[a]

[a] *Linköping University, Department of Physics, Chemistry and Biology, Linköping, 58183, Sweden*
[b] *Rensselaer Polytechnic Institute, Department of Materials Science and Engineering, Troy NY, 12180, USA*

Combining atomic and molecular layer deposition (ALD and MLD) processes is attractive for realizing multilayer stacks of inorganic nanolayers separated by organic nanolayers for accessing novel properties via interface effects. The inorganic nanolayers provide thermomechanical stability, and can be selected to obtain desired functionalities, e.g., optical, dielectric, electronic and thermal transport properties. The interfacial organic nanolayers allow possibilities for property tuning, structural flexibility, and accessing novel properties that are completely different from the component materials. Such multilayer thin film hybrid materials have been demonstrated by combining ALD-grown metal oxides with MLD-grown metalcone polymers using metal-organic precursors with reactive organic moieties, such as diols and triols [1]. Hybrid films of zincone exhibit novel properties, e.g., combination of optical transparency with high electrical conductivity, low thermal conductivity, and high mechanical flexibility [2]. Aluminium oxide and alucone using trimethylaluminum (TMA) as a metal precursor with H_2O and hydroquinone (HQ) as co-reactants have also been explored [3].

Here, we present for the first time, ALD-MLD of AlN-HQ multilayers using TMA together with a NH_3 plasma, and hydroquinone as co-reactants. We systematically varied the AlN thickness and the number of HQ interfaces. Results of X-ray reflectometry analyses support the multilayered nature of the films. Fourier transform infrared spectroscopy indicate the presence of Al-N, Al-O, C-C, C=C, C-O and C-H bonds. Peaks indicating the fingerprint region together with HQ signatures showed that the benzene rings in HQ were ensconced between the AlN layers as intended. X-ray photoelectron spectroscopy measurements provide insights into AlN-HQ interface chemistry. Materials property measurements are underway.

References

1. George, S. M., Lee, B. H., Yoon, B., Abdulagatov, A. I. & Hall, R. A. Metalcones: Hybrid organic-inorganic films fabricated using atomic and molecular layer deposition techniques. *J. Nanosci. Nanotechnol.* **11**, 7948–7955 (2011).
2. Liu, J., Yoon. B., Kuhlmann, E., Tian, M., Zhu, J., George, S. M., Lee, Y-C. & Yang, R.Ultralow thermal conductivity of atomic/molecular layer-deposited hybrid organic-inorganic zincone thin films. *Nano Lett.* **13**, 5594–5599 (2013).
3. Choudhury, D., Sarkar, S. K. & Mahuli, N. Molecular layer deposition of alucone films using trimethylaluminum and hydroquinone. *J. Vac. Sci. Technol. A Vacuum, Surfaces, Film.* **33**, 01A115 (2015).

[*] *Corresponding author e-mail:* pamburayi.mpofu@liu.se

Depositing ALD-oxides on MLD-metalcones: enhancing initial growth through O_2 plasma densification

Juan Santo Domingo Peñaranda[a], Matthias M. Minjauw[a], Sofie S. T. Vandenbroucke[a], Robin Petit[a,b], Jin Li[a], Jolien Dendooven[a], Christophe Detavernier[a,*]

[a.] *Department of Solid State Sciences, CoCooN group, Ghent University, Krijgslaan 281, S1, 9000 Gent, Belgium.*
[b.] *Department of Solid State Sciences, LumiLab group, Ghent University, Krijgslaan 281, S1, 9000 Gent, Belgium.*

Flexible devices for displays/battery applications are gaining traction every day, but moisture sensitivity can be a concern. For this, Thin-Film Encapsulation (TFE) moisture barriers need to be used. However, many current technologies rely on rigid barriers that crack and stop performing when flexing strain is applied. As a solution, organic/inorganic thin film stacks are now widely explored for TFE for flexible applications.

In this context, we have studied O_2 plasma densification of MLD alucone [1], titanicone, tincone and zincone. We also investigated the effect on the growth of ALD metal oxides on metalcones with or without a prior plasma densification to optimize the deposition of ALD/MLD multilayers.

Upon plasma treatment, all metalcone layers exhibited a similar behaviour. As shown in Figure 1, a bilayer structure was evidenced by X-ray reflectivity (XRR), composed of a (~2 nm thick) high-density layer on top of one with metalcone-similar density. The overall film thickness decreased and its evolution during treatment could be monitored with in-situ ellipsometry (Figure 2, left). Both in the dense and less-dense layer, a saturating behavior was revealed for increasing plasma exposure time. In Fourier-Transform Infrared Spectroscopy (FTIR), plasma-treated metalcones (PT-metalcones) showed a decrease in the C-O region and an increase in the C=O one (Figure 2, right), similar to aged metalcones. After several months of aging, only an increase in the O-H band was found. X-ray Photoelectron Spectroscopy (XPS) showed a significant decrease of C content in the near-surface region, and a higher C content in the underlying “bulk” of the film. Therefore, we conclude that O_2 plasma treatments on metalcones produce a partial densification of the layers. The near-surface region is transformed into a metal oxide (or oxycarbide), while preserving a hybrid layer underneath. The O_2 radical species oxidise the topmost region of the hybrid film into its corresponding, dense oxide. Some O_2 radicals penetrate deeper down the layer, oxidizing the original alcoholic structure into an intermediate ketonic one.

Secondly, metal oxides were grown on top of their respective metalcones, and pristine and PT-metalcones were compared. Using in-situ ellipsometry, growth on pristine metalcones always suffered a delay until the oxide thickness started to increase (Figure 3) [2]. However, an oxide layer immediately started growing on PT-metalcones, from the first cycle, offering a very accurate oxide thickness control. With this, we hope to have expanded the potential of using stacks of oxides and PT-metalcones for TFE applications. The use of O_2 plasma densifications could hold potential towards film-ratio optimisation for optimum performance at minimal film thicknesses.

Abstract figures

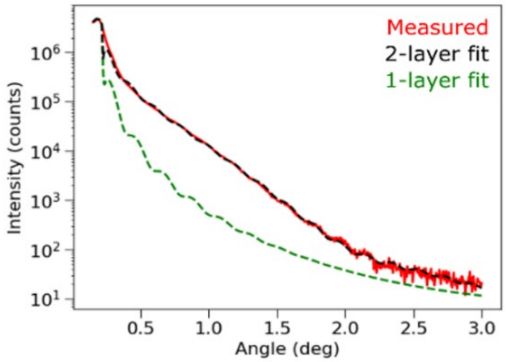

	Thickness (nm)	Roughness (nm)	Density (g/cm^3)
Si	-	0.3	2.3
SiO_2	1.8	1.5	2.7
Zincone	19.8	0.6	2.6
ZnO	2.0	0.3	7.4

Figure 1. XRR shows a bilayer formed upon densification. A dense layer is formed on top while the density of the bottom “bulk” remains close to the one expected for MLD metalcone.

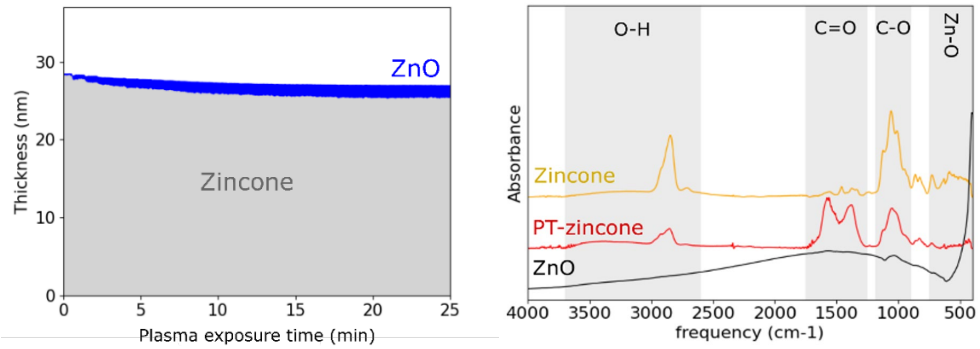

Figure 2. A metalcone film is densified upon O_2 plasma treatment, where in situ ellipsometry data (left) shows a bilayer formation and total thickness reduction with saturing behavior. On FTIR (right), the C=O region increases in intensity and the C-O band decreases, evidencing that the remaining structure is partially oxidised as well.

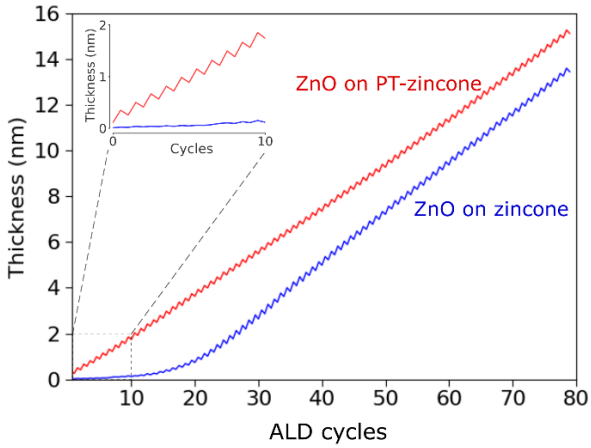

Figure 3. In situ ellipsometry data: When growing an oxide on top of a pristine metalcone, a delay is always found. In comparison, immediate growth on plasma-treated metalcones (PT-metalcones) occurs.

References

1. Santo Domingo Peñaranda et al. Dalt. Trans. 2021, **50** (4), 1224–1232
2. Choi et al. ACS Appl. Mater. Interfaces 2016, **8** (19), 12263–12271

* *Corresponding author e-mail: Christophe.Detavernier@ugent.be*

Engineering Biomimetic Biocompatible and Selectively Antibacterial Ultrathin Films by Vapor Phase Chemistry

[*]Karina Ashurbekova [a], Borja Alonso-Lerma [a], Kristina Ashurbekova [a], Arbresha Muriqi [c], Leire Barandiaran [a], Iva Šarić [d], Evgenii Modin [a], Raul Perez-Jimenez [e,b], Mladen Petravić [d], Michael Nolan [c], Mato Knez [a,b]

[a] *CIC nanoGUNE, Tolosa Hiribidea 76, Donostia-San Sebastián, E-20018, Spain.*
[b] *IKERBASQUE, Basque Foundation for Science, Plaza Euskadi 5, Bilbao, 48009, Spain.*
[c] *Tyndall National Institute, University College Cork, Lee Maltings, Dyke Parade, Cork, T12 R5CP, Ireland.*
[d] *Department of Physics and Centre for Micro- and Nanosciences and Technologies, University of Rijeka, Rijeka, 51000, Croatia.*
[e] *CIC bioGUNE, Bizkaia Science and Technology Park, building 800, Derio (Bizkaia) 48160 Derio, Biscay, Spain.*

Natural chitin and chitinoid materials have outstanding physical and biological properties, which inspired us to develop a process for biomimetic chitinoid organic and hybrid organic-inorganic thin film growth by Molecular Layer Deposition (MLD).
This work reveals a strategy for conformal growth of chitin and hybrid chitin-based biomaterials from the gas phase via Molecular Layer Deposition (MLD). We introduce a new type of organic-inorganic hybrid polymer, referred to as "metallosaccharides", based on sugar monomers as precursors. To ensure controlled growth, we couple N-Acetyl-D-mannosamine (ManNAc) with trimethylaluminum (TMA) or Titanium tetraisopropoxide (TTIP) from the vapor phase in repetitive cycles to obtain the respective biomimetic alumochitin or titanochitin thin films. To investigate these films, we utilize ATR-FTIR, X-ray photoelectron spectroscopy (XPS), Solid-state NMR (ssNMR), High resolution TEM (HRTEM) and Energy dispersive X-Ray spectroscopy (EDXS).
The antimicrobial activity of the alumochitin and titanochitin MLD films against Staphylococcus aureus and Escherichia coli were tested. Confocal microscopy allowed for analysis of attachment and proliferation of the bacteria on metallochitin-covered glass substrates. The results demonstrated high efficacy of both films, making them an attractive option for constructing bioactive surfaces.
Based on the in vitro proliferation of Human primary fibroblasts and HEK (Human Embryonic Kidney) 93 human cells, cultured on both alumochitin and titanochitin hybrid MLD films, the biocompatibility of the films was assessed. All MLD-coated substrates showed higher cell proliferation than the reference samples, namely uncoated coverslips.
Based on density functional theory (DFT), the chemical interactions between precursors ManNAc and TMA or TTIP, as well as the probability of the hybrid alumochitin or titanochitin film formation, were modeled and showed energetically favorable reaction mechanisms.

This project has received funding from the European Union´s Horizon 2020 research and innovation programme under the Marie Sklodowska -Curie grant agreement No 765378.

[*] *Corresponding author e-mail: ka.ashurbekova@nanogune.eu*

MOCVD of spinel ferrite film for applications in photoelectrochemical cells

Matteo Bombaci, Anna L.Pellegrino and Graziella Malandrino*

Dipartimento di Scienze Chimiche, Università di Catania, and INSTM UdR Catania, Viale A. Doria 6, 95125 Catania, Italy

Recently, spinel nanoferrites with general formula MFe_2O_4 have attracted great attention due to the potential application in hydrogen or oxygen production photoelectrochemical cells (PEC), due to their electrochemical and photochemical properties. The structure consists of M^{2+} cations, which usually occupy tetrahedral sites and Fe^{3+} which occupy octahedral sites in a face-centered cubic lattice formed by oxygens. Ferrites are active for the oxygen evolution reactions (OER) in PEC devices, through combined effects of electronic interactions between cations at octahedral and tetrahedral sites, as well as through the impact of different M^{2+} cations. Ferrites are also easily produced, have good chemical stability and redox activity, and the constituent elements are abundant in nature, non-toxic, and low-cost. Moreover, in this systems it is possible to tune the optoelectronic properties by replacing the divalent metal cation.[1] Several p-type ferrites, such as $CaFe_2O_4$, $CoFe_2O_4$ and $NiFe_2O_4$ and n-type like $ZnFe_2O_4$, have been investigated for applications in PEC cells [2].

In this work we present the MOCVD process of $NiFe_2O_4$, $CoFe_2O_4$ and $ZnFe_2O_4$ films, with variable thickness and morphology, depending on protocol's parameters, on Silicon (100), strontium titanate [STO (100)], ITO/quartz and "metallic foam" substrates. Those ferrites have been obtained at low pressure from the commercial iron(III) precursor [Iron(III)tris(2,2,6,6-tetramethyl-3,5-heptanedionate), $Fe(tmhd)_3$] and as second metal cation (M^{2+}), the synthetized β-diketonate precursors $M(tta)_2tmeda$ (M = Ni, Co, Zn), under flows of oxygen and Ar, as reactant and carrier gas, respectively. The three β-diketonate adducts $Ni(tta)_2tmeda$, $Zn(tta)_2tmeda$ and $Co(tta)_2tmeda$, (Htta = 2-thenoyltrifluoroacetone, tmeda = N,N,N',N'-tetramethyl-ethylendiamine), where the tmeda serves as a secondary Lewis base ligand, are nearly isomorphic and isostructural[3], and present small differences in the thermal behaviour when mixed in a proper ratio with $Fe(tmhd)_3$ precursor. In order to evaluate the thermal behaviour of the three different precursors mixtures, thermogravimetric (TG) and differential scanning calorimetry (DSC) analyses have been carried out, to allow the proper setting of temperature in the evaporation chamber. XRD measurements have confirmed the ferrite film formation, showing the production of polycrystalline ferrite phase on silicon, ITO/quartz and metallic-foam substrates, as well as the formation of oriented ferrite phase on single crystal substrates, like STO. The 1:2 stoichiometric ratio between the divalent cations M^{2+} (Ni^{2+}, Zn^{2+} and Co^{2+}) and Fe^{3+} is assessed via energy dispersive X-ray quantitative analysis (EDX). Moreover, the field-emission scanning electron microscopy (FE-SEM) images show the various morphology, texture, and thickness of the deposited ferrite films. The optical band gap has been evaluated through Tauc plot from the films deposited on ITO/quartz substrate. Preliminary measurements have been carried out to determine the catalytic activity in the oxygen evolution reaction (OER) and/or hydrogen evolution reaction (HER), which take place in photoelectrochemical water splitting devices.

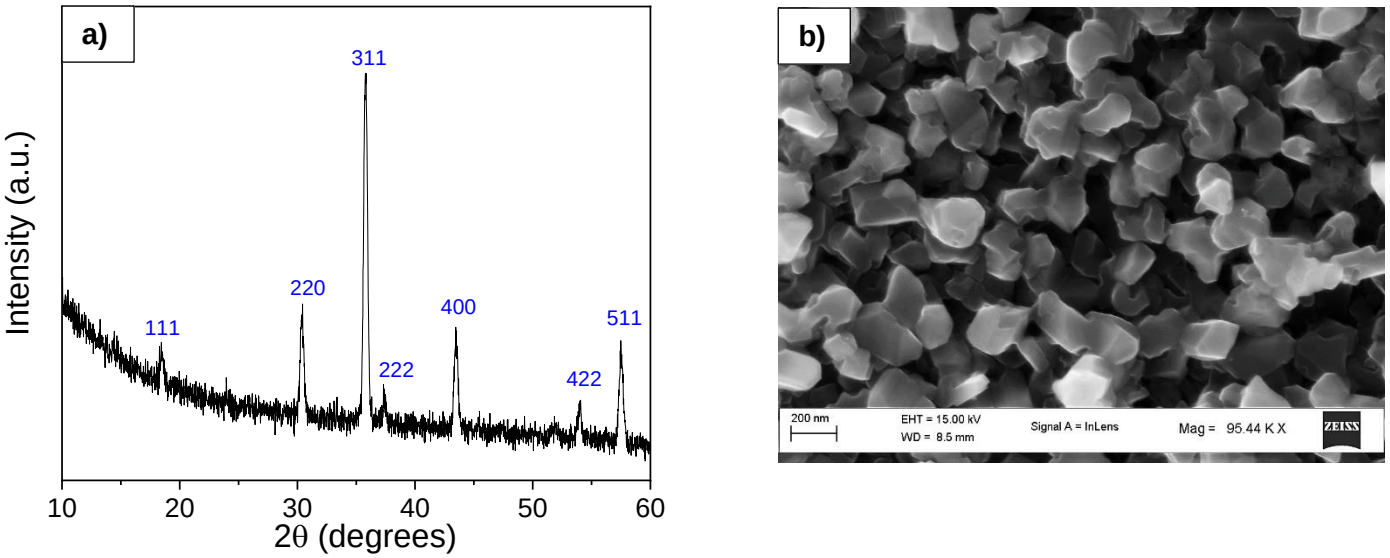

Fig. 1: a) XRD Pattern and b) FE-SEM image of a $NiFe_2O_4$ film deposited on Si (100).

References

1. S. Hussain, M.Mahdi Tavakoli, A. Waleed, U. Siddique Virk, S.Yang, A. Waseem, Z. Fan and M. Arif Nadeem. Langmuir 34, 3555–3564 (2018).
2. K. Malaie, Z. Heydari, M. R. Ganjali R. International Journal of Hydrogen Energy 46, 3510–3529 (2021).
3. G. Malandrino, L. M. S. Perdicaro, G. Condorelli, I. L. Fragalà, P. Rossi and P. Dapporto. Dalton Trans. 1101–1106 (2006).

* *Corresponding author e-mail:* gmalandrino@unict.it

Towards perovskite solar cells made by atomic layer deposition

Marianna Kemell*, Georgi Popov, Alexander Weiß, Mikko Ritala, Markku Leskelä

Department of Chemistry, University of Helsinki, FI-00014 Helsinki, Finland

Efficient and diverse utilization of solar energy is becoming increasingly important. The existing commercially available technologies must be accompanied by new ones to extend the range of applications towards flexible and lightweight devices, for example. With solar conversion efficiencies > 25%, halide perovskite solar cells show the highest promise among the emerging photovoltaic technologies.

Halide perovskites have the general formula ABX_3 where most often A = $CH_3NH_3^+$, $CH(NH_2)_2^+$ or Cs^+, B = Pb^{2+} or Sn^{2+} and X = I^-, Br^- or Cl^-. The most well-known member of this family is methylammonium lead iodide $CH_3NH_3PbI_3$ (MAPI). Its optical and electrical properties are ideal for photovoltaics. The properties can be adjusted to match other applications such as LEDs by tuning the composition. Moreover, halide perovskite solar cells are made from abundant and low-cost materials.

The perovskite solar cell technology is at the verge of commercialization but is still being impeded by scalability and stability issues. Atomic layer deposition (ALD) seems an obvious answer for solving the scalability issue and may contribute to improving the stability as well.

Our approach for depositing halide perovskite films relies on ALD of binary metal halides and their subsequent chemical conversion to the desired perovskites. Prior to this work ALD of metal halides other than fluorides was nonexistent. As the necessary first step, we developed ALD processes for binary metal halides PbI_2 [1], CsI [2], $PbCl_2$ [3] and $PbBr_2$ [3]. In all these processes, metal silylamides are used as metal precursors whereas different metal halides are used as halide precursors. Using the binary iodides as the starting point, we have developed the first ALD-based processes for the halide perovskites $CH_3NH_3PbI_3$ [1] and $CsPbI_3$ [2]. The former process involves treatment of an ALD-PbI_2 film with methylammonium iodide vapor whereas the latter converts an ALD-CsI film into $CsPbI_3$ by exposing it to the ALD process of PbI_2. Combining these processes with the ALD processes of $PbCl_2$ and $PbBr_2$ enables compositional engineering as a route to fine-tuned properties and improved stability.

Depositing the perovskite absorber only is not enough. No solar cell is complete without additional functional layers. In a halide perovskite solar cell, the perovskite layer is sandwiched between n- and p-type semiconductor films. Therefore, at least one material layer must be deposited on the halide perovskite, which is challenging due to their low thermal and chemical stability. We have contributed to this challenge by developing low-temperature ALD processes for PbS [4] by using Pb(II)amide precursors. Our processes enable deposition of p-type PbS on $CH_3NH_3PbI_3$ perovskite at temperatures below 100 °C, without damaging it. Furthermore, the PbS film also protects the underlying $CH_3NH_3PbI_3$ film from degradation under ambient conditions, acting thus in a dual role as a functional layer and as an encapsulant (Fig. 1). As another option, we have developed a two-step process for p-type CuI [5]. This process involves ALD of CuO at 80-140 °C and its conversion to CuI at RT, and is compatible with the $CsPbI_3$ perovskite (Fig. 2). Our processes form the first steps towards making a complete halide perovskite solar cell by ALD-based methods.

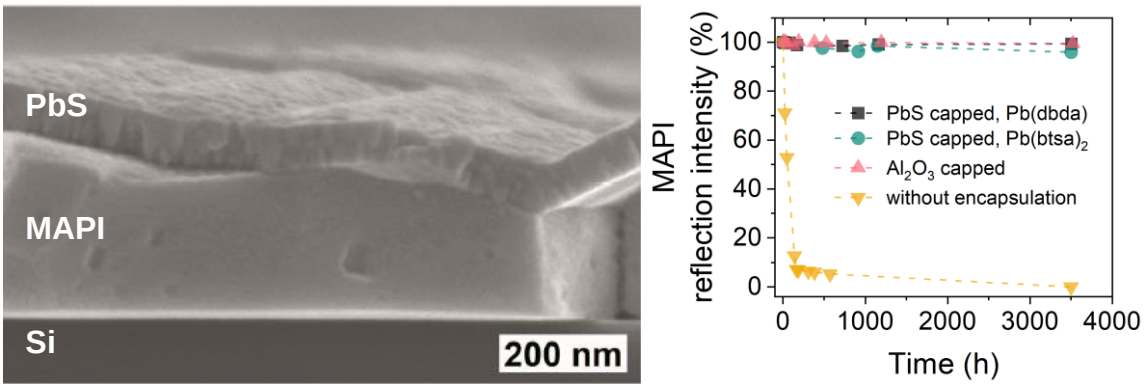

Figure 1. Left: Cross-sectional SEM image of a PbS-capped $CH_3NH_3PbI_3$ (MAPI). Right: MAPI film reflection intensity as a function of storage time in ambient air (open system) with and without different capping films [4].

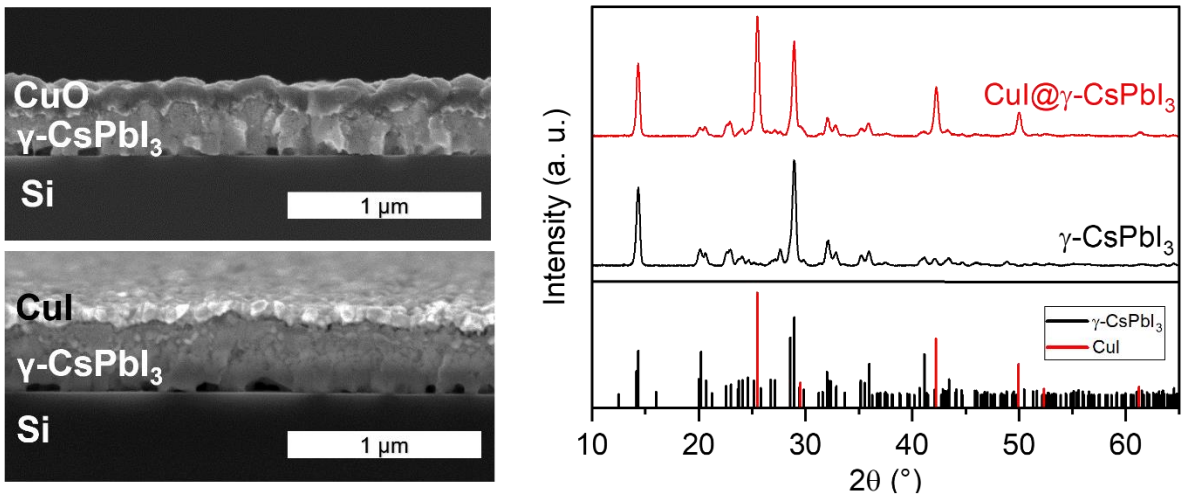

Figure 2. Left: Cross-sectional SEM images after deposition of ALD-CuO on γ-$CsPbI_3$ (top) and after the conversion of CuO into CuI (bottom). Right: GIXRD patterns of the γ-$CsPbI_3$ film before and after the deposition CuI on top of it [5].

References

1. G. Popov et al., *Chem. Mater.* **31** 1101 (2019).
2. A. Weiß et al., *Chem. Mater* **34** 6087 (2022).
3. G. Popov et al., *Dalton Trans*. **51**, 15142 (2022).
4. G. Popov et al., *Chem. Mater.* **32** 8216 (2020).
5. A. Weiß et al., *Adv. Mater. Interfaces* **2022**, 2201860.

* *Corresponding author e-mail:* marianna.kemell@helsinki.fi

Atomic Layer Deposition of $Li_4Ti_5O_{12}$: Towards High-Capacity 3D Thin-Film Batteries

Jan Speulmanns[a]*, Sascha Bönhardt[a], Malte Czernohorsky[a], Wenke Weinreich[a]

[a] *Fraunhofer Institute for Photonic Microsystems IPMS, Center Nanoelectronic Technologies (CNT), An der Bartlake 5, Dresden, 01109, Germany*

Atomic layer deposition (ALD) of lithium (Li)-compound thin films has aroused significant interest in recent years. Promising applications are Li-ion thin-film batteries (TFBs), protective particle coatings, interface model systems, and neuromorphic computing [1, 2]. Here, we evaluate the performance of $Li_4Ti_5O_{12}$ (LTO) anodes fabricated by ALD for three-dimensional (3D) solid-state TFBs to power upcoming autonomous sensor systems.

The simultaneous increase of power and energy density of full-cell 3D TFBs by coating the battery layer stack over micro-structured substrates was recently demonstrated [3]. The required conformal, pinhole-free deposition, and stoichiometric control of nanometer-thin films on highly structured surfaces are only accessible via ALD. The vapor-phase technique based on sequential, self-limiting surface reactions is well understood. However, the direct deposition of Li-compound anodes remains challenging [1].

In previous studies, we developed a thermal three-step ALD process for Li-containing mixed oxides on 200 mm silicon wafers [4, 5]. This process suppresses the undesired hygroscopic nature of lithium hydroxide during deposition with water as the oxygen source. Lithium-tert-butoxide (LTB) and lithium hexamethyldisilazide (LiHMDS) were both proven as suitable precursors forming high-quality spinel LTO with low impurities after rapid thermal processing. The electrochemical behavior of ALD LTO with LiHMDS was examined for the first time and linked to the film texture [5].

In this work, we optimize the LTO ALD process with LTB towards high-capacity 3D TFBs and evaluate the electrochemical performance for the first time. The effect of the substrate on the initial growth, crystallization behavior, and texture are investigated via in-situ spectroscopic ellipsometry and X-ray diffraction. A saturated growth per cycle of around 1.2 Å per cycle for a 7 s LTB pulse enables the required thick ALD films for high capacity. The ALD temperature window is explored between 220 and 320 °C.

Next, we evaluate two approaches to increase the footprint capacity. Planar ALD LTO films with a thickness of up to 100 nm are manufactured. 30 nm LTO films revealed excellent power capabilities with 50 % of the maximum capacity at extreme discharge rates of 200C. Outstanding cycle performance is demonstrated, exhibiting only 2 % capacity loss after 1000 cycles at 100C. By increasing the film thickness, the footprint capacity is raised from 1.8 to around 5.5 µAh cm^{-2}. However, the C-rate performance of thick films is inferior, which could be related to larger overpotentials due to the low conductivity of LTO. First results of LTO on micro-structured substrates with aspect ratios up to 20:1 show an increase in footprint capacity. However, the film conformality requires further optimization. The subsequent increase in energy and power density will be discussed.

Compared to other deposition techniques, the superior performance of ALD LTO is a key enabler for scalable high-volume production of on-chip high-capacity 3D TFBs.

References

1. O. Nilsen, K. B. Gandrud, R. Amund, F. Helmer, Wiley, Hoboken, NJ, 183-207 (2017).
2. Y. Zhu, J. C. Gonzalez-Rosillo, M. Balaish, Z. D. Hood, K. J. Kim, J. L. M. Rupp, Nat Rev Mater **6**, 313-331 (2021).
3. A. Pearse, T. Schmitt, E. Sahadeo, D. M. Stewart, A. Kozen, K. Gerasopoulos, A. A. Talin, S. B. Lee, G. W. Rubloff, K. E. Gregorczyk, ACS Nano **12**, 4286-4294 (2018).
4. S. Bönhardt, K. Kühnel, A. M. Kia, W. Weinreich, JVST A **37**, 31508 (2019).
5. J.Speulmanns, A.M. Kia, S. Bönhardt, W. Weinreich, P. Adelhelm, Small **17**, 2102635 (2021).

* *Corresponding author e-mail: jan.speulmanns@ipms.fraunhofer.de*

Macroscopically uniform distribution of platinum over mesoporous γ-alumina by a scalable atomic layer deposition process

Saeed Saedy[a,*], Jänis Järvilehto[b], Christine Gonsalves[b], Jorge Velasco[b], Thomas Grehl[c], Philipp Brüner[c], J. Ruud van Ommen[a], Riikka L. Puurunen[b]

[a] *Chemical Engineering Department, Delft University of Technology, Van der Maasweg 9, The Netherlands*
[b] *Department of Chemical and Metallurgical Engineering, Aalto University, Finland*
[c] *IONTOF GmbH, Münster, Germany*

Preparing supported catalysts is a gentle art, and the employed synthesis method determines the selectivity and activity of the catalyst. The size and shape homogeneity of supported nanoparticles have a decisive effect on catalyst efficiency. The nonuniformity of the supported metal/metal oxide clusters alters the catalyst's selectivity, activity, and stability; it also causes ambiguities when correlating the catalytic properties (selectivity/activity/stability) to its structure [1, 2]. The conventional methods of supported catalyst preparation, such as impregnation and deposition-precipitation, often fail to produce a uniform distribution of the active phase over the support. Furthermore, they may leave a significant amount of residues from the mother solution over the support, and these impurities can have a suppressive effect on the catalyst activity [2]. These liquid-phase methods also require several post-synthesis steps, such as filtration, drying, and calcination, which are energy and time intensive, and environmentally harmful because of waste production.

Atomic layer deposition (ALD) offers promising solutions for synthesizing well-defined advanced functional nanomaterials, such as supported catalysts. ALD makes it possible to deposit the catalytically active material with sub-nanometer control over the support, obtaining highly uniform catalysts [2, 3]. ALD has drawn much attention to preparing well-defined catalysts in the last few years. Numerous reports demonstrate this method's advantages for supported catalyst synthesis compared to conventional methods. However, most of these studies focus on the microscopic aspects of ALD-prepared catalysts, and the macroscopic uniformity of the obtained catalyst and the scalability of the synthesis procedure received little attention in recent years.

In this work, we report platinum ALD on commercial mesoporous alumina spheres (SASOL Limited, Fig. 1) as test vehicles with a 2.5 mm diameter and a specific surface area of 206 $m^2 \cdot g^{-1}$ (BET measurement). The alumina spheres were immersed in a bed of glass beads of 120 – 150 µm diameter and coated using an atmospheric pressure fluidized bed ALD (FB-ALD) reactor [4]. Fluidized bed reactors are widely used in the chemical industry because of excellent mixing and heat transfer, and applying them for ALD coating of powders and granules makes large-scale ALD processes for catalyst production feasible. (Trimethyl)methylcyclopentadienylplatinum(IV), $MeCpPtMe_3$, was used as the main reactant, and synthetic air was used as the counter-reactant for ALD of platinum at 110°C [5, 6]. Five samples of Pt/Al_2O_3 were obtained by varying the $MeCpPtMe_3$ pulse time (3, 6, 12, 24, and 48 min) while the oxidizer's pulse time was kept constant at 10 min; five cycles of ALD were used for all samples. The macroscopic distribution of platinum clusters over alumina was visualized using X-ray photoelectron spectroscopy (XPS, Thermo Scientific K Alpha X-ray photoelectron spectroscope) and low-energy ion scattering (LEIS, IONTOF Qtac 100 low-energy ion scattering spectrometer). The platinum's weight loading was also quantified using inductively coupled plasma - atomic emission spectroscopy (ICP-OES). The XPS line scans over the cross-section of alumina spheres (Fig. 2) demonstrate an adsorption front at the outer shell of the spheres, and the platinum concentration declines when moving toward the center. This trend is evident for the samples with $MeCpPtMe_3$ pulse times of 3, 6, and 12 min, and it fades off for the samples with longer exposure time.

The qualitative platinum surface coverage maps of cross-sections of the alumina spheres obtained using LEIS give a visual picture of the platinum distribution at the macroscopic level. In accordance with XPS results, the LEIS results (Fig. 3) showed an adsorption front for the samples with lower exposure time. This deposition front results in an egg-shell distribution of platinum in the samples with an exposure time of 3, 6, and 12 min, which fades off with the increase of exposure time.

The results of this work, to the best of our knowledge, for the first time visualize the macroscopic uniformity of an ALD-deposited noble-metal catalyst in a FB-ALD reactor. Also, this work reports the use of industry-relevant millimeter-sized spherical catalyst supports to attain macroscopic uniformity. The obtained results demonstrate that ALD can produce supported catalysts, attaining macroscopic uniformity. On the other hand, the scalable nature of the fluidized bed reactor employed in this study promises an environmentally friendly single-step large-scale catalyst production process.

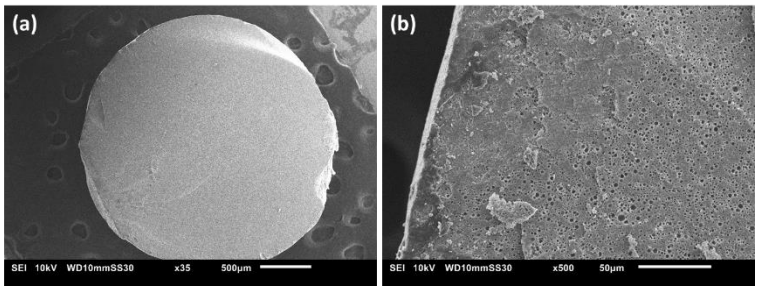

Fig. 1: The SEM image of the cleaved cross-section of a mesoporous alumina sphere.

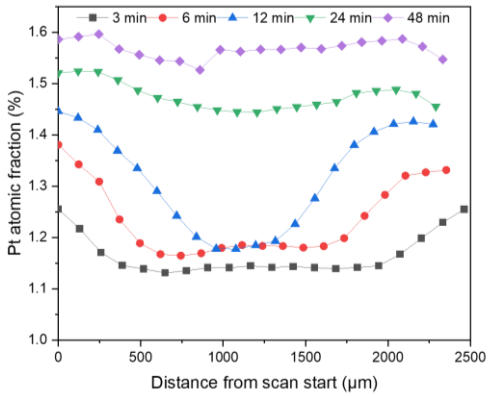

Fig. 2: The atomic fraction of platinum on the cleaved cross-section of 2.5 mm alumina spheres obtained using XPS line scans.

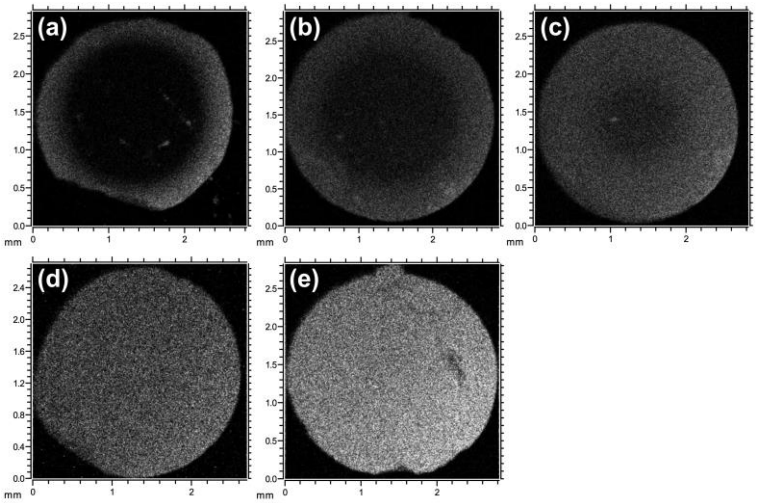

Fig. 3: The qualitative platinum surface coverage maps of cross-sections of alumina spheres with a platinum exposure time of a: 3 min, b: 6 min, c: 12 min, d: 24 min, and e: 48 min, obtained using LEIS.

References

1. P. Munnik, P. E. de Jongh, and K. P. de Jong, Chemical Reviews **115**, 6687 (2015).
2. B. J. O'Neill *et al.*, ACS Catalysis **5**, 1804 (2015).
3. J. R. van Ommen, A. Goulas, and R. L. Puurunen, in Kirk-Othmer Encyclopedia of Chemical Technology, pp. 1.
4. J. R. van Ommen and A. Goulas, Materials Today Chemistry **14**, 100183 (2019).
5. F. Grillo, H. Van Bui, D. La Zara, A. A. I. Aarnink, A. Y. Kovalgin, P. Kooyman, M. T. Kreutzer, and J. R. van Ommen, Small **14**, 1800765 (2018).
6. J. Järvilehto, Masters thesis, Aalto University, 2022.

* *Corresponding author e-mail: s.saedy@tudelft.nl*

Interplay between coordination sphere engineering and properties of nickel precursors for NiO thin films

Mattia Benedet,*[,a] Davide Barreca,[b] Ettore Fois,[c] Roberta Seraglia,[b] Gloria Tabacchi,[c] Marco Roverso,[a] Gioele Pagot,[d] Cristiano Invernizzi,[c] Alberto Gasparotto,[a,b] Alexandra Heidecker,[e] Alexander Pöthig,[e] Emanuela Callone,[f] Cinzia Sada,[g] Sandra Dirè,[f] Sara Bogialli,[a,b] Vito Di Noto,[d] Chiara Maccato[a,b]

[a] *Department of Chemical Sciences, Padova University, Via Marzolo 1, 35131 Padova, Italy*
[b] *CNR-ICMATE and INSTM, Department of Chemical Sciences, Padova University, Via Marzolo 1, 35131 Padova, Italy*
[c] *Department of Science and High Technology, Insubria University and INSTM, Via Valleggio 11, 22100 Como, Italy*
[d] *Department of Industrial Engineering, Padova University and INSTM, Via Marzolo 9, 35131 Padova, Italy*
[e] *Catalysis Research Center, Technische Universität München, Lichtenbergstr. 4, 85747 Garching, Germany*
[f] *Department of Industrial Engineering, Trento University, Via Sommarive 9, 38123 Trento, Italy*
[g] *Department of Physics and Astronomy, Padova University and INSTM, Via Marzolo 8, 35131 Padova, Italy*

Nickel oxide (NiO) is a *p*-type semiconducting material endowed with attractive properties, encompassing low-cost, excellent chemical stability and high transparency in the Vis region. Thanks to these favorable properties, NiO thin films are promising candidates for a variety of technological devices, including solar cells, solid state gas sensors, UV photodetectors, and light emitting diodes. Among the various physical and chemical preparation techniques for the growth of NiO films, chemical vapor deposition (CVD) is a favorable option thanks to the adaptability to large-scale production, good conformal coverage, and many degrees of freedom to tailor the system chemico-physical characteristics. Yet, its successful implementation is critically dependent on the availability of precursors endowed with suitable chemico-physical properties. In this regard, heteroleptic diketonate diamine adducts represent promising candidates, fulfilling the criteria of good stability under vaporization conditions, suitable volatility and reactivity, and suitable temperature range between volatilization and decomposition. In particular, precursor characteristics and behavior can be finely modulated either by changing the ligand sterical hindrance, or by introducing F-bearing groups, that can suppress the hydrolysis of moisture-sensitive complexes, reduce intermolecular interactions and improve mass-transport properties.
In this work, we have focused our attention on the development of three different Ni diketonate diamine precursors of general formula NiL_2TMEDA [L = 1,1,1-trifluoro-2,4-pentanedionate (tfa), 2,2-dimethyl-6,6,7,7,8,8,8-heptafluoro-3,5-octanedionate (fod), 2,2,6,6-tetramethyl-3,5-heptanedionate (dpm); TMEDA = *N*,*N*,*N′*,*N′*-tetramethylethylenediamine] obtained *via* an easy and reproducible two-step procedure (Fig. 1a). A main aim of the present study is to investigate the interplay between precursor molecular structure and the resulting chemico-physical properties, investigated by a variety of techniques (NMR, IR, optical absorption and IR spectroscopies, theoretical calculations), as well as with the thermal behavior and fragmentation patterns [analyzed by DSC, TGA (Figs. 1b-c) and mass spectrometry techniques]. As a matter of fact, NMR spectra (Fig. 1d) and single-crystal XRD analyses showed all the expected main features and accounted for the formation of monomeric compounds, endowed with a clean fragmentation pattern and attractive mass transport properties. TGA analyses showed a zero residual weight for all the precursors at temperatures higher than 300°C, and an increasing volatility upon changing L from dpm, to fod, to tfa. For all the investigated compounds, the linear vaporization rate trends in Fig. 1c indicated a clean vaporization free from undesired side decomposition processes, an amenable starting point for CVD applications.
The developed compounds have also been validated in thermal CVD experiments aimed at the fabrication of NiO films on Si(100) substrates under selected growth conditions, and the resulting materials have been characterized by complementary analytical techniques to investigate their chemical composition, structure and morphology. The clean precursor decomposition was assessed by XPS measurements (Fig. 2a), that provided evidence for the presence of Ni and O signals, whose detailed analyses confirmed the successful obtainment of pure NiO. XRD investigation (Fig. 2b) revealed the occurrence of cubic Ni(II) oxide as the sole crystalline phase. FE-SEM images (Fig. 2c) showed the formation of compact columnar films, with a morphology almost independent on the used precursor. The fluorination degree could be clearly appreciated by in-depth SIMS analyses (Fig. 2d). For $Ni(tfa)_2TMEDA$ and $Ni(fod)_2TMEDA$, fluorine appeared to be homogeneously distributed into NiO films, whereas in the case of $Ni(dpm)_2TMEDA$ no fluorine signal could be ever detected.
Taken together, the presently reported results highlight how $Ni(fod)_2TMEDA$, $Ni(tfa)_2TMEDA$ and $Ni(dpm)_2TMEDA$ can be deemed to be successful precursors for the CVD of nickel oxide-based nanomaterials, whose properties can be finely tailored in view of different functional applications [1].

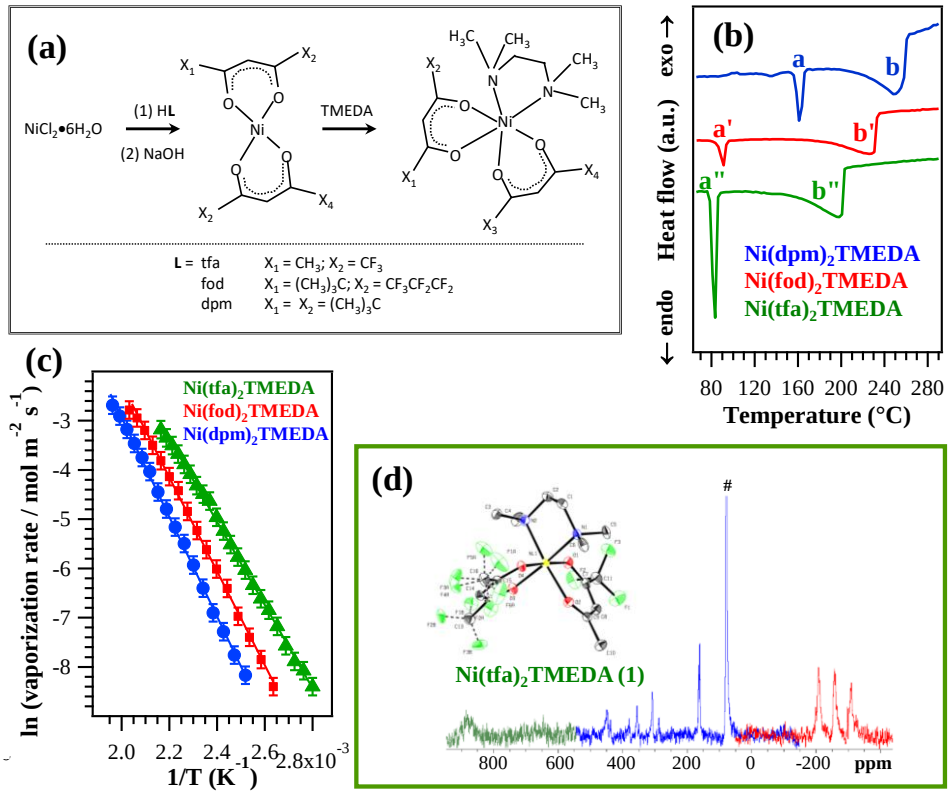

Figure 1. (a) Schematic procedure for the synthesis of the Ni-based precursors. (b) DSC curves and (c) Arrhenius plots for the compound vaporization. (d) ^{13}C NMR analysis of $Ni(tfa)_2TMEDA$ sample in $CDCl_3$ as a sum of four 800 ppm wide spectra ($CDCl_3$ signal at 77 ppm). Inset: compound molecular structure obtained by single crystal XRD analysis.

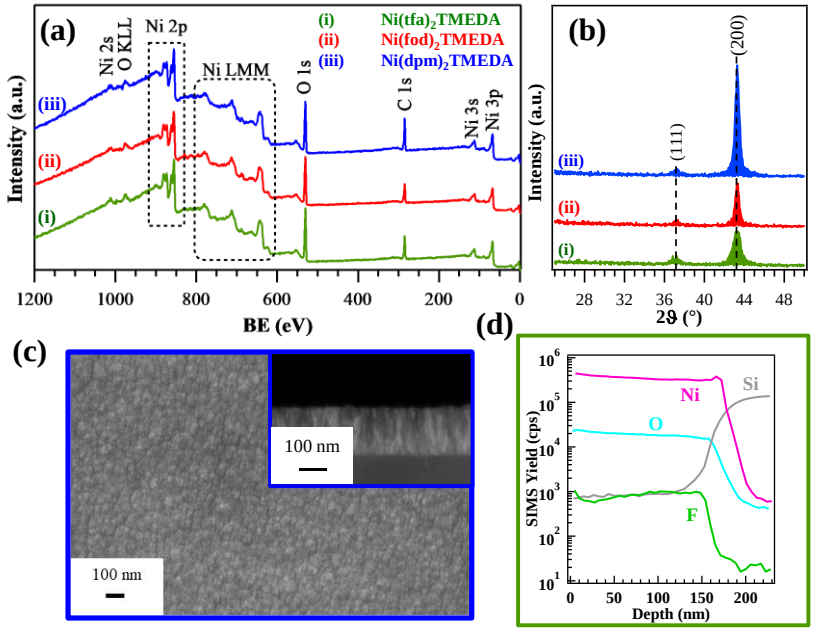

Figure 2. (a) Surface wide-scan XP spectra and (b) XRD patterns of NiO films grown on Si(100) under a wet O_2 atmosphere. (c) FE-SEM micrographs for NiO films obtained from $Ni(dpm)_2TMEDA$ under wet conditions. (d) SIMS depth profile of a $Ni(tfa)_2TMEDA$-derived NiO deposit on Si(100).

References

1. M. Benedet, D. Barreca, E. Fois, R. Seraglia, G. Tabacchi, M. Roverso, G. Pagot, C. Invernizzi, A. Gasparotto, A. Heidecker, A. Pöthig, E. Callone, C. Sada, S. Dirè, S. Bogialli, V. Di Noto, C. Maccato, *submitted*.

* *Corresponding author e-mail:* mattia.benedet@phd.unipd.it

Stabilized Aluminum Hydride Complexes as Potential Precursors for Vapor Phase Deposition Processes

Niklas Huster,[a,*] Anjana Devi[a]

[a] *Inorganic Materials Chemistry, Ruhr-University Bochum, Universitätsstr. 150, Bochum, D-44801, Germany*

Aluminium oxide (Al_2O_3) is one of the most studied and established material system owing to the wide range of its applications. Fabrication of thin films of Al_2O_3 via vapor phase deposition processes, namely atomic layer deposition (ALD) involves the most widely studied trimethylaluminium/water (TMA/H_2O) precursor system. This is often considered as an 'ideal' precursor combination. In comparison, the reports on deposition of aluminium nitride (AlN), and aluminium (Al) metal films are relatively limited which might be associated to the requirement of a reductive process environment. This can either be provided by a reducing co-reactant (e.g., NH_3, H_2) or taking advantage of the intrinsic reductive capabilities of the precursor itself. Lately aluminium hydrides (or *alanes*, AlH_3) have proven to be a suitable precursor class. A major drawback of alanes however is the limited thermal stability, which can be improved by introducing stabilizing ligands. Such stabilized alanes are long known as single source precursors (SSP) for Al metal films via chemical vapor deposition (CVD)[1] and have proven to be a versatile precursor class for ALD of AlN[2] and Al.[3] Thus, they are proposed to be promising for different aluminium based material systems just employing one precursor and varying process conditions and co-reactants.

Herein, we present the synthesis and characterization of a series of stabilized aluminium hydrides. These comprise structurally simpler amine stabilized alanes as well as structurally more complex compounds featuring multidentate ligands and intramolecular stabilized alanes by introducing e.g., *dimethylaminopropyl (DMP)* ligands. For evaluation as potential (single source) precursors for vapor phase deposition processes the compounds were evaluated by comprehensive thermal characterization and decomposition studies. The investigated compounds show significantly improved thermal stability alongside high volatility (Figure 1), while maintaining the high reactivity of aluminium hydride complexes. These properties qualify them as potential precursors for CVD as well as ALD, where well considered process conditions could be utilized to deposit different aluminium-based material systems.

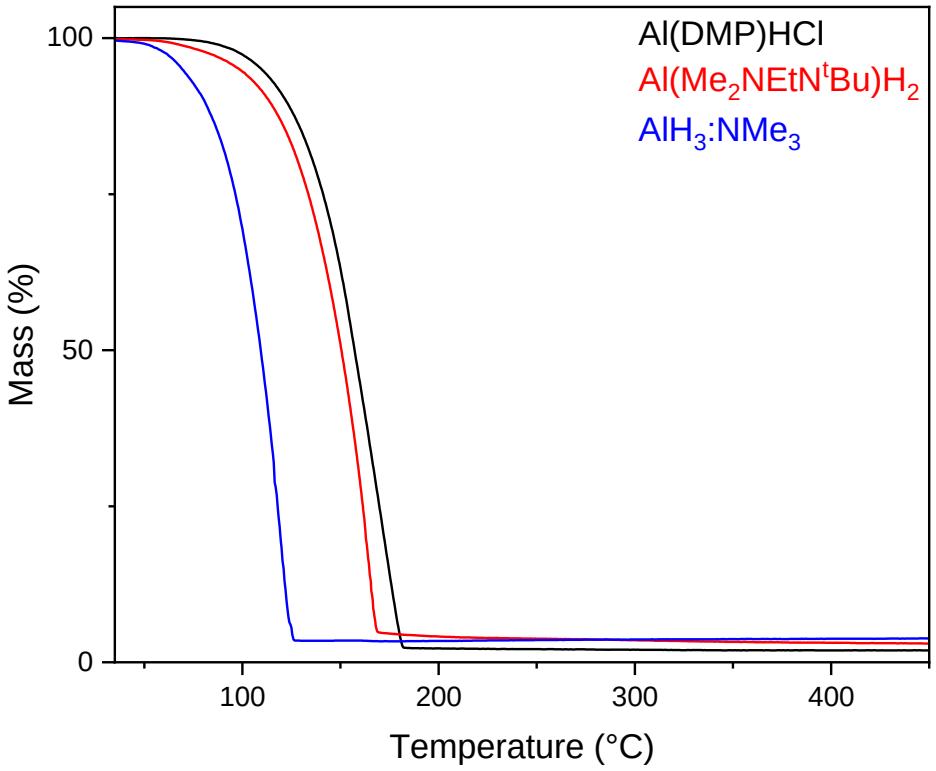

Figure 1 Selected stabilized alanes as potential precursors for vapor phase deposition. Temperature range from 35 – 450 °C with a heating rate of 5 K min^{-1} and a N_2 flow of 90 sccm.

References

1. I. Karpov, G. Bratina, L. Sorba, A. Franciosi, M. G. Simmonds, and W. L. Gladfelter, J. Appl. Phys., 76, 3471 (1994)
2. S. C. Buttera, P. Rouf, P. Deminskyi, N. J. O'Brien, H. Pedersen and S. T. Barry, Inorg. Chem., 11025 (2021)
3. K. J. Blakeney and C. H. Winter, Chem. Mater., 30, 1844 (2018).

* *Corresponding author e-mail: jan-niklas.huster@ruhr-uni-bochum.de*

ZnS Buffer Layers: Novel Precursors for AACVD

M. Robson[a], A. L. Johnson[a] *

[a] *University of Bath, Claverton Down, Bath, BA2 7AY, United Kingdom.*

Zinc sulfide, ZnS, presents an attractive non-toxic alternative to cadmium sulfide as a buffer layer material for thin film photovoltaic cells. The bandgap of ZnS can be tuned via oxygen doping, allowing for alignment with that of the solar absorber material deployed. This tunability requires control of Zn/S stoichiometry whilst also exercising high uniformity during fabrication, and given the intricate nature of thin film architectures, controllable and scalable fabrication methods must be considered. In this vein, aerosol-assisted chemical vapour deposition (AACVD) is a viable technique for thin film deposition as single-source precursors can afford stoichiometric control. Sustainable development of ZnS deposition via AACVD must be met with facile precursor synthesis and low deposition temperatures.

While metal amidates have been used for various deposition techniques, thioamidate-based metal sulfide precursors for chemical vapour deposition has gone largely unexplored, despite encouraging results.[1,2] Bismuth thioamidate was first explored for ALD of bismuth oxide. However, this precursor design was deemed to lack the required volatility, instead decomposing at 100 ˚C.[3] By contrast, AACVD precursors aren't confined by volatility. Tin(II) thioamide has been reported to deposit SnS at temperatures as low as 200 ˚C with minimal carbon content.[2] In light of this, formulation and analysis of zinc thioamides may provide insight into their viability for deposition of ZnS and Zn(O,S) buffer layers.

In this body of work, a novel single-source precursor design was explored as a basis for low-temperature deposition of zinc oxysulfides via AACVD. A series of zinc thioamidate complexes is presented as potential precursors for the deposition of ZnS. Viability studies were conducted using thermogravimetric and NMR experiments. Viable precursors were used for thin film deposition at temperatures 175 – 300 ˚C. Results give precedent for ZnO/ZnS co-deposition via AACVD for solar cell technology, and, more broadly, clean deposition of divalent-metal chalcogenide materials.

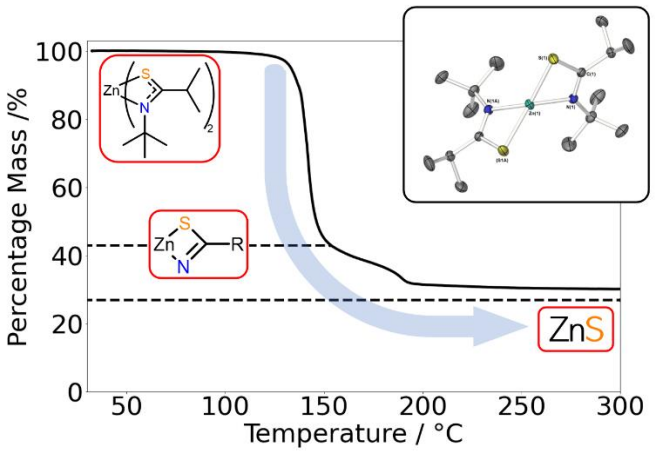

Fig. 1 *Decomposition profile of selected zinc thioamidate via thermogravimetric analysis. The resulting mass is indicative of ZnS deposition. The molecular structure of the selected precursor (insert).*

References

1. A. Catherall, S. Harris, M. Hill, A. Johnson, G. Kociok-Köhn, M. Mahon, *J. Mater. Chem. C*, **4**, 10731 (2016).
2. A. Catherall, S. Harris, M. Hill, A. Johnson, M. Mahon, *Cryst. Growth Des.*, **17**, 5544 (2017).
3. M. Vehkamäki, T. Hatanpää, M. Ritala, M. Leskelä, *J. Mater. Chem.*, **14**, 3191 (2004).

* *Corresponding author e-mail:* chsalj@bath.ac.uk

New Precursors to Printed Electronic Metal Oxides

Elinor T Vokes [a, b], Dr Andrew L Johnson [a]

[a] *Department of Chemistry, University of Bath, Claverton Down, Bath, BA2 7AY*

[b] *Centre for Doctoral Training in Aerosol Science, School of Chemistry, University of Bristol, Cantock's Close, Bristol, BS8 1TS*

Printing based thin film fabrication processes, such as aerosol jet printing (AJP), are an emerging area of technological interest within the electronics industry, as a cost-effective means to deposit functional materials on a range of substrates.[1] AJP involves the deposition of an ink containing an active functional pigment. The pigments of interest for this work are single-source precursors (SSPs) to n-type ZnO. ZnO has been used extensively as a material for the semiconducting channel in thin film transistors (TFTs), which are a type of field effect transistors that provide the basis for many electronics devices.[2] While ZnO is intrinsically n-type, the viability of forming p-type ZnO has been shown through doping with shallow acceptor alkali metals, thus ZnO exhibits the versatility required for next generation electronics.[3]

This work outlines the development of several novel precursor complexes compatible with deposition of ZnO *via* AJP. Based on successful ALD and CVD precursors, a series of heteroleptic and homoleptic Zn(II) aminoalkoxide complexes were synthesised as potential candidates for routes to printed ZnO films. Complexes were characterised by single crystal x-ray diffraction and multinuclear NMR. Preliminary studies, carried out to understand the viablilty of the complexes for thin film depostion, are described. Figure 1 shows the thermogravimetric traces of 4 of the synthesised complexes.

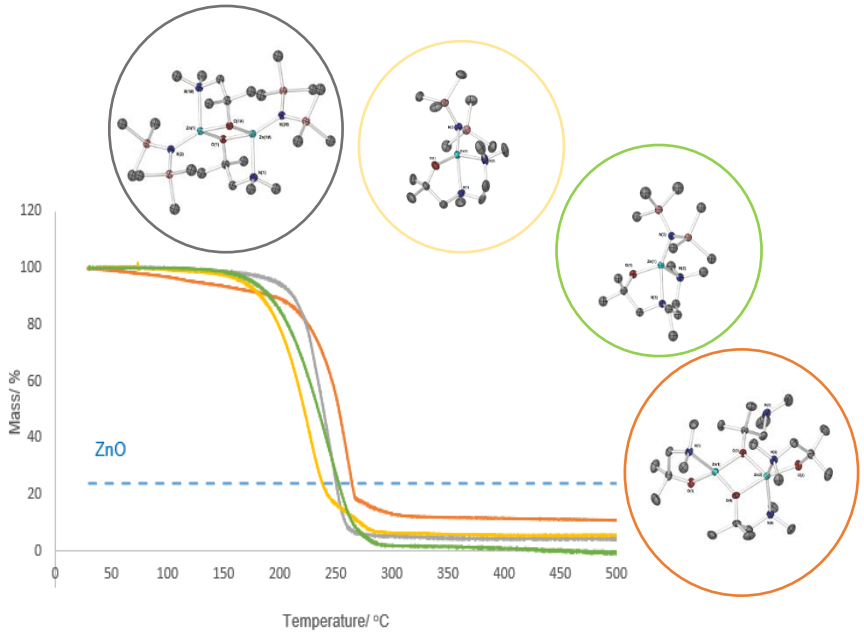

Fig. 1 Thermogravimetric traces of 4 of the synthesised Zn(II) aminoalkoxide complexes with corresponding structures shown.

References:

1. E. B. Secor, Flex. Print. Electron., **3**, (2018).
2. M. Pandey, M. Rashiku and S. Bhattacharya, *Chemical Solution Synthesis for Materials Design and Thin Film Device Applications*, (Elsevier, 2021), p. 349–368.
3. Ü. Özgür, Y. I. Alivov, C. Liu, A. Teke, M. A. Reshchikov, S. Doğan, V. Avrutin, S. J. Cho and H. Morkoç, *J. Appl. Phys.*, **98**, 41301 (2005).

* *Corresponding author e-mail: chsalj@bath.ac.uk*

Development of Single-Source Precursors for Chemical Vapour Deposition of Lithium Sulfide (Li_2S_x)

Daniel M. Mason[a,b], Andrew L. Johnson[a]*

[a] *University of Bath, Claverton Down, Bath, BA2 7AY, United Kingdom*
[b] *AAPS CDT, University of Bath, Claverton Down, Bath, BA2 7AY, United Kingdom*

Lithium-ion batteries are regarded as a revolutionary technology, widely used in portable devices, electric vehicles and large energy storage systems. Due to ever-growing energy needs, the demand for higher energy density storage devices has increased. However, the current intercalation-type cathodes used, such as $LiCoO_2$, have drawbacks. Capacities are limited to ~ 200 $mAh.g^{-1}$, costs are high and there are ethical implications from sourcing some materials [1,2]. To improve upon this, lithium-sulfur batteries are being considered part of the next generation of battery materials, using solid sulfur or lithium sulfide as the cathode [3]. Despite having a high capacity (1675 $mAh.g^{-1}$), sulfur cathodes are susceptible to volume changes during the discharge process and are prone to polysulfide shuttling and lithium dendritic growth. This results in a significant drop in capacity following the first discharge cycle [4,5]. Lithium sulfide has been proposed as a reasonable alternative cathodic material. The fully lithiated system (Li_2S) boasts a capacity of 1166 $mAh.g^{-1}$ [3]. However, it is subject to a high activation voltage, since the system is in a fully discharged state, prior to its first cycle. With chemical vapour deposition (CVD), a lithium sulfide film can be deposited onto a charge collector material with significant control. This allows for nanostructuring of the film, which could alter the reaction kinetics and lower the activation voltage. This can occur through the design of the precursor material. By using a single-source precursor for lithium sulfide, the energetic requirement of deposition is reduced, whilst the use of aerosol assisted CVD (AA-CVD) removes the necessity of a volatile precursor material; instead requiring solubility [6].

This work entailed the development of novel single-source precursors for deposition of metal chalcogenide thin films via AACVD. Multiple lithium organo-sulfide complexes are presented as potential precursors for the deposition of Li_2S_x ($1 \leq x \leq 8$). Studies included multinuclear-NMR and DOSY experiments, XRD and thermogravimetric analysis. Suitable precursor candidates, such as that shown in Fig. 1, are being taken forward for deposition studies to produce films for applications including use as charge carrying materials.

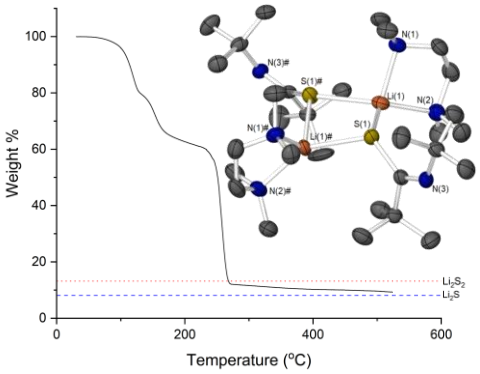

Fig. 1: TGA plot of lithium thioamidate precursor. Dotted lines highlight calculated Mass % of Li_2S_2 and Li_2S. Inset: Crystal structure of lithium thioamidate precursor. Thermal ellipsoids are shown at 50% probability. Hydrogens are omitted for clarity.

References

1. L. Zhou, W. Zhang, Y. Wang, S. Liang, Y. Gan, H. Huang, J. Zhang, Y. Xia, and C. Liang, Journal of Chemistry **2020**, 6904517 (2020).
2. S. G. Booth *et al.*, APL Materials **9**, 109201 (2021).
3. M. R. Kaiser, Z. Han, J. Liang, S.-X. Dou, and J. Wang, Energy Storage Materials **19**, 1 (2019).
4. H. Ye, M. Li, T. Liu, Y. Li, and J. Lu, ACS Energy Letters **5**, 2234 (2020).
5. H. Pan, Z. Cheng, P. He, and H. Zhou, Energy & Fuels **34**, 11942 (2020).
6. M. A. Bhide, K. L. Mears, C. J. Carmalt, and C. E. Knapp, in Nanomaterials via Single-Source Precursors, edited by A. W. Apblett, A. R. Barron, and A. F. Hepp (Elsevier, 2022), pp. 3.

* *Corresponding author e-mail:* chsalj@bath.ac.uk

Investigation of Bismuth ALD precursors

Jaroslav Charvot*, Filip Bureš

Institute of Organic Chemistry and Technology, Faculty of Chemical Technology, University of Pardubice, Studentská 573, 532 10 Pardubice, Czech Republic

Bismuth compounds have unique properties with high value in various technological fields. The most prominent are Bi_2Te_3 and Bi_2Se_3 used as thermoelectric materials. Additionally, both mentioned chalcogenides have been identified as topological insulators.[1] Elemental bismuth or Bi-Sb alloys also possess high order topology.[2] Some Bismuth-containing oxides or halides exhibit perovskite structure and can be used as superconductors, ferroelectric materials and show photoactivity.[3]

Atomic Layer Deposition (ALD) of bismuth-containing layers has been achieved using various precursors. $BiCl_3$ is a common compound, but it has considerably low volatility. Use of triphenylbismuth is often limited by its reactivity only under certain conditions for deposition of specific materials. Other bismuth compounds, such as alkoxides[4] or amides,[5] have also been investigated, with some successfully utilized precursors.

This work aims to further expand the bismuth precursors portfolio by investigation of new compounds that meet the general demands of ALD precursors (high volatility, thermal stability, appropriate reactivity) and can be easily and cheaply prepared in large quantities. For this purpose, fluorinated alcoholates were chosen with example of $[(CF_3)_2CH\text{-}O]_3Bi$, which was prepared by simple route as low-melting point distillable solid.[6] Another investigated class are tris(trialkylsilyl)bismuthides bearing atom of Bi with formally negative charge, which possibly enables new exciting materials in ALD.

The preparation of potential Bi precursors is followed by characterization by mass spectrometry and heteronuclear NMR. Determination of basic thermal properties, as key characteristic for ALD precursor was achieved by DSC and TGA. The best candidates with the most suitable properties are then tested in ALD.

This works is funded within the project THERMOS (TH80020009). We would like to thank M-ERA.NET and Technology Agency of the Czech Republic for support.

References

1. H. Zhang, C. X. Liu, X. L. Qi, X. Dai, Z. Fang, S. C. Zhang, Nat. Phys. **5**, 438–442 (2009).
2. L. Aggarwal, P. Zhu, T. L. Hughes, V. Madhavan, Nat. Commun. **12**, 8–13 (2021).
3. Z. Jin, Z. Zhang, J. Xiu, H. Song, T. Gatti, Z. He, J. Mater. Chem. **8**, 16166 (2020).
4. T. Hatanpää, M. Vehkamäki, M. Ritala, M. Leskelä, Dalt. Trans. **39**, 3219–3226 (2010).
5. M. Rusek, T. Komossa, G. Bendt, S. Schulz, J. Cryst. Growth **470**, 128–134 (2017).
6. P. C. Andrews, P. C. Junk, I. Nuzhnaya, L. Spiccia, Dalt. Trans., 2557–2568 (2008).

* *Corresponding author e-mail: jaroslav.charvot@upce.cz*

Modeling

Chair: Barry, Sean Thomas (Carleton University)

Time: 5/31/2023 8:30:00 AM
Location: Auditorium 1, Promotion Hall, Naamsestraat 22, Leuven

Mechanisms of atomic level processing from first principles simulations

Michael Nolan[a], Ji Liu[a], Arbresha Muriqi[a], Rita Mullins[a]

[a] *Tyndall National Institute, University College Cork, Lee Maltings, Cork, T12R5CP, Ireland.*

Atomic level processing, encompassing atomic layer deposition (ALD), thermal atomic layer etching (tALE), and molecular layer deposition (MLD) is widely used in semiconductor device production and is beginning to show its versatility in production of catalysis, battery materials, coatings for medical devices and novel hybrid materials with enhanced functionality. At the core of these processing technologies is chemistry that takes place at surfaces. First principles simulations, using density functional theory (DFT), are a powerful tool to understand and predict the chemistries of ALD, tALE and MLD to help chose new process chemistries or to understand why potential chemistries are successful or not.

In this contribution we will present an overview of our recent work on mechanisms of atomic level processing focussing on the following topics: **(i)** plasma ALD of cobalt[1-3], **(ii)** chemistries for MLD of hybrid inorganic-organic films[4-6] and **(iii)** mechanisms of thermal ALE of crystalline and amorphous HfO_2[7-8].

For Co plasma ALD we have determined the mechanism of a full deposition cycle using $Co(Cp)_2$ and NH_3/H_2 plasma (Figure 1) showing that the nitridation of the Co surface is crucial to promote Co deposition and that some incorporation of N into the deposited film is unavoidable.

For hybrid MLD we explain the experimental findings of poor film growth with typical aliphatic organics (ethylene glycol and glycerol) and show that aromatic precursors provide more stable and rigid films. We also discuss which functional groups on the organic impart higher stability and how functionalisation of the aromatic ring impacts on the fundamental MLD chemistry.

Finally, we use DFT simulations of the HF chemistry on model crystalline and amorphous HfO_2 surfaces to understand the differences in etch rates between $cHfO_2$ and a HfO_2 and provide an origin for enhanced etching of amorphous oxides compared to crystalline oxides.

If time allows, I will also discuss future directions in atomistic simulations of atomic level processing.

References

1. J. Liu and M. Nolan, J. Phys. Chem. C, **123**, 25166 (2019)
2. J. Liu, H. Lu, D. W. Zhang and M. Nolan, J. Phys. Chem., C, **124,** 11990 (2020)
3. J. Liu, H. Lu, D. W. Zhang and M. Nolan, Nanoscale, **14,** 4712 (2022)
4. A. Muriqi, M. Nolan, Dalton Transactions, **49,** 8710
5. A. Muriqi, M. Karppinen, M. Nolan, Dalton Transactions, **50,** 17583 (2020)
6. A. Tanskanen, P Sundberg, M Nolan and M Karppinen, Thin Solid Films, **736,** 138896 (2021)
7. R. Mullins, S. Kondati Natarajan, S. D. Elliott, M. Nolan, Chem. Mat., **32,** 3414 (2020)
8. R. Mullins, J. J. Gutierrez-Moreno, M. Nolan, J. Vac. Sci. Tech. A, **40,** 022604 (2022)

* *Corresponding author e-mail:* michael.nolan@tyndall.ie

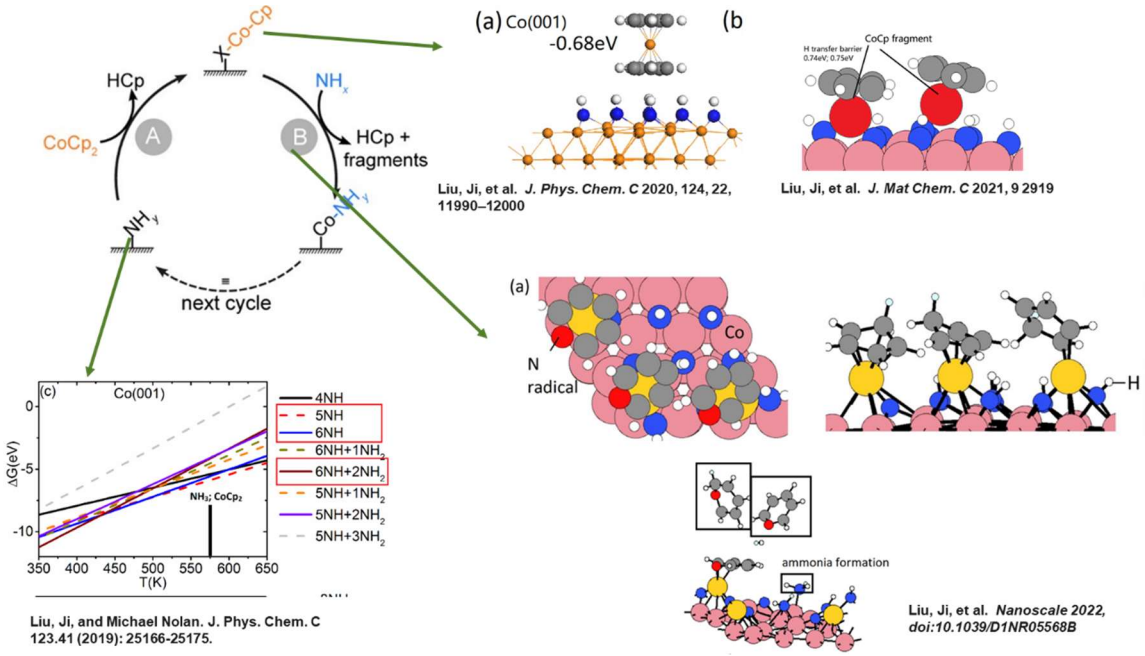

Figure 1: Summary of DFT calculations of a full plasma ALD cycle for Co deposition.

Predicting microstructural changes in a CVD reactor thanks to CFD simulation of the local supersaturation

Yann Gallou[a,*], Marie Dubois[a], Roman Reboud[a], Cyril Hassant[b] Alexandre Potier[b], Guy Chichignoud[a] Didier Chaussende[a]

[a] Université Grenoble Alpes, CNRS, Grenoble INP (Institute of Engineering), SIMaP, 38000 Grenoble, FRANCE
[b] MERSEN, 41 rue Jean Jaurès, Gennevilliers, 92230, FRANCE

Polycristalline silicon carbide (3C-SiC) can have multiple applications in harsh or high temperature environment owing to its outstanding strength, hardness, thermal shock resistance and inertness. Chemical vapor deposition is used for the production of pure and dense polycrystalline SiC coatings on various substrate compatible with the required temperature range for deposition (900°-1500°). For instance, deposition on graphite can serve as a protective coating for high temperature applications such as semiconductor annealing or doping furnaces. Coating on C/C composites intended for use in aerospace industry could protect them against oxidation and mechanical erosion.

Many properties of these SiC films depends on their microstructure, for instance grain size can influence the thermal conductivity [1], the hardness [2] and the Young modulus [2] of the material. Grain size evolution with thickness could also generates a stress gradient as intrinsic stress is often located at grain boundary as shown in other polycrystalline materials deposited via gas phase process [3,4]. In case doping agents are added in the film, electrical conductivity also depends on grain size as grain boundary acts as a carrier trap [5].

For the deposition of poly-SiC on complex shaped substrate, hot wall reactors are often used allowing a homogeneous heating of the loading thanks to radiation. The drawbacks of these reactors are the parasitic deposition on the hot wall that leads to the depletion of reactive species which makes it difficult to quickly assess the effect of a change in process conditions on the growth rate and the associated microstructure on the area of interest. Setting up new process conditions hence requires a lot of trials and errors which can be costly. Computational fluid dynamic (CFD) simulation is a powerful tool to evaluate gas flow, temperature distribution and even growth rate. However, only few studies relate the local growth conditions (temperature, gas composition…) to the microstructure of the deposit. The key parameter for film growth and its microstructure is the supersaturation. While supersaturation is hard to define for a binary material that does not evaporate as a single component, several propositions have been made in the literature. Most of them are based on thermodynamics consideration and consist of calculating separately the gas phase equilibrium composition while allowing the formation of the solid or not [6]. The ratio of both gives an estimation of the supersaturation value but consider the CVD process as a black box without accounting for gas flow, temperature gradient or reaction kinetics. To overcome this, some authors proposed a way to estimate local supersaturation based on CFD simulation and thermodynamic calculation [7]. This approach has only been applied to cold wall reactor while it would be of even greater interest for hot wall configuration, due to the evolution of the gas phase composition in the hot zone.

In this study we simulate a lab-scale CVD apparatus to relate local conditions to the corresponding microstructures at different position on the hot wall, upon changing the process conditions (temperature, pressure, H_2:MTS). The temperature distribution is simulated and calibrated via experimental measurement at different position in the reactor. The kinetic mechanism is compiled from several references [8–11] and some kinetic parameters are adjusted to take into account later findings and to fit experimental data. The simulation predicts well the experimental growth rate at every position in the hot wall reactor on a broad range of experimental conditions, including temperature, pressure, gas flow and H_2:MTS ratio. The estimation of the local supersaturation correlate well with the microstructure, for instance a higher grain size is observed at a lower supersaturation value. As the supersaturation depends exponentially on the temperature, this parameter has the most pronounced effect but interestingly, while the temperature is kept constant, a change of pressure or H_2:MTS ratio leads to a different growth rate profile and a shift in preferential orientation and grain size along the hot wall, associated to a variation of the local supersaturation.

Overall, we demonstrate that local conditions can be estimated via CFD simulation and related to the microstructural changes. Although the kinetic mechanism used contained about 40 species and 70 reactions it could be simplified to a smaller reactions scheme without losing much accuracy in determining the growth rate and the main gas-phase species. Some authors in the literature already succeeded in simulating complex hot wall reactor but with an oversimplified kinetic mechanism that would not allow an accurate determination of the local supersaturation [12]. It is then necessary to find a compromise between a very complex reaction scheme and an oversimplified one. Indeed, estimating

local super saturation in bigger reactor in 3 dimensions would help the design of new processes when a specific microstructure is looked for at a specific position in the reactor.

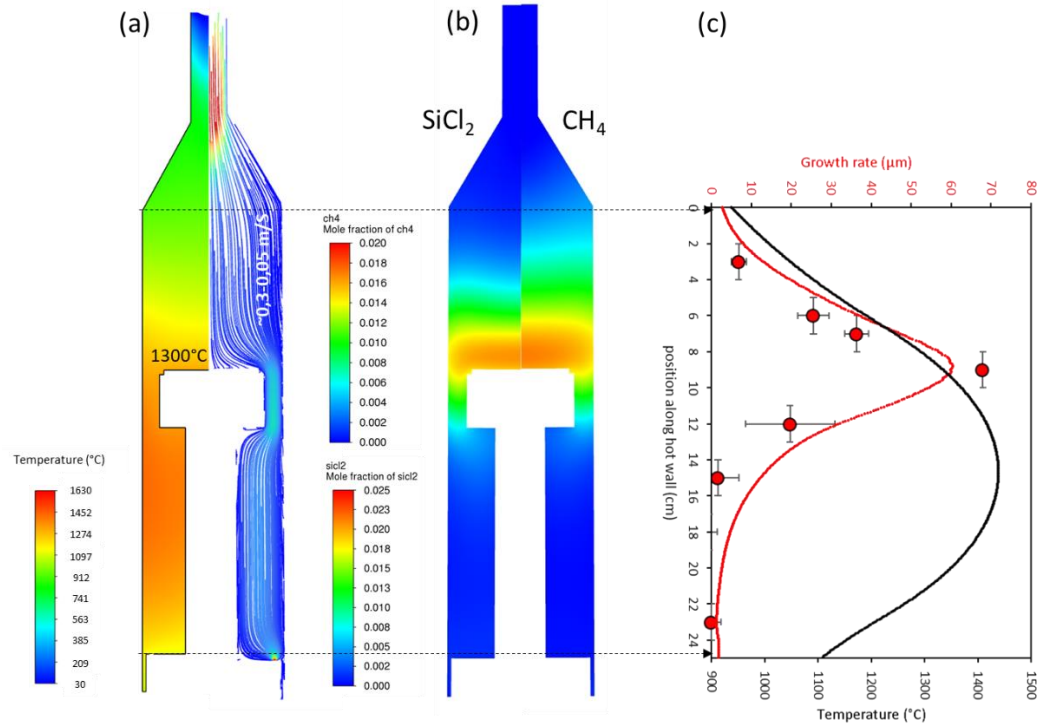

Fig 1. (a) temperature and gas flow in the CVD reactor, (b) simulated mole fraction for the two main species, CH_4 and $SiCl_2$, (c) Simulated temperature profile in black and growth rate in red. Red dots are the experimental growth rate.

References

1. A. K. Collins, M. A. Pickering, and R. L. Taylor, *Grain Size Dependence of the Thermal Conductivity of Polycrystalline Chemical Vapor Deposited B-SiC at Low Temperatures*, Journal of Applied Physics **68**, 6510 (1990).
2. Y. Long, *Deposition Rate, Texture, and Mechanical Properties of SiC Coatings Produced by Chemical Vapor Deposition at Different Temperatures*, International Journal of Applied Ceramic Technology **10**, 9 (2013).
3. P. Pobedinskas, J.-C. Bolsée, W. Dexters, B. Ruttens, V. Mortet, J. D'Haen, J. V. Manca, and K. Haenen, *Thickness Dependent Residual Stress in Sputtered AlN Thin Films*, Thin Solid Films **522**, 180 (2012).
4. G. C. A. M. Janssen, *Stress and Strain in Polycrystalline Thin Films*, Thin Solid Films **515**, 6654 (2007).
5. M. Eickhoff, H. Möller, J. Stoemenos, S. Zappe, G. Kroetz, and M. Stutzmann, *Influence of Crystal Quality on the Electronic Properties of* n *-Type 3C-SiC Grown by Low Temperature Low Pressure Chemical Vapor Deposition*, Journal of Applied Physics **95**, 7908 (2004).
6. G. Chichignoud, M. Ucar-Morais, M. Pons, and E. Blanquet, *Chlorinated Silicon Carbide CVD Revisited for Polycrystalline Bulk Growth*, Surface and Coatings Technology **201**, 22–23 (2007).
7. M. Pons, J. Su, M. Chubarov, R. Boichot, F. Mercier, E. Blanquet, G. Giusti, and D. Pique, *HVPE of Aluminum Nitride, Film Evaluation and Multiscale Modeling of the Growth Process*, Journal of Crystal Growth **468**, 235 (2017).
8. A. Veneroni and M. Masi, *Gas-Phase and Surface Kinetics of Epitaxial Silicon Carbide Growth Involving Chlorine-Containing Species*, Chem. Vap. Deposition 7 (2006).
9. R. Wang and R. Ma, *Kinetics of Halide Chemical Vapor Deposition of Silicon Carbide Film*, Journal of Crystal Growth **308**, 189 (2007).
10. P. Ho, A. Balakrishna, J. M. Chacin, A. Thilderkvist, B. Haas, P. B. Comita, and S. Clara, *CHEMICAL KINETICS FOR MODELING SILICON EPITAXY FROM CHLOROSILANES*, (n.d.).
11. M. D. Allendorf and R. J. Kee, *A Model of Silicon Carbide Chemical Vapor Deposition*, J. Electrochem. Soc. **138**, 841 (1991).
12. B. Deivendran, *3D Modeling and Optimization of SiC Deposition from CH3SiCl3/H2 in a Commercial Hot Wall Reactor*, Journal of Crystal Growth 10 (2021).

Corresponding author e-mail: **yann.gallou@grenoble-inp.fr

Diffusion-reaction model for conformality evolution in ALD on spherical porous catalyst particles

Niko Heikkinen[a,*], Juha Lehtonen[a], Jihong Yim[b], Riikka L. Puurunen[b]

[a] *VTT Technical Research Centre of Finland, Tietotie 4 C, Espoo, 02150, Finland*
[b] *Department of Chemical and Metallurgical Engineering, Aalto University School of Chemical Engineering, Kemistintie 1, Espoo, Finland.*

The ongoing transition from fossil feedstock based to renewable chemical industry and increasing precious metal scarcity [1] is creating demand for new catalyst preparation and modification methods. ALD is a versatile tool for heterogeneous catalyst preparation and modification [2–4]. The benefit is to add only desired amount of active metal(s) or functional overcoatings on the catalyst surface. Furthermore, the deposition conformality and control over the deposited material provides many catalyst finetuning opportunities. There are several fundamental publications [5,6] on modelling the ALD parameter effect on the conformality of the deposited thin film in model channels. However, less work has been done to resolve precursor and ALD process parameters effect on a porous, tortuous and spherical catalyst particle. Typically presented models have simplified the precursor transport into a cylindrical geometry model [7], whereas catalyst particle precursor transport is dependent also on the diminishing volume of the spherical geometry.

Our work presents a diffusion-reaction model fitted to a particle with spherical geometry. Table *1* presents model precursor related parameters (molecular mass, sticking probability, areal number density), ALD process parameters (temperature, precursor partial pressure) and catalyst support parameters (porosity, tortuosity, pore diameter, surface area, pore volume) to estimate the achieved precursor penetration into the catalyst particle with varying dose (mmol/g_{cat}). Figure *1* presents the modelled Zn ($Zn(acac)_2$ precursor) surface coverage profiles with varying exposure (precursor partial pressure x deposition time). In order to find a reasonable connection between model exposure and experimental dose, the model deposition time was first solved to result in 50 µm penetration depth. This penetration depth corresponded to 0.95 mmol/g_{cat} dose and SEM-EDS measurement penetration depth of zinc oxide coatings on alumina spheres. Lastly, the model deposition time was increased at the same ratio as with experimental dose to predict the remaining penetration depths.

Table 1, model parameters

Al_2O_3 support structural parameters		$Zn(acac)_2$ precursor parameters	
Parameter	**Value**	**Parameter**	**Value**
Porosity, ε	0.2	Temperature, T_P	393 K
Tortuosity, τ	4	Precursor mass, m_P	$263.61 \times 1.66 \times 10^{-27}$ kg
Mean pore diameter, d_{pore}	9.2×10^{-9} m	Maximum density of particles adhering to the surface, σ_P	2×10^{18} m^{-2}
BET surface area, A_O	158 m^2/g_{cat}	Precursor density outside the porous material, n_P (t, z = 0)	1.84×10^{22} m^{-3} *
Pore volume, V_P	5.4×10^{-7} m^3/g_{cat}	Sticking probability, β_0	1×10^{-2}

* Determined from estimated $Zn(acac)_2$ vapour pressure (100 Pa)

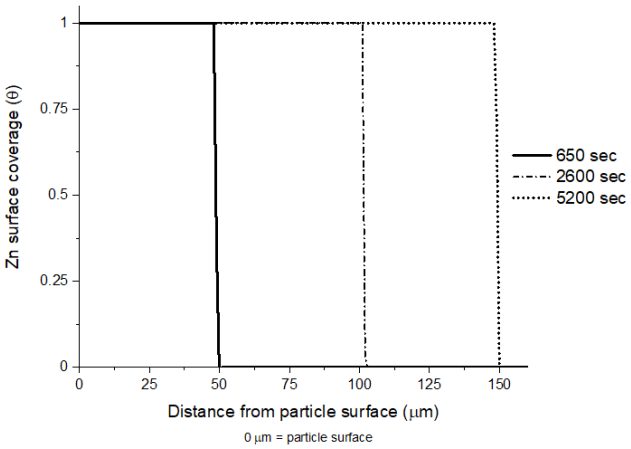

Model results	
Deposition time (seconds)	**Penetration depth (μm)**
650	50
2600	102
5200	149
Experimental results	
Dose (mmol/g_{cat})	**SEM-EDS penetration depth (μm)**
0,95	50
3,79	120
7,59	150

Figure 1, Left, modelled Zn surface coverage profiles with varying exposure. Exposure (partial pressure x time) having a fixed precursor partial pressure (100 Pa). Right, model deposition time (exposure) having the corresponding ratios with respect to the experimental dose of zinc acetylacetonate ALD reactant and resulting penetration depth of zinc oxide coatings inside the mesoporous alumina sphere particle.

According to the results in Figure *1*, the presented diffusion-reaction model, extended to spherical geometry (or shape factor) can be successfully used to design ALD processes for heterogeneous catalyst particles. This is especially useful, when designing novel catalyst compositions and structures for increased performance and catalyst life-time.

References

1. K. Cheng, L.C.J. Smulders, L.I. van der Wal, J. Oenema, J.D. Meeldijk, N.L. Visser, G. Sunley, T. Roberts, Z. Xu, E. Doskocil, H. Yoshida, Y. Zheng, J. Zečević, P.E. de Jongh, K.P. de Jong, Science (80-.). 377 (2022) 204–208.
2. H. Feng, J. Lu, P.C. Stair, J.W. Elam, Catal. Letters 141 (2011) 512–517.
3. B.J. O'Neill, D.H.K. Jackson, A.J. Crisci, C.A. Farberow, F. Shi, A.C. Alba-Rubio, J. Lu, P.J. Dietrich, X. Gu, C.L. Marshall, P.C. Stair, J.W. Elam, J.T. Miller, F.H. Ribeiro, P.M. Voyles, J. Greeley, M. Mavrikakis, S.L. Scott, T.F. Kuech, J.A. Dumesic, Angew. Chemie - Int. Ed. 52 (2013) 13808–13812.
4. J. Lu, B. Fu, M.C. Kung, G. Xiao, J.W. Elam, H.H. Kung, P.C. Stair, Science (80-.). 335 (2012) 1205–1208.
5. M. Ylilammi, O.M.E. Ylivaara, R.L. Puurunen, J. Appl. Phys. 123 (2018) 205301.
6. A. Yanguas-Gil, J.W. Elam, Chem. Vap. Depos. 18 (2012) 46–52.
7. T. Keuter, N.H. Menzler, G. Mauer, F. Vondahlen, R. Vaßen, H.P. Buchkremer, J. Vac. Sci. Technol. A Vacuum, Surfaces, Film. 33 (2015) 01A104.

* *Corresponding author e-mail:* niko.heikkinen@vtt.fi

DFT Modeling Study: Inhibition of Silica by Small Molecule Inhibitors in the AS-ALD of Al_2O_3

Philipp Wellmann[a]*

[a]*Wilhelm-Ostwald-Institut für Physikalische und Theoretische Chemie, Universität Leipzig, Linnéstraße 2, Leipzig 04103, Germany*

Through the development of AS-ALD technology, semiconductor manufacturing could be re-established as a bottom-up process. An easily accessible dielectric for ALD is Al_2O_3, which has advantageous properties compared to the natural oxide of silicon. To ensure the distinction between growth and non-growth areas, the selective shielding of surfaces employing gas-phase applicable small molecule inhibitors (SMI) is of much interest. Since the inhibition of the SiO_2 surface by methoxysilanes is spectroscopically almost inaccessible, DFT modeling has proven to be a valuable tool to unravel the structure of the blocking layer and the energetic aspects of its formation.
However, the significance of the DFT results strongly depends on the suitability of the deployed surface model used. Based on the highly idealized α-quartz model, previous studies could not satisfactorily explain key experimental features as the high efficiency of the trimethoxysilanes compared to the mono- and bifunctional silanes and the higher selectivities achievable with triethylaluminum (TEA) compared to trimethylaluminum (TMA). [1]

By employing more appropriate amorphous silica models, this DFT modeling study investigates how the reactions with trimethoxypropylsilane (TMPS) leads to the formation of the blocking layer and explores its interaction with the Al precursors TMA and TEA and the co-reactant water.
We show that TMPS exhibits unique bonding configurations with the amorphous system and that the full coverage of all silanols on the silica surface is feasible. The formation principles of the energetically most favorable full coverage configurations are derived. A theoretical limit for the closest packing of SMIs in the blocking layer is derived and evaluated regarding the permeability of Al precursors. This is achieved by calculating possible diffusion paths of the Al precursors undermining the blocking layer. Moreover, a reaction mechanism demonstrating the disintegration of the SMI-surface bond by the thus intruded Al precursors is described. We illustrate that the blocking layer is not inert to the Al precursors due to the presence of unreacted methoxy substituents and describe how the selectivity could be enhanced by their targeted substitution by inert alkyl groups. Furthermore, the role of the reactive bridge oxygen species regarding the loss of selectivity is evaluated, as well as methods for their preparatory removal. The work features reaction paths obtained by the nudged elastic band method and bonding analysis by the periodic energy decomposition analysis.

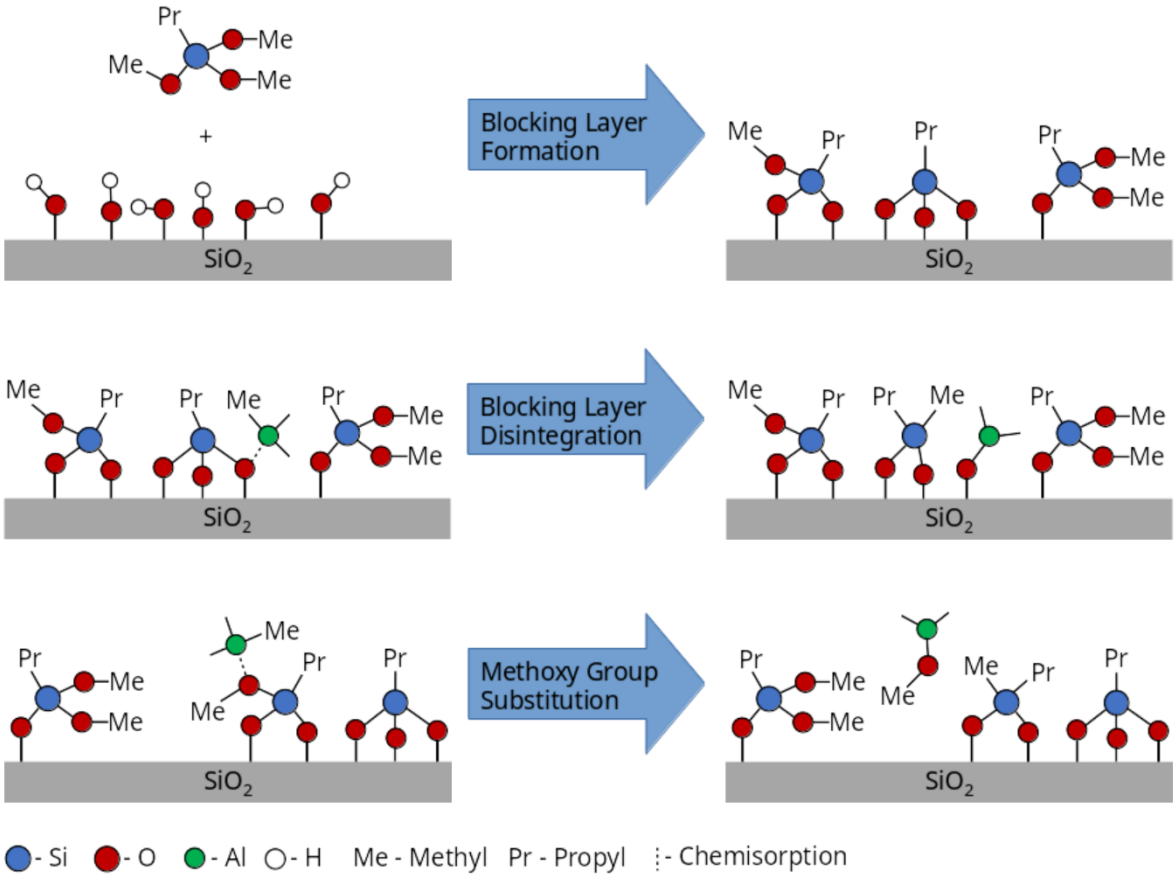

References
1. J. Yarbrough, *Chemistry of Materials* **2022** *34* (10), 4646-4659

* *Corresponding author e-mail:* p.wellmann@mailbox.org

Organic and hybrid materials

Chair: Nolan, Michael (Tyndall National Institute)

Time: 5/31/2023 10:30:00 AM
Location: Auditorium 1, Promotion Hall, Naamsestraat 22, Leuven

Vapor-Phase Synthesis and Modification of Porous Framework Thin Films

Junjie Zhao[a,*]

[a] *Zhejiang University, Rm. 1-409, Hetong Complex II, 866 Yuhangtang Rd, Hangzhou, 310027, China*

Engineering thin films of metal-organic frameworks (MOFs) and covalent organic frameworks (COFs) paves the way for fabrication of novel membrane structures, enabling separations for sustainability. Vapor-phase synthesis and modification of these porous framework materials avoid the swelling and dewetting issues that often appear in solution-based methods. In this talk, we will show vapor-phase processes for tuning COF pore sizes at sub-nm scale, preparing MOF thin films with controllable crystallinity, and constructing unique Janus film structures with MOFs and polymers. We explored atomic layer deposition (ALD) processes for pore engineering in two imine-based COFs. Changes in pore sizes were found to affect the gas adsorption behavior and the separation performance by COF membranes. We developed a vapor-phase synthesis method that can convert 2D nanosheets of hydroxy double salt into amorphous and crystallline zeolitic imidazolate framework (ZIF) thin films. Our amorphous mixed-metal ZIF-8 thin films possess similar composition and short-range order compared with the crystalline analogue, but exhibit higher separation selectivity for propylene over propane. Finally, we will present a strategy to obtain free-standing Janus MOF-polymer films using ALD-templated interfacial synthesis. This Janus film structure is flexible and stretchable, and can be easily transferred onto functional substrates for membranes and devices.

[*] *Corresponding author e-mail: junjiezhao@zju.edu.cn*

Molecular layer deposition of zeolitic imidazolate framework 8 films

Jorid Smets[a], Víctor Rubio-Giménez[a], Alexander John Cruz[a], Rob Ameloot[a,*]

[a] *Center for Membrane Separations, Adsorption, Catalysis, and Spectroscopy (cMACS), KU Leuven - University of Leuven, Celestijnenlaan 200F, Leuven, 3001, Belgium*

Vapor-phase film deposition of metal-organic frameworks (MOFs) would facilitate the integration of these materials into electronic devices. We studied the vapor-phase layer-by-layer deposition of zeolitic imidazolate framework 8 (ZIF-8) by consecutive self-saturating reactions of diethyl zinc, water, and 2-methyl imidazole. We developed two different methods: (1) Direct ZIF-8 'molecular layer deposition' (MLD) employs only self-saturating reactions, resulting in smooth films that are crystalline as-deposited, and (2) Two-step ZIF-8 MLD, in which crystallization occurs during a post-treatment step with additional linker vapor. The latter approach resulted in a reduced deposition time and an improved MOF quality, *i.e.*, increased crystallinity and probe molecule uptake, although the smoothness and thickness control were partially lost. Both approaches were developed in a modified atomic layer deposition reactor to ensure cleanroom compatibility. In this work, the effect of each step on the coating quality is evaluated, and the influence of the chemical nature of the substrate is studied.

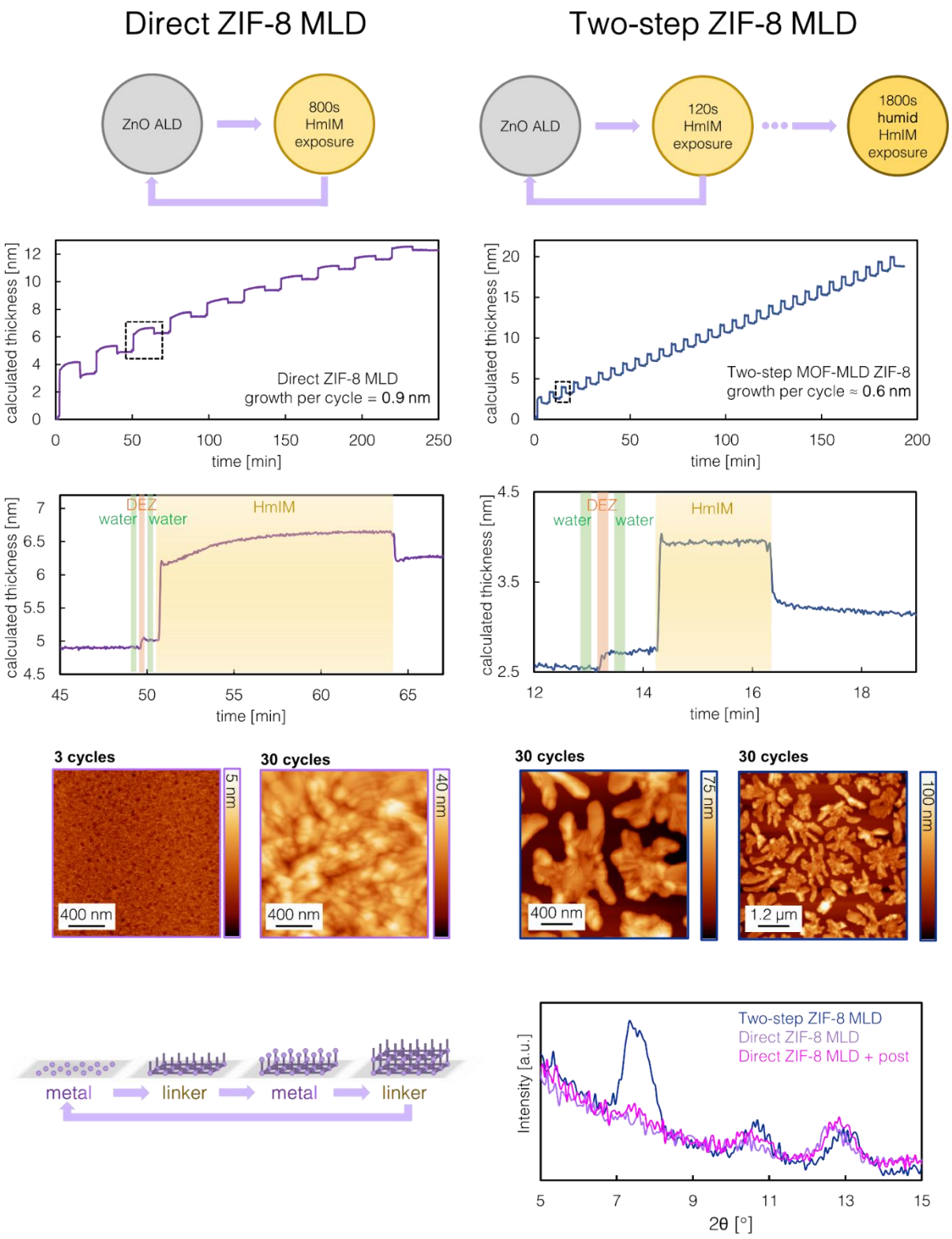

* *Corresponding author e-mail:* rob.ameloot@kuleuven.be

Towards high throughput spatial molecular layer deposition of alucone films

Hardik Jain[a,b], Mariadriana Creatore[a], Paul Poodt[a,*]

[a] *Department of Applied Physics, Eindhoven University of Technology, 5600 MB Eindhoven, The Netherlands*
[b] *TNO/Holst Centre, 5656 AE Eindhoven, Netherlands*

Molecular Layer Deposition (MLD) is a method, similar to ALD, to deposit organic- and hybrid inorganic/organic films making use of organic precursors and/or co-reactants. MLD holds great potential for applications requiring e.g. conformal deposition of organic/hybrid films inside 3D structures, for example for batteries [1-3] . However, scaling up MLD can often be challenging due to the necessity of very long cycle times (>100 s) and resulting low deposition rates. There are several MLD examples, like the common alucones, where very long purge times are required to outgas precursor that has infiltrated in the deposited film to avoid parasitic CVD reactions during the co-reactant exposure [4]. To minimize the effects of precursor infiltration, and to maximize deposition rates, a detailed understanding of the precursor infiltration, outgassing and subsequent CVD reactions is required.

For this purpose, we have studied the infiltration and outgassing kinetics of TMA in alucone films prepared with ethylene glycol in a Spatial ALD/MLD reactor, on both planar and 3D substrates [5,6]. By combining experimental data with a kinetic model, we have shown that for planar substrates, the extent of CVD reactions is mainly determined by the TMA dose and subsequent purge step, while being almost independent on the EG dose. Purge times exceeding 100 s are required to avoid CVD reactions and although purge times can be somewhat reduced by optimizing the TMA dose and purge gas flow, very long TMA purge times seem to be unavoidable to realize MLD of alucones without a CVD component. Using lateral high-aspect ratio trenches, we also investigated the effects of infiltration and outgassing on the conformality of MLD alucone films. The TMA infiltration, outgassing and parasitic CVD reactions, combined with diffusion limited transport of TMA out of and EG into the trenches lead to complex thickness profiles that have been explained using a simple diffusion-reaction model. Also in this case, very long purge times will be required to avoid non-conformal deposition.

However, a solution to increase the deposition rate of alucone MLD can be found in using di-methyl aluminium isopropoxide (DMAI) instead of TMA [7]. DMAI has a much lower vapor pressure and reactivity as compared to TMA, but DMAI does not infiltrate in the alucone film and therefore does not require long purge steps to avoid CVD reactions. Though an increase in DMAI exposure time as compared to TMA is required to compensate for a lower reactivity, the reduction in purge time effectively leads to an order of magnitude higher deposition rate as compared to using TMA. Furthermore, highly conformal alucone films inside high aspect ratio trenches have been realized as well. Finally, we will show that the film composition and properties of alucone films prepared using TMA and DMAI are very similar. These results indicate that high deposition rate and high conformality (Spatial) MLD of alucones is possible when using non-infiltrating precursors such as DMAI, helping to bring the scale-up of MLD one step closer.

References

1. Y. Zhao, X. Sun, ACS Energy Letters **3**, 899 (2018).
2. Y. Zhao et al, Nano Letters **17**, 5653 (2017)
3. D. Piper et al, Adv. Mater. **26**, 1596 (2014)
4. A. Dameron et al, Chem. Mater. **20**, 3315 (2008)
5. H. Jain, P. Poodt, Dalton Trans. **50**, 5807 (2021)
6. H. Jain, M. Creatore, P. Poodt, J. Vac. Sc. Technol. A **41**, 012401 (2023)
7. H. Jain, M. Creatore, P. Poodt, Dalton Trans. **51**, 7918 (2022)

[*] *Corresponding author e-mail: p.w.g.poodt@tue.nl*

.

Organic-Component and Ln-Ion Tailored White-Light Emitting Lanthanide-Organic Thin Films via ALD/MLD

Amr Ghazy[a], Mika Lastusaar[b] and Maarit Karppinen[a,*]

[a] *Department of Chemistry and Materials Science, Aalto University, Kemistintie 1, Espoo, FI-00076 Aalto, Finland*
[b] *Department of Chemistry, University of Turku, FI-20014, Turku, Finland*

Lanthanide (Ln) ions possess interesting photoluminescence properties, most importantly narrow band emissions at well-defined spectral ranges, e.g. red emission from Eu3+ ions and green emission from Tb3+ ions. Then, by combining several different Ln3+ ions mixed-lanthanide compounds with white light emission can be designed and synthesized. However, ALD-grown lanthanide oxide films are typically non-luminescent due to so-called concentration quenching effect. Our strategy to avoid this concentration quenching effect is to increase the Ln-Ln distances by separating the emissive Ln3+ ions by organic linkers. Indeed, we have realized interesting luminescence properties for various ALD/MLD-grown Ln-organic thin films. [1] Moreover, thanks to the organic components these films are mechanically flexible. [2]

White-light emitting materials are increasingly demanded for applications such as back light sources of displays to solar concentrators, biomedical imaging and photodynamic therapy. [3] Here we demonstrate warm white light emission for our ALD/MLD films grown using 1,4-benzene dicarboxylic acid (BDC) as the organic linker, in combination with Er3+, Eu3+, and Tb3+ ions. Moreover, the emission can be further enhanced by adding La3+ as seen in (Fig. 1a). (Fig. 1b) shows the comparison of the thus achieved light color with the colors coming from commercial fluorescent tube, incandescent bulb and LED lamp.

While the Ln-BDC films yield the desired warm white light emission, the absorption band (excitation range) is very narrow (centered around 250 nm) which limits their application potential. To tailor the absorption characteristics of our Ln-organic films we have investigated several different organic precursors. The absorption band can be shifted towards the higher wave-lengths by adding substituents to the benzene ring of the BDC backbone [4]; however, such films grown with 2,5-dihydroxy terephthalic acid and 2-amino terephthalic acid, turned out to be rough and non-homogenous, and not to show luminescence.

On the other hand, promising results were obtained for various nitrogen-containing aromatic organic molecules: nicotinic acid (NTA), 2,3-pyrazine dicarboxylic acid (PZC), uracil (URC), cytosine (CYS), and cyanuric acid (CUA). The newly developed ALD/MLD processes with these organic molecules yielded visually smooth and homogeneous Ln-organic films, showing intense luminescence. Most importantly, with these novel organic components it is now possible to cover a wide UV absorption/excitation range, up to ca. 380 nm, thus widening the potential application range. All the ALD/MLD processes reported here work in a relatively wide deposition temperature range, from 160 to 250 °C, and yield high quality films even on sensitive substrates such as polymers.

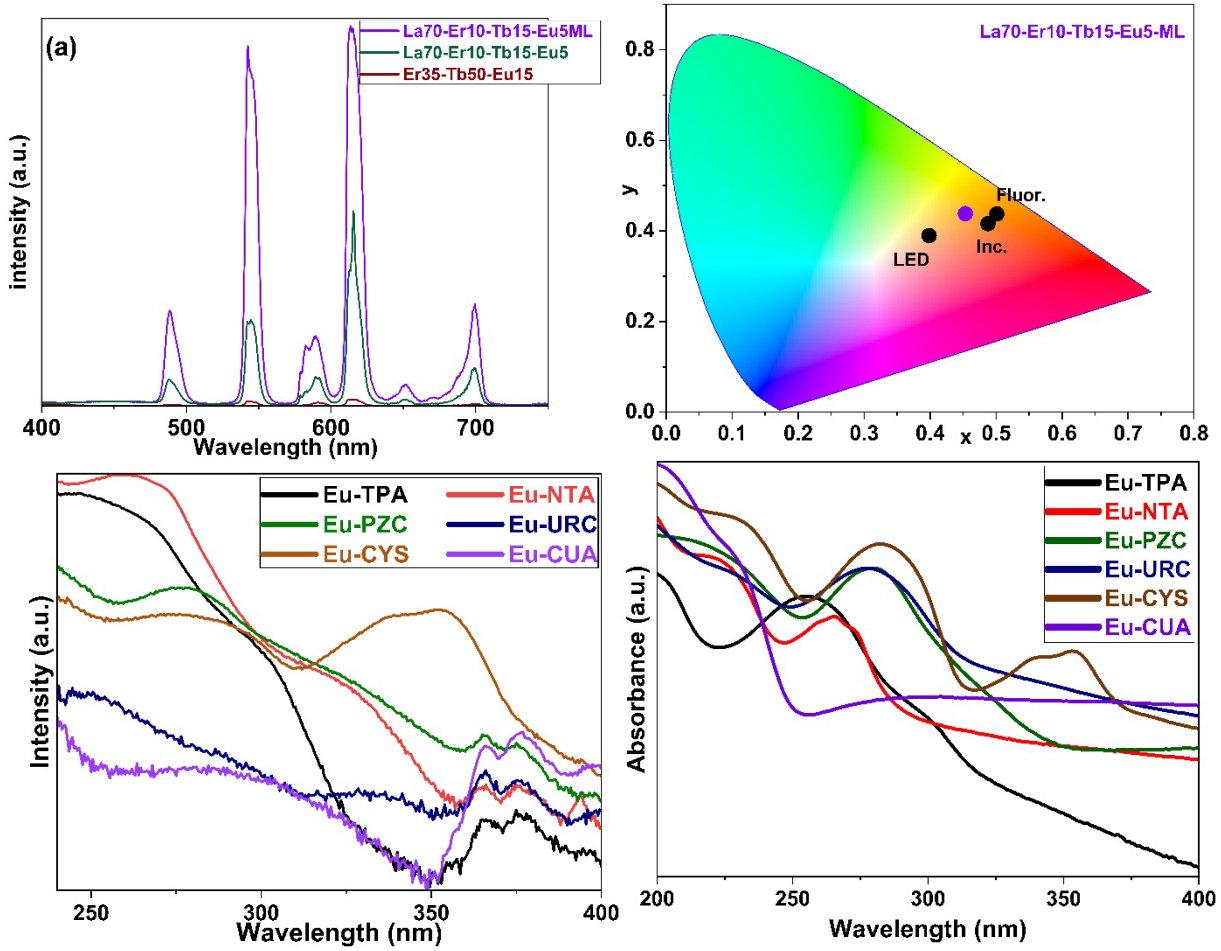

(**Fig. 1) (a)** Emission spectra of warm white emission of (La, Er, Tb, Eu)-TP samples showing peaks resembling transitions of Tb3+ and Eu3+. **(b)** Location of our ALD/MLD-grown white-light emitting thin film (purple circle) on the CIE 1931 color map, in comparison to commercial fluorescent lamp (Fluor.), incandescent lamp (Inc.) and LED lamp (LED). **(c)** Excitation spectra for our ALD/MLD Eu-organic thin films grown on silicon from different organic precursors. **(d)** Uv-vis absorption spectra of the ALD/MLD Eu-organic thin films from samples deposited on quartz glass

References

1. M. Safdar, A. Ghazy, M. Tuomisto, M. Lastusaari, and M. Karppinen, *Effect of Carbon Backbone on Luminescence Properties of Eu-Organic Hybrid Thin Films Prepared by ALD/MLD*, J. Mater. Sci. **56**, 12634 (2021).
2. Z. Giedraityte, P. Sundberg, and M. Karppinen, *Flexible Inorganic–Organic Thin Film Phosphors by ALD/MLD*, J. Mater. Chem. C **3**, 12316 (2015).
3. Y. Cui, B. Chen, and G. Qian, *Lanthanide Metal-Organic Frameworks for Luminescent Sensing and Light-Emitting Applications*, Coord. Chem. Rev. **273–274**, 76 (2014).
4. P. A. Hansen, J. Svendsen, H. Nesteng, and O. Nilsen, *Aromatic Sensitizers in Luminescent Hybrid Films*, RSC Adv. **12**, 18063 (2022).

* *Corresponding author e-mail:* maarit.karppinen@aalto.fi

Organic-inorganic hybrid thermoelectric materials through a new concept of vapor phase infiltration (VPI)

Kristina Ashurbekova[a,*], Mato Knez[a,b]

[a] *CIC nanoGUNE, Tolosa Hiribidea 76, Donostia-San Sebastián, E-20018, Spain.*
[b] *IKERBASQUE, Basque Foundation for Science, Plaza Euskadi 5, Bilbao, 48009, Spain.*

Thermoelectric (TE) devices have attracted great interest in waste heat recovery and solar heat utilization. Most ongoing research focuses on inorganic TEs for their high Seebeck coefficient (S) and electrical conductivity (σ). Their drawbacks are their low conversion efficiency, toxicity, and their high cost, which are serious obstacles for their broad use. Less attention has been paid to organic TEs, mainly because of their limited range of operating temperatures. The figure-of-merit (FoM) of organic TEs is usually 2-3 orders of magnitude lower than that of inorganic ones, due to their low S, σ, and, consequently, power factor (PF). However, organic materials have some key benefits over inorganic materials, including their low density, low cost, and low thermal conductivity. Very recently, hybrid organic-inorganic materials have been considered as promising candidates for exceptionally good TE materials as they opt for outperforming traditional TEs by combining the low thermal conductivity of organic materials with the high S and σ of inorganic materials. With the ability to offer flexible, inexpensive, and scalable energy conversion, hybrid materials are an unavoidable future perspective of TE technology. Still, currently available hybrid TE materials have serious limitations: 1) the dominantly physical interactions between the organic and inorganic phases reduce their long-term stability and greatly restrict the carrier transport in hybrid TE materials, 2) limited control of the distribution of the organic/inorganic phases at the nanoscale makes enhancement of phonon scattering in hybrid TE materials difficult. To advance these materials and overcome the challenges, in this work we are introducing revolutionary new hybrid TE materials by applying vapor phase infiltration (VPI) process to polymers.

VPI derives from atomic layer deposition (ALD) and bases on the same technology but is applied to polymeric substrates where the precursors not only bind to the surface, but also diffuse into the polymer through a vapor– solid dissolution process. In this way an inorganic–organic hybrid material is generated in the subsurface area of the polymer. The depth of this infiltrated area can be modified by changing the exposure times, but it also can vary in dependence on the diffusivity of the precursors inside the polymer. These key differences make VPI a unique technique for polymer modification/hybridization.

In the present work we created a new hybrid material set with covalently bound organic/inorganic interfaces by inclusion of high-performance inorganic TE hierarchical superlattice materials – various sulfides and tellurides into bulk of a set of semi-conducting polymers by VPI. For monitoring the hybridization process *in-situ*, a Quartz Crystal Microbalance (QCM) was integrated into the reactor for TE material synthesis. The *in-situ* monitoring allowed studying the saturation behavior of the VPI process and quantitatively controlling the loading of inorganic precursors into a polymer, thus providing precise control and an extra degree of flexibility for tuning the material properties. Ex-situ techniques was employed to characterize the PF of each material upon various stages of infiltration: sheet resistances were measured with four point probe measurements using the van-der-Pauw method and film thicknesses by cross-sectional SEM. The electrical conductivity was extracted from the sheet resistance and the thickness measurements.High resolution transmission electron microscopy (HRTEM) and X-ray photoelectron spectroscopy (XPS) results showed that VPI provides a great degree of control on the inorganic phase distribution and overall composition of VPI-generated materials by tuning the process parameters such as temperature, penetrant pressure, and exposure time. The obtained results offer new solutions for the waste-to-energy industry.

[*] *Corresponding author e-mail: kr.ashurbekova@nanogune.eu*

Energy-related applications and catalysis III

Chair: Knapp, Caroline (University College London)

Time: 6/1/2023 8:30:00 AM
Location: Auditorium 1, Promotion Hall, Naamsestraat 22, Leuven

Studying the effects of processing parameters in the chemical vapour deposition of TiO_2 coatings on glass for applications in photocatalytic NO_x remediation

Yanda Wong[a], Yuankai Li[a], Zhipeng Lin[a], Andreas Kafizas[a,b*]

[a] *Department of Chemistry, Molecular Science Research Hub, Imperial College London, W12 0BZ, U.K.*
[b] *London Centre for Nanotechnology, Imperial College London, SW7 2AZ, U.K.*

NO_x ($NO + NO_2$) pollution is a major cause of poor health, and has a range of detrimental environmental consequences [1]. One promising solution to remedy NO_x pollution is to use the photocatalytic material, TiO_2, which can use ambient sunlight to oxidise this toxin into comparatively benign nitrate (NO_3^-) [2]. Photocatalytic coatings of TiO_2 are mass produced on window glass using chemical vapour deposition (CVD), but currently show nominal activities towards NO_x remediation [3].

In this work, we employed both atmospheric pressure CVD (AP-CVD) and aerosol-assisted CVD (AA-CVD) to produce more than 100 unique TiO_2 coatings on window glass. We systematically studied how the process parameters influenced their photocatalytic activity for remediating NO_x pollution. A range of process parameters were explored, including the chemical precursor used (titanium ethoxide, titanium isopropoxide, titanium n-butoxide), deposition temperature (350 to 600 °C) and bubbler temperature (100 to 220 °C), reaction time, co-oxidant (methanol, ethanol, isopropanol) and solvent (methanol, ethanol, isopropanol and toluene). The coatings produced showed wide ranging physicochemical properties, including differences in phase composition (anatase/ anatase: rutile composite), preferred orientation of crystal growth, average crystallite size, surface roughness, optical bandgap energy, average visible light transmission, charge carrier generation and charge carrier lifetime. Their photocatalytic activity towards NO gas was measured using a similar protocol to those stated in the International Organisation for Standardisation test (ISO 22197-1:2016) [4].

Our findings showed that a TiO_2 coating produced by AP-CVD with the precursor titanium ethoxide was the most photocatalytically active, showing an average NO conversion rate of 22.7% that was ~85 times more active than a commercial self-cleaning window. The links between the process parameters, physicochemical properties and photocatalytic activity of these >100 TiO_2 coatings were explored in depth. Clear trends were seen between the processing parameters and the physicochemical properties and photocatalytic activity (Fig. 1a). Also, the use of a simple linear combination model showed that the three most influential physicochemical properties on the photocatalytic activity were surface roughness, charge carrier generation and charge carrier lifetime (Fig. 1b). We therefore conclude that these physicochemical properties be targeted in the rational design of more active coatings for applications in photocatalytic NO_x remediation.

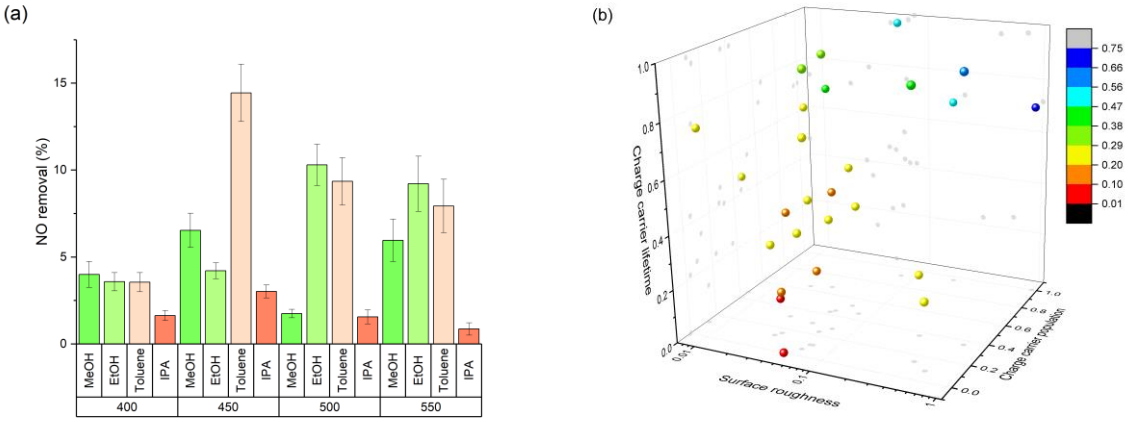

Figure 1: (a) An example bar chart to demonstrate the influence of reaction temperature and solvent used on the photocatalytic NO removal activity (%) for TiO_2 coatings produced by AA-CVD; error bars show 90% confidence intervals. (b) A normalised 4D scatter chart showing how the physicochemical

properties of surface roughness, charge carrier generation and charge carrier lifetime influence the photocatalytic NO removal activity (symbol colours).

Biography

Andreas Kafizas is a Senior Lecturer in the Department of Chemistry at Imperial College London (ICL). His research is focused on developing sustainable synthetic routes to photocatalytic coatings for a range of practical applications, including renewable fuels production (*e.g.* hydrogen fuel from water and carbon-based fuels from CO_2), air remediation (*e.g.* NO_x removal) and water remediation (*e.g.* arsenic removal).

Andreas completed his MSci in Chemistry in 2007, and PhD in Chemistry in 2011 at University College London. His PhD was focussed on the development of photocatalytic materials synthesised by chemical vapour deposition, and he was awarded the Ramsay Medal for best graduating doctor. In 2012, he was awarded the Ramsay Fellowship, where studied the charge carrier behaviour of photocatalytic materials for solar fuels at ICL. In 2016, he was awarded a Junior Research Fellowship at ICL to develop heterojunction photoelectrodes for solar water splitting and CO_2 reduction. In 2018, he was awarded a Lectureship at ICL, and now leads the Solar Coatings group (https://www.researchgate.net/lab/Solar-Coatings-Group-Andreas-Kafizas), is the theme lead in Sustainable Power and Renewable Fuels at the Energy Futures Lab, and is a board member and Chair of ED&I at the London Centre for Nanotechnology. Andreas has published over 90 peer-reviewed papers and has written 5 book chapters (>5,400 citations, h-index of 47).

References

1. J. Balbuena, M. Cruz-Yusta, L. Sánchez, J. Nanosci. Nanotechnol. **15**, 6373–6385 (2015).
2. J. Lasek, Y. H. Yu, J. C. S. Wu, J. Photochem. Photobiol. C Photochem. Rev. **14**, 29–52 (2013).
3. J. M. Langridge, R. J. Gustafsso, P. T. Griffiths, R. A. Cox, R. M. Lambert, R. L. Jones, Atmos. Environ. **43**, 5128–5131 (2009).
4. A. Mills, R. Andrews, R. Han, C. O'Rourke, S. Hodgen, J. Photochem. Photobiol. A Chem. **400**, 112734 (2020).

* *Corresponding author e-mail:* *a.kafizas@imperial.ac.uk*

Protection of platinum electrocatalysts for water electrolysis using atomic layer deposition of silicon dioxide

Ming Li[a], Saeed Saedy[a], Ruud Kortlever[b], J. Ruud van Ommen[a]

[a] *Chemical Engineering Department, Delft University of Technology, Van der Maasweg 9, The Netherlands*
[b] *Process & Energy Department, Delft University of Technology, Leeghwaterstraat 39, The Netherlands*

Atomic layer deposition (ALD) has become a powerful tool for catalyst research, benefiting from its atomically precise control and having less contamination issues than typical liquid-phase methods [1]. It has been used to elucidate the reaction mechanisms of various reactions by tuning the catalysts size, composition, nanostructure and active sites to reveal more insights into catalyst application aspect (e.g., catalyst protection and large-scale production)[2]. For instance, in our group, we used ALD to synthesize bimetallic catalysts (with core-shell and alloy morphologies), supported on a conductive substrate for CO_2 reduction. We demonstrated that using ALD to tailor the nanostructure of the catalyst enables tuning the catalyst selectivity[3]. Here, we show the potential of atomic layer deposited SiO_2 to protect Pt electrocatalysts for water electrolysis.

Hydrogen as a clean renewable energy carrier and a crucial feedstock for the chemical industry is considered an important building block for the energy transition[4]. Platinum is one of the most effective electrocatalysts for water reduction to hydrogen as well as for hydrogen oxidation and is widely used in the PEM electrolyzers and fuel cells. To deploy platinum based electrocatalysts in a cost-effective manner, it is crucial to protect the platinum catalyst from degradation and prolong its lifetime.

Here, we have applied an atomic layer deposited SiO_2 coating on the surface of platinum electrocatalysts to improve its durability. TEM, XPS, SEM-EDS mapping were used to characterize the catalyst and revealed the uniform deposition of SiO_2 on the surface of Pt nanoparticles. Linear sweep voltammetry (LSV), cyclic voltammetry (CV), and accelerated durability tests were applied to study the stability of the catalyst. We found that after 1000 cycles of CV scans in the water reduction potential range, the current density at -0.2 V vs. reversible hydrogen electrode (RHE) of the original catalyst was reduced by 34%. By contrast, after applying 2 cycles of SiO_2 ALD, the current density at the same voltage was reduced by only 7.3% after applying the same test procedure. After applying 5 cycles of SiO_2 ALD, the catalyst current density was only reduced by 1.9% after the accelerated durability test. Nevertheless, after applying 20 cycles of SiO_2 ALD, the activity of the Pt catalysts was inhibited by 64% compared with the unprotected catalyst. And the activity of the catalysts was partially restored after the accelerated durability test. The particle size of the unprotected catalyst (showed by TEM) increased by 16% after 1000 cycles CV scans, whereas it only increased by 1.6% after 1000 cycles scans protected by 5 cycles of SiO_2 ALD. Low-energy ion scattering (LEIS) will be used to reveal the deposition orientation between the Pt metal particles and the carbon black substrate.

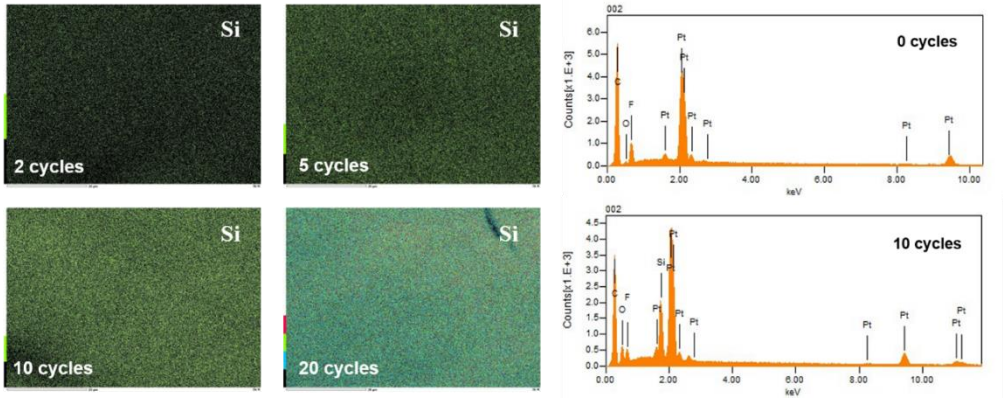

Figure 1: SEM and EDS characterization of the Pt catalyst with SiO_2 coating

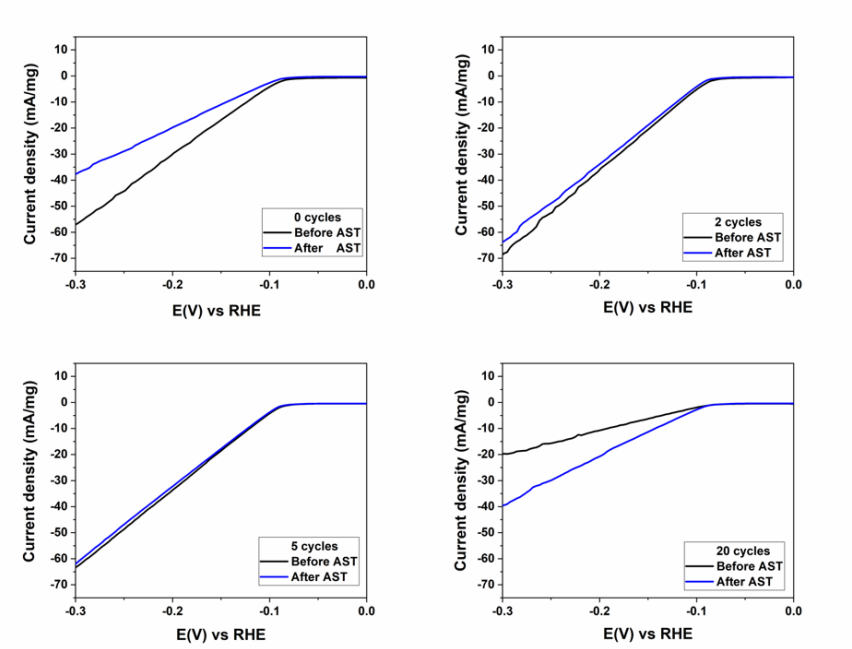

Figure 2: Linear sweep voltammetry tests of the Pt catalyst before and after accelerated stability tests

References

1. Van Bui, H., F. Grillo, and J.R. van Ommen, Atomic and molecular layer deposition: off the beaten track. Chem Commun (Camb), 2016. 53(1): p. 45-71.
2. O'Neill, B.J., et al., Catalyst Design with Atomic Layer Deposition. ACS Catalysis, 2015. 5(3): p. 1804-1825.
3. Li, M., et al., Nanostructuring Pt-Pd Bimetallic Electrocatalysts for CO2 Reduction Using Atmospheric Pressure Atomic Layer Deposition. ChemCatChem, 2022.
4. Cheng, N., et al., Platinum single-atom and cluster catalysis of the hydrogen evolution reaction. Nat Commun, 2016. 7: p. 13638.

* *Corresponding author e-mail:* *m.li-4@tudelft.nl*

Tin and Indium Sulfide by Plasma-Enhanced Atomic Layer Deposition for CO_2 Electroreduction

Femi Mathew, [a]* Järi Van Den Hoek,[b] Nithin Poonkottil, [a] Geert Rampelberg, [a] Nick Daems [b], Jonas Hereijgers,[b] Zeger Hens,[a] Tom Breugelmans,[b] Christophe Detavernier, [a] and Jolien Dendooven [a]

[a] *Ghent University, Krijgslaan 281, Ghent, 9000, Belgium*
[b] *University of Antwerp, Universiteitsplein 1, Wilrijk, 2160, Belgium*

The increase in concentration of CO_2 in the atmosphere continues to be an alarming environmental concern. Electrocatalytic reduction of CO_2 (CO_2RR) is a promising strategy that uses electrical energy to convert CO_2 to a range of carbon-based useful chemical products. Formate (HCOOH) is one of those products with great potential as a hydrogen carrier and as a precursor to produce industrially-relevant chemicals. In the quest to replace noble metal Pd electrocatalysts for formate production, researchers have identified In, Sn and Bi compounds as promising alternative candidates.[1] It is known that material properties such as crystallinity, surface chemical composition and surface morphology greatly impact electrocatalytic performance. Here, we explored thermal and plasma-enhanced atomic layer deposition (PE-ALD) to control these properties of SnS_2 and In_2S_3 films and evaluate their impact on CO_2RR.

Thin films of tin sulfide and indium sulfide have been deposited via thermal ALD using H_2S in combination with tetrakis(dimethylamido)tin (TDMASn) and indium acetylacetonate ($In(acac)_3$) respectively.[2][3] Inspired by several reports illustrating the significant influence of using plasma on the ALD growth characteristics and material properties of sulfides,[4][5] we employed H_2S plasma as the reactant in this work. The PE-ALD process for In_2S_3 using $In(acac)_3$ and H_2S plasma exhibits a growth per cycle of 0.36-0.14 Å/cycle in the temperature range of 145-260 °C. X-ray diffraction analysis reveals a tetragonal In_2S_3 phase in the whole temperature range. (Fig. 1) The surface morphology of the In_2S_3 films is identified to be rough with continuous crystallite structures. (Fig. 2)

The PE-ALD process for SnS_2 exhibits steady growth with a growth per cycle of 1.07-0.9 Å/cycle after a short incubation period in a temperature range of 80-180 °C. (Fig. 3) In comparison to the thermal ALD process which deposits amorphous SnS_2 thin films at 80°C and a mixture of SnS and SnS_2 phases at 180°C, the PE-ALD process deposits crystalline SnS_2 with strong c-axis oriented growth and most of the basal planes aligned parallel to the substrate in the temperature range of 80-180°C. (Fig. 4) Additionally, a transition in morphology from grain-like structures (30-50 nm) to out-of-plane oriented structures is found for SnS_2 deposited by PE-ALD at 80°C and 180°C, respectively.

To evaluate the sulfide thin films for CO_2RR, electrodes are prepared by applying thermal or PE-ALD directly on carbon gas diffusion electrodes (GDEs). Also on this substrate, the different ALD process conditions lead to differences in surface morphology, where the PE-ALD deposition of SnS_2 yields out-of-plane oriented structures at 180°C and continuous grains at 80°C whereas the thermal ALD process deposits amorphous SnS_2 films at 80°C. (Fig. 5(a-c)) The electrodes are evaluated in a flow-by reactor at 100 mA cm^{-2} with 0.5 M $KHCO_3$ as catholyte and 2.0 M KOH as anolyte. While CO_2RR experiments with In_2S_3 are ongoing, a comparison of the SnS_2 electrodes reveals that SnS_2 with out-of-plane oriented structures outperforms the other two SnS_2 morphologies in terms of its lower overpotential (i.e. 260 mV less negative) and maintaining structural stability even though its initial faradaic efficiency towards formate is lower (i.e. 64% vs. 80%). (Fig. 6,7) This result confirms the importance of optimizing the surface morphology for CO_2RR electrocatalysts.

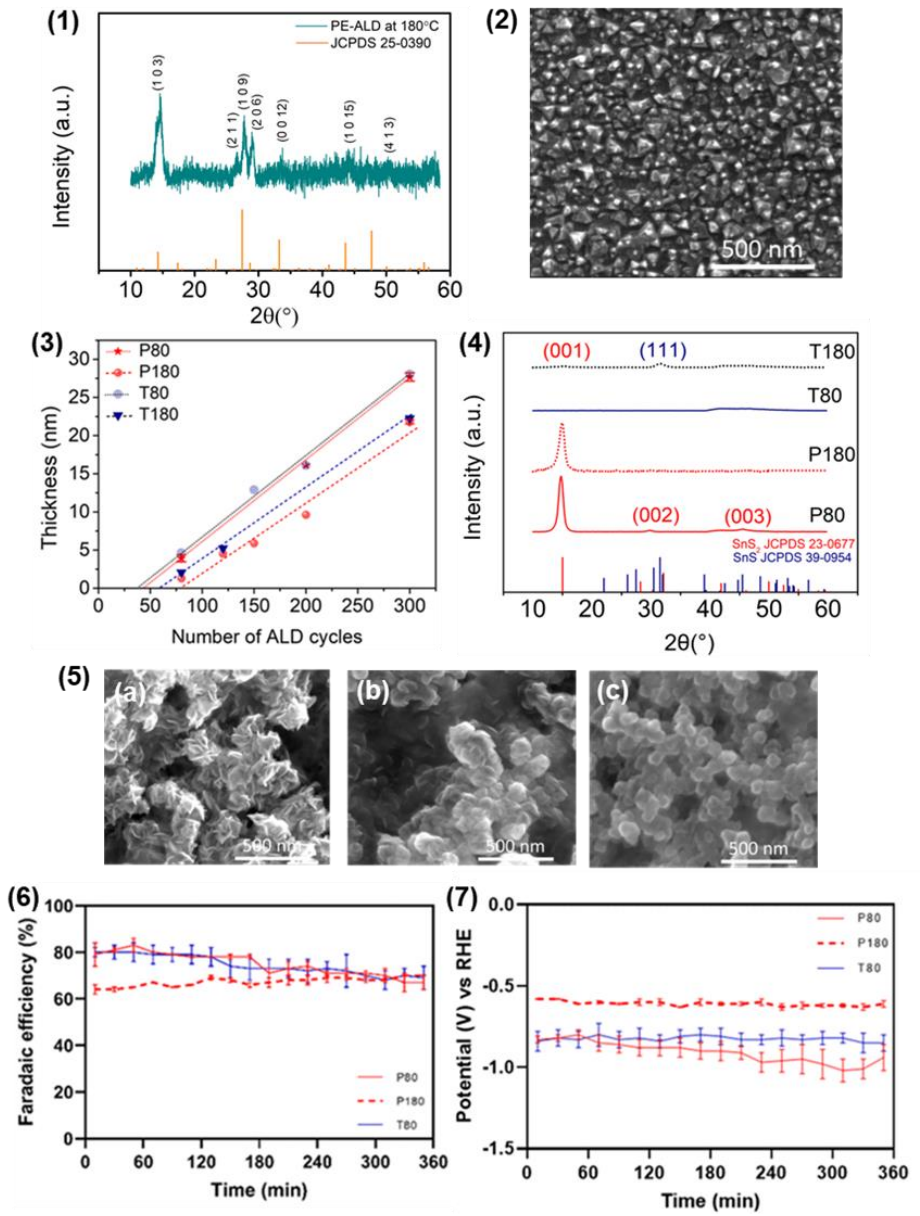

Fig. (1) XRD patterns of the In_2S_3 films grown by the PE-ALD process at 180 °C. Fig. (2) Top-view SEM image of In_2S_3 film deposited by the PE-ALD process at 180 °C. Fig. (3) Thickness against the number of ALD cycles for the PE-ALD process and the thermal ALD process at 80 °C and 180 °C. Fig. (4) XRD patterns of the SnS_x films grown by the PE-ALD and thermal ALD processes at 80 °C and 180 °C. Fig (5) Top-view SEM image of SnS_2 film deposited on gas diffusion electrode by the (a) PE-ALD process at 180 °C (b) PE-ALD process at 80°C , and (c) thermal ALD process at 80°C. CO_2RR results for SnS_2 films showing Faradaic efficiencies for formate [Fig. (6)] while measuring potentials [Fig. (7)] over six hours.

References

1. Shao. X, Zhang. X, Liu. Y, Qiao. J, Zhou. XD, Xu. N, Malcombe. JL, Yi. J, Zhang. J, Journal of Materials Chemistry A 2021,9(5),2526-59.
2. Ham. G, Shin. S, Park. J, Choi. H, Kim. J, Lee. Y. A, Seo. H, Jeon. H, ACS Applied Materials & Interfaces 2013, 5 (18), 8889-8896.
3. Naghavi. N, Henriquez. R, Laptev. V, & Lincot. D, Applied Surface Science 2004, *222*(1-4), 65-73.
4. Kuhs. J, Dobbelaere. T, Hens. Z, Detavernier. C, Journal of Vacuum Science & Technology A.Vacuum Surfaces and Films 2017, 35 (1), 01B111.
5. Mattinen. M, Gity. F, Coleman. E, Vonk. JF, Verheijen. MA, Duffy. R, Kessels. WM, Bol. AA. Chemistry of Materials 2022, 34(16),7280-7292.

* *Corresponding author e-mail:* femi.mathew@ugent.be

Effect of Processing Parameters and Electrolyte Concentration on the Electrochemical Performance of Spray Deposited $LiFePO_4$

Christina Floraki[a], Maria Androulidaki[b], Emmanuel Spanakis[c], Dimitra Vernardou[a,d*]

[a] *Department of Electrical and Computer Engineering, School of Engineering, Hellenic Mediterranean University, 71410 Heraklion, Greece*
[b] *Microelectronics Research Group, IESL-FORTH, P.O. Box 1385, 71110 Heraklion, Greece*
[c] *Department of Materials Science and Technology, University of Crete, 70013 Heraklion, Greece*
[d] *Institute of Emerging Technologies, Hellenic Mediterranean University Center, 71410 Heraklion, Greece*

Lithium iron phosphate ($LiFePO_4$) is an excellent cathode material for Li-ion batteries (LIBs) because it is extremely safe, thermally stable and low cost. Nevertheless, the electronic conductivity is poor and the diffusion coefficient is slow, which limit the development for high power devices. Hence, there is a lot of space for research to explore ways for the improvement of material's performance.

There are reports on the growth of $LiFePO_4$ thin film deposition including pulsed laser deposition, radio frequency magnetron sputtering, sol-gel, drop casting. The majority of these methods require high processing cost and annealing temperatures (i.e. ≥ 500 ^oC). In this work, a simple multiple-pass deposition technique will be utilized in which the spray-gun will be moved across the substrate creating a "wet film", which – after thermal annealing at very mild temperatures (i.e. 65 ^oC) – cathode materials will be formed on carbon component. Carbon component is chosen as a substrate because it is expected to act as a support for uniformly anchoring $LiFePO_4$ thin film increasing its stability. In that perspective, graphite is a suitable material because of its mixed electron-ion conductivity and structural stability. The best performing combination of electrode-electrolyte through the selective use of electrode and electrolyte materials will be evaluated.

**Corresponding and presenting author e-mail: dvernardou@hmu.gr*

Industry

Chair: Mackus, Adriaan J.M. (Eindhoven University of Technology)

Time: 6/1/2023 9:00:00 AM
Location: Auditorium 2, Maria-Theresiacollege, St. Michael's Street 6, Leuven

Dielectric gap-fill material and process challenges for future semiconductor technology

Alfonso Sepulveda[1,*], Antony Premkumar Peter[1], Venkat Sunil Kumar Channam[1], Pierre Morin[1], Johan Swerts[1]

[1]*imec, Leuven, 3000, Belgium*

As the semiconductor industry is shifting from finFET to nanosheet technology for the 3 nm and 2 nm generations new challenges are arising for several modules which include new material and process development. The key benefit that nanosheets bring for further CMOS scaling is the larger drive current per footprint compared to finFETs. In the ultimate 2D configuration the n- and p- type device separation, defined in the horizontal plane, is reduced by introducing a dielectric wall in between which brings along different gap-fill requirements. New architectures such as Complementary FET are defining the n- and p-type device separation in the vertical plane by introducing different isolation layers[1]. CFET consists of a very complex vertical integration that require new approaches for patterning, gap-fill and spacer depositions, and source/drain contact. This new technology is challenging existing dielectric spacers and gap-fill processes due to the high aspect ratio structures involved which can go up to AR ~15. Thin film deposition is relying in more advanced ALD and flowable-type of processes to provide with highly conformal, high-quality materials including lateral gap-fill capability up to 300 nm horizontal reach and also low temperature budgets. Dielectric depositions need to provide with a wide portfolio of functional materials which need to be thin enough to fit in narrow trenches down to ~12 nm and still provide with the necessary etch selectivity. In memory technology such as DRAM[2], architectures are also adding the third dimension to continue the scaling which brings together challenges that industry is now tackling to find effective solutions such as advanced ALD and area selective deposition (ASD). Here we cover the aspects of dielectric gap-fill material needs and process challenges for future CFET[1], 3D-DRAM and 3D heterogeneous integration technologies.

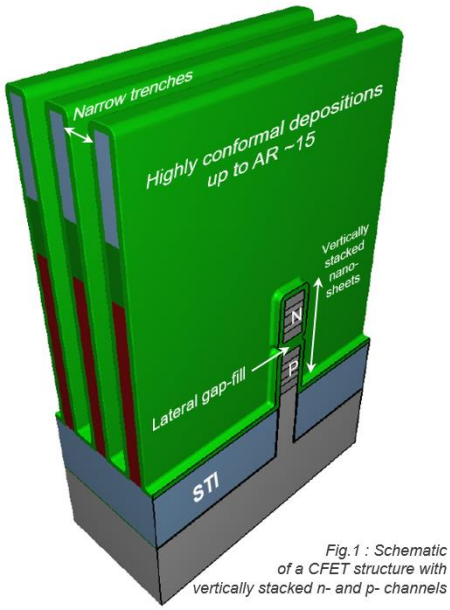

Fig.1 : Schematic of a CFET structure with vertically stacked n- and p- channels

References

1. *S. Subramanian et al., "First Monolithic Integration of 3D Complementary FET (CFET) on 300mm Wafers," 2020 IEEE Symposium on VLSI Technology, Honolulu, HI, USA, 2020, pp. 1-2, doi: 10.1109/VLSITechnology18217.2020.9265073.*
2. *A. Belmonte et al., "Tailoring IGZO-TFT architecture for capacitorless DRAM, demonstrating > 103s retention, >1011 cycles endurance and Lg scalability down to 14nm," 2021 IEEE International Electron Devices Meeting (IEDM), San Francisco, CA, USA, 2021, pp. 10.6.1-10.6.4, doi: 10.1109/IEDM19574.2021.9720596.*
3. *A. Jourdain et al., "Extreme Wafer Thinning and nano-TSV processing for 3D Heterogeneous Integration," 2020 IEEE 70th Electronic Components and Technology Conference (ECTC), Orlando, FL, USA, 2020, pp. 42-48, doi: 10.1109/ECTC32862.2020.00020.*

[*] *Corresponding author e-mail: alfonso.sepulvedamarquez@imec.be*

Green CVD—Toward a sustainable philosophy for thin film deposition by chemical vapor deposition

Henrik Pedersen[a], Seán T. Barry[b], and Jonas Sundqvist [a, c, d, e*]
[a]*Department of Physics, Chemistry and Biology, Linköping University, SE-581 83 Linköping, Sweden*
[b]*Department of Chemistry, Carleton University, 1125 Colonel By Drive, Ottawa, Ontario K1S 5B6, Canada*
[c]*BALD Engineering AB, Kanotvägen 4, SE-134 40 Värmdö, Sweden*
[d] *TECHCET CA LLC, 11622 El Camino Real, Suite #100, San Diego, California 92130*
[e] *AlixLabs AB, Ole Römers Väg 1, 1H, 223 62*

Thin films of materials are critical components for most areas of sustainable technologies, making thin film techniques, such as chemical vapor deposition (CVD), instrumental for a sustainable future. It is, therefore, of great importance to critically consider the sustainability aspects of CVD processes themselves used to make thin films for sustainable technologies. Recently [1], we point to several common practices in CVD that are not sustainable. From these, we offer a perspective on several principles for a sustainable “Green CVD” philosophy, which we hope will spur research on how to make CVD more sustainable without affecting the properties of the deposited film. We hope that these principles can be developed by the research community over time and be used to establish research on how to make CVD more sustainable and that a Green CVD philosophy can develop new research directions for both precursor and reactor design to reduce the precursor and energy consumption in CVD processes.

The total US$16-17 billion 2022 annual market for CVD processing equipment has a high forecasted growth rate (5-Year CAGR >8%, FIG.1) due to expansions in the global semiconductor and microelectronics industry. Especially high continued growth is expected for:

- Atomic Layer Deposition (ALD) needed for leading edge Processors and Memory (DRAM, 3DNAND flash)
- CVD of GaN and SiC for continued electrification and automotive applications (RF, Power Electronics)

Given the essential role of CVD methods for a circular economy and a sustainable society—in the production of the electronic devices needed for electric vehicles, energy storage in the form of lithium–ion batteries, energy-efficient lighting and communication, and solar cells, further development is required toward achieving more energy- and molecule-efficient processes. To do so, the full lifecycle of processes and products must be considered. Combined with the European industrial sustainability acts, Suschem [3] and Manufuture [4] focusing on the sustainable use of chemicals and sustainable manufacturing, respectively, and as stated above, in accordance with the UN Sustainability Goals, more sustainable CVD processes need to be developed. This need has recently been highlighted by the general finding that energy consumption and greenhouse gas emissions per 300 mm wafer for CMOS fabrication—and the included CVD processing steps in particular—increase with a decreasing node size. [5] Going from the 28 nm technology in 2011,6 typically in use at the event of smartphones and tablets, both energy consumption and greenhouse gas emission will more than double be going to the 2 nm node that is scheduled for high volume production at 2024 for 5G, AI, Autonomous driving electronics, and any type of high-end products such as laptops, phones, and internet servers.

Given the developing global energy crisis triggered by several geopolitical events, Europe has been hit extra hard with soaring energy costs and an immediate impact on the supply chain of energy fuels and industrial chemicals, which has put energy savings immediately on the short-term political agenda. All CVD processes use elevated temperatures. Some CVD processes for amorphous or polycrystalline films operate at a few hundred degrees Celsius, while epitaxial growth (e.g. Si, SiGe, GaN, SiC) of single-crystalline films, needed for some devices, use 1000−1500 °C. A reduction of the thermal budget in a CVD reactor is the obvious way to reduce energy consumption. From a Green CVD perspective, the question is then how to reduce the thermal budget of the CVD reactor without also altering the performance of the CVD process and how to use the excess heat generated from CVD equipment.

We appreciate that industry is reluctant to change established precursors and CVD processes that have been successfully brought into high volume production. Hence, the research area of Green CVD should

strive to make a given CVD process more sustainable without causing negative effects on the performance of the deposited film. Ideally, Green CVD should not affect the price of the CVD processing step either. It is very reasonable to expect that the demands for more sustainable production will increase and with that a need for more sustainable CVD. As in other research, a strong collaboration between industry and academia will strengthen the Green CVD development effort.

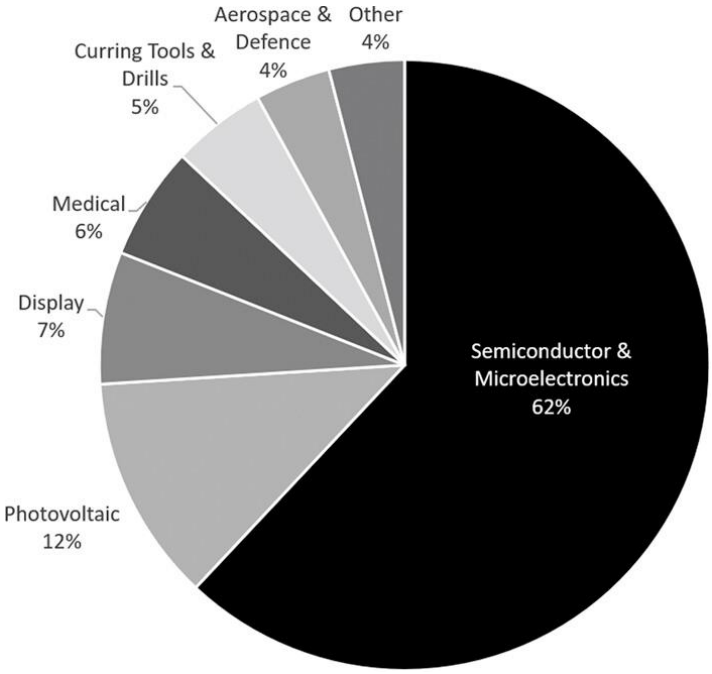

FIG. 1. CVD and ALD equipment market size and segmentation in 2022, US$16–$17 billion annual revenue and a forecasted 5-Year CAGR >8% as estimated by TECHCET CA LLC. [2]

References

1. Green CVD—Toward a sustainable philosophy for thin film deposition by chemical vapor deposition, Henrik Pedersen, Seán T. Barry, Jonas Sundqvist, JVSTA 39, 051001 (2021)
2. “CVD and ALD Metal and High-k Critical Materials Report 2022”,2022, see: www.techcet.com.
3. See: http://www.suschem.org/about.
4. See: http://www.manufuture.org/.
5. M. Garcia Bardon et al., in 2020 IEEE International Electron Devices Meeting (IEDM) San Fransisco, CA, 12–18 December 2020 (Virtual Event, IEEE, New York, NY, 2020), pp. 41.4.1–41.4.4. https://doi.org/10.1109/IEDM13553.2020.9372004,

* *Corresponding author e-mail: jonas@alixlabs.com*

Precursor design II

Chair: Hoffmann, Patrik (Empa)

Time: 6/1/2023 10:30:00 AM
Location: Auditorium 1, Promotion Hall, Naamsestraat 22, Leuven

Designing large aromatic molecules: Bringing colour to MLD

Per-Anders Hansen[a,*], Bhagyesh Purohit[a], Silje Holm Sørensen[a], Nicolas Depois[b], Claude Gros[b] and Ola Nilsen[a]

[a] *Department of Chemistry, University of Oslo, Sem Sælands vei 26, Oslo 0371, Norway*
[b] *Institute de Chimie Moléculaire de l'Université de Bourgogne, ICMUB, UCM CNRS 6302, Université Bourgogne France-Comté, 9, Avenue Alain Savary, BP 47870, 21078 Dijon Cedex, France*
** Corresponding author e-mail: p.a.hansen@kjemi.uio.no*

Atomic layer deposition (ALD) and its organic counterpart, molecular layer deposition (MLD), are incredibly powerful and flexible tools for designing completely new materials with novel and unique properties. The low temperature layer-by-layer approach and the use of highly reactive reactants allows one to combine vastly different organic and inorganic species and construct nanostructures with subnanometer precission. The possibilities are endless had we not been limited by the volatility of the precursors/molecules/reactants. This is most notable when using organic molecules as building blocks, since it severely limits the toolbox for available large molecules with interesting optical and electrical properties such as red-ox activity and optical conversion. In this work, we have investigated different strategies for molecular design of large molecules that allow vaporization while still having the necessary reactivity for ALD/MLD growth. Using these strategies, we succesfully achieve film growth with porphyrin and perylene derivatives, both molecules well known for their functional and optical properties. With this knowledge, we open for including much larger and more complex organic molecules into the world of vapor phase chemistry.

From a selection of porphyrin, perylene and other dye classes, we find that several dye classes either are suited for MLD or can be designed to be suited with special considerations. Figure 1 shows four successful MLD depositions using the pictured dye molecules and aluminium (film 1+3) and lanthanide (film 2+4) precursors. Successful MLD using such dyes opens up for another mechanism for tuning the dyes properties: In particular for perylene dyes the functional properties of the molecule is altered if the central oxygen is replaced by nitrogen on either end, a modification that is readily achieved by reacting the perylene acid anhydride with an amine. This way, perylene acid anhydrides can readily be turned into perylene diimides which are highly luminescent. MLD allows for readily available deposition of perylene acid anhydrides, diimides and even unsymmetrical mono-imides by adding amine groups either in-situ or pre-deposition to the perylene before reaction with metal precursors, or by reacting the perylene acid anhydride directly with the metal precursor. This way of readily obtaining different symmetrical or unsymmetrical perylene molecules in hybrid structures from the same starting perylene is unprecedent. Examples of four different perylene based hybrid films are shown in Figure 2, including two that show different optical properties if an amino acid is included in the reaction pathway or not.

Porphyrin dyes where more challenging, as commercially available reactive dyes containing -OH or -COOH groups rapidly degraded at temperatures high enough for sublimation. With the success from perylene depositions, we designed two new porphyrins with acid anhydride reactive groups and bulky alkyl chains to limit intermolecular packing efficiency. This decreased sublimation temperatures of about 100 °C compared to carboxylic acid porphyrins and resulted in partially successful MLD depositions. General strategies for such drastic decrease in sublimation temperature while maintaining reactivity will be discussed.

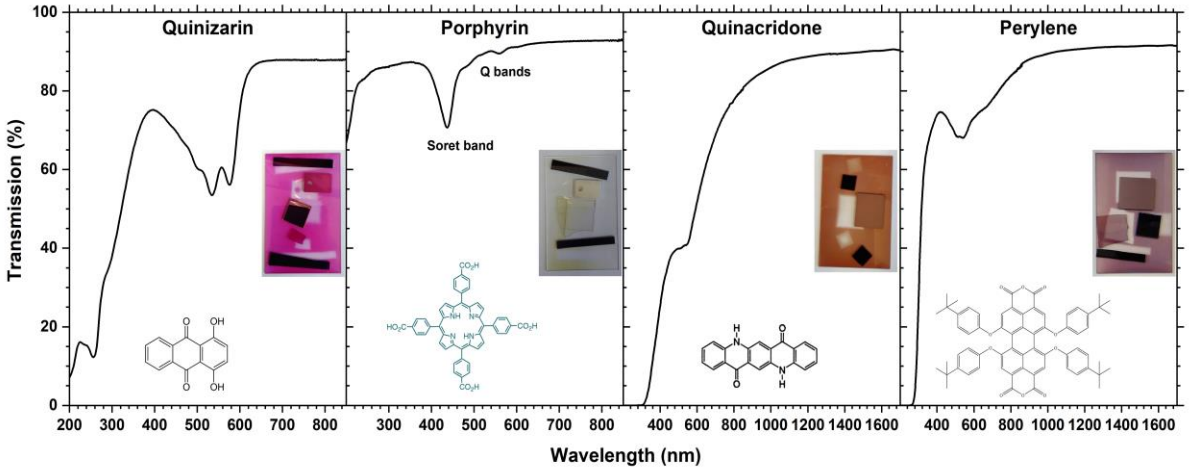

Figure 1: UV-Vis transmission spectra of silica substrates and photos of samples coated with MLD thin films of four different classes of strongly coloured dye molecules.

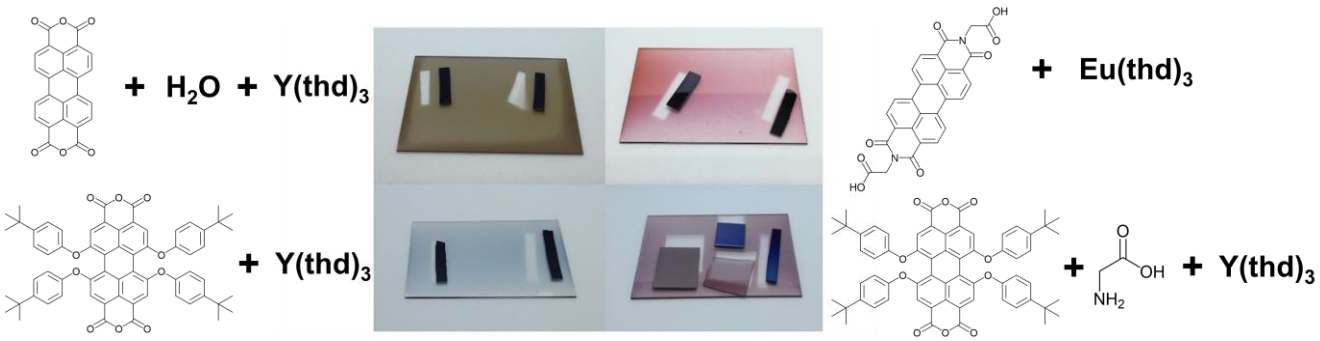

Figure 2: Photos of four different MLD film grown using perylene dyes and different reaction pathways, showing the possibility to obtain different optical properties.

Development of new Li-Nb precursors for DLI-CVD process of thin $LiNbO_3$ films

Anthony TACNET[a]*, Ausrine BARTASYTE[b], Quentin MICARD[b], Jean-Manuel DECAMS[c], Vincent ASTIE[c], Stéphane DANIELE[a]

[a] *CP2M CPE Lyon, University Claude Bernard Lyon 1, CNRS-UMR 5128, 4 Rue Victor Grignard, Villeurbanne, 69616, France;*
[b] *FEMTO-ST Institute, University of Bourgogne-Franche-Comté, CNRS-UMR6174, 26 rue de l'Epitaphe, Besancon, 25030, France;*
[c] *Annealsys, 139 Rue des Walkyries, 34000 Montpellier, France*

Reaching the full potential of the 5th generation of mobile telecommunications (5G) and the miniaturization of components require the development and improvement of thin piezoelectric layers present in high-frequency radio frequency (RF) acoustic filters. The bulk acoustic wave (BAW) filters are currently made of aluminum nitride films with a bandwidth limited at high frequencies by a low electromechanical coupling coefficient. **[1]** Single crystals of lithium niobate ($LiNbO_3$) and lithium tantalate represent around 70% of the piezoelectric materials used in the RF filters, based on surface acoustic waves, but their thin-film growth faces problems of composition homogeneity and Li:Nb stoichiometry. **[2]** Currently, thin films of $LiNbO_3$ or $LiTaO_3$ are elaborated from the single crystal wafers by bonding, ion slicing or polishing processes, which are limited by imperfect thickness control. Therefore, current research on the development of $LiNbO_3$ piezoelectric thin films for high frequency acoustic devices is oriented towards their elaboration by vapor phase deposition processes such as MOCVD. One of the major difficulties of these techniques is the control of the Li-Nb stoichiometry because lithium oxide is volatile, and film composition is highly dependent not only on the deposition conditions but also on the film orientation and thickness. This motivates a development new molecular precursors in which Li is already bonded to Nb and thus, limiting Li_2O loss during the film growth.

Our presentation will address new Li and Li-Nb precursors (Single source precursor or SSP) and their use in DLI-CVD applicable on an eventual industrial scale. A series of functional aminoalkoxide have been studied because of volatility compatible with the DLI-CVD and their ability to saturate the coordination sphere by chelation. For example, reacting the new homometallic $[Li(dmem)]_6$ precursor [dmemH = 2-{[2-(Dimethylamino)ethyl]methylamino}ethanol] with $[Nb(OEt)_5]_2$ led to an original heterometallic $[LiNbO(OEt)_3(dmem)]_2$ derivative (Fig. 1) with the right stoichiometry for $LiNbO_3$.

All precursors were fully characterized using multinuclear NMR, FTIR, single crystal XRD and TGA in order to determine their structures and applicability in DLI-MOCVD process. Selected precursors have been used for $LiNbO_3$ thin films elaboration by DLI-MOCVD.

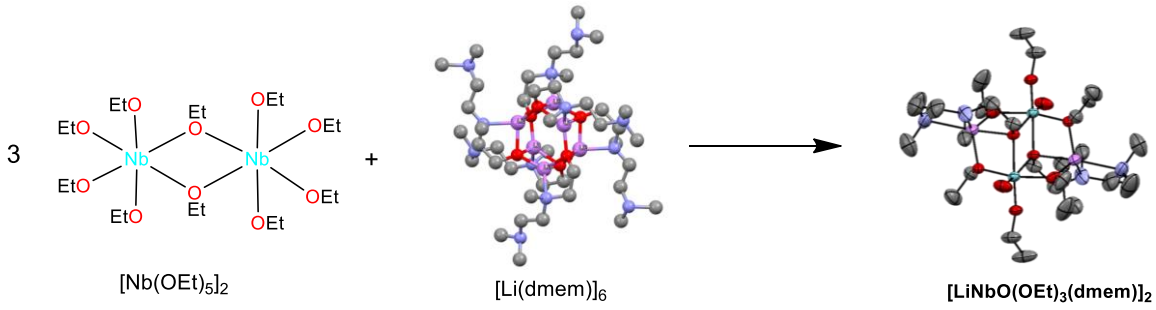

Figure 1: *Synthesis of the $[LiNbO(OEt)_3(dmem)]_2$ precursor.*

References

1. C. -M. Yang, K. Uehara, S. -K. Kim, S. Kameda, H. Nakase and K. Tsubouchi, IEEE Symposium on Ultrasonics,**1**, 170-173 (2003).
2. A. Bartasyte, S. Margueron, T. Baron, S. Oliveri, P. Boulet, Advanced Materials Interfaces, 4, 1600998 (2017).

* *Corresponding author e-mail:* *anthony.tacnet@etu.univ-lyon1.fr*

Atmospheric pressure vapor phase deposition of MgF_2 thin films: precursor thermal properties and their applications

Francesca Lo Presti[a], Anna Lucia Pellegrino[a], D. Muñoz-Rojas[b], and Graziella Malandrino[a,*],

[a] *Dipartimento di Scienze Chimiche, Università degli Studi di Catania,INSTM UdR Catania, Viale Andrea Doria 6, I-95125 Catania, Italy.*
[b]*Univ. Grenoble Alpes, CNRS, Grenoble INP, LMGP, 3, Parvis Louis Néel MINATEC, F-38000 Grenoble, Franc.*

The choice of proper molecular precursors is crucial to the performance of vapor phase deposition methods, including chemical vapor deposition (CVD) and atomic layer deposition (ALD), for the manufacture of functional thin films used in a variety of applications. [1] Alkaline-earth (AE) metalorganic precursors have proven to be the most intriguing and challenging to deal with since their large ionic radii require a customized coordination sphere to produce suitable thermal characteristics. Actually, the employment of AE precursors in the deposition of fluoride films has sparked even greater interest in them. [2,3] Magnesium fluoride (MgF_2), for example, stands out among the AE metal difluorides because of its intrinsic properties (low refractive index, hardness, durability, etc.) that are well suited even for hostile environments. These characteristics make it an excellent candidate among the UV transparent materials. [4,5]
It is well-known that the quality of the films produced with CVD or ALD approaches are strongly influenced by the chemical nature and structural design of the metalorganic precursors employed. Even more demanding, in terms of precursor thermal properties, is the spatial ALD (SALD), a variant of of the ALD method, which is being developed over the last 15 years. The main advantage of SALD is a faster deposition rate than conventional ALD, even at atmospheric pressure.. [6,7] Since the precursors used for atmospheric pressure (AP) processes should have a high volatility, the thermal requirements for precursors become even more strict. To have a reference point on whether a certain precursor is suitable for use in AP-vapor phase procedures, it is essential to optimize a simple method for evaluating the vapor pressures of complexes.
Hence, we propose a straightforward and efficient method for determining the vapor pressures of β-diketonate fluorinated compounds, focusing on the so-called "second generation" β-diketonate fluorinated complex, the [Mg(hfa)$_2$● 2H_2O● 2diglyme] Hhfa=1,1,1,5,5,5-hexafluoro-2,4-pentanedione and diglyme=bis-2-methoxyethyl-ether), [Mg(hfa)$_2$● 2H_2O● 2diglyme] adduct. The coordination sphere of the central metal ion is fully saturated by the presence of a number of anionic ligands necessary to neutralize the charge of the Mg ion and the addition of neutral ligands such as polyether which prevents oligomerization and water-coordination processes, thereby enhancing thermal stability. [8] For these reasons, it has been employed in MOCVD methods under low pressure conditions, [9] and because of its superior thermal properties this "second-generation" precursor should also suitable for ALD approaches. We fully investigate the possibilities of applying the Langmuir equation for the direct estimation of vapor pressure and enthalpy of vaporization of such metalorganic precursor starting from the experimental data of the thermogravimetric studies. This approach may be used to easily determine vapor pressures of complexes and thus evaluate “a priori” the suitability of a compound as precursor for AP-MOCVD and/or spatial ALD (SALD). [10]
The [Mg(hfa)$_2$● 2H_2O● 2diglyme] adduct has been successfully tested for the first time employing atmospheric pressure processes such AP-MOCVD and SCVD to produce nanostructured MgF_2 thin films on silicon substrates. An added value of this precursor is its single-source nature, since it represents a source of Mg and also of F, thus avoiding the use of an external fluorine source.

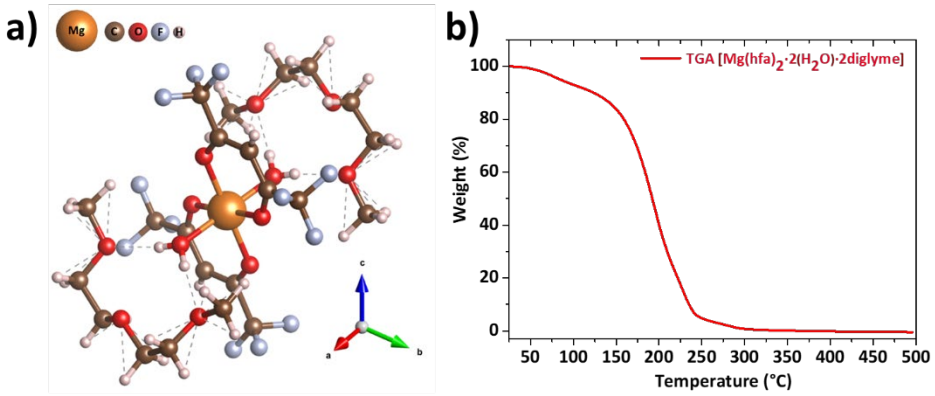

Fig. 1. Scheme of the [Mg(hfa)$_2$·2H$_2$O]·2diglyme (a) and TGA curve plot (b).

References

1. M. A. Malik and P. O'Brien, *Basic chemistry of CVD and ALD precursors in Chemical Vapour Deposition: Precursors, Processes and Applications*, ed. A. C. Jones and M. L. Hitchman, Royal Society of Chemistry Publishing, London, 207–271, (2009).
2. A. R. Barron and W. S. Rees, Adv. Mater. Opt. Electron., **2**, 271–288, (1993).
3. 7 A. C. Jones, H. C. Aspinall and P. R. Chalker, Surf. Coat. Technol., **201**, 9046–9054, (2007).
4. F. Perales, J. M. Herrero, D. Jaque, C. de las Heras, Opt. Mater., **29**, 783, (2007).
5. J. D. Bass, C. Boissiere, L. Nicole, D. Grosso, C. Sanchez, Chem. Mater., **20**, 5550, (2008).
6. D. Munoz-Rojas and J. MacManus-Driscoll, Mater. Horiz., **1**, 314–320, (2014).
7. P. Poodt, D. C. Cameron, E. Dickey, S. M. George, V. Kuznetsov, G. N. Parsons, F. Roozeboom, G. Sundaram and A. Vermeer, J. Vac. Sci. Technol., A, **30**, 010802, (2012).
8. M. E. Fragalà, R. G. Toro, P. Rossi, P. Dapporto and G. Malandrino, Chem. Mater., **21,** 2062–2069, (2009).
9. M. E. Fragalà, R. G. Toro, S. Privitera, and G. Malandrino, Chem. Vap. Deposition, **17**, 80-87, (2011).
10. F. Lo Presti, A. L. Pellegrino and G. Malandrino, Dalton Trans., **51**, 7352–7362, (2022).

* *Corresponding authors' e-mails:* graziella.malandrino@unict.it,

Cost-analysis and optimization of ALD and CVD processes for halide perovskites

Georgi Popov*, Alexander Weiß, Mikko Ritala, Marianna Kemell

Department of Chemistry, University of Helsinki, A.I. Virtasen aukio 1, Helsinki, 00014, Finland

Halide perovskites are compounds with remarkable properties that can deliver breakthroughs in multiple applications provided certain challenges can be resolved. Halide perovskites are ABX_3 type compounds with perovskite crystal structure and are most well-known for the unprecedentedly rapid development of perovskite solar cell efficiencies but also for their stability and scalability concerns. Photovoltaics is indeed the largest application of halide perovskites (65% in 2022 by publication volume), but the share of light emission, sensing, and microelectronic applications is significant and increasing (31 %). In these applications, the performance of halide perovskite laboratory devices exceeds that of the state-of-the-art devices. However, the poor stability and scalability of halide perovskites impede their practical use. The scalability issue is the primary focus of our work and is, in short, the challenge of preparing halide perovskite thin films on large areas and in large batches while maintaining the economic feasibility and quality necessary for cutting-edge performance.

We have advocated ALD as a solution for the scalability issue, but the idea is met with scepticism first based on the lack of ALD processes for halide perovskites and second, on the slowness and high cost of ALD. In recent years, we have developed ALD processes for binary iodides PbI_2 and CsI as well as a process for $CsPbI_3$ halide perovskite to demonstrate that these can be made with ALD.[1-2] A new wave of scepticism ensued speculating that it is not economically feasible to use ALD for a thick absorber layer in the solar cell. However, critics have not provided any definite values.

To objectively assess the outcomes of our work, we performed a cost analysis using a model described by Chang et al.[3] The model implements the Monte Carlo uncertainty approach, and the authors used it to evaluate the cost-effectiveness of ALD for heterojunction Si solar cells. We related the results of our cost analysis to the field of photovoltaics. Solar cells are high-volume, low-value products and, as such, represent the harshest application for evaluating the cost-effectiveness of ALD. From literature data and industrial reports, we deduced that the absorber cost must be in the range of 3 – 7 USD¢/W to be seriously considered. The cost analysis reveals that the criticism we received is justified, as a 400 nm absorber layer made with our $CsPbI_3$ process would cost 13.8 ¢/W (median).

The cost analysis result might seem disappointing, but it provides us with a useful reference point and enables further development. We identified bottlenecks in the existing process and developed solutions to overcome them. The $CsPbI_3$ process consists of CsI film deposition and PbI_2 deposition on top of CsI. PbI_2 reacts with CsI as it is being deposited, forming $CsPbI_3$. The deposition temperature of PbI_2 is chosen such that $CsPbI_3$ is stable, but PbI_2 is volatile, which conveniently avoids the deposition of any PbI_2 excess. The growth per cycle (GPC) of CsI is 3.3 Å, a large value for ALD, enabled by the deposition during both half-cycles (DBH), a unique feature of halide processes that rely on metal halides as precursors.[4] The PbI_2 deposition turns to be the bottleneck with a GPC of 0.14 Å. The PbI_2 process also benefits from the DBH mechanism, but PbI_2 is a 2D material with inert basal planes that retard growth and significantly decrease GPC.

We explored several alternatives to the PbI_2 ALD process. One example is the replacement of the second PbI_2 ALD step with a pulsed CVD (p-CVD) step. This approach allows the retention of uniformity and conformality from the first ALD step and increases the effective GPC to 1.5 Å bringing the cost down to 6.9 ¢/W, within the reasonable cost range. We believe that further study and optimization can increase the GPC and decrease the cost even more.

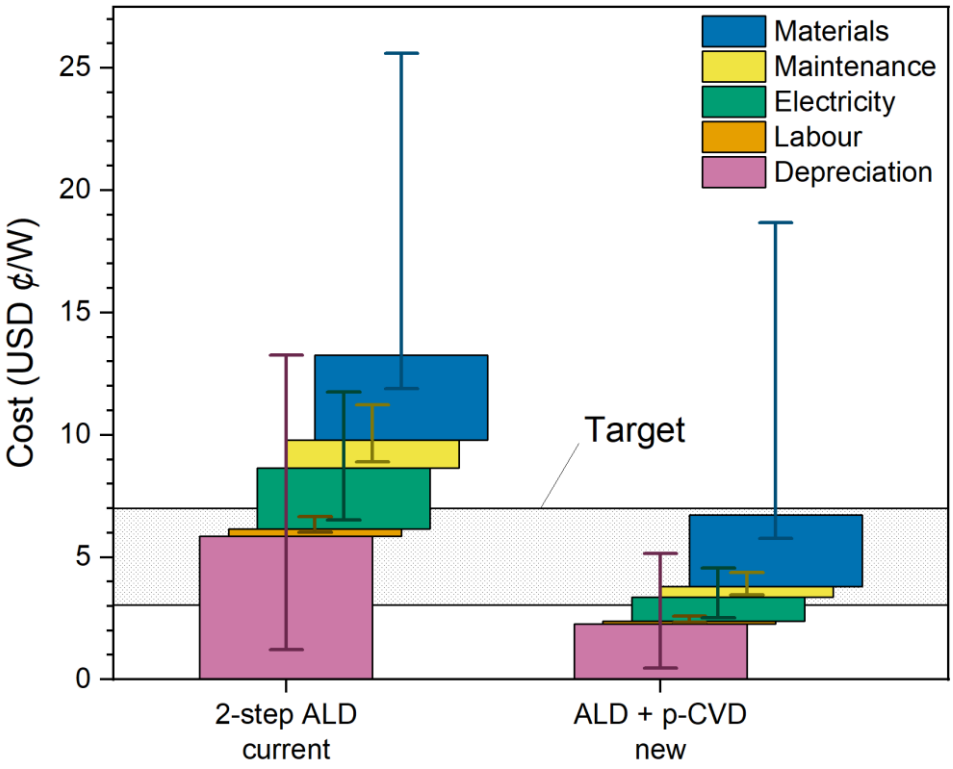

Figure 1. The cost breakdown for a 400 nm $CsPbI_3$ absorber layer deposited using the published two-step process and for a new process that substitutes the latter ALD step with p-CVD. For each cost component, the height is the median price, whereas the error bars represent the 10th and 90th percentile values of the cost component and represent uncertainty. The cost components are offset to prevent error bar overlap.

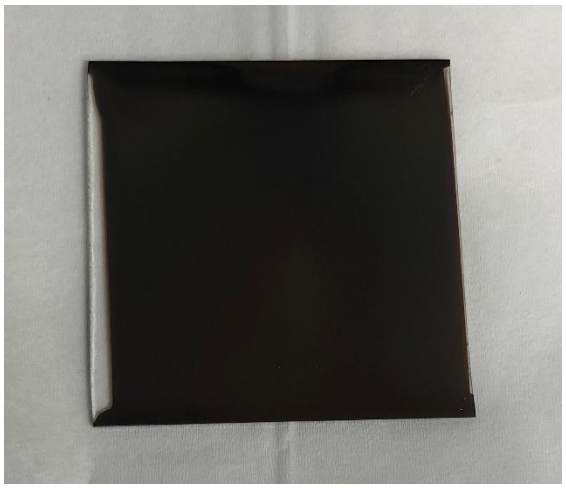

Figure 2. A halide perovskite film deposited on 5x5 cm soda lime glass substrate using the new ALD - p-CVD process scheme.

References

1. Chang et al., Prog. Photovolt. Res. Appl. **Early View**, (2022). DOI: 10.1002/pip.3553
2. Popov et al., Chem. Mater. **31**, 1101 (2019). DOI: 10.1021/acs.chemmater.8b04969
3. Weiss et al., Chem. Mater. **34**, 6087 (2022). DOI: 10.1021/acs.chemmater.2c01202
4. Pilvi et al., Chem. Mater. **19**, 3387 (2007). DOI: 10.1021/cm0629412

* *Corresponding author e-mail:* georgi.popov@helsinki.fi

Alkali β-Diketonate Glyme Adducts as Precursors for alkali niobate films: Synthesis, Characterization and Functional Validation

Francesca Lo Presti[a], Nishant Peddagopu[a], Anna L. Pellegrino[a], Ishamol Labbaveettil Basheer[b], Quentin Micard[b], Patrizia Rossi[c], Paola Paoli[c], Ausrine Bartasyte[b,d], and Graziella Malandrino[a,*]

[a] *Dipartimento Scienze Chimiche, Università degli Studi di Catania, and INSTM UdR Catania, Viale Andrea Doria 6, 95125 Catania, Italy*
[b] *FEMTO-ST Institute, Université Franche-Comté, ENSMM, CNRS UMR 6174, 25000 Besançon, France*
[c] *Dipartimento di Ingegneria Industriale, Università di Firenze, Via Santa Marta 3, 50136 Firenze, Italy*
[d] *Institut Universitaire de France*

Alkali niobate ($MNbO_3$, M = Li, Na, K) functional materials are of great interest due to their high technological potentials, e.g., in photonics ($LiNbO_3$) [1], in dielectrics (e.g., $NaNbO_3$) [2], and in piezoelectrics/ferroelectrics ($KNbO_3$, $K_{1-x}Na_xNbO_3$) [3]. Lithium niobate has been referred to as the "silicon of photonics" due to its exceptional optical properties. The interest in $MNbO_3$ has also been boosted by the need to look for lead-free piezoelectric materials due to the restriction of the European community on the use of PZT [$(PbZr)TiO_3$]. Nevertheless, applications for quantum photonics, surface acoustic wave devices, ferroelectric based devices etc. require the availability of $MNbO_3$ in thin film form.

To this aim various techniques have been applied such as capillary liquid epitaxial technique, RF-magnetron sputtering, spin-coating and metal–organic chemical vapour deposition (MOCVD).

Very few alkali precursors are known for vapour phase processes, either MOCVD or atomic layer deposition.

A very critical issue in the synthesis of an alkali metal complex is the large ionic radius of the cation, which requires high coordination numbers. In fact, except for Li^+, all the alkali metal ions from Na^+ to Cs^+ have an ionic radius larger than 1 Å, independently from the coordination number.

In this context, we focused our attention on the synthesis of new alkali precursors suitable for the growth of alkali niobate thin films. We report on the synthesis of novel lithium, sodium and potassium complexes of the type "M(hfa)•glyme", [Hhfa=1,1,1,5,5,5-hexafluoro-2,4-pentanedione, glyme=monoglyme (1,2-dimethoxyethane), diglyme (bis(2-methoxyethyl)ether), triglyme (2,5,8,11-tetraoxadodecane) and tetraglyme (2,5,8,11,14-pentaoxapentadecane)], with glymes performing like crown ethers in terms of coordinating/solvating ions, i. e. in terms of chelating properties.

Single-crystal X-ray diffraction studies enabled the identification of fascinating metal coordination framework for all the three ions. In particular, for the lithium ion a very complex structure was found with the asymmetric unit formed by $[Li_6(hfa)_6$•0.5monoglyme] with two water molecules coordinated, to give a structure of $[Li_{12}(hfa)_{12}$•monoglyme•$4H_2O]_n$ (Fig. 1a), while the diglyme adduct shows a dimeric unit $[Li_2(hfa)_2$•diglyme•$H_2O]$, where both lithium ions are five-coordinated [4].

In the case of sodium, the single-crystal studies evidence the formation of the ionic oligomeric structure $[Na_4(hfa)_6]_2^-$•$2[Na(diglyme_2]^+$ when the diglyme is coordinated, while a mononuclear seven-coordinated complex Na(hfa)•tetraglyme is formed with the tetraglyme. Reaction with the monoglyme does not occur, and the unadducted polymeric structure $[Na(hfa)]_n$ forms, while the triglyme gives rise to a liquid adduct, Na(hfa)•triglyme•H_2O [5].

In all the three investigated potassium complexes (with monoglyme, diglyme and tetraglyme), due to the presence of bridging μ^2 and μ^3 oxygen atoms, 1D polymers are formed. The compound of potassium with tetraglyme crystallizes giving an asymmetric unit which contains the $[K_4(hfa)_4$•tetraglyme] cluster (Fig.1b) [6].

Glymes play a crucial role in stabilizing complexes of alkali metals, analogously to what previously observed for alkaline-earth, transition and rare-earth metals through oxygen-ion complexation. In regard to their thermal properties, the novel alkali adducts are thermally stable enough to be applied in a conventional MOCVD process, but due to their excellent solubility, they perform better in liquid assisted MOCVD processes.

Preliminary studies have validated these precursors for the deposition of niobate films. Specifically, the $[Li_{12}(hfa)_{12}$•monoglyme•$4H_2O]_n$ and the $[K_4(hfa)_4$•tetraglyme] adducts have been applied to the deposition of $LiNbO_3$ and $KNbO_3$, respectively, through liquid delivery MOCVD. The X-ray diffraction (XRD) pattern of the $LiNbO_3$ film on Al_2O_3 (0001) (Fig. 2) shows the formation of a single-phase and a highly oriented film. The scanning electron microscopy (SEM) image (inset in Fig. 2) shows a nanostructured morphology.

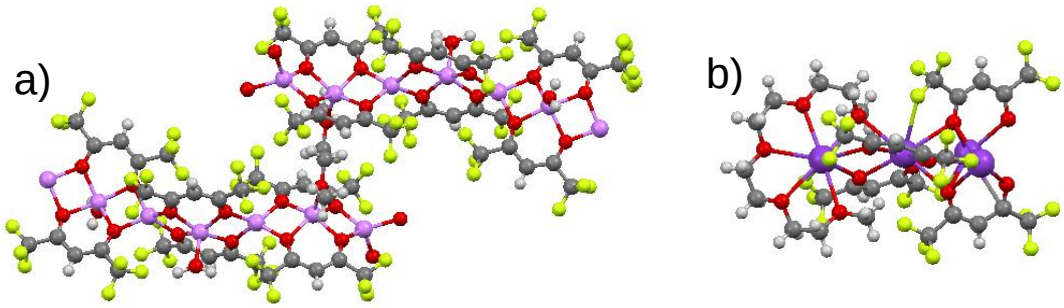

Fig. 1. ORTEP-3 views of the a) $[Li_{12}(hfa)_{12}•monoglyme•4H_2O]_n$ and b) the $[K_4(hfa)_4•tetraglyme]$ clusters.

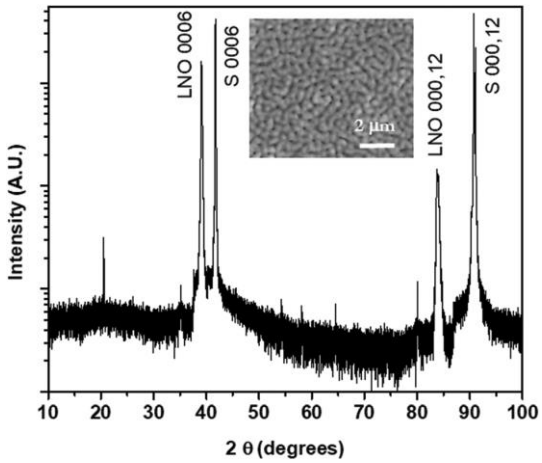

Fig. 2 X-ray diffraction pattern of a $LiNbO_3$ film deposited at 775 °C on C-sapphire (S) using the monoglyme adduct and the $Nb(tmhd)_4$. The inset reports the SEM image of the film.

References

1. A. Bartasyte, S. Margueron, T. Baron, S. Oliveri, and P. Boulet, Adv. Mater. Interfaces **4**, 1600998 (2017).
2. J. Schwarzkopf, M. Schmidbauer, T. Remmele, A. Duk, A. Kwasniewski, S. Bin Anooz, A. Devi, R. Fornari, J. Appl. Crystallogr. **45**, 1015 (2012).
3. Z. Cen, Z. Xu, L. Li, X. Wang, Dalton Trans. **50**, 8851 (2021)
4. N. Peddagopu, P. Rossi, C. Bonaccorso, A. Bartasyte, P. Paoli and G. Malandrino, Dalton Trans. **49**, 1002 (2020).
5. N. Peddagopu, A. L. Pellegrino, C. Bonaccorso, P. Rossi, P. Paoli and G. Malandrino, Molecules **27**, 6282 (2022).
6. N. Peddagopu, S. Sanzaro, P. Rossi, P. Paoli, and G. Malandrino, Eur. J. Inorg. Chem. 3776 (2021).

* *Corresponding author e-mail:* gmalandrino@unict.it

Semiconductor and nanomaterials II

Chair: Sepulveda Marquez, Alfonso (imec)

Time: 6/1/2023 10:30:00 AM
Location: Auditorium 2, Maria-Theresiacollege, St. Michael's Street 6, Leuven

Nucleation and initial growth in CVD of epitaxial Boron Nitride

Sachin Sharma*, Justinas Palisaitis, Henrik Pedersen and Hans Högberg

Department of Physics, Chemistry and Biology, Linköping University, SE-581 83, Linköping, Sweden

Thin films of epitaxially grown sp^2-hybridized boron nitride (sp^2-BN) in its hexagonal (h-BN) and rhombohedral (r-BN) phases have potential applications in UV devices, as piezoelectric materials, and in graphene technology. Thin film growth of sp^2-BN is typically done using CVD at temperatures above 1200 °C. A common substrate is oriented Al_2O_3(0001). We have recently studied the growth of sp^2-BN using thermal CVD, comparing the differences in growth on Al_2O_3(11-20) and Al_2O_3(0001) commonly known as *a*-cut and *c*-cut Al_2O_3 substrates. These films are grown with an AlN buffer layer which has been shown to improve crystallinity for the BN films in our past studies [1]. The B precursors utilized for growth are triethylborane (TEB) and trimethylborane (TMB), both used with NH_3 as nitrogen precursor to investigate different chemical pathways for the growth of BN films. XRD ω-scan show a FWHM of 0.98° r-BN film on *a*-cut Al_2O_3, contrasted by a FWHM of 1.15° r-BN film on *c*-cut Al_2O_3. The BN-polytype stability and epitaxial relationship were determined by XRD ϕ-scans to be r-BN[11-20]‖ w-AlN[11-20]‖ α-Al_2O_3[0001]the same on both *a*- and *c*-cut sapphire. These results from our last study recognizes *a*-cut sapphire as an evidently better substrate for the growth of r-BN [2].

To understand the influence of CVD process parameters leading to nucleation and initial growth of epitaxial sp^2-BN films on Al_2O_3, especially the precursors TEB or TMB. We now apply High Resolution Transmission Electron Microscopy (HRTEM) techniques, including interface focused STEM imaging, HRTEM imaging, EELS edge intensity distribution and line profiles which gives us the local film and interface information. These analyses are complimented with global film information acquired through FTIR and various thin film XRD techniques. Through this analytical analysis, we aim to methodically compare and investigate these sp^2-BN films grown using the different substrates and precursors.

From the HRTEM , we note that etching of the substrate surface is different between the substrates with a more significant etch pit formation on the surface of the *c*-cut vs *a*-cut Al_2O_3 substrates. Film delaminated substrates also show a difference in etch pit shapes. The HRTEM shows how the AlN layer forms bridging structures above the etch pits, i.e., AlN does not grow inside the pit, instead layers over it. The interface imaging shows that AlN crystal quality differs locally with less ordered intermediates at certain regions, more consistent AlN epitaxial growth is observed for the *a*-cut surface compared to the *c*-cut substrates. We observe BN polytype transition, past results showed the transition from h-BN to r-BN [3] during growth. As the sp^2-BN film grows thicker we see the onset of a less ordered growth with turbostatic sp^2-BN to amorphous material closer to the film vacuum interface. Our hypothesis is that carbon from the ligands incorporates into the BN film and disturbs the epitaxial growth. This was the reason for locally probing the films with analytical microscopy. We expect to learn more about all these film growth aspects through this ongoing study.

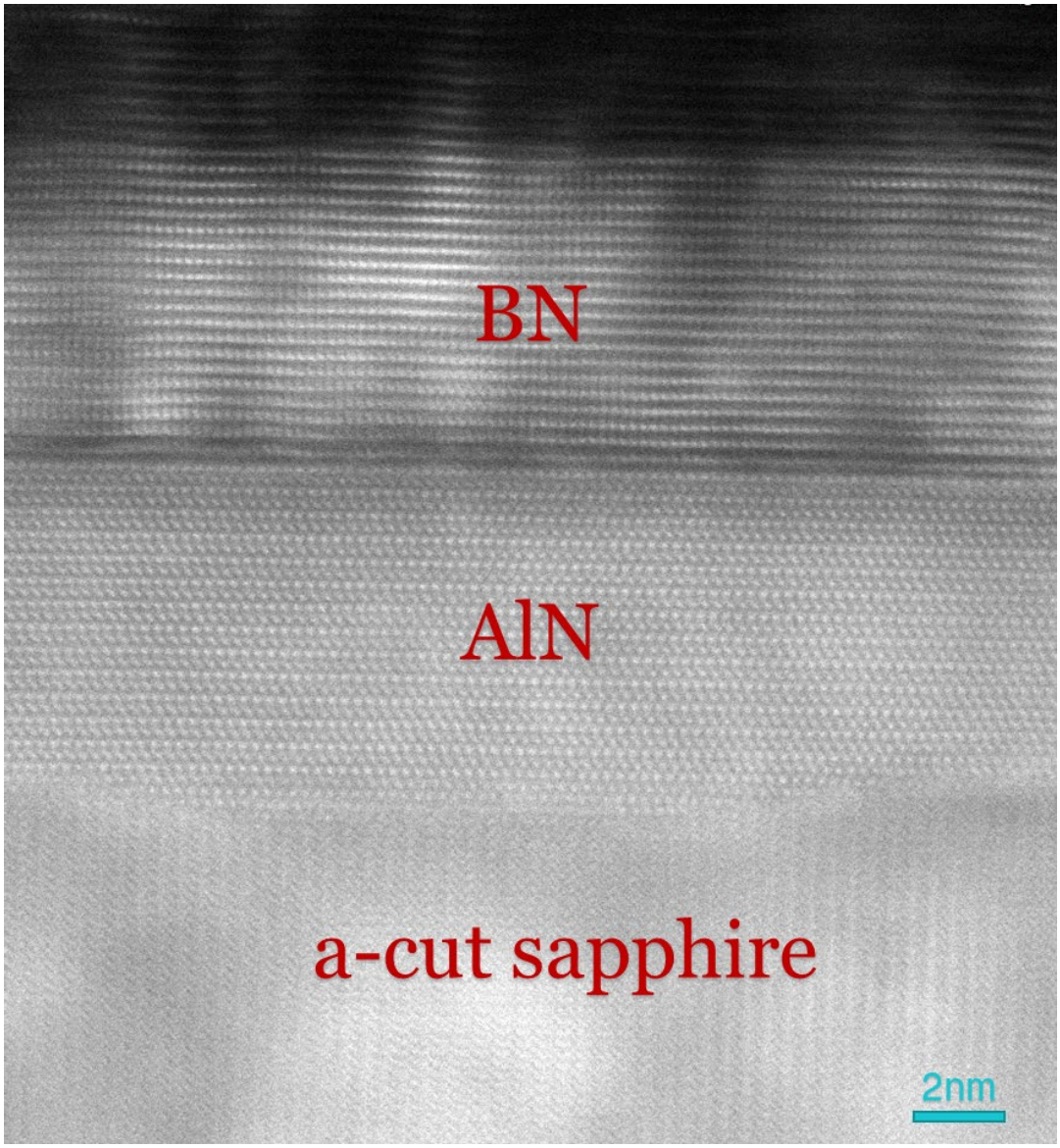

Fig. 1 STEM image of BN film growth using TMB precursor on a-plane Al_2O_3

References

1. M. Chubarov, H. Pedersen, H. Högberg, V. Darakchieva, J. Jensen, P. O. Å. Persson, and A. Henry, *Epitaxial CVD Growth of Sp2-Hybridized Boron Nitride Using Aluminum Nitride as Buffer Layer*, Phys. Status Solidi - Rapid Res. Lett. **5**, 397 (2011).
2. S. Sharma, L. Souqui, H. Pedersen, and H. Högberg, *Chemical Vapor Deposition of Sp2 -Boron Nitride Films on Al2 O3 (0001), (11-20), (1-102), and (10-10) Substrates*, J. Vac. Sci. Technol. A **40**, 033404 (2022).
3. M. Chubarov, H. Pedersen, H. Högberg, A. Henry, and Z. Czigány, *Initial Stages of Growth and the Influence of Temperature during Chemical Vapor Deposition of Sp2 -BN Films*, J. Vac. Sci. Technol. A **33**, 061520 (2015).

*Corresponding author e-mail: sachin.sharma@liu.se

Improving the quality of hexagonal boron nitride thin films grown on Ge(001)/Si substrates by CVD

Max Franck[a,*], Jarek Dabrowski[a], Markus Andreas Schubert[a], Walter Batista Pessoa[b], Dominique Vignaud[b], Mohamed Achehboune[c], Jean-François Colomer[c], Luc Henrard[c], Christian Wenger[a,d], and Mindaugas Lukosius[a]

[a] *IHP – Leibniz-Institut für innovative Mikroelektronik, Im Technologiepark 25, 15236 Frankfurt (Oder), Germany*
[b] *University Lille, CNRS, Centrale Lille, JUNIA ISEN, UPHdF, UMR 8520-IEMN F-59000 Lille, France*
[c] *Department of Physics, NISM Institute, University of Namur, Rue de Bruxelles 61, 5000 Namur, Belgium*
[d] *Semiconductor Materials, BTU Cottbus-Senftenberg, Platz der Deutschen Einheit 1, 03046 Cottbus, Germany*

Hexagonal boron nitride (hBN) is a two-dimensional material structurally analogous to graphene. It is an insulator with a bandgap of ~6 eV and has a range of promising applications, including deep ultraviolet optoelectronics, tunnel barriers in tunnel devices, and protection layers for high-mobility graphene. The most common method for synthesis of large-area, high-quality hBN, besides mechanical exfoliation, is chemical vapor deposition on catalytic transition metal substrates like Cu and Ni. However, for device fabrication, these methods require transfer of the hBN films to CMOS-compatible substrates, which leaves residual metal contaminations at concentrations unacceptable for Si technology integration.[1] Therefore, growth of hBN thin films directly on CMOS-compatible substrates, such as silicon, germanium or dielectrics, is desirable. In particular, germanium has proven suitable for CVD growth of high-quality 2D materials [2], due to its catalytic activity [3]. In fact, low pressure CVD growth of polycrystalline hBN monolayers using ammonia borane as the precursor has been reported previously.[4,5]

Here, we demonstrate CVD synthesis of well-oriented, few-layer hBN thin films on Ge(001)/Si substrates using borazine as a single-source precursor.[6] Morphology and crystalline quality were characterized using x-ray photoelectron spectroscopy, atomic force microscopy (AFM), Raman spectroscopy and transmission electron microscopy (TEM). The hBN films also contain nanocrystalline islands with crystallites 2-5 nm in size (Fig. 1), resulting in a root mean square (RMS) roughness of 12 nm (Fig. 3a). First experiments at slightly lower temperatures yielded fully nanocrystalline hBN films, ~50 nm in thickness and with smaller crystallite size. The crystalline quality was improved to the aforementioned state by increasing the growth temperature to near the melting point of germanium.

Subsequently, we focus on reducing the presence of nanocrystalline islands. By reducing the precursor flow to the substrate surface they can be eliminated (Fig. 2), leaving only small, amorphous islands at the Ge/hBN interface. This is accompanied by a reduced RMS roughness of 2.2 nm (Fig. 3b). The amorphous island density and size can be reduced by dilution of the borazine/Ar mixture from the bubbler with more Ar, resulting in an RMS roughness of 0.6 nm (Fig. 3c).

This work was funded by the FLAG-ERA grant 2DHetero, by the Deutsche Forschungsgemeinschaft (DFG, German Research Foundation) (436545422).

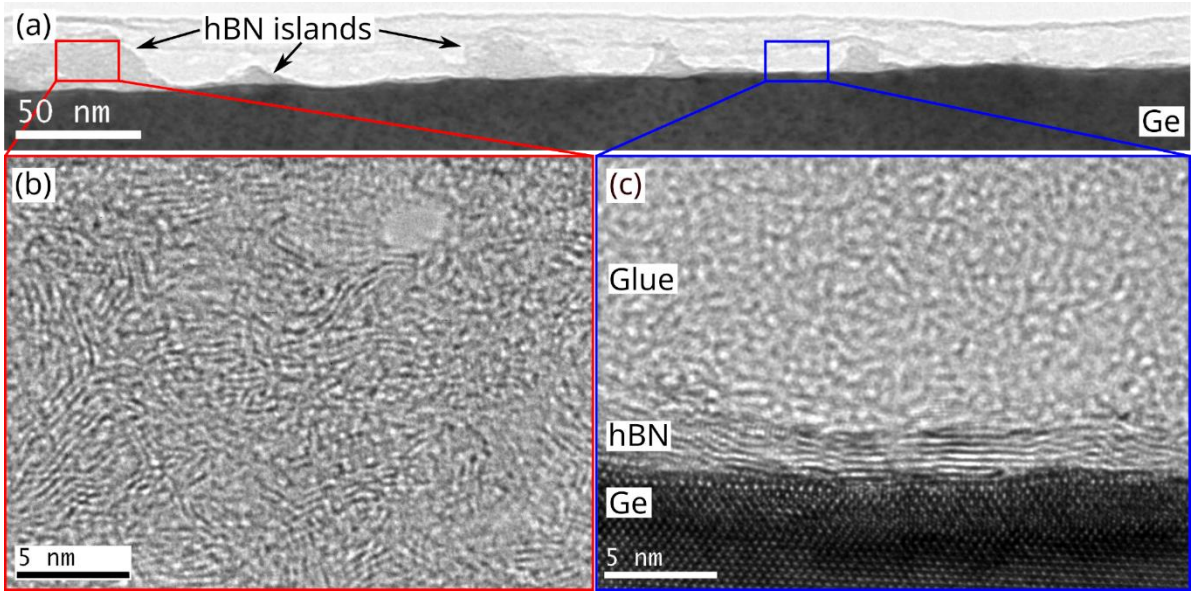

Figure 1. (a) Overview TEM image of hBN film grown on Ge(001)/Si at 980 °C setpoint temperature, showing islands and flat regions. (b) Detailed view of island marked by red box in (a). (c) Detailed view of vertically stacked hBN layers marked by blue box in (a). From [6].

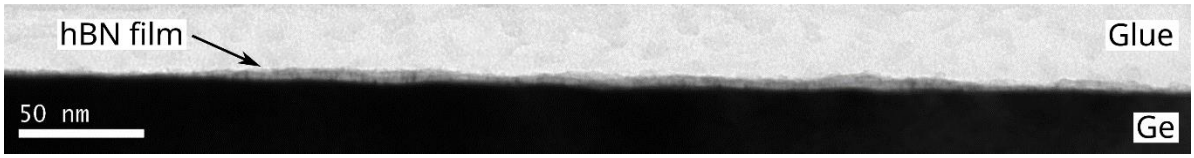

Figure 2. Overview TEM image of hBN film without nanocrystalline islands after reduction of precursor flow to the Ge surface.

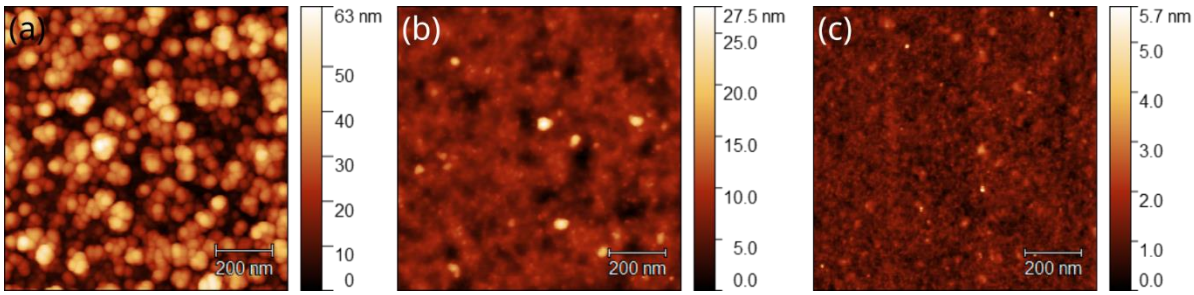

Figure 3. (a) AFM image corresponding to the sample shown in Fig. 1, showing a high density of larger, nanocrystalline islands, R_{RMS} = 12 nm. (b) AFM image corresponding to the sample shown in Fig. 2, showing a low density of smaller, amorphous islands, R_{RMS} = 2.2 nm. (c) AFM image of sample grown with a 3:1 dilution of the precursor, with further reduced island density and size, R_{RMS} = 0.6 nm.

References

1. G. Lupina *et al.*, ACS nano **9**, 4776 (2015).
2. J. Aprojanz *et al.*, ACS applied materials & interfaces **12**, 43065 (2020).
3. P. W. Loscutoff and S. F. Bent, Annual review of physical chemistry **57**, 467 (2006).
4. J. Yin *et al.*, Small **11**, 5375 (2015).
5. C. Zhang *et al.*, 2D Mater. **8** (2021).
6. M. Franck *et al.*, Nanomaterials **12**, 3260 (2022).

* *Corresponding author e-mail:* franck@ihp-microelectronics.com

AlScN/GaN heterostructures grown by metal-organic chemical vapour deposition using novel Sc-Precursors

Isabel Streicher[a,*], Stefano Leone[a], Christian Manz[a], Lutz Kirste[a], Patrik Straňák[a], Mario Prescher[a], Patrick Waltereit[a], Rüdiger Quay[a,b] and Oliver Ambacher[b]

[a] *Fraunhofer Institute for Applied Solid State Physics, Tullastrasse 72, 79108 Freiburg, Germany*
[b] *Institute for Sustainable Systems Engineering, University of Freiburg, Emmy-Noether-Strasse 2, 79110 Freiburg, Germany*

Nitride-based high-electron-mobility-transistors (HEMT) offer high power density and output power at high frequencies and play an important role in high-volume data transmission and efficient energy conversion. AlScN is a promising new barrier layer which provides a higher sheet charge carrier density (n_s) in the two-dimensional electron gas (2DEG) than conventional AlGaN layers thanks to its high spontaneous polarization and piezoelectric coefficients, reducing device channel resistance.
Both molecular beam epitaxy [1] and metal-organic chemical vapour deposition (MOCVD) [2] can be employed to grow AlScN HEMT structures. Growth by MOCVD makes AlScN-based devices accessible for industry-scale production but remains challenging due to the low vapour pressure of available Sc-precursors of about 3.07 x 10^{-6} mbar at room temperature. We developed a rearranged, heated gas mixing system to achieve a molar flow of 1-10 µmol/min which allows for Sc concentrations up to 30%. However, the growth rate (GR) remains low and the epilayers are exposed to a high thermal budget due to the extended growth time at high temperatures. This leads to the formation of AlGaN interlayers by Al atom diffusion. We investigate how the variation of the thermal budget affects interlayer formation by comparing AlScN/GaN heterostructures grown at different temperatures from 900 to 1200°C and with different GRs. The GR is varied by using two different Sc precursors, the conventional tris-cyclopentadienyl-scandium (Cp_3Sc) and the newly qualified bismethyl-cyclopentadienyl-scandiumchloride ($(MCp)_2ScCl$). $(MCp)_2ScCl$ allows for doubling the GR from the 0.006 nm/s typically achieved using Cp_3Sc to 0.015 nm/s [3]. Contactless Hall measurements show that, at fixed growth conditions, the sheet resistance R_{sh} can be decreased by approximately 20%. At 900°C, the average R_{sh} across the 4” wafer was decreased from 211 to 172 Ω/□, one of the lowest values reported in literature so far for AlScN/GaN heterostructures. The n_s was increased from 2.98 to 3.23 x 10^{13} cm^2 and the electron mobility µ from 998 to 1124 cm^2/Vs, see fig. 1. The values are homogeneous across the 4” wafers, see fig. 2. With increased growth temperature, R_{sh} increases, n_s and µ decrease (fig. 1).
The grown AlScN/GaN heterostructures are examined by transmission electron microscopy and energy-dispersive X-ray spectroscopy in combination with secondary ion mass spectrometry in order to determine the interlayer and barrier thicknesses and composition. The obtained information is used for 1D-Schrödinger-Poisson simulations of the 2DEG spatial distribution and charge density. We show that diffusion-induced AlGaN interlayers lead to a broadening of the potential well [4]. Reduction of the thermal budget by lowering the growth temperature from 1000 to 900°C or growing with increased GR allows for an improved confinement of the 2DEG and increases the n_s.
In order to improve the interfaces further we aim at GRs of about 0.13 nm/s, which is the typical GR of AlGaN barriers. To that end, we are currently testing new precursors with high vapor pressure of which we determine not only the maximum achievable GR but also Sc incorporation efficiency, effect of the C/Sc ratio of the precursor molecule, and impurity contamination such as oxygen. The electrical characteristics (R_{sh}, n_s and µ) of the epilayer structure at low barrier growth temperatures are very sensitive to precursor purity, as shown in fig. 3 for the standard precursor Cp_3Sc used in different purities. At 1000°C, we observed a change of R_{sh} from 1270 Ω/□ with the research grade precursor, to a much improved value of 211 Ω/□ with the production grade precursor.
First AlScN-based HEMTs fabricated from heterostructures grown with $(MCp)_2ScCl$ show a transconductance above 500 S mm^{-1} and a drain current of 1.8 mA mm^{-1} [5].

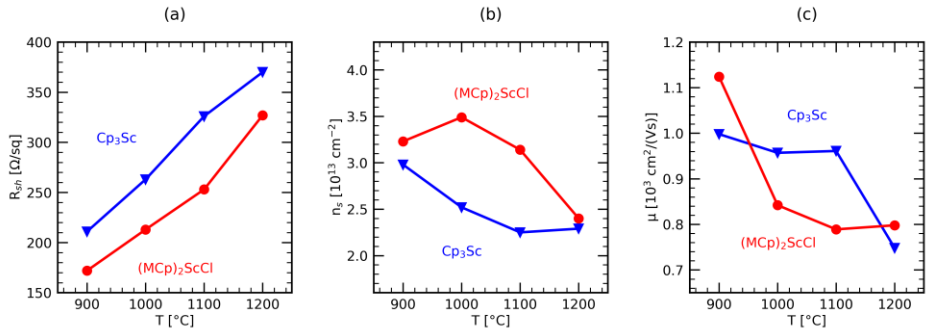

Figure 1: Contactless Hall measurements on AlScN HEMT structures grown with the conventional precursor Cp_3Sc and the novel precursor $(MCp)_2ScCl$ on 4” 4H-SiC wafers at different temperatures. (a) Sheet resistance R_{sh}, (b) sheet charge carrier density n_s and (c) electron mobility μ. The solid lines are a guide to the eye. Figure taken from [2].

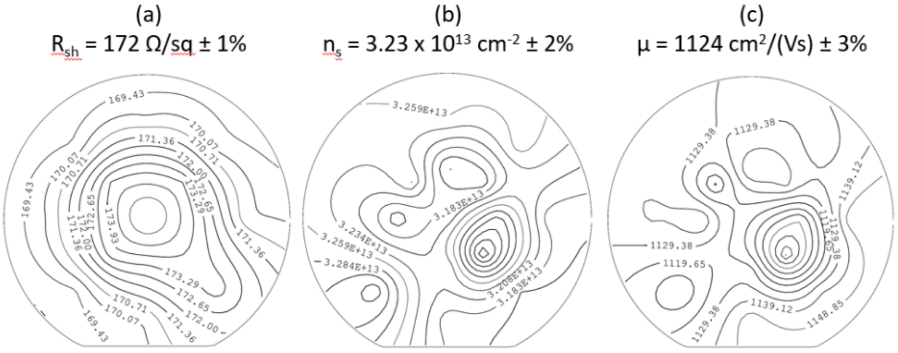

Figure 2: Map of R_{sh}, n_s and μ of a AlScN/GaN heterostructure grown at 900°C on a 4” wafer obtained with contactless Hall mapping.

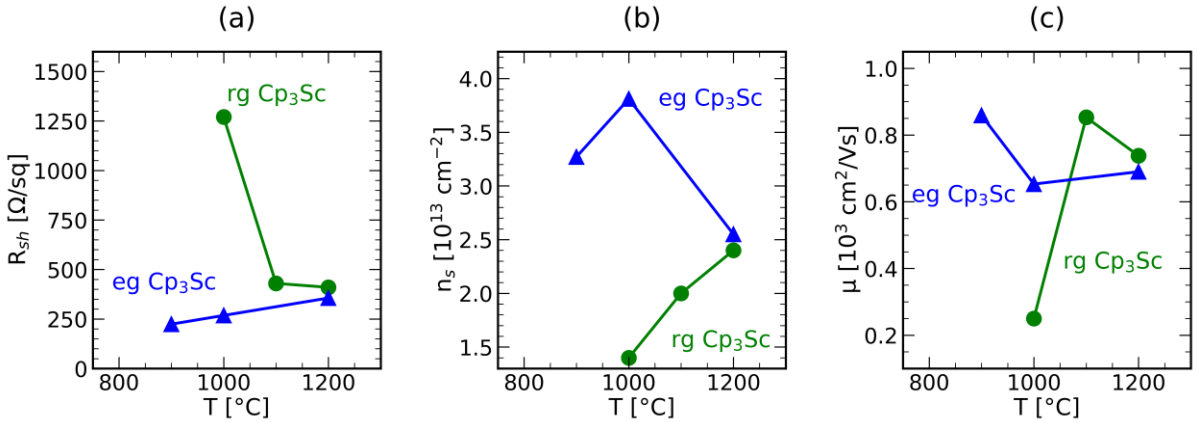

Figure 3: R_{sh}, n_s and μ determined by Hall measurements on AlScN HEMT structures grown on Al_2O_3 using research grade (rg) Cp_3Sc [6] and electronic grade (eg) Cp_3Sc [4] at different barrier layer growth temperature. The solid lines are a guide to the eye.

References

1. Tahhan M B, et al., IEEE Transactions on Electron Devices, **69**, 972 (2022).
2. Leone S, et al., Physica Status Solidi RRL **14**, 1900535 (2020).
3. Streicher I, et al., Physica Status Solidi RRL, 2200387 (2022).
4. Streicher I, et al., Crystal Growth & Design (2023).
5. Krause S, et al., IEEE Electron Device Letters **44**, 17 (2023).
6. Ligl J, et al., Journal of Applied Physics **127**, 195704 (2020).

* *Corresponding author e-mail:* *isabel.streicher@iaf.fraunhofer.de*

Group III-Nitride semiconductor materials made by low temperature plasma based Atomic Layer Deposition

Noureddine Adjeroud[a], , Jérôme Guillot[a], Christèle Vergne[a], Adrian-Marie Philippe[a], Yves Fleming[a] Jérôme Polesel-Maris[a]

[a] Materials Research and Technology Department, Luxembourg Institute of Science and Technology (LIST) 41, rue du Brill L-4422 Belvaux, Luxembourg

In the last few decades, there has been a phenomenal rise and progress in the field of III–Nitride semiconductors. Now, the materials group III-N is changing the path of high-performance integrated circuits (IC) technology in high power and high frequency regimes and has received much attention due to its wide and direct bandgap, high electron mobility and high breakdown electrical field.

III-N semiconductors are largely present in the industry, through chemical vapor deposition (CVD) techniques such as Metalorganic vapour-phase epitaxy (MOVPE). Those deposition techniques use conventionally the reaction of ammonia (NH_3) with industrially relevant precursors such as trimethylaluminum (TMA), trimethylgallium (TMG) or trimethylindium (TMI) at high temperatures (750-900 °C) [1]. Plasma-assisted Atomic Layer Deposition (PA ALD) is becoming a trustworthy alternative to the standard CVD deposition techniques, and it appears as a solution for highly conformal coating and low temperature processing as two important assets to tackle growth temperatures of the nitride films not interfering with CMOS circuitry.

This work is based on the optimization and engineering of the plasma ALD of c-axis highly oriented aluminium nitride (AlN) films we proposed [2]. The pathway was further extended to facilitate low temperature (<450 °C) deposition of other III-N materials, such as GaN and InN semiconductors with wide and small bandgap respectively. In this work we utilized a gas mixture of H_2/Ar/N_2 as nitrogen precursor for nitride thin films initiated by a plasma source. The mix of Ar and H_2 allows both to stabilize the plasma phase and to induce an optimized reducing of the ligands of the organometallic precursors reducing the carbon contaminants measured in the materials. We observed by XPS stoichiometric III-N films with no detectable carbon contaminants and also a low level (<5%) of oxygen contaminants in the nitride films. The XRD and TEM analysis confirm privileged hexagonal crystalline structure of the thin film below 100 nm thickness.

Insights on the ALD set-up and specific sequence of the deposition process will be presented for the growth of aluminium nitride (AlN), gallium nitride (GaN), indium nitride (InN), and ternary III-N films.

Those results have the potential to pave a way for both buffer-oriented seed films for post-growth, and also films with tailor made electronics properties for the next-generation of III-Nitride/CMOS components and functional coatings with piezoelectric and semiconducting properties for MEMS applications with transducing capabilities.

GaN				
Etch Time (s)	C 1s %	Ga %	N 1s %	O 1s %
t1	0.0	59.7	32.9	7.4
t2	0.0	54.2	41.8	4.0
t3	0.0	56.2	39.7	4.1
t4	0.0	54.6	41.9	3.5

Quantification of Ga(N,O) is not accurate due to N 1s-Ga LLM peaks overlaps as well as ga 2p - N KLL peaks overlaps

AlN				
Etch Time (s)	Al 2p %	C 1s %	N 1s %	O 1s %
t1'	29.7	23.9	21.3	25.1
t2'	48.4	0.0	45.9	5.7
t3'	49.1	0.0	46.7	4.2
t4'	48.8	0.0	47.1	4.1
t5'	48.8	0.0	46.8	4.4

TAB 1.: Elemental quantification. XPS analysis of nitride films ALD deposited

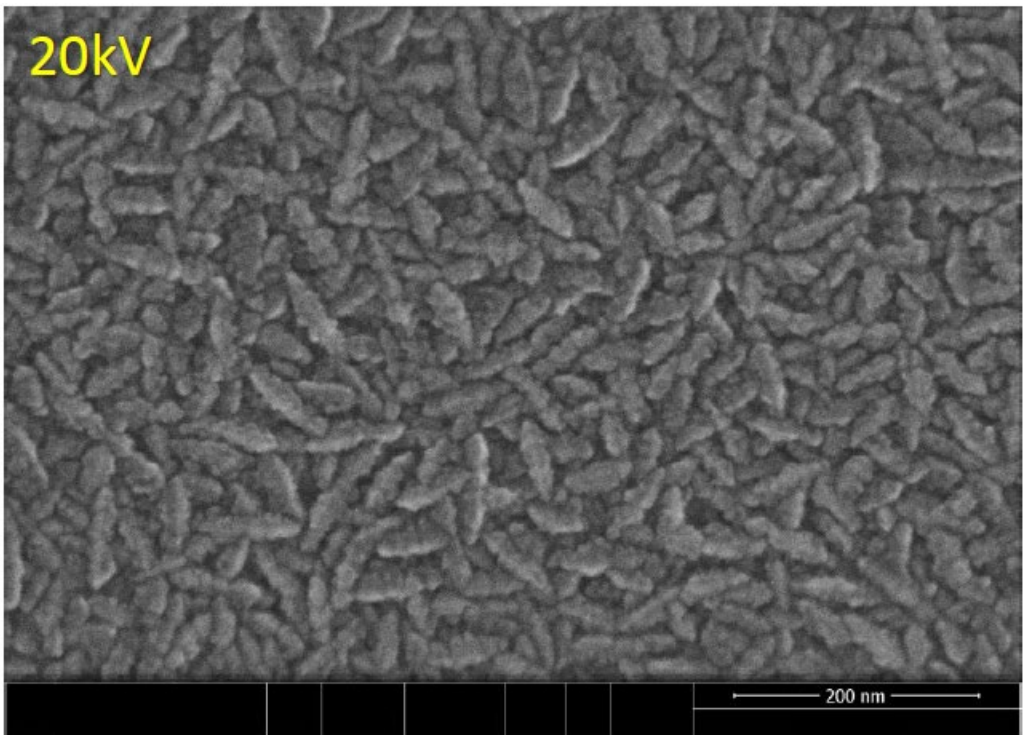

Fig. 1: SEM image of 150 nm thick GaN film deposited onto a silicon <100> substrate.

Reference
1. A. V. Kondratyev et al., physica status solidi (c), volume 5, issue 6 (2008)
2. Tai Nguyen, Noureddine Adjeroud, Sebastjan Glinsek, Yves Fleming, Jérôme Guillot, Patrick Grysan, and Jérôme Polesel-Maris, APL Materials 8, 071101 (2020)

* *Corresponding author e-mail:* noureddine.adjeroud@list.lu

ALD-AlO_x Monolayers for Modulation-Doping of Silicon Nanowires

Daniel Hiller[a,*], Soundarya Nagarajan[b], Ingmar Ratschinski[a], Somayeh Shams[a], Thomas Mikolajick[b,c], Jens Trommer[b], Dirk König[d]

[a] *Institute of Applied Physics (IAP), TU Bergakademie Freiberg, Germany*
[b] *Nanoelectronic Materials Laboratory (NaMLab) gGmbH, Dresden, Germany*
[c] *Institute of Semiconductors and Microsystems, TU Dresden, Germany*
[d] *Integrated Materials Design Lab (IMDL), Australian National University (ANU), Canberra, Australia*

Silicon nanowires (Si NWs) or nanosheets are the building blocks for future transistors but suffer from severe difficulties with efficient impurity doping due to a multitude of physical and technological problems when the diameters are reduced to a few nanometers (diffusion, dielectric and quantum confinement, statistics of small numbers, etc.). Especially junctionless nanowire transistors require high conductivities but high impurity doping concentrations cause a severely decreased mobility, which in turn implicates the need for higher operation voltages and increased electrical energy dissipation into heat. Therefore, alternative doping methods are desirable that separate doping-induced free carriers from their parent dopant atoms.

Here, we present a novel doping concept for Si NWs comparable to the modulation doping approach of III-V semiconductors. Based on results from density functional theory (DFT) calculations, we use Al-doped SiO_2 shells around the Si NWs, in which unoccupied Al-induced acceptor states are created with an energy level located below the Si valence band edge. These states can capture electrons from the Si, creating free holes as majority charge carriers [1-5]. Experimentally, the Al-doping of SiO_2 is realized by ALD to form (sub-)monolayers [6] of AlO_x.

In this presentation, recent results of this doping approach are shown. We demonstrate that Si NWs that were modulation-doped by SiO_2:Al-shells have several orders of magnitude lower electrical resistances as compared to NWs with undoped SiO_2-shells. Selected resistance results and schematic cross-sections of the Si NW test devices are shown in Fig. 1.

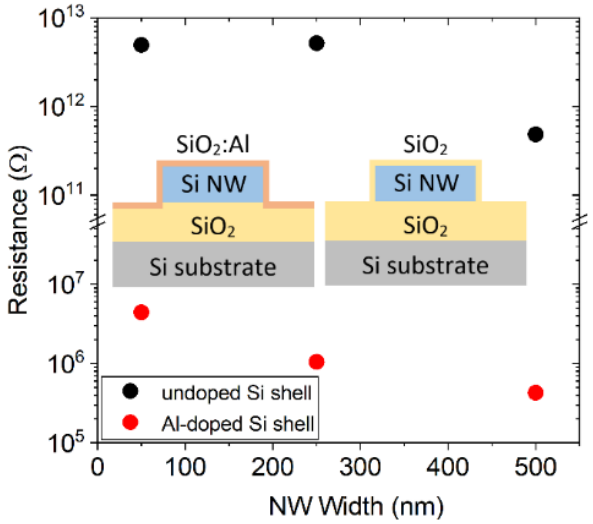

Fig. 1: Schematic cross-sections of the Si NW test devices and selected electrical resistance results.

References

1. D. König et al., Sci. Rep. **7**, 46703 (2017)
2. D. Hiller et al., ACS Appl. Mater. Interfaces **10**, 30495 (2018)
3. D. König et al., Phys. Rev. Appl. **10**, 054034 (2018)
4. D. Hiller et al., J. Appl. Phys. **125**, 015301 (2019)
5. D. Hiller et al., J. Phys. D Appl. Phys. **54**, 275304 (2021)
6. D. Hiller et al., Sol. Energy Mater. Sol. Cells **215**, 110654 (2020)

* *Corresponding author e-mail: daniel.hiller@physik.tu-freiberg.de*

ASD II

Chair: Detavernier, Christophe (Ghent University)

Time: 6/1/2023 1:30:00 PM
Location: Auditorium 1, Promotion Hall, Naamsestraat 22, Leuven

Is HV-CVD best for all coating challenges?

Patrik Hoffmann*, Wojciech Szmyt

Empa, Swiss federal labs for Materials Science and Technology, LAMP, Feuerwerkerstr. 39, Thun, CH-3602 and EPFL, STI, LPMAT, Station 12, Lausanne, 1015 Switzerland

High Vacuum Chemical Vapor Deposition (HV-CVD) is a deposition technique that combines the advantages of simple predictive precursor flow behaviour (i.e. Knudsen effusion), and strongly enhanced species mobility on the substrate surface of the coating composing ingredients. This translates into lower deposition temperatures, higher deposition rates and therefore higher quality price ratio as compared to other coating technologies for cutting edge performance coatings. Carrying out HV-CVD in a combinatorial manner allows for fast and efficient coating optimization.

The technology is based on parallel, carrier gas free, effusion of precursors onto a preheated substrate. The chemically reactive precursor molecules surface migrate and react with one another for growing films. Nucleation density and growth kinetics determine the "surface smoothness" of the growing films. Experimental proof of this effect is presented for two different cases of growth for two very different film growth challenges, a) epitaxial growth of Barium Titanate (BTO) crystalline films on $SrTiO_3$ buffered silicon substrates; and b) selective growth of TiO_2 on lithographically patterned perfluorosilanized naturally oxidized silicon wafers for selective growth of TiO_2.

200 nm thick heteroepitaxial BTO films need to be deposited at highest quality evidently with respect to stoichiometry and crystallinity but also with respect the surface roughness and waviness due to the function as optical on chip switches or other optical devices. Therefore the combinatorial study of the deposition of BTO films with $Ba(iPr_3Cp)_2$ and Titanium-tetraisopropoxide (TTIP), together with O_2 was carried out. The combinatorial character of the deposition experiments is characterized by the creation of two different gradients of the two metal containing precursor gas fluxes, the precursor flux ratio between the two precursors and the second gradient, the total precursor flux onto the substrate, corresponding to a gradient in precursor impinging rate of the molecules. These two gradients are achieved by a selection of effusion holes openings in the precursor supplying precursor rings as schematically presented in Fig.1. This opening arrangement results in the also shown precursor ratio and total flux gradients on the 4 inch Silicon wafer.

Deposition at 450°C substrate temperature resulted in the growth of BTO films of thicknesses around 200nm (depending on the deposition time) with very low surface roughness (see. Fig 2) only at the correct impinging rates of both precursors, and evidently the correct ratio. The found ideal conditions are then applied on full wafer scale and this achievement is presently evaluated for the industrial fabrication of optical devices, by a Swiss start-up company.

Our HV-CVD set-up was conceived to perform in-situ patterned deposition by laser mask projection and therefore selective growth of materials with "reactive" precursors was also carried out.[1] Again, nucleation probability to initiate growth and growth rates will determine the "selectivity" of the growth process. Here a selective "monolayer" perfluorsilanization was carried out in order to create a low sticking surface for both precursors, which was removed with a mask pattern resulting on naturally oxidized silicon at the deposition "active" surface. Especially the adsorption of water with very high sticking probability will initiate the nucleation of the TiO_2 growth with TTIP as deposition partner. (see schematic presentation in Fig 3b) The specific impinging rates of the precursors together with the substrate temperature define the window of selectivity. At low impinging rates (precursor flow) and low substrate temperature, 100 nm selective TiO_2 growth could be obtained, as shown in figure 3c. With increasing film growth, the probability of nucleation on the "intert" surface is increasing and constant height different growth appears after full coverage of the originally inert surface. Together with the formerly reported thermodynamic and kinetic information for this deposition system, deep understanding of nucleation rates could be experimentally indirectly obtained.

References

1. M. Reinke, Y. Kuzminykh, P. Hoffmann, ACS Appl. Mater. Interfaces, **7**, 9736 (2015).

* *Corresponding author e-mail: patrik.hoffmann@empa.ch*

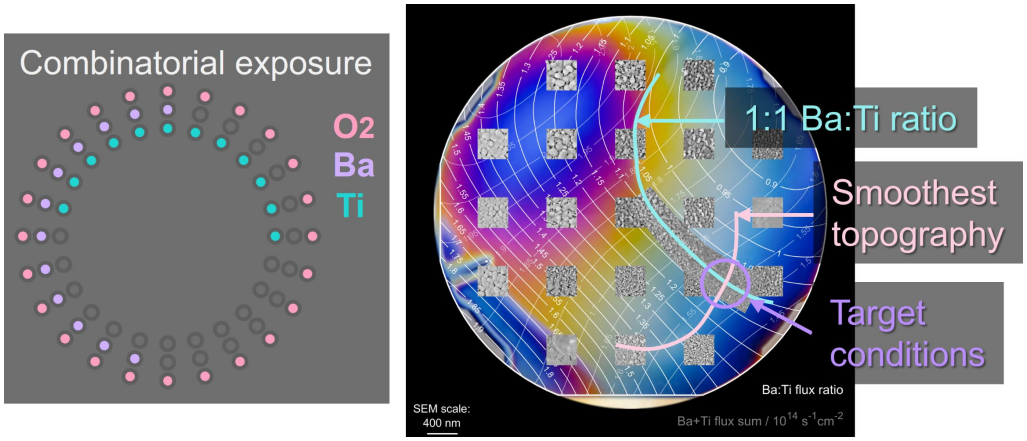

Fig. 1. Effusion orifice opening configuration schematic (left) and the resulting synthesis result on a 4" test Si wafer (right). The combinatorial deposition allowed to identify the optimized conditions for the growth of smoothest and stoichiometric BTO films.

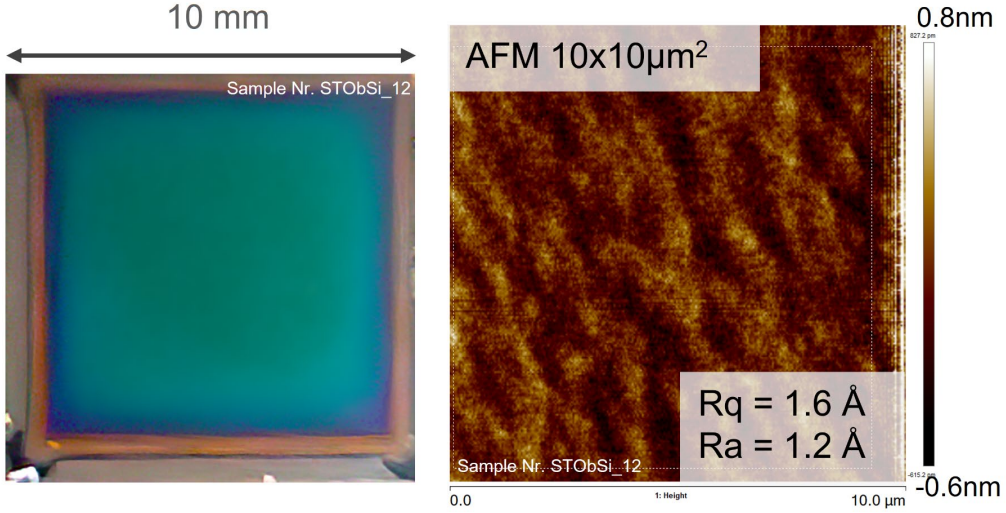

Fig. 2. Optimized conditions found by combinatorial deposition were transferred into a uniform deposition on SrTiO3-buffered substrate (left). The synthesized BTO films were epitaxial, stoichiometric, pure and near atomically smooth (right).

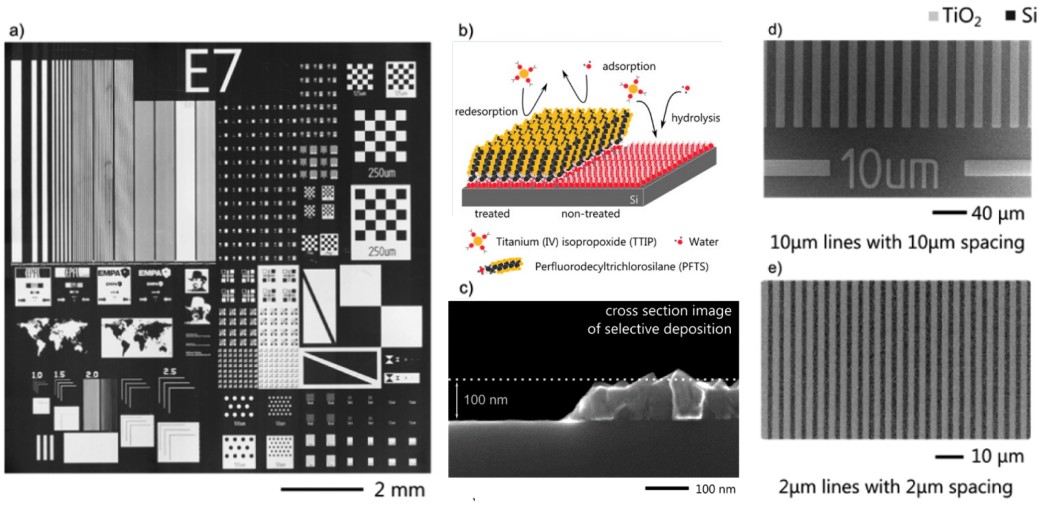

Fig. 3. Selective area deposition of TiO_2 on PFTS reacted/patterned Si wafer. a) overview, b) schematic of selective deposition, c) cross section of optimized growth, d,e) zoom in a). from [1]

Area-Selective Etching of Polymers for Self-Aligned Patterning

Valtteri Lasonen[a], Chao Zhang[a], Marko Vehkamäki[a], Anton Vihervaara[a], Mikko Ritala[a,*]

[a] *Department of Chemistry. University of Helsinki, A.I.Virtasen aukio 1, Helsinki, FIN-00014, Finland*

Patterning by area-selective etching of polymers, first presented by Zhang et al. [1], is a self-aligning technique which is based on different catalytic properties of different surfaces (Fig. 1). A thin polymer film is patterned and used as a resist similar to many common patterning processes, but it may also remain as part of the structure being made. The area-selective etching of polymer is done by annealing in the presence of an etchant gas. The polymer is decomposed from top of catalytically active materials, while on top of non-catalytic materials the polymer stays intact. This makes the technique self-aligned, thus avoiding placement errors and other defects. Different etching gases, such as O_2 and H_2, can be used. These small molecules diffuse through polymers onto the catalytically active surface that activates them to react with the polymer locally. Also, some materials can catalytically decompose the polymer directly in an inert atmosphere without the use of any etchant gas. After the self-aligned patterning step, many deposition methods can be used, for example, area-selective ALD or CVD or line-of-sight PVD followed by lift-off.

Several catalytic and non-catalytic materials have been identified. The catalytic effect of these materials depends on the temperature, the polymer, and the etching gas. This means that by carefully choosing the temperature, polymer, and atmosphere we can modify different surfaces to be catalytically active or inactive. Finding alternative atmospheres is important because, for example, many materials used in semiconductor devices cannot withstand high temperatures in oxidative atmospheres.

Here, we demonstrate that a very thin layer, even down to a fraction of a monolayer, of catalytically active material shows clear catalytic effect (Fig. 2). This is important because many of the catalytically active materials identified, like Pt and CeO_2, are not commonly used in semiconductor devices. However, thin layers of Pt can be used to catalytically activate metals, and CeO_2 to catalytically activate insulators.

Feasibility of the overall self-aligned patterning process is demonstrated in nanometer scale with two polymers, poly(methyl methacrylate) (PMMA) and polyimide (Fig. 3). Pt was used as a catalytic surface and native SiO_2 as a non-catalytic surface. ALD-Ni was deposited using PMMA as a resist for lift-off and ALD-Ir using polyimide as a growth inhibiting layer.

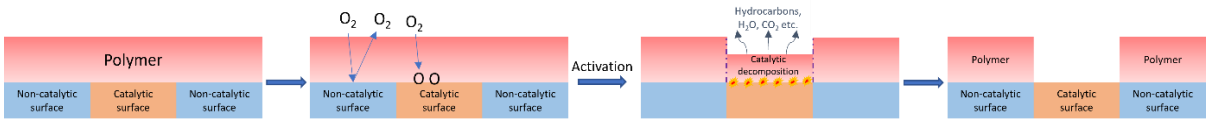

Figure 1 - Schematic of the self-aligned patterning by area-selective etching of polymers

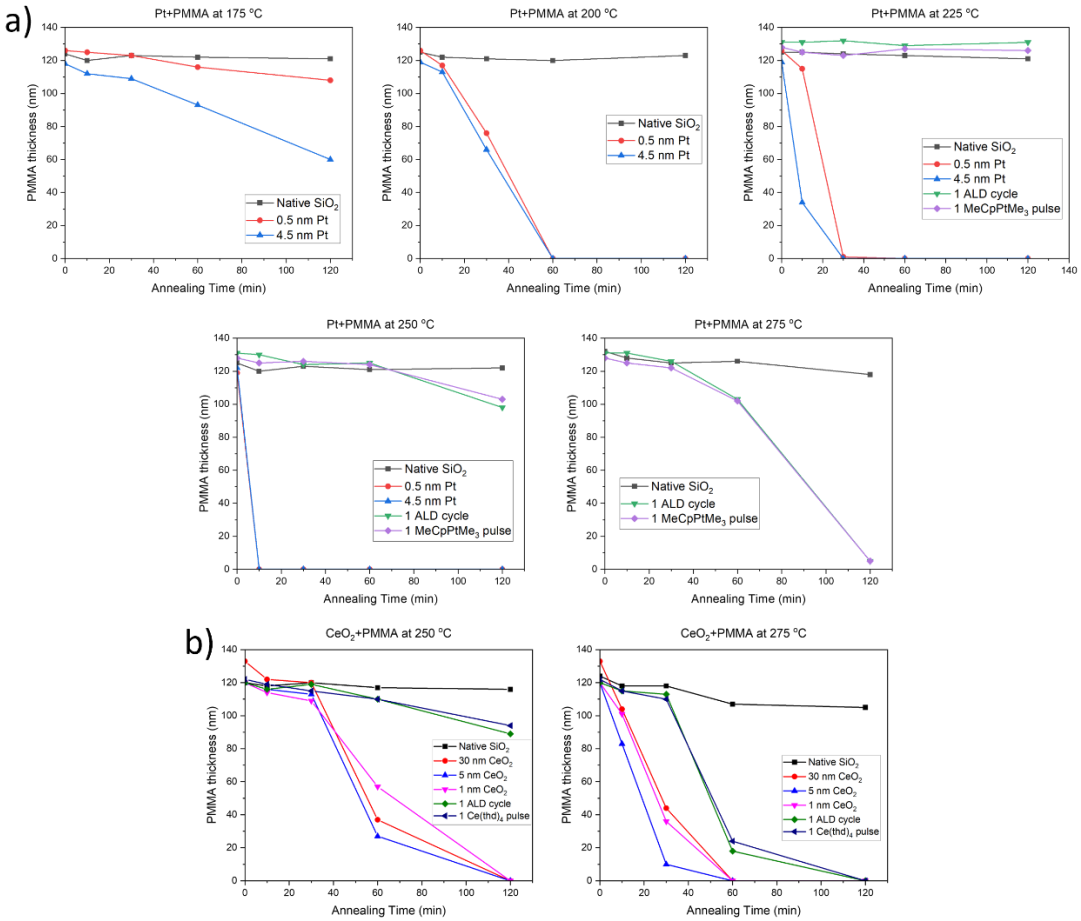

Figure 2 - Changes in the thicknesses of PMMA thin films over time on native SiO_2 and (a) Pt or (b) CeO_2 films of different thicknesses in air at different temperatures.

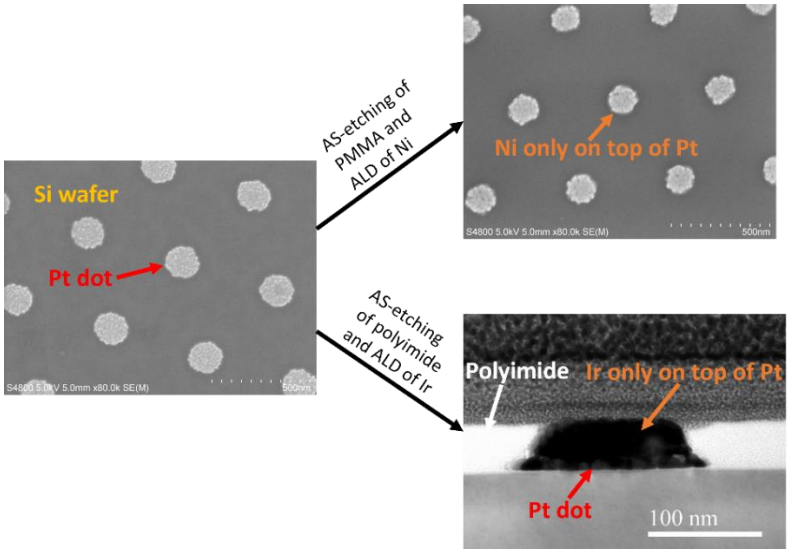

Figure 3 - SEM images of patterned Pt/SiO_2 before the area-selective etching process and after the area-selective etching of PMMA followed by ALD of Ni and removal of PMMA. TEM image after the area-selective etching of polyimide followed by ALD of Ir without removing polyimide.

References

1. C. Zhang, M. Leskelä and M. Ritala, Coatings, **11**, 1124 (2021).

* *Corresponding author e-mail: mikko.ritala@helsinki.fi*

Area-selective ALD involving sputter yield amplification by heavy elements

A.A. de Jong[a,*], M.J.M. Merkx[a], N.J. Chittock[a], W.M.M Kessels[a], A.J.M. Mackus[a]

[a] *Eindhoven university of technology, P.O. Box 513, Eindhoven, 5600 MB, The Netherlands*

As feature sizes in nanoelectronics continue to shrink, replacing lithography-etch schemes by area-selective atomic layer deposition (AS-ALD) will allow for self-aligned fabrication [1]. During AS-ALD, material is only deposited on the growth area while no deposition takes place on the non-growth area. Currently, most approaches to AS-ALD exploit a chemical pathway [2]. As an alternative, a supercycle combining ALD and sputter etching by ions can be used as a physical mechanism in achieving AS-ALD, see Fig. 1. For this to work, the non-growth area should contain heavy elements, in contrast to the growth area. Then, ALD has a similar growth per cycle (GPC) on the growth area and non-growth area, while the etch rate by sputtering is larger on the non-growth area, leading to a difference in net deposition. The difference in etch rate is caused by the so-called sputter yield amplification effect, where heavy substrate atoms reflect ions more efficiently and subsequently sputter the deposited material on top [3].

In this work, the potential of combining ALD of metal oxides with sputtering by low energy Ar ions (<100 eV) to achieve AS-ALD is investigated. Al_2O_3 is used as growth area and HfO_2 as non-growth area, considering that Al weighs 27 amu and Hf 178 amu (i.e. much larger than the Ar mass of 40 amu). On both substrates, two SiO_2 ALD cycles have been performed (BDEAS precursor and O_2 plasma coreactant at 250°C, reported in [4]). Subsequently, both substrates were exposed to an Ar ion bombardment with a 47.0 eV average ion energy. A difference in sputter etch rate of SiO_2 has been revealed using X-ray photoelectron spectroscopy (XPS) by plotting the decrease in Si2p photoelectron peak area as function of ion dose (see Fig. 2). On HfO_2, a significant sputter etch rate is observed, while no sputter etching occurs on Al_2O_3.

As a demonstrator, ten supercycles consisting of two SiO_2 ALD cycles followed by a $1.6 \cdot 10^{17}$ cm^{-2} Ar ion dose have been performed on Al_2O_3 and HfO_2. The SiO_2 thickness on both substrates is tracked by in-situ spectroscopic ellipsometry, see Fig. 3. During each supercycle, a thickness increase can be seen after the ALD cycles and a thickness decrease after the ion etch step. This thickness decrease is larger on the HfO_2 substrate. Finally, 1.1 nm of SiO_2 has been grown on Al_2O_3, while no significant SiO_2 thickness is observed on HfO_2.

In this contribution, the selective sputter etch results and the design of the deposition-etch supercycles exploiting sputter yield amplification will be discussed. Increasing the number of ALD cycles per supercycle can increase the net deposition on the growth area, while tuning the ion energies and doses accordingly can improve the selectivity. Moreover, it will be shown that this AS-ALD process can be extended to different combinations of materials, such as TiO_2 ALD and WO_3 as non-growth area. Substrate-selective ion sputtering can thus provide an unique pathway to AS-ALD which can distinguish between novel combinations of light growth areas and heavy non-growth areas.

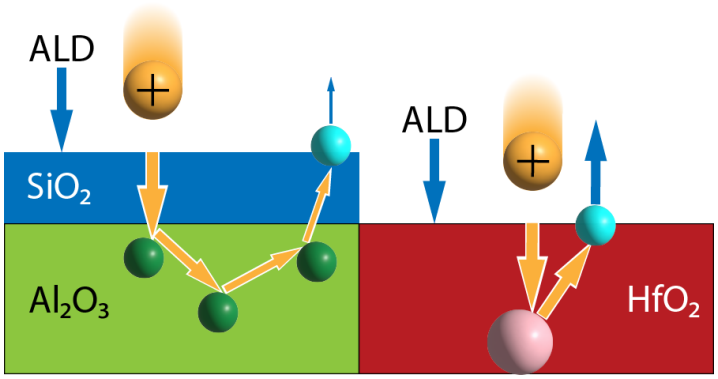

Fig. 1: Area selective ALD of SiO_2 by combining ALD and ion sputtering. The GPC (blue arrow pointing downwards) is similar on both Al_2O_3 and HfO_2 while the sputter yield (blue arrow pointing upwards) is amplified on the heavier HfO_2. Ions undergo fewer collisions (orange arrows) before they can sputter in HfO_2 due to the large mass of the Hf atoms, as compared to Al (also drawn by the orange arrows). The result is a net deposition on Al_2O_3 and not on HfO_2.

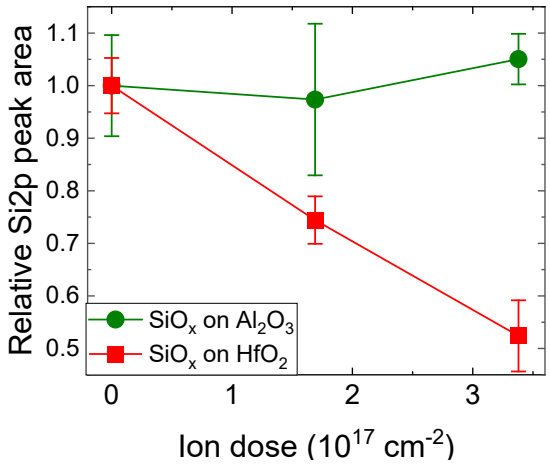

Fig. 2: Relative Si2p XPS peak areas before and after various ion doses. Ion sputtering occurs readily on HfO_2, while no significant decrease in Si counts on Al_2O_3 is observed. A relative peak area of 1.0 corresponds to 2 Å of SiO_2, deposited by two ALD cycles.

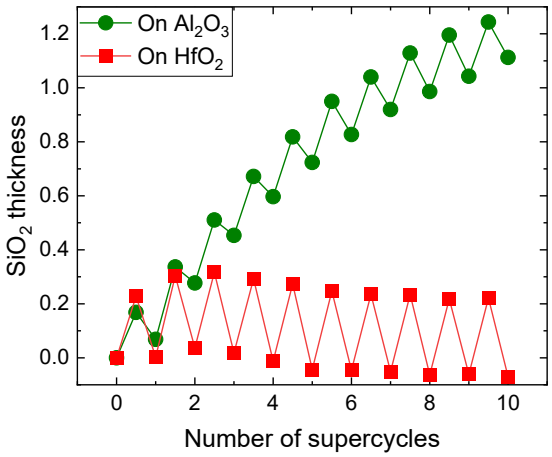

Fig. 3: SiO_2 thickness on Al_2O_3 and HfO_2 during the 10 area selective ALD supercycles, as determined by in-situ spectroscopic ellipsometry. The thickness after the two ALD cycles and the ion etch step are shown for both substrates.

References

1. R. Clark, K. Tapily, K.-H. Yu, T. Hakamata, S. Consiglio, D. O'Meara, C. Wajda, J. Smith, and G. Leusink, *Perspective: New Process Technologies Required for Future Devices and Scaling*, APL Mater **6**, 058203 (2018).
2. A. J. M. Mackus, M. J. M. Merkx, and W. M. M. Kessels, *From the Bottom-Up: Toward Area-Selective Atomic Layer Deposition with High Selectivity*, Chemistry of Materials **31**, 2 (2019).
3. S. Berg, A. M. Barklund, B. Gelin, C. Nender, and I. Katardjiev, *Atom Assisted Sputtering Yield Amplification*, Journal of Vacuum Science & Technology A: Vacuum, Surfaces, and Films **10**, 1592 (1992).
4. Seok-Jun Won, Sungin Suh, Myung Soo Huh, and Hyeong Joon Kim, *High-Quality Low-Temperature Silicon Oxide by Plasma-Enhanced Atomic Layer Deposition Using a Metal–Organic Silicon Precursor and Oxygen Radical*, IEEE Electron Device Letters **31**, 857 (2010).

* *Corresponding author e-mail:* a.a.d.jong@tue.nl

Selective ALD-Deposition of IrO_x on Platinum Neural Electrodes

Nicolai Simon [a,b,*], Thomas Stieglitz [b], Volker Bucher [a],

[a] *Institute for Microsystems Technology (iMST), Furtwangen University, Neckartal 142, Rottweil, 78628, Germany*
[b] *Laboratory for Biomedical Microtechnology, IMTEK and BrainLinks-BrainTools Center, Albert-Ludwigs-University, Freiburg i. Brsg., Georges-Köhler-Allee 201, Freiburg, 79110, Germany*

Neural interfaces are used to interact with neurons from the body for clinical purposes. These interfaces consist of a polymer sheet with embedded electrodes. The electrodes are in direct contact with the biological tissue and in case of stimulation, they convert the electrical currents into ionic currents through cell membranes. The effectiveness of this process is determined by the electrode material, which is often platinum. To lower the impedance, iridium oxide is sputtered on top of the platinum electrodes [1]. However, this process requires lithography to protect the polymer surfaces from the electrically conductive iridium oxide. This takes time and involves misalignment errors.
With the help of area-selective atomic layer deposition (AS-ALD), only the platinum electrodes are coated with iridium oxide. Here, the catalytic property of the platinum is exploited to initiate layer growth on the surface due to the atomic dissociation of oxygen [2].
In this work, a polyimide 2611 surface and platinum substrates were selectively coated using the iridium precursor (Methylcyclopentadienyl)(1,5-cyclooctadiene) iridium(I) ((MeCp)Ir(COD)) and oxygen as the co-reactant in a thermal ALD process at 225 °C with 500 cycles. In a previous study, it was shown that ALD could be performed with this precursor [3]. The Cp group of the precursor is resistant to ligand exchange and requires a high-energy metallic surface such as platinum to react. A low-energy surface such as that of the polymer does not have the necessary energy to break the aromatic ring and thus cannot initiate layer growth [4]. A nucleation delay occurs on the polymer surface resulting in selectivity.
In situ ellipsometry was performed to investigate the selectivity. Figure 1 shows the measurement results of ellipsometry. For polyimide, the two curves are coincident, indicating no growth of the layer on the surface of the polyimide. In the case of platinum, there is a shift in the curve, which indicates layer growth. In addition to the experiments, AFM images were also taken, which are shown in Fig. 2, to compare the surface topography. The roughness of the polyimide changed only slightly, whereas there was a drastic change in the surface of the platinum. Nucleation clusters were formed, which also indicate layer growth. Using ellipsometry and AFM, area-selective growth of iridium oxide films on platinum and polyimide were shown.

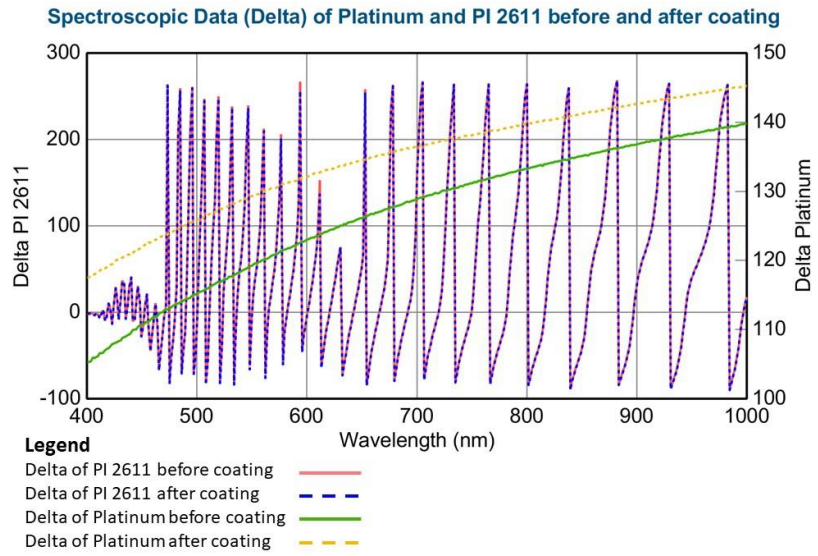

Figure 1. Spectroscopic data (delta) of the substrates before and after coating. No shift of delta is observed in polyimide 2611, while a shift of delta is clearly seen in platinum, which indicates layer growth on platinum.

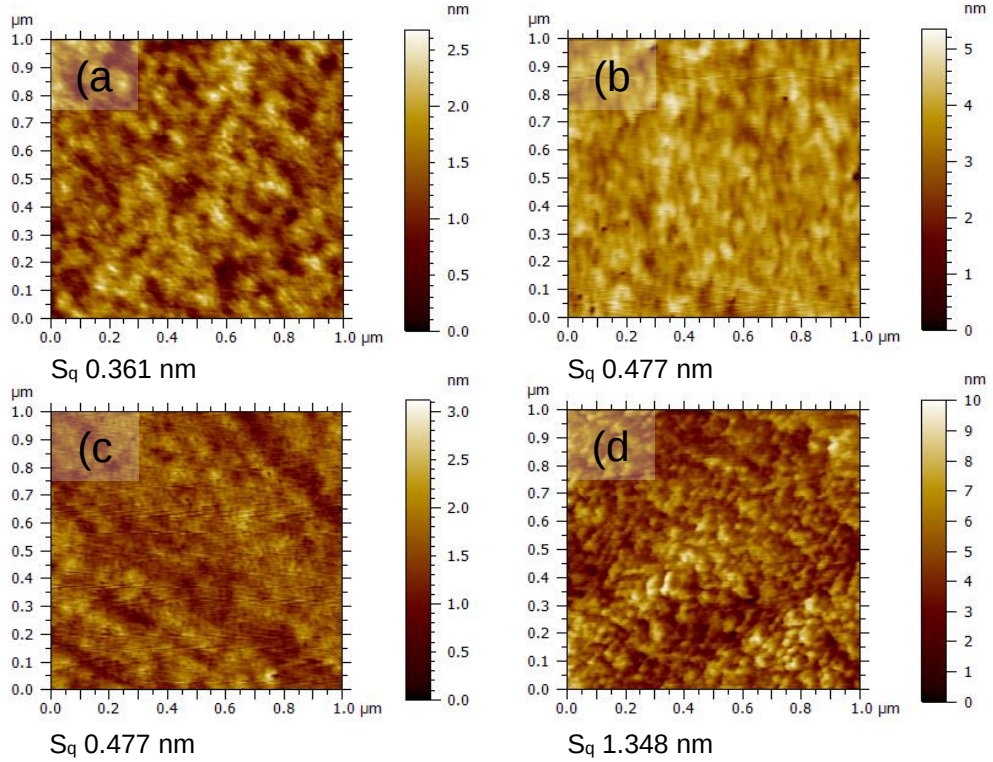

Figure 2. AFM images of substrate surface (reference and after coating) with 512 sample/lines and 1 μm^2. (a) Polyimide 2611 reference (b) Polyimide 2611 after coating (c) Platinum reference (d) Platinum after coating

References

1. S. F. Cogan, T. D. Plante, and J. Ehrlich, Conference proceedings : … Annual International Conference of the IEEE Engineering in Medicine and Biology Society. IEEE Engineering in Medicine and Biology Society. Annual Conference **2004**, 4153 (2004).
2. J. A. Singh et al., Chem. Mater. **30**, 663 (2018).
3. N. Simon, M. Asplund, T. Stieglitz, and V. Bucher, Current Directions in Biomedical Engineering **7**, 539 (2021).
4. T. Aaltonen, P. Alén, M. Ritala, and M. Leskelä, Chem. Vap. Deposition **9**, 45 (2003).

* *Corresponding author e-mail: n.simon@hs-furtwangen.de*

Functional materials III

Chair: Coclite, Anna Maria (Graz University of Technology)

Time: 6/1/2023 1:30:00 PM
Location: Auditorium 2, Maria-Theresiacollege, St. Michael's Street 6, Leuven

Self-healing of Metal Oxides enabled by Vapor Phase Infiltration

Oksana Yurkevich [a], Evgeny Modin[a], Iva Šarić [c], Robert Peter [c], Mladen Petravić [c], Mato Knez [a,b,*]

[a] *CIC nanoGUNE BRTA, Tolosa Hiribidea 76, Donostia-San Sebastián E-20018, Spain;*
[b] *IKERBASQUE, Basque Foundation for Science, Maria Diaz de Haro 3, Bilbao E-48013, Spain*
[c] *Department of Physics and Centre for Micro- and Nanosciences and Technologies University of Rijeka, Radmile Matejčić 2, 51000 Rijeka, Croatia*

Sustainability is a greatly important issue for current and future technological developments. This becomes important especially in view of consumer electronics which are essential part of our society and become more and more disposable goods. One way to minimize the waste is to extend the lifetime of devices. This can be done through self-healing approaches in case of defects in the materials. However, the vast majority of these works are devoted to the self-healing of organic materials. Implementing such functionality to the inorganic materials is highly demanded in recent times, not at least due to the rapid development in the area of flexible electronics. The few existent examples for inorganic materials rely on liquid healing agents, such as liquid metals or liquid precursors. The progress in this field remains very challenging, mainly because of a lack of feasible healing agents and suitable ways to supply them to the damaged site. In this work, we propose an approach to form self-healing metal oxides (MeO) by applying the vapor phase infiltration (VPI) method.

We used VPI as a tool to induce self-healing properties into hybrid organic-inorganic materials. This was achieved by infiltration of metal organics into the polymers which do not possess reactive oxygen-containing functional groups. Application of a typical VPI process to a functional polymeric substrate will result in the formation of dispersed metal oxide clusters and nanoparticles (NPs) inside the polymer along with an inorganic thin film of the same MeO on the surface. This hybrid polymer matrix with dispersed NPs can serve as a reservoir with healing agents for a repair of a cracked MeO film. Self-healing of inorganic materials and structures was realized also without liquid agents by making use of the mobility of inorganic NPs within polymers, as the spatial distribution of NPs can be tuned by means of harnessing both enthalpy and entropy.

After the infiltration process, samples were transferred into the microscope chamber and cut in a controllable way by a Focused Ion Beam (FIB). Usage of FIB and SEM allowed inspecting the ruptured area of the hybrid structure prior to and after its exposure to the ambient atmosphere. X-ray photoelectron spectroscopy (XPS), energy-dispersive x-ray spectroscopy (EDX), and transmission electron microscopy (TEM) were used to analyze the chemical structure and composition of the obtained hybrids. The self-healing effect after exposure of the FIB-cut sample to air was observed for zinc and indium metal oxides (Fig.1). Hereby, we introduce an alternative materials architecture and construction framework for designing inorganic materials capable to self-heal.

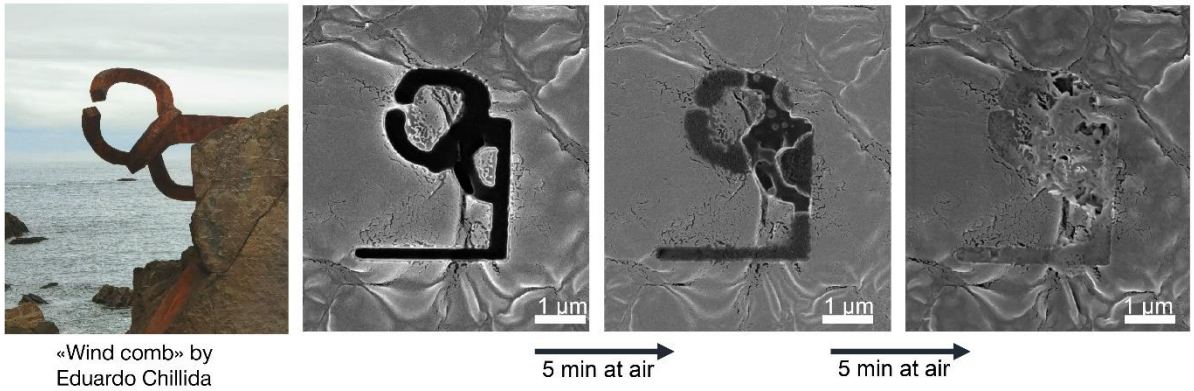

Fig. 1. Healing of selectively FIB-etched patterns on the PVC/ZnO surface over time. The left image is a photo of the sculpture “Wind comb”, created by Eduardo Chillida.

* *Corresponding author e-mail:* m.knez@nanogune.eu

Thick ZrO_2 thermal barrier coatings produced by DLI-MOCVD on plastic molds

Alexandre Jaud[a], Laura Montalban[b], Diane Samélor[a], Daniel Sadowski[a], Abderrahime Sekkat[c], Hugues Vergnes[c], Anne Catherine Brulez[d], Cédric Boschard[d], Constantin Vahlas[a], Stephane Benayoun[b], Brigitte Caussat[c*]

[a] CIRIMAT - CNRS, University of Toulouse, 4, Allée Emile Monso, BP-44362, 31030 Toulouse Cedex 4, France
[b] LTDS- CNRS, ECL, 36 avenue Guy-de-Collongues, 69134 Écully cedex, France
[c] LGC - CNRS, University of Toulouse, 4, Allée Emile Monso, BP-44362, 31030 Toulouse Cedex 4, France
[d] Institut Textile et Chimique de Lyon, 87 chemin des Mouilles, 69134 Écully cedex, France

The quality of injection molded plastic parts strongly depends on the control of heat exchange between the mold and the molten polymer [1]. The addition of a thermal barrier on the surface of the mold allows a delay in the cooling of the molten polymer, a decrease in its viscosity and thus an improved quality of the molded parts. If thermal barriers are mainly studied in the aeronautic field, works on thermal barriers for plastic molds are less frequent [2]. In this case, the barrier layer must be non-toxic, inert and stable over time with respect to the polymer and steel of the molds, while having a low thermal conductivity. Thermal barrier coatings made of ZrO_2 layers meet these requirements. The deposition process must be carried out under conditions that are compatible with the steel of the molds to be coated and it must produce coatings with 2 µm minimum thickness, even on molds with patterns (grooves, studs).

Due to the use of gaseous reactants under reduced pressure, metal organic chemical vapor deposition (MOCVD) provides conformal coatings on complex substrates . Associated with a direct liquid injection (DLI) technology, this process produces relatively high deposition rates. In the present study we first focus on crystallized and by such porous ZrO_2 coatings deposited on planar, Si and steel substrates. $Zr(O^iPr)_2(tbaoac)_2]$ was chosen as a Zr precursor since it allows deposition in the presence of O_2 at temperatures below 570°C that are compatible with the steel of the molds. This precursor has already been used successfully to deposit ZrO_2 by DLI-MOCVD [3].

The process has been developed to deposit micron thick layers in 1.5h. The reactor used is a horizontal tubular type with hot walls, with and a temperature gradient in its inlet zone, which allows to coat in a single experiment multiple Si coupons and thus to obtain many results (combinatorial approach).

Fig. 1 shows the thickness profile of the films along the reactor estimated by spectroscopic ellipsometry and checked by scanning electron microscopy (SEM). The thickness of the films strongly depends on the position of the samples, because the local deposition temperature and precursor concentration evolve along the reactor. X-ray diffraction shows that the ZrO_2 films are crystallized, mainly in monoclinic phase. It can be noticed, on the sample section observed in SEM (Fig. 1b and 1c), that they display a columnar structure and that films deposited in the isothermal zone towards the reactor outlet are thinner and more porous than those deposited near the inlet, at a lower temperature.

Based on these operating conditions, thicker films, between 0.3 and 18 µm were produced by increasing deposition time, namely to 1.5, 8.33 and 29h. SEM micrographs (Fig. 2) reveal their columnar structure.

The thermal conductivity of the ZrO_2 coatings deposited by CVD was evaluated using a custom-made device based on the experimental work by Atakan et al. [1]. It consists of two main components: a cold part including a sample holder at room temperature and a hot part including a copper insert maintained at a temperature range that spans between 80 °C and 200 °C. Heat transfer occurs when the surface of the coated sample is placed into contact with the hot copper insert. The evolution of the contact temperature as a function of the time is measured using a PT100 sensor located at the surface interface. Preliminary results indicate that the presence of a 15 µm thick ZrO_2 coating delays the heat transfer up to 6°C with respect to a reference steel sample (Fig. 3). These results are promising for the development of future thermal barrier coatings for diverse industrial applications including plastic injection molding processes.

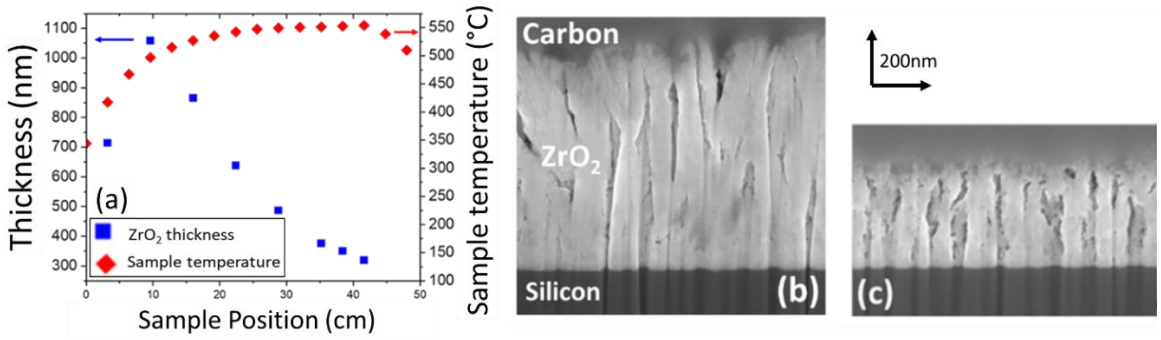

Figure 1: (a) Evolution of thickness of ZrO_2 film and samples temperature as a function of the position from the reactor inlet. (b) and (c) Focused ion beam - field emission gun SEM images of the cross-section of a ZrO_2 film deposited on Si at 16 cm from the reactor inlet (local temperature: 527°C) (b) and at 32 cm (local temperature: 550°C) (c).

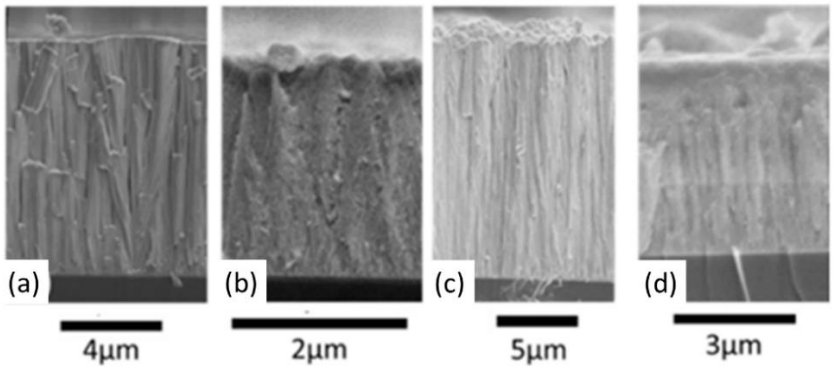

Figure 2: Cross-sectional SEM images of ZrO_2 films. (a) Deposition of 8h20 at 12 cm from the reactor inlet (local temperature: 510°C) (b) Deposition of 8h20 at 28 cm from the reactor inlet (local temperature: 546°C) (c) Deposition of 29h at 12 cm (d) Deposition of 29h at 28 cm.

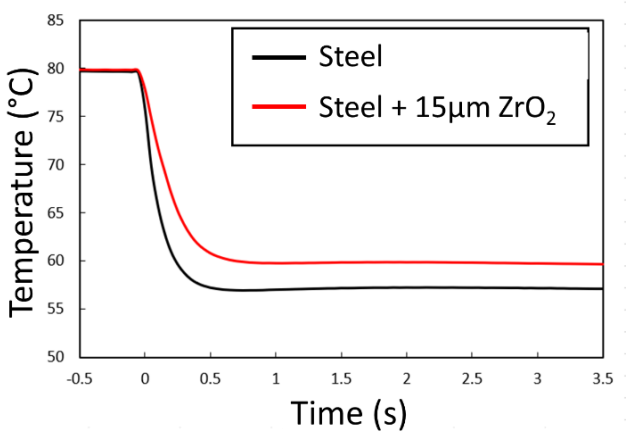

Figure 3. Comparison of the temperature at the interface of the copper insert as a function of time for a reference steel sample and a coated sample (15 µm of ZrO_2).

References

1. B. Atakan, V. Khlopyanova, S. Mausberg , F. Mumme, A. Kandzia, and C. Pflitsch, Phys. Status Solidi C **12**, **7,** 878-885 (2015).
2. V. Frettlöh, F. Mumme, G. Fornalczyk, M. Sommer, C. Beck and M. Korres, *HTM J. Heat Treatm. Mat.*, **75, 2**, 121-133 (2020).
3. S. Beer, D. Samelor, A.-A. Aal, J. Etzkorn, D. Rogalla, A. E.Turgambaeva, J. Esvan, A. Kostka, C. Vahlas and A. Devi, Journal of Materials Research and Technology, 13, 1599-1614 (2021).

* *Corresponding author e-mail: brigitte.caussat@ensiacet.fr*

Y_2O_3 and YF_3 thermal ALD for anti-corrosion coating

Sunao Kamimura[a], Takashi Teramoto [a], Takashi Ono [b], Christian Dussarrat [a*], Nicolas Blasco [b], Nicolas Gosset [a], Grigory Nikiforov [b]

[a]*Air Liquide Laboratories, Tokyo Innovation Campus, 2-2 Hikarinooka, Yokosuka, Kanagawa 239-0847, Japan*
[b]*Air Liquide Advanced Materials, 3121 Route 22 East, Branch Estates, Suite 200, Branchburg, NJ 08876, USA*

1. INTRODUCTION

Aluminum-based ceramics have been extensively used in semiconductor plasma processing equipment as plasma-facing materials. However, these materials are eroded by corrosive fluorocarbon plasmas, resulting in the production of contaminant particles on the wafer. In order to solve this problem, yttrium oxide (Y_2O_3) and yttrium fluoride (YF_3) coatings have recently attracted substantial attention due to their high resistance to erosion in plasma, especially plasma etch, avoiding the generation of fluoride particles from the chamber wall surface, thereby reducing particulate contamination [1].

Atomic layer deposition (ALD) is a thin film coating method that enables conformal dense and pinhole-free film deposition even for the complex structures like showerheads. However, the formation YF_3 thin films by ALD has been challenging since common fluorine sources such as HF are generally dangerous and corrosive, hence could lead to permanent damage to the chamber of semiconductor plasma processing equipment.

We have carried out the screening of several types of organometallic yttrium precursors for ALD, and have succeeded in depositing an ALD YF_3 film using a novel F containing yttrium organometallic precursor called Ybeta-prime in combination with O_3 as the co-reactant. These precursors are introduced sequentially, leading to a HF-free YF_3 thin film coating process. The object of this study is the investigation of YF_3 ALD and the investigation of the film dry etch resistance property using CF_4/O_2 plasma. Furthermore, Y_2O_3 thin film prepared using an ALD technique was used to compare the surface erosion behaviors with YF_3 film.

2. Experiments / Results

The YF_3 thin film deposition is performed on Si coupons using a cross-flow type reactor. The reactor pressure is controlled at 10 Torr, and the reactor temperature is varied from 225°C to 350°C. The YF_3 thin film growth was confirmed by XPS measurements, and it revealed that growth per cycle (GPC) increases as reactor temperature increases. The refractive index of deposited YF_3 thin film was constant with the deposition temperature, its value being consistent with bulk YF_3 value (1.5 @632.8 nm). Dense, uniform, conformal hydrophobic (WCA > 90 degrees) films are obtained at the range of temperature between 225°C and 300°C. SEM was used to measure step coverage of the ALD YF_3 film deposited at 275°C in a 1:6.25 aspect ratio structure. The SEM image shows excellent step coverage (top: 22 nm/bottom: 22 nm), opening interesting perspectives for industrial applications requiring high conformality. This contrasts with YF_3 films obtained through CVD processes (step coverage was less than 50 % at deposition T = 350°C). The YF_3 film sample was introduced into an inductively coupled plasma (ICP) etching tool (200 mm Alcatel MS100) together with a Al_2O_3 sample as a reference. The erosion behaviors of those coupons were analyzed under representative plasma etching conditions, using the same bias power and processing gases (CF_4 and O_2) where high density CF_4/O_2 plasma are produced (RF source power: 1300 W. RF bias power: 200 W [2]. Chamber pressure: 1.1 Pa. The CF_4/O_2 flow rates: 30:5 sccm. Etching time: up to 4 min). As shown Fig. 3, YF_3 thin film was found to be etched at least one order of magnitude slower than the Al_2O_3 .

3. Summary

We succeeded in developing a YF_3 ALD process without HF usage. Deposited YF_3 thin film shows high uniformity and conformality, and this YF_3 thin film showed strong resistance to fluorine-containing plasma, outperforming other etch-resistant materials, such as alumina. Such described YF_3 ALD films are thus promising candidates for potential applications in the field of anticorrosive coatings.

Table 1. Summary of physical and chemical properties of newly developed Yttrium precursors and ALD processes

Target Layer	Y_2O_3	YF_3
AL Molecule	Arya™	YBeta-Prime™
Melting point	Liquid	42°C
Volatility	1Torr @ 155°C	1Torr @ 119°C
ALD GPC w/O_3	0.9-1.4 A/cycle @ 300-450°C	0.6A/cycle @ 300°C
Other co-reactant tested	H_2O (positive), O_2 (positive)	n.a.
ALD window	450°C	250-300°C

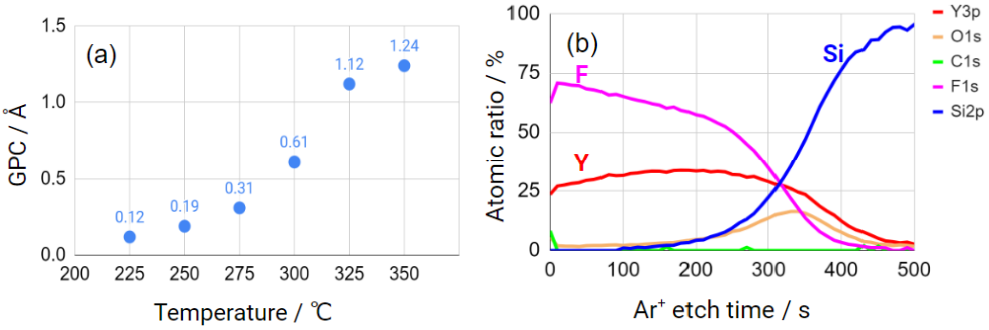

Figure 1. (a) The dependence of the GPC on the reactor temperature. The Y-beta prime precursor and O_3 co-reactant are used for this experiment. (b) XPS depth profile of deposited film (the reactor temperature was 300°C).

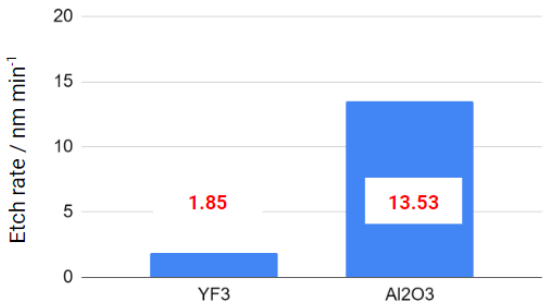

Parameter	Value
Source power [W]	1300
Bias power/voltage [W/V]	200 / ~ 160 to 180
Pressure [Pa]	1.1
CF_4 /O_2 [sccm]	30 / 5
Substrate temperature [℃]	~ 30 (not regulated)

Figure 2. Etch rates of YF_3 thin film (35 nm) and Al_2O_3 thin film (500 nm). The Al_2O_3 film was provided by Beneq. The experiment conditions are summarized in the right table.

References

1. T-K. Lin, W-K. Wang, S-Y. Huang, C-T. Tasi, and D-S Wuu, *Nanomaterials* **7**, 183 (2017)
2. C. Dussarrat, N. Blasco, W. Noh, J. Lee, J. Greer, T. Teramoto, S. Kamimura, N. Gosset and T. Ono. *Coatings* **11**, 497 (2021).

*Corresponding author e-mail: christian.dussarrat@airliquide.com

Dielectrics I

Chair: Tamm, Aile (University of Tartu)

Time: 6/1/2023 3:30:00 PM
Location: Auditorium 1, Promotion Hall, Naamsestraat 22, Leuven

Metastable nickelates by ALD - Advantages of low temperature epitaxy

Henrik H. Sønsteby[a,*], Yani L. Amedjkouh[a], Mathilde I. N. Verne[a], Ola Nilsen[a]

[a] *University of Oslo, Department of Chemistry, Postbokds 1033, Blindern, NO-0315, Oslo, Norway*

Rare-earth nickelates (*RE*NiO_3, *RE* = trivalent rare-earth cation) is a group of perovskite oxides that have received a surge of interest over the last decade or so. This is mostly due to the existence of a sharp metal-to-insulator transition (MIT) that is correlated to the Ni-O-Ni bond angle, which varies with the size of the rare-earth cation. The Ni-O-Ni bond angle determines the O_{2p} – Ni_{3d} orbital overlap, with bands widening when the angle is large (*i.e.* large orbital overlap).[1,2] Materials that possess sharp electronic functional transitions that can be controlled are highly sought after in creating future generations of devices.

One issue with the rare-earth nickelates is that they are notoriously difficult to prepare. Ni^{3+} is rarely stable, and the perovskite phase is often in competition with binary oxides and more stable Ruddlesden-Popper (RP) phases.

Some of the lighter rare-earth nickelates, particularly $LaNiO_3$, $NdNiO_3$ and $SmNiO_3$ have been prepared with success both as bulk crystals and as films. The heavier, albeit just as interesting compounds, such as $EuNiO_3$, $GdNiO_3$ and $TbNiO_3$ have proven much more difficult to prepare. This is likely partially due to the decreased stability of the perovskite compared to competing phases, and due to the increased difficulty of stabilizing Ni^{3+} in these structures. Keep in mind that most rare-earth nickelates have been prepared by high temperature techniques.

We have recently prepared $LaNiO_3$, $NdNiO_3$ and $SmNiO_3$ by atomic layer deposition (ALD), observing direct epitaxy at low temperatures.[3] The back-end-of-line (BEOL) compatible conditions that these films were prepared in, has opened the door for implementation in electronic devices. But there is another, and more fundamental possibility that has presented itself: Preparation of metastable nickelates that are stabilized by a combination of cation composition control, low temperature of deposition and strain engineering. This allows the exploration of exotic nickelates, that are very difficult to prepare and study by conventional techniques.

In this talk, I will show how low-temperature epitaxy by ALD has been used to deposit high-quality films of $EuNiO_3$ and $GdNiO_3$, and cation substituted variants thereof. $EuNiO_3$ is interesting due to the extreme response in electronic resistivity as a function of strain. Highly strained films are impossible to reach at higher temperatures; the films immediately relax. We show how $EuNiO_3$ is an insulator on $SrTiO_3$ substrates, but a good metal on $YAlO_3$. $GdNiO_3$ is another interesting nickelate with an MIT of around 200 °C. It is however, notoriously hard to prepare due to the much higher stability of Gd_2O_3 and NiO. We show how $GdNiO_3$ can be prepared using low-temperature epitaxy by ALD, and also how it decomposes upon annealing, confirming the low stability at higher temperatures.

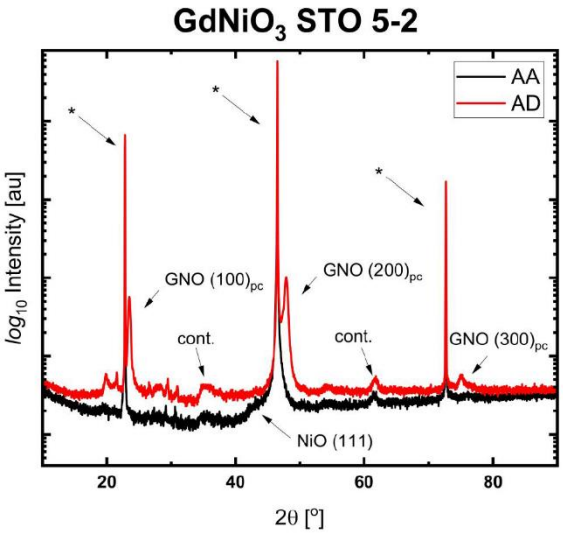

This line of thought is not only interesting for rare-earth nickelates, but for all classes of complex oxides that are either hard to prepare or cannot be prepared at higher temperatures. Low-temperature epitaxy by ALD opens for highly conformal, uniform and high-quality films of such compounds, with the added bonus of being BEOL compatible.

References

1. S. Catalano *et al.*, Rep. Prog. Phys. **81**, 046501, (2018).
2. J. Varignon *et al.*, npj Quant. Mater. **2**, 21, (2017)
3. H. H. Sønsteby *et al.*, Nat. Mater. **11**, 2872 (2020)

* *Corresponding author e-mail:* henrik.sonsteby@kjemi.uio.no

Effects of Interlayer Formation by Oxidants and Substrates on Properties of ALD ZrO_2 Thin Film

Seonyeong Park[a], Seunggyu Na[a], Yujin Lee[a, b], Seung-min Chung[a], Hyungjun Kim[a,*]

[a]*School of Electrical and Electronic Engineering, Yonsei University, Seodaemun-Gu, Seoul 03722, Korea*
[b]*Department of Chemical Engineering, Stanford University, Stanford, California 94305, United States*

In the early stage of dynamic random access-memory (DRAM) development, the thickness of the dielectric SiO_2 has been reduced in the Si based two-dimensional structure to obtain high integration density and capacitance. However, as the DRAM devices have been continuously scaled down, thickness of SiO_2 reached a fatal limit of reaching the physical thickness at which leakage current due to tunnelling effect occurs. To break through this, SiO_2 was replaced by high dielectric constant(*k*) materials [1]. Among the various high-*k* materials, ZrO_2 is one of the promising materials since it has good thermal stability, high dielectric constant (*k*~30) and wide bandgap (5.16-7.8 eV) [2,3]. However, when the film is deposited with oxygen plasma (O_2 plasma) to obtain high-density and high-*k* film, the leakage current density may be increased due to the interlayer formed between high-k dielectric film and substrate because of the plasma energy. Since the interlayer is formed due to the oxidation of the electrode during the film deposition process, which is affected by the potential barrier height of the oxidation reaction [4], proper selection of the electrode is also required. Currently used TiN deteriorates the electrical properties such as increased leakage current density due to the interlayer formed between high-*k* film and TiN [5,6]. Recently, noble metals such as Pt, Au, Ag, etc., reported as ideal substrate to reduce the interlayer formation [4], are difficult to easily apply to real industry because of its high price.

In this study, we conducted research on lowering the leakage current density at the same time as increasing the *k*-value. To do that, we compared two oxidants (O_2 plasma and hydroperoxide) and two substrates (Ru and TiN). Hydroperoxide (H_2O_2) was selected as a comparison with O_2 plasma since the oxidizing power of H_2O_2 is stronger than that of water and smaller than that of O_2 plasma. Ru was select as a comparison with TiN because it has good thermal stability, low resistance, high work function, and relatively inexpensive among noble metals [7].

For ultrathin high quality ZrO_2, atomic layer deposition (ALD) has been used, which can secure atomic layer controlled ZrO_2 film with high conformality and high uniformity. Several physical properties of ZrO_2 thin film were examined such as chemical composition, crystallinity, and film density. As seen in Fig. 1(left), it was confirmed that a large difference in crystallinity appeared depending on oxidants. These crystallinity difference also affects the *k*-value (Fig. 1(right)). ZrO_2 thin film using O_2 plasma as oxidant showed much higher *k*-value than using H_2O_2 as oxidant. The reason why the *k*-value varies depending on the substrate can be explained through Fig. 2. Although ZrO_2 thin film using O_2 plasma showed higher crystallinity, it has a rather low *k*-value because it has a thick interlayer on TiN. However, since a negligible interlayer was formed on the Ru substrate, it was considered to have a high *k*-value.

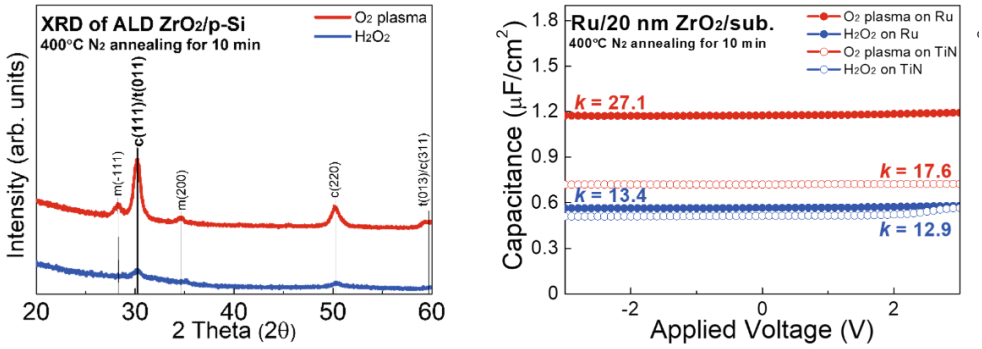

Figure 1. (left) crystallinity results according to oxidants using XRD analysis, (right) capacitance according to oxidants and substrates.

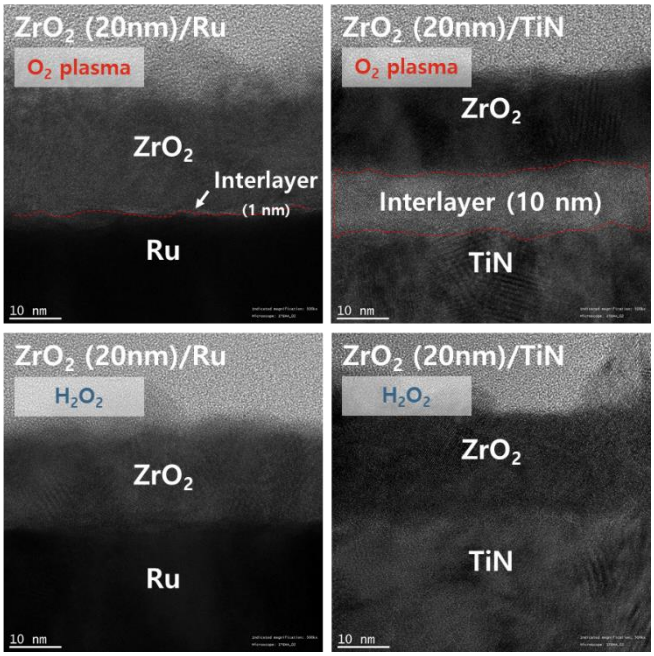

Figure 2. Cross-section TEM image of ALD ZrO_2 films; (top 2 images) using O_2 plasma as an oxidant, (bottom 2 images) using H_2O_2 as an oxidant, (left 2 images) on Ru substrate, and (right 2 images) on TiN substrate.

References

1. Y. Xia, J. A. Rogers, K. E. Paul, and G. M. Whitesides, Unconventional Methods for Fabricating and Patterning Nanostructures, Chem. Rev. 99(7) 1823 (1999).
2. R. M. Wallace, and G. D. Wilk, High-k Dielectric Materials for Microelectronics, Crit. Rev. Solid State Mater. Sci. 28, 231 (2003).
3. J. Robertson, High dielectric constant gate oxides for metal oxide Si transistors, Rep. Prog. Phys. 69, 327 (2006).
4. W. G. Kim and S. W. Rhee Effect of the top electrode material on the resistive switching of TiO_2 thin film, Microelectron. Eng. 87, 98 (2010).
5. C. Jorel, C. Vallée, E. Gourvest, B. Pelissier, M. Kahn, M. Bonvalot, and P. Gonon, Physicochemical and electrical characterizations of atomic layer deposition grown HfO_2 on TiN and Pt for metal-insulator-metal application, J. Vac. Sci. Technol. B 27, 378 (2009).
6. M. Pešić, S. Knebel, K. Cho, C. Jung, J. Chang, H. Lim, N. Kolomiiets, V. V. Afanas'ev, T. Mikolajick, and U. Schroeder, Conduction barrier offset engineering for DRAM capacitor scaling, Solid State Electron 115, 133 (2016).
7. S. J. Park, W. H. Kim, H. B. R. Lee, W. J. Maeng, and H. Kim, Thermal and plasma enhanced atomic layer deposition ruthenium and electrical characterization as a metal electrode, Microelectron. Eng. 85, 39 (2008).

* *Corresponding author e-mail: hyungjun@yonsei.ac.kr*

HfZrO-based structures by ALD for embedded ferroelectric non-volatile memories

Amanda Mallmann Tonelli[a*], Julien Mercier[a], Léonard François[a], Nicolas Gauthier[a], Laurent Grenouillet[a], Vincent Jousseaume[a], Messaoud Bedjaoui[a]

[a]*Univ. Grenoble Alpes, CEA, Leti, F-38000 Grenoble, France*

Ferroelectric HfO_2-based materials have been intensively studied since 2011, thanks to their excellent CMOS compatibility and potential for scalability [1]. Recently, TiN/$Hf_{0.5}Zr_{0.5}O_2$/TiN ferroelectric capacitors were successfully integrated in the Back-End-Of-Line (BEOL) of 130 nm CMOS technology [1]. $Hf_{0.5}Zr_{0.5}O_2$ (HfZrO) has shown robust ferroelectricity, high dielectric constant and low-temperature preparation, which is a crucial aspect for its integration into the semiconductor-based industry and a promising material for the non-volatile memories [1]. Since atomic layer deposition (ALD) processes are extremely conformal, ALD is the recommended approach in the production of 3D ferroelectric random access memory.

Among the methods for depositing thin films, ALD is unique for its capability of growing conformal thin films of compounds with a control of composition and thickness at the atomic level [2]. This technique enables the development of complex systems such as nanolaminates, periodic stacking of bilayer structures to form thicker multilayers. In particular, the deposition of nanolaminates for microelectronics applications demonstrated that such structures acquire particular physical properties, such as enhanced dielectric constant [2].

The aim of this study is to develop ultrathin ferroelectric layers by ALD for MFM (Metal Ferroelectric Metal) capacitors for non-volatile memories. Within this work, two different types of structures were developed and investigated: 10 nm thick HfZrO, made through supercycles of alternating layers of HfO_2 and ZrO_2, and 10 nm thick HfO_2/ZrO_2 nanolaminates consisting of stacked 2 nm thin HfO_2 and 2 nm thin ZrO_2. At first, the objective of this project is to investigate the intrinsic characteristics of the material in the two different structures through the study of its morphology. For this, X-ray reflectometry (XRR) analysis was performed to estimate thickness, density and roughness; grazing incidence and in-plane X-ray diffraction (XRD) were carried out on the different films to analyze crystallinity; time-of-flight secondary ion mass spectrometry (ToF-SIMS) was made to extract information about the composition of the layers. In addition, a mercury contact probe analysis was performed to provide an estimation of the dielectric constant of the obtained material. After annealing, through electrical positive-up-negative-down (PUND) measurement, it was possible to obtain evidence of ferroelectricity. The project perspective will be to analyze the material evolution at each stage of the MFM stacked structure on 300 mm Si substrates and relate to the electrical results.

The experimental analysis of the as-deposited films allowed some preliminary conclusions. The XRD results presented in (Fig. 1) reveal that the films are nanocrystalline, as expected for these materials in the absence of annealing. The diffraction peaks around 30.5° and 35.3° stand for a mixture of tetragonal and orthorhombic phase and could be evidence of the beginning of crystallization of a ferroelectric material. ToF-SIMS data in (Fig. 2) allows the observation of the stacking of different interfaces through consistent Hf/Zr profiles. Finally, the analysis with the mercury probe at 10 kHz indicated the C-V dispersion characteristics showed in (Fig. 3), from which it was possible to extract a dielectric constant of 13.6 and 12.3, for the as-deposited film of 10 nm HfZrO and 10 nm HfO_2/ZrO_2 multilayers stack respectively. The reported results are different from the monoclinic HfO_2 phase, stable at room temperature, which has a dielectric constant (k) of ~20 to 25, and from the monoclinic ZrO_2 phase, in which k is ~25 to 30 [3].

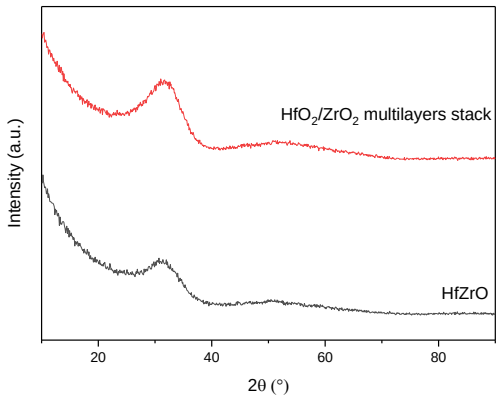

Figure 1. In plane XRD of the as-deposited 10 nm HfZrO and 10 nm HfO_2/ZrO_2 multilayers stack.

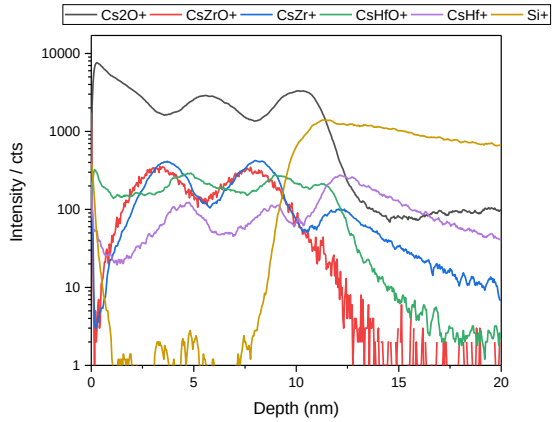

Figure 2. Frontside ToF-SIMS depth profiles of the as-deposited 10 nm HfO_2/ZrO_2 multilayers stack.

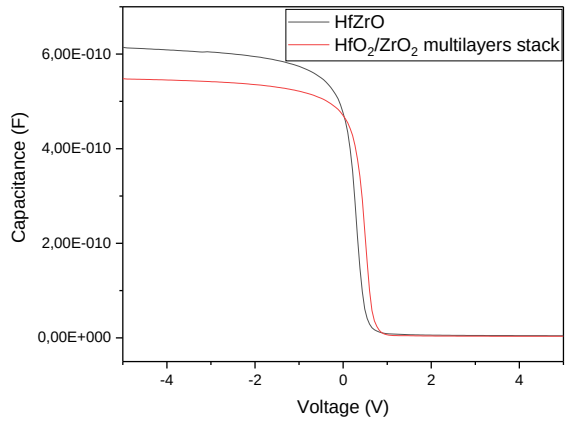

Figure 3. C-V characteristics obtained of the as-deposited films.

References

1. T. François *et al.*, « Demonstration of BEOL-compatible ferroelectric Hf0.5Zr0.5O2 scaled FeRAM co-integrated with 130nm CMOS for embedded NVM applications », présenté à 2019 IEEE International Electron Devices Meeting (IEDM), San Francisco, CA, USA, déc. 2019. doi: 10.1109/IEDM19573.2019.8993485.
2. M. Tallarida, M. Weisheit, K. Kolanek, M. Michling, H. J. Engelmann, et D. Schmeisser, « Atomic layer deposition of nanolaminate oxide films on Si », *Journal of Nanoparticle Research*, p. 5975–5983, 17 mars 2011.
3. L. Lamagna *et al.*, « Thermally induced permittivity enhancement in La-doped ZrO2 grown by atomic layer deposition on Ge(100) », *Applied Physics Letters*, p. 122902, 23 septembre 2009.

* *Corresponding author e-mail: amanda.mallmanntonelli@cea.fr*

Evaluation of ALD Films of Y_2O_3, Al_2O_3 and Their Combinations for Hydrogen Permeation Barrier Applications

Alexandru C. Pavel[a*], Harold Dekkers[a], Pierre Morin[a], Johan Swerts[a], Alexis Franquet[a], Valentina Spampinato[a], Johan Meersschaut[t]

[a] *Imec, Kapeldreef 75, Leuven 3001, Belgium*

Films of Yttrium Oxide, Aluminium Oxide and various combinations of the two had been deposited on a 10 nm thermally grown SiO_2 substrate in a thermal crossflow ALD reactor. The depositions were done using 300 mm Si wafers at reactor temperatures between 290 and 320 degrees Celsius. Aluminium Oxide was considered in this study as a baseline reference, and as a source of crystalline order scattering that prevented the crystallization of Yttrium Oxide in its thermodynamically stable cubic bixbyite type. The depositions used tris-Ethyl Cyclopentadienyl Yttrium (III) (TECY) and Trimethyl Aluminium (TMA) for the metal precursors, and deionized Water and Ozone for the oxidizers of the metal precursors. The Ozone generator used a high intake of Nitrogen flow (10% v/v) during the generation of Ozone from the Oxygen source. The films had a thickness ranging from 30 nm to 75 nm, and in a subsequent step, a few selected depositions underwent Oxygen anneal treatment for 60 minutes at 500 Celsius degrees. The formulations developed with Ozone had a higher content in Carbon and Hydrogen contaminants, than their deionized Water counterparts.

The combinations of the two metal oxides were delivered in the form of nanolaminates (Fig. 1) and co-deposited films. The nanolaminate formulations varied in the Yttrium (III) to Aluminium (III) molar ratio, and the structure of their respective super cycles. The classic type of nanolaminates used 5 to 10, 10 to 10 and 10 to 5 cycles of TECY and TMA, respectively. The other type of nanolaminate explored was of the compositionally graded structure, which was designed with a dual, simultaneous, and opposite in direction step size gradients of 10% and 20% over a predefined set of composition ranges. The compositionally graded nanolaminate was further developed for targeting the maximal degree of intermixing of the two metal oxide components.

All films were subjected to a Deuterium anneal for 5 minutes at 400 degrees Celsius, using a flow of 10 slm 5% (v/v) D_2 in N_2. In a different set of experiments, wafer coupons of the same films were subjected to an identical anneal treatment, but using H_2 instead of D_2. The Deuterium exposed films were then analysed using ToF-SIMS for the determination of the penetration depth profile. The Hydrogen exposed films were subjected to ERD analysis for the quantification of the Hydrogen content. All films showed complete penetration of the Deuterium species. The compositionally graded nanolaminates that had a higher content in Yttrium Oxide by recipe structure, showed periodic modulation of the Deuterium intake, with a parallel evolution of the two signals (Y and D, see Fig.2). Also, the bicomponent films of the nanolaminate and co-deposition types made with Ozone and subsequently annealed in Oxygen, showed lesser uptake of the Deuterium species when compared to the Aluminium Oxide films.

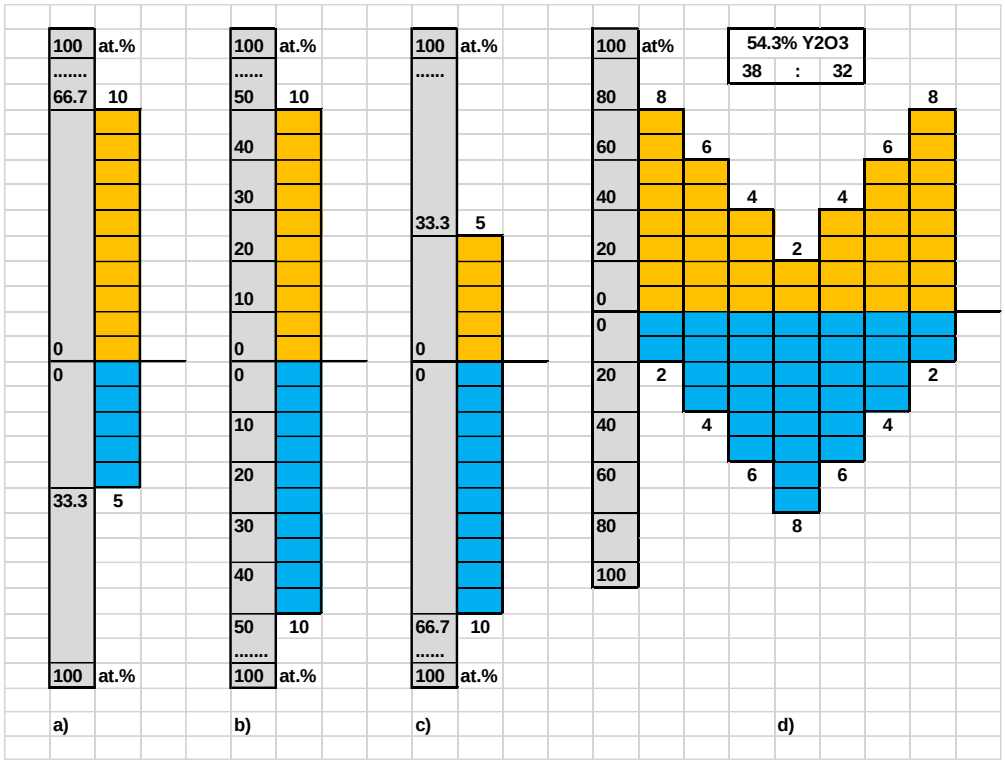

Figure 1. Schematic of super cycle for some nanolaminate structures (Y_2O_3 in yellow and Al_2O_3 in blue): a) 10x to 5x; b) 10x to 10x; c) 5x to 10x; d) compositionally graded with a step size of 20%.

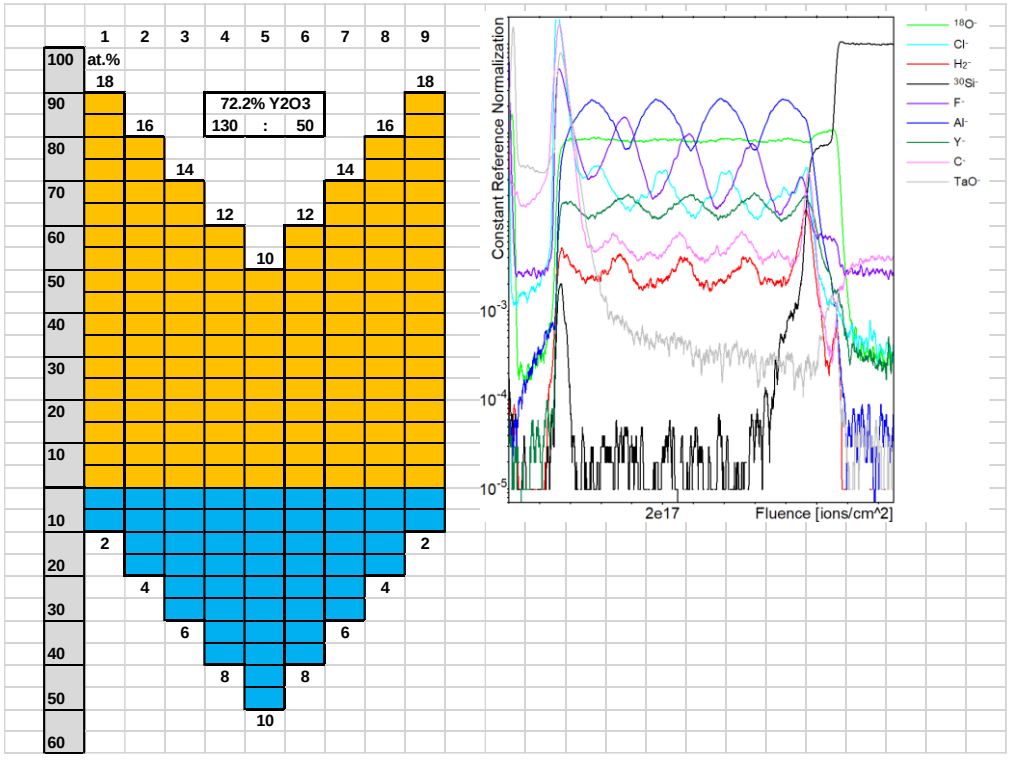

Figure 2. ToF-SIMS profiles of the chemical species present in the analysed sample of a compositionally graded nanolaminate with a step size of 10%.

*Corresponding author e-mail: alexandru.pavel@imec.be

Poster session II

Time: 6/1/2023 5:00:00 PM
Location: Jubilee Hall, Naamsestraat 22, Leuven

SMI layer decomposition - a theoretical investigation on the deposition of Al_2O_3

Patrick Maue[a]*, Ralf Tonner-Zech[a]

[a]*Leipzig University, Linnéstraße 2, Leipzig, 04103, Germany*

Small molecule inhibitors (SMIs) are an alternative to Self-assembled monolayers (SAMs) for the inhibition of non-growth surfaces in area-selective ALD and currently gaining interest for certain applications. [1] Their advantage is that they can be applied via the gas phase and might be sterically less demanding than SAMs what opens the possibility to develop new processes of AS-ALD. However, like other inhibitor approaches, especially SMIs suffer from the loss of selectivity after a certain number of ALD-cycles. [2] Interaction with precursor compounds and the following chemical decomposition of the SMI layer can be the reason for such a loss in selectivity (Fig. 1). [2,3] The mechanisms of such SMI-layer decomposition are not yet fully understood and further research is necessary to get insight into the chemistry behind those processes. [2] Here, theoretical approaches like DFT simulations for molecules and surfaces can be a helpful tool to investigate the decomposition of the blocking layer as it is difficult to gain insight into the relevant processes on a molecular level, experimentally. In this study the SMI-coverage of a SiO_2-surface and its interaction with aluminum precursors and water were investigated. For this the reaction of inhibitor molecules with Al-precursors and water were investigated by simulations in gas phase and on the surface. The energetics of SMI adsorption and the physisorption of precursors were also calculated. Apart from the precursor-SMI interaction the influence of dimerization for different Al-precursors was considered and thermochemical data for the dimerization calculated.

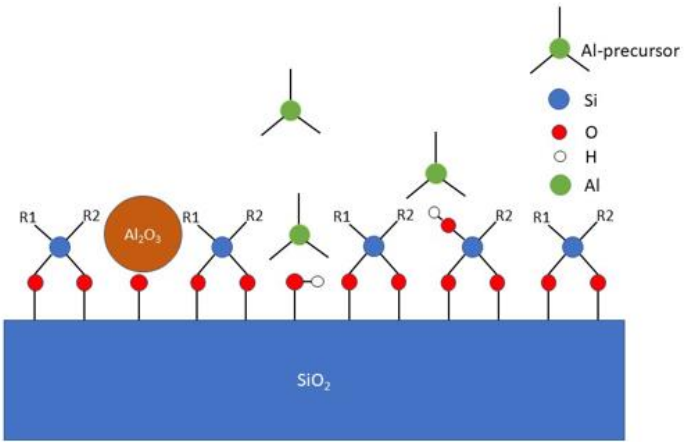

Figure 1: Schematic illustration of the SMI blocking layer on SiO_2 and its defects. Free surface hydroxyl groups or reactive functionalities on SMIs resulting from decomposition reactions can initiate growth of ALD material (Al_2O_3).

References

1. Merkx, Marc JM, et al. "Insight into the removal and reapplication of small inhibitor molecules during area-selective atomic layer deposition of SiO_2." *Journal of Vacuum Science & Technology A: Vacuum, Surfaces, and Films* 39.1 (2021): 012402.
2. Yarbrough, Josiah, Alex B. Shearer, and Stacey F. Bent. "Next generation nanopatterning using small molecule inhibitors for area-selective atomic layer deposition." *Journal of Vacuum Science & Technology A: Vacuum, Surfaces, and Films* 39.2 (2021): 021002.
3. J. Yarbrough, F. Pieck, D. Grigjanis, Il-Kwon Oh, P. Maue, R. Tonner-Zech, and St. F. Bent *Chem. Mater.* 2022, 34, 10, 4646–4659

* *Corresponding author e-mail:* patrick.maue@uni-leipzig.de

Area-selective ALD/MLD of noble metals and polyimide through surface-dependent film nucleation and growth

C. Zhang*, M. Leskelä and M. Ritala*

Department of Chemistry, University of Helsinki, Helsinki, Uusimaa 00014, Finland

In semiconductor industry, there is an urgent need to develop self-aligned thin film patterning processes to keep up with the pace of device scaling set by Moore's law. Conventional photolithography is facing unprecedented challenges in terms of more severe edge placement error (EPE) and the rocketing manufacturing cost. Area selective atomic layer deposition (AS-ALD) is a self-aligned thin film deposition and patterning process that has the capability to realize thin film patterning cost-effectively yet without concern of EPE issues. In this work, AS-ALD of noble metals and area-selective molecular layer deposition (AS-MLD) of polyimide was achieved through surface-dependent film growth. The surface-dependent growth was found in the polyimide process using PMDA and DAH as precursors [1] and the noble metal processes using metal β-diketonates, i.e., $Ir(acac)_3$, $Ru(thd)_3$, and $Rh(acac)_3$, as precursors with either O_2 or air as a coreactant [2]. A range of technically relevant substrate surfaces from conductive metals (Cu, Co, Ru) to dielectrics (SiO_2, Al_2O_3, ZrO_2, HfO_2, SiOC) were studied. These surfaces are different from each other in terms of surface termination, catalytic activity, and Lewis acidity. These intrinsic chemical differences were found to be efficient in controlling the film nucleation and growth, and were therefore utilized to achieve the desired selective deposition. The film nucleation and growth were investigated on growth- and nongrowth-surfaces with various characterization methods, including SEM, EDS, XPS, ellipsometry, TEM, etc. The selectivity was successfully demonstrated on nanometer-scale patterns at optimized deposition conditions (Fig. 1). Furthermore, an insight into the selectivity mechanism was obtained based on our experimental observations and literature knowledge.

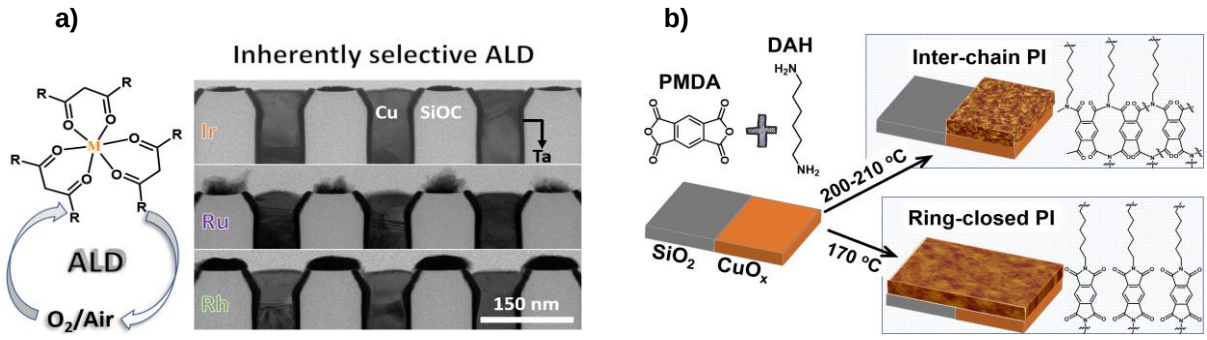

Figure 1. Area-selective ALD of noble metals on Cu/SiOC patterns and the schematic drawing showing AS-MLD of polyimide on Cu versus native SiO_2.

References

1. C. Zhang, M. Vehkamäki, M. Pietikäinen, M. Leskelä, M. Ritala, Chem. Mater. **32**, 5073 (2020).
2. C. Zhang, *E, Tois,* M. Leskelä, M. Ritala, Chem. Mater. **34**, 8379 (2022).

* *Corresponding author e-mail:* chao.zhang@helsinki.fi; mikko.ritala@helsinki.fi

Correlating In-Situ Photoluminescence and Ellipsometry: A Novel approach to Analyze ALD Materials for Photovoltaic Applications

Nao HARADA[a], Alexandra LEVTCHENKO[a], Damien COUTANCIER[b], Frederique DONSANTI[a], Julie GOFFARD[a], Corentin DOMENEGHETTY[a], Jean-François GUILLEMOLES[b], Daniel SUCHET[b], Géraud DELPORT[b], Nathanaelle SCHNEIDER[b,*]

[a] *IPVF, Institut Photovoltaïque d'Île de France, 18 Boulevard Thomas Gobert, 91120 Palaiseau, France*
[b] *IPVF, UMR 9006, CNRS, IPVF SAS, Ecole Polytechnique, PSL U., 18 Bld Th. Gobert, 91120 Palaiseau, France*

For the last decades, Atomic Layer Deposition (ALD) has undoubtedly become a key technique to deposit thin films in various research fields. As the deposition is sequential and self-limited, a high control over the films' thickness can be reached together with a high conformality. Moreover, the deposition can be done at low temperatures (below 100 °C) and allows the growth of a large panel of materials on different substrates. In the field of PV, ALD films are already used at an industrial scale (for instance in PERC solar cells) but their use also extends to buffer layers for CIGS cells, transparent conductive oxides (TCO), passivation or charge transport layers (ETL & HTL) for perovskite solar cells … [1]

In-situ ellipsometry together with photoluminescence (PL) were considered as relevant techniques to correlate film's growth properties and its functionalization. Indeed, by acquiring Spectroscopic Ellipsometry (SE) data, the film's thickness and optical constants are addressed during the growth [2], while its function is determined by analysing PL spectra or PL decays (by Time Resolved Photoluminescence TRPL) [3]. While in-situ SE is commonly used during ALD growth, only one example of in-situ PL has been developed to our knowledge and none combines the two techniques [4], making our approach original. In-situ characterizations would also be very useful for pre-industrialization, by reducing the number of samples required to totally take advantages of ALD specificities and generate highly performant devices. This presentation will introduce our experimental set-up in more details, as well as some first analysis results on the growth of ALD thin films on halide perovskite solar cells correlating SE and PL measurements (Fig. 1).

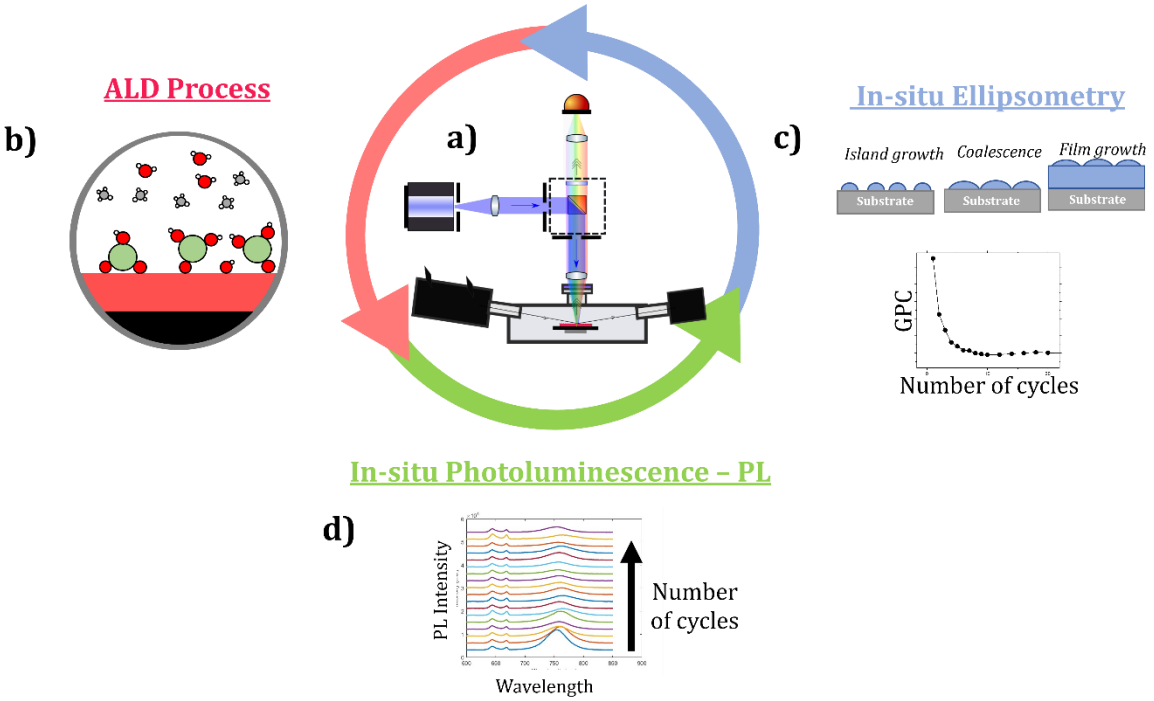

Fig. 1 a) Experimental set-up with in-situ PL and ellipsometry in an ALD reactor b) ALD growth c) In situ ellipsometry - Thickness, optical constants, and growth mechanisms d) In situ PL – Functionalization properties (passivation, carrier behaviour)

References

1. "Atomic Layer Deposition (ALD). Principes Généraux, matériaux et applications" *Ouvrage spécial des Techniques de l'Ingénieur : Principes et applications de la technique ALD (Atomic Layer Deposition)*
2. Langereis, E. *et al. J. Phys. Appl. Phys.* **42**, 073001 (2009).
3. Unold, T. & Gütay, L. in *Advanced Characterization Techniques for Thin Film Solar Cells* -275–297.
4. Kuhs, J. *et al. ACS Appl. Mater. Interfaces* **11**, 26277–26287 (2019).

* *Corresponding author e-mail:* nathanaelle.schneider@cnrs.fr

Electronic structure, optical and electrical properties of APCVD SnO_2 films. Influence of thermal cycling.

Christos Petaroudis[a,b], Ioannis Kostis[b], Petros-Panagis Filippatos[a,c], Alexander Chroneos[c], Anastasia Soultati[a], Maria Vasilopoulou[a] and Dimitris Davazoglou[a]*

[a] *NCSR "Demokritos", Institute of Nanoscience and Nanotechnology, POB 60228, 15310 Agia Paraskevi, Greece*
[b] *University of West Attica, Dpt. of Electrical Engineering 250, Thivon Av., Aegaleo 122 44, Greece.*
[c] *Department of Electrical and Computer Engineering, University of Thessaly, Volos, 38333, Greece*

Tin oxide (SnO_2) films were chemically vapor deposited at atmospheric pressure (APCVD) and temperatures between 380 and 420 ^oC on oxidized silicon substrates, using $SnCl_4$ vapors as metallic precursor and water or methanol vapors as oxidizers. As seen in Fig. 1, films deposited using methanol as oxidizer exhibit significantly enhanced grain size relatively to those with water.
Electrical and optical properties of films were studied using simultaneously spectroscopic ellipsometry (SE) and electrical resistivity (current-voltage, I-V) measurements in air and at temperatures up to 400 ^oC. The optical measurements were analyzed using the T-L and the Drude physical models and in this way, except of the optical constants also information related to details of the electronic structure of these films were obtained, which were correlated to their electrical properties.
Within the Tauc-Lorentz (T-L) model the imaginary part of the dielectric constant, ε_2, is given as a function of photon energy, E, by [1]:

$$\varepsilon_2(E) = \frac{1}{E}\frac{AE_nC(E_{gTL}-E)^2}{\left[(E_n^2-E^2)^2+C^2E^2\right]}$$ for $E>E_{gTL}$ and $\varepsilon_2(E)=0$ for $E<E_{gTL}$

The real part of the dielectric constant is calculated by Kramers-Kronig analysis integrating ε_2 within all energies [1]. The physical meaning of parameters, A, E_n, E_{gTL} and C is shown in Fig. 2 where E_{gT} represents the Tauc gap obtained by extrapolating the linear part of the quantity $(\alpha.E)^{1/2}$ to E=0 (α is the absorption coefficient). Thus the difference E_{gTL}-E_{gT} gives a measure of the localized electronic states within the gap, which is related to the number of oxygen vacancies. The Drude model foresees a variation of ε_2 of [1]: $\varepsilon_2 = \frac{\omega_p^2}{\omega}\frac{\gamma}{\omega^2+\gamma^2}$ where ω is the frequency (proportional to the photon energy, $E=\hbar\omega$, $\hbar$ is the reduced Plank constant), γ the broadening which simulates the friction during oscillation $\omega_p^2 = \frac{N e^2}{m^*\varepsilon_0}$ is the plasma frequency related to the number of free electrons N, and their effective mass m* (e and ε_0 are the electron charge and the vacuum dielectric constant respectively).
The optical modelling turned out to reproduce very accurately the SE quantities (psi and delta) and therefore the dispersion of the refractive index (n*=n-ik, real and imaginary part) of SnO_2 films at various temperatures was obtained. In Fig. 3 n and k dispersions are reported and the corresponding calculated transmission spectra for films deposited on glass substrates.
The density of electronic states near the gap is shown in Fig. 2 and was related to the optical and electrical properties of SnO_2 films. Thus, it was found that the average energy of optical transitions En and the broadening C, related to the average energy distance between VB and CB and to the width of the CB respectively, are the crucial parameters that influence the light absorption within the visible range of SnO_2 films. Thus highly transparent large-grained SnO_2 samples exhibit large values of En and C. The parameters that influence mostly the surface conduction are the broadening C and the amplitude factor A, related to the extent of the overlapping of wave-functions. Small values of these parameters, observed for small-grained SnO_2 samples, indicate the strong localization of wave-functions in the CB and high effective mass of electrons therein, which lead to a linear-quadratic shape of the I-V curve shown in Fig. 4(a) contrary to large-grained films where linear I-V curves were obtained (Fig. 4(b)). The extent of gap states (expressed by the difference E_{gT}-E_{gTL}) decrease fast with heating in air and caused shifts of ω_p the magnitude and the direction of which also depend on the effective mass of carriers, i.e., on the values of A and C [2, 3].

Fig. 1. SEM images taken on two APCVD SnO2 samples grown at 390 °C using water (left) and methanol (right) as oxidizing agents. Larger grains are can be observed on the latter sample.

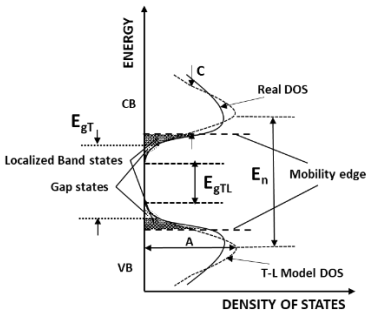

Fig. 2. Schematic representation (not in scale) of the actual DOS (solid line) and of that of the T-L model (dashed line).

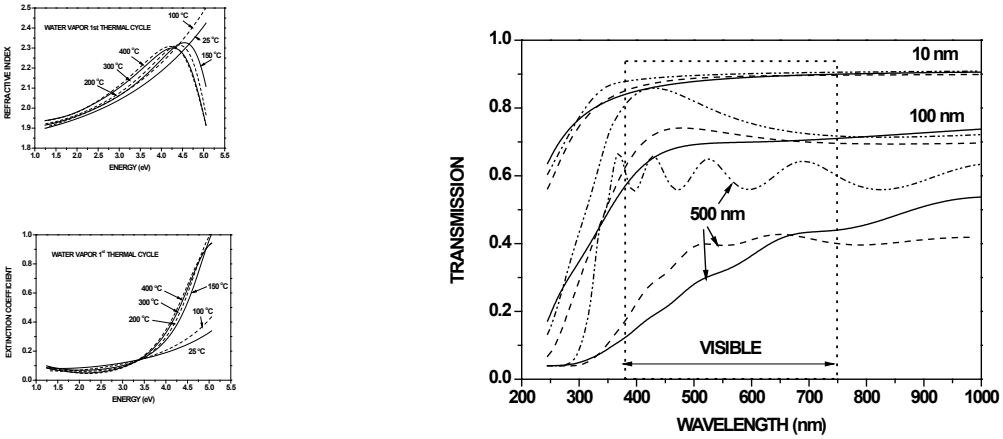

Fig. 3. Left, dispersions of the real (upper) and of the imaginary (lower) parts of refractive index of an APCVD SnO2 sample grown using water vapor as oxidizer at various temperatures. Right, Calculated transmission of the system SnO_2/glass substrate for various film thicknesses. Continuous lines correspond to the water as-deposited SnO_2 films and the dashed ones of the same films after the first thermal cycle. Dash-dotted lines correspond to methanol vapor as-deposited SnO_2 films.

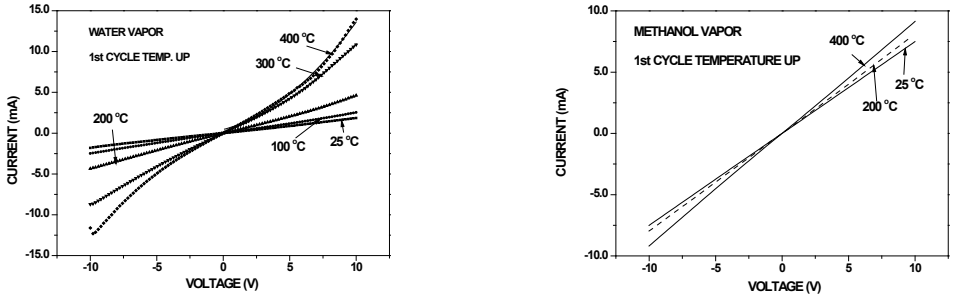

Fig. 4 Typical I-V curves taken on a water- (a) and a methanol vapor- (b) deposited SnO_2 samples with thickness of 120 and 90 nm respectively, at various temperatures.

References
1. G. E. Jellison, Jr. and F. A. Modine, Appl. Phys. Lett. 69, (1996) 371.
2. C. Petaroudis et al Th. Sol. Films, Vol. 734, 2021 Art. No. 138841
3. C. Petaroudis et al Th. Sol. Films Vol. 741, 2021 Art. No. 139039

* *Corresponding author e-mail:* d.davazoglou@inn.demokritos.gr

Thin film conformality characterization using imaging spectroscopic ellipsometry with the PillarHall LHAR-method

Anish Philip [a *], Arash Mirhamed[b], Jussi Kinnunen[a], Mikko Utriainen[a]

[a] *Chipmetrics Ltd, Yliopistokatu 7, Joensuu, 80130, Finland*
[b] *Park Systems GmbH, Stresemannstr. 30, 37079 Göttingen, Germany*

The conformal ultra-thin film deposition on high aspect ratio structures has become an indispensable demand for the fabrication of next-generation-semiconductor 3D devices, such as 3D NAND and DRAM. The state-of-the-art thin film techniques to achieve conformal thin films are chemical vapor deposition based, especially atomic layer deposition (ALD) where conformality is considered as an inherent property due to the surface limited layer-by-layer growth mechanism. However, the quantitative data for conformality of ALD thin film processes is sparse. The conformality, which is also often referred as step coverage, requires high aspect ratio (HAR) substrates for characterization. In conventional testing approach, the test wafer with patterned and etched vertical cavities is used and the measurement is carried out by cross sectional sample preparation and advanced SEM or TEM measurements. Unfortunately, this approach is time consuming and highly expensive. However, the cross-sectional sampling can be avoided with the use of lateral high aspect ratio (LHAR) test structures [1] instead of vertical HAR structures. The LHAR method utilizes faster, and less tedious conventional optical thin film analysis tools to measure the film thickness and penetration depth as a function of aspect ratio.

An advanced solution for the LHAR method uses the PillarHall® LHAR4 silicon test chips (made commercially available by Chipmetrics Ltd) in combination of optical microscopy or line-scan spectrometry. Multiple LHAR test structures with variable aspect ratio (up to 10000:1) enable accurate determination of maximum conformal aspect ratio as well as the step coverage for any defined aspect ratio. The obtained conformality data can be further converted to any target structures with known geometrical dimensions and shapes by following the physical modelling, i.e., kinetic model for step coverage by atomic layer deposition in narrow holes or trenches by Gordon et al. [2]. The easily removable silicon membrane roof in LHAR chips makes the method compatible with conventional planar optical metrology tools such as optical microscopy or line-scan reflectometry. Unfortunately, the thin film detection limit for white light optical microscope is usually restricted and highly material dependent, e.g., for Al_2O_3 film on silicon substrate the limit is approximately ≥ 20 nm. However, in semiconductor devices the film thicknesses are often less; typically below 10 nm. Therefore, it is a need for optical analytical tools without compromising the spot size and lateral resolution. A novel and promising highly sensitive, high spatial and lateral resolution film characterization tool for PillarHall can be imaging spectroscopic ellipsometry (ISE) [3], i.e., it combines the benefits of both ellipsometry and optical microscopy in a single device. The unification of the two technologies creates a metrology tool that redefines the limits of both ellipsometric measurements and polarization-contrast microscopy. In this study, we implemented for the first time the imaging ellipsometer to characterize the film penetration depth (PD) measurements in LHAR for ultra-thin films.

In the current research, two PillarHall® LHAR4 substrates coated via ALD (Beneq TFS-200, 300 °C) with ultrathin Al_2O_3 layers of thickness 5 and 20 nm were used. Samples were characterized using ISE (Park Systems, Accurion_EP4), optical microscopy (Olympus MX51) and line-scan reflectometer (Filmetrics F40-UVX). The unique features including high spatial resolution, quick and accurate detection of film thickness (intrinsic ellipsometric contrast-enhanced microscopy, Fig. 1.) image to identify the sub-nanometre thickness makes ISE highly beneficial for LHAR method. Furthermore, the possibility to operate the ISE device in wide UV-NIR wavelength range allows the measurement of film thickness and penetration depth profile for ultra-thin films even through the LHAR silicon roof. The initial results of the measurements through silicon roof are promising and will be the topic for further studies. The current study showed the benefits of using PillarHall® LHAR4 substrates in combination of imaging ellipsometer for accurate conformality measurement independent of film thickness or material. The imaging ellipsometer expands the PillarHall use to film thickness ranges below 10 nm and we foresee that the combination will improve the accuracy of the conformality studies considerably.

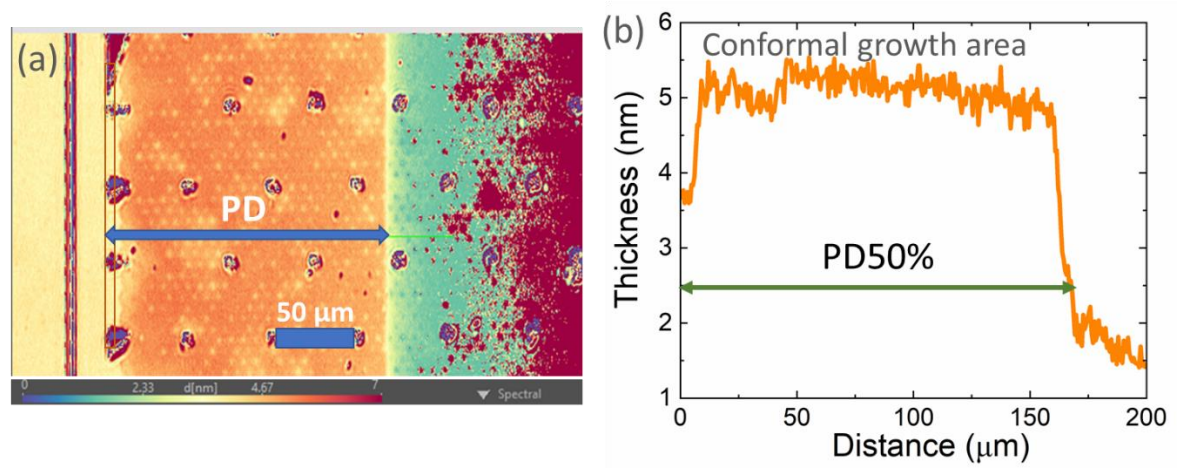

Fig.1. Imaging ellipsometer results for a 5 nm thick Al_2O_3 grown on the PillarHall® LHAR4 substrate. (a) Spectroscopic ellipsometer image after peeling off the top silicon roof from LHAR substrate. (b)Thickness mapping obtained from the same film, indicating the conformal growth area matching with the penetration depth. The arrows indicate penetration depth at 50% of film thickness (PD50%).

References

1. J. Yim, O. M. E. Ylivaara, M. Ylilammi, V. Korpelainen, E. Haimi, E. Verkama, M. Utriainen, R. L. Puurunen, Phys. Chem. Chem. Phys., **22**, 23107 (2020).
2. R. G. Gordon, D. Hausmann, E. Kim, J. Shepard, Chem. Vap. Deposition, **9**, 73 (2003).
3. S. Funke, U. Wurstbauer, B. Miller, A. Matkovic, A. Green, A. Diebold, C. Röling, P. H. Thiesen, Appl. Surf. Sci., **421**, 435 (2017).

* *Corresponding author e-mail:* anish.philip@chipmetrics.com

In Vacuo XPS Study of Al_2O_3 ALD Deposition Processes on GaN

Sofie S. T. Vandenbroucke[a,*], Eldad B. Treidel[b], Liad Tadmor[b], Enrico Brusaterra[b], Paul Plate[c], Nicole Bickel[b], Frank Brunner[b], Joachim Würfl[b], Oliver Hilt[b], Jolien Dendooven[a], Christophe Detavernier[a]

[a] *Department of Solid State Sciences, CoCooN group, Ghent University, Krijgslaan 281/S1 9000 Ghent, Belgium*
[b] *Ferdinand Braun Institut (FBH), Gustav Kirchhoff Str. 4, 12489 Berlin, Germany*
[c] *Plasma Process Technology Department, SENTECH Instruments GmbH, 12489 Berlin, Germany*

Vertical GaN-based switching transistors are currently receiving increased attention as an alternative to Si and SiC-based devices. Vertical fin metal insulator semiconductor field effect transistors (finFETs) are among the most promising GaN-based power switching transistor architectures.[1] For secure typically OFF operation, a broad gate positive voltage span up to 10 V and a stable threshold voltage, power switching devices need reliable gate insulators. For this reason, an Al_2O_3 ALD layer is often used as a gate insulator because of its relatively high permittivity, large band gap, and high breakdown electric field. Jackson *et al.[*2] demonstrated that different wet surface treatments of GaN prior to Al_2O_3 ALD influence the chemical composition and affect the electrical device performance. In this work, *in vacuo* X-ray Photoelectron Spectroscopy (XPS) is used to study the GaN surface during plasma pre-treatment and during the initial ALD cycles for both thermal (using water as precursor) and plasma-enhanced (using O_2-plasma) ALD growth of Al_2O_3 onto GaN, without exposing the sample to air.

First, the effect of the plasma treatment prior to ALD is investigated. Both NH_3- and H_2-plasma pre-treatment can successfully remove spurious carbon contamination from the pristine GaN surface while a 30 min heat treatment at 400 °C alone is not sufficient (Fig. 1). In addition, NH_3-plasma is found to remove a large fraction of the oxygen species that are present on the pristine GaN surface. After both plasma pre-treatments, the formation of N-H species is observed in the N1s spectra. In the case of NH_3-plasma these N-H species are not removed from the surface after the first ALD half-cycle (i.e. exposure to trimethylaluminium (TMA)). Both the C1s and Al2p XPS spectra after TMA exposure are consistent with the adsorption of TMA to the surface (data not shown here). During the second ALD half-cycle, the TMA treated surface is exposed to water (for thermal ALD) or O_2-plasma (for the plasma-enhanced ALD process). In both cases, the data (Fig. 2) is consistent with the growth of Al_2O_3. Water exposure removes most but not all of the adsorbed TMA ligands from the surface, while O_2-plasma is found to offer sufficient reactivity to remove all detectable carbon. Further it is observed that the O concentration in the near-surface region increases dramatically after O_2-plasma exposure. This increase coincides with the formation of O-Al, O-Ga and NO-Ga species on the surface.

Electrical data show that the density of trap states is lower for the NH_3-plasma treated samples, which could possibly be assigned to the enhanced removal of Ga_xO_y of the pristine GaN surface.[3] In addition, more trap states were observed for samples deposited using the thermal ALD process. Possibly these are caused by the presence of carbon impurities, caused by the incomplete removal of the TMA ligands by water as detected by XPS. For the plasma-enhanced ALD process more hysteresis is observed between the forward and reverse bias stress sweep CV cycles indicating a high content of stress indued interface traps. This might be explained by the presence of oxygen defects created during the O_2-plasma pulse. The best electrical data were achieved when combining a NH_3-plasma pre-treatment, followed by initial Al_2O_3 growth using thermal ALD, and then switching to plasma-enhanced ALD to thicken the Al_2O_3 layer.

This work was funded by the ECSEL JU Grant No 101007229. The JU receives support from the European Union's Horizon 2020 research and innovation program and Germany, France, Belgium, Austria, Sweden, Spain, Italy.

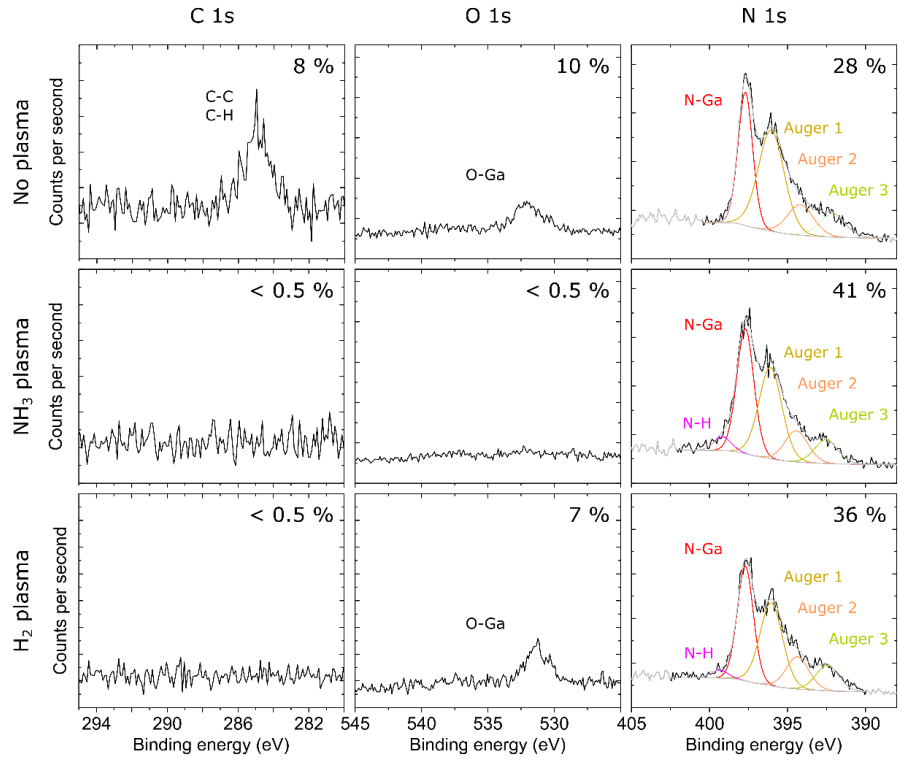

Figure 1 In vacuo XPS spectra acquired after heat pre-treatment and no plasma (top), NH_3-plasma (middle) and H_2-plasma (bottom) of a n-GaN surface.

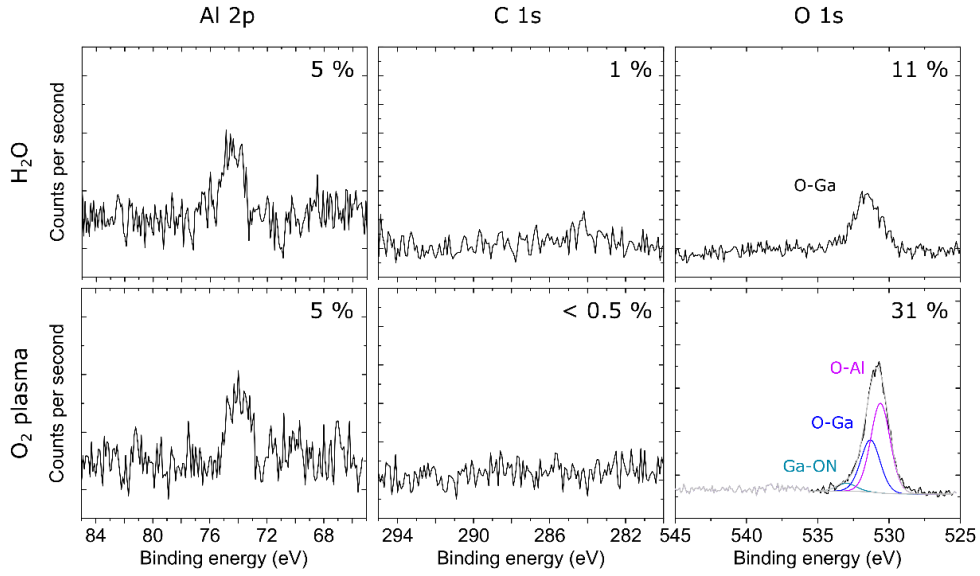

Figure 2 In vacuo XPS spectra acquired after water exposure (top) and O_2-plasma (bottom) during respectively the thermal and plasma-enhanced Al_2O_3 ALD process on a H_2-plasma pre-treated GaN surface.

References

1. Y. Zhang, M. Sun, J. Perozek, Z. Liu, A. Zubair, D. Piedra, N. Chowdhury, X. Gao, K. Shepard, T. Palacios, IEEE Electron Device Lett. **40**, 75 (2018).
2. C. M. Jackson, A. R. Arehart, T. J. Grassman, B. McSkimming, J. S. Speck, S. A. Ringel, ECS J. Solid State Sci. Technol. **6**, 489 (2017).
3. S. B. Bae, K. W. Kim, Y. S. Lee, J. H. Lee, Y. Bae, S. Cristoloveanu, Microelectron. eng. **109**, 10 (2013).

* *Corresponding author e-mail:* Sofie.Vandenbroucke@ugent.be

Specific characterization of III-nitride thin film deposits by Plasma Enhanced Atomic Layer Deposition

Yves Fleming[a*], Adrian Marie Philippe[a], Jérôme Guillot[a], Christèle Vergne[a], Noureddine Adjeroud[a], Jérôme Polesel-Maris[a,]

[a] *Luxembourg Institute of Science and Technology, rue du Brill 41, Belvaux, L-4422, Luxembourg*

Group III nitrides are materials with unique physical properties for light emitting devices as well as high-frequency electronics devices [1]. Due to these unique physical properties, a lot of research has been carried out in recent years to make group III nitrides compatible to CMOS technologies. III-nitrides and CMOS technologies need to be combined on the same die to make realistic miniaturization on the same chipset of several functionalities for sensors, actuators, energy harvesting, RF amplifier, signal treatment, machine learning and wireless communication on the mmWave frequency ranges of 5G. Since such devices are small, low power consumption and can be integrated with CMOS technology, the latter becomes highly promising for IoT (Internet of Things) applications. To achieve this goal, growth temperatures of the nitride films need to stay below 450°C in order not to interfere with CMOS circuitry [2]. Advances in research on Atomic Layer Deposition (ALD) and Physical Vapor Deposition (PVD) processing of III nitrides suggests low temperature deposition of thin films compatible with this thermal requirement. At the current stage, the associated physical properties do not yet fully achieve expectations [3,4]. PVD magnetron sputtering, for instance, is a deposition method known to be difficult for delivering thickness control at the nanometre scale leading to a weaker control of thin film thickness [5]. ALD deposition on the other side offers a unique control and reliable stoichiometry and conformality of the film in comparison to PVD. Thus, the self-limiting process of growth allows an excellent uniformity and thickness control of the film in a wide temperature window. Currently, literature about nitride deposition by ALD is much less extensive than that of the oxide processes [6].

Recently, it has been shown that Plasma Enhanced (PE) ALD deposited AlN films can be grown at 250 °C with a high quality (002) orientation while maintaining piezoelectric response [7]. In this publication, it was shown that the preferred orientation can be changed between an (100) oriented film and an (002) oriented film depending on process parameters such as the purging time between the precursor delivery and the plasma discharge. This opens the promising way of processing wide bandgap nitride thin film at growth temperature compatible with CMOS circuitry. The semiconductor industry is highly demanding for the manufacture of oriented nitride thin films below 100 nm. Hence, advanced characterizations are mandatory for the investigation of film thickness, strain, crystal growth and orientation as well as average crystallite domain size. In this work, we investigate the influence of the purging time as a growth parameter onto the III-nitride films. Specific characterisation methodologies based on X-Ray Diffraction (Fig. 1), Transmission Electron Microscopy (Fig. 2), and X-ray Photoelectron Spectroscopy will be detailed about the crystal growth, the strain and the quantification of the film quality. Apart from AlN and GaN, various other nitride films, deposited by PE-ALD, are presented.

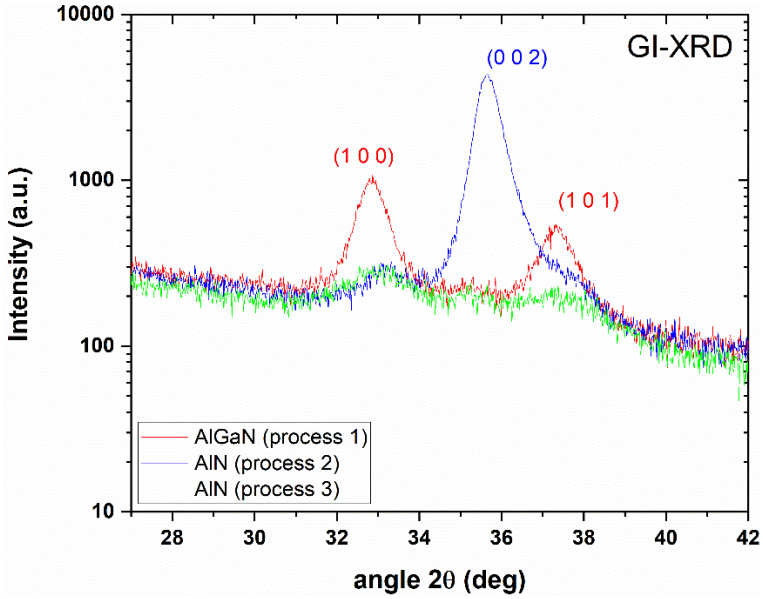

Fig 1.: XRD spectra of textured III-nitride thin films recorded in grazing incidence deposited using 3 different processes. The planes of the main reflection peaks observed are marked.

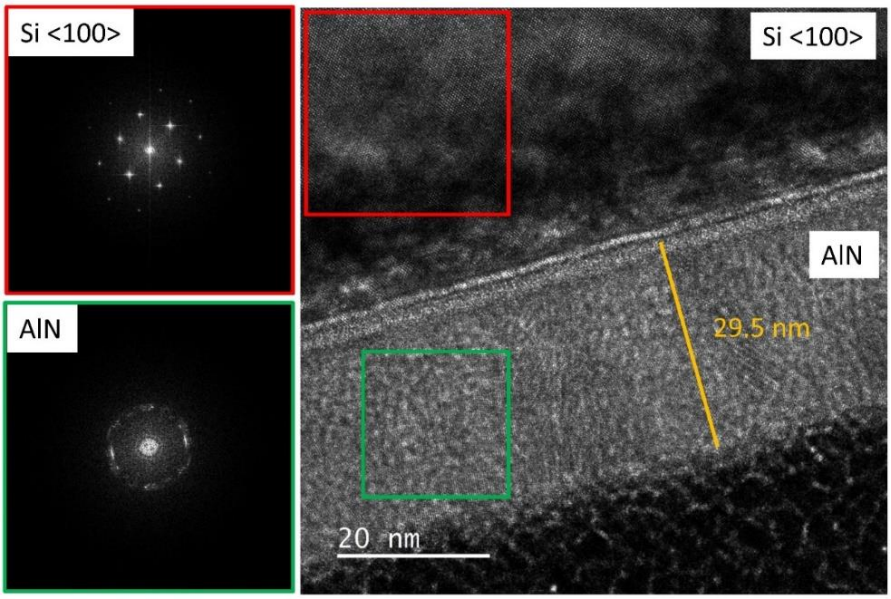

Fig. 2: TEM image of 30 nm thick AlN film deposited onto a silicon <100> substrate. The inset shows the diffraction pattern of the textured polycrystalline AlN film.

Reference list:

1. Website: https://vandewalle.materials.ucsb.edu/research/nitride-semiconductors (last viewed on 04/01/2022).
2. S. Kizir et al., Substrate impact on the low-temperature growth of GaN thin films by plasma-assisted atomic layer deposition, J. Vac. Sci. Technol. A Vacuum, Surfaces, Film. 34 (2016) 041511. doi:10.1116/1.4953463.
3. C. Ozgit et al., Atomic layer deposition of GaN at low temperatures, J. Vac. Sci. Technol. A Vacuum, Surfaces, Film. 30 (2012) 01A124. doi:10.1116/1.3664102.
4. A. Prabaswara, et al., Review of GaN Thin Film and Nanorod Growth Using Magnetron Sputter Epitaxy, Appl. Sci. 10 (2020) 3050. doi:10.3390/APP10093050.
5. C. Liu et al., Plasma-enhanced atomic layer deposition of AlN epitaxial thin film for AlN/GaN heterostructure TFTs, IEEE Electron Device Lett. 34 (2013) 1106–1108. doi:10.1109/LED.2013.2271973.
6. R.W. Johnson et al., A brief review of atomic layer deposition: From fundamentals to applications, Mater. Today. 17 (2014) 236–246. doi:10.1016/j.mattod.2014.04.026.
7. T. Nguyen et al., APL Materials 8, 071101 (2020).

* *Corresponding author e-mail: yves.fleming@list.lu*

Characterization Method of Sticking Probability for Various ALD Chemistries Relevant for Artificial Solid Electrolyte Interphases

Léo Lapeyre[a*], Krzysztof Mackosz[a], Wojciech Szmyt[a,b], Laszlo Pethö[a], Johann Michler[a], Patrice Raynaud[c], Ivo Utke[a]

[a] *Empa, Feuerwerkerstrasse 39, CH3602 Thun, Switzerland*
[b] *EPFL, Station 17, CH1015 Lausanne, Switzerland*
[c] *LAPLACE, Université de Toulouse, CNRS, INPT, UPS, 31062 Toulouse, France*

With the increasing demand for longer life time and safer batteries, atomic layer deposition (ALD) has become the method of choice for the synthesis of artificial solid electrolyte interfaces [1-3] (SEIs) due to its outstanding thickness control and conformality of deposited films, allowing the surface modification of porous cathode active material (CAM) from batteries electrodes in a unique way. In this context, the ALD process has to be optimized in order for precursors to diffuse in the high aspect ratio (AR) and porous 3D structures of CAMs, aiming for the full coverage of the active material. Namely, the diffusivity of precursors must be maximized to ensure a proper insulation of the CAM by the ALD thin films and prevent the CAM degradation induced by the electrochemical reaction with the electrolyte.

Szmyt *et al.* (2022) [4] developed a set of scaling laws describing the different ALD regimes (reaction- or diffusion-limited) and their corresponding surface coverage with respect to coating depth and sticking probability. Eq. (1) shows the expression of the coverage in the diffusion-limited regime, i.e. the dominating regime when depositing on high AR and porous substrates.

$$\theta(t) = \frac{\lambda_c}{L}\sqrt{\frac{J\beta_0}{n_0}t} \tag{1}$$

With θ - the surface coverage, λ_c - the reaction front width, L - total length of the pores, n_0 - the substrate surface sites density, J - the flux of molecules to surface, β_0 - the sticking coefficient and t - the time. From coverage profiles, this regime allows to determine the sticking probability of precursors, by measuring the coverage profile of the chemisorbed film and obtaining λ_c. Consequently, the relation between λ_c and the sticking coefficient β_0 described by Eq. (2) enables us to determine β_0.

$$\lambda_c = \frac{4}{\bar{s}}\sqrt{\frac{2}{3\beta_0}} \tag{2}$$

Where $\bar{s}$ is the surface area to void volume ratio.
In our work, we apply this model to porous Si structures (series of cylindrical holes, see Fig. 1), allowing to determine the reaction front of the coating inside the pores. The penetration depth and, therefore, the sticking coefficient of given precursors can be determined, following Eq (2). By selecting specific ALD process parameters, such as the precursor pressure and the exposure time in the reactor, the penetration depth and coverage rate can be maximised. The influence of substrate temperature on the chemisorption probability is additionally investigated, in the objective of modifying the ALD regime and improve the conformality of deposited films. This optimisation step is then applied to various ALD processes involving different precursors and coating materials, including Li-based films.

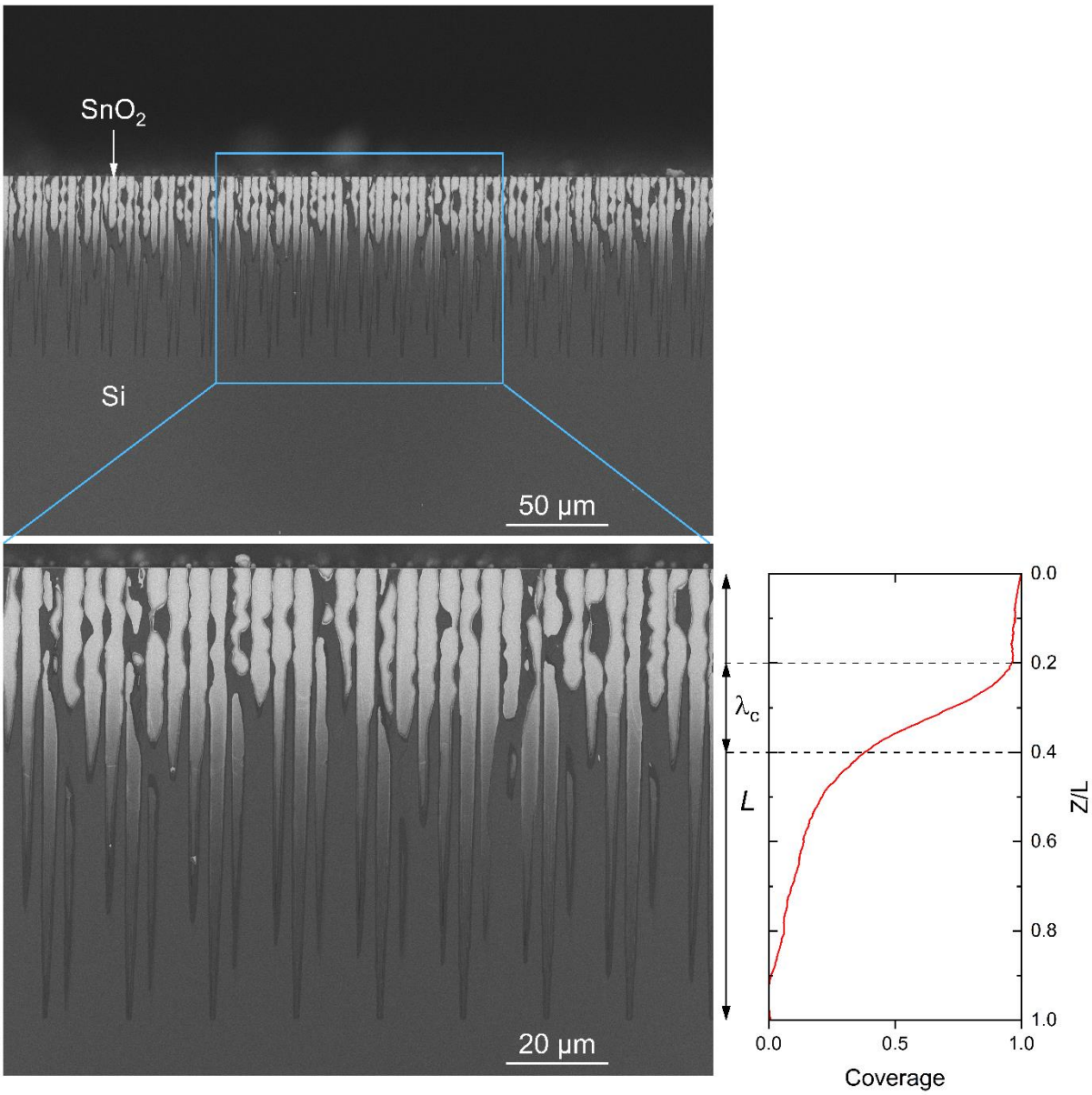

Figure 1 Cross-section topography of porous Si substrate coated with SnO2 by ALD. The pores opening and the holes depth are about 2 and 100 µm, respectively, providing an aspect ratio of 50. Pictures were acquired by scanning electron microscope (SEM) employing in-beam back scattered electron sensor.

References

1. Ma *et al.,* Adv. Mater. Interfaces, 2016, 3, 1600564; DOI: 10.1002/admi.201600564
2. Wang *et al.,* Journal of Power Sources, 2013, 233, 1-5; DOI: 10.1016/j.jpowsour.2013.01.134
3. Gao *et al.,* Materials Today, 2020, 40, 140-159; DOI: 10.1016/j.mattod.2020.06.011
4. Szmyt *et al.*, Chem. Mater. 2022, 34, 203−216; DOI: 10.1021/acs.chemmater.1c03164

* *Corresponding author e-mail: leo.lapeyre@empa.ch*

Alumina layers deposited by atomic layer deposition with different precursors for different microelectronic applications

Pauline Dill [a*], Vladimir Kolkovsky [a*], *Mathias Franz* [b]

[a]*Fraunhofer Institute IPMS, Maria-Reiche Str.2, Dresden, 01109, Germany*
[b]*Fraunhofer Institute ENAS, Technologie-Campus 3, Chemnitz, 09126, Germany*

Aluminium oxide thin films deposited by using the atomic layer deposition (ALD) technique on p- and n-type Si can be widely used in photovoltaics and modern microelectronics. In photovoltaics the passivation properties of alumina layers should be usually activated by annealing at around 350-450 °C. Such annealing steps lead to the reduction of the surface recombination velocity and to the increase of the density of negative charge. However, the existence of the negative charge in alumina layers could be undesirable for other microelectronic applications such as capacitive micromachined ultrasonic transducers or bimorph actuators where the shielding effects should be avoided. In the present study we analyze the electrical and passivation properties of alumina layers deposited by ALD with different precursors at different temperatures. We demonstrate that the effective surface recombination velocity is below 2 cm/s in all as-deposited alumina layers independently on the deposition conditions. However, it is significantly smaller in Al2O3 layers prepared with water in comparison to those prepared with ozone. We correlate this observation with the higher density of the interface states in alumina samples deposited with ozone as obtained from impedance measurements performed at different ac frequencies and at different biases. We also observe a significantly larger density of the negative fixed charge in alumina layers deposited with ozone whereas the leakage currents in these alumina films are significantly lower in comparison to the layers prepared with water. We analyze the conduction mechanisms in the films and discuss the origin of the negative charge. In addition, the influence of the annealing temperatures on the density of the negative fixed charge in Al2O3 layers is investigated.

[*] *Corresponding author e-mail: pauline.dill@ipms.fraunhofer.de / uladzimir.kalkouski@ipms.fraunhofer.de*

In-situ investigation of the physico-chemical mechanisms driving Al_2O_3 growth into PMMA during sequential infiltration synthesis

Alessia Motta [a,b], Gabriele Seguini [a], Claudia Wiemer [a], and Michele Perego [a,*]

[a] CNR-IMM, Unit of Agrate Brianza, Via C. Olivetti 2, I-20864 Agrate Brianza, Italy

[b] Politecnico di Milano, Dipartimento di Energia, Via Ponzio 34/3, 20133 Milano, Italy

Sequential Infiltration Synthesis (SIS) is a vapor-phase infiltration technique, derived from atomic layer deposition (ALD) on polymers, that is widely employed for the fabrication of hybrid organic-inorganic materials and/or inorganic nanostructures starting from a polymer template [1]. During SIS, an organic matrix is alternatively exposed to a precursor and a co-precursor of the inorganic material. The exposure steps are intercalated by purge in N_2 flux to remove un-reacted molecules and reaction by-products. The SIS process is quite complex as it involves several thermally activated physico-chemical phenomena: (1) sorption of the precursor molecules, (2) diffusion and (3) subsequent entrapment of the absorbed precursors into the polymer matrix. Understanding these fundamental phenomena is crucial to tune and maximize the incorporation of the inorganic species, potentially increasing SIS applications [2]. In this work, in-situ real-time dynamic spectroscopic ellipsometry (SE) is used to study the effect of temperature (70-110°C) in the case of the well-studied SIS process for the Al_2O_3 growth into poly(methyl methacrylate) (PMMA) thin films infiltrated by trimethylaluminum (TMA) and water (H_2O). By monitoring the evolution of the film thickness and refractive index during the first SIS cycle (Figure 1a), it is possible to obtain qualitative and quantitative information about the different phenomena occurring during the SIS process. In particular, according to Henry's law, the sorption of TMA molecules leads to an increase in PMMA thickness that is directly proportional to the concentration of TMA molecules in the films. Therefore, by properly fitting the sorption coefficient (S_{max}) with Van't Hoff equation it is possible to estimate the sorption enthalpy of the process [3][4], as shown in Figure 1b. Moreover, the initial thickness evolution during TMA exposure shows a time dependence $1/t^{1/2}$ which points to a Fickian diffusion behavior of TMA molecules [5]. Accordingly, the diffusion coefficient (D) can be determined by fitting the swelling curves ε(t) reported in figure 1c by the following equation:

$$\varepsilon(t) \sim 4\varepsilon_{max}\sqrt{D/\pi}\sqrt{t/h_0^2}$$

where h_0 and ε_{max} are the initial thickness of the PMMA film and the maximum swelling. The extracted D values correspond to effective diffusion coefficients since they describe a process with diffusion and reaction of TMA molecules taking place simultaneously during the TMA exposure step [3][6]. Accordingly, these D values are expected to be lower than pure diffusion coefficient due to the reduction in diffusion flux. By fitting the effective diffusion coefficient to an Arrhenius-type relationship, the activation energy of the diffusion process is determined, as shown in Figure 1d. Finally, the analysis of the purge step after TMA exposure indicates that the PMMA layer thickness decreases due to the out-diffusion of un-reacted TMA molecules. This thickness evolution is well described by an exponential function with a characteristic decay time τ [5]. The τ values at different temperatures are reported in the inset of figure 2. Accordingly, the residual thickness and, consequently, the residual swelling ε_∞ after an infinite purging time is extrapolated. The ε_∞ value is directly associated to the TMA molecules covalently bonded to the PMMA matrix. Figure 2 reports ε_{max} and ε_∞ values as a function of temperature, showing that the fraction of TMA molecules chemically trapped in the polymer is fairly constant. In conclusion, monitoring the real-time thickness evolution of the PMMA film during the SIS process by in-situ SE allows to fully characterize the phenomena involved in the SIS process. This study sheds light on the role of temperature in this system and provides information to better tailor the process parameters.

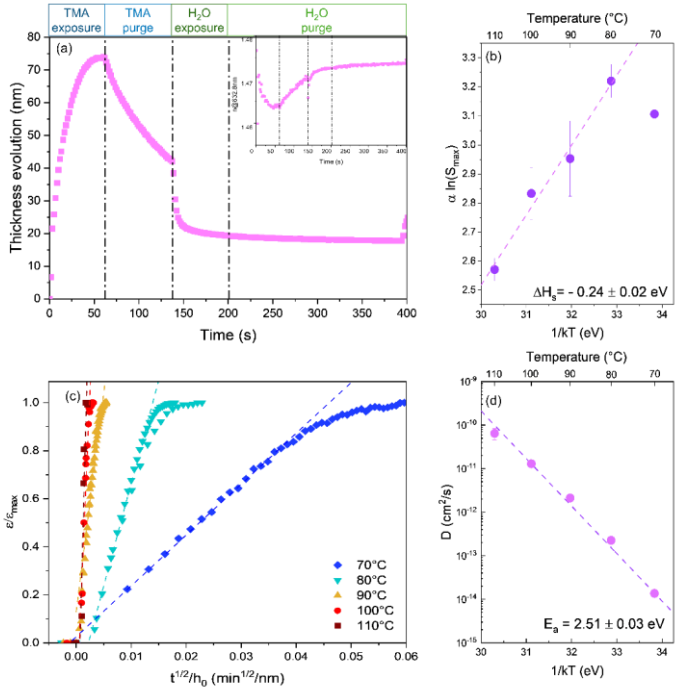

Figure 1. (a) Thickness evolution of 180 nm thick PMMA layer during the 1st SIS cycle at 90°C. In the inlet the refractive index at 632.8 nm evolution. Dotted lines are reported to distinguish the process steps. (b) Van't Hoff plot of the maximum TMA solubility in PMMA as a function of the SIS process temperature. Sorption enthalpy based on the Van't Hoff slope is reported. (c) $\varepsilon(t)/\varepsilon_{max}$ curves during the 1st TMA exposure phase as a function of $\sqrt{t}/h_0$ for all saturated PMMA thicknesses at the SIS process temperature (d) Effective diffusion coefficient of TMA in PMMA as a function of the temperature. The diffusion activation energy based on the Arrhenius slope is reported.

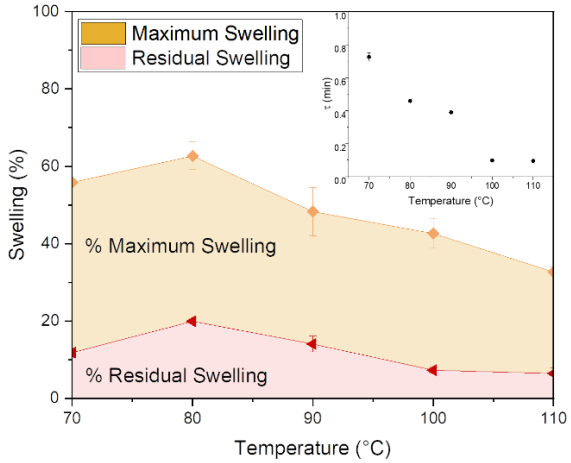

Figure 2. Maximum swelling percentage during the TMA hold step and residual swelling percentage after infinite purging time as a function of the SIS process temperature. In the inlet the characteristic desorption time (τ) as a function of the SIS process temperature during the 1st cycle TMA purging step in PMMA films.

References

1. R.Z. Waldman *et al.*, J. Chem. Phys. 151, 190901 (2019)
2. Rotem Azoulay *et al.*, Small, 1904657 (2019)
3. C.Z. Leng *et al.*, Phys.Chem.Chem.Phys., 20, 21506 (2018)
4. J. Ham *et al.*, Sensors, 22, 6132 (2022)
5. E. Cianci *et al.*, Adv. Mater. Interfaces, 1801016 (2018)
6. R.R. Petit *et al.*, ACS Appl. Mater. Interfaces, 13, 46151−46163 (2021)

* *Corresponding author e-mail: michele.perego@cnr.it*

Evidence of a twin mediated growth in CVD of polycrystalline silicon carbide (3C-SiC)

Yann Gallou[a,*], Marie Dubois[a], Alexandre Potier[b], Didier Chaussende[a]

[a] *Université Grenoble Alpes, CNRS, Grenoble INP (Institute of Engineering), SIMaP, 38000 Grenoble, FRANCE*
[b] *MERSEN, 41 rue Jean Jaurès, Gennevilliers, 92230, FRANCE*

Polycristalline silicon carbide (3C-SiC) can have multiple applications in harsh or high temperature environment owing to its outstanding strength, hardness, thermal shock resistance and inertness. Chemical vapor deposition is used for the production of pure and dense polycrystalline SiC coatings on various substrate compatible with the required temperature range for deposition (900°-1500°). For instance, deposition on graphite can serve as a protective coating for high temperature applications such as semiconductor annealing or doping furnace. Coating on C/C composites intended for use in aerospace industry could protect them against oxidation and mechanical erosion. Deposition on silicon allows the fabrication of structure for MEMS applications dedicated to harsh environment applications where standard silicon-based MEMS would fail [1]. Production of thick free-standing polycrystalline film can also serve as substrate for the production of quasi-wafer intended for power electronics semiconductor industry [2].

When deposited by CVD at a temperature above 1100°C, preferential orientations often form in polycrystalline SiC according to the Van der Drift mechanism [3], most of the time <111> or <110>. Among the critical properties for the final coating, many of them depends on the preferential orientation such as hardness [4] young modulus [4], and surface quality after polishing [5]. For all these reason, understanding preferential orientation formation, and relate it with process parameters is of key importance.

In spite of an extensive number of studies, the origin for these orientations are still in debate [6–10]. While most authors agree for the <111> orientation, stating that the selection of the {111} planes is due to a low surface energy and a high number of Si-C pair, the origin for the <110> orientation is less understood. Some authors propose that the selection of this orientation is made by a twin mediated growth, also referred as TPRE mechanism [7,11,12]. Their hypothesis is mainly based on morphological observations but lack of characterization at the grain scale. To fill this gap, we performed thorough EBSD characterization of the <110> oriented films. EBSD revealed a very high fraction of twin boundary (Σ3), up to 60% for the <110> oriented samples. Pentagonal cluster of grains separated by high angle grain boundary were visible, in which mainly Σ3, Σ9 and Σ27 CSL GB coexist. Pole figure on these clusters confirmed a double pseudo 5-fold symmetry axis, typical of a cross-twinned structure in FCC crystal although a much higher number of grains were visible in these cluster.

Overall, we propose a growth scenario taking into consideration the deviation from a perfect cross-twinned structure.

We also try to relate the switch from one orientation to another to the growth mechanism associated with the change in temperature in our hot-wall CVD reactor (1070°C to 1500°C). This was done by characterizing the microstructure at different position in the deposition chamber in a single experiment.

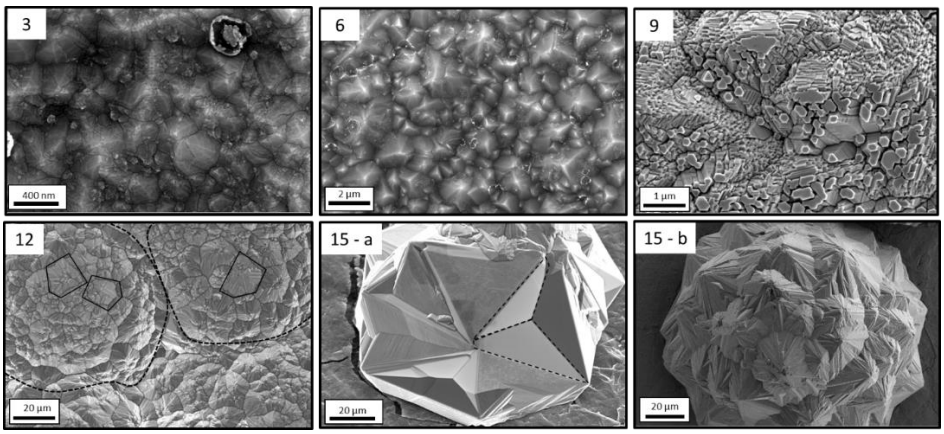

Fig. 1: SEM-secondary electron surface morphology observation of samples taken at position 3, 6, 9 , 12 , 15 cm. The corresponding temperature are 1070°C, 1250°C, 1390°C, 1460°C and 1490°C.

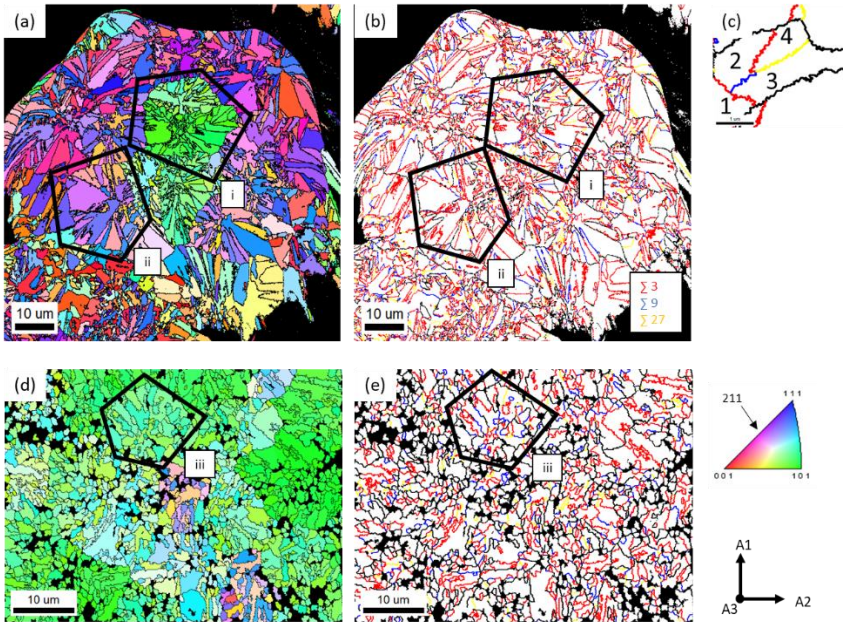

Fig. 2: EBSD Inverse pole figure map for sample taken at 15 cm (a) and at 12 cm (c) and the corresponding grain boundary maps (b), (e). (c) shows CSL relationship in a cluster of 4 twinned grains. Orientations are given along axis A3 in the IPF maps.

References

1. C. A. Zorman and M. Mehregany, *Silicon Carbide for MEMS and NEMS - an Overview*, in *Proceedings of IEEE Sensors*, Vol. 2 (IEEE, Orlando, FL, USA, 2002), pp. 1109–1114.
2. O. Bonnin, E. Guiot, and W. Schwarzenbach, *A Greener SiC Wafer with Smart Cut Technology*, 7 (n.d.).
3. Van der Drift, *Evolutionary Selection, a Principle Governing Growth Orientation in Vapourdeposited Layers. Philips Res. Rep 1967, 22 (3), 267.*, (n.d.).
4. Y. Long, *Deposition Rate, Texture, and Mechanical Properties of SiC Coatings Produced by Chemical Vapor Deposition at Different Temperatures*, International Journal of Applied Ceramic Technology **10**, 9 (2013).
5. G. Chichignoud et al., *Processing of Poly-SiC Substrates with Large Grains for Wafer-Bonding*, MSF **527–529**, 71 (2006).
6. J. Chin, P. K. Gantzel, and R. G. Hudson, *The Structure of Chemical Vapor Deposited Silicon Carbide*, Thin Solid Films **40**, 57 (1977).
7. D. J. Cheng, W. J. Shyy, D. H. Kuo, and M. H. Hon, *Growth Characteristics of CVD Beta-Silicon Carbide*, J. Electrochem. Soc. **134**, 3145 (1987).
8. M. G. So and J. S. Chun, *Growth and Structure of Chemical Vapor Deposited Silicon Carbide from Methyltrichlorosilane and Hydrogen in the Temperature Range of 1100 to 1400°C*, Journal of Vacuum Science and Technology A: Vacuum, Surfaces and Films **6**, 1 (1988).
9. Y. Kajikawa, S. Noda, and H. Komiyama, *Preferred Orientation of Chemical Vapor Deposited Polycrystalline Silicon Carbide Films*, Chemical Vapor Deposition **8**, 3 (2002).
10. Y. Lai et al., *Microstructure and Texture of Polycrystalline 3C–SiC Thick Films Characterized via EBSD*, Ceramics International **46**, 27000 (2020).
11. H. Cheng, T.-T. Lin, and M.-H. Hon, *Multiple Twind Induced <110> Preferred Growth in TiN and SiC Films Prepared by CVD*, **35**, 4 (1996).
12. Hon, *Growth Characteristics of SiC 3C*, Journal of Materials Science 27 3883-3888 (1992).

*Corresponding author e-mail: yann.gallou@grenoble-inp.fr

Comprehensive study of the early growth stages of copper films

Krzysztof Maćkosz[a,b,*], Camilla Minzoni[a], Aleksandra Szkudlarek[b], Sylwia Klejna[b], Marcin Sikora[b], Ivo Utke[a]

[a] *Empa, Feuerwerkerstrasse 39, Thun, CH-3602, Switzerland*
[b] *AGH University of Science and Technology, al. A. Mickiewicza 30, Kraków, 30-059, Poland*

The nucleation of ALD metal layers shows several key problems, among others, are nucleation delay and island growth, which prohibit the formation of thin compact metal films. To shed more light on the process of nucleation, we have performed a comprehensive study of the early growth stages of copper films prepared by means of the ALD. For the metal precursor, the general view is that electron-rich surface sites are required for its dissociative adsorption and thus for high nucleation density: metals, suboxides, hydroxyl-free substrates or reducing agents like the hydride anion. Delay in the steady-state growth is a common observation attributed to the changing surface during the first few ALD cycles [1]. This suggests that not only the starting surface but also that of the growing film needs to be characterized in-situ for insight into nucleation, coalescence, and film formation.

Based on the protocol reported by the group of Karppinen [1] $Cu(dmap)_2$ and HQ were used to grow copper, varying the growth temperature in the range of 120-160°C. Copper layers were probed globally using synchrotron methods: (X-ray Absorption Spectroscopy and X-ray Fluorescence) and locally using microscopic methods (Scanning Electron microscopy and Transmission Electron Microscopy). The results show island growth irrespective of substrate type for a few hundreds of ALD cycles. Coverage density, distribution of island size and chemical composition differs depending on growth conditions. However, for the first stage of copper film growth, the key element is to determine the oxidation state of the layers. We have resolved mixed compositions varying from metallic copper to copper oxide based on TEM studies. Both Cu(I) and Cu(II) oxides are present. It is uncertain whether the oxide phase was deposited or it is formed upon exposure to air during samples transfer from ALD reactor to TEM experimental chamber.

Systematic ex-situ XAS investigations of naturally air-exposed Cu films, deposited by means of ALD performed at the PIRX beamline at the Solaris synchrotron confirmed the rapid surface oxidation by air of copper films. They revealed the reduction of Cu under X-ray irradiation in majority of the studied films. Both effects were significantly more pronounced in early ALD nucleation of Cu films, which shows the necessity of in-situ and operando measurements (without breaking vacuum) and mitigating the irradiation effects. We aim to track the evolution of chemical composition as a function of coverage with a particular focus on the possible formation of metallic copper at any stage of the deposition process.

Our planned studies, together with SEM/TEM support, provide a comprehensive understanding of the nucleation process, which is the key mechanism to understanding the growth of ultrathin metallic Cu films by ALD

References

1. D. J. Hagen, M. E. Pemble, M. Karppinen, Appl. Phys. Rev. **6**, 041309 (2019).

[*] *Corresponding author e-mail: krzysztof.mackosz@empa.ch*

High resolution imaging optical thickness metrology for ALD

Oyunbolor, Binderiya[a], Christophe Defranoux[a], Attila Sütő[a*]

Marco Dibenedetto[b] , Fidel Toldra-Reig et Octavio Graniel[b] , Carmen Jiménez[b] , Matthieu Weber[b] , David Munoz Rojas[b] , Mikko Utriainen[c], Jussi Kinnunen[c]

[a] Semilab Co. Ltd, Prielle Kornélia street 4/A ,Budapest, 1117, Hungary
[b] Laboratoire des Matériaux et du Génie Physique, 73 Rue Félix Esclangon, Grenoble, 38000, France
[c] Chipmetrics Ltd, Ylipistokatu 7, Joensuu, 80130, Finland

The growing interest of spatial atomic layer deposition (ALD) grown thin films in semiconductor industry leads to a search for precise optical characterization techniques such as spectroscopic ellipsometry and reflectometry. Imaging spectroscopic methods provide not only thickness and optical properties, but also enables to determine surface homogeneity variation over the given area. With its microscope type configuration, Semilab imaging spectroscopic reflectometer is sensitive enough to detect thickness variation in sub-nanometer scale, with high resolution and fast scanning speed. These techniques enable not only thickness and optical properties determination, but also high-resolution surface images, as compared to conventional optical metrology of 3D thin film conformality [1].

The studied samples were deposited by spatial atomic layer deposition (SALD) [1] using different deposition heads. The ZnO lines were obtained using Diethylzinc $(C_2H_5)_2Zn$ (DEZ) and water using an SALD pen instead of the standard head, as described previously [4]. It is demonstrated that by cross scanning over different regions of ZnO surface, a large thickness variation is observed: a maximum thickness measured at the edge and center of ZnO deposited line was 213.9 nm and 381 nm, respectively. Fig. 1 shows the SALD microscope image and optical thickness 2D map by using imaging spectroscopic reflectometer (iSR).
PillarHall® test chips were also characterized to determine the penetration depth and get uniformity information. Fig. 2 shows the deposited layer uniformity and penetration information using iSR method.

Overall conclusion is the atomic layer deposition can be characterized by iSR/iSE [4,5] metrology including high lateral resolution imaging system and wide wavelength range monochromator provided reflectivity measurement at given wavelengths. The reflectivity versus wavelength is evaluated by model-based approach. The specification and advantage of the method over the conventional scanning methods are discussed.

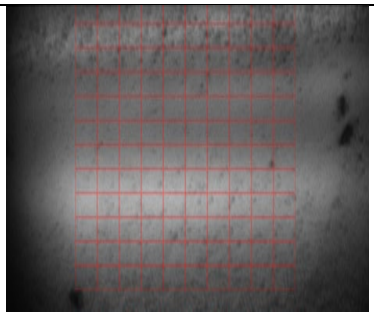

A surface image of SALD grown ZnO taken with Imaging spectroscopic reflectometry.
Red boxes indicate the scanning region.

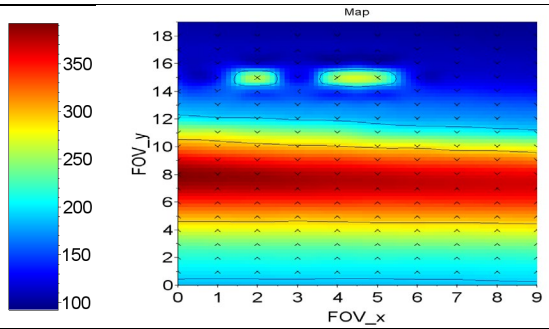

A plot of thickness variation over the scanning area. Lateral resolution is 10 μm in x direction and 5 μm in y direction. Total Field of View is 100 by 100 μm

Fig. 1 Spatial ALD application

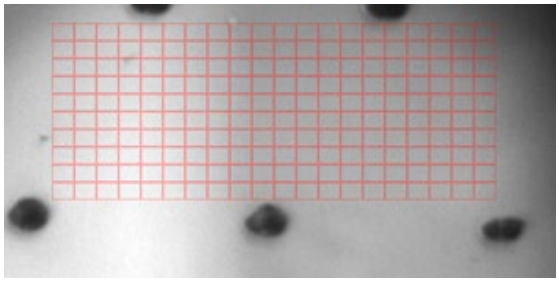	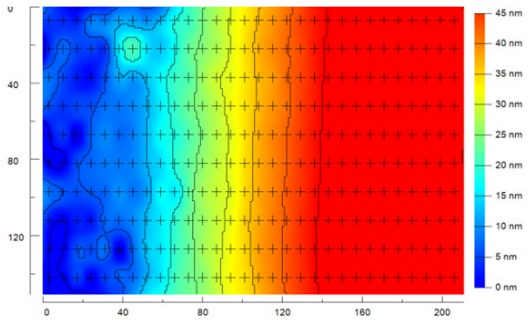
PillarHall LHAR4 silicon test chip contains Lateral High Aspect Ratio test structures for ALD and CVD thin film characterization.	Deposited layer uniformity check over 100 by 70 μm. The scale is given in pixels on CCD camera.

Fig. 2 Pillar Hall application

References

1. Proceedings Volume 12008, Photonic Instrumentation Engineering IX; 120080D (2022)
2. Commun Mater 2, 78 (2021)
3. Advanced Materials Technologies, 2020, 5 (12), 2000657.
4. Applied Optics Vol.46, No. 25 (2007)
5. Applied Optics Vol.41, No. 22 (2002)

* *Corresponding author e-mail:* attila.suto@semilab.hu

Ion beam analysis of ALD and CVD thin films and nanostructures

Johan Meersschaut[a,*]

[a] *imec, Kapeldreef 75, Leuven, BE-3001, Belgium*

ALD and CVD processes are cornerstones for the semiconductor technology. During their development it is essential to have access to sensitive characterization techniques to probe the elemental, structural, electronic, and optical properties of the developed materials. Over the years, ion beam analysis has proven to be a valuable tool to obtain complementary quantitative information about the deposited materials. In this contribution, we will review the different experimental approaches in ion beam analysis that are being used at imec, and how they may contribute to the development of new ALD and CVD processes.

Rutherford backscattering spectrometry (RBS) is a well-known ion beam analysis method. The method relies on impinging a highly energetic beam of light ions, typically He^+, on the sample, and one detects the energy and intensity of the backscattered light ions. RBS is sensitive to the areal density (atoms / cm^2) of elements heavier than the substrate in a wide range of thicknesses. It has been used to determine, for example, the growth per cycle, or the surface-dependent growth inhibition. Besides, Rutherford backscattering spectrometry in channeling mode can be used to probe the epitaxial properties or defect density of a thin film. Recent advancements of Rutherford backscattering spectrometry are the use of multi-detector data-acquisition [1] and using modern data-analysis algorithms [2]. Also, we have demonstrated the potential of Rutherford backscattering spectrometry to probe the area-selective deposition on patterns of nanostructures [3].

Elastic recoil detection analysis (ERD) is another ion beam analysis technique which has strongly supported the ALD and CVD communities. Here, a beam of high energy heavy ion projectiles impinges on the sample at a shallow angle, and one detects the ions of the sample that are recoiled in the forward direction. If one uses a two-parameter detection system, like the simultaneous detection of time-of-flight and energy (ToF-E), then it enables the accurate quantification of the atomic fraction of the various low-Z elements in the layer simultaneously. ToF-E elastic recoil detection analysis is often used to quantify – reference free – the stoichiometry of layers containing for example hydrogen, carbon, nitrogen, and oxygen.

In certain cases, nuclear reaction analysis (NRA) may prove to be very useful. The resonant nuclear reaction occurs when certain energetic ions collide with other specific nuclei in the target, and a nuclear reaction is occurring. A given nuclear reaction is very sensitive to probe one specific element. We use a proton beam to measure ^{11}B and ^{27}Al, and a ^{15}N ion beam to profile hydrogen in the samples.

We will give an overview of the ion beam analysis techniques at imec. We will also present recent improvements and new capabilities.

References

1. G. Laricchiuta et al., J. Vac. Science & Technology A 36, 02D407 (2018); doi: 10.1116/1.5016033
2. R. Heller et al., J. Appl. Phys. 132, 165302 (2022); doi.org/10.1063/5.0096497
3. N. Claessens et al., Scientific Reports 12 (2022) 17770; doi.org/10.1038/s41598-022-22645-8

* *Corresponding author e-mail:* Johan.Meersschaut@imec.be

Development of a cobalt atomic layer deposition process using $Co_2(CO)_6HC{\equiv}CC_5H_{11}$ as precursor

Mathias Franz[a*], Marcus Daniel[b], Stefan E. Schulz[ac]

[a] *Fraunhofer Institute for Electronic Nano Systems ENAS, Technologie-Campus 3, Chemnitz, 09126, Germany*
[b] *scia Systems GmbH, Clemens-Winkler-Str. 6c, Chemnitz, 09116, Germany*
[c] *Center for Microtechnologies, Chemnitz University of Technology, Straße der Nationen 62, Chemnitz, 09111, Germany*

The deposition of ultra-thin metallic cobalt films is an ongoing topic of research. Cobalt is a promising candidate to replace copper in modern interconnect systems with feature sizes below 20 nm.[1] Another application is the use of metallic cobalt in the nanometre scale in magnetic sensors.[2] Especially the atomic layer deposition (ALD) gives the opportunity to deposit thin films homogeneously even in structures with a high aspect ratio or small feature sizes.

Thermal ALD processes for metallic cobalt require typically temperatures of at least 150 °C [3]–[5], while plasma enhanced (PE) ALD processes are reported for temperatures above 100 °C.[6], [7] Here, we present the development of a low temperature PEALD process with an ALD window in the temperature region between 50 °C and 110 °C.

For the deposition of cobalt we used $Co_2(CO)_6HC{\equiv}CC_5H_{11}$ as precursor. A schematic sketch of the structure of the complex is shown in
. The synthesis and the basic characteristics had been described by Georgi et al. [8]. The process development took place in a scia Atol 200 machine from scia Systems GmbH. The precursor was evaporated by bubbling. The second precursor pulse was a hydrogen plasma pulse. Both pulses were separated by purging with pure Argon.

Figure *2* shows the temperature dependence of the developed ALD process. The growth rate is mainly temperature independent in the investigated region. The measured growth per cycle is roughly 0.1 Å/cycle for temperatures between 50 °C and 110 °C. For higher temperatures the deposition rate rises. This is likely correlated to a precursor decomposition at the substrate surface. This means, that the typical self-limiting behaviour of an ALD mode is not present anymore. This has been verified by continuous processes with the cobalt precursor only in a thermal induced process in CVD-mode (Chemical Vapour Deposition). Here, a deposition rate of 0.3 Å/min was measured.

The films had been analysed by X-ray photoelectron spectroscopy. Figure *3* shows the normalised spectra of a reference CVD process and an optimised ALD process in comparison. The precursor decomposition in CVD mode resulted in a film with high carbon and oxygen contamination. The line shape of the cobalt peak shows that the cobalt is in an oxidised state. However, the ALD process with H_2 plasma pulse resulted in a film with metallic cobalt with low contamination of oxygen and carbon.

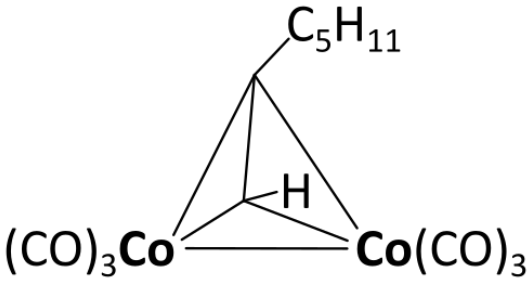

Figure 1: Schematic structure of the used cobalt precursor [$Co_2(CO)_6HC{\equiv}CC_5H_{11}$].

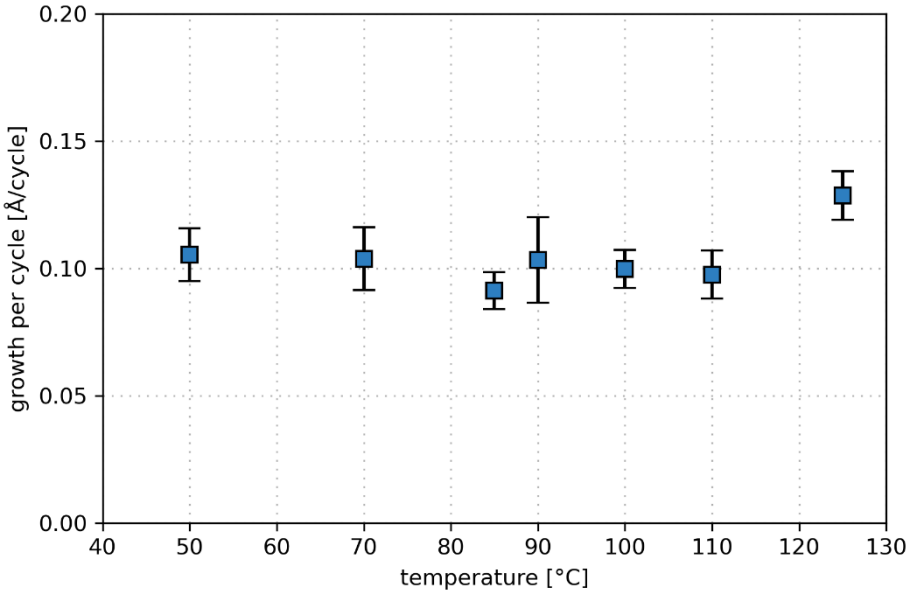

Figure 2: Temperature dependence of the deposition rate of the metallic cobalt ALD process.

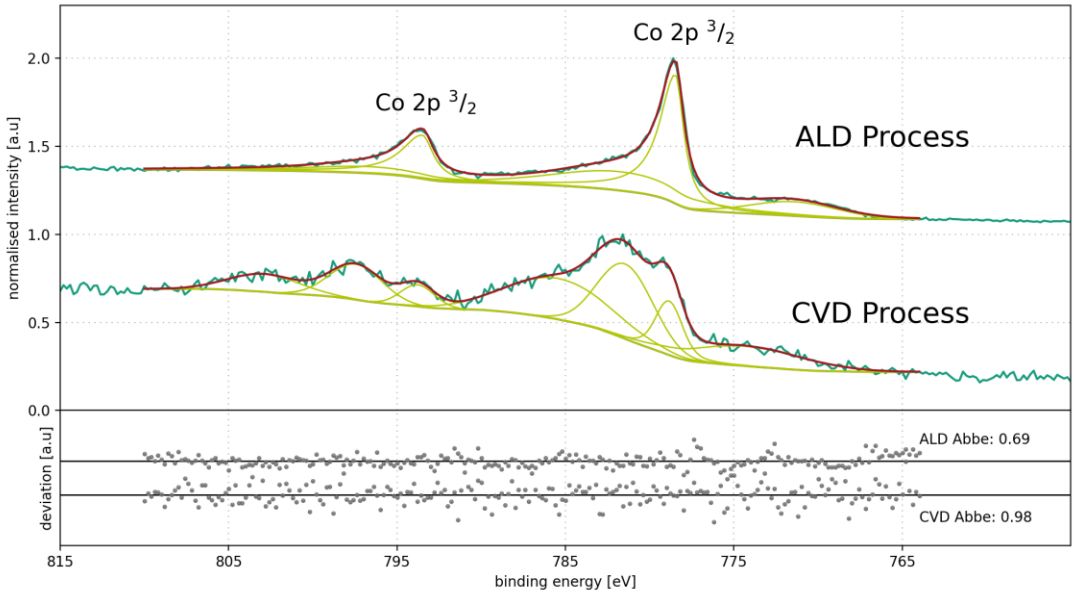

Figure 3: Normalised XPS spectra of the cobalt peaks of deposited films with an ALD process at 85 °C and a CVD process at 125 °C.

References

1. N. A. Lanzillo *et al.*, *IEEE Trans. Very Large Scale Integr. VLSI Syst.*, vol. 30, no. 1, pp. 60–67, Jan. 2022, doi: 10.1109/TVLSI.2021.3126541.
2. A. Sharma *et al.*, *J. Mater. Chem. C*, vol. 8, no. 34, pp. 11822–11829, 2020, doi: 10.1039/D0TC02734K.
3. D. Zanders *et al.*, *Chem. Mater.*, vol. 33, no. 13, pp. 5045–5057, Jul. 2021, doi: 10.1021/acs.chemmater.1c00877.
4. E. Longo *et al.*, *Nano Res.*, vol. 13, no. 2, pp. 570–575, Feb. 2020, doi: 10.1007/s12274-020-2657-4.
5. K. Väyrynen *et al.*, *Adv. Mater. Interfaces*, vol. 6, no. 3, p. 1801291, Feb. 2019, doi: 10.1002/admi.201801291.
6. B. Zhu *et al.*, *Nanos. Res. Lett.*, vol. 14, no. 1, p. 76, Dec. 2019, doi: 10.1186/s11671-019-2913-2.
7. J. You *et al.*, *J. Alloys Compd.*, vol. 758, pp. 116–121, Aug. 2018, doi: 10.1016/j.jallcom.2018.05.075.
8. C. Georgi *et al.*, *J. Mater. Chem. C*, vol. 2, no. 23, pp. 4676–4682, 2014, doi: 10.1039/c4tc00288a.

* *Corresponding author e-mail:* *mathias.franz@enas.fraunhofer.de*

Conformality of plasma-enhanced atomic layer deposition of silver films into lateral high aspect ratio microstructures

Renaud Leturcq[a,*], Sabrina Wack[a], Petru Lunca Popa[a], Noureddine Adjeroud[a], Christèle Vergne[a]

[a] *Material Research and Technology (MRT) Department, Luxembourg Institute of Science and Technology (LIST), Belvaux, Luxembourg*

Atomic layer deposition (ALD) of metals offers great opportunities in many fields, from catalysis to microelectronics, due to potential advantages to deposit ultra-thin films in complex structures. While ALD of metals has been demonstrated for a large range of materials [1], the deposition mechanism is usually not well understood, which limits the technique for large scale production. Silver is one example of highly interesting materials for its optical and electrical performances, and the deposition of highly uniform and conformal conductive ultra-thin Ag films is of great interest due to the miniaturization and three-dimensional architecture of semiconductor devices [1,2]. Although ALD of silver has been investigated by several groups recently, it is usually limited to discontinuous films made of islands [1,3].

We have investigated the conformal deposition of silver films by plasma-enhanced atomic layer deposition (PE-ALD) using lateral horizontal aspect ratio (LHAR) microstructures from Pillarhall® and compared it with a new process involving pulsed-plasma chemical vapor deposition (PP-CVD) and post-processing, showing conformal deposition of ultra-thin conductive silver films [4]. While the standard PEALD process shows an exponential decrease of the deposited material in the LHAR structure, presumably limited by the recombination of plasma radicals on the walls, our new approach demonstrates high conformality of the deposited film on complex lateral high aspect ratio structures (up to 100). Moreover, the obtained layer remains continuous inside the structure. More than showing the limitations of ALD of metals, the use of LHAR can further give important information on the deposition mechanisms, including diffusion and reaction kinetics [5].

References

1. A. N. Example, Journ. Nam. **53**, 1256 (2007).
2. D. J. Hagen *et al.*, Appl. Phys. Rev. **6**, 041309 (2019).
3. V. Cremers *et al.*, Appl. Phys. Rev. **6**, 021302 (2019).
4. S. Wack *et al.*, J. Phys. Chem. C **123**, 27196 (2019).
5. S. Wack *et al.*, ACS Appl. Mater. Interfaces **12**, 36329 (2020).
6. M. Ylilammi *et al.*, J. Appl. Phys 123, 205301 (2018).

[*] *Corresponding author e-mail:* renaud.leturcq@list.lu

Growth and Nucleation Study of ALD Copper Thin Films

Camilla Minzoni[a,b] *, Krzysztof Mackosz[a], Marcin Sikora[c], Patrik Hoffmann[b], Ivo Utke[a]

[a] *EMPA, Feuerwerkerstrasse 39, Thun, 3602, Switzerland*
[b] *EPFL Swiss Federal Institute of Technology Lausanne, Lausanne, 1015, Switzerland*
[c] *AGH University of Science and Technology, al. A. Mickiewicza 30, Krakow, 30-059, Poland*

Atomic Layer Deposition (ALD) is one of the most suitable and promising techniques for the fabrication of uniform, ultrathin films. Based on sequential self-limiting surface reactions, ALD allows to achieve homogeneous and conformal thin films with thickness control.
However, while metal oxides ALD is already a well-established fabrication process, the ALD of elemental metals faces several challenges: lack of the mechanistic understanding of the reactions in control, poor nucleation, difficulty in the reduction of the metallic center, and tendency to island growth. These are issues that metal ALD is still facing [1]. Copper ALD has been studied extensively for several advanced technologies as copper has a good electrical and thermal conductivity.
We investigated the deposition of metallic copper on (300 nm) SiO_2/Si substrates and TEM carbon membrane grids.
The copper thin films were deposited using $Cu(dmap)_2$ ($C_{10}H_{24}CuN_2O_2$) as the source of copper, while two different compounds were tested as the reducing agent; diethyl zinc Et_2Zn, a metal-containing reactant, and hydroquinone HQ ($C_6H_6O_2$), an organic reducing agent.
The two different reducing agents employed in these ALD processes enable us to study in detail the role of the reactant and to evaluate its influence on the reaction mechanism (Fig. 1 – Fig. 2). The choice of the reducing agent could be the key to achieve a controlled Cu deposition.

SEM imaging was used to evaluate the morphology of the Cu films deposited on SiO_2/Si (300 nm) substrate, while composition analysis was carried out by SEM-EDX. The characterization reported here (Fig. 3), illustrates the film nucleation observed during the two ALD processes (same number of cycles and same Cu precursor and reducing agent pulse time used). During the $Cu(dmap)_2$ and HQ process, 3D islands were observed which can coalesce to form a continuous film by increasing the number of cycles performed. In general, this type of growth occurs when the metal adatoms are much more strongly bound to each other than to the substrate, as is often the case for metal films on SiO_2 substrate. The ALD process of $Cu(dmap)_2$ and Et_2Zn occured in as a more compact film; however, the resulting film is characterized by zinc contamination, as shown in the EDX analysis.

We also studied the nucleation process with conventional ex-situ TEM for the the $Cu(dmap)_2$ + HQ ALD process on the TEM carbon membrane grid. (Fig. 4). Thanks to this approach, imaging, diffraction and microanalytical information were easily obtained and then combined to give detailed information.
In agreement with SEM imaging in Fig. 3a, the ALD process results in 3D island growth. By TEM a bimodal size distribution of the crystal Cu particles was resolved. Moreover, diffraction analysis confirmed the crystallinity of the Cu particles. A quick sample transfer between ALD reactor and TEM reduced the post-oxidation at ambient conditions.

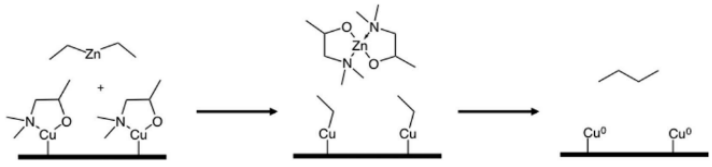

Fig. 1: Reduction of $Cu(dmap)_2$ by Et_2Zn through ligand exchange and subsequent reductive elimination process. [2]

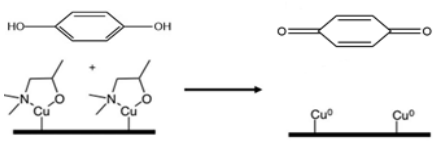

Fig. 2: Reduction of $Cu(dmap)_2$ by HQ through a redox reaction with the formation of metallic Cu [3].

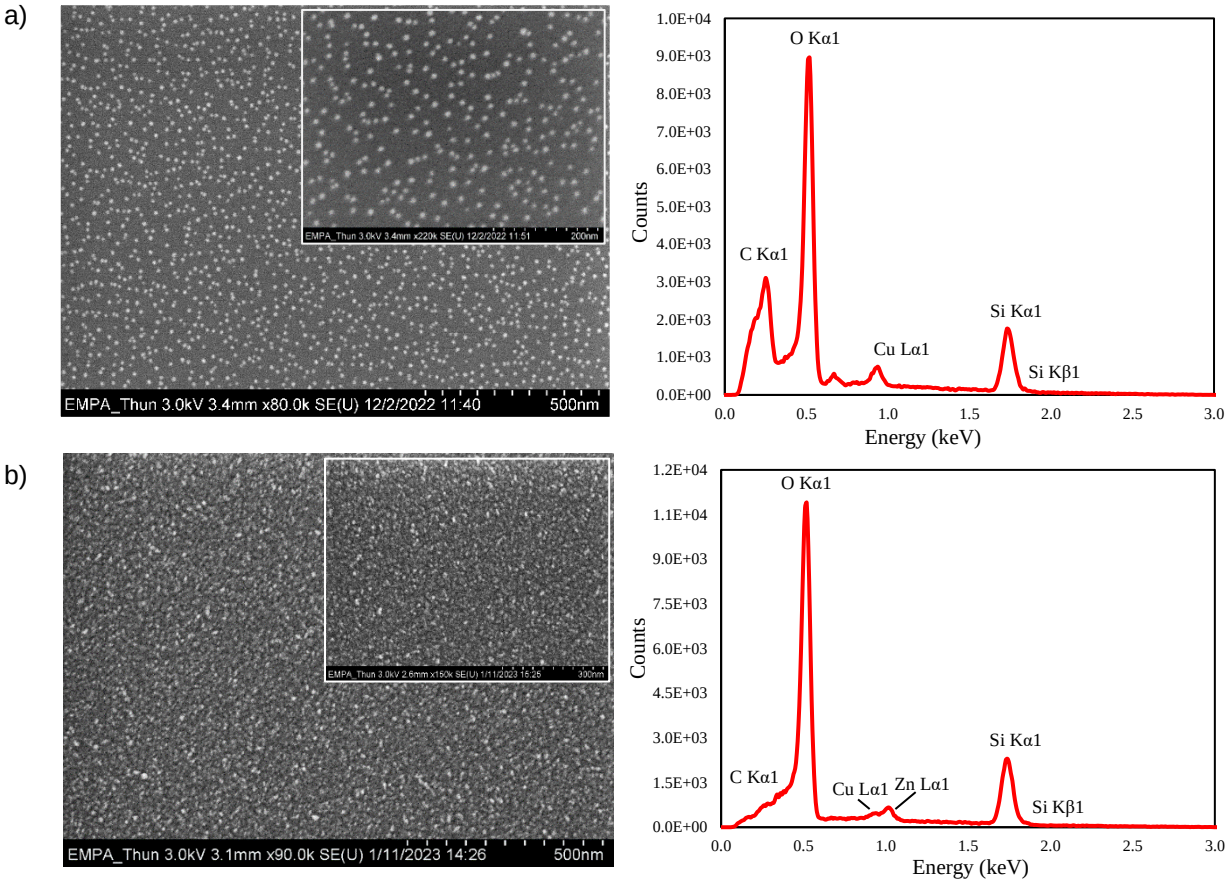

Fig. 3: SEM imaging and EDX characterization of Cu thin film obtained by using a) $Cu(dmap)_2$ + HQ, b) $Cu(dmap)_2$ + Et_2Zn. The oxygen peaks are due to oxidation at ambient atmosphere after ALD.

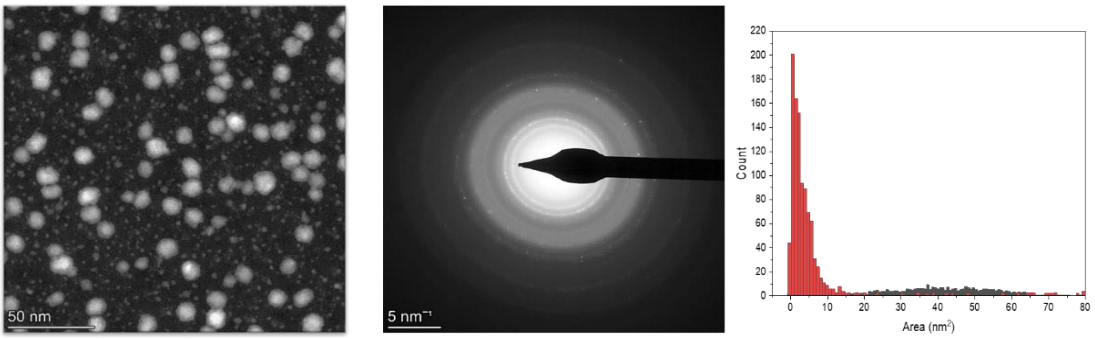

Fig. 4: TEM image and diffraction analysis of crystal Cu deposited by the ALD process $Cu(dmap)_2$ + HQ on TEM Carbon grids. A bimodal size distribution is observed.

References
1. D. J. Hagen, M. E. Pemble, M. Karppinen, Atomic Layer Deposition of Metals: Precursors and Film Growth, Appl. Phys. Rev. **6**, 041309 (2019).
2. P. G. Gordon, A. Kurek and S. Barry, Trends in Copper Precursor Development for CVD and ALD Applications, ECS Journ. of Solid State Science and Technology **4**, N3188-N3197 (2015).
3. D. J. Hagen, L. Mai, A. Devi, J. Sainio, M Karppinen, Atomic/Molecular Layer Deposition of Cu-Organic Thin Films, Dalton Trans., 47, 15791-15800 (2018)

* *Corresponding author e-mail:* camilla.minzoni@empa.ch

Twovalent Ru diazadienyls:A promising precursor class for the MOCVD of low resistivity Ru thin films

David Zanders[a*], Jorit Obenlüneschloß[a], Niklas Huster[a], Michael Gock[b], Michael Unkrig-Bau[b], Anjana Devi[a]

[a] *Inorganic Materials Chemistry, Ruhr University Bochum, Universitätsstraße 150, Bochum, Germany 44780*
[b] *Global Business Unit Heraeus Precious Metals, Heraeus Deutschland GmbH & Co. KG, Heraeusstraße 12-14, Hanau, Germany 63450*

Ruthenium thin films are garnering interest as next-generation interconnects to replace Cu in future nanoelectronic devices. Especially in the back end of line (BEOL) and middle of line (MOL), ongoing scale down has motivated alternative metallization approaches such as semi-damascene in which Ru outperforms Cu and Co.[1] Here, main advantages of Ru over other interconnect materials comprise high resistance towards electromigration allowing designs without barrier layers as well as high resistance towards scaling effects.[2,3]

For thin film fabrication, chemical vapor deposition (CVD) has been established as one of the most viable approaches to deposit coatings of a plethora of material systems, including metals, in thicknesses as low as sub-nanometers. A paramount factor in each CVD process is the choice of precursor: Its specific chemistry in interplay with substrate surfaces and co-reactants savors high relevance regarding layer formation and material quality. A review of the current CVD processes for Ru shows that a considerable number of often closely related precursors with their individual advantages and drawbacks have been employed.[4] Yet, none of them could fully satisfy academic and industrial demands alike.

This presentation introduces an alternative, new and a promising Ru precursor class, namely Ru diazadienyl cymenes [Ru(DAD)(Cym)] and underlines its potential for vapor deposition-based applications by the demonstration of a single source precursor (SSP) and ammonia (NH_3) assisted CVD process.[5] Ru thin films obtained by these two processes from the Ru(^{tBu2}DAD)(Cym) precursor (Figure 1) are subjected to various analyses and their film growth behaviour is carefully analysed (Figure 2). Structural and morphological methods such as XRD, AFM and SEM (c.f. Figure 3), are hereby complemented by compositional techniques such as RBS, NRA as well as XPS. In the context of a potential large-scale introduction of Ru as interconnect in integrated circuits, the importance and challenges to establish an efficient recycling cycle will be thematised furthermore.

A direct comparison of Ru thin films obtained from both processes reveals the NH_3 assisted one to produce layers with enhanced crystallinity in a temperature range of 350 – 500 °C which exhibit an overall more textured surface and possess a higher purity (> 90 at.% Ru). On SiO_2 substrates, 30 – 35 nm thick Ru layers with resistivity values in the range of 12 – 16 µΩ cm (Ru bulk = 8 µΩ cm) are successfully grown by the NH_3. Especially the former performance is on par with established Ru CVD processes relying on problematic, oxidative film growth chemistry. In a consecutive case study, CVD grown Ru thin films are subjected to catalysis assessment in the acidic OER. Promising performance of the layers is demonstrated, and this proof-of-concept investigation supports the utilization of CVD processes for the synthesis of catalyst materials comprising thin layers of Ru.

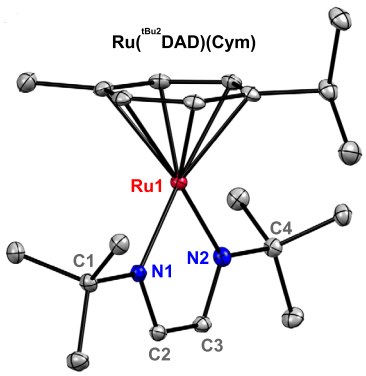

Figure 1: Solid state crystal structure of Ru(^{tBu2}DAD)(Cym). Thermal ellipsoids are set to 50% probability level and hydrogens are omitted for clarity.

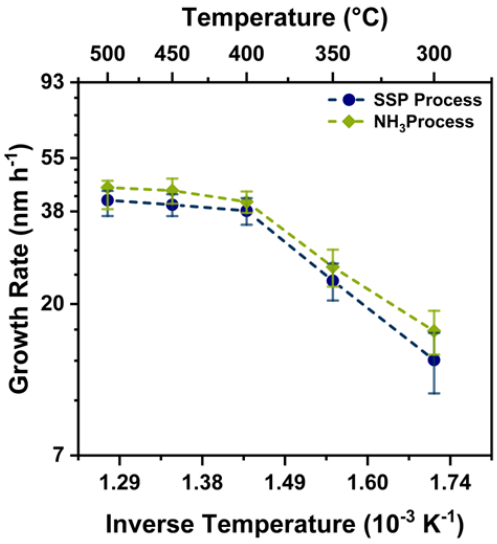

Figure 2: Arrhenius plot with growth rates of Ru thin films grown on Si(100) substrates by the SSP; (blue) and NH_3 (green) process using Ru(^{tBu2}DAD)(Cym).

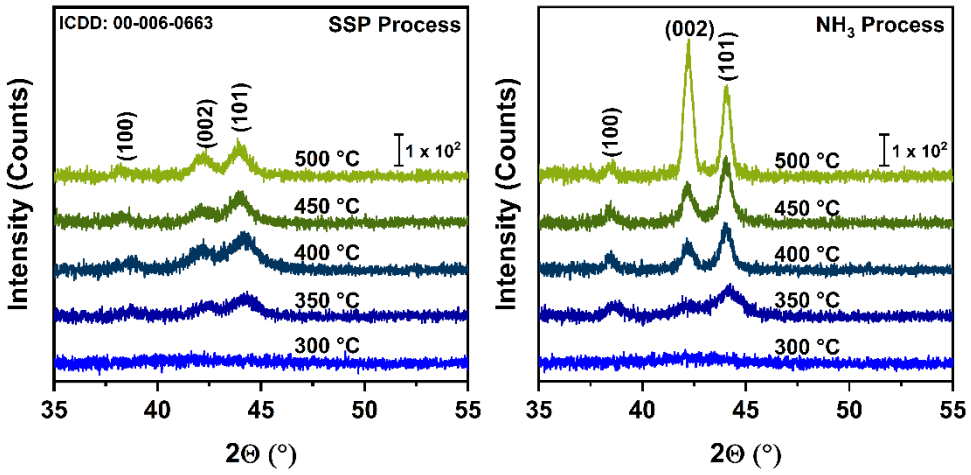

Figure 3: XRD patterns for Ru thin films grown by the SSP and NH_3 process.

References
1. G. Murdoch, et al., in **2020** *IEEE IITC 1052020.*
2. M. Siniscalchi, et al., *Appl. Phys. Lett.,* **2020**, *117, 43104.*
3. O. V. Pedreira, et al., in **2020** *IEEE IRPS 9129087*
4. https://www.atomiclimits.com/alddatabase/.
5. D. Zanders, et al., *Adv. Mater. Interfaces,* **2022**, *9, 35, 2201709.*

* *Corresponding author e-mail:* david.zanders@rub.de

Scanning-Tunneling Microscopy Simulation through an Online Platform

Mads Engelund*[a], Stanislav Kharitonov[a], Georg Graf[a] and Horst Laubenthal[a]

[a] *Espeem SARL, 12 Cité Franz Leesbierg, L-4206, Esch-sur-Alzette, Luxembourg*

In on-surface synthesis research, it is crucial to identify molecules by comparing experimental Scanning-Tunneling Microscopy (STM) images with simulated ones. However, accessing simulated STM images of molecules is a task that requires significant effort in practice. Despite the fundamental techniques of Tersoff-Hamann[1] and Bardeen-theory[2] being known for a long time, poor applications of these theories are prevalent in the experimental scientific literature.

We at Espeem have identified three common problems that contribute to this difficulty: (1) tip distance - the scanning tip is assumed to be unrealistically close to the molecule/surface due to constraints of modeling programs; (2) spatial noise - the uncertainty in the lateral tip position is not included or is included incorrectly; and (3) non-planarity - non-planar molecules are difficult to deal with, as the surface is not included in the calculation and arbitrary choices of molecular rotation are often used.

To support our experimental collaborators[3-5] (see Fig. 1) we have created a practical simulation method that produces STM images to aid experimental researchers. Our expert-curated solution solves the three practical simulation problems as follows: (1) tip distance - the wave-functions are evaluated with the atomic-centered orbital code SIESTA[6] to save calculation time over plane-wave codes, and we overcome long-range inaccuracy by explicitly extending the wavefunction into vacuum using the efficient Paz/Soler method[7]; (2) spatial noise - a gaussian 2D filter is applied to a 3D map of the current vs. tip position, and the iso-surface of the current is found to create the final image, which allows for the reproduction of abrupt jumps in the tip height; and (3) non-planarity - a model potential is used to emulate a generic surface, and the weak potential is chosen to align the molecule with the surface but cause minimal distortion.

To further improve the convenience, we have recently created a Software-as-a-Service web-app[8] which allows us to manage hardware and software for our clients. We believe that this service will remove an important practical obstacle to experimental on-surface synthesis and crystal growth studies, helping experimental researchers to deliver results both faster and better.

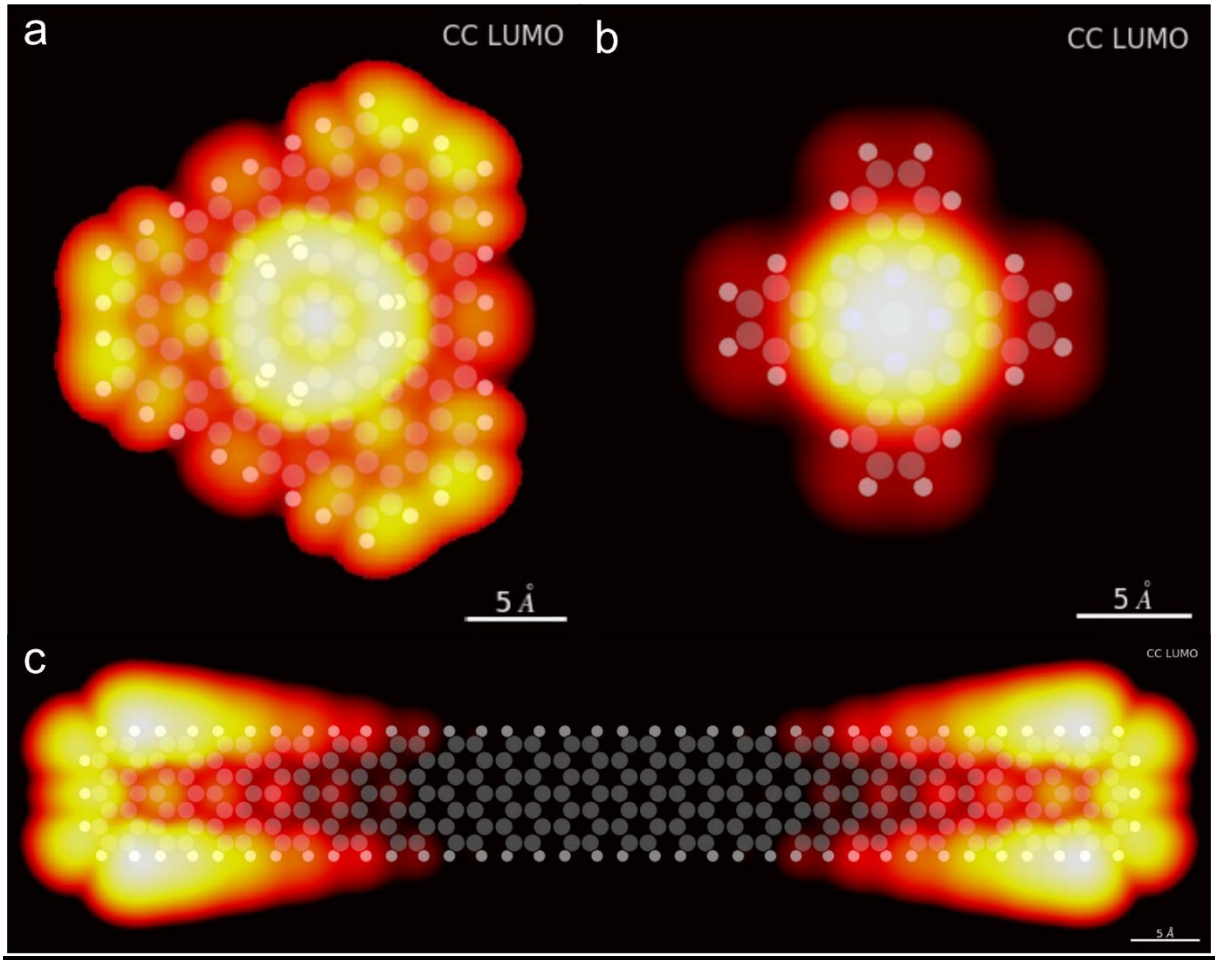

Figure 1. Simulated STM images of the LUMO frontier orbital created to support the identification of (a); a graphene flake with three nano-pores, (b); a tin phthalocyanine, and (c); a finite graphene nano-ribbon.

References

1. J. Tersoff et al., Phys. Rev. Lett. **50**, 1998 (1983)
2. J. Bardeen, Phys. Rev. Lett. **6**, 57 (1961)
3. R. Zuzak et al., Chem. Science **10**, 10143 (2019)
4. L. Bodek et al., B. Beilstein J. Nanotechnol. **11**, 821 (2020)
5. M. Kolmer et al., Science **369**, 571 (2020)
6. J. M. Soler et al., Journ. Phys.: Condensed Matter **14**, 2745 (2002)
7. O. Paz et al., Phys. Rev. Lett. **94**, 056103 (2005)
8. https://app.espeem.com

* *Corresponding author e-mail:* mads.engelund@espeem.com

The automatic modelling system for reaction mechanisms using multi-objective optimization algorithms

Takahiro Takahashi[a,*], Tenichiro Arai[b], Shinsuke Kubota[b], Eisuke Nakazawa[b]

[a] *Department of Electrical and Electronic Engineering, Faculty of Engineering, Shizuoka University, 3-5-1 Johoku, Naka-ku, Hamamatsu 432-8561, Japan*
[b] *Department of Engineering, Graduate School of Integrated Science and Technology, Shizuoka University, 3-5-1 Johoku, Naka-ku, Hamamatsu 432-8561, Japan*

The identification of a suitable reaction model (reaction mechanism) that describes the reaction pathways from the source gases to the films is one of the most important facets in the development of CVD processes [1,2]. In order to accelerate developments in this area and to reduce the workload involved, we have developed a system that automatically identifies the reaction models involved in the experimental results of CVD processes [3,4]. The reaction models have been determined both quantitatively and qualitatively based on chemical kinetics.

In this study, we developed the automatic modelling system to analyse the deposition profiles in the macroscopic cavity (*Macrocavity*) (Fig.1) [3,5]. The inference engine to model the reaction mechanism in the system was developed using NSGA-III, which is one of the most powerful and finest algorithms among multi-objective optimization problems [6].

We demonstrated the performance and validity of the system using the deposition profiles of TEOS (Tetraethoxysilane) thermal CVD [7,8]. The system successfully proposed a number of candidate reaction models, both in terms of reproducibility and model simplicity, as Pareto optimal solutions to the multi-objective optimisation problems. In addition, screening among the candidate reaction models was necessary to determine the optimal reaction model in the current situation.

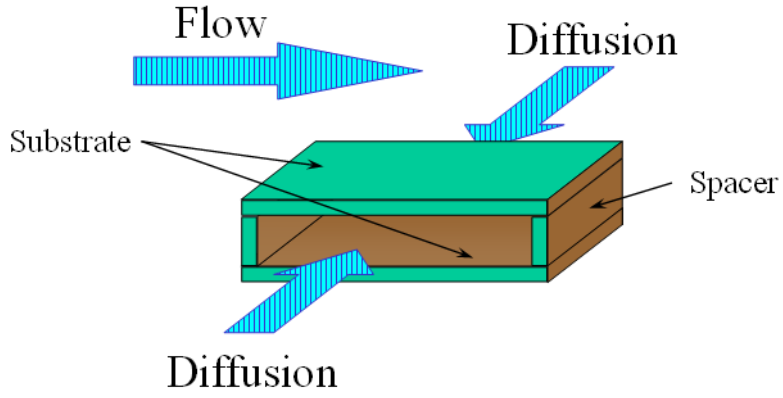

Figure 1. Schematic structure of Macrocavity.

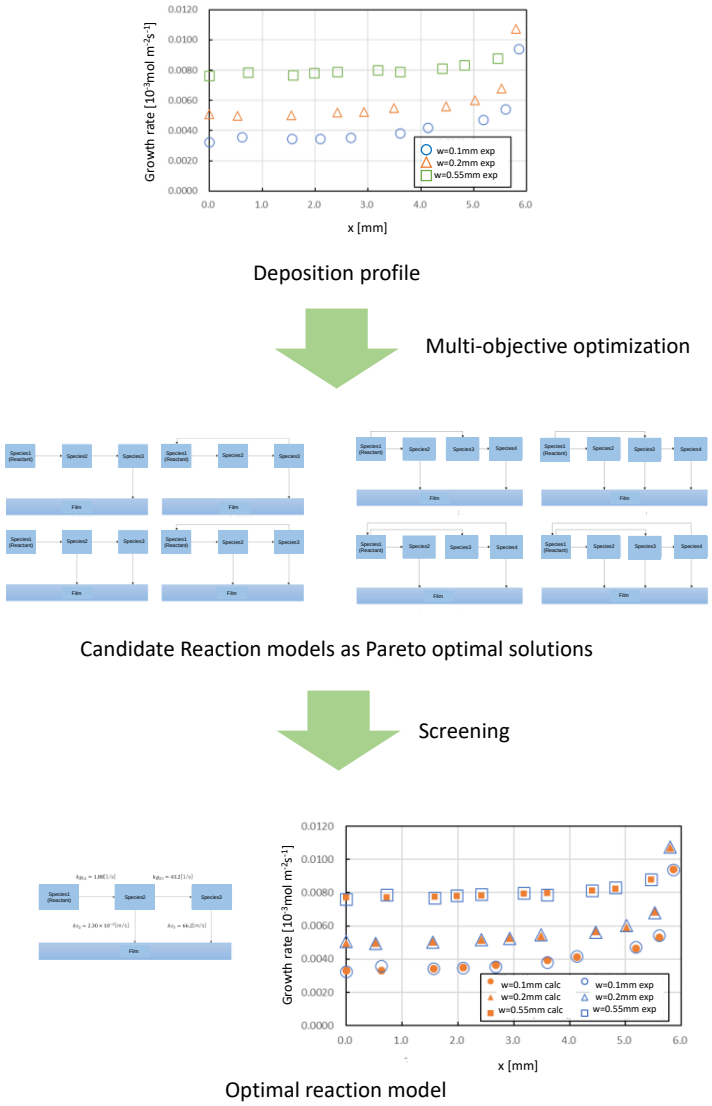

Figure 2. Schematic process of modelling using multi-objective optimisation algorithms.

References

1. H. Komiyama, Y. Shimogaki and Y. Egashira, Chem. Eng. Sci. **54**, 1941 (1999).
2. H. Liao and T. S. Cale, Thin Solid Films **236**, 352 (1993).
3. T. Takahashi, K. Funatsu and Y. Ema, Meas. Sci. Technol. **16**, 278 (2005).
4. T. Takahashi, H. Nakai, H. Kinpara and Y. Ema, J. Nanosci. Nanotechnol. **11**, 8044 (2011).
5. K. Watanabe and H. Komiyama, J. Electrochem. Soc. **137**, 1222 (1990).
6. K. Deb and H. Jain, "An evolutionary many-objective optimization algorithm using reference-point based non-dominated sorting approach, part I: solving problems with box constraints," IEEE Trans. on Evolutionary Computation (TEVC), vol.18, no.4, pp.577–601 (2014).
7. T. Sorita, S. Shiga, K. Ikuta, Y. Egashira and H. Komiyama, J. Electrochem. Soc. **140**, 2952 (1993).
8. T. Sorita, PhD Thesis, University of Tokyo (in Japanese) (1995).

* *Corresponding author e-mail:* takahashi.takahiro@shizuoka.ac.jp

Using SOLIDWORKS Flow Simulation as a tool to optimise the deposition pattern of a combinatorial air pressure CVD.

Yuankai Li[a], Andreas Kafizas[a]

[a] Imperial College London, Exhibition Rd, South Kensington, London, SW7 2AZ, UK

Combinatorial CVD can create novel products with high throughput and relatively lower cost (Maier, Stöwe, & Sieg, 2007). This is because combinatorial CVD allows for multiple depositions to occur simultaneously, resulting in thin films with different compositions and thicknesses (Kafizas & Parkin, 2011). However, the carrier gas flow inside the reactor can severely impact the entire deposition process. Therefore, modifying the gas flow in the reactor is critical for a successful deposition.

In our air pressure CVD system, there are three bubblers mounted in three gas lines that are joined together at the end of a manifold. The gas flows then go through a small mixing chamber where a baffle is placed to alter the gas flow. As a result, the deposition pattern of chemicals will vary based on the patterns of holes drilled on the baffle.

In this study, we utilized SolidWorks Flow software to conduct a computational fluid dynamics (CFD) simulation. The purpose was to investigate the relationship between the hole patterns on the baffles (samples are shown in the figure 1) and the aerodynamic properties of the gas on the sample surface. For instance, we analysed the overall density of the fluids and volume fraction of one carrier gas flow based on the sample surface, as shown in Figure 2. The former could reflect the thickness of the depositions, and the latter could show the distribution of a certain deposition.

With the assistance of the simulation studies, the experimental results of the combinatorial deposition can be optimised. In the future works, more detailed simulations and experimental results will be compared and contrasted. Eventually, this work may provide guidance to help researchers modify APCVD deposition patterns.

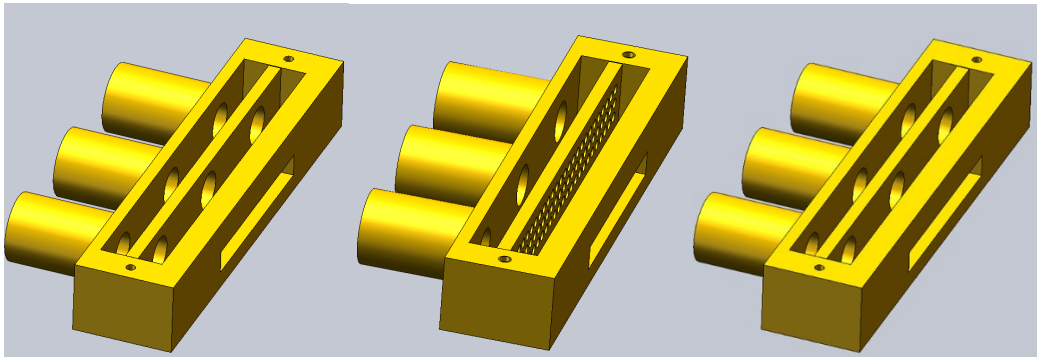

Figure 1.

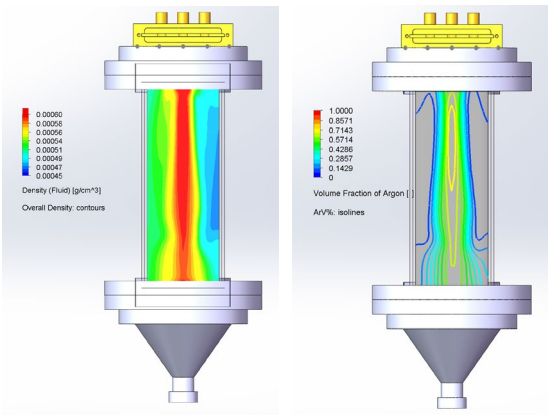

Figure 2.

References:

1. Maier, W. F., Stöwe, K., & Sieg, S. (2007). Combinatorial and High-Throughput Materials Science. *Angewandte Chemie International Edition, 46*(32), 6016-6067. doi: https://doi.org/10.1002/anie.200603675
2. Kafizas, A., & Parkin, I. P. (2011). Combinatorial Atmospheric Pressure Chemical Vapor Deposition (cAPCVD): A Route to Functional Property Optimization. *Journal of the American Chemical Society, 133*(50), 20458-20467. doi: 10.1021/ja208633g
3.

Flash lamp enabled atomic layer deposition of titanium oxide employing titanium isopropoxide as a single-source precursor

Yuanhe Cui[a*], Rumen Deltschew[a], Thomas Mikolajick[a], Martin Knaut[a]

[a] *Technische Universität Dresden, Institute of Semiconductors and Microsystems, 01062 Dresden, Germany*

Atomic layer deposition (ALD) is a thin film deposition technique used to produce thin films, which are formed by the sequential deposition of sub-atomic layers of the desired film material. Nowadays, a variety of materials can be deposited by using thermal or energy enhanced atomic layer deposition. However, common ALD is facing several limitations and one of the main limitations of ALD is the reactivity of precursors and their co-reactants. Especially at low process temperatures it is challenging to find suitable precursors to achieve specific material properties like minimized contamination levels, low sheet resistances, high film densities or a specific crystal structure.

To address these limitations of common ALD processes, we developed a novel flash lamp enabled atomic layer deposition (FLE-ALD) process. This approach combines the self-limiting chemisorption of precursor molecules in the first half-cycle with a millisecond flash lamp annealing (FLA) during the second half-cycle (Fig. 1c). The heat applied during the second half-cycle enables single-source ALD processes by inducing thermal decomposition of the chemisorbed molecules resulting in the desired film material. In addition, the FLA step helps to improve the quality of the resulting films, such as film density and crystallinity.

This paper demonstrates the FLE-ALD approach for the deposition of titanium oxide in a single-source process by employing titanium isopropoxide as the precursor. In every second half-cycle, the substrate surface is exposed to short time light flashes with a pulse length in the millisecond range and the chemisorbed molecules are decomposed during the FLA step. The heat induced in the FLA step is distributed to the substrate's bulk and the process chamber during the subsequent purging and/or cooling step, resulting in a constant substrate temperature and maintaining the self-limiting behavior of the precursor chemisorption for the next cycle.

The process development confirmed the FLE-ALD principle and the typical self-limiting mechanism as well as the constant growth per cycle of ALD by varying and characterizing process parameters like precursor dose, purge time, flash lamp power, substrate temperature (Fig. 2), and cycle number. Spectroscopic ellipsometry was used to measure the film thicknesses and to investigate the optical properties of the deposited films. The film composition was analyzed by X-ray photoelectron spectroscopy and scanning electron microscopy was used to analyze the step coverage in high aspect ratio structures. In addition, the actual film densities were derived from X-ray reflectivity and the film crystallinities were confirmed by X-ray diffraction and Raman spectroscopy.

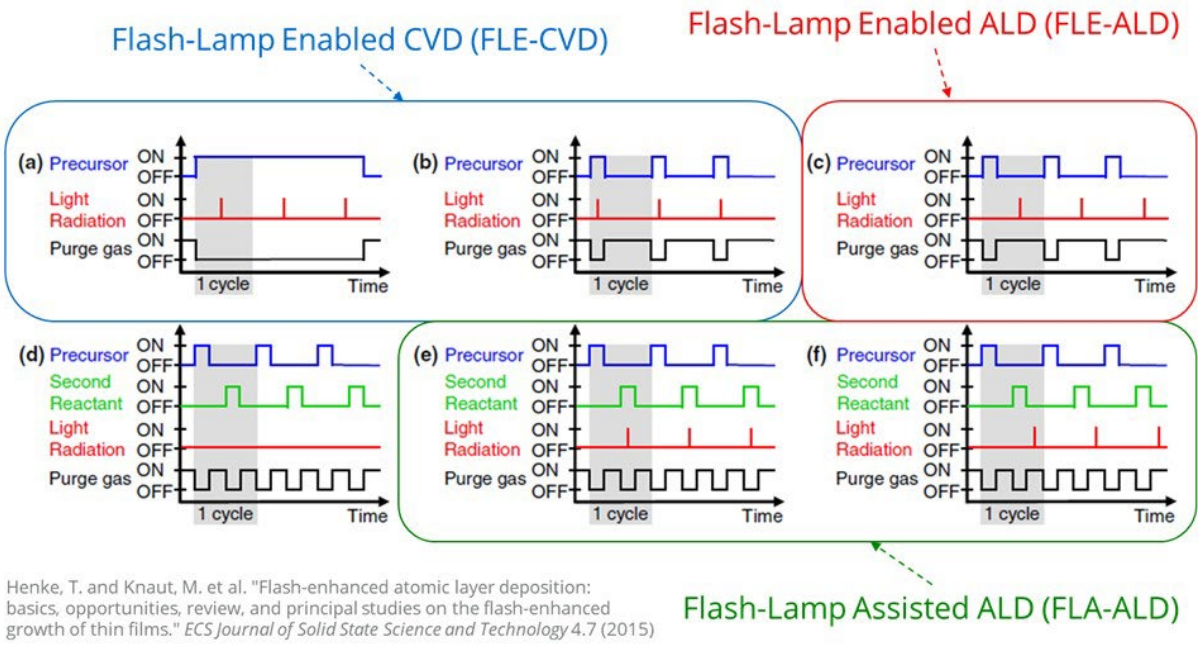

Fig. 1: Process sequences for different variants of FLA based ALD and conventional thermal ALD [1]

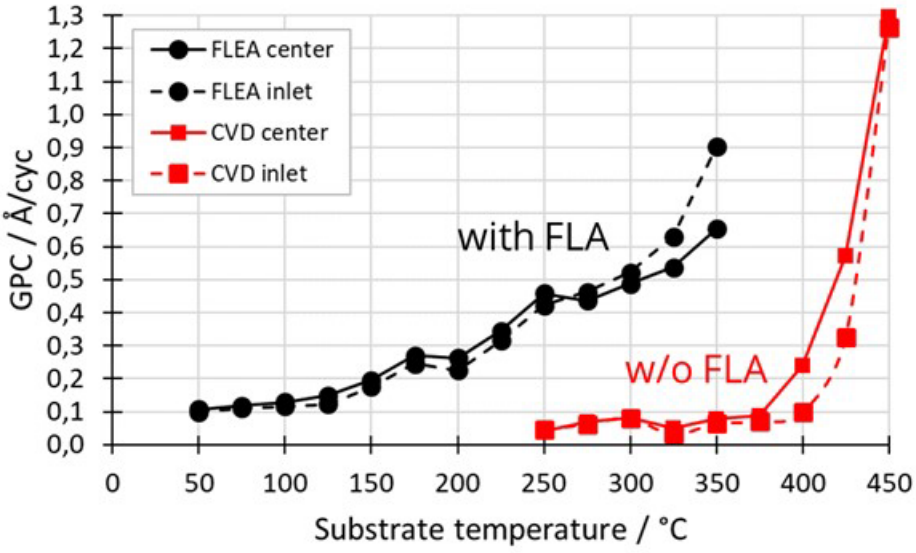

Fig. 2: Growth per cycle as function of the substrate temperature for FLE-ALD processes (black lines) and single-source CVD processes without any FLA treatment (red lines).

References

1. T. Henke, M. Knaut, C. Hossbach, M. Geidel, L. Rebohle, M. Albert, W. Skorupa, and J. W. Bartha, ECS J. Solid State Sci. Technol. 4, P278 (2015).

* *Corresponding author e-mail:* yuanhe.cui@tu-dresden.de

Mechanical Behavior upon Annealing-induced Blistering of Atomic Layer Deposited Alumina Thin Film Layered with Tantala

Helle-Mai Piirsoo*, Taivo Jõgiaas, Kaupo Kukli, Aile Tamm

Institute of Physics, University of Tartu, W. Ostwaldi str 1, 50411 Tartu, Estonia

Flexible electronics and microelectromechanical systems require investigations and advancement of the mechanical properties of thin oxide films [1,2]. Layering and wrinkling of thin films enables to modify their hardness, ductility, elasticity [1,3]. Post-deposition annealing of atomic layer deposited Al_2O_3 films on silicon substrate leads to blistering due to H_2 build up beneath the film (Fig. 1) [4]. Density and diameter of blisters can be influenced with process parameters and additional top layers [4,5]. Blistering increases the residual tensile stress and induces microcracks in the film [6,7], which might provide local elastic relaxation in the case of bending of the film – substrate system, similarly to the mechanics of wrinkles in ceramic film – flexible substrate systems [1,8].

In the present work, Al_2O_3 and Ta_2O_5 layered films were ALD on silicon substrates and post-deposition rapid thermal annealing at 700 and 800 ºC was implemented. Hardness of as-deposited layered Al_2O_3 – Ta_2O_5 thin films depended on the layer sequence from substrate to surface and on the layer thicknesses, while Young's modulus remained similar for all deposited films [9]. Hardness and Young's modulus of Al_2O_3-Ta_2O_5 films depended strongly on the sequence of the oxide layers following the annealing treatments, with the highest hardness (~ 16 GPa) achieved for double-layered film with Al_2O_3 bottom and Ta_2O_5 top layers. Reversal of the layers resulted in hardness below 15 GPa and the film did not blister.

Hardness and Young's modulus of blisters were lower compared to regular material (Fig. 2). Further studies are to be conducted to determine the potential influence of blistering to the mechanical behaviour of layered Al_2O_3 – Ta_2O_5 thin films.

We demonstrate nanoengineering the structure and mechanical properties of layered oxides by modifying the sequence of chemically distinct ALD-grown layers, accompanied by implementation of annealing to induce crystallization and blistering.

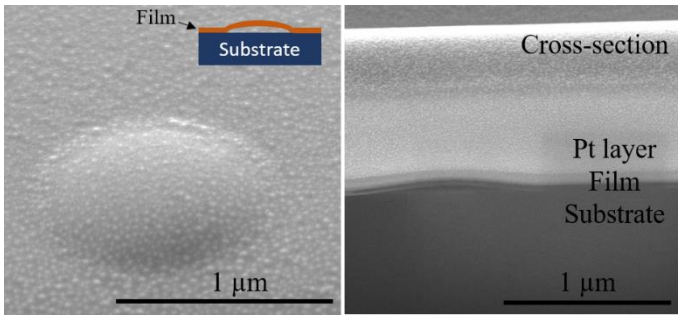

Figure 1. Scanning electron microscope image of surface morphology and cross-section of a blister of Ta_2O_5/Al_2O_3 film after annealing 10 min in air at 700 ºC.

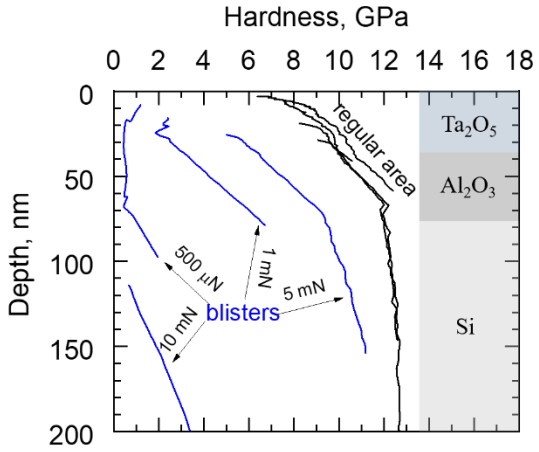

Figure 2. Hardness of blisters and regular area of Ta_2O_5/Al_2O_3 film after annealing 10 min in air at 700 ºC measured with various indentation forces.

References

1. Y. Mei, S. Kiravittaya, S. Harazim, O.G. Schmidt, Mater. Sci. Eng. R Rep. **70**, 209 (2010).
2. Y. Huang, A. Sai Sarathi Vasan, R. Doraiswami, M. Osterman, M. Pecht, IEEE Trans. Device Mater. Reliab. **12**, 482 (2012).
3. M. Nasim, Y. Li, M. Wen, C. Wen, J. Mater. Sci. Technol. **50**, 215 (2020).
4. R. Matsumura, N. Fukata, ACS Appl. Mater. Interfaces. **14**, 1472 (2022).
5. L. Hennen, E.H.A. Granneman, W.M.M. Kessels, 2012 38th IEEE Photovolt. Spec. Conf., 001049 (2012).
6. B. Vermang, H. Goverde, A. Uruena, A. Lorenz, E. Cornagliotti, A. Rothschild, J. John, J. Poortmans, R. Mertens, Sol. Energy Mater. Sol. Cells. **101**, 204 (2012).
7. M. Broas, H. Jiang, A. Graff, T. Sajavaara, V. Vuorinen, M. Paulasto-Kröckel, Appl. Phys. Lett. **111**, 141606 (2017).
8. M. Shahbaz Alam, M. Khan, Sk. Faruque Ahmed, Mater. Today Proc. **49**, 1401 (2022).
9. H.-M. Piirsoo, T. Jõgiaas, P. Ritslaid, K. Kukli, A. Tamm, Coatings. **12**, 404 (2022).

* *Corresponding author e-mail:* *helle-mai.piirsoo@ut.ee*

Minority carrier lifetime of more than 1.2ms for commercial Cz-Si(111) wafers, through ALD Al_2O_3 passivation

Namitha Dsouza[a], Ashish K. Singh[b], Rajesh Maurya[a], Jatindra K. Rath[a,b,*]

[a]*Department of Physics, Indian Institute of Technology Madras, Chennai, 600036, India*
[b]*DST Solar Energy Harnessing Centre, Indian Institute of Technology Madras, Chennai, 600036, India*

The passivation of c-Si surface plays a vital role in reducing the recombination losses of photo-electrons at the interface of Si and the adjacent layer in silicon heterojunction solar cell. This study aims to improve the efficiency of c-Si based carrier selective contact solar cells by depositing a passivation layer of Al_2O_3 using Atomic Layer Deposition (ALD). Excellent uniformity of the films over large area substrates, conformance, and control over depositing ultrathin films with a low temperature ALD growth process, will satisfy our requirement of developing layers of c-Si based carrier selective contact solar cell. To that end, the passivation characteristics of Al_2O_3 films deposited at 200 °C by thermal ALD were studied. The chosen temperature (200 °C) ensures that the film growth is saturated and lies in the optimum ALD temperature window for Al_2O_3 films. This is confirmed by the measured growth per cycle of 0.1±0.01 nm on c-Si wafer, obtained using spectroscopic ellipsometry. To study the passivation quality of these Al_2O_3 layers, n-type c-Si (111) Cz wafers with a resistivity of 2 Ω cm and a thickness of 170 μm was subjected to saw damage removal, standard RCA clean, and HF dip following which Al_2O_3 films were deposited using thermal ALD. The thermal activation required for the passivation process was provided by post-deposition annealing of these samples in forming gas environment. The enhancement in the passivation quality after annealing at different temperatures and different time spans was studied. This was done using the lifetime measured by the WCT-120 Sinton lifetime tester. For samples annealed in forming gas environment at 310 °C for 120mins, minority carrier lifetime at a minority carrier concentration of 1×10^{15} cm^{-3} showed an excellent value of about 1.24ms (Figure 1), reaching very near to the measured bulk lifetime ~2.9 ms for these industrial type Cz Si wafers, demonstrating excellent passivation quality of Si surface by our ALD Al_2O_3. Thus, an effective surface recombination velocity of 3.7 cm/s is obtained which gives an impressive implied open circuit voltage (iV_{OC}) of 0.704 V even for our commercial type Cz wafer. The development of carrier selective layers with ALD, along with the device quality passivation which is already obtained enables the fabrication of a complete solar cell without any vacuum break in ALD at a lower thermal budget.

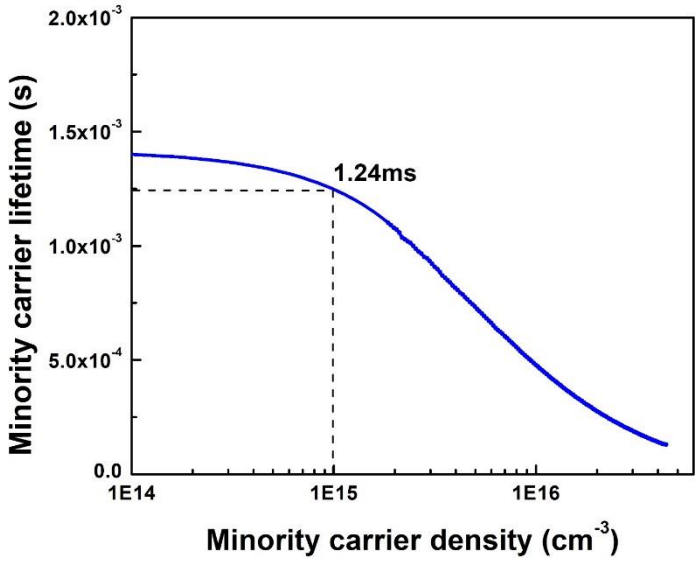

Figure 1. Injection level dependent effective lifetime of n-type Cz Si(111) wafer symmetrically passivated with Al_2O_3 and annealed in forming gas.

* *Corresponding author e-mail: jkr@iitm.ac.in*

Wafer scale growth of transition metal dichalkogenide films by MOCVD

Sergej Pasko[a], Simonas Krotkus[a], Jan Mischke[a], Moez Ounis[a], Haonan Tang[a], Cornelia Wockel[a], Alex Henning[a], Michael Heuken[a]*

[a] *AIXTRON SE, Dornkaulstr. 2, Herzogenrath, 52134, Germany*

Two-dimensional (2D) materials including transition metal dichalcogenides (TMDCs) such as tungsten or molybdenum disulfides (WS_2, MoS_2) and diselenides (WSe_2, $MoSe_2$) are considered as promising materials for future heterogeneous electronics due to their unique properties [1], for example 2D materials are predicted to retain a high charge carrier mobility even at the monolayer scale, at which silicon transport properties degrade [2].
Metal-Organic Chemical Vapor Deposition (MOCVD) is a proven method for the growth and development of semiconductor materials (including 2D materials) on an industrial scale [3-4].

In this contribution we present our recent progress on the uniform deposition of transition-metal dichalcogenides by MOCVD on up to 200 mm wafer scale with commercial AIXTRON Close-Coupled Showerhead (CCS®) systems (Fig. 1a). The nucleation and growth of TMDC domains is monitored using in-situ reflectometry. The influence of growth parameters such as nucleation/deposition temperature, reactor pressure, carrier gas composition and precursor molar flows on the growth of TMDC crystallites has been investigated. The coverage and average size of TMDC crystallites (Fig. 1b) have been determined from segmentation analysis of SEM images. The coalescence behavior of TMDC domains has been studied and the quality and uniformity of the obtained monolayer TMDC films have been determined by complementary optical spectroscopy and scanning probe techniques including Raman spectroscopy (Fig.1c), AFM and SEM.

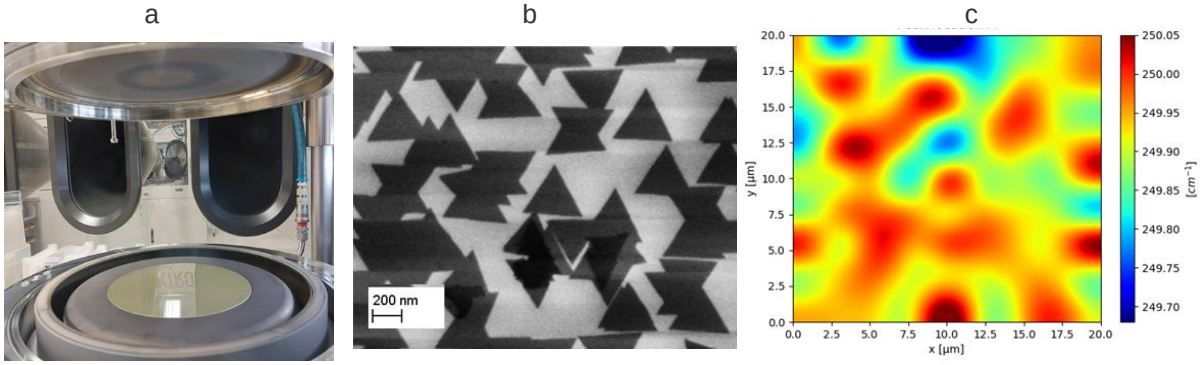

Fig.1.(a) MoS_2 monolayer grown on 200 mm sapphire in CCS AIXTRON system; (b) nucleated WSe_2 domains on c-plane sapphire by SEM; c) Raman A_{1g} peak position uniformity of monolayer WSe_2 on sapphire by µ-Raman mapping

References

1. M. C. Lemme et al., Nature Comm. **13**, 1392 (2022)
2. D. Akinwande et al., Nature, **573,** 507 (2019).
3. M. Heuken et al., Proc. SPIE, **10940,** Light-Emitting Devices, Materials and Applications, 109400Y (2019)
4. S. Rahimi et al., ACS Nano, **8,** 10, 10471 (2014)

* *Corresponding author e-mail:* m.heuken@aixtron.com

Titanium Nitride Thin Film Fabricated by Atomic Layer Deposition with Hydrazine and Metal-Organic Precursors

Jeffrey Spiegelman[a] Adrian Alverez[a],
Andrew C. Kummel [b] Cheng-Hsuan Kuo[b], Aaron J Mcleod[b], James Huang[b], Victor Wang[b],
SeongUK Yun[b], and Zichen Zhang[b],

[a] *RASIRC, 7815 Silverton Ave, San Diego, CA 92126, USA*
[b] *University of California San Diego, 9500 Gilman Dr, La Jolla, CA 92093, USA*

Titanium nitride (TiN) thin films are utilized as diffusion barriers for Co and W metal layers, as well as the gate metal barrier in CMOS and memory devices due to the material's low resistivity; TiN is also used as a coating for hard disk drives [1]. In the present work, it is shown that the resistivity can be decreased below 220 μΩ-cm with a non-halogenated precursor at 425 °C by using a Ti precursor with high thermal stability and by reducing the oxygen and carbon contents in the films using a highly reactive co-reactant, anhydrous hydrazine (N_2H_4). Titanium tetrachloride ($TiCl_4$), as well as three metal-organic precursors and anhydrous hydrazine (N_2H_4, Rasirc, Brute Hydrazine), were employed with ultra-high purity nitrogen purge gas. Films formed with the three halogen-free precursors, TDMAT (tetrakis (dimethylamino) titanium), TDEAT (tetrakis (diethylamino) titanium), and TEMATi (tetrakis (ethylmethylamido) titanium) were compared to $TiCl_4$ for resistivity and conformality. The TiN ALD chamber was connected to an *in-situ* Auger electron spectrometer (RBD Instruments), which determined the atomic composition of ALD TiN. Pulse lengths and purge times were optimized on HF-cleaned Si (100) or degreased SiO_2. For $TiCl_4$, the optimized deposition temperature was 425 °C and the optimal pulse times were 300 ms for $TiCl_4$ and 3600 ms for N_2H_4, but for the metal-organic precursors, different optimized pulsed lengths and deposition temperatures were needed. Four-point probe (Ossila) measurements were performed to determine the resistivity of TiN thin films on degreased SiO_2 substrates. Nanoscale patterned samples with horizontal vias (aspect ratio: 1:5) were used to verify the conformality of the low resistivity TiN thin films. TEM was employed to analyze the conformality of TiN thin films. Comparisons of TiN using N_2H_4 with $TiCl_4$ and TEMATi using in-situ Auger and ex-situ resistivity are shown in (Fig. 1-2) The data in (Fig.1) for $TiCl_4$ was employed as a benchmark; the low resistivity, (~89 μohm-cm) was ascribed to the high deposition temperature (500 °C) and low O and C contaminant content allowing for good crystalline structures.
Note, the resistivity was only constant for N_2H_4 pulse lengths greater than 3.6 s consistent with the need for excess N_2H_4 to reduce O and Cl contaminants.

The optimal metal-organic precursor was found to be TEMATi as shown in (Fig.2). TEMATi is still thermally stable at 425 °C; therefore, it is hypothesized that the crystallinity can be improved relative to TDEAT or TDMAT by higher temperature processing without carbon incorporation. It is noted that the residual C and O in the optimized TEMATi + N_2H_4 films are comparable to that in the optimized $TiCl_4$ + N_2H_4 films. A comparison of resistivity for TiN using $TiCl_4$ as well as metal-organic precursors is shown in (Fig. 3) As the thickness decreased, resistivity increased, consistent with surface oxidation and surface scatting in the thin films. Among all metal-organic precursors, TEMATi had the lowest resistivity, ~220 μΩ-cm at 425 °C.

As shown in (Fig 3) a conformal TiN thin film (~3.8 nm) was deposited in horizontal vias using $TiCl_4$ +N_2H_4 at 425°C. EDX results support that a TiN thin film was grown on the walls in the horizontal vias. Bright-field TEM (BF-TEM) is shown in (Fig 3 a-c). EDX mapping showed that the fin was SiO2/SiCOH and the thin film conformally grown in the horizontal via was TiO_xN_y (Fig 3 d-g). BF TEM images of TiN using TEMATi + N_2H_4 at 425°C are shown in (Fig 4) Conformal TiN was again deposited on the fins with thickness around 5.5 nm.

Previously Wolf *et al.* demonstrated 400 °C, ALD of TiN with $TiCl_4$ and N_2H_4 with a resistivity of 500 μΩ- cm [2]. The lowest resistivity thermal ALD TiN films reported using a metal-organic precursor employed TDEAT and NH_3 and had 450 μΩ-cm resistivity [3]. Elam et. al. synthesized TiN using TDMAT and NH_3 had 10000 μΩ-cm [4]. The lowest resistivity PEALD TiN films reported using a metal-organic precursor employed TDMAT and NH_3 had 180 Four-point μΩ-cm resistivity [5]. The lowest resistivity

thermal ALD TiN films reported using $TiCl_4$ and NH_3 and had 120 μΩ-cm resistivity but employed a toxic chemical, H_2S, to minimize the residual Cl [6]. Therefore, the present work with TEMATi + N_2H_4 at 425 °C showing resistivity below 220 μΩ-cm represents the lowest reported TiN resistivity for thermal ALD with a non-halogenated precursor. The reported ALD films using $TiCl_4$ and N_2H_4 represent the lowest reported TiN resistivity for thermal ALD with a halogenated precursor while avoiding the use of H_2S. It is hypothesized that the extremely high reactivity of N_2H_4 enabled both high nucleation in the horizontal vias and enable exclusion of oxygen and carbon in the TiN thereby lowering resistivity.

Acknowledgment: Special thanks to Micron for the patterned samples.

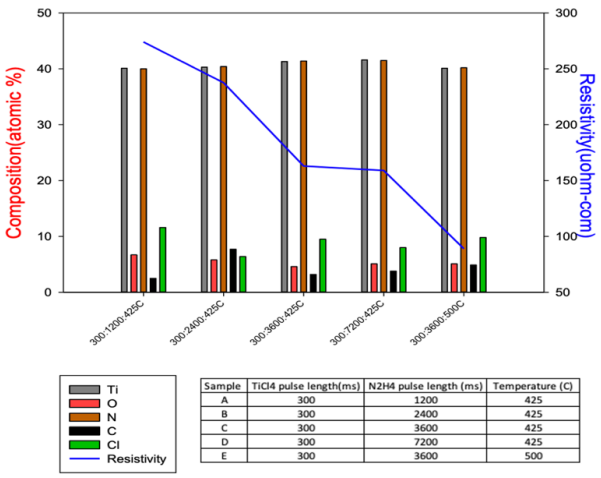

Sample	TiCl4 pulse length(ms)	N2H4 pulse length (ms)	Temperature (C)
A	300	1200	425
B	300	2400	425
C	300	3600	425
D	300	7200	425
E	300	3600	500

(Fig. 1) Pulse length study of TiN using $TiCl_4$ and N_2H_4.

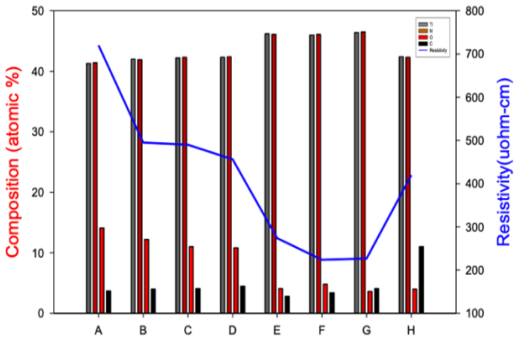

Sample	Pulse length TEMATi	Pulse length N2H4	Temp
A	300	1200	300
B	300	1200	350
C	300	3600	350
D	300	3600	400
E	300	6000	400
F	300	6000	425
G	200	6000	425
H	300	6000	450

(Fig. 2) Pulse length study of TiN using TEMATi and N_2H_4.

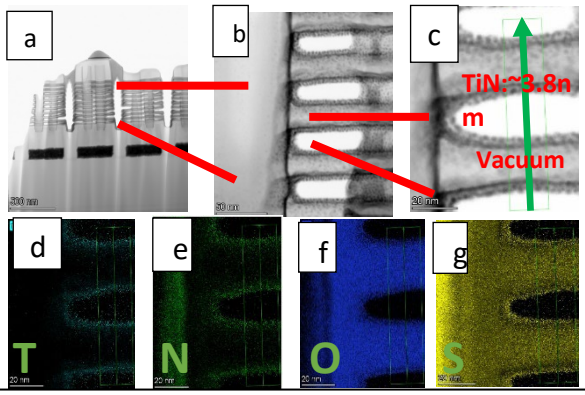

(Fig. 3 a-c) Bright-field TEM and d-g, EDX mapping analysis of TiN thin film in horizontal vias using TiCl4 + N2H4 at 425 oC.

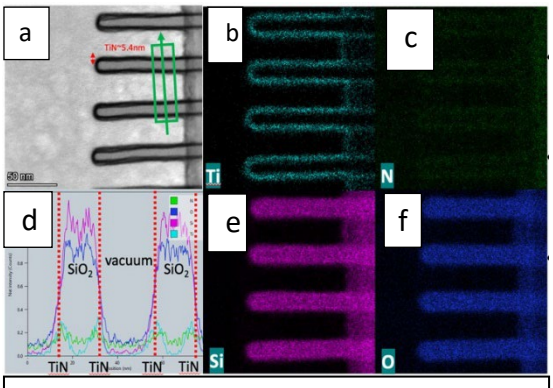

(Fig. 4a) Bright-field TEM images and b-f EDX mapping of TiN using TEMATi + N2H4 at 425 oC in the horizontal vias.

References:
1. C. H. Ahn. et al. *Metals and Materials International*, 7 (2001).
2. Steven Wolf et al. *Applied Surface Science* 462 (2018).
3. ECS Transactions, 22 (1) 167-173 (2009).
4. Thin Solid Films, 436, 145-156 (2003).
5. Microelectronic Engineering, 86, 72-77 (2009).
6. ACS Appl. Electron. Mater 3, 2, 999-1005 (2021).

*Corresponding author e-mail: JS@rasirc.com or info@rasirc.com

Functionalization of gCN-based electrocatalysts with metal and metal oxide nanoparticles for the enhancement of the oxygen evolution reaction

Mattia Benedet,[a,*] Davide Barreca,[b] Alberto Gasparotto,[a,b] Gian Andrea Rizzi,[a,b] Chiara Maccato[a,b]

[a] *Department of Chemical Sciences, Padova University and INSTM, Via Marzolo 1, 35131 Padova, Italy*
[b] *CNR-ICMATE and INSTM, Department of Chemical Sciences, Padova University, Via Marzolo 1, 35131 Padova, Italy*

The relentless environmental pollution brought about by the overreliance on fossil fuels requires the development of sustainable approaches to meet the ever-growing energy demand in a carbon-neutral fashion. In this context, water splitting activated by sunlight, a virtually inexhaustible natural resource, has emerged as an amenable route for a green production of molecular hydrogen, an important energy vector. Yet, the overall process efficiency is limited by the anodic oxygen evolution reaction (OER), and an ongoing challenge concerns the design and fabrication of eco-friendly, cheap and earth-abundant OER electrocatalysts as alternatives to noble metals-based ones. In the current tide of possible candidates, graphitic carbon nitride (gCN) presents a range of attractive properties, encompassing thermal and physico-chemical stability, amenable reactivity, and band gap enabling Vis light harvesting. It is worthwhile highlighting that g-CN consists of earth-abundant and non-toxic elements, a relevant feature to reduce the environmental footprint and improve the process sustainability.

In the present work, we propose original and versatile preparation routes for the obtainment of supported gCN-based OER photoelectrocatalysts. After the synthesis of precursor powders from melamine (M) or melamine + cyanuric acid (CM), the target systems are deposited on fluorine-doped tin oxide substrates (FTO) by electrophoresis or decantation. The gCN matrixes are then functionalized with low amounts of metals (Au, Ag or Au+Ag) or metal oxides (CoO or $CoFe_2O_4$) by means of radio frequency (RF)-sputtering from weakly ionized plasmas under mild operational conditions. A thorough structural, morphological, compositional and optical investigation by complementary analytical tools evidenced a direct dependence of the system chemico-physical features on the adopted gCN precursor (M *vs*. CM) and experimental parameters. An advanced TEM characterization revealed that metal particles had a nanometer-scale size (Fig. 1a). Whereas silver was, to a certain extent, atomically spread in gCN-Ag specimens, a feature paving the way to single-atom catalysis, the presence of alloyed core-shell Au-Ag nanoaggregates was observed for bimetallic systems. The samples featured an optical band gap of ≈2.7 eV (Fig. 1b) and, for gCN-Au, an enhancement of Vis-light absorption attributed to the surface plasmon resonance (SPR). Even for oxide-containing gCN, analyses evidenced the formation of nanostructured particles for the functionalizing agents (Fig. 1c). All the target specimens featured an appreciable defectivity degree, as indicated by the presence of uncondensed amino groups ($-NH_x$, x = 1,2; components **ii** and **iv** in C1s and N1s photopeaks, Fig. 1d), possessing a beneficial effect on the ultimate performances.

The introduction of both metal and oxide co-catalysts had a favorable influence on photoelectrochemical behavior in comparison to the pristine gCN systems. Among noble metal-containing electrocatalysts, gCN(CM)-Au showed the best performances (Fig. 2a), thanks to the formation of Schottky barriers, suppressing electron-hole recombination and increasing photoactivity, especially when coupled with SPR (Fig. 2b). As concerns metal oxide-functionalized samples, the improved gCN-$CoFe_2O_4$ activity (Fig. 2c) was rationalized basing on the formation of *Z*-scheme gCN/$CoFe_2O_4$ junctions, more efficient than *p*-*n* gCN/CoO ones in promoting charge carrier separation (Fig. 2d).

The obtained results, critically discussed basing on the interrelations with material characteristics, may act as pointers towards further implementation of stable, cost-effective and active OER photoanodes for solar hydrogen production. In perspective, the strategies presented in this study offer promising opportunities even for manufacturing photoelectrocatalysts for H_2O remediation, one of the most urgent global priorities to reduce water stress and promote an enhanced societal wellbeing.

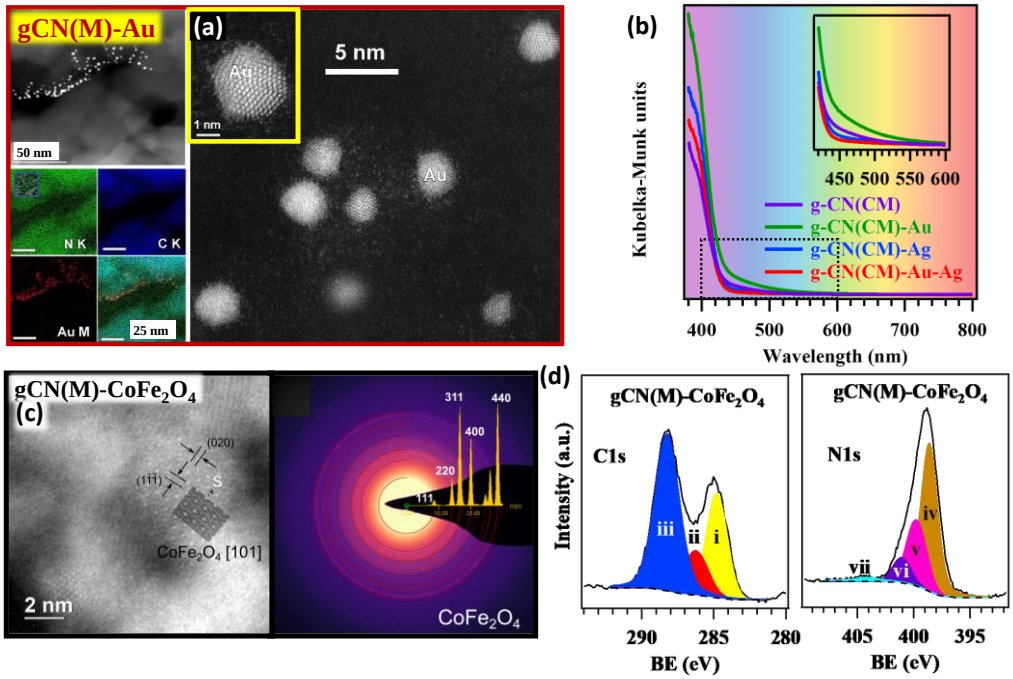

Figure 1. (a) Representative TEM micrographs for gCN(M)-Au and corresponding EDXS-STEM elemental maps (N K: green; C K: blue; Au M: red). (b) Optical spectra of gCN(M) systems [1]. (c) Experimental and simulated TEM image and SAED pattern for gCN-$CoFe_2O_4$. (d) C1s and N1s photopeaks for gCN-$CoFe_2O_4$ [2].

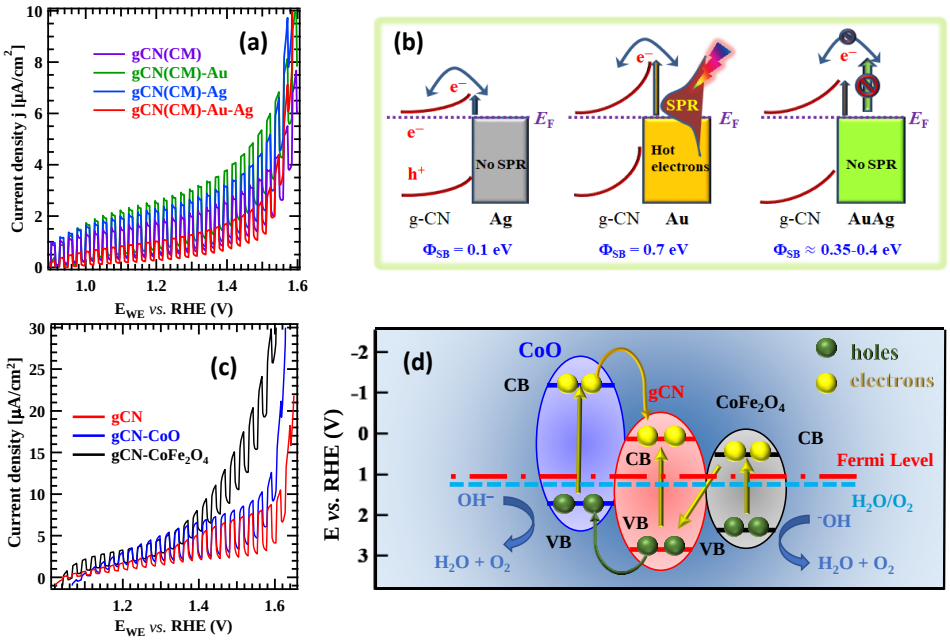

Figure 2. (a) Chopped linear sweep voltammetry (LSV) scans for gCN(CM) systems functionalized with noble metals. (b) Sketch of the Schottky barrier height (Φ_{SB}) for the same systems [1]. (c) Chopped LSV scans for oxide-containing gCN materials. (d) Sketch of the junction between gCN and CoO (left) or $CoFe_2O_4$ (right) [2].

References

1. M. Benedet, G. A. Rizzi, A. Gasparotto, O. I. Lebedev, L. Girardi, C. Maccato, D. Barreca, Chem. Eng. J. **448**, 137645 (2022).
2. M. Benedet, G. A. Rizzi, A. Gasparotto, N. Gauquelin, A. Orekhov, J. Veerbeck, C. Maccato, D. Barreca, *submitted*.

* *Corresponding author e-mail:* mattia.benedet@phd.unipd.it

Development of Ternary ALD Chalcogenides for Memory Applications

Tobias Peissker [a,*], Wouter Devulder [a], Venkateswara R. Pallem [b], Jean-Marc Girard [c], and Laura Nyns [a]

[a] IMEC, 3001 Leuven, Belgium
[b] Air Liquide Advanced Materials, Innovation Campus Delaware, Newark, DE 19702, US
[c] Air Liquide Advanced Materials, 75 quai d'Orsay, 75007 Paris, France

To bridge the gap between a fast latency, volatile memory such as DRAM, and non-volatile, slow, but high-density memory like NAND, Storage Class Memory (SCM) is one of the most promising concepts. It combines fast latency with non-volatility and the possibility to integrate these type of memory devices with a high density. SCM devices based on 3D cross point architecture have already been established, using phase change materials (PCM) as memory element and Ovonic Threshold Switch (OTS) materials as selector element. The selector element needs to be highly selective, i.e., showing a high $I_{ON/OFF}$ ratio, to be able to withstand high driving currents, and to show high amorphous stability to program the PCM element. For future devices, 3D vertical integration of SCM devices is required to achieve the high storage density.
For these advanced device architectures, Atomic Layer Deposition (ALD) is the preferred deposition technique as it can enable highly conformal layers of PCM and OTS materials, even for high aspect ratio structures. The capability of ALD to deposit highly conformal films for a wide range of applications has been shown extensively in the past [e.g., 1]. Unfortunately, the ALD deposition of materials such as germanium chalcogenides is challenging. A binary compound like GeSe might not fulfil all requirements to be used as OTS in a SCM device [4], and ternary or even quaternary compounds will be needed to improve the memory cell performance, increase its thermal robustness, and tune the $I_{ON/OFF}$ ratio. In this conference contribution we will address the ALD of (doped) germanium chalcogenides, which are a class of materials being explored as PCM and selector elements. We used the dechlorosilylation chemistry for the low-temperature ALD reaction of (nonmetal) alkylsilyl compounds with metal chlorides, which resulted in amorphous chalcogenide layers [2,3]. Here, we will report on the development of a ternary ALD process targeting a GeAsSe film. We have investigated in detail the growth of ALD GeAsSe on various substrate materials which are important for device integration. In general, we have observed nanometer-sized circular nucleation islands (Fig. 1). Even after high cycle counts of ([GeSe][As_2Se_3]) ALD super cycles the nucleation islands persist, and no closed layer was formed under the conditions investigated. The islands are characterized in view of morphology and elemental composition in relation to the substrate surface properties (surface termination) and critical deposition parameters.

Acknowledgement
The authors would like to thank Andrea Illiberi, Michael Givens and Jerome Innocent from ASM Belgium for their support in process development.

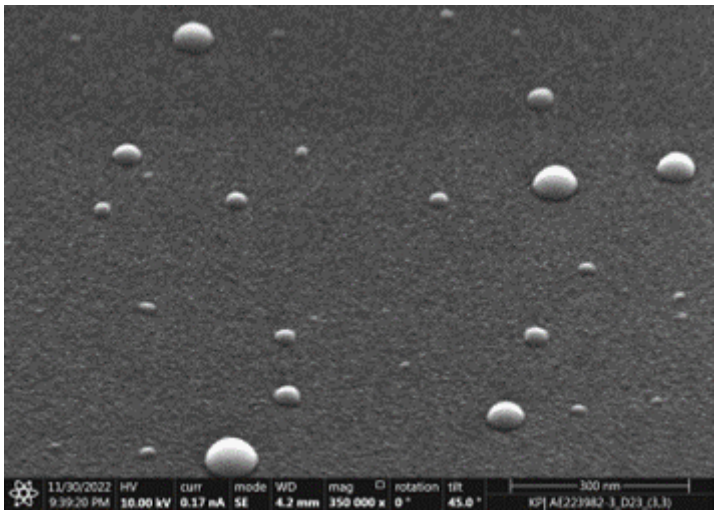

Fig.1: SEM tilted-view image (350kx) of 200 ALD super cycles of ([GeSe][As2Se3]) showing GeAsSe islands on a flat TiN bottom layer.

References

1. George, Chem. Rev. **110**, 1, 111–131 (2010)
2. Pore et al, J. Am. Chem. Soc., **131**, 3478-3480 (2009)
3. Haider et al**,** Mater. Adv., **2**, 1635-1643 (2021)
4. Yoo et al, ACS Appl. Mater. Interfaces, **12**, 20, 23110–23118 (2020)

* *Corresponding author e-mail:* tobias.peissker@imec.be

Nucleation and initial growth stages of MoS_2 by plasma-ALD

Jeff J.P.M. Schulpen[a], Wilhelmus M.M. Kessels,[a] Ageeth A. Bol[a,b]*

[a] *Eindhoven University of Technology, Groene Loper 3, Eindhoven, 5612 AE, The Netherlands*
[b] *University of Michigan, 500 S. State St., Ann Arbor, MI 48109, USA*

The controlled growth of monolayer and few-layer 2D TMDs remains an important challenge to realize electronic and opto-electronic applications based on 2D TMDs. While (MO)CVD has emerged as a powerful method of growing high-quality 2D TMD films, these films typically have to be transferred from a growth substrate to a device substrate, complicating the manufacturing process and prohibiting compatibility with nanostructured substrates. Alternatively, ALD enables highly controlled growth of 2D TMDs at relatively low temperatures and hence can be used to deposit directly on (nanostructured) device substrates. For such direct growth of monolayer or few-layer TMDs, nucleation effects on the substrate play an especially large role in determining the key properties like grain size of the resulting film. In this work, we elucidate the nucleation stage of plasma-ALD MoS_2 using a combination of in-situ and ex-situ characterization techniques. First, we critically re-evaluate the saturation behavior of this ALD process which is an important requirement for its reproducibility. We find that while no thermal decomposition of the precursor is observed in the heterodeposition regime at a substrate table temperature of 400℃, some nonsaturating component remains during the homodeposition regime. Next, we show how spectroscopic ellipsometry can be used to monitor the MoS_2 nucleation and monolayer closure *in situ,* which we verify through correlation of the data with *ex-situ* XPS and photoluminescence measurements. The fingerprint of crystalline MoS_2 is observed in the Raman spectra, with the A_{1g}-E^1_{2g} separation increasing as with film thickness as expected. Even for submonolayer films, the A_{1g}-E^1_{2g} separation remains larger than the 19 per cm expected for monolayer MoS_2, which may indicate substrate-induced strain or defectivity of the submonolayer films. Furthermore, we obtain insight into the oxidation of the sub-monolayer films from XPS scans of the Mo3d orbital region, which indicate that especially the edge sites of MoS_2 islands are prone to oxidation.

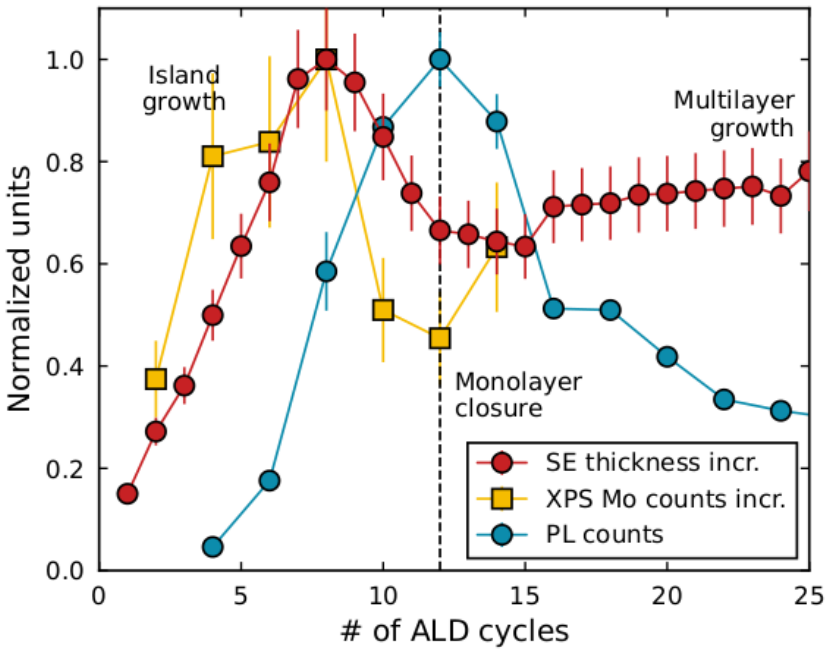

Figure 1: In-situ spectroscopic ellipsometry as probe of MoS_2 nucleation and initial growth. An initially enhanced growth rate converges to steady-state growth, indicative of film closure. The stabilization of the growth rate coincides with the maximum photoluminescence yield at monolayer closure.

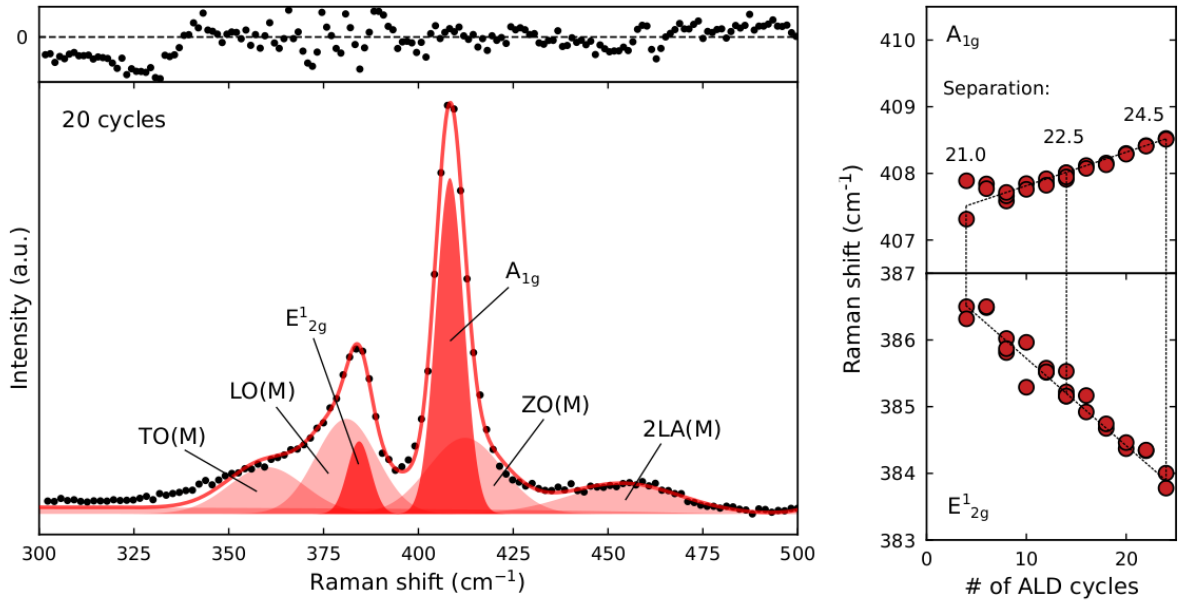

Figure 2: Raman spectra taken after different number of ALD cycles show the characteristic peaks of crystalline MoS_2. The A_{1g}-E^1_{2g} separation increases with number of ALD cycles. The small separation of 19 per cm characteristic for monolayer MoS_2 is not observed which may be related to strain or defectivity of the submonolayer film.

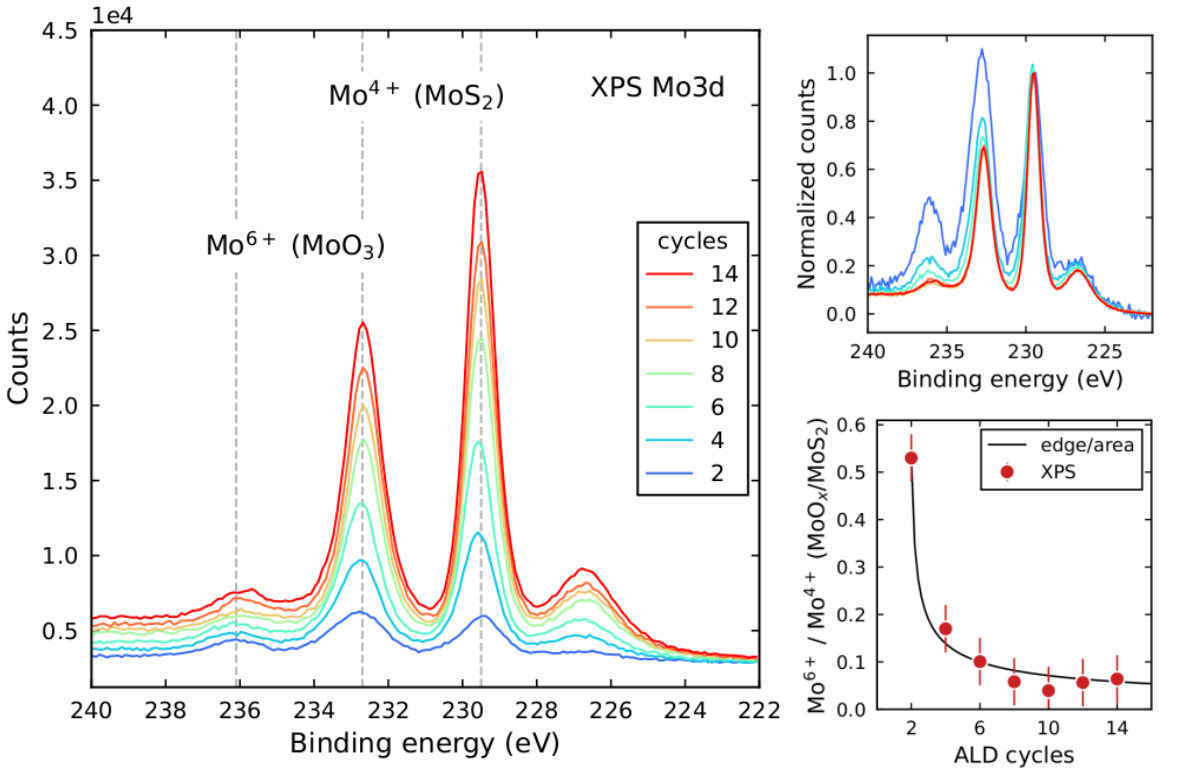

Figure 3: XPS elemental scan of the Mo3d orbital region shows increasing Mo counts with increasing number of ALD cycles. Furthermore, presence of 6+ oxidation state Mo can be quantified, indicating oxidized MoO_3. The relative amount of oxidation decreases with number of ALD cycles, indicating that especially the MoS_2 island edges are sensitive to oxidation.

* *Corresponding author e-mail:* aabol@umich.edu

Fast Plasma ALD for Quantum: Superconducting NbN

Dmytro Besprozvannyy*, Michael Powell, Louise Bailey, Harm Knoops, Agnieszka Kurek, Russ Renzas, and Andrew Newton

Oxford Instruments Plasma Technology, North End, Yatton, Bristol, BS49 4AP, UK

In recent years, plasma ALD has become an essential technique for nanoscale fabrication, including high-volume manufacturing,[1] due to its self-limiting behaviour and low temperature operating regimes. Multiple ALD applications in the quantum segment, including the deposition of superconducting nitrides, are moving from the research field into production where fast deposition times and product throughput is critical. Additionally, highly conformal films are required to coat demanding 3D structures.[2]

The challenge is to deliver fast processes while maintaining and improving the film properties. This is particularly important in new technology areas, such as superconducting quantum devices, where device performance is closely tied to materials and processing, and required thicknesses are frequently in the 50-200 nm regime.

Here, we will share recent development of a high-quality superconducting NbN for quantum applications, such as resonators and interconnects, capable of depositing > 50 nm film thickness in two hours. The process uses (t-Butylimido)tris(diethylamino)niobium(V) (TBTDEN) precursor and a N_2/H_2/Ar plasma at a relatively low temperature of 320° C. The RF-driven remote plasma source design and chamber of our system is optimized for ALD and short cycle times.

The high quality of the deposited films was demonstrated by the electrical resistivity measurements, a conformality of 100% on 8:1 aspect ratio trenches and superconducting transition temperature (T_c) showing > 11K.Thickness uniformity of < ±5% across a 150 mm Si wafer was achieved with 1% repeatability. We will also show how film stress can be tuned as a function of process parameters, such as the RF power.

Emerging quantum technologies based on superconducting nitride materials are showing great promise and will benefit not only from the uniformity of the deposition, conformality and film quality, but also from the speed and control provided by this ALD process.

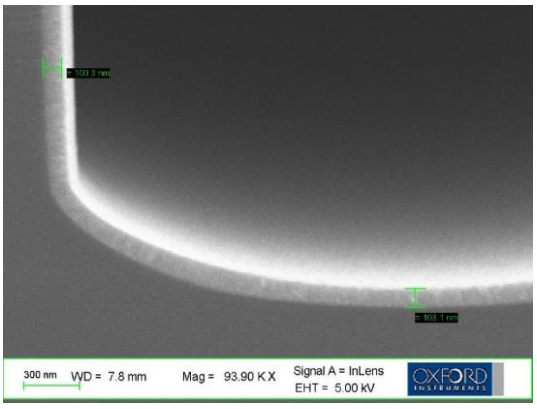

Plasma ALD NbN (100 nm) on 8:1 aspect ratio trench.
The thickness on the side walls, the bottom of the trench and the top of the structure is comparable.

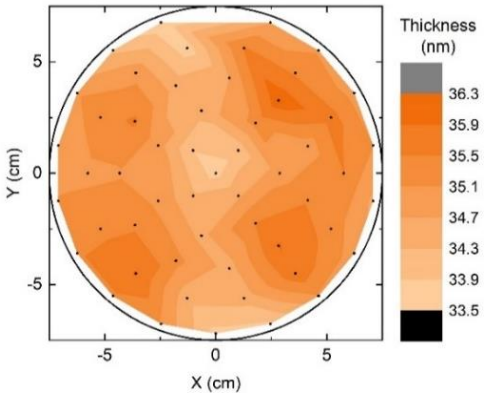

NbN thickness distribution map with a 3 mm edge exclusion showing a ± 1.4 nm non-uniformity across a 150 mm wafer.

References

1. Knoops et al., J. Vac. Sci. Technol. A, Vol. 37, No. 3, May/Jun 2019
2. Arts et al., J. Vac. Sci. Technol. A 37(3), May/Jun 2019

* *Corresponding author e-mail: dmytro.besprozvannyy@oxinst.com*

Dielectrics II

Chair: Van Elshocht, Sven (imec)

Time: 6/2/2023 8:30:00 AM
Location: Auditorium 1, Promotion Hall, Naamsestraat 22, Leuven

Atomic Layer Deposition of Functional Complex Oxides for Next-generation Electronics?

Mari Napari[a,†,*], Andrew Caruana[b], Mikko Heikkilä[c], Simo Huotari[d], Jaakko Julin[e], Christy Kinane[b], Sami Kinnunen[e], Otto Mustonen[f], Gavin Stenning[b]

[a] *School of Electronics and Computer Science, University of Southampton, Southampton SO17 1BJ, U. K.*
[b] *STFC ISIS Pulsed Spallation Neutron and Muon Facility, Harwell OX11 0QX, U. K.*
[c] *Department of Chemistry, University of Helsinki, 00014 Helsinki, Finland*
[d] *Department of Physics, University of Helsinki, 00014 Helsinki, Finland*
[e] *Department of Physics, University of Jyvaskyla, 40500 Jyvaskyla, Finland*
[f] *School of Chemistry, University of Birmingham, Birmingham B15 2TT U. K.*

Throughout the 21st century the researchers have been developing new concepts, strategies, and materials, that could replace the silicon-based CMOS technologies used today. While we do not know yet, what are the major technologies that will take over in the Beyond-CMOS / Beyond-Moore era, it is certain, that these technologies, like the semiconductor-based electronics, will rely on high-quality thin films. However, in the next-generation technologies it is not only the quality, but also the functionality and the performance of these thin film materials, that make the difference. One particularly intriguing family of materials for the electronics applications are oxides and their heterostructures, thanks to their extreme diversity[1]. Similar to the semiconductor technologies, the realisation of the new device concepts will require thin film fabrication methods that are compatible with the material systems and are scalable to large scale device production without compromising in the film quality. This is where the atomic layer deposition (ALD) has the most to offer.

In this talk I will discuss the potential of ALD for emerging nanoelectronic technologies based on functional oxide thin films. As a more detailed case study example I will present spinel ferrite films that can be used as spin-filtering layers for spintronic devices that operate with spin-polarised currents. In this work plasma-enhanced ALD was used to deposit cobalt ferrite ($CoFe_2O_4$, CFO) and iron-rich nickel ferrite ($Ni_{0.75}Fe_{2.25}O_4$, NFO) thin films. Due to the additional kinetic energy provided by the plasma species generated by the direct capacitively coupled plasma, the films grown on sapphire wafers were epitaxial with correct cationic arrangements with minimal amount of light element impurities and showed ferrimagnetic behaviour at room temperature. Additionally, the polarized neutron reflectometry measurements showed that the thin films of both CFO and NFO have a high structural and magnetic uniformity over the film thickness at film thicknesses <10 nm. However, as the film thickness is increased, a magnetic gradient appears, which can be linked to the structural changes in the growing ALD film.

References

[1] M. Coll et al. "Towards Oxide Electronics: A Roadmap" *Appl. Surf. Sci. 482 (2019) 1*
[2] M. Coll & M. Napari "Atomic Layer Deposition of Functional Multicomponent Oxides" *APL Materials 7 (2019) 110901*

[*] *Corresponding author e-mail: mari.napari@kcl.ac.uk*
[†] *Present address: Department of Physics and Astronomy, King's College London, London WC2R 2LS, U. K.*

Plasma Enhanced-Atomic Layer Deposition of nanolaminates and nanocomposites Al_2O_3/HfO_2 layers on wide band gap semiconductors

B. Galizia[a,b*], P. Fiorenza[a], E. Schilirò[a], G. Greco[a], S. Di Franco[a], M. Saggio[c], F. Giannazzo[a], F. Roccaforte[a], G. Malandrino[b], R. Lo Nigro[a]

[a] *Consiglio Nazionale delle Ricerche – Istituto per la Microelettronica e Microsistemi (CNR-IMM); Strada Ottava, 5, Catania 95121, Italy*
[b] *Dipartimento di Scienze Chimiche, Università di Catania, Viale Andrea Doria, 6, Catania 95125, Italy*
[c] *STMicroelectronics, Stradale Primosole, n50 – 95121 Catania, Italy*

One of the biggest challenges in modern power electronics is represented by power losses in semiconductor devices causing an increase of energy consumption. Overcoming the physical limits of traditional Silicon-based technologies by using wide band gap (WBG) semiconductors, such as silicon carbide (SiC) and gallium nitride (GaN), the energetic efficiency and electrical performances could be both improved. [1–3] Nevertheless, several issues still need to be addressed such as the finding of an appropriate gate insulator [4]. Moreover, since device frequency performance is strongly dependent on maintaining a high geometric aspect ratio between gate length and barrier width, precise control over the thickness of gate insulators is very important. In this context, atomic layer deposition (ALD) is considered as a key enabling technique because of its controlled layer-by-layer growth. [5] Huge efforts are nowadays devoted to the fabrication of multicomponent gate insulators having high dielectric constants and good chemical stability. Notably, the growth of Al_2O_3-HfO_2 laminated layers is among the most interesting combinations because of the possibility to mix the complementary characteristics of the two materials [6,7], i.e. the thermal stability of the Al_2O_3 and the high dielectric constant of the HfO_2 materials.

In this work, Plasma Enhanced-ALD growth of different Al_2O_3/HfO_2 combinations has been considered, specifically fabricating both nanolaminated stacked Al_2O_3-HfO_2 layers and a homogeneous nanocomposite HfAlO layer (Fig. 1). Nanolaminated Al_2O_3/HfO_2 thin films consisted in alternated and well-defined nanosub-layers (thickness lower than 3 nm) of each oxide, and the number of alternated layers has been changed while maintaining the same total film thickness of 30 nm. The nanolaminated system demonstrated higher dielectric constants compared with single Al_2O_3 layer, a better thermal stability compared with the raw HfO_2 and a general decrease of dielectric defects such as trapped charges. [8,9] Finally, 30 nm nanocomposite Al_2O_3-HfO_2 layers, having no alternating structures but homogeneous HfAlO composition, have been deposited as well. In this case the dielectric properties have been compared by varying the Hf:Al ratio stoichiometric composition and higher dielectric constant has been associated with higher Hf:Al ratio, up to 4:1. On the basis, of all the collected data the nanocomposite Hf-rich layer can be considered the most promising system. In fact, it showed better dielectric behavior in terms of dielectric constant value and charge traps amounts, as it can be seen from electrical characterization (Fig. 2).

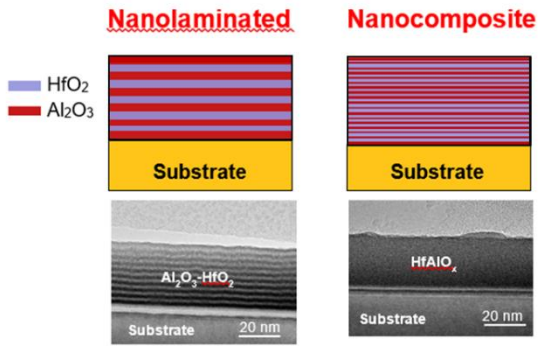

Fig. 1: Scheme of Al_2O_3 and HfO_2 thin layer combinations as nanolaminated and nacomposite systems and the related cross-section TEM images of the samples deposited by pasma ehnanced-ALD method.

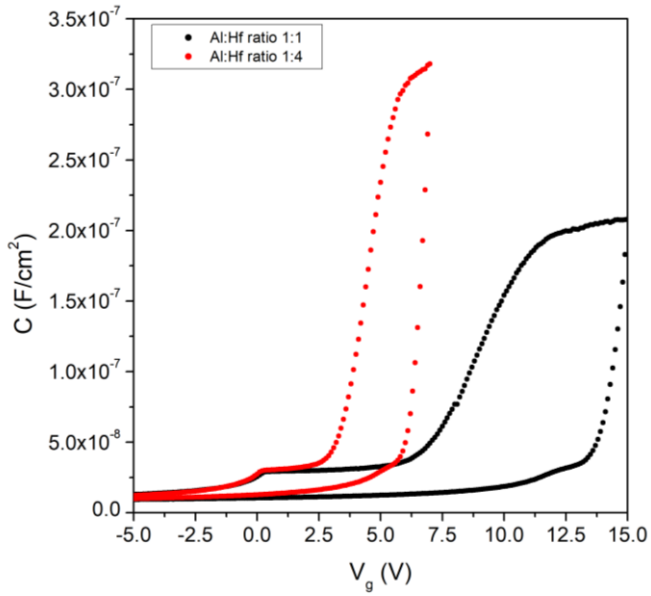

Fig. 2: Capacitance-Voltage measurements of nanocomposite samples with different stoichiometry dielectrics on the same WBG 4H-SiC substrate.

References

1. F. Roccaforte, P. Fiorenza, G. Greco, R. Lo Nigro, F. Giannazzo, F. Iucolano, and M. Saggio, *Emerging Trends in Wide Band Gap Semiconductors (SiC and GaN) Technology for Power Devices*, Microelectronic Engineering **187–188**, 66 (2018).
2. J. Millán, P. Godignon, X. Perpiñà, A. Pérez-Tomás, and J. Rebollo, *A Survey of Wide Bandgap Power Semiconductor Devices*, IEEE Transactions on Power Electronics **29**, 2155 (2014).
3. F. Roccaforte, P. Fiorenza, R. Lo Nigro, F. Giannazzo, and G. Greco, *Physics and Technology of Gallium Nitride Materials for Power Electronics*, La Rivista Del Nuovo Cimento **41**, 625 (2018).
4. R. Lo Nigro, P. Fiorenza, G. Greco, E. Schilirò, and F. Roccaforte, *Structural and Insulating Behaviour of High-Permittivity Binary Oxide Thin Films for Silicon Carbide and Gallium Nitride Electronic Devices*, Materials **15**, 3 (2022).
5. M. Ritala and J. Niinistö, *Industrial Applications of Atomic Layer Deposition*, ECS Trans. **25**, 641 (2009).
6. P. Eklund, M. Sridharan, G. Singh, and J. Bøttiger, *Thermal Stability and Phase Transformations of γ-/Amorphous-Al_2O_3 Thin Films*, Plasma Processes and Polymers **6**, S907 (2009).
7. K. Kukli et al., *Effect of Selected Atomic Layer Deposition Parameters on the Structure and Dielectric Properties of Hafnium Oxide Films*, Journal of Applied Physics **96**, 5298 (2004).
8. R. Lo Nigro, E. Schilirò, P. Fiorenza, and F. Roccaforte, *Nanolaminated Al_2O_3/HfO_2 Dielectrics for Silicon Carbide Based Devices*, Journal of Vacuum Science & Technology A **38**, 032410 (2020).
9. R. Lo Nigro, E. Schilirò, P. Fiorenza, and F. Roccaforte, *Comparison between Single Al2O3 or HfO2 Single Dielectric Layers and Their Nanolaminated Systems*, Adv. Mater. Lett. **11**, 1, 20011460 (2020).

* *Corresponding author e-mail:* bruno.galizia@imm.cnr.it

Tuning the crystallinity of Boron Nitride using Chemical Vapor Deposition

Thomas Souvignet (Phd)[a], Bérangère Toury[a], Catherine Journet[a*], Catherine Marichy[a*]

[a] *Laboratoire des Multimarériaux et Interfaces, 6 rue Victor Grignard, Villeurbanne, 69622, France*

2D materials are excellent candidates for current and future electronic devices. Among them, hexagonal boron nitride (hBN) is proving to be a key material for future graphene-based optoelectronic devices,[1] as it is an insulator and an isostructural of graphene. It appears to be a substrate of choice to boost the properties of graphene and thus enable the implementation of this later in real-life applications. Recently, it has been shown that controlling the degree of crystallinity of BN can have a significant impact on its intrinsic properties. For example, amorphous BN displays an ultra-low dielectric constant of 1.16, whereas a value of 4.0 at 1MHz is observed for hBN.[2] Therefore, tailoring the structure of BN and thus its properties would permit widening its application areas, from isolating interconnects and high-performance electronics in optoelectronic to spintronics.[3]

Among the synthesis approaches, Chemical Vapor Deposition (CVD) of hBN has been widely reported in the literature and thin films have been obtained from different precursors such as ammonia-borane, diborane, BCl_3 and borazine (formula $B_3N_3H_6$).

In the present contribution, BN films with different degrees of crystallinity deposited by CVD are introduced. The impact of the different growth parameters on the final material is presented using the borazine as a single source precursor. Four different gases are investigated: Ammonia, Nitrogen, Ar/H_2 95/5 and Ar/H_2 90/10. Particular attention is paid to the influence of the carrier gas flow rate, the type of substrates and the deposition temperature. The obtained films are characterized by ellipsometry, X-ray diffraction, scanning electron microscopy, electron dispersion, Raman and Infra-red spectroscopy.

As expected, the deposition temperature plays a crucial role, although the nature of the carrier gas strongly influences the reactivity of the borazine and thus the final structure of BN. The results show a stoichiometric B:N ratio of 1:1 with very low carbon and oxygen contamination on the films deposited with an Ar/H_2 mixture on the copper foil, while higher oxygen impurities and lower crystallinity are noted on Si(100). Films grown at 1000°C show the presence of small crystallites. Control of the crystallinity of BN films can be achieved by regulating the temperature during the process, allowing the deposition of films within a wide range of crystallinity. Not only copper but also Si 100 has been used as a substrate with similar results without cleaning nor treatment of the substrates.

References

1. K. K. Kim *et al.*, ACS Nano, Synthesis and Characterization of Hexagonal Boron Nitride Film as a Dielectric Layer for Graphene Devices, **6**, 8583–8590 (2012)
2. S. Hong *et al.*, Nature, Ultralow-dielectric-constant amorphous boron nitride, **582**, 511–514 (2020)
3. A. Antidormi *et al*., Nano Mater. Sci., Emerging Properties of Non-Crystalline Phases of Graphene and Boron Nitride Based Materials, **4**, 10-17 (2022)

[*] *Corresponding author e-mail: catherine.journet@univ-lyon1.fr, catherine.marichy@univ-lyon1.fr*

Comparison of Thermal and Plasma Enhanced ALD growth of Al_2O_3/AlN dielectric stacks on silicon carbide

R. Lo Nigro[a*], B. Galizia[a,b], P. Fiorenza[a], E. Schilirò[a], G. Greco[a], Z. Fogarassy[c], B. Pecz[c], G. Malandrino[b], M. Saggio[d], F. Giannazzo[a], F. Roccaforte[a]

[a] *Consiglio Nazionale delle Ricerche – Istituto per Microelettronica e Microsistemi (CNR-IMM); Strada Ottava, 5, Zona Industriale, Catania 95121, Italy*
[b] *Dipartimento di Scienze Chimiche, Università di Catania, Viale Andrea Doria, 6, Catania 95125, Italy*
[c] *Centre for Energy Research, Institute of Technical Physics and Materials Science, Konkoly-Thege ut 29-33, 1121 Budapest, Hungary*
[d] *STMicroelectronics; Stradale Primosole, 50 – 95121 Catania, Italy*

Over the last years, silicon carbide (4H-SiC) semiconductor has become suitable for high-power applications due to its superior properties compared with silicon, such as lower intrinsic carrier concentration, higher breakdown field, saturation velocity, and thermal conductivity.[1,2] Nevertheless, there are still some open topics related to the exploitation of the full potentiality of this material and among them the nature of the dielectric layer in metal-insulator-semiconductor (MIS) devices is a crucial issue to be faced.[3,4] In fact, the traditionally used SiO_2 dielectric suffers from low dielectric constant (≈3.9) compared to the one of 4H-SiC (≈9.7), so that, according to Gauss' law, the high breakdown field of 4H-SiC (3 MV/cm) cannot be fully exploited because of the earlier breakdown of SiO_2 layer.[5] Consequently, high dielectric constant, large band-offset and good thermal stability as well as low density of defects are the ideal properties for gate dielectric in 4H-SiC power devices.[3,4]
Aluminum oxide (Al_2O_3) possesses most of the ideal dielectric properties, nevertheless, Al_2O_3 thin films demonstrated do not possess a better interface quality than SiO_2 layers.[6,7] In this context, another high-κ insulator of interest is the aluminium nitride (AlN) having not only high dielectric constant, but also a low lattice mismatch to 4H-SiC (~0.9%).[8-10] These properties make it promising for a very good interface quality if epitaxially grown on (0001)4H-SiC (Fig.1). On the otherhand, it has been demonstrated that AlN thin layers can be obtained as epitaxially grown layers only for film thickness of few nanometers and that after 6 nm critical thickness value, the polycrystalline structure becomes predominant currently making AlN unsuitable as MIS dielectric.[8,9]
In this work, a new solution is proposed to exploit advantageous features of both Al_2O_3 and AlN dielectrics: Al_2O_3/AlN bilayers (Fig.1) were fabricated on 4H-SiC via Atomic Layer Deposition (ALD) methods. ALD is widely recognized as one of the best synthesis techniques, because of its excellent precision on thickness control, high uniformity, reproducibility and conformality even on high aspect-ratio substrates.[11] Moreover, it represents probably the best trade-off between good film's properties and suitable industrial scaling of the process and in some cases the Plasma-Enhanced ALD (PE-ALD) growth is considered the best solution for deposition on flat substrates.
In this work, we studied and compared the effect of thermal-ALD and PE-ALD Al_2O_3 layers on AlN thin interfacial layer grown on 4H-SiC at 250°C. The AlN interfacial layer has been deposited via PE-ALD growth, since it is well known that plasma processes produce higher purity and denser nitride films with respect the thermal ALD method.[10] In this context, structural and electrical characterization of the two Al_2O_3/AlN bilayers obtained by T-ALD or PE-ALD depositions of the Al_2O_3 layers, are reported. Poor electrical behavior of the PE-ALD Al_2O_3/AlN bilayer has been correlated to its structural characteristics (Fig.2). In particular, the presence of degradation at the interface between plasma-deposited Al_2O_3 and AlN has been detected probably due to an oxidation interaction caused by oxygen plasma even at deposition temperature as low as 250°C.
By contrast, the structural and electrical properties of the T-ALD Al_2O_3/AlN bilayers showed promising characteristics (Fig2). In particular, the investigated samples demonstrated a reduction of the oxide trapped charges (almost one order of magnitude down to 10^{11}-10^{12}), a slight reduced amount of interface traps density and an increase of dielectric constant (from ~7.5 to ~8.5) compared with a single Al_2O_3 reference layer. These preliminary results encourage the investigation of Al_2O_3/AlN bilayers as a candidate for future 4H-SiC power MIS applications.

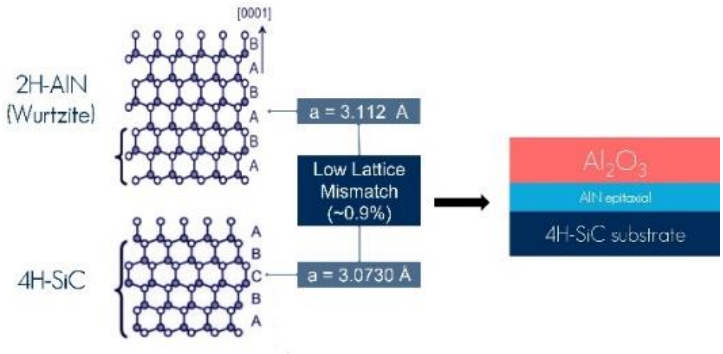

Fig. 2: Crystalline structures of 2H-AlN and 4H-SiC materials and their lattice parameters and relationship as well as a scheme of the proposed Al_2O_3/AlN dielectric stack on 4H-Sic substrates..

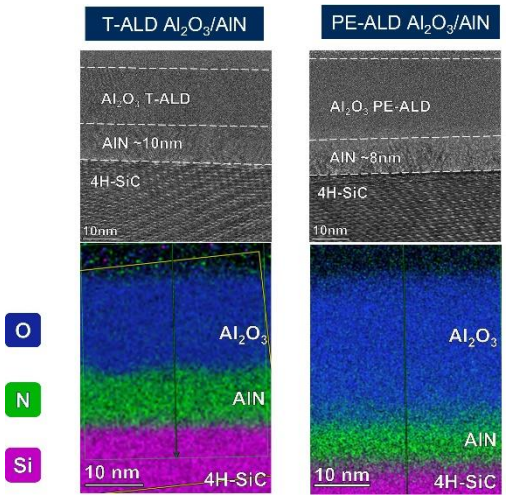

Fig. 2: STEM images and the relative EDX chemical maps of the two Al_2O_3/AlN dielectric stacks obatined by deposition of Al_2O_3 layers by thernal-ALd or PE-ALD methods

References

1. F. Roccaforte, P. Fiorenza, G. Greco, R. Lo Nigro, F. Giannazzo, F. Iucolano, and M. Saggio, *Emerging Trends in Wide Band Gap Semiconductors (SiC and GaN) Technology for Power Devices*, Microelectronic Engineering **187–188**, 66 (2018).
2. J. Millán, P. Godignon, X. Perpiñà, A. Pérez-Tomás, and J. Rebollo, *A Survey of Wide Bandgap Power Semiconductor Devices*, IEEE Transactions on Power Electronics **29**, 2155 (2014).
3. R. Lo Nigro, P. Fiorenza, G. Greco, E. Schilirò, and F. Roccaforte, *Structural and Insulating Behaviour of High-Permittivity Binary Oxide Thin Films for Silicon Carbide and Gallium Nitride Electronic Devices*, Materials **15**, 3 (2022).
4. A. Siddiqui, R. Y. Khosa, and M. Usman, *High-k Dielectrics for 4H-Silicon Carbide: Present Status and Future Perspectives*, J. Mater. Chem. C **9**, 5055 (2021).
5. P. Fiorenza, F. Giannazzo, and F. Roccaforte, *Characterization of SiO_2/4H-SiC Interfaces in 4H-SiC MOSFETs: A Review*, Energies **12**, 12 (2019).
6. F. Zhang et al., *Interfacial Study and Energy-Band Alignment of Annealed Al_2O_3 Films Prepared by Atomic Layer Deposition on 4H-SiC*, Journal of Applied Physics **113**, 044112 (2013).
7. . E. Schilirò, R. Lo Nigro, P. Fiorenza, and F. Roccaforte, *Negative Charge Trapping Effects in Al_2O_3 Films Grown by Atomic Layer Deposition onto Thermally Oxidized 4H-SiC*, AIP Advances **6**, 075021 (2016).
8. J. Choi and J. P. Chang, *Band Structure and Alignment of the AlN/SiC Heterostructure: Applied Physics Letters, **86**,*192101 (2005).
9. R. Y. Khosa, J. T. Chen, K. Pálsson, R. Karhu, J. Hassan, N. Rorsman, and E. Ö. Sveinbjörnsson, *Electrical Properties of 4H-SiC MIS Capacitors with AlN Gate Dielectric Grown by MOCVD*, Solid-State Electronics **153**, 52 (2019)
10. W.-C. Kao, W.-H. Lee, S.-H. Yi, T.-H. Shen, H.-C. Lin, and M.-J. Chen, *AlN Epitaxy on SiC by Low-Temperature Atomic Layer Deposition via Layer-by-Layer, in Situ Atomic Layer Annealing*, RSC Adv. **9**, 12226 (2019).
11. M. Ritala and J. Niinistö, *Industrial Applications of Atomic Layer Deposition*, ECS Trans. **25**, 641 (2009).

* *Corresponding author e-mail:* raffaella.lonigro@imm.cnr.it

Novel concepts

Chair: Bahlawane, Naoufal (Luxembourg Institute of Science and technology)

Time: 6/2/2023 10:30:00 AM
Location: Auditorium 1, Promotion Hall, Naamsestraat 22, Leuven

Synthesis of mixed anion oxynitride thin films as visible light active self-cleaning photocatalytic coatings

Geoffrey Hyett[a*], Samuel D. Cosham[a], Alex N. Kulak[b], Antonio Iborra-Torres[a], Kelly Rees[a], Karl M. Kaye [a], and Nathanya J Platt.[a]

[a] *School of Chemistry, University of Southampton, SOUTHAMPTON, UK*
[b] *School of Chemistry, University of Leeds, Leeds, UK*

Cutting-edge materials research is increasingly focused on compounds containing multiple anions, and with more complex compositions. This interest is driven by the increased structural and compositional diversity, and difference in anion properties which allows for greater control of the electronic structure and optimization of functional properties, with examples in photocatalysis,[1,2] superconductivity,[3,4] and thermoelectrics.[5] It is vital that thin film techniques suitable for large area, low-cost applications such as CVD can keep pace with the developments in these areas of materials chemistry and are able to supply depsoiton methods for complex multicomponent and mixed anion films. To help address this we have investigated routes to thin films of oxynitride and other ternary composition materials, with a particular emphasis on their application as visible light active photocatalysts.

In this presentation we will report on our use AACVD to synthesis the established visible light photocatalyst TaON as a thin film from the reaction of tantalum ethoxide and ammonia. The self-cleaning ability of this film was assessed using stearic acid as the model pollutant.[6] We have also investigated the perovskite tantalum and niobium oxynitrides, which are likewise known visible light photocatalysts form work carried out on bulk particles. We establish a route for the deposition of thin films for seven perovskite oxynitrides. A cobalt oxide co-catalyst was deposited onto each film by drop casting. Catalytic tests were conducted using stearic acid degradation, and this found the film of $SrNbO_2N$ with the cobalt oxide co-catalyst to be the most active for complete mineralization of this model pollutant. Using a real-world loading of greasy contamination on a surface we can estimate the time to completely remove this contamination under conditions of the bright sunlight, as 13.4 h for the $SrNbO_2N$ film,[7] and 28 h for the TaON film.[6]

We can also report on a novel CVD approach to the formation and control of composition of mixed anion materials, as applied to titanium oxynitride thin films. The method used is the AACVD of a mixture of single source precursors. By combining tetrakis(dimethylamido) titanium and titanium tetraisopropoxide in specific ratios in a series of AACVD reactions at 400 °C, we are able to deposit thin films of titanium oxynitride with three different structure types and a wide range of compositions. Using this precursor system, we can observe films of nitrogen doped anatase, with 25% anion doping of nitrogen; a new composition of pseudobrookite titanium oxynitride with a composition of $Ti_3O_{3.5}N_{1.5}$, identified as being a UV photocatalyst; and rock-salt titanium oxynitride in the range $TiO_{0.41}N_{0.59}$ to $TiO_{0.05}N_{0.95}$. This work shows that a dual single-source CVD approach is an effective method for the deposition of ternary mixed anion ceramic films through simple control of the ratio of the precursors.[8]

Finally, we can report on use of AACVD to form thin films of the zinc titanate phases using zinc acetate and titanium isopropoxide as precursors. Using a technique previously reported with powders, the mixed ZnO and Zn_2TiO_4 films were treated with acid to produce porous Zn_2TiO_4 which, through reduction and vapour leaching of zinc, were converted to hierarchically porous thin films of anatase TiO_2. This conversion was monitored by XRD. Analysis of photocatalytic activity of the hierarchically porous titania, using dye and stearic acid degradation tests, found a factor of 12 to 14 increase in rates of photocatalysis over conventional TiO_2 thin films.[9]

References

1. Q. Wang *et al.*, Nat. Mater**.** 18**,** 827 (2019). **2**. C. Pan, T. Takata, and K. Domen, Chemistry – A European Journal 22, 1854 (2016). **3**. D. Johrendt and R. Pottgen, Angew. Chem., Int. Ed. 47, 4782 (2008). **4**. H. Ogino, S. Sato, K. Kishio, J. Shimoyama, T. Tohei, and Y. Ikuhara, Appl. Phys. Lett. 97, 3, 072506 (2010). **5**. L. D. Zhao, D. Berardan, Y. L. Pei, C. Byl, L. Pinsard-Gaudart, and N. Dragoe, Appl. Phys. Lett. 97, 092118 (2010). **6**. S. D. Cosham, V. Celorrio, A. N. Kulak, and G. Hyett, Dalton Trans. 48, 10619 (2019). **7**. A. Iborra-Torres, A. N. Kulak, R. G. Palgrave, and G. Hyett, Acs Applied Materials & Interfaces 12, 33603 (2020). **8**. K. Rees, E. Lorusso, S. D. Cosham, A. N. Kulak, and G. Hyett, Dalton Trans. 47, 10536 (2018). **9**. N. J. Platt, K. M. Kaye, G. J. Limburn, S. D. Cosham, A. N. Kulak, R. G. Palgrave, and G. Hyett, Dalton Trans. 46, 1975 (2017).

[*] *Corresponding author e-mail: g.hyett@soton.ac.uk*

Stimuli-responsive thin films and their applications as actuators and on-skin sensors

Anna Maria Coclite [a,*]

[a] *Graz University of Technology, Petergsasse 16, Graz, 8010, Austria*

Stimuli-responsive materials are those that change their properties, as shape, wettability, optical properties depending on environmental cues, like pH, temperature, humidity. Such dynamic property can be used in several modern devices. In addition, when the stimuli-responsive material has the shape of a thin film, the response, which is based on diffusion, is very fast and reversible.

Functional and responsive surfaces have been successfully deposited by initiated Chemical Vapor Deposition (iCVD) on a variety of substrates.[1] Such method allows the full retention of the functional groups of the monomer structure and this is important to obtain a large responsiveness amplitude. This presentation will focus on the applications of stimuli-responsive nanofilms for sensors and actuators. The high versatility of iCVD in driving application-specific properties into the material, creating a platform for the implementation of polymeric coatings into device fabrication, will be discussed.

Fast response and large signal amplitude are fundamental requirements for good sensors. Fast and ultra-fast humidity sensors based on the optical detection of the change in thickness of the iCVD hydrogels will be shown.[2] The implemented sensor prototype delivered reproducible relative humidity values and the achieved response time for an abrupt change of the humidity was about three times faster compared to one of the fastest commercially available sensors on the market.

The combination of materials with different properties in nanostructures is required to meet the needs of modern intelligent devices. Several examples of such type of hybrid devices will be presented. In particular, an electronic skin concept was realized by combining stimuli-responsive thin films with piezoelectric zinc oxide in core-shell geometries.[3] Such device geometry was obtained by templated atomic layer deposition of the ZnO followed by the iCVD of the stimuli-responsive film. The nanostructuration of the films lead to a location-specific signal detection. In addition, the combination of two different materials allowed the detection of three stimuli: force, humidity and temperature. The whole sensor device could be deposited on flexible substrates and used for on-skin sensor or as electronic skin. While the piezoelectricity of ZnO provides sensitivity to external force, the thermoresponsiveness of the hydrogel core provides sensitivity to surrounding temperature and humidity changes. The hydrogel core exerts mechanical stress onto the ZnO shell, which is translated to a measurable piezoelectric signal. A localized force sensitivity of 364 pC N^{-1} is achieved with very low cross talk between 0.25 mm^2 pixels. Additionally, the sensor's sensitivity to humidity is demonstrated at 20° and 40 °C, i.e., above and below the hydrogel's lower critical solution temperature (LCST) of 34 °C. The largest response to temperature is obtained at high humidity and below the hydrogel's LCST. The sensor response to force, humidity, and temperature is significantly faster than the system's intrinsic or excitation-induced time scale. Finally, the sensor response to touch and breath demonstrates its applicability as e-skin in real- life environment.

Another example of device that will be shown is a pH-sensor, again based on a pH-responsive thin film deposited by iCVD, and deposited on tattoo paper, so that it can be easily applied to the skin to measure physiological signals.[4] When the tattoo sensor is transferred on skin it maintains full functionality, and shows excellent conformability to topographical features of epidermis. The investigation of the morphology of all layers within the sensor verifies full control of the desired width of electrodes, thickness of hydrogel, and deposition shielded areas. The hydrogel layer exhibits a reversible pH-responsive swelling of 24.7 ± 0.3% to 38 ± 1%, with respect to the dry state, at pH 4 to pH 6, respectively. Impedance spectroscopy identifies the phase shift at 10 and 1000 Hz as an excellent pH-related property of the sensor, which can be only ascribed to the presence of the hydrogel. The sensors ability to be operated with non-sophisticated read-out hardware and software is also demonstrated.

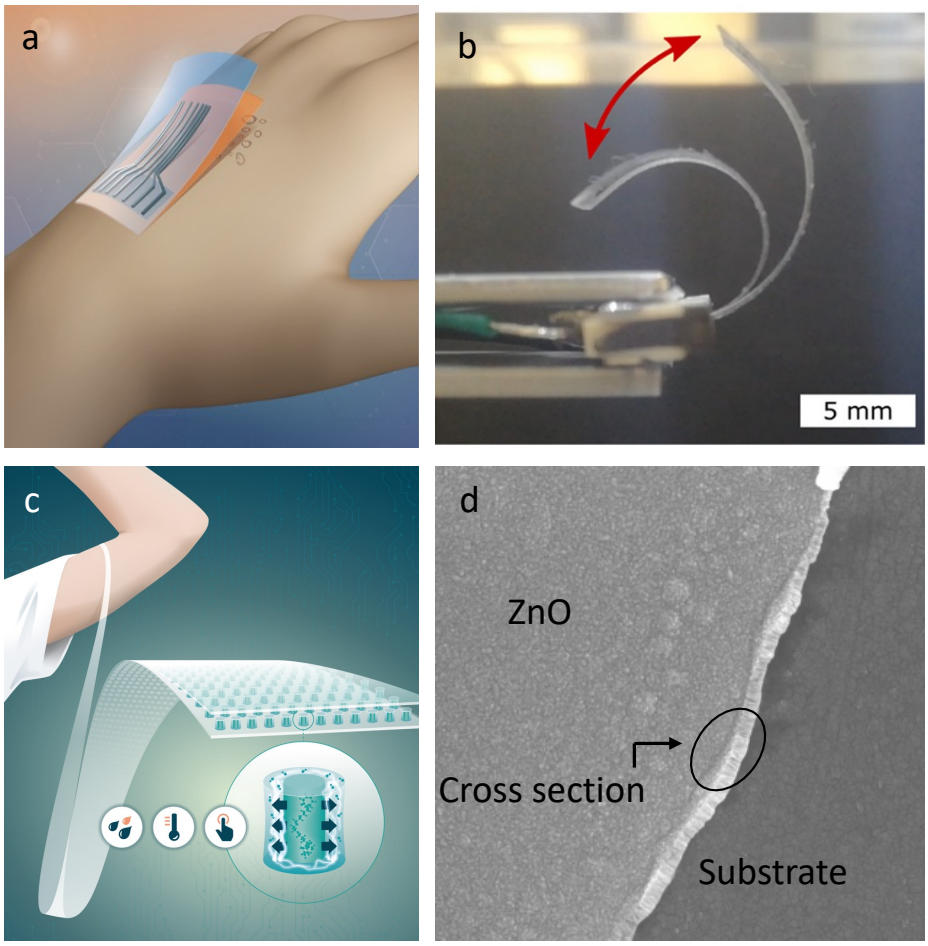

Figure 1: Sensors based on stimuli-responsive hydrogels: (a) electronic tattoo responsive to pH change [4] (b) actuator based on a bilayer of an inert material and a humidity-responsive one [5] (c) electronic skin responsive to force, temperature and humidity [3] (d) SEM cross section of a zinc oxide thin film with columnar growth [6].

References

1. Coclite AM, Howden RM, Borrelli DC, et al (2013) 25th anniversary article: CVD polymers: a new paradigm for surface modification and device fabrication. Adv Mater 25:5392–5423. https://doi.org/10.1002/adma.201301878
2. Buchberger A, Peterka S, Coclite AM, Bergmann A (2019) Fast optical humidity sensor based on hydrogel thin film expansion for harsh environment. Sensors (Switzerland) 19:1–11. https://doi.org/10.3390/s19050999
3. Abu Ali T, Schäffner P, Belegratis M, et al (2022) Smart Core-Shell Nanostructures for Force, Humidity, and Temperature Multi-Stimuli Responsiveness. Adv Mater Technol 7:2200246. https://doi.org/10.1002/admt.202200246
4. Unger K, Greco F, Coclite AM (2022) Temporary Tattoo pH Sensor with pH-Responsive Hydrogel via Initiated Chemical Vapor Deposition. Adv Mater Technol 7:2100717. https://doi.org/10.1002/admt.202100717
5. Dallinger A, Kindlhofer P, Greco F, Coclite AM (2021) Multiresponsive Soft Actuators Based on a Thermoresponsive Hydrogel and Embedded Laser-Induced Graphene. ACS Appl Polym Mater 3:1809–1818. https://doi.org/10.1021/acsapm.0c01385
6. Abu Ali T, Pilz J, Schäffner P, et al (2020) Piezoelectric Properties of Zinc Oxide Thin Films Grown by Plasma-Enhanced Atomic Layer Deposition. Phys status solidi 217:2000319. https://doi.org/10.1002/pssa.202000319

* *Corresponding author e-mail: anna.coclite@tugraz.at*

Competitive diffusion as a route to enhance step coverage in CVD

Arun Haridas Choolakkal,* Pentti Niiranen, Hans Högberg, Jens Birch and Henrik Pedersen

Department of Physics, Chemistry and Biology, Linköping University, SE-581 83 Linköping, Sweden

Molecules with a lower mass diffuses faster than heavier molecules in a mixture of gases at local thermodynamic equilibrium. We hypothesize that this phenomenon can be used to improve film uniformity and step coverage (SC) in CVD. We define SC as the film thickness at the sidewall in the bottom of a feature divided by the film thickness at the side wall at the top of the feature. Our concept is to add a heavy non-reactive molecule, as diffusion additive, to promote diffusion of the reactive gas species. We test this in a single precursor thermal CVD process.

We have recently shown that perfectly conformal, i.e., SC = 1, B_xC films can be deposited in 8:1 aspect ratio features from triethyl boron, $B(C_2H_5)_3$ (TEB), in a hydrogen ambient at 450 °C substrate temperature and 5 kPa total pressure.[1] However, we noted that 450 °C is the upper temperature limit for SC = 1 and that the SC decreases with higher temperature. The film density and composition improved close to B_4C at temperatures above 450 °C, making higher temperature deposition desirable.

Here, we present our studies on adding a diffusion additive to the B_xC CVD process. The molecular mass of TEB is 98 g/mole. A diffusion additive must thus have a molecular mass > 98 g/mole and be non-reactive at the CVD conditions, making Xenon (Xe), with an atomic mass of 131 g/mole, a suitable choice. We therefore added a co-flow of Xe to the TEB and hydrogen flows in the conformal B_xC process. We note an increase in SC from 0.71 to 0.97 with the addition of Xe gas at 550 °C. We also note that the area of uniform film thickness in the reactor increased, while the film-substrate interface roughness decreased by a factor of about 50 % with the addition of Xe. These results indicate that our hypothesis of enhanced diffusion is correct. X-ray photoelectron spectroscopy measurements show no changes in the chemical state of the films with and without addition of Xe.

References

1. A.H. Choolakkal, H. Högberg, J. Birch, and H. Pedersen, J. Vac. Sci. Technol. A 41, 013401 (2023).

* *Corresponding author e-mail: arun.haridas.choolakkal@liu.se*

Superconductivity in Chromium Oxide Thin Films Embedding Silver

Markus Otus[a]*, Gunta Kunakova[b], Taivo Jõgiaas[a], Donāts Erts[b], Jekaterina Kozlova[a] Kaupo Kukli[a],Aile Tamm[a]

[a] *University of Tartu, Institute of Physics, W.Ostwaldi 1, 50411 Tartu, Estonia*
[b] *University of Latvia, Institute of Chemical Physics, 19 Raina boulevard, Riga, LV-1586, Latvia*

Beginning with the experiments of H. Kamerlingh Onnes [1] over a hundred years ago and sparked further with the discoveries by Bednorz and Müller [2], superconductivity has become one of the most thoroughly researched and utilised quantum mechanical phenomena, with the search for novel materials which exhibit the necessary properties being an ongoing process for more than a century. Recently, Stanev *et al*. [3] implemented machine learning modelling to propose novel materials which might exhibit superconductivity. In this work, we have attempted to synthesize $AgCrO_2$, one of the materials listed by Stanev *et al.*, as a candidate material, and investigate its properties.

To synthesize the stacked nanostructures, we produced a number of thin film and/or particle combinations starting with either a Si or a Si/TiN substrate, onto which we deposited a layer of chromium oxide in various combinations with either dispersed Ag nanoparticles or an Ag thin film. Chromium oxide layers were produced in an atomic layer deposition process via surface reactions between tris(2,2,6,6-tetramethyl-3,5-heptanedionato)chromium(III) [$Cr(TMHD)_3$] and O_3, using an in-house built flow type hot wall reactor. Prefabricated Ag nanoparticles were dispersed in an aqueous solution, and introduced to the sample surface by air-drying droplets from the dispersion. Ag thin films were deposited using thermal evaporation. After various combinations of chromium oxide and Ag, an electrode of gold, was deposited using electron beam evaporation and, afterwards, maskless photolithography was used to design the electrodes. Figure 1 presents the disain of the stacked nanostructures.

To evaluate the structure, morphology and the distribution of Ag NPs (in samples that contained them), the samples were investigated with scanning electron microscopy, energy-dispersive X-ray spectroscopy and scanning transmission electron microscopy, both before and after the resistivity measurements. Based on preliminary evaluations of the samples, an initial set of samples was selected to measure their resistivity at temperatures down to 2 K. These measurements were carried out using a physical property measurement system. Through these measurements, some of the samples were found to exhibit superconductivity, with a T_c at around 3.5 K (Figure 2).

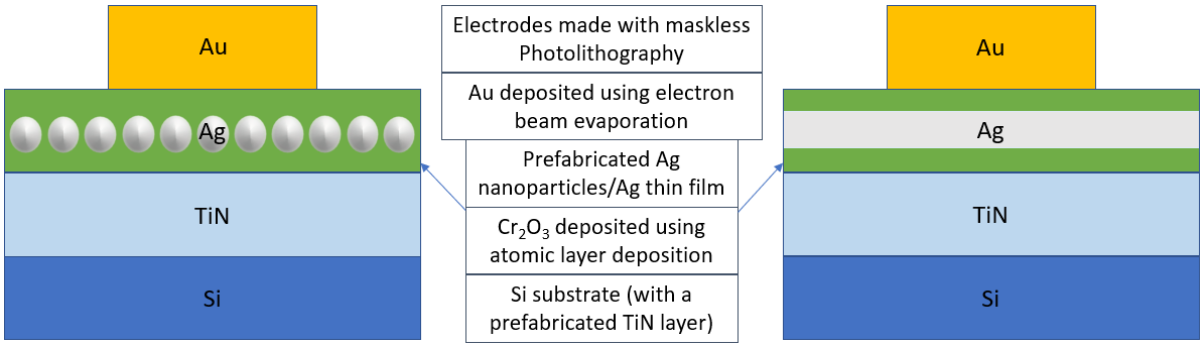

Figure 1 A schematic overview of the prepared samples and the methods used to produce them. Chrome oxide is depicted in green.

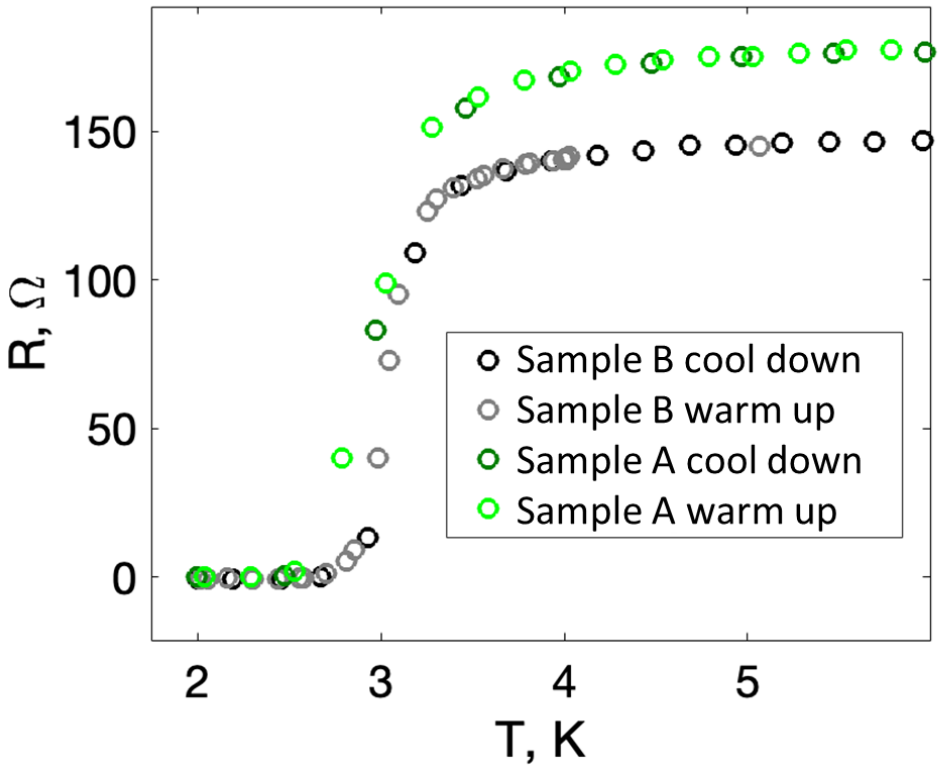

Figure 2 Resistance measurements for two samples with a structure of Si|Tin|Cr_xO_x|Ag(thin film)|Cr_xO_x, showing T_c at around 3.5K. A and B in the sample names indicate a difference in electrode distances, with a distance of 250 µm for sample A and 100 µm for sample B.

References

1. Kamerlingh Onnes, H. The resistance of pure mercury at helium temperatures. *Proc. Koninklijke Akademie van Wetenschappen, Amsterdam* 261–272 (1911).
2. Bednorz, J. G. & Müller, K. A. Susceptibility measurements support high-tc superconductivity in the ba-la-cu-o system. *Zeitschrift für Phys. B - Condens. Matter* **64**, 189–193 (1986). https://doi.org/10.1007/BF01303701
3. Stanev, V., Oses, C., Kusne, A.G. et al. Machine learning modeling of superconducting critical temperature. npj Comput Mater 4, 29 (2018). https://doi.org/10.1038/s41524-018-0085-8

* *Corresponding author e-mail:* markus.otsus@ut.ee

Novel metal-polymer interface engineering via combined atomic layer and physical vapor deposition

Johanna Byloff[a,d], Pierre-Olivier Renault[b], Damien Faurie[c], S. Altaf Husain[b], Thomas E. J. Edwards[a],Barbara Putz[a,e,*]

[a] *Empa, Feuerwerkerstrasse 39, Thun, 3602, Switzerland*
[b] *Université de Poitiers, 11 Bd Marie et Pierre Curie, Poitiers, 86073, France*
[c] *Université Sorbonne Paris Nord, 99 avenue Jean Baptiste Clément, Paris, 93340, France*
[d] *ETH Zürich, Rämistrasse 101, Zurich, 8092, Switzerland*
[e] *Montanuniversität Leoben, Franz-Josef-Strasse 18, Leoben, 8700, Austria*

Metal thin films on polymers serve a variety of applications in industry, medicine and space travel. The Al-Polyimide (PI) system investigated in this study offers high temperature resistance and good adhesion properties between substrate and coating. Previous studies [1, 2] attributed the favourable adhesive properties to the natural formation of a thin amorphous Al-O-C interlayer [3] (IL, 5 nm thick) between metal film and PI substrate. A novel cluster deposition setup at Empa Thun (SC-1, Swiss Cluster) allows combining atomic layer (ALD) and physical vapour deposition (PVD) without breaking vacuum. Using this system, we are uniquely able to mimic natural interlayers artificially, with resemblance in thickness, microstructure and eventually also chemistry. Overview and high-resolution TEM images of the natural interlayer (IL) in the Al-PI system are shown in Fig. 1, together with a model of artificial interlayer deposition using ALD/PVD.

To study the mechanical and interfacial benefits of interlayers over a wide thickness range, Al thin films (150 nm, PVD) were deposited on a polyimide substrate with different Al_2O_3 interlayer thicknesses (ALD at room temperature, precursor sequence: $Al(CH_3)_3$ (TMA) + H_2O, 1, 8, 42, and 208 cycles, nominal thicknesses: 0.12, 1, 5, and 25 nm). Ongoing work includes thorough analysis of the resulting interlayer chemistry (hydrogen-content) and high-resolution cross-sectional FIB/TEM analysis of the local interface structure, focusing on ALD surface coverage, growth per cycle (GPC) and potential post-deposition diffusion and oxidation phenomena. Specifically, the comparison of a reference sample (natural interlayer) with the 5 nm artificial Al_2O_3 interlayer film system will show to what extend synthetic interlayer deposition can resemble natural interlayer formation.

For mechanical testing, the Al/Al_2O_3 bi-layer films on polyimide were subjected to equi-biaxial tensile loading [4] and unloading with in-situ X-ray diffraction and electrical resistivity measurements at Synchrotron SOLEIL. All samples were tested up to a maximum applied strain of 8%. Thus, the evolution of Al film stress, width of the Al diffraction peak and electrical resistivity as a function of the strain and IL thickness could be determined. Additionally, post-mortem SEM images were analysed to obtain crack density and spacing, and correlate well to observed differences in the shape of the film stress-strain curves. Notably, all artificial bilayer systems show good adhesion, comparable to the reference film, and no delamination was observed. Significant embrittlement of the Al film due to the presence of a brittle interlayer [5, 6] was observed only for an Al_2O_3 thickness of 25 nm. This can be seen by a higher crack density indicated by orange arrows in Fig. 2 a and b. Regarding interface design, the comparison of 5 nm artificial versus natural interlayer reveals similar electrical resistivity but a difference in Al yield strength.

Future work in this direction will include implementing molecular layer deposition (MLD) into our cluster deposition system, aiming for full chemical resemblance at the interface through the deposition of Alucones and further advancing towards gradient and intelligent interface structures for dissimilar composite materials.

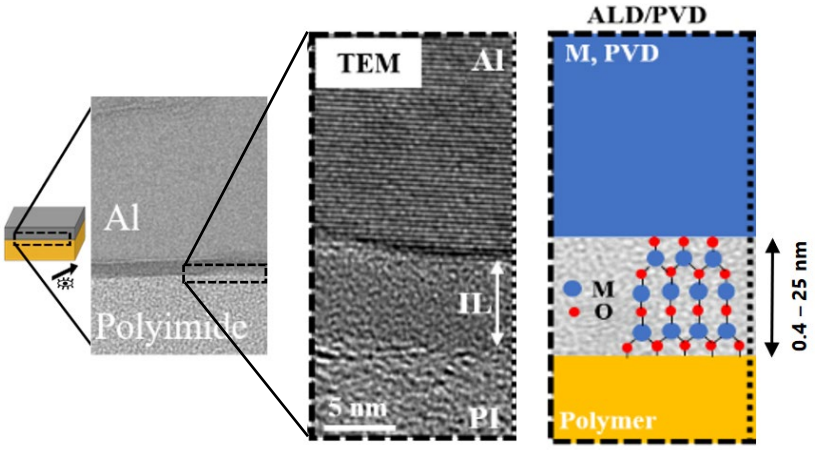

Fig 1: Overview and high-resolution TEM images of a natural interlayer (IL) between Al and polyimide (left), model of artificial interlayer deposited using ALD (right). TEM images are adapted from Ref [1].

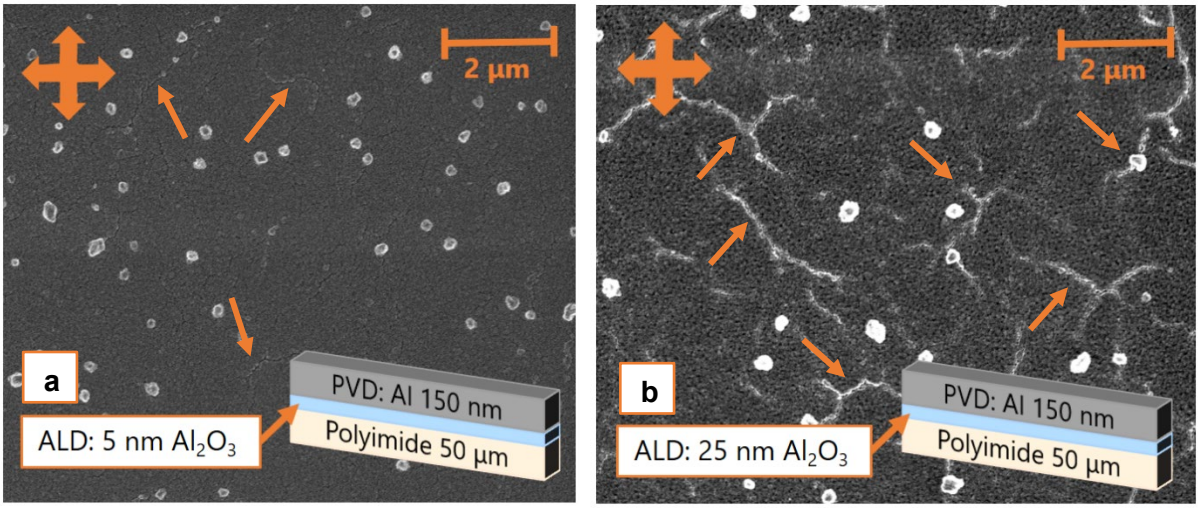

Fig 2: Post-mortem SEM images of biaxially strained Al thin films with (a) 5 nm and (b) 25 nm artificial Al_2O_3 interlayers. Tensile directions are indicated by the orange cross on the top-right corner of the images and cracks are marked with orange arrows. Both samples were tested up to a maximum applied strain of 8%. A higher crack density is observed in the 25 nm artificial interlayer sample, signalling significant embrittlement of the Al top layer.

References

1. B. Putz, G. Milassin, Y. Butenko, B. Völker, C. Gammer, C. Semprimoschnig, and M. J. Cordill, Surface and Coatings Technology **332**, 368 (2017).
2. S. H. Oh, C. Rentenberger, J. Im, C. Motz, D. Kiener, H.-P. Karnthaler, and G. Dehm, Scripta Materialia **65**, 456 (2011).
3. L. Atanasoska, S. G. Anderson, H. M. Meyer, Z. Lin, and J. H. Weaver, Journal of Vacuum Science & Technology A: Vacuum, Surfaces, and Films **5**, 3325 (1987).
4. G. Geandier, D. Thiaudière, R. N. Randriamazaoro, R. Chiron, S. Djaziri, B. Lamongie, Y. Diot, E. Le Bourhis, P. O. Renault, P. Goudeau, A. Bouaffad, O. Castelnau, D. Faurie, and F. Hild, Review of Scientific Instruments **81**, 103903 (2010).
5. B. Putz, R. L. Schoeppner, O. Glushko, D. F. Bahr, and M. J. Cordill, Scripta Materialia **102**, 23 (2015).
6. V. M. Marx, F. Toth, A. Wiesinger, J. Berger, C. Kirchlechner, M. J. Cordill, F. D. Fischer, F. G. Rammerstorfer, and G. Dehm, Acta Materialia **89**, 278 (2015).

* *Corresponding author e-mail:* barbara.putz@empa.ch

SPONSORS

Premium Sponsor

Pegasus

Silver Sponsor

ASM

DOCK/CHEMICALS
SEMICONDUCTORS DECISION

euris

Bronze Sponsor

EpiValence
Building Chemical Bonds

OXFORD INSTRUMENTS

Exhibitor

STREM CATALOG
An Ascensus Specialties Product

HIDEN ANALYTICAL

ANNEALSYS
SEMCO TECHNOLOGIES

SEMILAB

Dedicated item

Air Liquide